397 p.

CAT. 32

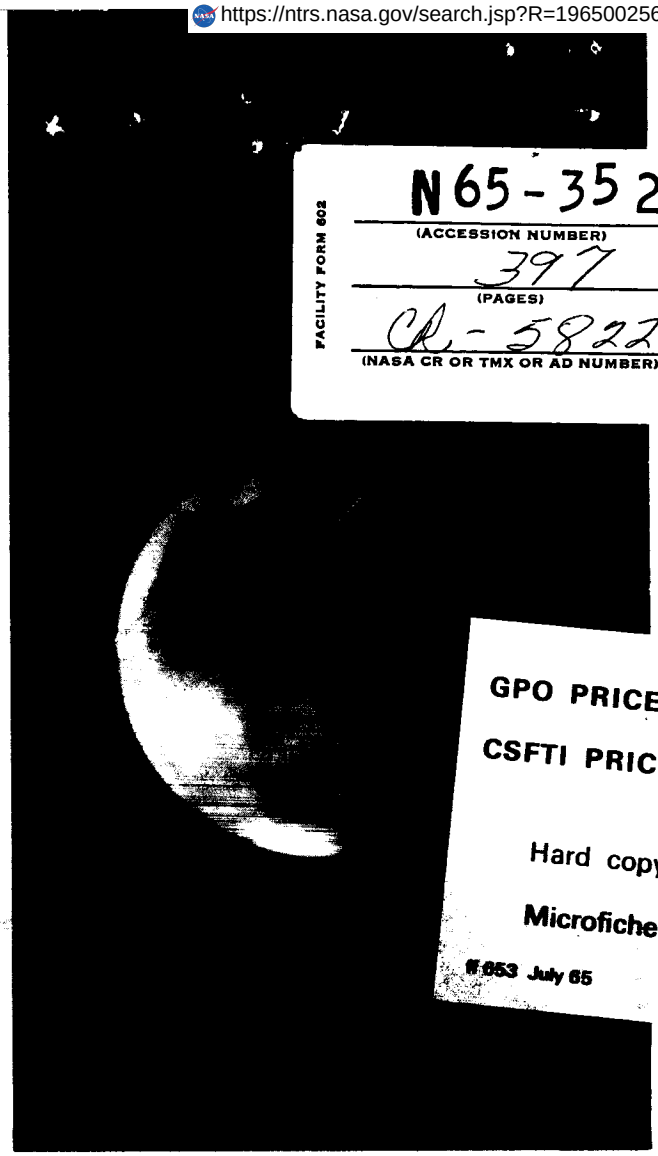

VOYAGER
DESIGN STUDIES

Volume Five: Lander Design
Part Two

Prepared Under Contract Number NASw 697 ■ Research and Advanced Development Division ■ Avco Corporation ■ Wilmington, Massachusetts ■ National Aeronautics and Space Administration ■ Avco/RAD ■ TR-63-34 ■ 15 October 1963

This document consists of 400 pages
Copy No. of 150 copies, Series A

VOYAGER DESIGN STUDIES

Volume V: Lander Design

Part II

Avco RAD-TR-63-34

15 October 1963

Prepared under Contract No. NASw 697 by

RESEARCH AND ADVANCED DEVELOPMENT DIVISION
AVCO CORPORATION
Wilmington, Massachusetts
for
NATIONAL AERONAUTICS AND SPACE ADMINISTRATION

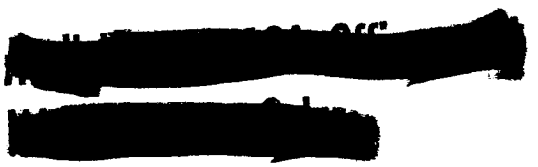

FOREWORD

The Voyager Design Study final report is divided into six volumes, for convenience in handling. A brief description of the contents of each volume is listed below.

Volume I -- Summary

A completely self-contained synopsis of the entire study.

Volume II -- Scientific Mission Analysis

Mission analysis, evolution of the Voyager program, and science payload.

Volume III -- Systems Analysis

Mission and system tradeoff studies; trajectory analysis; orbit and landing site selection; reliability; sterilization

Volume IV -- Orbiter-Bus System Design

Engineering and design details of the orbiter-bus

Volume V -- Lander System Design

Engineering and design details of the lander.

Volume VI -- Development Plan

Proposed development plan, schedules, costs, problem areas.

TABLE OF CONTENTS

LIST OF TABLES

LIST OF TABLES (Cont'd)

LIST OF TABLES (Cont'd)

LIST OF TABLES (Concl'd)

LIST OF FIGURES

LIST OF FIGURES (Cont'd)

LIST OF FIGURES (Cont'd)

LIST OF FIGURES (Cont'd)

LIST OF FIGURES (Cont'd)

LIST OF FIGURES (Cont'd)

LIST OF FIGURES (Cont'd)

LIST OF FIGURES (Cont'd)

LIST OF FIGURES (Cont'd)

LIST OF FIGURES (Cont'd)

LIST OF FIGURES (Cont'd)

LIST OF FIGURES (Cont'd)

LIST OF FIGURES (Cont'd)

LIST OF FIGURES (Cont'd)

LIST OF FIGURES (Cont'd)

LIST OF FIGURES (Cont'd)

LIST OF FIGURES (Concl'd)

6. POWER SUPPLY

6. 1 Constraints

The selection of a power source for the Mars lander was made by referring a number of candidate systems to the criteria that the system must be sterilizable, capable of providing long life service within the weight limitations, and compatable with the scientific mission. The following sections briefly describe the performance features of the several power systems which were considered and provide a discussion of the selected 110-watt radioisotope (Pu-238) thermoelectric (Ge - Si) generator, nickel cadmium battery system.

1. Temperature. The temperature range on the Martian surface is generally estimated to be from -65 to +50 ^{o}F. For most power sources which have been examined, these low temperatures constitute favorable conditions. For batteries, however, any reduction below +70 ^{o}F is reflected in capacity loss and the obvious ways to compensate result in a large weight penalty. A further aspect for the temperature constraint is the dry heat sterilization requirement at 135 ^{o}C of all lander components. This specification is particularly severe on solid fuel propellants which would be used for a certain class of short life mission and on silver zinc batteries which, were it not for their intolerance to sterilization, would otherwise be the most desirable storage device.

2. Scientific instruments. Included among the instruments in the scientific package is a gas chromatograph, which imposes a condition that the atmosphere remain clean of contaminants that may be provided by any products of imperfect combustion. This condition eliminates a large number of possible power sources; for instance, the internal combustion engines, although sterilizable and concordant with the low ambient temperatures, cannot be used on the first lander.

These last two constraints, sterilization and exhaust, have themselves effectively made the selection of the radioisotope-fueled thermoelectric generator and a nickel cadmium battery as the power source of the Mars lander.

6. 2 Power Supply Selection

The salient performance features of the various power systems examined for the Mars lander are given below.

a. Silver zinc batteries. A battery is the simplest and therefore probably the most reliable power source that can be conceived of to satisfy the lander profiles. Silver zinc batteries are particularly attractive because of their high energy density, which, in the energy regime needed to satisfy the minimum profile, is approximately 40 useable watt hours per pound. At the present state of the art, a silver zinc system is not suited due to the long wet storage shelf life as would be required by the 300-day flight. Because of this limitation, automatic activation would probably be resorted to, although this technique is not particularly attractive because no prelaunch checkout with the flight system is possible and therefore some confidence would be sacrificed. Further, for the scientific mission selected, which involves about 5,600 watt hours, 185 pounds of battery would be needed. In addition to this burden, 162 pounds would be required to transmit the 1.4×10^8 bits which have been assimilated. A 347-pound battery, without redundancy, does not seem to be a rational choice, particularly in light of the fact that the estimate is low by reason of the insulation needed to maintain temperatures above +30° F and the self heating drain that might be required.

Therefore, the silver zinc system is not feasible as a primary source. As a secondary source, to be recharged by some other primary source, it is definitely applicable since only a few cycles are needed.

In any case, silver zinc batteries are not presently sterilizable. Delco appears to be making progress in the development of one but, at present, when silver zinc is subjected to this treatment, the failure is catastrophic; silver oxide and silver peroxide decompose from the positive electrode and the separators warp. Losses of less then 50 percent are seldom encountered.

b. Hydrogen-oxygen fuel cell. The medium temperature (500 °F) hydrogen oxygen fuel cell of Pratt and Whitney was, for a time, considered as a possible power source for the lander mission. Other fuel cells such as the G. E. ion exchange membrane cell, were found to be neither lighter nor sterilizable nor further developed. The fuel consumption of 1 lb/kw-hr results in very small tankage size and weight. Gaseous storage of the fuel would therefore be acceptable thus avoiding the boiloff problem with the cryogenic technique. The product of the H_2 - O_2 reaction is water which would have to be contained, but this does not represent a difficulty because of the small quantity of fuel involved. The Pratt and Whitney fuel cell can easily tolerate the 145 °C qualification treatment.

There are two primary factors which militate against selection of this device for the Voyager mission: (1) the state of the art is not well advanced. Costly development programs would have to be undertaken and no assurance exists that acceptable flight models will be available, and (2) the system would weigh 466 pounds, which is the immediate and more dominant reason.

This weight consists of the three modules that are needed in order to achieve the assigned power system reliability of 0.99679. A reliability of 0.9 could have been accommodated with about 150 pounds.

c. Internal combustion engine. Dynamic engines are optimally suited to higher power ($\geq$ 1 kw) and short life ($\leq$ 2, 3 days) applications. High power is desirable with the dynamic engine because efficiency increases with power while fixed weight increases at a rate significantly less than power. A short life mission would definitely be preferable because of the added fuel burden of long mission.

Basically, two kinds of internal combustion engines were investigated: hydrogen-oxygen fueled systems and hydrocarbon fueled systems. The H_2 - O_2 system examined was the two-stroke engine with direct injection of O_2 into a previously admitted change of H_2. At the present time, the energy consumption rate is about 1.7 lb/kw-hr while 1.47 lb/kw-hr is established as the design goal. While this BSPL is quite attractive, a number of problems exist particularly in the area of oxygen injector operation, combustion chamber design, high heat rejection and excessive throttling losses at the hydrogen inlet value. Internal combustion engines are sterilizable and are attractive from a weight aspect (fixed weight for a 1 kw system is 35 pounds), but the state of development is not sufficiently advanced with the H_2 - O_2 fueled systems.

The second internal combustion system considered uses the more conventional hydrocarbon fuels of methanol or kerosene. These fuels can be stored in the liquid state and use a liquid oxidizer such as hydrogen peroxide. Methanol will provide about 4.7 kw-hr while kerosene is slightly higher at 5 lb/kw-hr. As in the case of the H_2 - O_2 system, the liquid fuel system is sterilizable and, also, from weight consideration, acceptable. Figure 141a provides a comparison of several lander systems at the 1-kw level. The accessory weights of generator and fuel tankage are included in the graph.

The major obstacle to acceptance of the liquid fueled internal combustion engine are the compromising exhaust products of CO, CO_2 and H_2O. The weight for the basic system, as shown in the figure, is not prohibitive (a 60-hour mission for continuous delivery of 1 kw weighs approximately 305 pounds). Nonetheless, this weight is very much greater than the weight of the RTG-Nicad battery combination which was selected for the lander power source. However, containment of the exhaust handicaps the system and reduces output by the virture of the back pressure. In addition, a compressor may be required which further complicates and reduces reliability.

The technology necessary to produce a flight model of a suitable internal combustion engine is already well established and, for lander missions after the first when the atmosphere has been satisfactorily established, this power source is quite attractive.

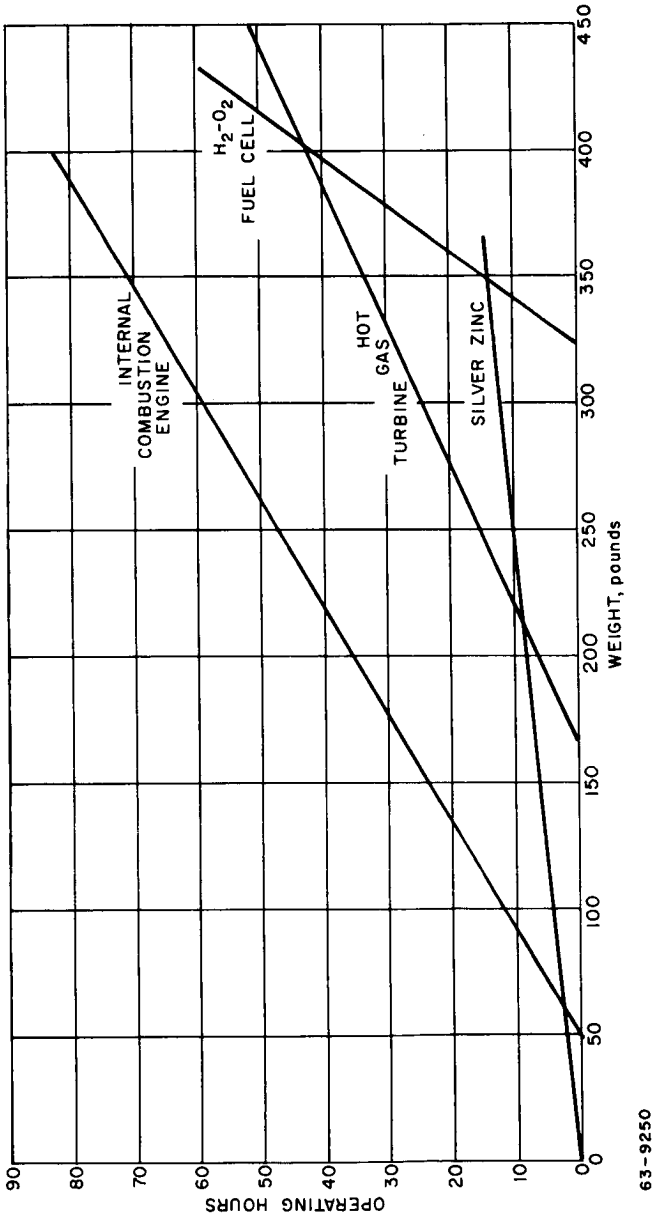

Figure 141a COMPARISON OF SOME LANDER POWER SUPPLY SOURCES

d. Hot gas turbine. The design for the hot gas turbine involves use of a series of solid propellant fuel cylinders which would be initiated on command, producing high pressure gas that drives a turbo alternator.

As the first gas generator is exhausted, a control circuit senses the drop in system pressure, or in the line frequency from the generator, and initiates the next gas generator. The line frequency is controlled by regulation of the hot gas supply system pressure by a control valve. Since the minimum burn time of a single stick is a function of its diameter and length (100 watts for 0.5 hour can be provided by a propellant 0.75-inch in diameter and 43 inches long) and each propellant must be individually contained and suitably insulated from its neighbors lest premature and inadvertent ignition occur, it was established that the fuel compartment size needed to satisfy the energy requirement of the mission would be a cylinder 1.5 feet in diameter and 3-1/2 feet long, weighing about 395 pounds.

On that basis, the system is not competitive.

Relative to the sterilization question, one fuel was found which, when sterilized at 135 °C, did not evolve gas for 82 hours. This may or may not be compatible in that the flight-proof article must sustain a qualification sterilization of three cycles at 145 °C for 36 hours and a terminal sterilization at 135 °C for 24 hours sterilization procedure.

e. Reactor systems. Nuclear reactor systems are definitely out of their weight class for the Voyager missions considered during this study.

f. Static heat engine. A limited life mission (few hours) can be provided by the combustion of magnesium or beryllium using suitable conversion. Since combustion of magnesium takes place at near 3000 °F, full advantage of this temperature can be taken only by a thermionic converter. Ignition would be established by supplying a spark in an oxygen atmosphere and thereafter the system would operate until either the fuel is wholly consumed or heat transfer through the chamber walls is reduced to the level at which the thermionic action fails to be sustained. The reduction in heat transfer occurs because of the fact that the magnesium monoxide deposited upon the chamber wall is a good insulator. This restriction to operating life may be circumvented by resorting to multiple combustion chambers which are ignited on a programed basis, as in the case of the solid propellant fueled turbine in paragraph d.

This system has already operated and provides an overall energy density of 155 watt hours per pound. The device is essentially a high power source and its fixed weight is extremely low: the basic 500-watt engine weighs about 1 pound, whereas the kilowatt size is slightly more than 2 pounds. From the standpoint of both sterilization and exhaust, MnO, the system is acceptable.

One less obvious advantage with this system is that although the thermionic diode is not a fully developed convertor, it needn't be, because in this case, the operating life of any one engine will not exceed a few hours. The low basic weight of the system will be increased by the addition of a dc - dc converter to accommodate the stepup of the 1 volt output of the generator to a nominal 28 volts. The converter would weigh about 18 pounds.

The limitations of the system, some of which are mentioned above are:

1) Not restartable. Ignition is accomplished by supplying a spark. In practice, this would be done by passing a current through a fuzable platinum wire in an oxygen atmosphere. Although this is simple enough, once started, the system cannot be restarted because all other start wires would have been melted during combustion.

2) Reliability. The daughter of 1) above is a considerable loss in confidence because the flight model cannot be checked out.

3) Short Life. Life can be extended by using additional engines but programing and load sharing problems complicate the system.

4) Limited mission selection. Though lightweight, the engine occupies a space about 6 inches in diameter by 6 inches in height and an extended mission would require considerable volume for power source. For example, an extended mission of say, 100 hours at 500 watts, would weigh about 325 pounds.

g. Solar Cells. The solar cell array is probably the least likely candidate for a power source in an unmanned lander mission. Operation is limited to sunlit periods, cloud cover is sparse but random and would interupt transmission and mission operation which is probably intolerable. Further, the landing attitude and, to a lesser extent, the lander latitude of the spacecraft are contingencies which bear heavily on effectiveness. The array must be deployed and, most likely, oriented. The small solar constant at Mars, neglecting the unknown reduction due to atmospheric absorption, would impose an array size too large to be stored and unfolded.

During the period of the study in which no battery was acceptable and the RTG is power limited by thermal reasons, the prospect was considered of utilizing the inner surface of the lander petals for mounting of a fixed solar array. This surface comprises 49 ft.^{2}. The results of an exact analysis which predicts the performance of a flat, nonoriented, horizontal solar panel at an arbitrary landing site on Mars as a function of season is shown in figure 142 for the specific case of a landing at the desirable latitude of 30 degrees south. The figure illustrates the hourly variation in performance and it is obvious that the scheme is not useable. Examine the winter solstice (arrival for a January 1969 launch). The falloff power on either side of the midday

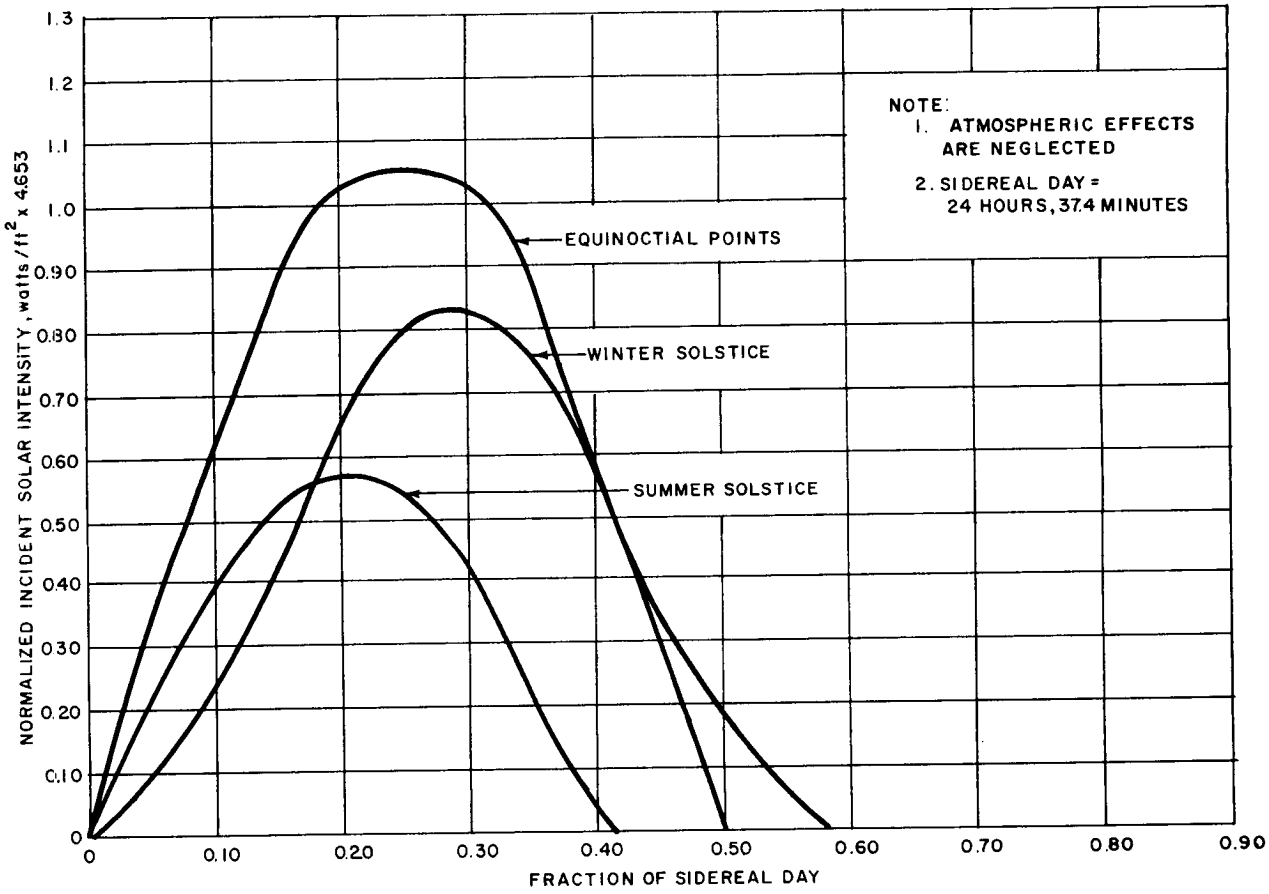

63-9320

Figure 142 INCIDENT SOLAR INTENSITY VERSUS TIME AT 30°S LATITUDE ON MARS

print is rapid. Assuming that voltages beyond the half power point are unusable, 180 watt hours/ft^2/day are obtainable and these occur during 5 to 7 hours which have been assumed to be cloudless.

As a last resort, if no other primary power source were available, this technique could be used for battery charging if a longer but reduced bit content mission were acceptable.

h. Radio-isotope thermoelectric generator. The RTG was selected as the primary power source for the Mars lander because it has many desirable features, long life, good power density, and provides a heat sink for maintenance of operating temperatures in a cold environment (it also happens to be the only candidate in the election). It is the present intention to use Pu-238 as the fuel element and germanium silicon thermoelectric conversion elements. Thermionic conversion has not been selected for two reasons:

1) There is no weight advantage because of the need to encapsulate the entire T/I package. Encapsulation is imposed because of the safety requirement that the system enter intact so that no radioactive material will be dispersed on the planet, and

2) Operating temperature, operating life and reliability are almost synonymous terms and serious material problems should be anticipated when operating at the 1600 to 1700 ^{o}K required by the thermionic diode. All information in the open literature relating to life describe failure before 1000 hours, although the classified SNAP 13 program has achieved operating lifetimes longer than this. The Voyager mission life is about 11,000 hours. In any case, no environmental tests have as yet been conducted on the SNAP program and considerable time and development effort may be required before a diode is qualified.

Technological advancement from the present state of the art merits close attention but until such time when the converter is established as a reliable, rugged, long-life device, the Voyager program shall assume the more established thermoelectric conversion.

i. Fuel selection. Fuel selection, from the availability aspect, is not the problem it was with the Mars orbiter. Power levels in the order of 110 watts rather than 800 watts are considered. Refer to figure 143 which tabulates some of the critical data on the more important isotopes.

Cesium 137 has a very low power density; 70 pounds of isotope material would be required for a 1.5-year mission at 110 watts.

Cesium 144, Curium 242 and Polonium 210 may be dismissed on the basis that their half lives are too short and would present severe, possibly insolvable, thermal control problems at the outset of the mission.

ISOTOPE	$T^{1/2}$	DECAY	W_T/ GRAM	W_T/ CC	ENERGIES (Mev)		@$T^{1/2}$ lbs/KWe	@T=1.5yr lbs/KWe	AVAIL. KWe '67	'68	'69	COST KWe	(1)LANDER WT/lbs RTG WEIGHT	(2) ORBITER RTG WT.	HEALTH ASPECTS
Cesium 137	33.0yr		0.07	0.22	0.52 0.66	weak	632.0	326.0	0.85	1.8	1.8	2.7	145	551	Bad
Cerium 144	285.0d		2.3	13.8	0.3 2.98	weak	19.2	36.2	1.2	17.5	35.0	0.28	71	261	Very Bad
Curium 242	162.0d		120.0	1170.0	6.1	weak	0.368	1.91	2.8	2.8	2.8	7.1	63	244	Fair
Curium 244	18.5yr		2.3	22.4	5.8	weak	19.2	10.1	0.01	0.07	2.05	12.7	53	235*	Bad
Polonium 210	138.0d		140.0	1320.0	5.3	8	11.1	24.6	0.28	2.8	2.8	9.3	84	235	Very Bad
Plutonium 238	86.0yr		0.48	9.3	5.5	weak	92.0	47.0	0.53	0.7	0.79	22.5	76	272*	Very Bad
Promethium 147	2.6yr		18.0	1.0	0.2	weak	245.0	183.0	0.01	0.05	0.05	10.0	93	409	Good
Strontium 90	28.0yr		0.2	0.7	0.61 2.4	weak	221.0	114.0	1.6 0.01	2.5	2.5	2.0	100	339	Very Bad
Thullium 171	1.9yr		0.2	1.5	0.1	none	221.0	190.0	UNKNOWN				110	415	Excellent
Cobalt 60	5.3		16.6	1.87	0.3	1.33	2.68	1.63	UNKNOWN					235*	Very Bad

(1) 110 watt RTG, shield neglected.

(2) Shield Weight Neglected
Battery Weight Not Included

63-8510

Figure 143 ISOTOPE AVAILABILITY CHART

Curium 244 is a seemingly excellent fuel for the Mars lander mission. Shield weight neglected, about 2 watts per pound may be achieved at the 100 watt level resulting in the lightest weight RTG in column 11 of the figure.

Promising though the fuel may be, the unshielded dose rates, although tolerable for electronic hardware, appear excessive for some of the scientific instrumentation and make necessary a heavy shield. On this basis, a more satisfactory fuel appears to be Plutonium 238.

Plutonium 238 removes the dose rate objections to Cm 244. The dose rate in rem/hr is between 2 and 3 orders of magnitude less than that which would be observed from a Cm 244 source. It is also sufficiently available.

Dose levels and equipment radiation tolerance had been receiving a great deal of attention toward the conclusion of the study. Though shielding requirements for specific instrument packages had not yet been established, it appears that the overall system weight with Plutonium 238 is less than with any other isotope in the power levels of interest.

Promethium 147 is a beta emitter which has a relatively low power density and would most probably require considerable shielding due to its contamination by other materials. In any case, the anticipated availability will not permit its consideration.

Strontium 90 is a reasonable fuel in spite of the health hazard involved. The half life is long and has a reasonable power density; about 12 pounds would be needed for a 110 watt, 1-1/2-year mission. The fact to be considered, however, is that in the decay process, emission of very strong Bremstrahlung takes place and indicates the need for considerable shielding.

Thulium 171 Isotope selection is plagued by the fact that availability, high power density, long half life, and low shielding requirements are not now achievable in a single isotope. Thulium has a short half life of 1.9 years and an acceptable power density. Its outstanding features have been purported to be its extremely low background, its low cost, and great abundance. These latter two features are now looked upon with considerable doubt due to the fact that 1) flux levels of 10^{15} neutrons/cm^2/sec are needed to produce Tm 171 from Tm 169 by the cold encapsulation method and reactors at this level will not be available for 2 years. At that time, the production capacity of these reactors is estimated to be about 200 thermal watts per year, and production by the hot encapsulation route using Erbium 170, would require approximately a 5-year lead time to develop the separation process. At that time, although the production cost is small, the separation cost is high. Even then not very much more than 200 thermal watts will be available per year.

j. Nickel cadmium batteries. The RTG is a watts device and cannot deliver large power for short periods of time. For thermal reasons, no more than 140 watts can be accommodated by the spacecraft. Since the load demand exceeds this limitation, there is need for an energy storage device.

The nickel cadmium battery is sterilizable with an 8-percent capacity loss and, though its energy density is a maximum of 14 watt-hr/lb, no alternatives exist. In spite of the higher weight necessitated by the NiCad system, it offers the advantage that it is capable of sustaining the 300-day flight in the wetted state without capacity loss. It has, in addition, demonstrated the capability to be fully discharged without damage and, were it necessary, many (>100) such deep discharges could be tolerated. The OGO satellite is presently using a 30-percent depth of discharge; for the Mars lander a 50-percent depth of discharge will be used. Since only about 10 cycles are contemplated, 75-percent discharge depth could later be resorted to in order to conserve weight.

6.3 System Description

There are two distinct phases of the Mars lander mission, each of which places different demands upon the power system. The scientific phase begins after the landing checkout and lasts for approximately 55 hours. During this period, there is a need to supply relatively small energy requirements for short periods of time. After the initial 55 hours, many of the instruments may be shut down and the scientific load will be reduced to about 10 watts. The communication phase follows the scientific phase and begins on the first pass of the orbiter or, if the relay link fails, on command from DSIF. The direct link alternative places a more severe burden on the system and therefore will be considered in discussion rather than the relay case.

1. Scientific phase. The loader profile for the scientific mission is shown in figure 144. This profile was prepared from 1) a list of scientific instruments that provided duty cycle, power consumption and number of samples required, 2) a knowledge that several instruments must operate in sequence or are limited to daytime operation, and 3) the thermal control fact that a maximum of 140 watts of RTG (assuming 7-percent efficiency) can be accommodated.

It is apparent, and will be proven in the next section, that the minimum weight which can be achieved with an RTG-battery combination is obtained by choosing an RTG which is slightly larger than that which is needed to accommodate the constant power drain and choosing, also a very low duty cycle profile, that is, one in which a given energy is spread over a very long time. This arrangement will allow the battery to be charged slowly and then quickly discharged as it delivers a small amount of energy. The practical limitations

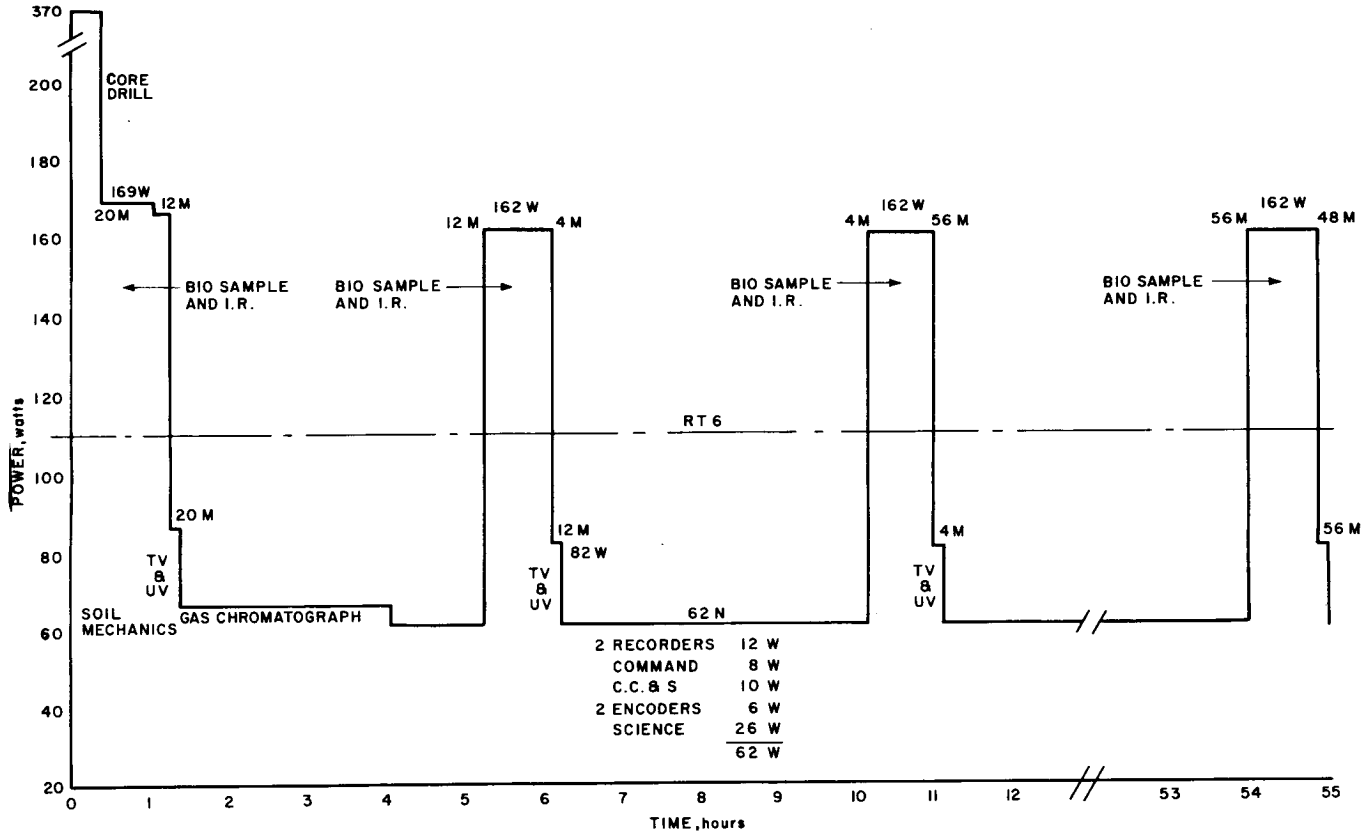

Figure 144 MARS LANDER INSTRUMENTATION PROFILE

to this approach are numerous, e. g., short discharge times and/or very long charge time cannot generally be selected arbitrarily. The load profile is usually established by other considerations such as equipment warmup time, operating period, sampling rate, etc., as is the case in the scientific instrumentation load profile of figure 144.

The minimum RTG size needed to satisfy the situation can be calculated by the following technique:

a. Load watt hours (Battery Contribution)

$$\left(\frac{162}{0.85} - P_G\right) \frac{52 \text{ min}}{60 \text{ min/hr}} = 161 - 0.867\ P_G$$

P_G is the generator power in watts

where

0.85 is the converter regulator efficiency

162 is the load in watts requirement during battery discharge

52 is the discharge time in minutes.

b. Recharge watt hours needed from RTG

$$\frac{161 - 0.867\ P_G}{(0.8)\ (0.85)} = 238 - 1.27\ P_G$$

where

0.8 represents the battery storage efficiency

0.85 represents the converter regulater efficiency

c. Recharge watt hours available from RTG

$$\left(P_G - \frac{62}{0.85}\right) 4h = 4\ P_G - 291$$

where

0.85 represents the battery storage efficiency

4 represents the charge time in hours

62 represents the constant load power drain in watts

d. Available watt hours ≥ required watt hours

$4 P_G - 291 \geq 238 - 1.27 P_G$

$5.27 P_G \geq 529$

$P_G = 100$ watts

110 watts is chosen as the reference design value.

e. $$\frac{(161 - 0.867 P_G)}{(14\,\text{wh/lb.})\ (0.5\ (0.9)\ (0.635)} = \frac{66.7\ \text{wh}}{3.92\ \text{wh/lb}} = 17\ \text{pounds}$$

where 14 wh/lb refer to the maximum achievable energy density from a nickel cadmium battery

0.5 is the depth of discharge

0.9 is the effective capacity after sterilization

0.635 represents the decrease in capacity due to the 52-minute discharge time (figure 145)

f. Power source weight

25 pounds power conditioning

47 pounds battery

80 lbs RTG

152 lbs

The zero redundancy battery weight needed to accommodate the largest of the scientific energy requirements which occurs at the beginning of the profile, as computed by the methods of a. and e., is 47 pounds.

2. Communication phase. The loadprofile for the communication phase is given in figure 146. The length of transmission time per day is established, on the short side, by the 47-pound nickel cadmium battery used for the science phase which will permit 1 hour of communication time. One hour of playout time requires an energy contribution of $\frac{(251)}{0.85} - (110) = 186$ watt hours. This corresponds exactly to a 47-pound nickel cadmium battery.

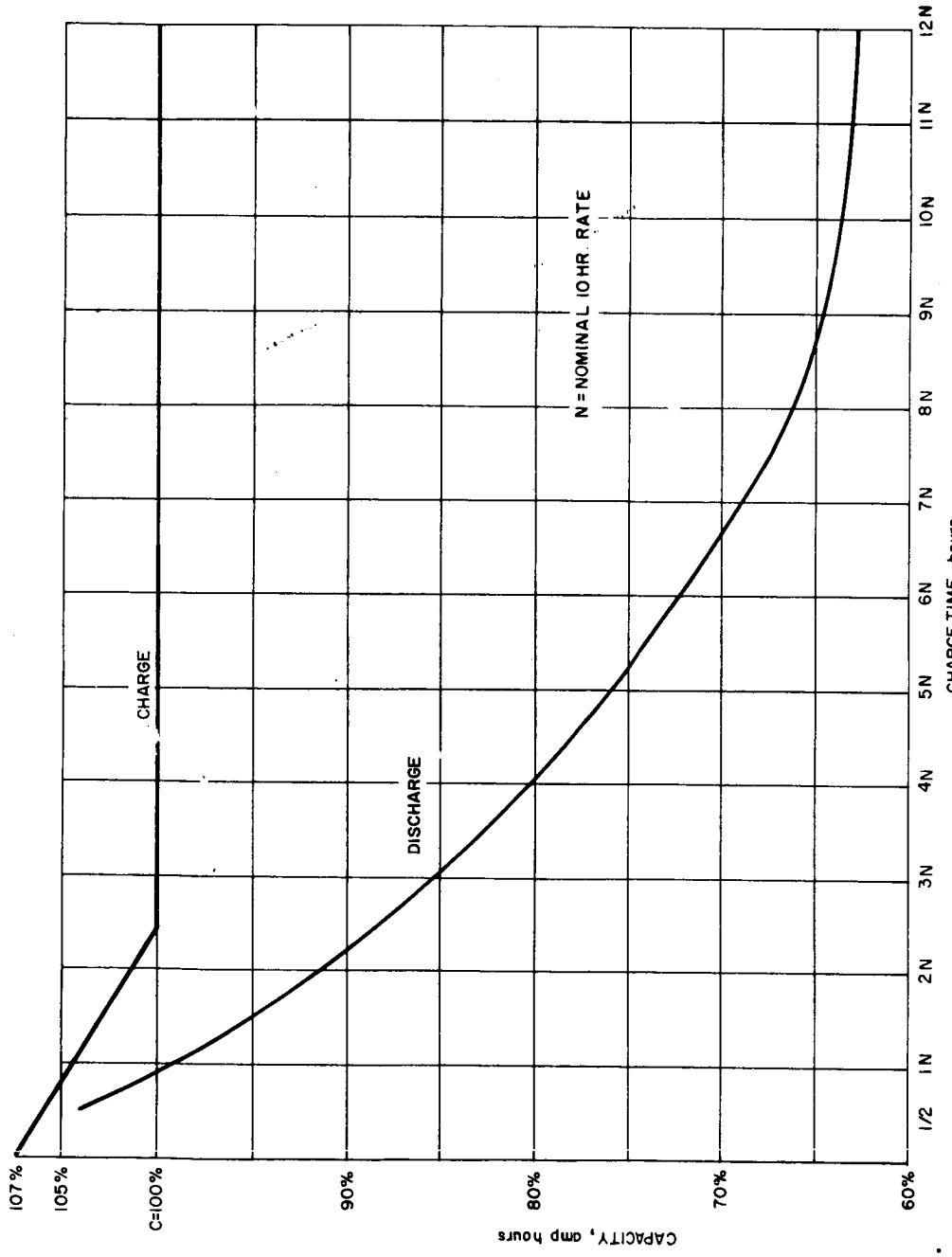

Figure 145 MARS LANDER COMMUNICATION PROFILE

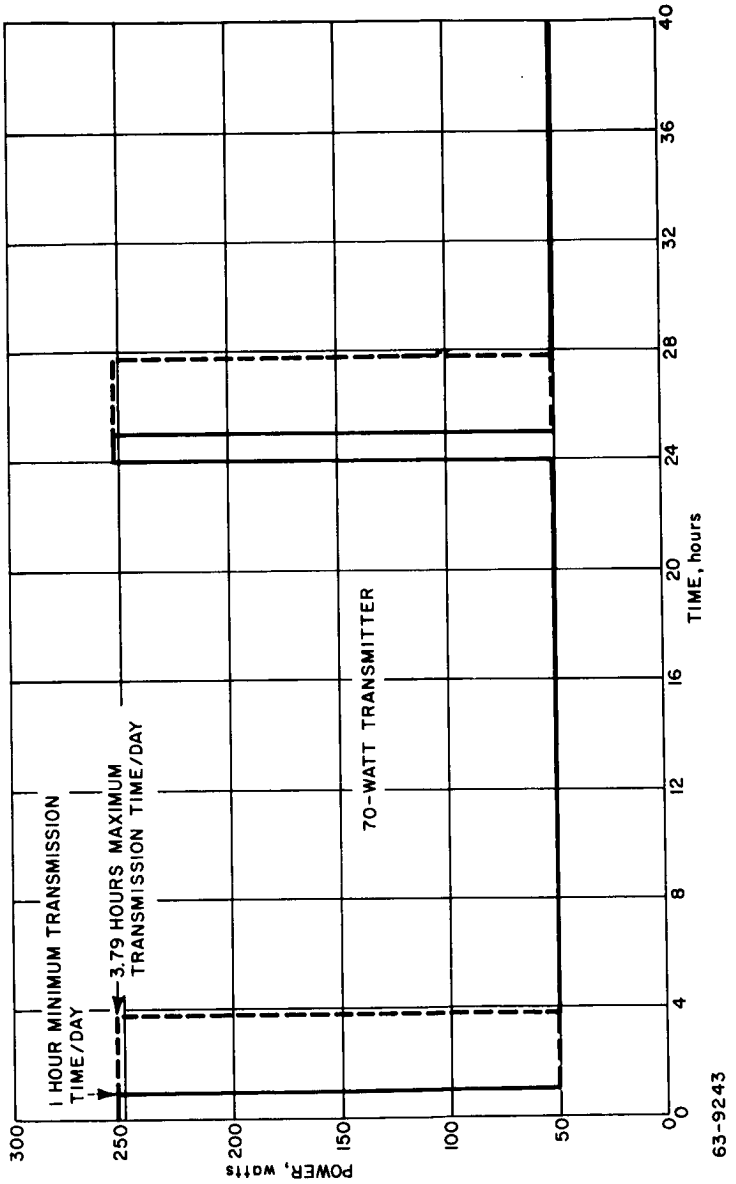

Figure 146 LOAD PROFILE FOR THE COMMUNICATION PHASE

The maximum transmission time per day is established by the recharge capability of the 110-watt RTG. This time may be calculated as follows:

a. Battery contribution. $\left[\frac{251 - (110)(185)}{0.85}\right] T = 186\,T$

b. Necessary recharge WH. From RTG $\frac{186\,T}{(0.8)(0.85)} = 273\,T$

where

0.8 = battery storage efficiency

0.85 = converter regulator efficiency.

c. Available recharge WH. $\left[110 - \frac{50}{0.85}\right](24 - T) = 1220 - 51\,T$

d. Recharge available $\geq$ recharge needed

$1220 - 51\,T \geq 273\,T$

$T \leq 3.79$ Hours

Hence, the maximum transmission time per day, under the constraint that the RTG is limited to 110 watts, is 3.79 hours.

e. Corresponding battery size = $\frac{(186)(3.79)}{(6.4\text{ wh/lb.})(0.875)} = 126$ pounds

Notice that for this long transmission time, the power system weight would increase by 79 pounds (excluding battery redundancy) over the 1-hour transmission time case. Similar calculations may be made for intermediate transmission times and for different RTG power levels. These results of this tradeoff are shown in figure 146A.

The advantage of using a higher power RTG is evident from the figure which illustrates that considerably less battery weight will be needed to achieve longer playout times. However, if short playout times are acceptable, the lower power RTG will result in the minimum weight system. The 300-watt RTG is insensitive to playout time because the peak load condition never exceeds the generator output and consequently batteries are not required.

For the case at hand, the minimum battery weight of 47 pounds which is needed for the scientific mission results in a transmission time of slightly less than 1 hour/day; however, 3 hours of transmission time per day has

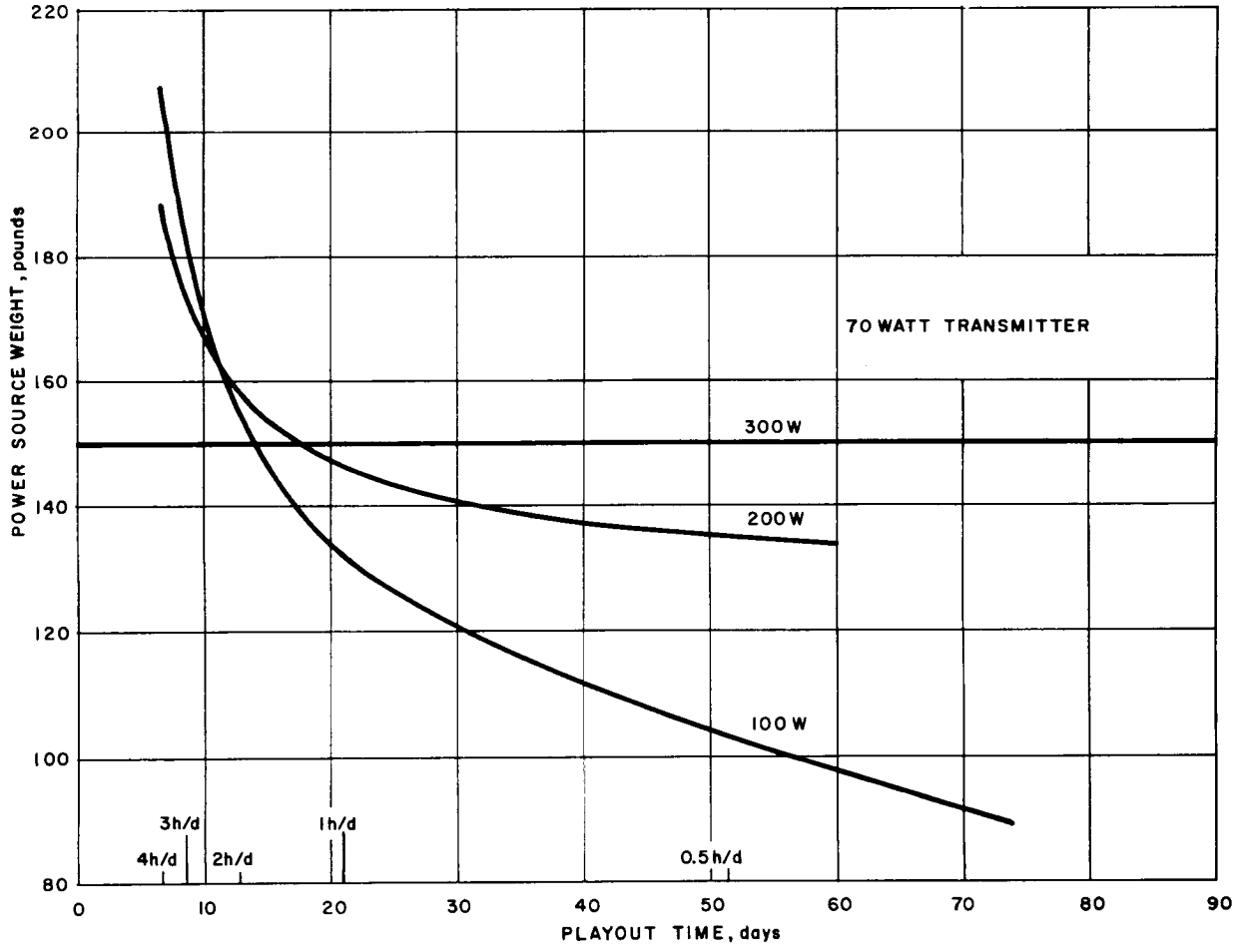

63-9322

Figure 146a POWERPLANT WEIGHT versus PLAYOUT TIME AND RTG SIZE

been established as a reasonable mission duration and in order to meet that situation, 104 pounds of batteries are needed.

3. System weights. The weights for the reference design Mars Lander power system is:

110-w RTG	80 pounds
Batteries	167 pounds (104 pounds plus 60-percent redundancy)
Power conditioner	25 pounds
Total	272 pounds

7. COMMUNICATION SYSTEMS

7.1 System Requirements

The Mars lander communication system is required to transfer to Earth all scientific and engineering data acquired by the lander during its operational life. The operational life of the lander begins with its separation from the orbiter-lander bus at approximately one million kilometers from the planet. After separation, the status of critical items in the lander must be determined. These items include the internal temperature profile of the lander, the RTG power supply, the battery, the power conditioning equipment, and the data handling equipment.

Upon entering the atmosphere approximately 60 hours after separation, additional engineering and scientific measurements must be made to determine the dynamic performance of the lander vehicle, the performance of the heat shield, and the atmospheric characteristics. The dynamic measurements include pitch, yaw, roll, and triaxial accelerations, while the static measurements include ablation of the heat shield material, and pressures. The atmospheric measurements will consist of a spectrographic analysis. At a specific, preprogramed deceleration level, a signal must be provided which will deploy the drogue chute. The main parachute is deployed by use of an altimeter. After the main parachute is deployed and the heat shield and its supporting structure jettisoned, the lander must take terrain pictures from various altitudes during descent provided it enters on the sunlit side of the planet. The total entry and parachute descent time varies with entry angle and atmospheric uncertainties. A minimum of 10 minutes descent time on the main chute is provided; the maximum total entry time is 23 minutes. The data acquired by the lander during this time must be transmitted from the lander to Earth either directly or by relay through the orbiter, before the lander impacts the planet, in order to circumvent the possibility of failure of the communications system following impact.

When the lander comes to rest on the planet surface, a complete engineering status check must be made of all lander equipment before the lander begins its main scientific mission. This status check consists of monitoring 210 functions which include all scientific instruments and data transmitting equipment and all engineering functions mentioned previously. This data must be transmitted to Earth as soon as possible to allow corrective action or modifications to be made in preprogramed operations in the event of subsystem failure. The status check will be completed in approximately 5 minutes.

The main scientific mission of the lander will commence on the completion of the engineering status check. The communication system must monitor and

store all information collected by 23 scientific instruments during the first 48 hours on the planet surface. While on the planet surface, the lander must be capable of receiving commands from Earth at any time.

When the main scientific mission of the lander has been completed, the total data acquired must be transmitted to Earth as soon as possible, either directly or by relay through the orbiter.

When all main scientific data have been transmitted from the lander, a reduced scientific mission designed to acquire planet seasonal data must be started. The information content of this reduced mission will not exceed that taken during the first 48 hours and will last for approximately 150 days. Data acquired during this phase must be stored and transmitted to Earth whenever it is convenient.

An added requirement is imposed on the lander communications system in that the lander must be sterilized to prevent the planet from being contaminated by Earth-originating organisms.

7.2 Communication System Description

1. General description. The Mars lander communication system will transmit all data acquired by the lander during its operational life either directly to Earth through a highly directional S-band link or by means of a VHF relay link through the Mars orbiter. The highly directional link consists of a steerable 5-foot parabolic antenna and a 70-watt transmitter. At a transmitted bit rate of approximately 1500 bits/sec, a worst case performance margin of +2.51db can be expected at a worst case range of 3.6×10^8 km. The relay link consists of a pair of orthogonal, crossed loaded slots and a 50-watt transmitter. This system will transmit data on command from the orbiter when the orbiter is near periapsis and within the line of sight of the lander. At a transmitted bit rate of 10,000 bits/sec a worst case performance margin of +8.34 db can be expected at a worst case slant range of 2500 km. These two links serve as redundant backups to each other. With the direct link, approximately 10 days will be required to transmit all data to Earth. With the relay link, approximately 25 days will be required to transmit the same information to the orbiter. The S-band link includes a coherent command receiver to receive commands from Earth. Commands will normally be received through a separate command system. This system consists of a gimballed S-band slot antenna having a beam width of 140 degrees. The modulation scheme used in the direct link is PSK/PM. The modulation scheme in the relay link is pulsed linear chirp. This modulation scheme is used to minimize the effects of multipath. An X-band radar altimeter will be used by the lander to obtain altitude correlation of atmospheric measurements taken during entry. It will also provide signals for deploying the

parachutes and for jettisoning the lander heat shield. A separate pulsed linear chirped communication system will be used to relay information to the orbiter during entry. The data handling equipment on board the lander will be capable of operating in any one of seven modes, different modes being used in the different phases of the lander operational life. Data requiring storage will be stored in two tape recorders, one to store data acquired at relatively low sampling rates and the other to store high sampling rate data.

The main source of power for the lander equipment will be a 117-watt radio isotope thermoelectric generator (RTG). To handle peak power conditions, rechargeable storage batteries will be used. The lander communications system will be sterilized to prevent contaminating Mars with Earth-originating organisms. To meet the reliability figure requirement of the lander, the communication system will be 100 percent redundant, except for antennas, the RTG, and the battery. However, multielement arrangements required for the battery to produce sizable powers will be connected such that the failure of a single element or a group of elements will only reduce the capacity slightly. All redundancies in the communication system will be passive, except for the command system which requires active redundancy. The total weights, volumes, and power consumptions of the lander communication system equipment are listed in tables 12 and 13.

2. Detailed system description. A simplified block diagram of a lander communication system which will meet all of the requirements stated is shown in figure 147. This system has 300 data channels; 30 allotted to the scientific measurements listed in table 14, and 270 for the engineering measurements listed in table 15. This system is capable of operating in any one of seven modes, consisting of three engineering modes, two science modes, and two data transmission modes. The three engineering modes are a critical engineering data mode, a complete engineering data mode, and an engineering data mode associated with the separation and entry phases of the Mars lander operational life. The two science modes are associated with the entry and parachute descent phase and main science mission phase of the lander operational life. The two transmission modes are modes associated with transmitting data through either a VHF link to the orbiter or an S-band direct link to Earth. In any mode, the monitored data can be stored in tape recorders, while in selected modes the lander has the capability of transmitting monitored data in real time. The lander communication system also has the capability of receiving commands from Earth.

A simplified block diagram of the lander data handling equipment is shown in figure 148. The data sampling portion of this equipment consists of seven commutator decks of varying channel capacities. During each of the seven operational modes, a different combination of these seven commutators are activated.

TABLE 12

MARS LANDER (DIRECT AND RELAY)
MAJOR SUBSYSTEM WEIGHT, VOLUME AND POWER

Major Subsystem	Redundancy	Volume (in^3)	Weight (pounds)	Power Consumed (watts)
VHF Omni Antenna System (Heat Shield)	0	---	6.0	---
5-ft S-Band Parabola	0	---	18.5	---
Gimballed Antenna System	0	---	10	---
Antenna Driver Amp.	1	144	5.0	---
Antenna Angle - Command Computer	---	---	---	42
Central Programmer and Sequencer	---	---	---	
50-watt VHF Transmitter (Linear Chirp)	1	440	24.0	120
70-watt S-Band P. A	1 (degraded)	275	16.0	140
S-Band Transceiver Hi Gain	1 (Active)	600	20.0	20
S-Band Command Receiver Lo Gain	1 (Active)	400	14.0	28
PCM Command Receiver (S-Band, Orbiter Altimeter Operated)	1	200	11.0	5
Mars Lo-Speed Recorder	0	1000	12.0	4
Mars Hi-Speed Recorder	0	1200	14	6
Command Decoder	1 (Active)	22	2.0	12
Subcarrier Modulator	1	80	4.0	3

TABLE 12 (Concl'd)

Major Subsystem	Redundancy	Volume (in^3)	Weight (pounds)	Power Consumed (watts)
Multiplexer/Encoder	1	300	18.0	3
Power Conditioning Equipment 20 W/lb (Based on Peak Total)	1	680	25.0	---
Cabling			10.0	---
X-Band Altimeter + Antenna		30	5	35
Subtotals		4971	207.5	438

TABLE 13

MARS LANDER (DIRECT AND RELAY)
DATA HANDLING SUBSYSTEMS
WEIGHT, VOLUME, AND POWER

Major Subsystem	Volume (in^3)	Weight (pounds)	Power Consumed (watts)
50-watt VHF Transmitter (Linear Chirp)	440	24.0	120
70-watt S-Band P. A	275	16.0	140
S-Band Transceiver Hi Gain	600	20.0	20
Mars Lo-Speed Recorder	1,000	12.0	4
Mars Hi-Speed Recorder	1,200	14	6
Subcarrier Modulator	80	4.0	3
Multiplexer/Encoder	300	18.0	3
TOTALS	3,895	108.0	296

TABLE 14

SAMPLING RATES AND DUTY CYCLES FOR
MARS LANDER SCIENTIFIC AND ENGINEERING MEASUREMENTS

NO.	Measurement	Sampling Rate (samples)	Duty Cycle
1.	TV	12,500/sec	12 pictures in 48 hours during daylight
2.	Ultraviolet	12,500/sec	10 pictures/sample. 12 samples in 48 hours.
3.	Petromicroscope	12,500/sec	4 pictures in 48 hours
4.	Infrared	53/sec	12 samples in 48 hours 47 min/sample
5.	3-axis seismograph	4.0/sec	continuous
6.	Sun spectrometer	3.0/sec	sunrise to sunset
7.	Cell growth	1.0/min	1 sample in 24 hours
8.	Gas chromatograph	1.0/min	1 sample in 48 hours
9.	X-ray diffractometer	28/min	1 sample every 12 hours 4 samples
10.	Turbidity and pH Growth	2/hr	continuous
11.	Soil mechanics	3.3/min	1 sample in 48 hours
12.	X-ray spectrometer	0.33/sec	continuous
13.	Advanced mass spectrometer	0.33/sec	12 samples in 48 hours.
14.	Biosample acquisition	0.33/sec	continuous
15.	Emission	0.33/sec	12 samples in 48 hours
16.	Atmosphere	17/min	24 samples in 48 hours
17.	Microphone	2/min	continuous
18.	Anemometer	8/hr	continuous
19.	H_2O detector	8/hr	continuous
20.	Velocity of sound	8/hr	continuous
21.	Temperature	8/hr	continuous
22.	Density	8/hr	continuous
23.	Pressure	8/hr	continuous
24.	Engineering	1/min	200 measurements continuous

TABLE 15

MARS LANDER
ENGINEERING DATA CHANNEL REQUIREMENTS

Item	Quantity	Channel Requirements
3-axis accelerometer	1	3
3-axis rate gyroscope	1	3
Ablation gauge	14	14
Resistance thermometer	25	25
Pressure	15	15
Drogue chute deploy switch	1	
Main chute deploy switch	1	
Heat shield separation switch	1 Digital	9
Discrete switch closures	40	
TV camera	1	5
UV camera	1	5
Petromicroscope camera	1	5
3-axis spectrometer	1	3
X-ray diffractometer	1	3
X-ray spectrometer	1	3
Sun spectrometer	1	2
Gas chromatograph	1	2
Soil mechanics	1	1
Advanced mass spectrometer	1	2
Biosample acquisition	1	1

TABLE 15 (Concl'd)

Item	Quantity	Channel Requrements
Emission	1	2
Atmosphere	1	1
H_2O detector	1	1
Altimeter	1	3
VHF transmitter	4	3
S-Band power amplifiers	4	3
S-Band transponder	2	6
Parabolic antenna drive	1	2
Antenna angle computer	2	2
Tape recorder	2	8
Multiplexer/encoder	2	3
VHF command receiver	2	4
Command decoder	2	6
Central programer and sequencer	2	6
Power conditioning equipment	2	4
Battery	2	4
RTG	1	2

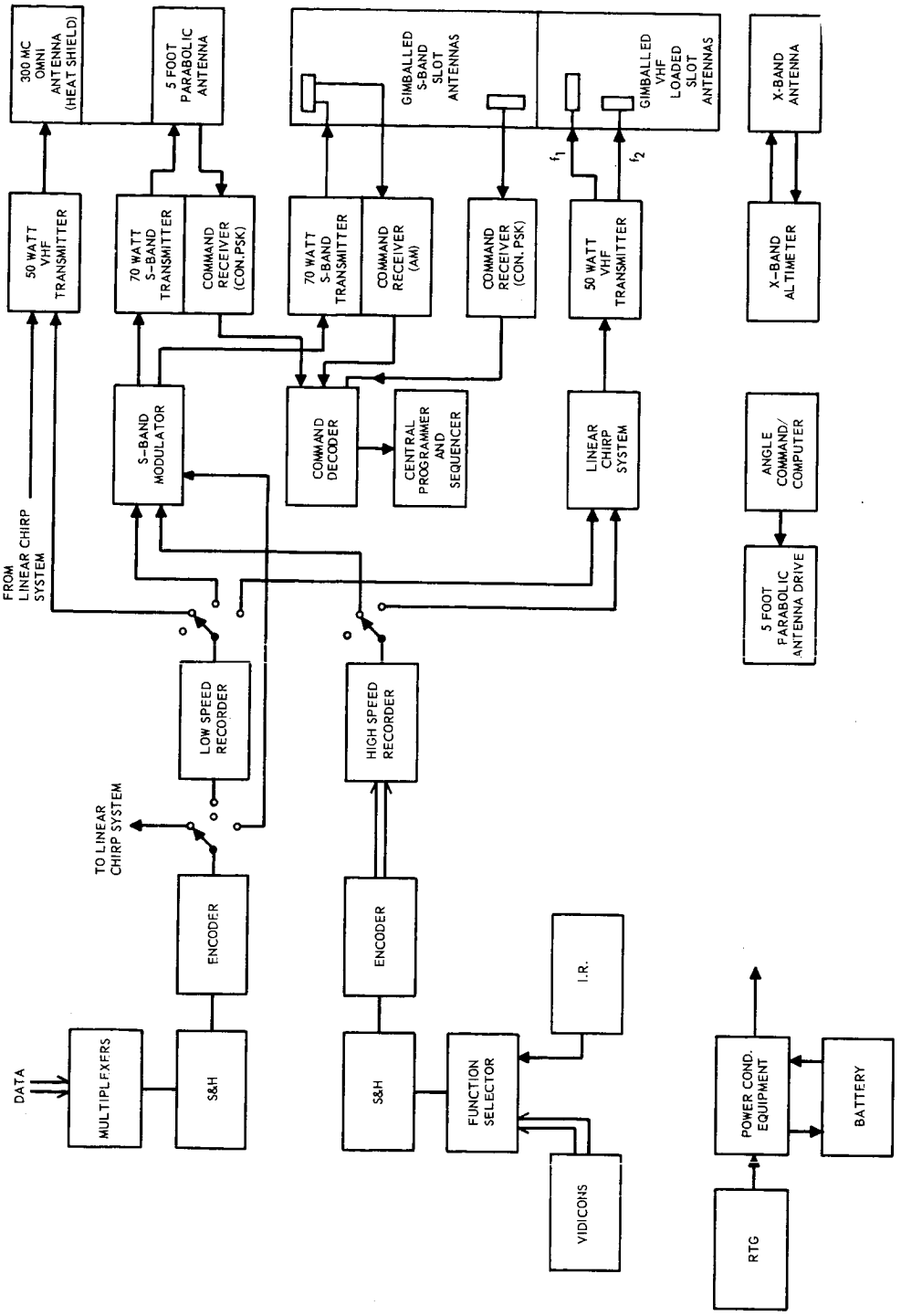

Figure 147 LANDER DATA MULTIPLEXER SIMPLIFIED BLOCK DIAGRAM

63-9626

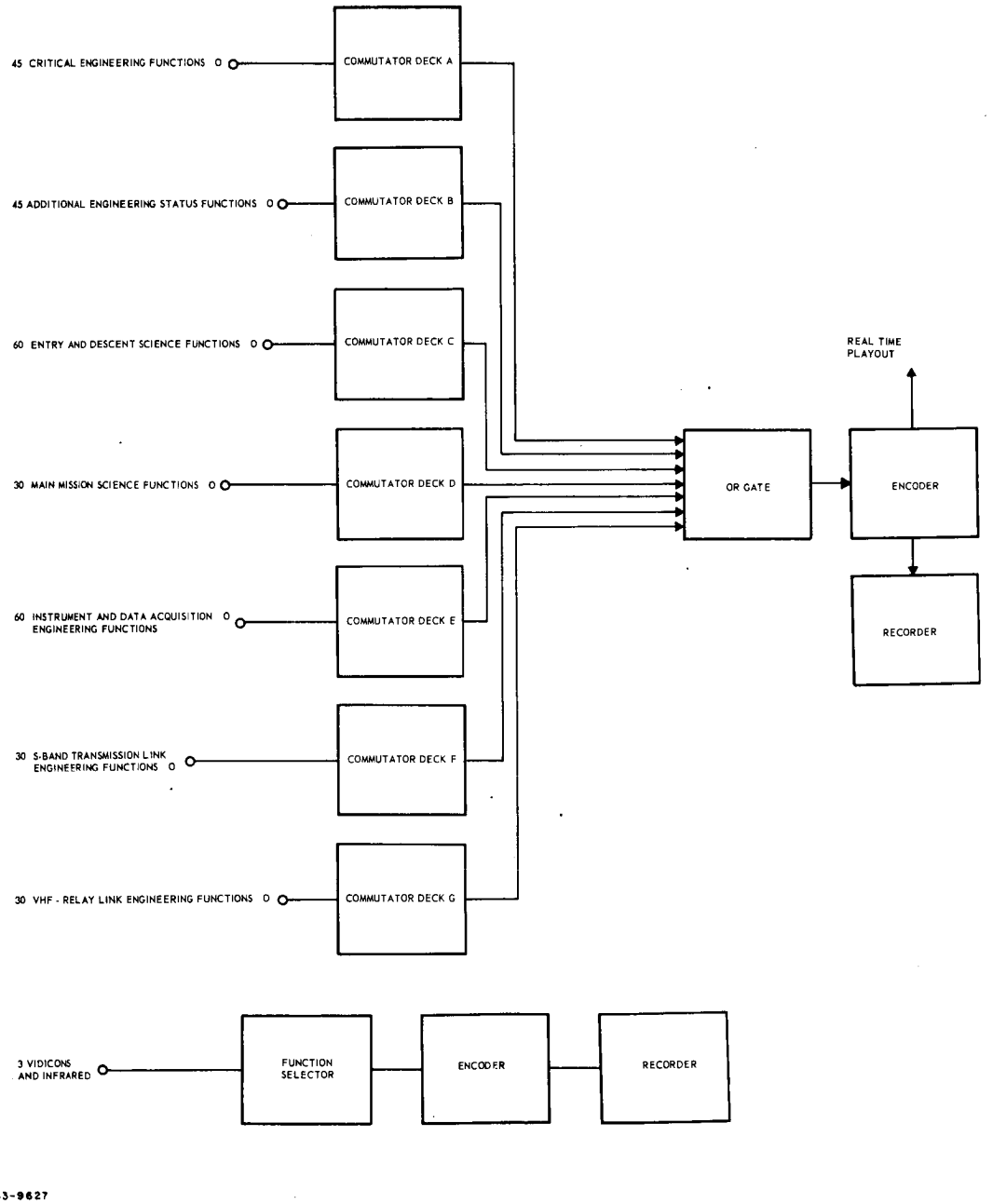

63-9627

Figure 148 LANDER DATA MULTIPLEXER SIMPLIFIED BLOCK DIAGRAM

a. Separation to entry. At separation from the lander-orbiter bus, the data handling equipment will switch to mode 1, the separation to entry to entry mode. In this mode, commutator decks A and B are activated. As shown in figure 148, these commutators monitor 45 critical engineering functions and 45 additional engineering status functions. The 45 critical engineering functions include critical lander internal temperatures, the power system, the central programmer and sequencer, the command system, and several sequence-of-event functions. The 45 additional engineering status functions include equipment temperatures, the data handling equipment, and the VHF transmitter. During this phase, the lander is completely enclosed in a heat shield and is not attitude controlled. To transmit the acquired data in real time directly to Earth would require a radiated power of 20 watts/bit/sec, using an isotropic radiator on the lander heat shield. If a directive antenna was used to reduce the energy per bit per second requirement, the lander would accrue a weight penalty due to the antenna and the control system to point it.

The orbiter during this phase is always in relatively close proximity to the lander. The signal energy per bit per second required to transmit the acquired data to the orbiter is only a small fraction of the energy required to transmit the same data directly to Earth. For this reason, the orbiter will be used as a relay station. Table 16 lists the design parameters required to establish a communications link between the lander and orbiter. The modulation scheme selected for this phase is pulsed linear chirp. The reason for selecting this modulation scheme rather than say PM/PSK, is a matter of convenience. As will be explained later, after the lander lands on the planet, the lander to orbiter communications link may be plagued by severe multipath effects. A pulsed linear chirp modulation scheme minimizes these effects. Since the orbiter will be required to receive pulsed linear chirped data during the landed phase, to prevent undue complexity it is reasonable to use the same modulation scheme for all communications with the orbiter. The receiver on board the orbiter has a 1 mc bandwidth which is required to receive the landed phase data at a much higher bit rate than is required during separation to entry. A sampling rate of 2 samples/min is considered an acceptable sampling rate for the separation to entry phase. As shown in figure 149, alternate channels of commutator decks A and B are monitored sequentially at a rate of 4 samples/sec. A complete frame of both commutators A and B is sampled once every 22.5 seconds which exceeds the acceptable sampling rate. Each of the sampled functions in this phase will be converted to a five-bit binary code word which will exceed a reasonable accuracy requirement of 5 percent. The codes data will be transmitted to the orbiter in real time at 20 bits/sec.

After separation, the lander is given a differential velocity with respect to the orbiter. Some 60 hours later when the lander begins to enter the Martian atmosphere, the slant range between the lander and orbiter will be a maximum of 14,000 km. This range is the worst case value representing the worst case entry angle of the lander and all other positioning errors. The best case slant

TABLE 16

TELECOMMUNICATIONS DESIGN CONTROL CHART

(Mars, Lander-to-Orbiter Separation to Entry)

No.	Parameter		Nominal Value	Tolerance	Source	Worst Value
1	Total transmitter power	50 watts	+47.0 dbm	$^{+0.0}_{-0.5}$ db		+46.5 dbm
2	Transmitting circuit loss		-0.25 db	$^{+0.0}_{-0.05}$ db		-0.3 db
3	Transmitting antenna gain		+0.0 db	$^{+0.0}_{-0.5}$ db		-0.5 db
4	Transmitting antenna pointing loss		---	---		---
5	Space loss = 32.46 20 log F+20 log R F 300 mc, R 14,00 km		-164.92 db	---		-164.92 db
6	Polarization loss		-0.0 db	±0.5 db		-0.5 db
7	Receiving antenna gain	Helix	+5.0 db	±0.5 db		+4.5 db
8	Receiving antenna pointing loss	21 degrees	-0.5 db	±0.5 db		-1.0 db
9	Receiving circuit loss		-0.1 db	Max.		-0.1 db
10	Net circuit loss		-160.77 db	$^{+1.5}_{-2.05}$ db		-162.82 db

TABLE 16 (Concl'd)

No.	Parameter	Nominal Value	Tolerance	Source	Worst Value
11	Total received power	-113.77 dbm	$^{+1.5}_{-2.55}$ db		-116.32 dbm
12	Receiver noise spectral density (N/B) T system_____NF 4 db	-169.8 dbm	$^{+1.0}_{-0.0}$ db		-168.8 dbm
13	Predetection bandwidth (10^6 cps)	+60 db	---		+60 db
14	Required ST/N/R $p_e = 5 \times 10^{-4}$	+4.6 db	$^{+1.0}_{-0.0}$ db		+15.6 db
15	Detector threshold power required	-95.2 dbm	$^{+2.0}_{-0.0}$ db		-93.2 db
16	Pulse compression gain	+25 db	$^{+0.0}_{-1.0}$ db		+19 db
17	Integration improvement (500 bits/data bit)	+10.0 db	$^{+1.0}_{-1.0}$ db		+9 db
18	Required received power	-125.2 db	$^{+4.0}_{-1.0}$ db		-121.2
19	Performance Margin	+11.43	$^{+2.5}_{-6.55}$ db		+4.88

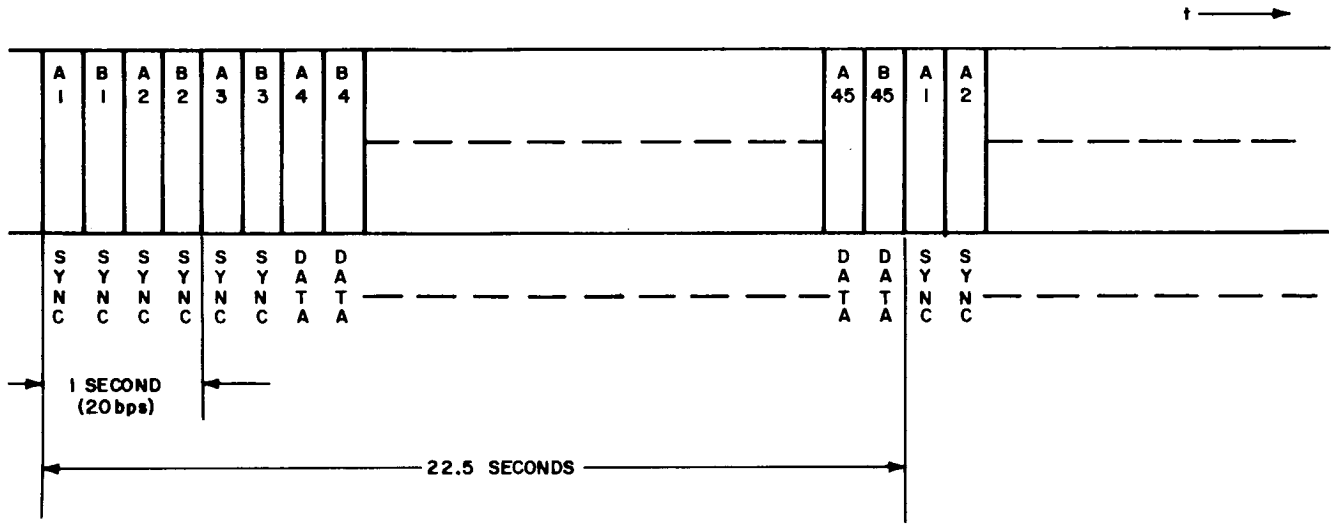

63-9628

Figure 149 SEPARATION TO ENTRY CRITICAL ENGINEERING STATUS MODE

range will occur if the lander enters the atmosphere at a shallow entry angle. The slant range for this case would be a maximum of some 4000 km.

At 14,000 km table 16 shows that a worst case performance margin of +4.88 db could be expected, by integrating 500 chirp pulses representing one data bit. At 20 data bits per second the chirp rate would be 10,000 pulses per second. This results from the fact that with the linear pulsed chirped system, selected for the lander, each transmitted bit has a duration of 100 μsec regardless of bit rate up to a bit rate of 10,000 bits/sec. The received bits in the orbiter antenna are compressed to 1 μsec duration with a resultant gain in signal to noise ratio of +20 db. The 1 μsec pulses account for the 1 mc bandwidth in the orbiter receiver. The details of the chirped system operation are covered in the discussion of VHF relay. A -4.12 db worst case performance margin would result if one chirpred pulse per data bit was transmitted to the orbiter for detection.

b. Improvement of error rate. If pulses are received at a 10 kc rate, but information is only received at a 20 bit rate, it should be possible to integrate 500 successive pulses. This must be done after detection and, therefore, is not the optimum way to make use of the redundant pulses. Nevertheless, a considerable reduction will be thus achieved in the error rate of the information bits, without additional equipment.

System waveforms are shown in figure 150 showing the original PCM data representing lander entry instrument readings. In B, each A bit has been converted to a pair of bits, a +1, -1 pair representing +1 in A, a -1, +1 pair a 0 in A. In C, the B waveform has been modulated in a 10 kc pulse sequence. Positive pulses excite one of the two transmitted chirp waveforms, negative pulses excite the others. (The waveforms may, of course, be identical except for frequency translation.) Therefore, C also represents the output of the chirp receiver in the orbiter, in the absence of noise or multipath disturbance. D shows the receiver input when noise or multipath effects are present. If we knew when the baud intervals ΔT began and ended, the best way to make a decision as to which type of bit was transmitted during ΔT would be to count the number of positive and the number of negative pulses occurring in the baud. If there are more plus than minus pulses, the bit is called a 1. If the reverse, the bit is called a -1. Thus waveform B is reconstructed. To derive A from B, frame coding pulses must be inserted in the A message at regular intervals. Using these for synchronization, B may be connected to A by standard methods.

There seems to be no reason of any consequence why the reduction of D to A must be accomplished aboard the orbiter. Instead, let the D waveform be recorded and transmitted to Earth just as it is during the transmission and retransmission of lander TV pictures. All postdetection operations are then accomplished in Earth. This permits us to find the beginning and end of the baud intervals by rerunning the record as often as necessary. The differences between the number of positive and negative pulses in each band is measured.

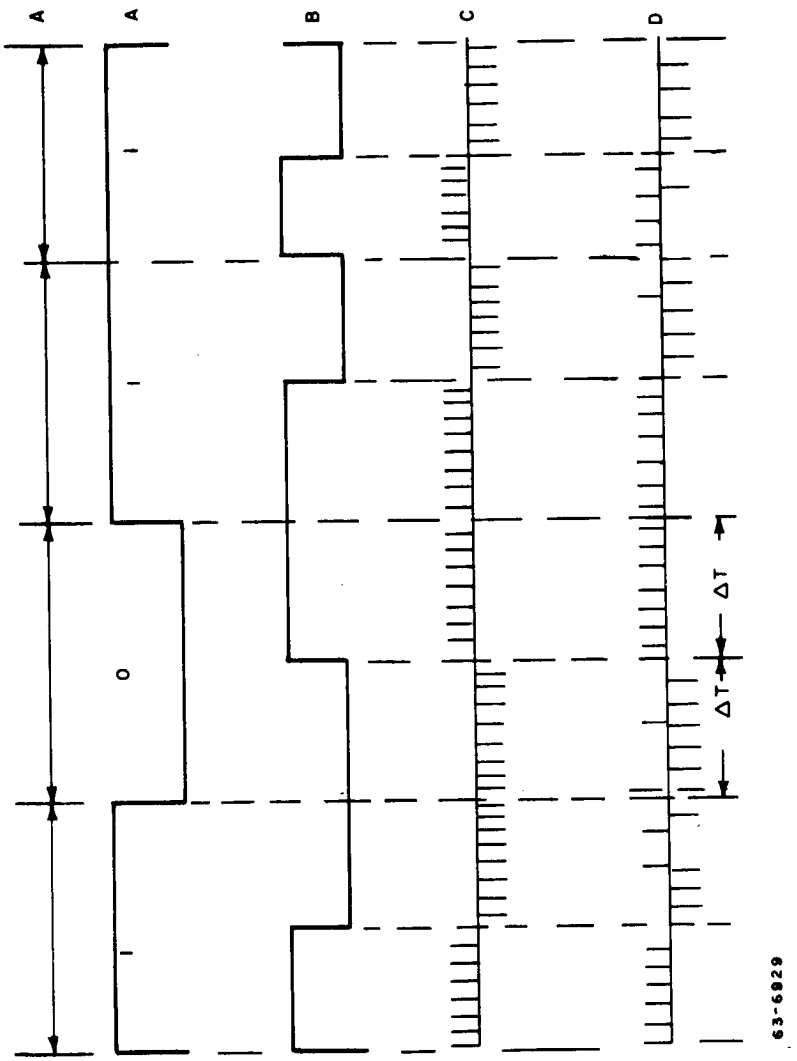

Figure 150 CHIRP ERROR REDUCTION AT LOW BIT RATES

The absolute value of this difference is integrated over the whole record. The phasing of the baud sync (shown dotted in figure 150)is readjusted between runs. When the integral is maximized, the baud sync phasing is correct.

The expected improvement from this system should be in the neighborhood of 10 db, as indicated in table 16.

The data monitored by commutator decks A and B will only be transmitted to the orbiter in real time for 5 minutes every hour beginning 1 hour after separation. The reasons for transmitting intermittently every hour are twofold. First, the lander is RTG power limited to 117 watts raw unregulated power which is not sufficient to operate the transmitter. Since the battery is used to make up the difference between the RTG power and the required power, a recharge time must be allowed. Second, during the first few hours, the slant range between the lander and orbiter is relatively short; therefore, the performance margin will be significantly higher.

To receive data from the lander, the orbiter antenna system must be planet vertically oriented. Since the orbiter has a planet vertically oriented camera system on board for mapping the planet surface, it serves as an ideal mounting structure for the VHF receiving antenna. This antenna is a 65-degree beam helix which, again, is required in the landed phase. During the separation to entry phase, the lander is always within 10 degrees of axis. The resulting antenna pointing loss in this phase is, therefore, less than can be expected in the landed phase.

The antenna system design for the lander consists of two radiating elements, each covering 2π steradians. The pattern is essentially isotropic over a large area surrounding the vehicle and is required since the lander is not altitude controlled. With an isotropic radiator in the lander and a fixed beamwidth antenna in the orbiter, it is desirable to use as low a carrier frequency as possible to reduce the free space attenuation. However, due to constraints on antenna size, a VHF carrier is considered a practical lower limit. Due to a corona problem that will exist during the entry phase, a 50-watt VHF transmitter was selected as an upper limit on power.

The signal energy per bit per second required is determined for a bit error probability of 5 bits in 10^4 ($P_e = 5 \times 10^{-4}$). This P_e is determined for a desired P_e at the DSIF of $P_e = 1 \times 10^{-3}$. In a relay mode through the orbiter, two detection systems will contribute errors, one in the orbiter and the other at the DSIF.

$$[1 - P_e(\text{DSIF})] = [1 - P_e(\text{LANDER/ORBITER})]\,[1 - P_e(\text{ORBITER/DSIF})]$$

$$= 1 - 2P_e - P_e^2 \quad .$$

The third term in this equation is negligible, therefore:

$$2P_e = P_e\,(\mathrm{DSIF})$$

$$P_e = \frac{P_e\,(\mathrm{DSIF})}{2} = \frac{1 \times 10^{-3}}{2}$$

$$P_e = 5 \times 10^{-4}$$

At this error probability, the required signal energy per bit per second is +15.6 db.

3. Entry and descent. The start of the lander entry into the Martian atmosphere will be signalled by closure of a highly sensitive g switch. At this time, the data handling equipment will switch to mode 2, the entry and descent science mode. In this mode, commutator decks A, B, C, and G will be activated. Commutator deck C monitors 60 entry and descent science functions. These functions include dynamic performance measurements on the vehicle, ablation of the heat shield material, a pressure profile on the lander structure, and atmospheric measurement. Commutator deck G monitors 30 functions associated with the VHF transmission link. The data acquired during entry will be played out to the orbiter in real time using the same transmission system employed in the previous phase. However, at peak heating during entry, the lander will ionize the gases surrounding the heat shield. During this time, the lander data transmission system will experience a phenomenon commonly called blackout which will severely attenuate the radiated energy to the orbiter. Since the environmental conditions experienced by the lander at this time are most critical, the acquired data must also be stored for subsequent playout when blackout ends and normal communication link conditions are reestablished. Since it is not known precisely when blackout will occur, the real time data link will serve the dual purpose of providing engineering performance and atmospheric condition information until blackout and an indication of when blackout occurs. In the event the lander does not survive the critical environmental conditions experienced during blackout, the real time data may provide indications of the causes of failure. As shown in figure 151, segments of commutator decks A, B, C, and G are alternately sampled in sequence at a minimum frame rate of one frame every 1.2 seconds. Due to the difference in channel capacities between deck C and decks A, B, and G, the same sequence of channel sampling repeats every ninth frame of deck C. The accuracy required by most of the data sampled by these commutators is 5 percent or less. There are selected measurements, however, requiring accuracies of 2 percent or better. For this reason, the sampled data is converted to a nine-bit binary code word in an analog-to-digital converter. Since this data will also be stored, to minimize the storage requirement, only the five most significant bits of the nine-bit encoded word will be stored for those measurements requiring 5 percent accuracy.

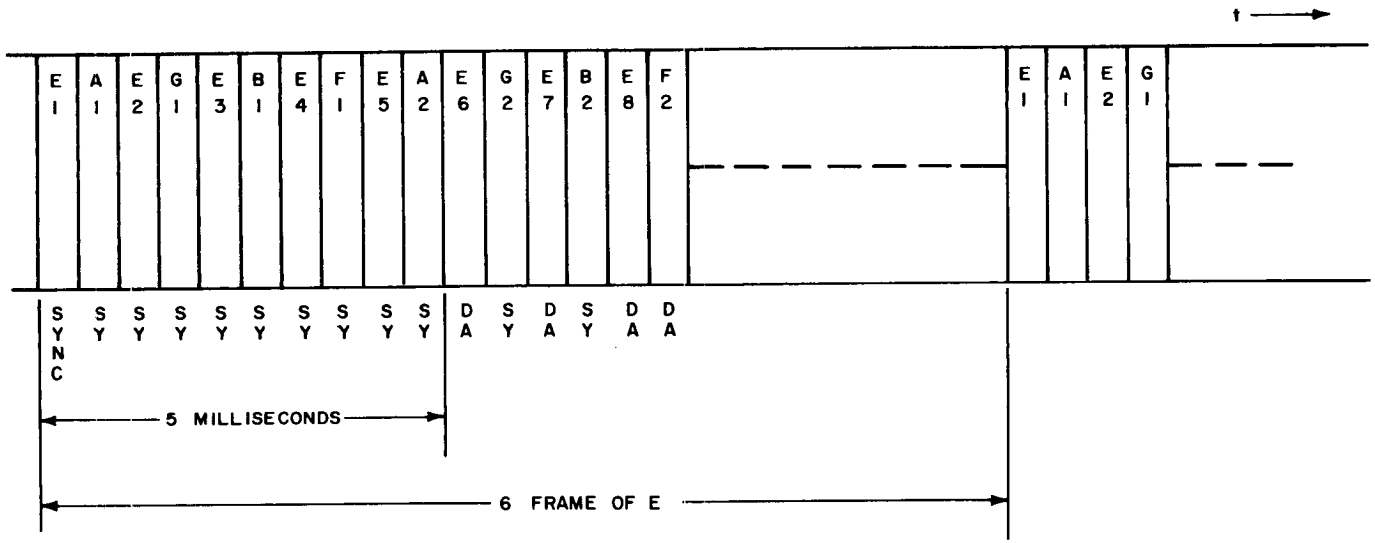

63—9634

Figure 151 ENTRY AND DESCENT SCIENCE MODE

To store the complete nine-bit word for those measurements requiring 2 percent accuracy, two adjacent commutator channels will be used; the first to store the five most significant bits, and the second to store the four least significant bits. As shown in figure 151, adjacent channels on say commutator C are not sampled concurrently in time due to the interleaving of commutators A, B, and G. A solid state storage register will be used to store the four least significant bits initially. During the time normally allocated for the storage of an adjacent channel, those four bits will be inserted. During real time playout, the same technique will be employed to maintain a constant five bits per word data format.

The same sequence of data shown in figure 151 for real time playout will be used to store the data, with the important difference, shown in figure 152. In this figure, the channel allocations for commutator deck G are blank; that is, they will not be stored. When the stored information is played out after blackout, those gaps will be filled with real time data on the performance of the transmission link.

A parallel recording, serial playback magnetic tape recorder will be used to store the data and later provide it in a form suitable for synchronous transmission. A signal and power flow diagram for this machine is shown in figure 153. Seven tracks are required to store the encoded five bit data words, five tracks for recording each coded word in parallel form, one track for recording clock pulses appearing in synchronism with the coded word rate, and one track for recording clock pulses indicating the blanks shown in figure 152. Also, on this last track, a pulse will be inserted which indicates the correct position for the insertion of channel G1 in the sequence shown in figure 152. This is required to maintain the same sequence of channel sampling every ninth frame of deck C. During playout, the five data tracks are fed to a five-bit parallel register which compensates for the skew or the phase differences in the five parallel bits. The bits are then dumped simultaneously into a five-stage shift register which shifts them out one at a time at the required bit rate. Synchronism is obtained by phase comparing the recorded version of the word rate clock with the real time clock and using the resultant error signal to control motor speed thereby closing the loop. This loop is designed to compensate for all expected errors due to speed changes, tape stretching, tape skewing, etc. However, if in the final design it is found that these errors make excessive demands on the output loop, an additional loop can be added which will lock the motor speed to the spacecraft clock during recording. This will eliminate the major source of error.

During this phase, the input word rate to the recorder is 80 words/sec or 80 bits/sec/track. Recorders are currently available having bit packing

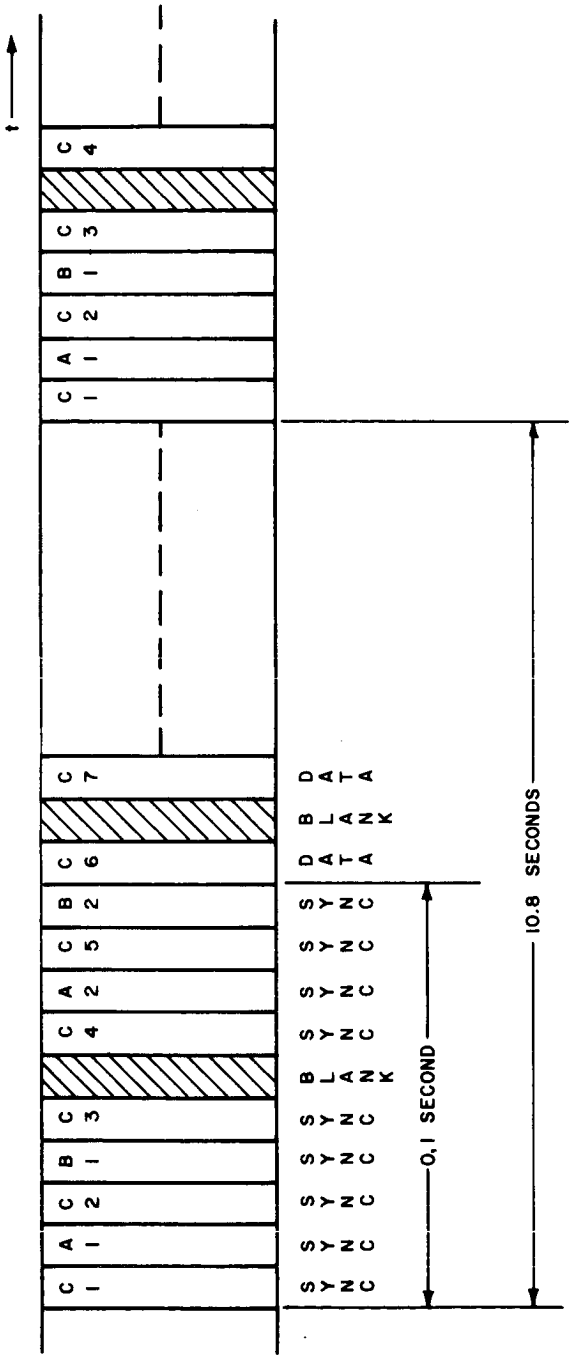

Figure 152 DATA ACQUISITION AND STORAGE ENTRY AND DESCENT SCIENCE MODE

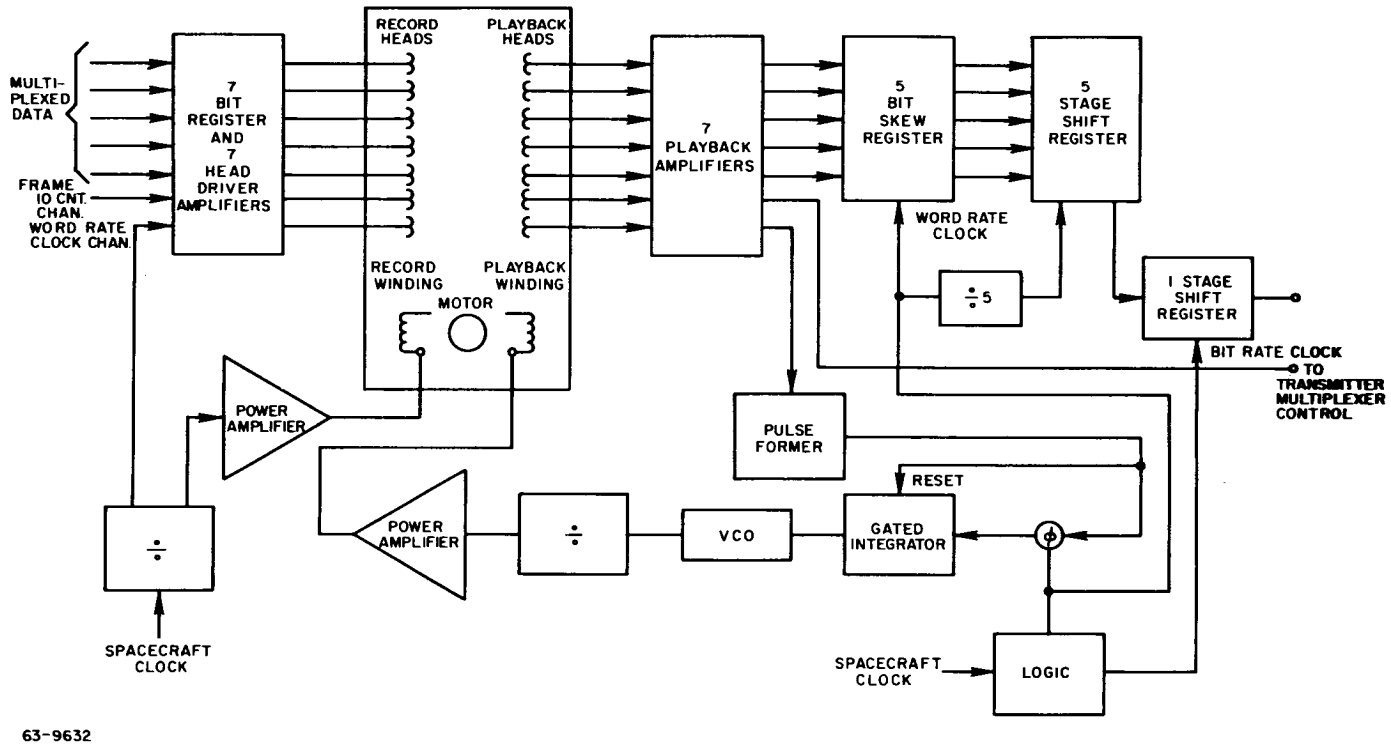

Figure 153 SIGNAL AND POWER FLOW DIAGRAM MARS LANDER
TAPE RECORDER 1

densities exceeding 1000 bits/in. However, at 1000 bits/in, the tape record speed during this phase can be:

$$\frac{80 \text{ bits/sec}}{1000 \text{ bits/in}} = 0.08 \text{ in/sec} .$$

Recorders are currently available which can record at this speed.

At a preprogramed time interval from the closure of the g switch, a radar altimeter will be turned on. This altimeter will be used to satisfy the requirements to supply signals to deploy the drogue chute, main chute, and jettison the heat shield. It will also provide altitude correlation for scientific measurements in the atmosphere. The parachutes are deployed at altitudes near 20,000 feet; therefore, the altimeter will be capable of measuring altitude starting at approximately 40,000 feet.

An X-band altimeter was considered a practical choice for the lander. Since the altimeter antenna must have a window in the portion of the heat shield which will experience peak heating, the aperture size of the antenna should be kept to a minimum. Alternately, the free space attenuation increases as frequency squared. To maintain a reasonable peak power, X-band was considered a reasonable choice.

4. Lander Altimeter, General Description. The X-band lander altimeter measures altitude from 40,000 to 1,000 feet with a continuous readout of altitude data in a pulse train format. Sensitivity computations are summarized in table 17.

TABLE 17

MARS LANDER ALTIMETER SENSITIVITY CALCULATIONS

$$P_t = \frac{(4\pi H)^2 \text{ KTB (NF) (S/N) L}}{G_t \lambda^2 \sigma} = 865 \text{ watts}$$

P_t = Peak power
H = Altitude 12.2 km (40,000 feet)
K = Boltzmann's constant $1.38(10^{-23})$ joules/degree Kelvin
t = Temperature 300°K
B = Receiver Bandwidth 3 mc.
NF = System Noise Figure 11.5 db
S/N = Signal-to-noise Ratio 15.5 db
L = System losses 1.5 db

G = Antenna Gain 4.7 db
λ = Wavelength $3(10^{-5})$ km
σ° = Reflectivity 0.1
P_{fd} = False alarm probability 10^{-10}
P_d = Probability of detection 0.90

In the conceptual design for a lander altimeter, reliability, minimum weight, size and power consumption have been emphasized. Solid state and microminiaturization techniques have been employed where feasible. The proposed system is a noncoherent pulse altimeter.

The transmitter is a magnetron operating at 9.3 kmc with a peak power output of 1 kw. System pulse repetition frequency is 2.5 kc with a 1 μ sec pulse giving a duty cycle of 0.0025. The magnetron, currently in production, would be integrated with a solid-state modulator to provide a 5-pound, 55 in^3 package.

A branch duplexer is used for isolation with a gas TR tube mounted in the waveguide. The recovery time of this tube is less than 1 μ sec, thus permitting operation of the system to 500 feet. The output of the duplexer is fed to a crystal mixer for heterodyning with the local oscillator.

The local oscillator is a crystal oscillator with a five-stage multiplier chain multiplying the oscillator at 32.19 mc to a final output of 1 milliwatt minimum at 9.27 kmc. Four stages of IF at 30 mc with 3 mc bandwidth provide 100+ db of gain, and two stages of AGC supply a 60-db dynamic range.

A crystal detector and one stage of video amplification provide the stop pulses to the transmission gate for range measurement and to a seven-stage binary counter for ejection of the parachute at 20,224 feet. The accuracy of this system is $\pm$ 1 bit. A 3.165 mc crystal oscillator serves as the clock for the range measurement. Range data are acquired at a rate of 158 ft/bit for each altitude measurement. A schematic of the system is outlined in figure 154 with design parameters listed in table 18.

TABLE 18

MARS LANDER ALTIMETER DESIGN PARAMETERS

1.	Average Power Output	2.5 watts
2.	Frequency	9.3 kmc
3.	Pulse Width	1 μ sec
4.	PRF	2.5 kc
5.	Range	40,000 feet (max.)
6.	Accuracy	$\pm$ 158 feet
7.	Modulation	Pulse
8.	Weight	8 pounds
9.	Volume	117 in^3
10.	Power Consumption	25.8 watts
11.	Antenna Gain	5.7 db

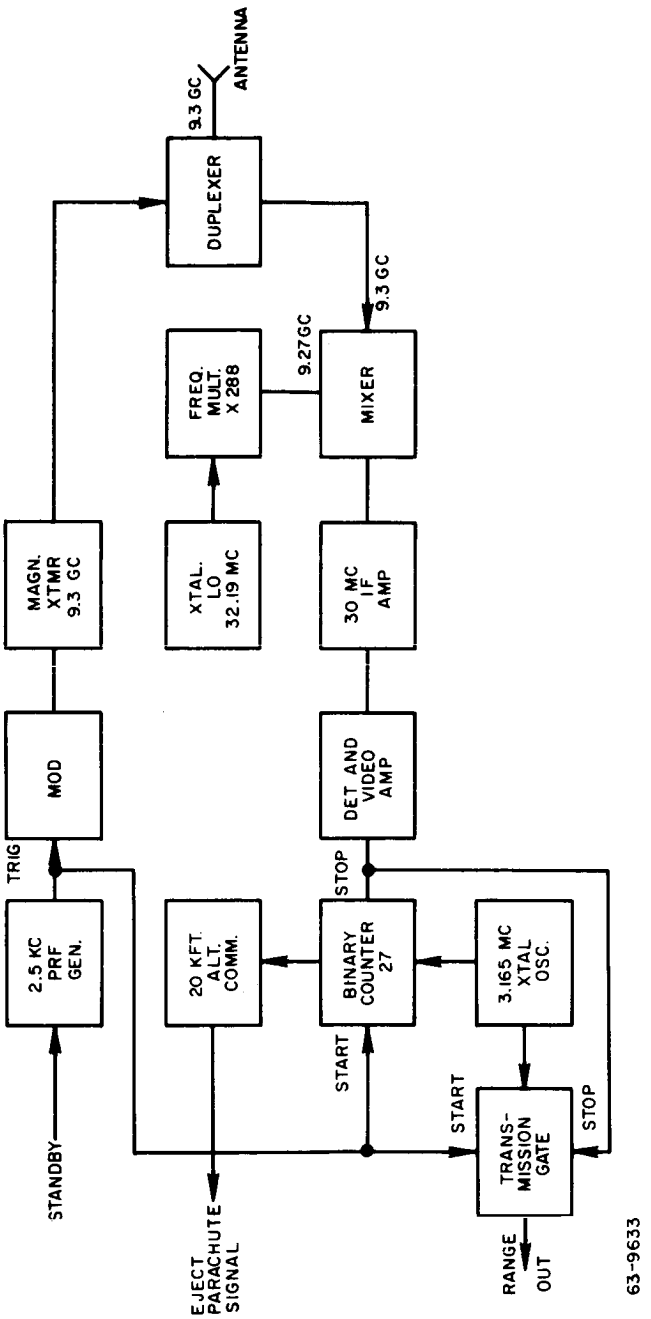

Figure 154 LANDER ALTIMETER BLOCK DIAGRAM

a. Transmitter/Modulator. The transmitter is a pulsed magnetron integrated with a solid-state line type modulator. The operating frequency is 9,300 mc with 1 kw peak output transmitter power. No AFC loop is required. The maximum drift of the tube is 75/kc/°C and results in a maximum drift of 375/kc in a 5°C controlled temperature environment. The L3812 magnetron is an off-the-shelf item weighing 16 ounces maximum with a 0.005 maximum duty cycle. Duty cycle of the lander transmitter will be 0.00025 using a 2.5 kc pulse repetition rate and a 1 μsec pulse width.

Combining the modulator and magnetron provides a 5-pound 55 in^3 package requiring approximately 20 watts of input power. The modulator operates from 23 vdc and supplies a 1,400 volt, 2.2 ampere pulse, and 6.3 volts 0.85 ampere filament power to the magnetron. A 2.5 kc synchronizer will trigger the modulator. Design parameters of the transmitter/modulator are tabulated in table 19.

TABLE 19

DESIGN PARAMETERS FOR
TRANSMITTER MODULATOR -- MARS LANDER ALTIMETER

Transmitter Frequency	9.3 kmc
Peak Power Output	1 kw (min.)
Pulse Width	1 μsec
PRF	2.5 kc
Magnetron/Modulator Integrated Weight	5 pounds
Magnetron/Modulator Integrated Volume	55 in^3
Frequency Drift 75 kc/°C	375 kc (max.)
Efficiency	34 percent
Peak Pulse Voltage	1.4 kv
Peak Pulse Current	2.2 Amperes
Filament Power(at 6.3 volts)	5.4 watts
Integrated Magnetron/Modulator Est. MTBF	4,000 hours
Power Input	20 watts (max.)

A branch duplexer with a TR tube mounted on aluminum waveguide will program the antenna signals. An ATR tube will not be required. Weight of the duplexer and waveguide will be approximately 10 ounces. Insertion loss will be 0.5 db each way.

b. Local Oscillator. A solid-state local oscillator/multiplier chain with a crystal oscillator at 32.19 mc and two triplers, two quadruplers, and one doubler provides a minimum of 1 milliwatt at 9.270 mc. Weight of the unit is less than one pound and power requirements are approximately 0.5 watt. The crystal is stable to $\pm$ 5 parts in 10^5 for a temperature range of -55 to + 90 °C without an oven.

c. Mixer/IF Amplifier. A hermetically sealed crystal mixer designed for 150 °C operation will be used for the first detector. Conversion loss of the crystal mixer is 6.0 db and burnout rating is 5 ergs.

The four-stage subminiaturized 30 mc IF amplifier has a bandwidth of 3 mc, gain of 100+ db and 60 db AGC. The IF amplifier noise figure is less than 4 db giving a total receiver noise figure of 11.5 db from:

$F_{db} = Lc + 10 \log (F_{if} + t - 1)$

F_{db} = receiver noise figure

Lc = crystal conversion loss 6.0 db

F_{if} = IF amplifier noise figure 2.5

t = crystal noise/temperature ratio 2

d. Range Processor. The 30 mc IF amplifier feeds the second detector and video amplifier for generation of the range stop pulse for the computer gate. A 3.165 mc clock is used to generate a signal for measuring the range. The selected clock provides an accuracy of ± 158 feet. Readout will be made at a 2.5 kc rate for the train of 3.165 mc pulses with the number of bits proportional to range. Each bit will be valued at 158 feet increments. A seven-stage binary counter will be used to determine when to eject the parachute. The 128-bit counter will provide the signal to eject the parachute at 20,224 feet. Accuracy of measurements will be ± 1 bit or ± 158 feet. Size weight, and power requirements for the lander altimeter are tabulated in table 20.

TABLE 20

MARS LANDER ALTIMETER (X-BAND)
COMPONENT SIZE, WEIGHT, AND POWER

	Size (Volume)	Weight	Power
PRF Generator	2.0 in^3	3 ounces	0.10 watt
Solid-State Mod.	55 in^3	5 pounds	20 watts
Magnetron Transmitter			(MTBF: 4,000 hrs)
Altimeter Command	3 in^3	4.0 ounces	0.5 watts (MTBF: 500,000 hrs)
Crystal L. O.	30.0 in^3	1.0 pound	2.0 watts
Frequency Multiplier			(MTBF: 10,000 hrs)
Duplexer (Type Varian BL965)	18.0 in^3	10.0 ounces	.10 watt
Range Comp:	4 in^3 (3 x 2 x .5 x 2)	8.0 pounds	3.0 watts (MTBF: 500,000 hrs)
X-TAL OSC.	1.5 in^3	1.5 ounces	0.5 watts
Det. & Vid. Amp.			
30 mc. IF Amp (4 stages)	3.3 in^3	5.0 ounces	1.5 watts
Mixer	116.8 in^3	8.0 pounds	26.8 watts

5. Data Handling. After the main parachute is deployed, the lander is required to take terrain pictures from specific altitudes during descent. These pictures will be taken with a vidicon type TV camera. The pictures taken will be 400 by 400 element rasters with a 3 bit gray scale. The vidicon has a useable readout or charge retention time of 20 seconds. The sampling rate required to read out the raster in 20 seconds is 8000 samples/sec. There is a great disparity between this sampling rate and that associated with commutators A, B, and C. For this reason, a separate sampled data was selected to handle the TV information. The sampled data system used with the vidicon includes a 3-bit encoder and a tape recorder for storage. Since the terrain pictures are acquired intermittently at selected altitudes, this sampled data system will be operated intermittently to minimize the data storage requirements and also allow the data to be played back at a reduced bit rate. The sweep control circuits in the vidicon are controlled by the central programmer and sequencer and the vidicon output is time division multiplexed by a Sample and Hold circuit preceding the encoder. At 8000 samples/sec each sample must be encoded and stored within 125 μsec. During this 125 μsec, the sampled amplitude could change, causing an error in the encoded output. To prevent this error, the Sample and Hold circuit will have a minimum sampling time of 1 μsec, a holding time of 123 μsec and a discharge time of 1 μsec. An encoder having a 1 mc frequency response was selected for use with the Sample and Hold circuit. During the 123 μsec that the sampled analog input is held constant, the corresponding digital output of the encoder will be fed in parallel form to a tape recorder for storage.

The recorder used to store the intermittent TV data will employ the same speed control techniques discussed previously. The main differences will be in the number of data channels and in the recording speed. The data, consisting of three-bit words will be recorded in parallel on three tracks. Again, an additional track will be used for recording clock pulses appearing in synchronism with the coded word rate. With a packing density of 1000 bits/track-inch, the recording tape speed will be:

$$\frac{8000 \text{ bits/sec}}{1000 \text{ bits/in}} = 8 \text{ in/sec}$$

Five TV pictures will be taken during descent. Using a three-bit gray scale, the total recorded information bits including line and frame synchronization is:

(8000 samples/sec) (3 bits) (20 seconds) (5 pictures) = 2.4×10^6 bits.

Allowing 10 percent for tape waste, the total played out bits is 2.64×10^6 bits.

Since the data input is not continuous, the recorder will only be run during readout of a picture. Without dynamic braking, the recorder start/stop time is about 1 second. Since 20 seconds are required to read out the vidicon,

the tape waste due to stopping and starting is only 10 percent. Due to starting and stopping, however, the data bits and the word clock associated with one picture will not be phase coherent on the tape with the bits from the previous picture. Since, on playout, it is desirable to maintain the output bit rate continuous and synchronous, a few bits will be lost between the recorded stop/start times before the output phase-lock loop can lock on to the recorded clock. No data need be lost, however, since the recorder can be allowed to get to speed and remain at speed, recording only the clock for a very short time before data are played in.

The lander is required to transmit to the orbiter all the recorded data before it impacts the planet. This will be done during a 5-mintue interval just prior to impact. To accomplish this, the orbiter must not have passed beyond the line of sight of the lander. It is for this reason that the lander is positioned ahead of the orbiter. The degree to which the lander must lead the orbiter is also the result of the requirement to determine the status of the lander during the first 5 minutes after impact. The orbiter in the worst case condition will be at a slant range of 14,000 km from the lander and be in sight for the 10 minutes required to play out the stored entry and descent information and the status information after impact.

6. Communications. When the heat shield is jettisoned at a preprogrammed altitude, the VHF antenna system and transmitter associated with the separation to entry phase will be jettisoned along with it. In order to play out the recorded entry and descent information, a new VHF communication link must be established with the orbiter. This will be done by means of a gimballed VHF antenna system consisting of two orthoganal slots with loaded dipoles. This antenna system is required during the landed transmission phases for communications with the orbiter. It is gimballed to allow a vertical orientation. During the entry and descent phases, however, this antenna will be rigidly supported to prevent movement and damage by the entry vibration and shock environments.

Table 21 lists the design parameters required to establish this communication link with the orbiter. The orbiter receiving system is the same one used in the separation to entry phase. A 50-watt VHF transmitter was selected for this and the subsequent landing phase since the Martian atmospheric pressure is much lower than on Earth and corona will result at high transmitter power levels. To overcome this problem, the VHF antenna system will be evacuated to a pressure where corona is no longer a problem. To do this, the VHF antenna will be enclosed in a dielectric chamber, the dimensions of which are restricted by space and thermal limitations. The system will be evacuated rather than pressurized since, during transit, the lander will be in free space vacuum. Any leakage during transit would be a problem with a pressurized system, but is actually an advantage for an evacuated system. A 50-watt transmitter power level was considered a practical compromise

TABLE 21

TELECOMMUNICATIONS DESIGN CONTROL CHART
(Mars Lander-to-Orbiter, Descent, Gimballed VHF Slot Antennas)

No.	Parameter		Nominal Value	Tolerance	Source	Worst Value
1	Total transmitter power	50 watts	+47.0 dbm	+0.0 -0.5 db		+46.5 dbm
2	Transmitting circuit loss		-0.25 db	+0.0 -0.5 db		-0.3 db
3	Transmitting antenna gain	140 degrees	+4.5 db	+0.0 -0.5 db		+4.0 db
4	Transmitting antenna pointing loss		-1.5 db	±1.5 db		-3.0 db
5	Space loss = 32.46+20 log F+20 log R F 300 mc, R 14,000 km		-164.92 db	---		-164.92 db
6	Polarization loss		-0.0 db	±0.5 db		-0.5 db
7	Receiving antenna gain	Helix	+5.0 db	±0.5 db		+4.5 db
8	Receiving antenna pointing loss	21 degrees	-0.5 db	±0.5 db		-1.0 db
9	Receiving circuit loss		-0.1 db	Max.		-0.1 db
10	Net circuit loss		-157.77 dbm	+3.0 -3.55 db		-161.32 db

TABLE 21 (Concl'd)

No.	Parameter	Nominal Value	Tolerance	Source	Worst Value
11	Total received power	-110.77 dbm	+3.0 -4.05 db		-114.82 dbm
12	Receiver noise spectral density (N/B) T system_____ NF 4 db	-169.8 dbm	+1.0 -0.0 db		-168.8 dbm
13	Predetection Bandwidth (10^6 cps)	+60 db	---		+60 db
14	Required ST/N/B $p_e = 5 \times 10^{-4}$	+14.6db	+1.0 -0.0 db		+15.6 db
15	Detector threshold required	-95.2 dbm	+2.0 -0.0 db		-93.2 dbm
16	Pulse Compression gain	+20 db	---		+20 db
17	Required received power	-115.2 dbm	+2.0 -4.05 db		-113.2 dbm
18	Performance margin	+4.43 db	+2.0 -6.05 db		-1.62 db

between thermal, corona, and space limitations. Using the pulsed linear chirped modulation scheme, a bit rate of 10,000 bits/sec is achievable. The detailed discussion of this system will be made in the discussion of the landed phase.

The worst case performance margin that can be expected with this link is -1.62 db. This worst case figure, if experienced, will simply reduce the bit error probability to approximately 1×10^{-3}, which is certainly an acceptable margin for the data recorded in this phase. At 10,000 bits/sec, the total transmitted bit content at 5 minutes will be:

$$5 \times 60 \times 10,000 = 3 \times 10^6 \text{ bits.}$$

The total recorded TV information, including tape wastage is 2.64×10^6 bits. The total recorded information due to sampling commutator deck A, B and C and the gaps left for the insertion of real time transmission system parameters on deck G is:

$$100 \text{ samples/sec} \times 5 \text{ bits} \times 600 \text{ seconds} = 300,000 \text{ bits.}$$

The total bit content to be played out is the summation of the recorded information in both recorders or 2.94×10^6 bits. The data will be played out by first playing out the 300, 000 bits from the commutators and secondly, the 2.64×10^6 bits from the vidicon. If for some reason the playout time is less than 5 mintues, all the engineering status information will have been played out and the most that will be lost in the event of lander failure on impact is some of the TV pictures.

The data stored during the descent phase will not be erased as it is played out. This is done to guard against the contingency that the orbiter is unable to receive the lander data at this time. If this happens, the data can be re-transmitted after the orbiter has gone into orbit. If the orbiter fails to go into orbit, the DSIF can command the lander to play out the data to Earth.

7. Landing. Upon landing and after comint to rest, the lander may have assumed any orientation due to terrain features. It will try to right itself to a normal orientation by opening its petals. The supporting structure for the gimballed antenna system will be removed and the antenna will assume a planet vertical orientation by means of the gimbal.

The data handling equipment will switch to mode 3, the complete engineering data mode. In this mode, the status of all equipment aboard the lander is monitored by commutator decks A, B, E, F, and G. Commutator E monitors 60 scientific instrument and data acquisition engineering functions. Commutator F monitors 30 functions associated with the S-band transmission equipment used in the direct link to Earth, while commutator G monitors

30 functions associated with the VHF transmission equipment used in the relay link to the orbiter. As shown in figure 155, alternate channels of commutator decks A, B, E, F, and G are monitored sequentially at a sampling rate of 2000 samples per second. At this rate, a given commutator segment is sampled at a minimum rate of 167 samples/sec. Again, due to the difference between the channel capacity of commutator deck E and decks A, B, F, and G, the same sequence of samples appears every sixth frame of commutator deck E or once every 360 msec. The lander will remain in this mode for 5 minutes, during which the data will be transmitted to the orbiter in real time using the same communications link as in the descent phase.

8. Main Scientific Mission. When the lander completes the engineering status check, it will start recharging its batteries. During this time, the lander will await commands from Earth which may alter the preprogramed scientific mission in the event of equipment failures as indicated by the engineering status check. Unless altered by command, the lander will begin its main scientific mission on the preprogramed basis.

9. Data Acquisition and Storage. At this time, the data handling equipment will switch to mode 4, the main science mode. In this mode commutator decks, A, D, and E are activated. Also, the vidicon sampled date system is activated. Commutator deck D monitors all scientific instruments requiring sampling rates less than 5 samples/sec. The sampling rates and duty cycles for all scientific instruments are listed in table 14. Except for the infrared bolometer and the vidicons, the sampling rates required by these instruments are less than 5 samples/sec. In addition to the TV, ultraviolet, and petro-microscope vidicons, the vidicon sampled data system will monitor the infrared bolometer. The duty cycles of these four instruments are such that no more than one is on at a given time.

As shown in figure 156, alternate channels of commutator decks A, D, and E are monitored sequentially at a rate of 40 samples/sec. One complete frame of commutator D will be sampled every 1.5 seconds. This rate exceeds the requirements for all instruments except the 3-axis seismograph and the Sun spectrometer which require 4 and 3 samples/sec, respectively. These rates can be achieved by super commutation. As in the previous phases requiring data storage, gaps are left in the recorded data for the insertion of real time information on the transmission link during playout. The tape recorders used to store this data are the same ones used during entry and descent. The data monitored by commutators A, D, and E will be recorded continuously throughout the 48 hour scientific mission. At 40 samples/sec, the total bit content recorded during this phase is:

$$(40 \text{ samples/sec})\ (5 \text{ bits})\ (48 \text{ hours})\ (3600 \text{ sec/hr}) = 0.345 \times 10^8 \text{ bits.}$$

At a bit packing density of 1000 bits/in/track, the record speed is:

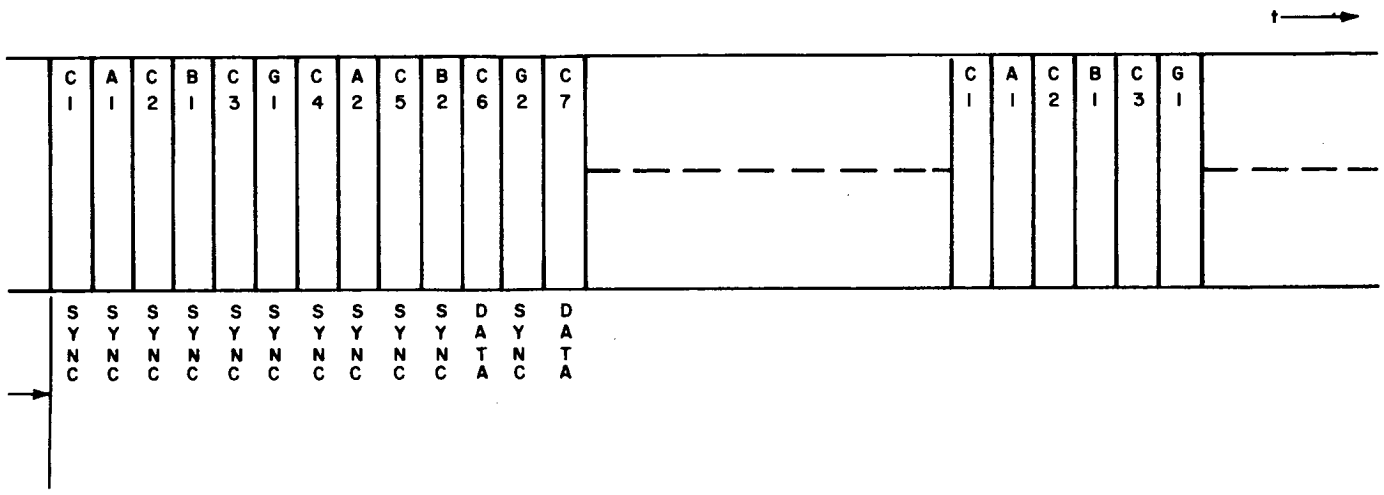

63-9830

Figure 155 LANDING, COMPLETE ENGINEERING STATUS MODE

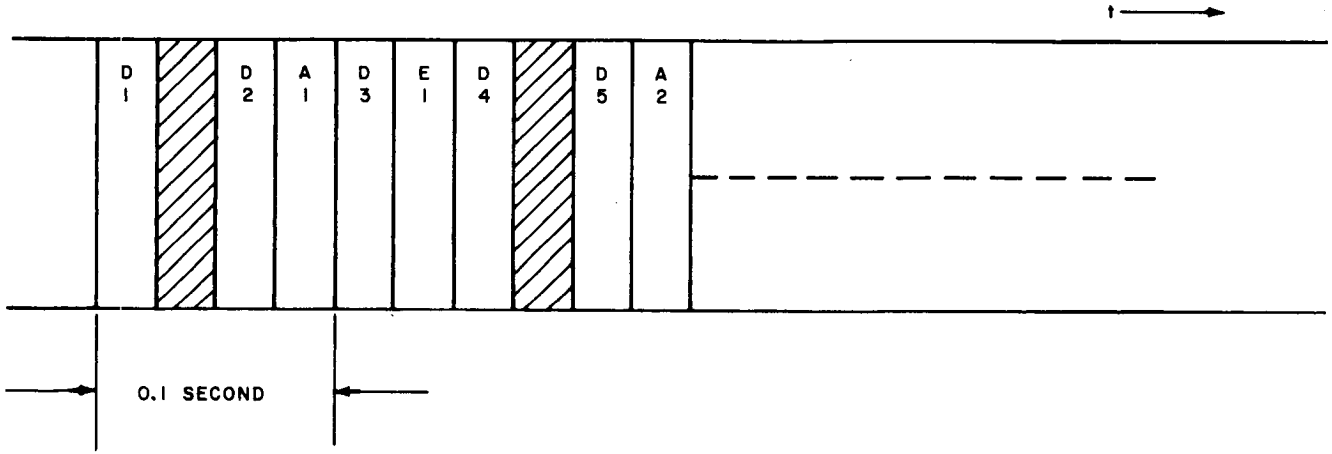

Figure 156 MAIN SCIENCE MODE

$$\frac{40 \text{ bits/sec}}{1000 \text{ bits/sec}} = 0.04 \text{ in/sec}$$

At 0.04 in/sec the total tape length required is:

(0.04 in/sec) (3600 sec/hr) (48 hrs) (1/12) - 576 feet.

The seven tracks required by this recorder can easily be accommodated on 1/2-inch wide tape. The machine would weigh approximately 10 pounds, including electronics, and would occupy about 1000 in^3. The power consumption during the record mode would be about 2 watts with 4 to 6 watts being consumed during playback.

The TV pictures taken of the terrain surrounding the lander will have 500 x 500 element rasters at a three-bit gray level. The same rasters size will be employed in the ultraviolet and petromicroscope vidicons. To read out these rasters in 20 seconds will require a sampling rate of 12,500 samples/sec. As in the descent phase, the sample and hold circuit will be used. The holding time, however, is reduced to 78 μsec due to the higher sampling rate. The same tape recorder used to store vidicon information in the descent phase will be used in this phase. With a bit packing density of 1000 bits/in/track, the record speed is:

$$\frac{12,500 \text{ bits/sec}}{1000 \text{ bits/in.}} = 12.5 \text{ in/sec}$$

There are 12 TV pictures, 120 ultraviolet pictures, and 4 petromicroscope pictures taken during the main science mission. Since these pictures are identical in raster size, the total recorded information bits including frame and line synchronization is:

(136 pictures) (250,000 samples/picture) (3 bits) = 1.02×10^8 bits.

Allowing for 10 percent tape waste during the stop/start times, the total recorded bits for the vidicon information is 1.12×10^8 bits. There is the added requirement to sample the infrared bolometer with this system. There are 12 samples taken of the bolometer, each lasting 47 minutes. During this time, the required sampling rate is approximately 60 samples/sec. The tape speed while monitoring the bolometer will be:

$$\frac{60 \text{ bits/sec}}{1000 \text{ bits/in.}} = 0.06 \text{ in/sec}$$

At 12.5 in./sec, the total tape length required is:

(12.5 in./sec fps) (22 sec/picture) (136 pictures) (1/12) = 3120 feet.

The total recorded information bits for the bolometer is:

(12 samples) (47 min/sample) (60 samples/sec) (60 sec/min) (3 bits) =

6.1×10^6 bits

Allowing 10 percent for tape waste, the total recorded bits is 6.7×10^6 bits.

At 0.06 in./sec, the total tape length required is:

$$(0.06 \text{ in./sec})(60 \text{ sec/min})(12 \times 47 \text{ min})\left(\frac{1.1}{12}\right) = 186 \text{ feet}$$

The total required tape length to accommodate both recording speeds is 3300 feet. However, as indicated for the previous recorder, seven tracks can be accommodated on 1/2-inch wide tape. By using seven tracks, the tape length required would be reduced to 1650 feet. This machine would weigh approximately 16 pounds, including electronics, and would occupy about 1500 in.^{3} The power consumption during recording and playback would be about 6 watts.

The total stored bits is the summation of the stored bits in each recorder or,

$$\begin{array}{r} 1.12 \times 10^8 \text{ bits} \\ 0.067 \times 10^8 \text{ bits} \\ 0.345 \times 10^8 \text{ bits} \\ \hline 1.532 \times 10^8 \text{ bits} \end{array}$$

As mentioned in the descent phase, the data acquired during that phase will not be erased. The amount of data acquired is only 3×10^6 bits and the resultant increase in recorder capacities is negligible.

10. Main scientific data transmission. The stored main scientific data will be transmitted to Earth by means of an S-band direct link or a VHF band relay link through the orbiter. There is a requirement to establish a direct link capability since some of the later Mars missions are landing missions only. This direct link will require a steerable high gain directional antenna to play out the stored information in a reasonable length of time. During the earlier missions, this link may not operate satisfactorily due to environmental

contingencies not presently known. However, the scientific data acquired during these earlier missions will provide the information required to improve the direct link design for later missions. It is for this reason that a VHF relay link capability through the orbiter is included in the early mission lander design. The weight penalty accrued by the lander for this capability is a small percentage of the total lander communications system weight, mainly because the energy required to relay information to the orbiter is a small fraction of the energy required to transmit the same information directly to earth and thus no additional power source weight is required.

The relay link has definite advantages over the direct link, specifically a much lower energy per bit requirement and the ability to use a nonsteerable wide beamwidth antenna. By using a wide beamwidth antenna, the lander does not have to track the orbiter thus eliminating the contingencies associated with the direct link.

The antenna system selected for the lander in the relay link is a pair of orthogonal loaded slots having a beamwidth of 140 degrees. At this beamwidth, the relay link will suffer from the effects of multipath.

11. The relay link.

a. Multipath disturbance.

1) General. The Voyager Mars lander vehicle might find itself in terrain which provides good propagation paths other than the line-of-sight path. If the power transmitted via these alternate routes is a significant part of the total power, the data error rate will increase.

Prolonged fades may occur due to near-cancellation of the direct signal by the sum of the reflected signals. If the delay via reflected paths is comparable with the baud interval in digital transmission, intersymbol interference may occur. The effects of multipath propagation would appear to be particularly significant in the case of sinusoidally phase modulated signals of low modulation index, because reflections from all parts of the terrain can add so as to cause interference. In the case of a rapidly moving receiver such as the orbiter, the path geometries would change rapidly. The result of this would be to reduce the coherence between direct-path signals and reflected-path interference, but with enough power arriving via reflected paths, the "noise" so produced may be high enough to increase the error rate.

2) The effect of pulse transmission. An effective way of reducing the amount of reflected power is to send signals as sharp pulses with a low duty factor. This prevents vectorial addition of scattered signals except for those which are delayed by multiples of the pulse repetition rate. If we assume that the scattered power is proportional to the area over which scattering takes place, figure 157 shows the amount of multipath interference reduction caused

by pulsing the signal. The pulse length is and the repetition interval T. Scattered signals can add vectorially only if they originate in the circle of radius R about the transmitter and successive annular rings of the thickness τ separated by radial distances T, 2T, etc. If the number of rings is large, the ratio of power scattered from the rings to power scattered from the vehicle surface is

$$\left(R \approx \frac{1}{\pi} \frac{\tau}{1} = \frac{1}{\pi D} \right) \tag{12}$$

where D is the inverse of the duty cycle.

If the received pulses are gated, the small pulses scattered from the area between the rings are completely eliminated. In that case, equation (12) represents the reduction in power received via scatterers when the signal is pulsed. It is assumed that the average direct-path power remains the same. Hence (12) also represents the reduction in the ratio of scattered power to direct-path power.

3) Use of the pulse compression system. Transmitter size and weight rise when a C. W. signal is converted to a pulsed signal with the same average power. For this reason a pulse - compression system is recommended. Present-day art permits compression ratios of the order of 100; the compression ratio is approximately equal to the factor D in (12). Therefore a reduction of the order of 25 db in power received via scatter paths is possible with pulse compression, the only increase in tramsmitter and receiver weight being due to the dispersive filters required by a chirp keying system and somewhat more complex amplifiers.

Manufacturers of these filters indicate that size and weight are within reason. Weight for a pair of dispersive lines (the receiver needs two) is expected to be under 2 pounds.

The transmitted baud will be identical for either 1 or 0, except that the carrier frequency will be shifted by an amount large compared with the bandwidth. Since the bit rate is to be 10 kc, the bandwidth will be D times as great, or 1 mc.

In the receiver, (see figure 158) 1 and 0 signals are separable by virtue of their differing center frequencies. Each signal passes through a separate but identical IF strip with its own automatic gain control. Wide-band IF noise will be used as a pilot signal to hold gain constant. Each IF feeds one of the two dispersive delay lines. These compress the signal. The compressed outputs of the lines are rectified and sampled by the synch circuit at the end of each baud. The polarity of the sampled output determines whether the signal is a 1 or 0.

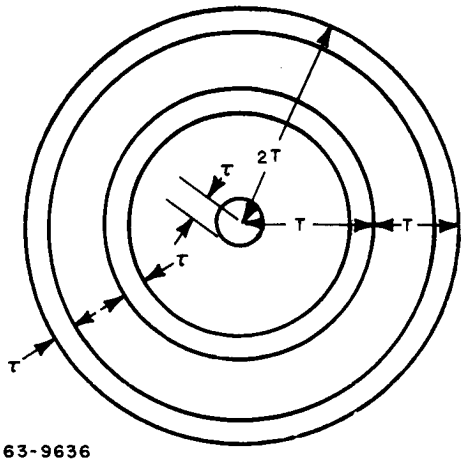

Figure 157 MULTIPATH INTERFERENCE REDUCTION

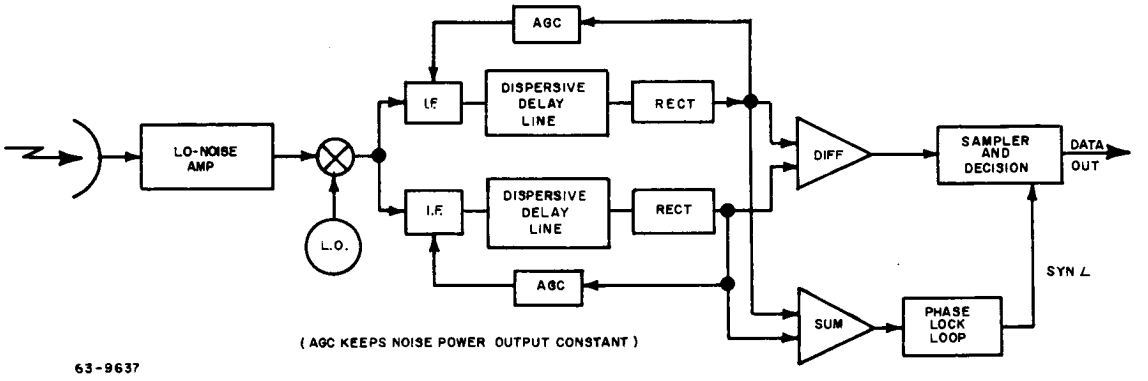

Figure 158 CHIRP RECEIVER

Synchronization is derived from a narrow-band phase lock loop. The rectified outputs of the lines are added and the sum is the input to the phase-lock loop. The spectrum of this signal contains a line at the pulse repetition frequency, and this line is tracked by the phase-lock loop. The bandwidth of this loop will be made as small as necessary to avoid significant degradation due to synch jitter.

The chirp system will not be as efficient a communication system as would be a biorthogonal one of the type used between Earth and orbiter. The difference in efficiency will be about 4 db, if sync is derived in the manner stated. It is also possible to derive synch from each compressed pulse by comparing it with a threshold. If multipath problems are to be severe despite the use of a pulsed system, the threshold system has an advantage in that its recovery from a disturbance is complete after one pulse (i.e., one data bit) while a flywheel synch system will have to relock after a disturbance. However, this system is considerably less efficient in terms of energy required per bit for a given noise power density. Error rates for the two systems are compared below.

4) Error rates for chirp keying. Each transmitted baud consists of a constant-loop-transmission wherein frequency varies linearly with time. Mark and space symbols differ in center frequency, but otherwise consist of identical waveforms. At the receiver, mark and space are sorted into two parallel IF channels by virtue of their differing carrier frequencies. Each IF channel terminates in an IF filter matched to the transmitted waveform. This waveform is so selected that the output of the matched filter is much shorter in duration than the received baud, as in "pulse compression" radar. The envelopes of the mark and space filter outputs are subtracted and the result of subtraction is sampled at the instant when the signal envelope is known a priori to be at its peak. If the sample is of one polarity, the baud is declared a one; if the other polarity, it is declared a zero.

While the direct-path radiated waveform of each baud is not a pulse, its spectrum is calculated to produce a narrow pulse at the output of the matched filter. Multipath signals form similar pulses, but delayed and of smaller amplitude than would be the case if they could vectorially or algebraically add.

Additive Gaussian noise in the communication channel leads to error in the decision regarding whether mark or space was transmitted. The probability of this error as a function of signal-noise ratio in the information bandwidth will now be computed.

5) Synchronous sampling. It will be shown that the relationship between error rate and SNR for chirp keying is identical with that for noncoherent frequency-shift keying. We consider first the case where (in either type of transmission) we know when to sample the filter outputs.

In the case on non-coherent FSK the envelopes of the outputs of the mark and space filters are compared and the decision goes to the one with the larger outputs. The probability density function of the envelope of signal plus noise is that of a sinusoid plus Gaussian noise, the modified Gaussian distribution (ref. 33). The probability density function of the envelope of Gaussian noise alone is the Rayleigh distribution.

For a given envelope voltage from the channel-containing signal, the conditional probability density function of error is the probability that the envelope voltage from the other channel will be greater than v.

$$dp = \int_{v}^{\infty} \rho_N (e)\, de \tag{13}$$

where ρ_N is the probability density function for envelope of noise alone. The total probability of error is the integral of the conditional probability over all possible values of v. Since v arises in the channel containing signal, the integral is weighted by the probability density function for signal plus noise

$$\rho = \int_{0}^{\infty} \rho_{S+N} \left[\int_{v}^{\infty} P_N (e)\, de \right] dv \tag{14}$$

By substituting the Rayleigh and modified Gaussian distributions in (13), it can be shown that the result is

$$\rho = \frac{1}{2} e^{-\frac{S}{2N}} \tag{15}$$

where S is the IF signal power at the filter output at time of sampling, and N is the average IF noise power at the filter output in the noise bandwidth of the filter.

The only difference between the statistics of chirp keying and noncoherent FSK arises because the frequency of the chirp signal at the filter output is not quite constant, while in the case of FSK it is constant. However, the frequency variation is very small for reasonably large compression ratios (ref. 34) and this difference will be neglected here. In that case, the probability density function for the channel containing signal plus noise is the same modified Gaussian one applicable to FSK. Similarly the probability density function for the other channel is the Rayleigh. Thus, the probability of error at time of sampling is given by (14) and (15) for the chirp system. It has been assumed

that it is known a priori when peak signal is to occur in the channel containing the signal based, and that sampling of both channels takes place at this time. The only remaining question concerns what value of $\frac{S}{N}$ should be applied in (15). Remember that this is the IF SNR at the output of a channel filter, and is defined here as the ratio of half the peak instantaneous power in the signal (at the time of sampling) to the mean noise power. But since the filter is matched to the signal, it can be shown that the IF SNR defined in this way is related to the input signal and noise by:

$$\frac{S}{N} = \frac{E}{N_o} \tag{16}$$

where E is the signal energy in one baud and N_o is the single-sided noise power density, both measured at the filter input. Therefore, if the non-coherent FSK system and the chirp system both are subject to the same N_o and both have identical baud energy E, they also have the same SNR in the filter output, hence, finally, the same probability of error per baud.

6) Continuous Comparison. If there is no way of knowing when to sample the filter outputs, each one must be compared continuously with a threshold. At any time when the envelope of one or the other filter rises above the threshold, mark or space are declared according to which filter output passed the threshold. The statistics of this case differ from that previously considered. Here a comparison must be made between the envelope of each filter output and a threshold, rather than between the two envelopes. The optimum threshold is not fixed but varies with SNR. Finally, in each baud interval there are twice as many opportunities for error as there are independent samples of envelope noise in the baud interval (twice because the noise in the two filter outputs is independent; therefore, each output contributes equal numbers of errors). This is in contrast with synchronous sampling, where there is only one opportunity for error per baud.

The two probability density function of the envelopes are the same as before; the Rayleigh distribution for noise alone and the modified Gaussian for signal plus noise. As before, designate these $P_N(e)$ and $P_{S+N}(e)$. The probability of any noise sample exceeding the threshold will be designated P_N, where

$$P_N(v) = \int_0^\infty P_n(e)\ de \tag{17}$$

being the threshold level.

The probability of any signal not exceeding the threshold will be designated

$$P_{S+N}(v) = \int_0^v P_{S+N}(e)\, de \qquad (17a)$$

Since we are looking at the filter outputs, the signals are narrow pulses, appearing rather like radar blips. Although either mark or space waveform is always in the receiver the signals at the filter outputs are "present" only when all components of the transmitted waveform add algebraically to produce a pulse. Two kinds of error can occur: a type A error happens when a signal is received (either mark or space) but noise subtracts from the signal so that the threshold is not reached; a type B error happens when no pulse appears at either filter output, but noise exceeds the threshold, causing a false alarm.

This is much like the problem of determining the probability of detection and probability of false alarms at the output of an incoherent radar. The only difference is that the cost of either type of error is the same in our case, whereas this is not usually the case in radar.

The probability of at least one type B error during a baud interval is:

$$P_B = (1 - \text{probability of no type B errors}) \qquad (18)$$

$$P_B = \{1 - [1 - P_N(v)^{2n}]\} \approx 2n\, P_N(v) \quad \text{for large } n \qquad (19)$$

where n is the equivalent number of independent noise samples in the envelope of each filter output. For matched filters with large compression ratios, n is also nearly equal to the compression ratio.

(For large compression ratios, and no "weighting", the amplitude part of the filter IF transfer characteristic is nearly square, and its width is n/T where T is the baud interval. It can be shown that in a time T, the equivalent of n independent noise samples emerge from a square filter with bandwidth n/T.)

The probability of a type A error during the baud interval is

$$P_A = P_{S+N}(v) \qquad (20)$$

Since errors of type A or type B are equally important, the threshold should be set so that each are equally likely, hence a constraint on v is:

$$P_A = P_B \quad \text{or} \qquad (21)$$

$$2n\, P_N(v) = P_{S+N}(v) \tag{22}$$

$$2n \int_v^\infty \frac{e}{N} \epsilon^{-\frac{R^2}{2N}} de = \int_0^v \frac{e}{N} \epsilon^{-\left(\frac{e^2}{2N} + \frac{S}{N}\right)} I_o\left(\frac{\sqrt{25}\, e}{N}\right) de \tag{23}$$

S/N is the signal-to-noise ratio in the IF output of either filter, at the peak of the pulse. Thus, the earlier arguments given in the synchronous case can be used to show that (5) applies, whence

$$\frac{S}{N} = \frac{E}{N_o} = \frac{\rho_S T}{N_o} \tag{24}$$

where P_S is the average signal power entering the filter, T is the baud interval, and N_o the noise power per cps (signal-sided) entering the filter. For a given value of the compression ratio n (23) can be solved for v as a function of S/N. The total probability of error (probability of either type A or type B error) is:

$$P = P_A + P_B - P_A P_B \tag{25}$$

since P_A and P_B are independent, P_A and P must be quite small, so that we may with high accuracy write:

$$P = P_A + P_B = 2P_A = 2P_B \quad , \tag{26}$$

the final two equalities occurring because of the constraint on the threshold given by (21), (22), and (23).

Combining (26) and (27) we find for the total probability of error:

$$P = 4n \int_v^\infty \frac{e}{N} \epsilon^{-\frac{e^2}{2N}} de = 2 \int_0^v \frac{e}{N} \epsilon^{-\left(\frac{e^2}{2N} + \frac{S}{N}\right)} I_o\left(\frac{\sqrt{25}\, e}{N}\right) de \tag{27}$$

is plotted as a function of $\frac{S}{N}$, for the case n = 100, in figure 159.

7) Dispersive ultrasonic delay lines. Present lines are of aluminum tapered strip. Typical performances are

Bandwidth	2 mc
Center frequency	5 mc
Delay	30 μ s
Compression	100/1
Volume	81 in.^{3}
Weight	12 ounces
Temperature requirements	nominal ± 0.01°C

It is expected that within 9 months, "zero TC" glass lines will be available with

Center frequency	30 mc
Bandwidth	6 to 8 mc
Compression	100/1
Insertion loss	35 db
Temperature requirements	70 ± 15°C

Glass can be obtained suitable for other nominal temperatures.

The sterilization temperature does not pose a serious problem, and suitable ceramics and bonders are available.

8) Wideband FM.

a) Summary. Wideband FM can reduce the effects of multipath provided the bandwidth of the modulating signal is greater than the reciprocal of the minimum path delay time; however, when the amplitude of the delayed path is comparable to that of the direct path, the FM or FMFB system has difficulty in overcoming the multipath effects.

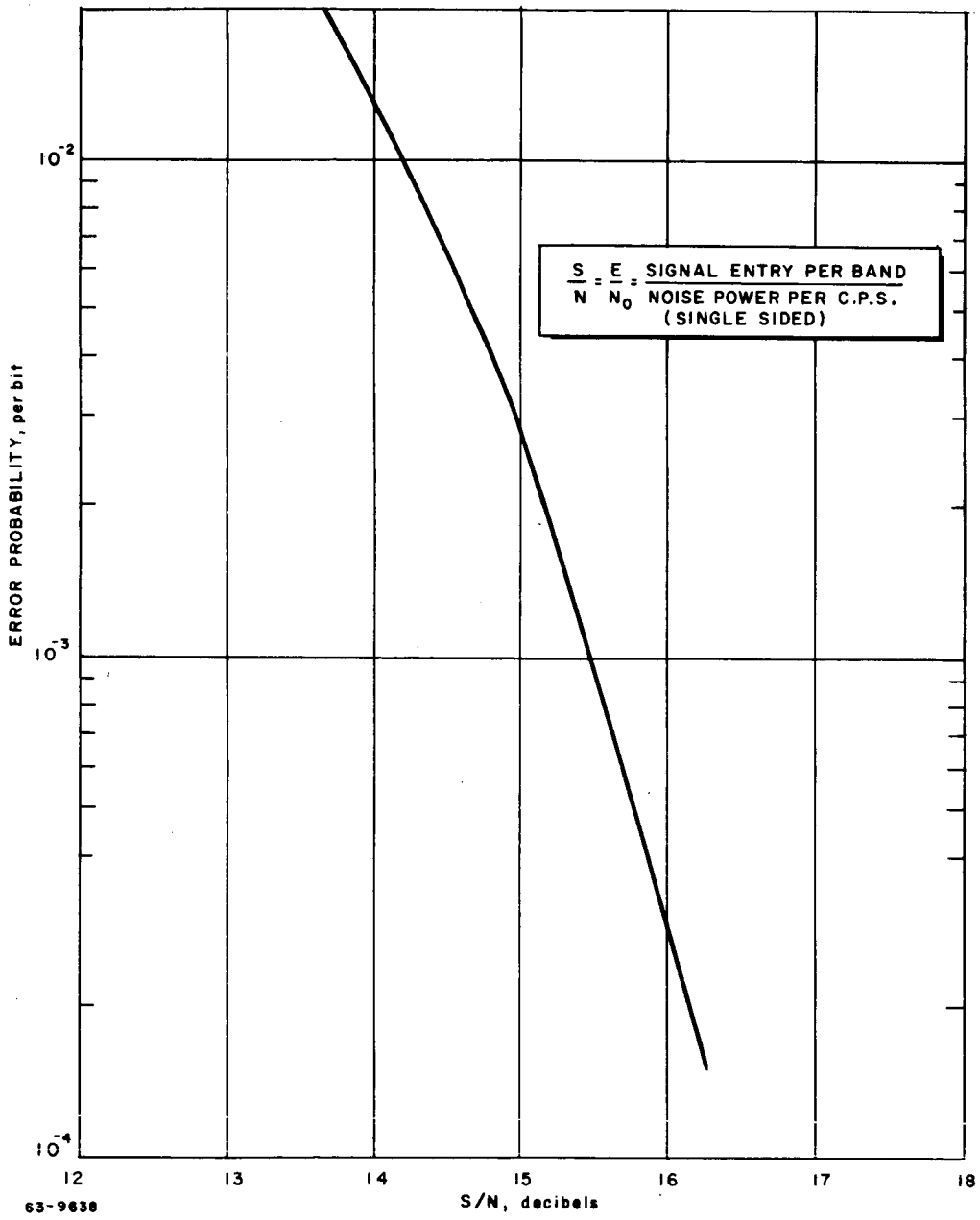

Figure 159 ERROR PROBABILITY

b) Discussion. FM has the following interference reducing properties:

1 Interference sidebands are ordinarily so related in amplitude, frequency and phase with respect to the desired carrier that they are inefficient in producing frequency modulation as compared with the sidebands of the desired signal.

2 The frequency modulation produced by the most effective sidebands of the interference is of too high a frequency to pass through the audio portion of the receiver.

If the minimum multipath delay is so large that the delayed and direct path signals cannot be considered coherent, and if the instantaneous modulation has had time to change, then the stated interference-reduction effects of FM will come into play. If these conditions are not met, the delayed signals can act directly against the sidebands and cause considerable distortion.

To further consider the effects of multipath, suppose we consider a two-path case. Over a short interval of time the frequency of the direct and delayed signal can be considered constant. Suppose the frequency of the direct signal is p and that of the delayed signal is $p + r$. The vector diagram for the two-signal interference is: Figure 160.

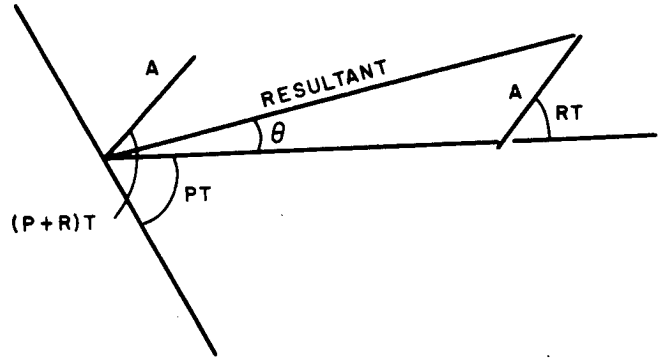

Figure 160 TWO-SIGNAL INTERFERENCE VECTOR DIAGRAM

where the amplitude of the direct path is 1 and the amplitude of the delayed path is a. The instantaneous angular frequency of the resultant signal is:

$$\omega = \frac{d\theta}{dt} = \frac{a\,r\,(a + \cos\,rt)}{1 + 2a\,\cos\,rt + a^2} \quad . \tag{28}$$

A plot of instantaneous angular frequency versus time is shown below.

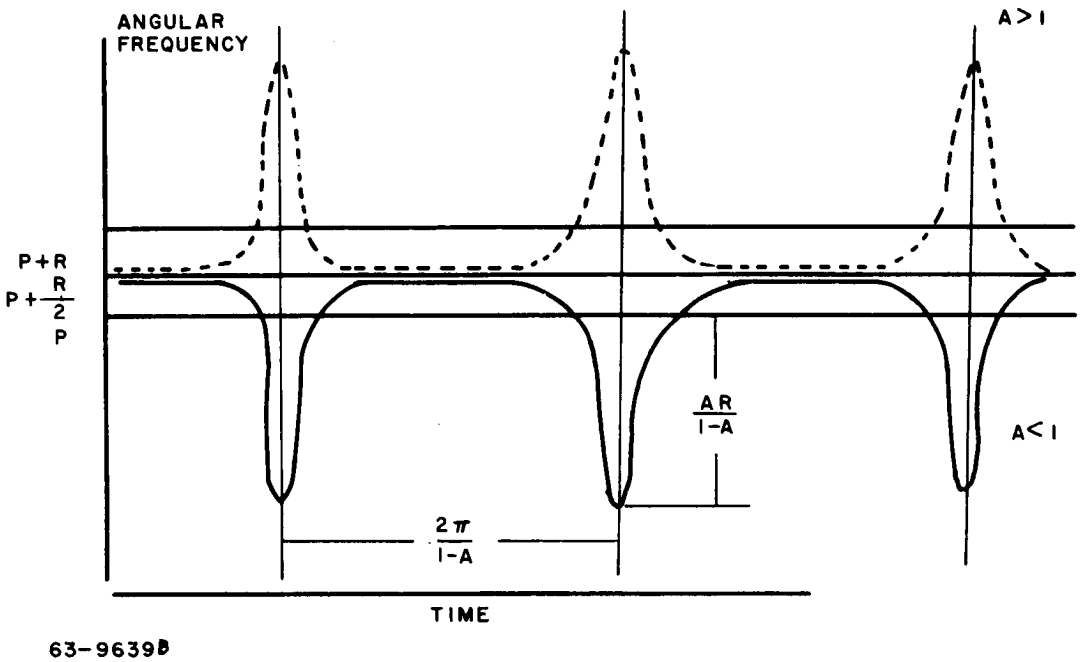

Figure 161 INSTANTANEOUS ANGULAR FREQUENCY

In practice i is always large compared to r so that the average frequency of the resultant is the same as that of the wanted signal. However, in order to preserve this average frequency, it is necessary to preserve the spikes; therefore, the frequency detector must be linear over this wide range, or if feedback is used in the receiver, the feedback loop must be able to track these rapid changes in instantaneous frequency. When the two components are in antiphase, not only is there a rapid variation in instantaneous frequency, but there is also a sharp dip in amplitude. When a is close to unity, this decrease in amplitude will not be able to be removed by the limiters, and fading will result. By increasing the modulation index, and going to a wide-band FM system, one may increase the spike recurrence rate above the resolving power of the system. Thus, a wideband FM system helps remove some of the effects of multipath, but cannot completely remove these effects.

If the delayed signal is greater in amplitude than the direct signal, the instantaneous angular frequency has spikes indicated by the dotted line rather than the solid line in the previous plot. If a feedback loop is used in the receiver, the loop will lock on to the stronger signal, and if the relative amplitudes of the delayed and direct path signals keep changing, additional distortion may be introduced in an FMFB system due to the loop alternating which of the two signals it stays locked on to.

If the amplitude of the delayed signal is much smaller than that of the direct signal, the multipath introduces an additional term:

$$D\,[s(t) = s(t+ri]\cos\left(\lambda\int_{t}^{t+r} s(x)\right)dx \qquad (29)$$

in the output signal of an FMFB receiver.

Note:

D = $\dfrac{\text{amplitude of delayed signal}}{\text{amplitude of direct signal}} \ll 1$

$s(t)$ = modulating signal

r = modulatory index

λ = delay associated with delayed path.

12. Detailed system description (Mars lander). Assuming that the orbiting receiver utilizes a circularly-polarized rigid antenna which is fixed to point at the Martian surface due to stabilization of the orbiting vehicle itself, a beamwidth of 84 degrees is required for Mars to fill the receiver beamwidth at periapsis. Ideally, the lander's transmitting antenna should have a beamwidth of 180 degrees so that it could communicate with the orbiter from horizon to horizon. However, such a wide beamwidth would produce multipath reflections from all objects within the view of the lander and would be extremely difficult to combat. Therefore, it is necessary to keep the main transmitter beam several degrees above the horizon at the sacrifice of some communication time. Without a precise knowledge of the fine-grain structure of the Martian terrain, a minimum beam elevation of 20 degrees appears a reasonable choice. Such a beam would clear a 170-foot ridge located 500 feet from the lander. Therefore, a transmitting antenna beamwidth of 140 degrees has been chosen.

A model of this transmitting antenna has been constructed and tested in a simulated Martian atmosphere to determine its breakdown characteristics. These tests have shown that 50 watts of peak input power is the maximum such an antenna can safely handle without breakdown. The dissipated power is within the thermal limitations of the antenna structure. This antenna also has an effective bandwidth of 1 mc.

At the maximum communication range (2500 km), a power level of 50 watts is compatible with the desired signalling rate of 10,000 bits/sec. However, a 10 kc RF bandwidth has an essential resolution of 100 μsec, or 16.4 nm. This means that all multipath signals which are delayed up to 100 μsec from the direct signal, due to terrain reflectors up to roughly 8.2 nm from the lander, cannot be resolved. For the transmitter beamwidth of 140 degrees, a mountain 17,000 feet high would be needed at a distance of 8.2 nm in order to lie within

the beam and produce appreciable interference. Since it is most unlikely that a mountain this tall will be encountered, multipath reflections will occur much closer to the lander and thus will be unresolvable. This means that the spectral bandwidth must be wider than 10 kc and, if possible, should utilize the full 1 mc bandwidth of the antenna.

A 1 mc bandwidth would produce a resolution of 1 μsec, and would allow effective discrimination of multipath reflections from objects beyond roughly 500 feet from the lander. This resolving power, plus the beamwidth characteristics of the antenna, would allow quite effective multipath rejections.

One method of achieving this result would be to signal with 1 μsec pulses with a repetition rate of 10,000 pulses/sec. The direct-path signal would then be time gated to eliminate later multipath. Because of the 100:1 increase in bandwidth (1 mc: 10 kc), however, a 5,000 watt peak signal would be required.

As a result, this approach is unacceptable because of the excess peak power.

A second approach would be to utilize high deviation FM with code tones designating the binary digits. Although this approach would allow operation below 5,000 watts due to FM processing gain, the FM receiver's threshold would force the use of powers above 50 watts. This is true even if an FM/FB receiver is used to maintain a low threshold. Furthermore, FM does not suppress multipath effects as effectively as time gating techniques.

On the basis of these considerations, the optimum modulation is one which spreads a 10,000 bits/sec message to occupy 1 mc, keeps the peak radiated power constant at 50 watts through receiver processing equal to the bandwidth spreading. The receiver should not be threshold limited, receiver time gating should be possible for multipath discrimination, and both signalling bits should be capable of occupying the total RF bandwidth with minimum cross-character interference. The closest practical modulation to this ideal is linear frequency pulse compression ("chirp"). As applied to the lander telemetry system, a binary digit 0 is represented by a 100 μsec rectangular pulse whose frequency linearly increases through 1 mc during this period. The digit 1 is represented by a decreasing sweep of frequency during the signalling interval. These two signalling waveforms are shown in figure 162 and are orthogonal to one another within 20 db.

At the receiver, a matched correlation filter for each waveform compresses each digit into a 1 μsec pulse whose effective peak power is 20 db higher than the transmitted average power of 50 watts. The matched filter consists of an all-pass network whose time delay characteristics vary linearly with frequency. For the 0 waveform, the filter's delay decreases with frequency over the 1 mc signalling band, while the 1 filter's delay increases with frequency. The compressed signal outputs from the two channels are then time gated to reject multipath signals which follow.

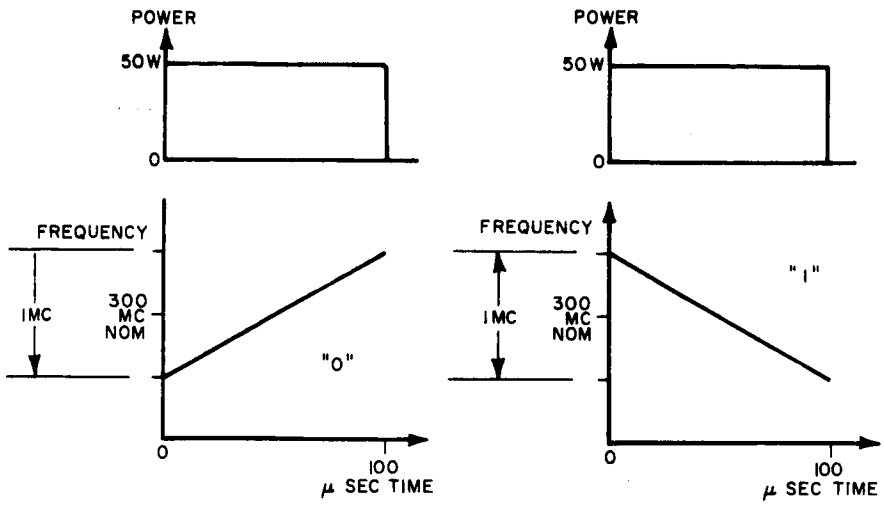

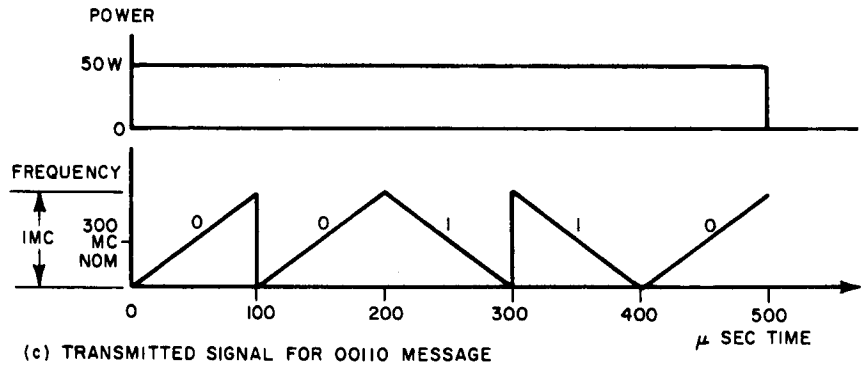

63-9640

Figure 162 TRANSMITTER WAVEFORMS

The technique is not threshold limited (since it relies upon matched filter correlation of phase relations established at the transmitter), is highly efficient in its utilization of bandwidth since all information is concentrated within the main RF bandwidth and not spread into redundant sidebands), allows operation at low average powers, and yet allows time-gated elimination of spurious signals at the receiver.

The approach has a beamwidth spreading of 100:1 and a power enhancement of 20 db. The codes chosen for the signalling bits are independent from one another by a factor of 20 db. That is, when a 0 is being transmitted, a spurious signal 20 db down from the 0 channel's output will occur at the output of the L channel. Therefore, a 20 db signal-to-noise ratio (where noise is a primarily spurious signal) is the maximum achievable. Since the desired error probability of 5×10^{-4} requires a signal-to-noise ratio of 15.6 db, the coding will perform adequately. Tests have shown that a 4-db spurious-signal margin is more than adequate for compression system degradation.

The normal output of a pulse compression communication system is a $\sin x/x$ time pulse. Since the main sidelobes of such a pulse are only 13 db down from the main response, shaping is necessary to make these sidelobes at least 15.6 db down. This is accomplished by frequency shaping of the incoming spectrum with a Tchebycheff weighting filter. This filter can be designed to reduce the sidelobes to a level greater than 25 db below the main response at the expense of a slight widening of the output pulse.

A basic block diagram for the chosen lander telemetry system is shown in figure 163 and the performance of this system is shown in table 22. As noted, the system has a 17-db loss margin under nominal propagation conditions. Since the link is line of sight at VHF, the losses actually encountered will be associated with the equipment itself and not the propagation path. This margin is considered adequate to include matched filter realization losses, antenna losses, processing losses, transmission line losses, environmental performance losses, and so on.

13. Telemetry transmitter.

a) Transmitter encoder. The general configuration of the chirp encoder used in the transmitter is shown in figure 164. The purpose of this unit is to produce the chirp waveforms corresponding to the 1's and 0's of the PCM information signal and the carrier frequency required for transmission. This is accomplished in the following manner:

The master clock, consisting of a stable oscillator and waveform-shaping circuits, is used to produce the timing pulses employed throughout the system. The repetition rate of the pulse train is 10 kc, corresponding to the data rate of the transmission link. This pulse train is fed, among other places, to a short-pulse generator, which produces an output waveform with essentially

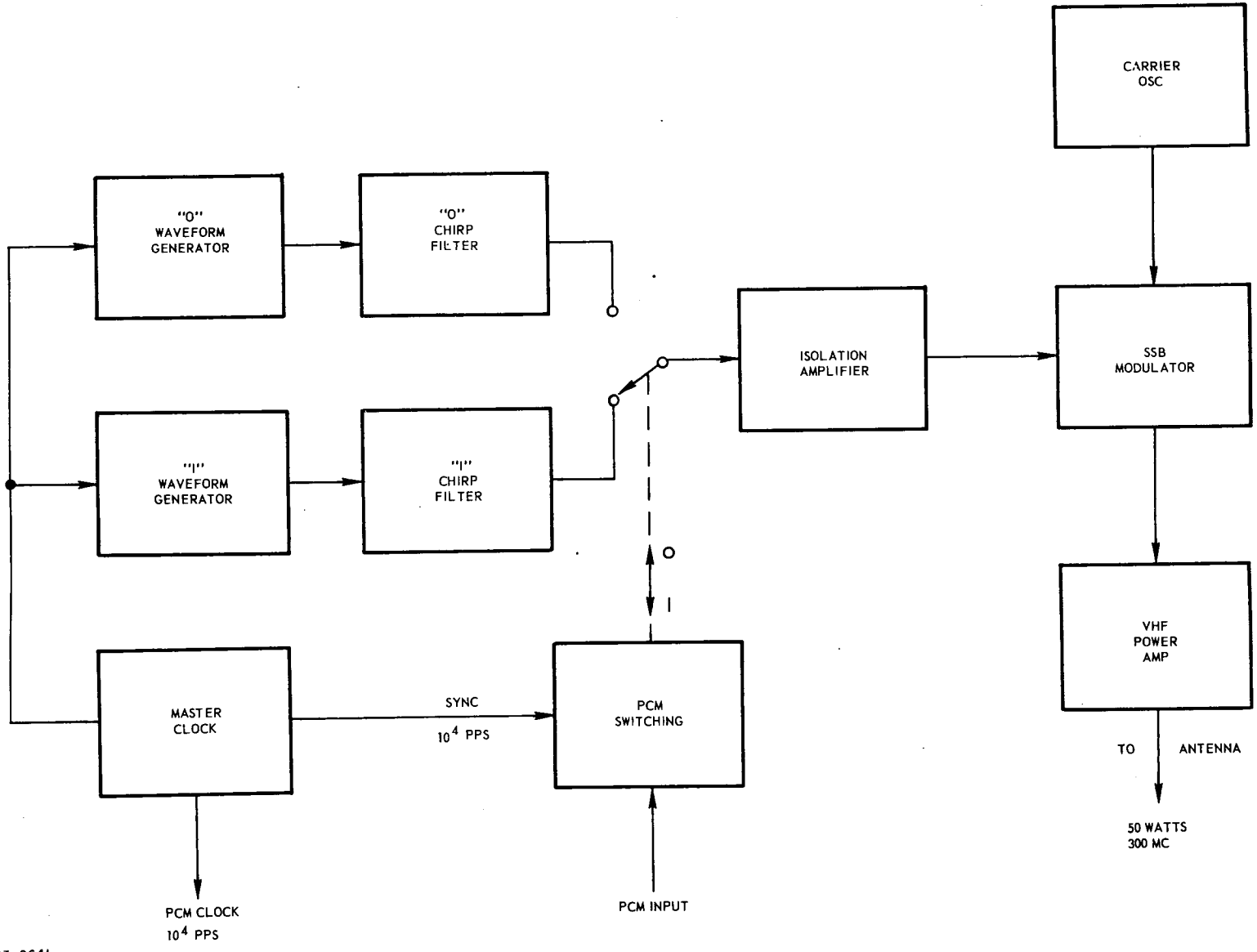

Figure 163 LANDER TRANSMITTER

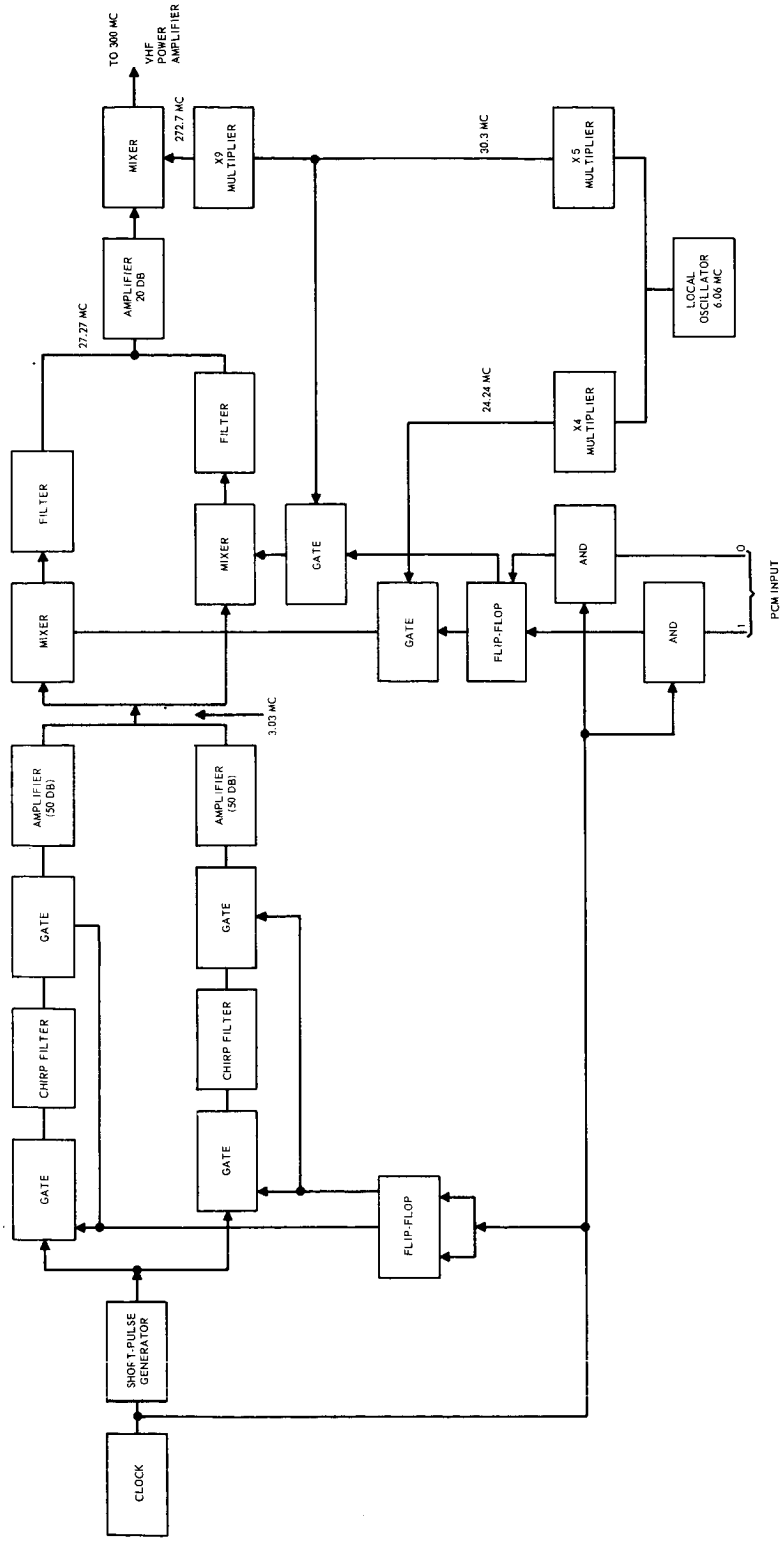

Figure 164 TRANSMITTER ENCODER BLOCK DIAGRAM

TABLE 22

TELECOMMUNICATIONS DESIGN CONTROL CHART

Mars Lander-to-Orbiter, Transfer of 48 Hr Science Data, Gimballed VHF Slot Antennas)

No.	Parameter		Nominal Value	Tolerance	Source	Worst Value
1	Total transmitter power	50 watts	+47 dbm	+0.0 -0.5 db		+46.5 dbm
2	Transmitting circuit loss		-0.25 db	+0.0 -0.05 db		-0.3 db
3	Transmitting antenna gain	140 degrees Loaded Slots	+4.5 db	+0.0 -0.5 db		+4.0 db
4	Transmitting antenna pointing loss		-1.5 db	±1.5 db		-3.0 db
5	Space loss = 32.46 20 log F+20 log R F 300 mc, R 2500 km		-149.96 db	---		-149.96 db
6	Polarization loss		0.0 db	±1.5 db		-1.5 db
7	Receiving antenna gain	65 degrees Helix	+5.0 db	±0.5 db		+4.5 db
8	Receiving antenna pointing loss	at 84 degrees	-3.0 db	+0.0 -1.0		-4.0 db
9	Receiving circuit loss		-0.1 db	Max.		-0.1 db

TABLE 22 (Concl'd)

No.	Parameter	Nominal Value	Tolerance	Source	Worst Value
10	Net circuit loss	-145.31 db	+3.50 -5.05 db		-150.36 db
11	Total received power	-98.31 dbm	+3.50 -5.55 db		-103.86 dbm
12	Receiver noise spectral density (N/B) T system_____ NF 4 db	-169.8 dbm	+1.0 -0.0 db		-168.8 dbm
13	Predetection Bandwidth	+60 db	---		+60 db
14	Required ST/N/B $p_e = 5 \times 10^{-4}$	+14.6 db	+1.0 -0.0 db		+15.6 db
15	Detector threshold required	-95.2 dbm	+2.0 -0.0 db		-93.2 dbm
16	Pulse compression gain	+20 db	+0.0 -1.0 db		+19 db
17	Required rec'd power	-115.2 dbm	+3.0 -0.0 db		-112.2 dbm
18	Performance margin	+16.89 db	+6.5 -8.55 db		+8.34 db

constant spectral energy density over the region between 2.5 and 3.5 mc. To meet this requirement, the waveform may be either a very short video pulse (approximately 0.1μsec) or a longer RF pulse with a 3-mc carrier. In the latter case, the pulse would consist of approximately a half cycle of the carrier, which could be generated by gating a 3-mc ringing circuit.

In either event, the pulse is applied to a pair of gates, each of which feeds a filter matched to a descending-frequency chirp waveform. Before going into the details of the gating operation, first consider the type of waveform which will appear at the filter output when excited by the short pulse.

The filters are required to generate a signal with a 1-mc bandwidth. Since frequencies outside this desired region do not contribute to the output signal within the 100μsec interval over which the output pulse is defined, the only significant input frequencies are those within $\pm$0.5 mc of the center frequency of the filter. Since this is true, any signal which has a uniform spectral distribution over this region produces the same effect as an impulse of voltage, which has a uniform spectral distribution over all frequencies. The short pulse applied to the filters has this characteristic and therefore the filter output will be its impulse response which, since the filter is matched to a chirped pulse, will be a chirped pulse.

At this point, it is appropriate to discuss the proposed methods for implementing these filters. Several rather commonly used procedures are available, but of these the use of either a cascade of all-pass filters sections or a linearly dispersive delay line are the most useful. For high-resolution radar systems, the former method is favored, since it can be used to produce waveforms with greater bandwidths. The latter method, however, possesses the advantages of simplicity and inherent reliability. Since the rather modest bandwidth requirements of the proposed system is well suited to these devices, the dispersive delay-line filter has been selected for this application.

The type of delay line which will be used is a zero TC glass line down which acoustic waves propagate with an almost linear frequency dispersion. In other words, low frequencies are delayed by a greater amount than are high frequencies, so the impulse-response of the line is a downward-chirped waveform. The weight of each line would be less than 1 pound. For best operation, a center frequency of about 3 mc is desirable, which accounts for the specifications previously given regarding the pulse spectrum.

Two chirp filters are employed in the design because of the requirement for contiguous output pulses. The required pulse envelope shape is rectangular, but the filter is incapable of actually generating such an output in response to an impulse. The waveform is actually quite rounded and is elongated considerably beyond the prescribed duration. In order to produce the desired shape, clipping and squaring circuits must be employed. The gates which follow the chirp filters are actuated by a flip-flop controlled by the clock, and therefore,

limit the duration of the output pulses to the desired 100μsec. The gates at the filter inputs are controlled by the same flip-flop, and these serve to attenuate the input between the lines, thereby permitting the output signals to die down before the next input is applied. The outputs from the pair of filters are amplified and then combined to give a continuous sequence of downward-chirped pulses of 100μsec duration and 1 mc bandwidth.

The set of mixers and filters which appears next in the block diagram is used to apply the PCM coding to this waveform. The sequence of chirped pulses is applied to two mixers simultaneously. The local oscillator signal of one mixer is at a frequency of 24.24 mc, while that of the other is at 30.3 mc. Filters are employed to select the upper sideband from the upper mixer and the lower sideband from the lower mixer. It is apparent that the center frequency of the selected sideband will be 27.27 mc in both cases. However, because of the manner in which they are produced, the upper output will chirp downward and the lower output will chirp upward. These signals may now be used to represent 1 and 0 in the desired manner. Selection of a 1 or a 0 is accomplished by gating the local-oscillators to the mixers. A flip-flop controls these gates and the flip-flop itself is synchronized with the clock by means of the "and" gates in series with its input lines.

The encoded signal, now at a center frequency of 27.27 mc, is translated to the desired frequency of transmission by a single-sideband generator described in the next section dealing with the transmitter RF circuits. The local-oscillator signals required for this mixer and the two used in the encoder are derived from a frequency-synthesizer consisting of a 6.06 mc crystal-controlled oscillator, and three frequency multipliers, providing multiplication factors of 4, 5, and 9, respectively.

It is estimated that the entire encoder package will include 75 transistor stages, about equally divided between analog and digital types, 130 resistors, 95 condensors, 40 inductors, 2 delay lines, 3 transformers and a crystal, and will weigh approximately 3.5 pounds. It will occupy a total of about 25 in.^{3}. The power consumption of the circuitry will be about 1.4 watts (50 ma at 28 volts). There will probably be some requirement for temperature control of the oscillator crystal and the dispersive delay lines. Since it is not known at this time how accurately the internal temperature of the vehicle will be maintained, the power required for temperature control cannot be estimated with accuracy at this time. Current expectations are that if temperature variation around nominal is only $\pm$ 15°C, no oven will be required for glass lines operating at 100:1 compression ratio. Higher variations would necessitate but crude temperature control. It may be assumed, therefore, that a nominal allocation of about 5 watts for temperature control will be sufficient for the purpose. This leads to a total power consumption of 6.4 watts for the entire encoder unit.

b) Transmitter power amplifier. The transmitter power amplifier section is shown in figure 165. This section amplifies the chirp digital signals and produces a single-sideband transmission at 50 watts.

The single sideband generator will be of the filter type, using a balanced modulator for local oscillator suppression, and an output filter for unwanted sideband suppression and additional local oscillator suppression. The balanced mixer is a hybrid T using coaxial lines and varactor diodes, and will give 30 db of LO suppression. The output filter will consist of 2 coaxial lines forming a bandpass filter at 300 mc. Sixty db of unwanted sideband suppression can be obtained in this way, and better than 40 db total of LO suppression. The filter method of single sideband generation was chosen over the phasing method because of its lesser critical characteristics, and its adaptability to different input signals. Good results have been obtained at these frequencies and bandwidths in previous feasibility breadboards using this technique.

The low level output signal of the SSB generator will be amplified up to the drive power required by the power amplifier by a driver stage employing techniques similar to those that are used in the final amplifier. For the latter, the 50 watts of final output power are readily realized with class C power amplifier stages using ceramic-metal tubes.

The estimated weight and size of the balanced modulator are, respectively, 1 pound and 6 $in.^3$ and, for the SSB filter, 1 pound and 15 $in.^3$. The driver will weigh about 0.7 pound and occupy about 15 $in.^3$ while the final amplifier will weigh about 1.8 pounds and have a volume of about 32 $in.^3$. Approximately 125 watts at 28 volts will be drawn from the power supply by this transmitter power amplifier section.

c) Relay link data playout control. The stored main scientific data will only be played out to the orbiter when the orbiter is within the line of sight of the lander. To do this, the lander will be commanded from the orbiter by means of the orbiter radar altimeter. To prevent the lander from transmitting when the range is beyond 2500 km, the orbiter altimeter will send bursts of five pulses at altitudes lower than 1800 km and single pulses at altitudes above 1800 km. The lander command receiver is designed to operate on the burst of five pulses. The transmitting range of 2500 km represents the maximum slant range expected when the orbiter is at 1800 km altitude. The details of the command pulse characteristics are discussed in the Mars orbiter integrated altimeter command system. The details of the receiver in the lander are discussed below.

14. Lander altimeter command receiver. Design of the low capacity lander command receiver is similar to the orbiter altimeter receiver. The solid-state local oscillator with the 30 mc crystal oscillator and varactor multiplication is identical. A crystal mixer is also used for heterodyning with the incoming signal to 30 mc. The 30-mc IF amplifier has a 3 mc bandwidth and is a three-stage unit

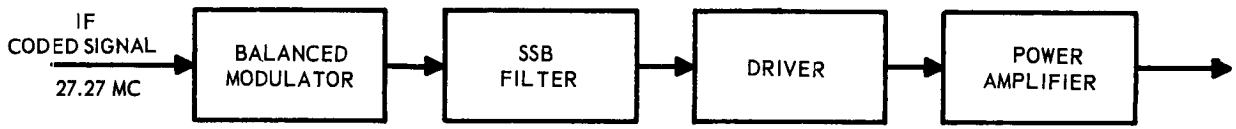

63-9643

Figure 165 VHF TRANSMITTER RF CIRCUITS

with one stage of AGC. A crystal detector, and one stage of video amplification follows the IF amplifier.

The decoder is based on a four-code pulse with two 1 μsec pulses spaced 2 μsec apart. Schematically, the decoder consists of three flip-flops, three "and" gates and two lumped constant delay lines of 3 μsec delay each. Pertinent design parameters are listed in table 23 and the system is diagramed in figure 166.

TABLE 23

LANDER ALTIMETER COMMANDED RECEIVER DESIGN PARAMETERS

Electrical	Compatible with orbiter at 1500 to 1800 km
Weight	19.25 ounces
Volume	25.3 in.^{3}
Power Consumption	3 watts

15. Low capacity command receiver. The low capacity command receiver consists of a solid-state local oscillator, a crystal mixer, a subminiaturized IF amplifier, a second detector, video amplifier and decoder. The receiver is similar in design to the orbiter altimeter receiver.

A three-stage 30 mc IF amplifier with a gain of 80 + db and 30 db of AGC has a 3 mc bandwidth and an IF noise figure less than 4 db. Overall receiver noise figure is 11 db. Figure 167 is a simplified block diagram of the decoder for the command receiver. Table 24 summarizes the size, weight, and power requirements.

TABLE 24

MARS LANDER LOW-CAPACITY COMMAND RECEIVER (S-BAND)
(Size, Weight, and Power Requirements)

	(Size)	Weight (ounces)	Power
Frequency Multipliers	20.0 in.^{3} (2 x 5 x 2)	12.0	1.0 watt (MIBF: 10,000 hrs.)
5 Pulse Decoders 4 f/p. 5 gates)	2.0 in.^{3} (2 x 2 x .5)	3.5	1.0 watt (MIBF: 500,000 hrs.)
Det. & Vid. Amp.: 30 mc IF amp (3 st): mixer	5.3 in.^{3} (1.3 x 1.3 x 2)	3.75	1.0 watt
	25.3 in.^{3}	19.25	3.0 watts

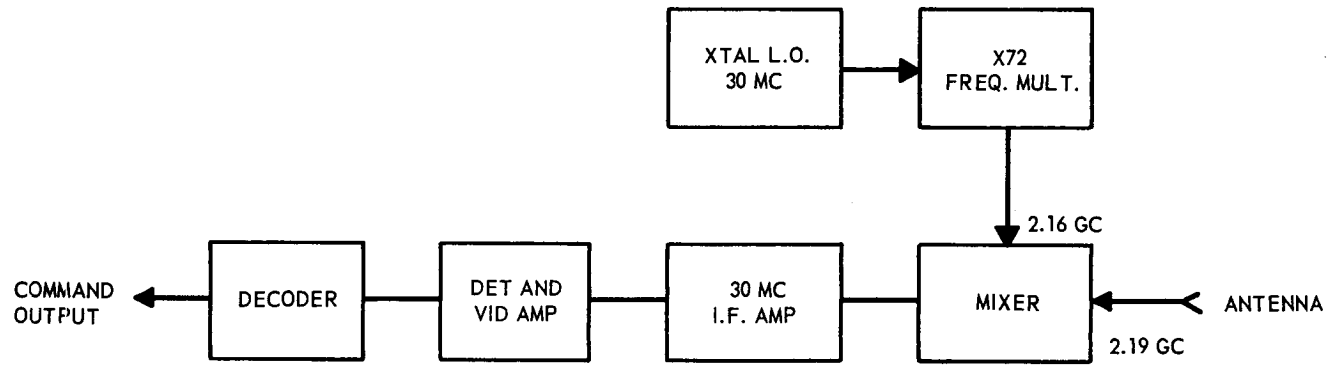

Figure 166 LANDER COMMAND RECEIVER

63-9644

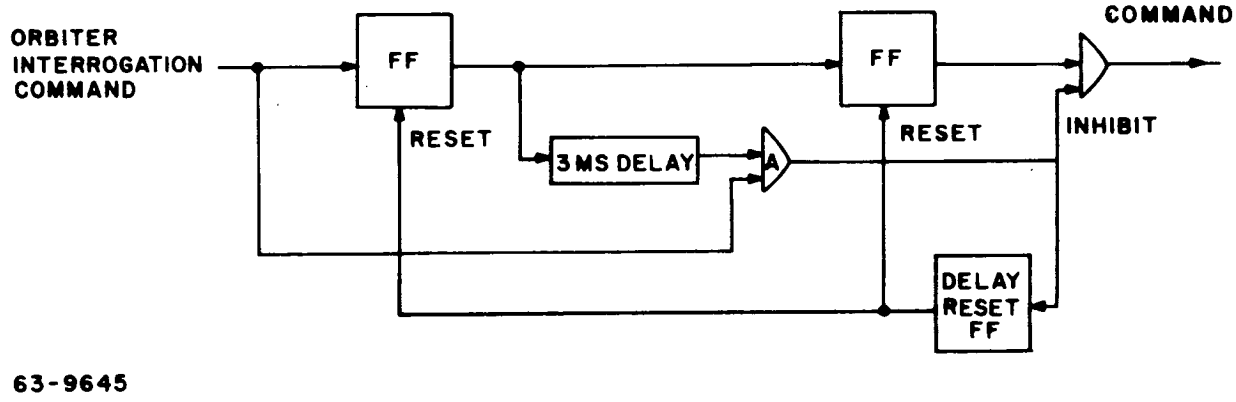

Figure 167 LANDER COMMAND RECEIVER DECODER

16. The direct link.

a. General discussion. Two direct link communication systems were selected for the lander, a high data rate system using a directive antenna, and a low data rate system using gimballed slot antennas. The high rate data system uses a steerable 5-foot parabolic antenna and a 70-watt S-band transmitter. With this system, a worst case performance margin of +2.51 can be expected at a transmission rate of 1500 bits/sec and an expected worst case range of 3.6×10^8 km.

The low rate data system uses a 70-watt S-band transmitter and a wide beamwidth gimballed S-band slot antenna system. With this system, a worst case performance margin of -0.33 db can be expected at a bit rate of 4 bits/sec and a range of 3.6×10^8 km.

The low rate system will be used to transmit diagnostic data in the event of subsystem failure, for subsequent corrective action to be commanded from Earth.

The lander will be visible to Earth approximately 4 hours per day. Due to power profile requirements a maximum of 3 hours per day will be allowed for data transmission. With this limitation, it will take 10 days to transmit the stored main science data to Earth.

b. Detailed system description.

1) High data rate system. A block diagram of the high data rate transmission system on board the lander is shown in figure 168. The communication link parameters associated with this system to establish a link with the DSIF are listed in table 25.

PSK/PM modulation will be used in this link and will be coherently detected at the DSIF. The carrier component will be synchronously detected at the DSIF in a phase-locked loop while bit synchronism for detection will be derived from a PN coded sequence which is multiplexed with the data during transmission. The power required for carrier detection and the PN sequence is negligible compared to the power required for the data.

2) Carrier loop threshold during receipt of high rate lander data. Assume that $2 B_L = 10$ cps. It is desirable that the carrier should remain in lock for at least the duration of one longest complete frame, and preferably for much longer times.

Bits per biosample picture = 750,000.

Bit rate = 1500 bits/sec

TABLE 25

TELECOMMUNICATIONS DESIGN CONTROL CHART
(Mars Lander to DSIF, High Gain) Directive Antenna)

No.	Parameter	Nominal Value	Tolerance	Source	Worst Value
1	Total transmitter power 70 watts	+48.45 dbm	+0.0 -0.5 db		+47.95 dbm
2	Transmitting circuit loss with diplexer	-1.0 db	+0.0 -0.5 db		-1.5 db
3	Transmitting antenna gain 5-foot parabola	+28.7 db	±0.6 db		+28.1 db
4	Transmitting antenna pointing loss	-0.2 db	±0.2 db		-0.4 db
5	Space loss = 32.46 +20 log F+20 log R F 2300 mc, R 3.6×10^8 km	-270.83 db	---		-270.83 db
6	Polarization loss	-0.0 db	+0.0 -0.08 db		-0.08 db
7	Receiving antenna gain	+61.0 db	+0.0 -0.5 db		+60.5 db
8	Receiving antenna pointing loss	---	---		---
9	Receiving circuit loss	-0.1 db	Max.		-0.1 db
10	Net circuit loss	-182.43 db	+0.8 -1.88 db		-184.31 db

TABLE 25 (Cont'd)

No.	Parameter	Nominal Value	Tolerance	Source	Worst . Value
11	Total received power	-133.98 dbm	+0.8 -2.38 db		-136.36 dbm
12	Receiver noise spectral density (N/B) T system 50 °K NF _____	-181.43 dbm	±0.7 db		-180.73 dbm
CARRIER PERFORMANCE -					
13	Carrier modulation loss				
14	Received carrier power	negligible			
15	Carrier APC noise BW ($2B_{LO}$)				
	Carrier track (1-way)				
16	Threshold SNR in $2B_{LO}$				
17	Threshold carrier power				
18	Performance margin				
	Carrier - Track (2-way)				
19	Threshold SNR in $2B_{LO}$				
20	Threshold carrier power				
21	Performance margin				

TABLE 25 (Cont'd)

No.	Parameter	Nominal Value	Tolerance	Source	Worst Value
	Carrier - Telemetry				
22	Threshold SNR in $2B_{LO}$				
23	Threshold carrier power				
24	Performance margin corresponds to subcarrier degradation of 1.5 db				+3.0 db
SUBCARRIER PERFORMANCE					
	Data Channel				
25	Bit rate (1/t) 1500 bits/sec	+31.76 db	---		+31.76 db
26	Required ST/N/B $P_e = 1 \times 10^{-3}$	(6.8+1.5)db	$^{+2.0}_{-0.0}$ db		+10.3 db
27	Threshold subcarrier power	-140.77 dbm	±1.9 db		-138.87 dbm
28	Modulation loss				
29	Received data subcarrier power	-133.98 dbm			-136.36 dbm
30	Performance margin	+6.79 db	$^{+2.7}_{-4.28}$		+2.51 db
	Sync channel				
31	Sync APC noise BW ($2B_{LO}$)				

TABLE 25 (Concl'd)

No.	Parameter	Nominal Value	Tolerance	Source	Worst Value
32	Threshold SNR in $2B_{LO}$				
33	Threshold subcarrier power				
34	Modulation Loss				
35	Received sync subcarrier power	negligible			
36	Performance margin				

Then frame duration = $\frac{750,000}{1500}$

= 500 seconds .

Then for a cumulative probability of 80 percent that 90 degrees will not be exceeded over this period, where 90 degrees is an arbitrary choice based on certain available pactical data,

$(1 - p)^{500 \times 10} = 0.20$

Thus $p \cong \frac{.20}{5000} = 4 \times 10^{-5}$.

The rms value, corresponding to 4.05p is

$\frac{90}{4.05}$ = 22.2 degrees.

The additional threshold = $\left(\frac{55}{22.2}\right)^2$

= 6.1

= 7.85 db .

Hence, the required carrier threshold is

7.85 + 5 = 12.85 db

Receiver Noise Spectral density = -180.73 dbm

Carrier APC Noise BW (10c/s) = 10 db

Threshold = 12.85 db

Performance margin = 3 db

Received carrier power = -154.88 dbm

Net circuit loss = 184.31 db

Transmitter carrier power = 29.43 dbm ,

which is negligible compared to available power, even if a few db's of additional power are used to ensure much longer lock durations.

3) Sync threshold power. The power required for sync can be shown to be negligible also.

4) Data threshold.

For

$$P_E = 1 \times 10^{-3}$$

use 6.8 db + 1.5 degradation due to carrier S/N

= 8.3 db

The 5-foot parabolic antenna selected for this system is not the optimum diameter antenna required to minimize the direct link system weight. The optimum antenna is 9 feet in diameter. The lander cannot conveniently accomodate an antenna size larger than 5 feet.

The determination of this optimum antenna size and the weight penalty accured by the lander as a result of using a 5-foot antenna are discussed below.

5) Determination of optimum antenna diameter. The objective is to minimize that part of the total weight of communications equipment which is a function of the antenna diameter. These weights are

a) weight of storage battery

b) weight of the RTC power source

c) weight of the antenna.

The transmission time per day (1969) at the encounter region is a maximum of approximately 4 hours.

In transmission we have

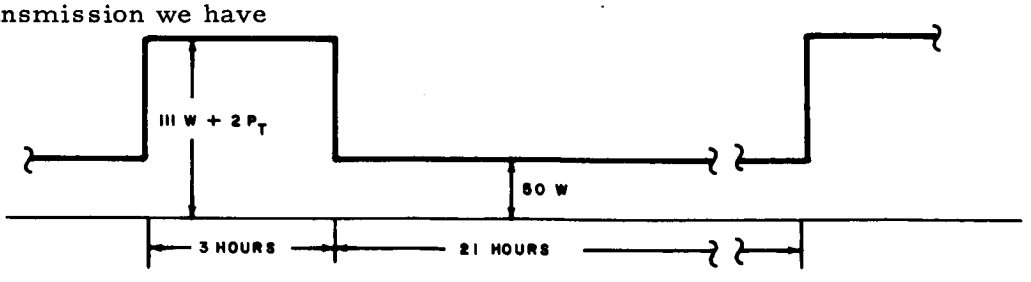

63-9647

Figure 169 LOAD PROFILE

Because of thermal limitations on RTG power and battery weig t, a time of 3 hours for playout is close to the maximum possible. The power requirements were obtained as follows (tables 26 and 27).

TABLE 26

MARS LANDER POWER LOADING DURING TRANSMISSION

Transmitter (eff. = 0.5)	$2P_T$ watts
1 of 2 recorders	6 w
Command set	28 w
Command decoder	12 w
Central computer and sequencer	42 w
Sub carrier modulator	3 w
Transponder (up to 3 w level)	20 w
Total	111 w + 2 P_T

TABLE 27

MARS LANDER CONSTANT-POWER LOADING BETWEEN TRANSMISSION

Command set	28 w
Decoder	12
Modified central computer and sequencer (less Sun seeker)	10
Total	50 w

Let amplitron eff = 0.50

P_G = RTG raw power output

P_T = transmitter power output

0.85 = power convertor efficiency (typical)

$$\text{Battery WH} = \left[\frac{P_T}{0.85 \times 0.5} + \frac{111}{0.85} - P_G\right] 3$$

$$= [2.36\ P_T + 131 - P_G]\ 3$$

$$= 7.08\ P_T + 393 - 3\ P_G \qquad (30)$$

using a discharge capacity factor of 0.84

Battery weight

$$= \frac{\text{WH}}{6.4 \times 0.84}$$

$$= \frac{\text{WH}}{5.4} = 1.31\ P_T + 72.7 - 0.56\ P_G \qquad (31)$$

Also, with a battery recharge efficiency of 0.8,

$$0.85\ P_G = \left[\frac{50}{0.85}\right] 21 = \frac{7.08\ P_T + 393 - 3\ P_G}{0.8}$$

Thus $17.9\ P_G - 1240 = 8.85\ P_T + 491 - 3.76\ P_G$

$$P_G = \frac{8.85\ P_T + 1731}{21.66}$$

$$P_G = 0.409\ P_T + 80.0 \qquad (32)$$

From (22)

$$P_T \quad 2.45\ P_G - 195 \qquad (33)$$

Weight of RTG 1.4 w/lb (Plutonium in region of 100 w level)

$$W_G = 0.292\ P_T + 57.1 \tag{34}$$

Weight of antenna = 3.7 D (feet) (From figure 170) (35)

Totat variable weight

$$= 1.31\ P_T + 72.7 - 0.56\ P_G + 0.292\ P_T + 57.1 + 3.7D$$

$$= 1.602\ P_T + 129.8 + 3.7D - 0.56\ (0.409\ P_T + 80)$$

$$= 1.373\ P_T + 84.9 + 3.7D \quad . \tag{36}$$

We now express P_T as a function of

B = bit rate

D = antenna diam

and R = range .

From the design control chart, table 28 (using worst case tolerances) the required transmitter power in lbm is

$$10 \log P_T = -167.13 + 10\ \mathrm{Log}_{10} B + 146.37 + 20 \log R - 18.75 \log D + 0.5 - 30$$

$$= 10 \log_{10} B + 20 \log_{10} R - 18.75 \log_{10} D - 50.76$$

$$= 10 \log_{10} B + \log_{10} R^2 - 10 \log_{10} D\ 1.875 - 10 \log_{10} (1.19 \times 10^5)$$

$$= 10 \log_{10} \left[\frac{BR^2}{1.19 \times 10^5 \times D\ 1.875} \right]$$

whence $P_T = \dfrac{BR^2}{1.19 \times 10^5\ D 1.875}$. (37)

Total variable wt

$$= \frac{1.373\ BR^2}{1.19 \times 10^5\ D^{1.875}} + 84.9 + 3.7D \quad . \tag{38}$$

Differentiating for a minimum, we have

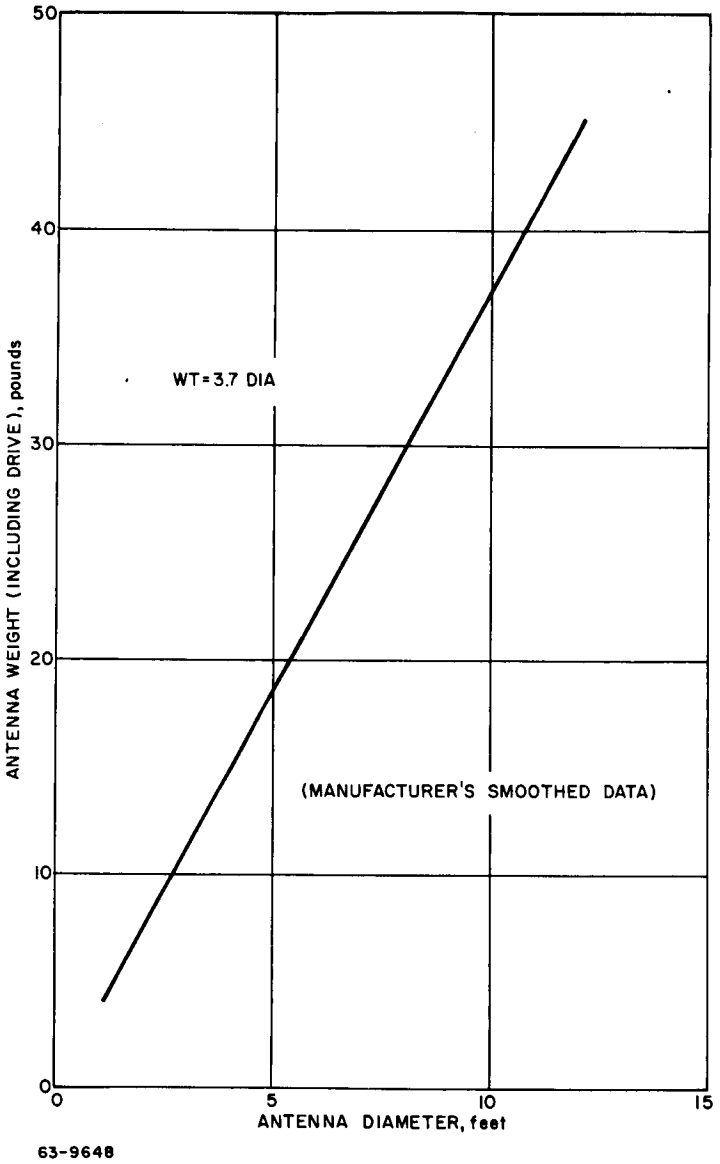

Figure 170 PARABOLIC ANTENNA WEIGHT

TABLE 28

GENERAL TELECOMMUNICATIONS DESIGN CONTROL CHART
(Lander or Orbiter High Gain Links to DSIF--General Expression)

No.	Parameter	Nominal Value	Tolerance	Source	Worst Value
1	Total transmitter power		$^{+0.0}_{-0.5}$ db		
2	Transmitting circuit loss				-1.5 db
3	Transmitting antenna gain *see Figs. 171 & 172			$15.34 + 18.75 \log_{10} D$	
4	Transmitting antenna pointing loss				-0.4 db
5	Space loss = 32.46+20 log F+20 log R F 2300 mc, R $Rx10^6$ km			$219.70 + 20 \log_{10} R$	
6	Polarization loss				-0.08
7	Receiving Antenna gain				+60.50
8	Receiving Antenna pointing loss				-0.48
9	Receiving circuit loss				-0.10
10	Net circuit loss	(-146.37 + 20 Log R - 18.75 doz D) Items 2 thru 9			
11	Total received power (neglecting carrier power)			-167.13	$+10 \log_{10} B$

TABLE 28 (cont'd)

No.	Parameter	Nominal Value	Tolerance	Source	Worst Value
12	Receiver noise spectral density (N/B T system 50°K NF_____				-180.73 dbm/cps
CARRIER PERFORMANCE					
13	Carrier modulation loss				
14	Received carrier power				
15	Carrier APC noise BW ($2B_{LO}$				
	Carrier track (1-way)				
16	Threshold SNR in $2B_{LO}$				
17	Threshold carrier power				
18	Performance margin				
19	Threshold SNR in $2B_{LO}$				
20	Threshold carrier power				
21	Performance margin				
	Carrier - Telemetry				
22	Threshold SNR in $2B_{LO}$				

TABLE 28 (cont'd)

No.	Parameter	Nominal Value	Tolerance	Source	Worst Value
23	Threshold carrier power				
24	Performance margin for s/c degradation of 116 db				310
SUBCARRIER PERFORMANCE					
	Data channel				
25	Bit rate (1/t) B bps				$+10\text{Log}_{10}B$
26	Required ST/N/B $1/10^{-3}$ Bit Rate				+9.6db
27	Threshold subcarrier power			-171.13	$+10\text{Log}10^{B}$
28	Modulation loss				
29	Received data subcarrier power			-167.13	$+10\text{Log}_{10}B$
30	Performance margin				+4db
	SYNC channel				
31	SYNC APC noise BW ($2B_{LO}$				
32	Threshold SNR in $2B_{LO}$				

TABLE 28 (concl'd)

No.	Parameter		Tolerance	Source	Worst Value
33	Threshold subcarrier power				
34	Modulation loss				
35	Received SYNC subcarrier power				
36	Performance margin				

$$\frac{1.373 \times 1.875\ BR^2}{1.19 \times 10^5\ D_{OPT}\ 2.875} = 3.7$$

whence

$$D_{OPT}^{2.875} = \frac{1.875 \times 1.373\ BR^2}{1.19 \times 10^5 \times 3.7}$$

$$= \frac{BR^2}{2.35 \times 10^5}$$

$$D_{OPT}^{2.875} = 4.25 \times BR^2 \times 10^{-6} \quad . \tag{39}$$

Thus

$$D_{OPT}^{2.875} = 4.25 \times {}_{opt}P_T \times 1.19 \times 10^5 \times D_{opt}\ 1.875 \times 10^{-6}$$

$$D_{opt} = 0.51\ {}_{opt}P_T \quad . \tag{40}$$

The minimum weight obtained with D_{OPT} is from (38)

$$= \frac{1.373\ BR^2\ D_{OPT}}{1.19 \times 10^5 \times 4.25\ BR^2 \times 10^{-6}} + 84.9 + 3.7\ D_{OPT}$$

$$= 2.72\ D_{OPT} + 84.9 + 3.7\ D_{OPT}$$

$$= 6.42\ D_{OPT} + 84.9\ \text{lbs} \quad . \tag{41}$$

The weight penalty incurred in using a nonoptimum diameter D is

$$= \frac{1.373\ BR^2}{1.19 \times 10^5\ D1.875} + 84.9 + 3.7D - 6.42\ D_{OPT} - 84.9$$

$$- \frac{1.373\ D_{OPT}}{1.19 \times 10^5 \times 4.25 \times 10^{-6} \times D1.875} + 3.7\ D - 6.42\ D_{OPT}$$

$$= \frac{2.72\ D_{OPT}^{2.875}}{D1.875} + 3.7D - 6.42\ D_{OPT}$$

$$= D\left[2.72\ \frac{(D_{OPT})^{2.875}}{D} = 6.42\ \frac{(D_{OPT})}{D} + 3.7\right] \quad . \tag{42}$$

For $R = 300 \times 10^6$

$B = 1500$ BPS .

From (8) we have

$$P_T \; D1.875 = \frac{(300)^2 \; 1500}{1.19 \times 10^5}$$

$$= 1130 \qquad (43)$$

Dividing (43) by (40) we have

$$\frac{D1.875}{0.51} = \frac{1130}{D}$$

$$D_{OPT}^{2.875} = 576$$

$$D_{OPT} = 9 \text{ ft} \quad .$$

Weight penalty incurred in using a 5 ft antenna is from (42)

$$5 \left[2.72 \left(\frac{(9)}{5}\right)^{2.875} - 6.42 \left(\frac{(9)}{5}\right) + 3.7 \right]$$

$$= 34.5 \text{ lbs} \quad .$$

The weight penalty involved in not using the optimum antenna diameter is small. In addition, a 9-foot antenna would have to be stowed in a collapsed condition, since the overall lander dimensions could not accommodate its erected size. Such a feature is felt to be undesirable due to the difficulty of maintaining the accuracy of tolerance required for high gain. Curves of antenna gain versus diameter are shown in figures 171 and 172.

6) S-band power amplifiers. The requirements for telecommunications of the Voyager mission include higher power than has been previously required for space missions and extreme reliability and long operating life. When operating at increased transmitter powers, the transmitter electrical efficiency becomes a dominant consideration due to its influence on the size and weight of the primary spacecraft electrical system.

An amplitron power amplifier was selected for the S-band transmitters.

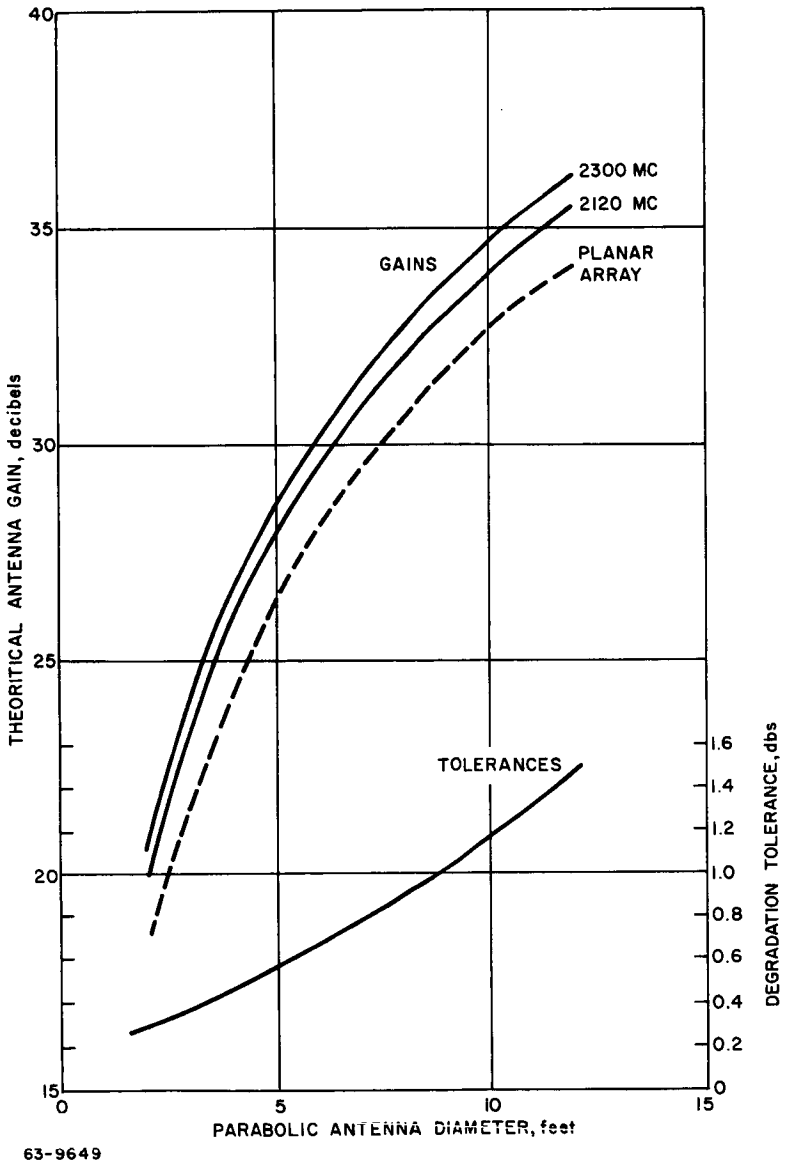

Figure 171 THEORETICAL PARABOLIC ANTENNA GAIN

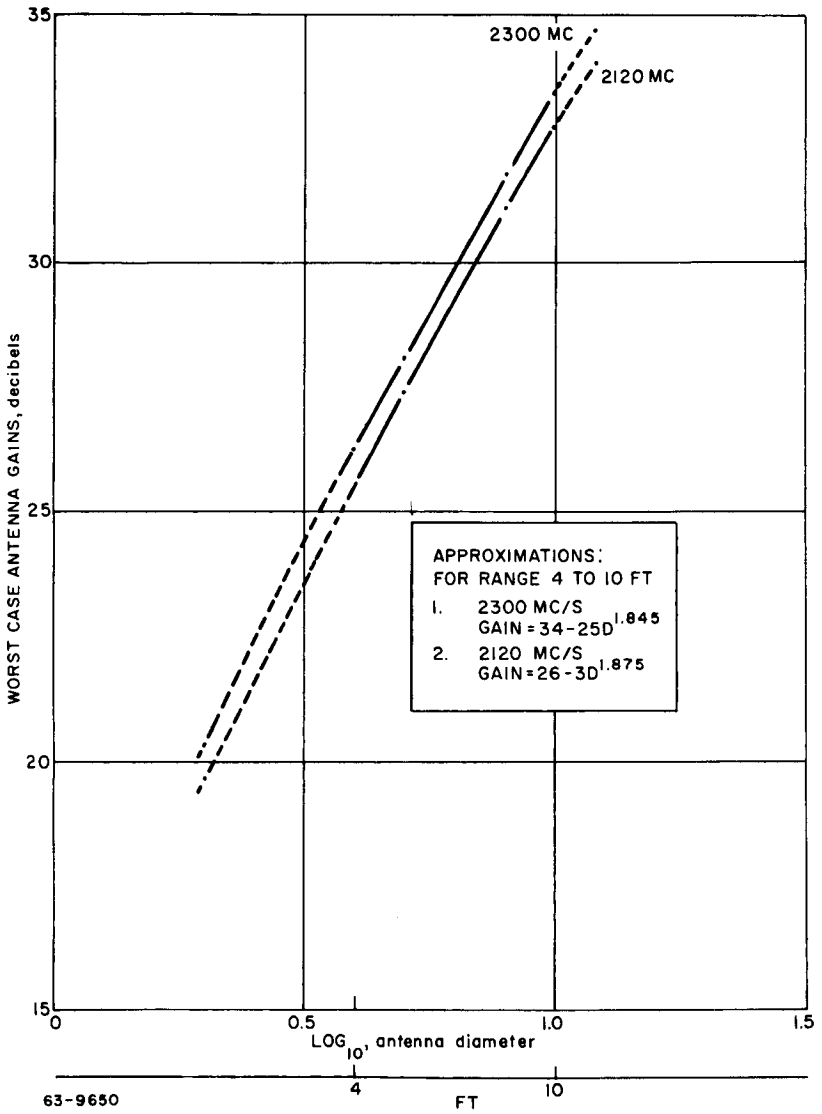

Figure 172 WORST CASE PARABOLIC ANTENNA GAIN

This device has an overall efficiency of 50 percent including filament power.

Two cascaded amplitrons will be operated from an individual, conservatively designed power supply. The two halves of the amplifier will essentially be identical, consisting of an amplitron and its power supply. Due to the unique feedthrough feature of the amplitron, when either of the amplitrons is not operated, the power output from the amplifier will be one-half (3 db down) the maximum output power of 70 watts.

7) The 70-watt amplitron amplifier. The 70-watt amplifier will, in effect, be a slightly modified version of the 120-watt amplifier used in the orbiter. The output will be obtained with only one of the amplitrons on. This form of redundancy will lead to almost identical output power for each condition, the only loss being that due to the insertion loss of the series cavity. The detailed discussion of amplitrons is included in the orbiter section.

In the relay link discussion it was indicated that an upper limit on the VHF transmitter power is approximately 50 watts due to thermal dissipation. The amplitron has a higher efficiency than power tubes available at VHF. For this reason a 70-watt limit in amplitron power is reached for the same thermal dissipation, in the gimballed S-band system. In the direct link the antenna is cassegrainian, however, 70 watts is again considered a pratical upper limit on power.

8) Modulator. The modulator in this transmitter is contained in a frequency multiplication chain identical to the frequency multiplication in the orbiter transponder, with the exception that the transmission frequency will be derived from a stable oscillator rather than a phase locked loop voltage controlled oscillator. The details of the modulator and the frequency multiplication chain are discussed in the orbiter section.

c. Low data rate system. The low data rate transmission system on board the lander is identical to the high data rate system with the exception of the antenna. Unlike the high rate system, the carrier and PN synchronization channel powers are not negligible. The communication link parameters associated with this system are listed in table 29.

Although the worst case performance margins are such that the system will not perform as desired under worst case conditions, the nominal operation of the system has a satisfactory performance margin. Under worst case conditions, the system will suffer a slight degradation in bit error probability.

The derivation of thresholds in the carrier and Pn synchronization loops are derived in the following section.

TABLE 29

TELECOMMUNICATIONS DESIGN CONTROL CHART
(Mars Lander, Transfer of Eng'g Status Data to DSIF Gimballed S-Band Slots)

No.	Parameter	Nominal Value	Tolerance	Source	Worst Value
1	Total transmitter power 70 watts	+48.45	+0.0 -0.5 db		+47.45 dbm
2	Transmitting circuit loss with diplexer	-1.0 db	+0.0 -0.5 db		-1.5 db
3	Transmitting antenna gain 140 degrees	+3.5 db	+0.0 -0.5 db		+3.0 db
4	Transmitting antenna pointing loss	-1.5 db	±1.5 db		-3.0 db
5	Space loss = 32.46+20 log F+20 log R F 2300 mc, R 3.6×10^8 km	-270.83 db	---		-270.83 db
6	Polarization loss	-0.0 db	+0.0 -0.08 db		-0.08 db
7	Receiving antenna gain	+61.0 db	+0.0 -0.5 db		+60.5 db
8	Receiving antenna pointing loss	---	---		---
9	Receiving circuit loss	-0.1 db	max		-0.1 db
10	Net circuit loss	-208.93 db	+1.5 -3.08		-212.01 db
11	Total received power	-160.48 dbm	+1.5 -3.58 db		-164.06 dbm

TABLE 29 (Cont'd)

No.	Parameters	Nominal Value	Tolerance	Source	Worst Value
12	Receiver noise spectral density (N/B) T system 50 °K NF _____	-181.43 dbm	±0.7 db		-180.73 dbm
CARRIER PERFORMANCE -					
13	Carrier modulation loss	-2.0 db	---		-2.0 db
14	Received carrier power	-162.48 dbm			-166.06
15	Carrier APC noise BW ($2B_{LO}$ = cps)	+7.0 db	in 12		+7.0 db
	Carrier track (1-way)				
16	Threshold SNR in $2B_{LO}$				
17	Threshold carrier power				
18	Performance margin				
	Carrier - Track (2-way)				
19	Threshold SNR in $2B_{LO}$				
20	Threshold carrier power				
21	Performance margin				
	Carrier - Telemetry				
22	Threshold SNR in $2B_{LO}$	+10.27	---		+10.27

TABLE 29 (Cont'd)

No.	Parameters	Nominal Value	Tolerance	Source	Worst Value
23	Threshold carrier power	-164.16 dbm			-163.46 dbm
24	Performance margin	+1.68 db			-2.60 db
SUBCARRIER PERFORMANCE					
	Data channel				
25	Bit rate (1/t) 4 bps	+6.0 db	---		+6.0 db
26	Required ST/N/B $P_e = 10^{-3}$	+7.2 db	$^{+0.8}_{-0.0}$ db		+8.0 db
27	Threshold subcarrier power	-168.23 dbm	$^{+1.5}_{-0.7}$ db		-166.73 dbm
28	Modulation loss	-3.0 db	---		-3.0 db
29	Received data subcarrier power	-163.48 dbm	$^{+1.5}_{-3.58}$ db		-167.06
30	Performance margin	+4.75 db	$^{+1.2}_{-5.08}$		-0.33
	SYNC channel				
31	SYNC APC noise BW ($2B_{LO}$ = 0.5 cps)	-3.0 db	---		-3.0 db
32	Threshold SNR in $2B_{LO}$	+16.0 db	$^{+1.0}_{-0.0}$ db		+17.0 db

TABLE 29 (Cont'd)

No.	Parameters	Nominal Value	Tolerance	Source	Worst Value
33	Threshold subcarrier power	-168.43 dbm	$^{+1.7}_{-0.7}$ db		-166.73
34	Modulation loss	-3.0 db	---		-3.0 db
35	Received SYNC subcarrier power	-163.48 db	$^{+1.5}_{-3.58}$ db		-167.06
36	Performance margin	+4.95 db	$^{+2.2}_{-5.28}$ db		-0.33

1) Carrier loop threshold during DSIF receipt of low rate lander data. The design technique is identical to that used for the Mars orbiter. The doppler rate is extremely low. The maximum doppler is ± ·930 cps. A typical figure for the uncertainty in carrier frequency could be ± 1000 cps.

Let us assume $2B_L = 5$ cps

$$W_N = 2B_L 4 = 4.72 \text{ rad/sec} \quad .$$

Then the maximum permissible sweep rate would be

$$R = 0.22\,(4.72)^2$$

$$= 4.89 \text{ cps} \quad . \tag{44}$$

The time to sweep for lock =

$$= \frac{2(1930)}{4.89 \times 60} \tag{45}$$

$$= 13.1 \text{ mts} \quad .$$

For a transmission time of 3 to 4 hours, and a very slowly changing data rate, this time is allowable.

$$\Omega = 2\sqrt{(0.71)\,(4.72)\,(429{,}000)}$$

$$= 1200 \text{ rad/sec}$$

$$= 190 \text{ cps} \quad . \tag{46}$$

The approximate hold in range

$$= 68.3 \text{ kc} \quad . \tag{47}$$

The highest offset due to Doppler

$$\text{is } \theta = \sin^{-1} \frac{930 \times 2\pi}{429{,}000} = \sin^{-1} (0.014)$$

$$= 0.8 \text{ degrees} \quad . \tag{48}$$

The degradation due to doppler is therefore negligible.

There are approximately 45 critical engineering measurements to be made and transmitted during the emergency engineering made for the Mars lander. This

mode would utilize a low gain gimballed antenna on the lander for communication to the DSIF of some status and diagnostic engineering data. It is anticipated that there will be a transmission capability of approximately 4 bits/sec. The data will require five-bit accuracy. If we assume that no longer than 100 seconds will be required for locking the PN sync, then the time for which the carrier should stay in lock if there is to be reception of at least one frame of this data will be

$$100 + 5 \times 45 \times 1/4 = 156 \text{ seconds} . \tag{49}$$

Thus, for a cumulative probability of 80 percent, that 90 degrees will not be exceeded over a period of 156 seconds, we have

$$P_{CUM} = 1 - (1 - P)^{156 \times 2B_L}$$

$$0.20 = 1 - (1 - P)^{78}$$

$$P = \frac{0.20}{78}$$

$$P = 2.56 \times 10^{-3} .$$

The rms value corresponding to 3ρ, must then be $\frac{90}{3} = 30$ degrees.

The additional threshold[1] $= \left(\frac{55}{30}\right)^2$

$$= 3.37$$

$$= 5.27 \text{ db} . \tag{50}$$

Hence the required carrier threshold will be 5.27 + 5 = 10.27 db.

2) The PN sync loop threshold. The probability of losing lock in the sync loop during a frame should not exceed 10^{-3}.

Hence $(1 - P_L)^{450} \times 2B_L = 0.999$.

Where the length of the data frame is 56.25 seconds. For $2B_L = 1/2$ cps

$(1 - P_L)^{28.13} = 0.999$

whence

$$P_L = \frac{0.001}{28.13}$$

$$= 3.55 \times 10^{-5} .$$

[1] For further details see carrier threshold calculations carried out in the Mars orbiter section on the transponder. The 55 degree rms figure corresponded to a measured threshold of 5 db.

Using the same technique as that in the design of the carrier loop, we find the rms angle is $\frac{90}{4.05} = 22.2$.

This requires an increase in threshold by $\left(\frac{55}{22.2}\right)^2 = 6.1$ i.e., by 7.9 dbs.

Thus, the sync threshold (with the additional degradation of 3 db due to PN correlation) is 5 + 7.9 + 3 = 15.9 db.

3) Data threshold. For $P_E = 10^{-3}$ we have E/No = 8 db, using differentially coherent case due to relative noisiness of sync channel for worst case conditions.

17. Command system.

a. Command demodulation and detection.

1) General system characteristics. A block diagram of the command demodulator and detector (CDD) is shown in figure 173. The signal removed from the transponder phase detector output can be represented as the product of D, the command data, PN a psuedonoise code and $2f_s$ the clock, multiplied by two in frequency. All three of these are binary waveforms taking on only the values +1 or -1. A PN generator, driven by the loop VCO, is included in the CDD. If it is assumed that the locally generated PN signal is in phase with the PN component of the incoming signal, then their product will be +1 and the PN factors throughout can be disregarded. The input signal is run through parallel channels, one of which is shifted in frequency by f_s . The two channels are then filtered leaving D times the fundamental of the f_s . (The period of D is much longer than that of f_s .) Multiplication of these paralleled signals cancels D, since $D^2 = 1$, and leaves only f_s which is acquired by the phase-lock loop. The PN generator has associated with it a word detector which produces a sync pulse once each cycle of the PN code. This code period is also the bit period of D.

The sync pulse is used in the command bit detector to discharge the integrate-and-dump filter and for sampling. The quadrature detector produces an output whenever the sync phase-lock loop loses lock. This output is used to prevent the acceptance of a command word. If the locally generated PN code is not in phase with the received PN code, the loop input will be noise-like, preventing lock. In this case, the VCO will generate a frequency slightly higher than twice the clock frequency. This will cause the PN generator to speed up until its output is in phase with the received PN code. The CDD, thefore, has three outputs which are fed to the command decoder: the sequence of command bits, the sync pulse and the out-of-lock signals. The primary difference between this subsystem and that used in the Mariner is that here one input signal contains both the sync and data information.

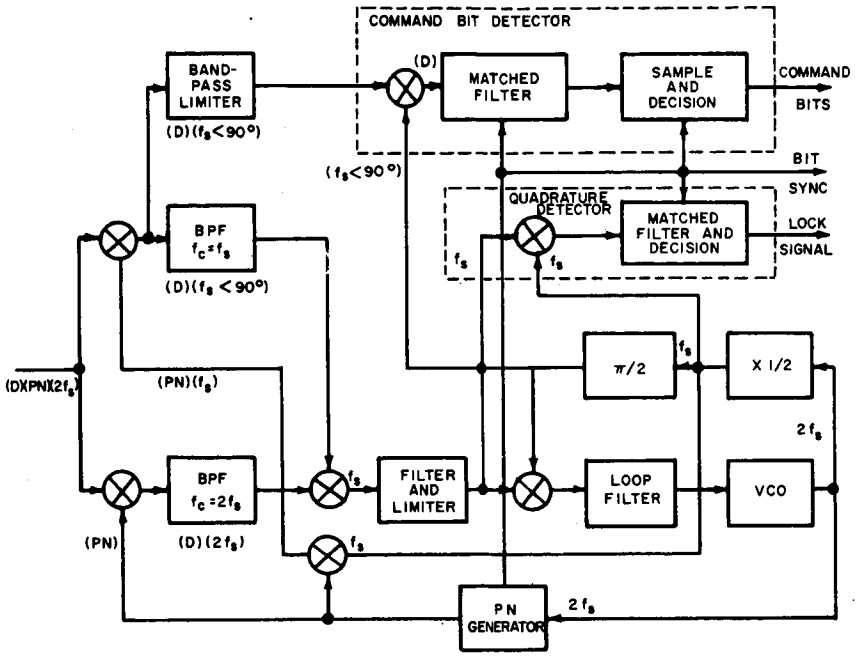

Figure 173 COMMAND DEMODULATOR AND DETECTOR

The transmission rate for the information bits is 2/3 bits/sec. The noise bandwidth in the sync loop was set at 1.0 cps which leads to an acquisition time in the sync loop of 38.8 seconds which is longer by 8.8 seconds than the transmission time for a 20-bit command word.

The performance margins for the Mars lander are slightly positive for the worst combination of tolerances and the maximum expected end of mission range. Those for the Mars orbiter are approximately -0.5 db under the same conditions. Performance margin can be defined as the additional system degradation in db that could occur before performance would be degraded.

The detection scheme illustrated in figure 173 is that proposed in ref. 35. It has the advantage that less power is required than for the arrangment used for Mariner R. A comparative analysis of the synchronization properties of the two systems is now performed.

2) The lander command link. Table 30 lists the design parameters required to establish a command link between the DSIF and the lander. The details of the system are discussed in following sections.

a. The carrier loop. For $2\,B_L = 10$ cps and with a cumulative probability of not losing carrier lock of 0.999 for a duration of 68 seconds (1 command word plus 38 seconds to acquire lock) we have

$$(1 - P)\,68 \times 10 = 0.999$$

$$P = \frac{0.001}{680} = 1.47 \times 10^{-6}$$

$$\text{rms} = \frac{90^\circ}{4.3} = 21 \text{ degrees} \quad \bullet$$

$$\text{Additional threshold} = \left(\frac{55}{21}\right)^2 = 6.9$$

$$= 8.4 \text{ db} \quad \bullet$$

$$\text{Carrier threshold} = 5 + 8.4 = 13.4 \text{ db} \quad \bullet$$

b. The sync loop. It was given that the probability of losing lock in the sync loop during a command could not exceed 10^{-3}.

$$\text{Hence } (1 - P_L)^{30 \times 2B_L} = 0.999$$

where the length of the command frame is 30 seconds. For $2B_L = 1$ cps

TABLE 30

TELECOMMUNICATIONS DESIGN CONTROL CHART
(Mars Lander, Command Link Gimballed S-Band Slots)

No.	Parameter	Nominal Value	Tolerance	Source	Worst Value
1	Total transmitter power	+80.0 dbm	±0.1 db		+79.9 dbm
2	Transmitting circuit loss	-0.6 db	±0.2 db		-0.8 db
3	Transmitting antenna gain	+51.0 db	±0.5 db		+50.5 db
4	Transmitting antenna pointing loss	---			---
5	Space loss = 32.46+20 log F+20 log R F 2120 MC, R 3.6×10^8 KM	-270.18 db	---		-270.18 db
6	Polarization loss	-1.5 db	±1.5 db		-3.0 db
7	Receiving Antenna gain	+4.0 db	$^{+0.0}_{-1.0}$ db		+3.0 db
8	Receiving Antenna pointing loss	-1.5 db	±1.5 db		-3.0 db
9	Receiving circuit loss	-0.1 db	Max		-0.1 db
10	Net circuit loss	-218.88 db	$^{+3.7}_{-4.7}$ db		-223.58 db

TABLE 30 (Cont'd)

No.	Parameter	Nominal Value	Tolerance	Source	Worst Value
11	Total received power	-138.88 dbm	+3.8 -4.8 db		-143.68 dbm
12	Receiver noise spectral density (N/B) T system_____NF 4 db	-169.8 dbm	±1.0 db		-168.8 dbm
CARRIER PERFORMANCE					
13	Carrier modulation loss	-3.0 db	---		-3.0 db
14	Received carrier power	-141.88 dbm	+3.8 -4.8 db		-146.68 dbm
15	Carrier APC noise BW ($2B_{LO}$ = 10 cps)	+10.0 db	in 12		+10.0 db
	Carrier Track (1-way)				
16	Threshold SNR in $2B_{LO}$				
17	Threshold carrier power				
18	Performance margin				

TABLE 30 (Cont'd)

No.	Parameter	Nominal Value	Tolerance	Source	Worst Value
	Carrier - Track (2-way)				
19	Threshold SNR in $2B_{LO}$				
20	Threshold carrier power				
21	Performance margin				
	Carrier - Telemetry				
22	Threshold SNR in $2B_{LO}$	+12.4 db	$\pm$1.0 db		+13.4 db
23	Threshold carrier power	-147.4 dbm	$\pm$2.0 db		-145.4 dbm
24	Performance margin	+5.72 db	$^{+5.8}_{-6.8}$ db		-1.28 db
SUBCARRIER PERFORMANCE					
	Data channel				
25	Bit rate (1/5) 2/3 bps	-1.76 db	---		-1.76 db
26	Required ST/N/B $p_e = 2.6 \times 10^{-3}$	+7.22 db	$^{+1.5}_{-0.0}$ db		+8.72 db
27	Threshold subcarrier power	-160.82 dbm	$^{+2.0}_{-1.0}$ db		-158.32 dbm

TABLE 30 (Concl'd)

No.	Parameter	Nominal Value	Tolerance	Source	Worst Value
28	Modulation loss	-3.0 db	---		-3.0 db
29	Received data subcarrier power	-141.88 dbm	$^{+3.8}_{-4.8}$ db		-146.68 dbm
30	Performance	+18.94 db			+11.64 db
	Sync channel				
31	Sync APC noise BW ($2B_{LO}$ = 1 cps)	+0.0 db	±0.2 db		+0.2 db
32	Threshold SNR in $2B_{LO}$	+14.85 db	±1.0 db		+15.85 db
33	Threshold subcarrier power	-154.95 dbm	±2.2 db		-151.75 dbm
34	Modulation loss	-3.0 db	---		-3.0 db
35	Received Sync subcarrier power	-141.88 dbm	$^{+3.8}_{-9.8}$ db		-146.68 dbm
36	Performance margin	+13.07 db			+5.07 db

$$(1 - P_L)^{30} = 0.999$$

$$\text{whence } P_L = \frac{0.001}{30}$$

$$= 0.0000333$$

$$= 3.3 \times 10^{-5} .$$

Using the same technique as that in the design of the carrier loop, we find the rms angle is 22.2 degrees. This requires an increase in threshold by

$$= \left(\frac{55}{22.2}\right)^2 = 6.1$$

i.e. by 7.85 dbs.

Thus, the sync threshold (with the additional degradation of 3 db due to PN correlation) is 5 + 7.25 + 3 = 15.85 db.

c. Data threshold. Using parity for every information bit, we require a bit error probability of 2.6×10^{-3}.

Due to the noisiness of the sync loop, we use the differentially coherent curve.

Threshold = 7.22 + 1.5 = 8.72 db .

Data Rate = 2/3 information bit/sec.

3) Selection of required error detection technique. It is shown that for the required probability of losing lock in the sync loop, and for the lowest value of probability of receiving without error a command word consistent with the required minimum word acceptance probability, that the command decoder needs an error detection capability. Three error detection techniques were considered: 1) a simple parity check on the information bits, 2) a parity check bit for each information bit, and 3) a combination of the first two. Number one was inadequate, number two was satisfactory and number three was appreciably better than required.

let P_I be the probability of a "data" bit error

P_B be the probability of an "information bit error"

Q_w be the probability of a word being received correctly

P_w be the probability of a word being received incorrectly

Q_B be the probability of no error in an "information" bit

Q_A be the joint probability of not losing sync and not detecting an error

P_o be the probability of losing sync lock during a command word.

It is required that the probability of not losing lock in the sync loop during a command word be 0.999. It is also required that Q_A shall be 0.9. Finally, the word error rate for a system using an error detection scheme shall be the same as for a system without such a scheme in which the bit error rate is 10^{-5}.

For a non-error-correcting system with 20 bits per word, we have a word error rate.

$$P_w = 1 - Q_w$$

$$= 1 - (1 - P_B)^{20}$$

$$= 1 - (1 - 10^{-5})^{20}$$

$$= 20 \times 10^{-5} \quad .$$

a) Simple parity check on total number of information bits. In this case, 21 information bits are received.

$$Q_w = (1 - P_1)^{21}$$

Also $Q_A = (1 - P_o)(Q_w + P_w) = 0.9$.

Approximately $(1 - P_o)(Q_w) = 0.9$.

Hence $Q_w = \frac{0.9}{0.999} = 0.9009009$.

whence $P_1 = 4.95 \times 10^{-3}$.

For this format

$$P_w \cong 1/2\,(k)\,(k+1)\,P_1^2\,(1 - P_1)^{k-1}$$

where $k = 20$

$$P_w = 1/2\,(20)\,(21)\,P_1^2\,(1 - P_1)^{19} = 4.68 \times 10^{-3} \quad .$$

This word error probability is too high.

b) Parity check for each information bit. In this case, 40 data bits are received. A parity check bit is sent with each information bit. That is, a 0 is sent as 10 and a 1 as 01. This means that an information bit will be incorrectly interpreted if and only if both the information bit and its parity check bit are incorrectly detected. Such a scheme will always detect an odd number of errors and it will detect most combinations of an even number of errors.

Then the probability of an error in an information bit is $P_B = P_I^2$. The probability of a k bit word being received correctly is

$Q_w = Q_B^k = [(1 - P_I)^2]^k \cong (1 - 2k P_I)$ while the probability of receiving it incorrectly is $P_w = [P_I^2 + (1 - P_I)^2]^k - (1 - P_I)^{2k}$

whence

$$P_w \cong k P_I^2 [1 - (2k - 2) P_I]$$

$$Q_w = (1 - P_I)^{40} = 0.90090$$

$$P_I = 2.6 \times 10^{-3}$$

$$P_w = 20 P_I^2 [1 - 38 P_I]$$

$$= 1.22 \times 10^{-4} \quad .$$

This is very close to the required value.

c) Combination of the first two methods. The value of P_w can be reduced even more at low cost by transmitting a parity check bit for all the information bits. (This bit would be treated as an information bit and would therefore have its own parity check bit.) This code would then detect odd numbers of errors in the reconstructed information bits. The result of combining these two error detecting schemes is a triple error detecting code that will also detect many other errors. In this case $P_B = P_I^2$, $Q_w = Q_B^{k+1} = [(1 - P_I)^2]^{k+1}$

or

$$Q_w = 1 - 2(k+1)P_1$$

$$P_w = \binom{k+1}{2}(P_1^2)^2[(1-P_1)^2]^{(k-1)} + \binom{k+1}{4}(P_1^2)^4[(1-P_1)^2]^{(k-3)} + \binom{k+1}{6}(P_1^2)^6[(1-P_1)^2]^{k-5} + \ldots$$

$$= 1/2\,(k)(k+1)P_1^4[1-(2k-2)P_1] .$$

Notice that the probability of incorrectly receiving a command word has been greatly decreased by the addition of two more redundant bits.

$$Q_w = 1 - 2(k+1)P_1 = 0.9009009$$

$$= 1 - 42P_1$$

$$P_1 = 2.5 \times 10^{-3}$$

$$P_w = 1/2\,(20)(21)P_1^4[1-38P_1]$$

$$= 7.46 \times 10^{-9}$$

which is considerably less than the required value of 20×10^{-5}.

b) Command decoder. The last component to be discussed is the command decoder. Command words are assumed to be made up of 20 information bits. Each of these information bits is transmitted as a pair of bits which will be called data bits for purposes of differentiation. The decoder has two bit reconstructors which convert the received data bits to information bits. Two bit reconstructors are necessary since it is not known initially which pairing of the data bits should be made. The decoder programmer prevents the use of a command word either if an error is detected in reconstructing the information bits, or if the sync loop loses lock. The reconstructed command word moves into a shift register which is just long enough to store the command address (7 bits for the orbiter, 6 for the lander). This shift register is connected to an address recognition matrix which, when the shift register is filled, opens a gate to route the remainder of the command word. Since the only transmitted pairs are (1, -1) and (-1, 1), the system has an error detection capability. The primary purpose of sending an information bit as two short bits is to reduce the acquisition time of the sync phase lock loop by a factor of two.

The lander command decoder should weigh one pound, occupy 11 $in.^3$ and take 5.5 watts. The orbiter requires twice as much power; however, weight and volume are only about 20 percent greater.

The period of an information bit has been set at 1.5 seconds. Each information bit will be sent as a pair of data bits each of which has a period of 0.75 second. Only the pairs (1, -1) and (-1, 1) will be used to represent information bits. The PN generator will go through a complete cycle in 0.75 second. If n_i is the number of PN bits per cycle, the clock frequency, f_s, will be $\frac{n_i}{1.5}$ cps with 2 PN bits per clock cycle. For convenience in building the narrow band filters in the parallel branches at the CCD input, n_i should probably be greater than 15. The code length n_i must satisfy the relation $n_i = 2^n - 1$ where n is some integer. As has been shown, the average acquisition time in the sync loop is directly proportional to the clock frequency, and hence to n_i. For these reasons, n_i will be picked to be 31 making $f_s = 20\ 2/3$ cps. The primary advantage in sending each information bit as a pair of bits is that it halves the period of the PN cycle and, therefore, the sync loop acquisition time. There is also, a small power savings, due to the error detection inherent in this scheme. The space craft decoder is shown in figure 174.

It is the function of the bit reconstructor to interpret the pair (1, -1) as a -1, the pair (-1, 1) as a + 1 and the pairs (1, 1) and (-1, -1) as errors. Notice of a detected error would then be sent to the programmer which clears the shift register, SR, associated with the matrix and gates off its input until the command word is begun again. Notice that the bit reconstructor must know which pair of data bits corresponds to a given information bit. This information could be provided in more than one way. 1) The command word could be preceded by a short code word which would, upon recognition, activate the decoder and provide the bit reconstructor with its needed information. A possible prefix, suggested by JPL, is (-1, -1, -1, 1, 1, 1). When no command is being sent, the decoder continually receives plus ones. The above prefix could never be misinterpreted as a set of data bits but use of this word would effectively lengthen the command word by three bits and decrease its probability of acceptance. 2) Two bit reconstructors could be used in such a way that they would examine different pairings of the data bits. In this case, an error would not be indicated until both bit reconstructors had found an error. If no command word was permitted to begin with two plus ones or two minus ones, (as information bits) one of the bit reconstructors would find an error within three data bits and it could stop reconstructing bits, thereby reducing memory requirements.

It seems that the mechanization of the second method would be simpler than that of the first and, as mentioned before, it requires two less information bits in the command word. For these reasons, method (2) is suggested in which case the word Sync Recognition Block in figure 174 would be identical to the bit

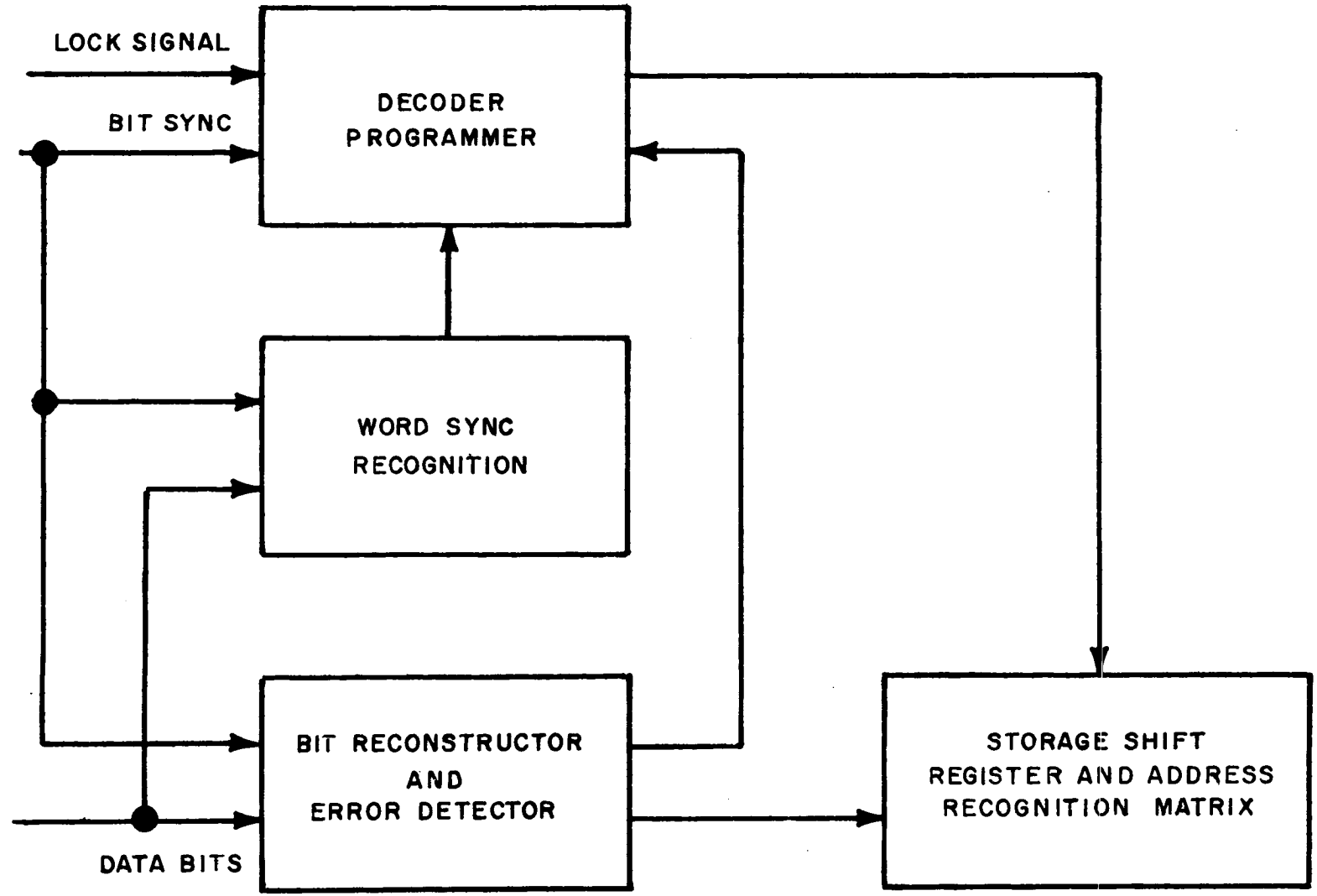

Figure 174 COMMAND DECODER

reconstructor and error detector:

A noise-like pulse train is transmitted from the Earth to the spacecraft which upon being decoded provides sync pulses and a coherent reference for the command detector. This pulse train is a modified maximal length shift register sequence or m-sequence. M-sequences are often referred to as pseudo-noise and will therefore be represented by the letters PN. The PN is modified by multiplication with a square wave which has a period equal to the period of one PN bit. The effect of this is to replace each +1 in the PN by the pair (-1, +1) and each -1 by the pair (+1, -1). Also, the period of the product is twice that of the PN since the PN contains an odd number of bits (2^{n-1}). Perhaps it should be emphasized that the sync waveform is periodic.

Consider the waveform shown in figure 175.

Woodward has defined the rect function as,

$$\text{rect } t = \begin{cases} 1, \text{ for } |t| < \frac{1}{2} \\ 0, \text{ for } |t| > \frac{1}{2} \end{cases}$$

$$f_1(t) = \text{rect}\left(\frac{t - \frac{\tau}{2}}{\tau}\right) - \text{rect}\left(\frac{t - \frac{3\tau}{2}}{\tau}\right) \tag{51}$$

The voltage spectrum of $f_1(t)$ is given by

$$F_1(w) = (\tau \operatorname{sinc} f\tau)\left[e^{-\pi i f \tau} - e^{-\pi i f 3\tau}\right] \tag{52}$$

where

$$\operatorname{sinc} f\tau = \frac{\sin \pi f \tau}{\pi f \tau}$$

Equation (52) can also be written as

$$F_1(w) = \frac{2}{\pi f}(\sin^2 \pi f \tau)\, e^{-2\pi i f \tau + i\frac{\pi}{2}} \tag{53}$$

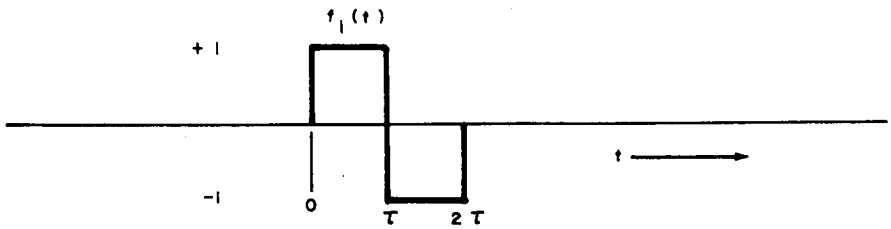

Figure 175 RECT FUNCTION

The sync waveform consists of a train of pulse pairs like those of figure 175 with polarity determined by PN so it can be written as,

$$f(t) = \sum_{k=1}^{2^n-1} a_k \left\{ \text{rect}\left[\frac{t-(4k-3)\frac{\tau}{2}}{\tau}\right] - \text{rect}\left[\frac{t-(4k-1)\frac{\tau}{2}}{\tau}\right] \right\} \tag{54}$$

where $\sum_{k=1}^{2^n-1} a_k$ is the PN waveform and a_k is either plus one or minus one. By analogy with equations (52) and (53) the voltage spectrum of $f(t)$ can be written as,

$$F(w) = \left(\frac{2}{\pi f}\right)(\sin^2 \pi f \tau) \sum_{k=1}^{2^n-1} e^{-\pi i f(4k-2)\tau + i\frac{\pi}{2}} \tag{55}$$

The envelope of the power spectrum is now proportional to,

$$G(f) = \frac{\sin^4 \pi f \tau}{(\pi f \tau)^2} \quad . \tag{56}$$

The sync waveform $f(t)$ which is defined in equation (54) phase modulates the carrier w_o with a modulation index m, giving as the transmitted signal,

$$s(t) = \sin [w_o t + m f'(t)] \quad \text{or} \tag{57}$$

$$s(t) = \sin w_o t \cos mf + \cos w_o t \sin mf \quad .$$

Notice that $f(t)$ takes on only two values, +1 and -1. Therefore, $\cos mf = \cos m$ while $\sin mf = f \sin m$.

$$s(t) = (\cos m) \sin w_o t + f(\sin m) \cos w_o t \quad . \tag{58}$$

When $m = \frac{\pi}{2}$, the first term which is the carrier is supressed and

$$s(t) = f(t) \cos w_o t . \tag{59}$$

The transponder loop locks onto the carrier and suppresses it at the output of the loop phase detector as a plot of $\left| \frac{\epsilon(s)}{\theta_i(s)} \right| = \left| 1 - H(s) \right|$ shows.

(See Figure 100 on page 128 of Ref. B). Therefore, the portion of the spectrum that is taken from the transponder phase detector output is just the second term of equation 48 shifted down in frequency by w_o.

$$s(t) = f(t) (\sin m) \sim f(t) \tag{60}$$

The signal is then processed by the command detector.

In the Voyager, the command word will modulate the function $f(t)$. The command word is made up of a sequence of plus ones and minus ones which change polarity only once during each period of $f(t)$. This does not alter the previous results except that $f(t)$ should be replaced by $D(t) f(t)$ in equations 47, 48, 50, (57,) (58), and (60) where $D(t)$ is the command word.

18. Coding Voyager communications. The ranges over which the Voyager communications will work are large. Naturally, the question of coding command or information data arises. And, if this feature were shown to be necessary, the selection of a method of coding poses a problem. The requirements for the command link are examined first. One of the primary functions of the command link would be to rectify failures that could occur in many of the equipments on the lander. In the case of the Martian lander, which has, and requires a self-righting capability, a hemi-omni-antenna will be used.

At the greatest ranges, of the order of 360 million km, it can be shown that the power required for carrier lock exceeds that required for data and sync by some 8 to 10 db. This fact, coupled with the desire to maintain a high degree of reliability and simplicity in the command receiver, indicates that any complex coding of the command data is not merited.

A very similar argument applies to the transmission of low rate engineering status data through the lander's low gain antenna directly to the DSIF. In addition, the slow rate of change of this data, and the fact that communication times exceeding 4 hours are possible, suggests that alternative methods of data reduction at the DSIF would be possible.

Coding could be applied with advantage to the high gain lander data link with only slight additional complexity. The extra equipment required at the DSIF is

not considered to be a problem.

Coding methods can be divided into two broad categories depending on whether or not coherent detection is an integral part of the decoding process.

1) Incoherent error detecting and correcting codes are decoded subsequent to coherent detection of individual bits.

2) Coherent biorthogonal codes are decoded coherently by maximum likelihood detectors. The coherent codes are really extensions of the ordinary PCM-PSK transmissions, having a more complex envelope. As an example of the latter, the digilock coding system consists of an alphabet of 32 different pulse trains. Each group of five information bits, taken together, determines which of the 32 biorthogonal waveforms will be transmitted. The selected pulse train modulates the phase of the transmitter. At the receiver, the incoming I. F. waveform is passed through 32 matched filters, each matched to one of the permissible transmitted waveforms. It is hypothesized that the signal which was transmitted is the one matched to the filter having the greatest output. This decision results in the emission of a particular five-bit pulse train from the receiver, corresponding to the original group of five information bits in the transmitter.

The incoherent codes are efficient as long as the SNR does not fall below the design value. If it does, the probability of more errors occuring per word than the code was designed to handle becomes large, and the error rate rapidly increases. The coherent coding methods do not show the same kind of improvement threshold.

The digilock coding system requires only a small investment in extra equipment and power at the transmitter. The receiving equipment is relatively complex. It appears well suited to the task of transmitting data from vehicle to DSIF, where the heavier decoding equipment is located on Earth. When the data rate is high and almost all the power in the transmitted signal resides in the data, and when the received bit error rate is in the order of 10^{-3}, use of a five-bit digilock system will reduce the transmitted power requirement by 3 db or increase the system margin by the same amount. (see refs. 35 and 36)

To our knowledge, error correcting codes with equal improvement possibilities have not been instrumented for space vehicles.

In the case of transmission from vehicle to Earth via the omni-antenna, where most of the transmitted power resides in the carrier and relatively little is the data, improvement, due to coding is hardly worth the effort because it improves only the SNR in the data channel, whereas improvement is really needed in the carrier channel.

19. Antenna systems

a. VHF isotropic antenna. A VHF link will be provided between the orbiter and the lander from the separation of the two vehicles up to the parachute phase of the lander's descent onto the surface of Mars. In order to maintain this RF link, omnidirectional coverage in the hemisphere above the lander is required. This will be obtained by means of a four-element array mounted on the lander vehicle. Any number of elements fewer than four would produce large null areas inconsistent with omnidirectional coverage. The individual elements must be capable of transmitting RF energy at 300 mc, with a bandwidth of approximately 4 mc. Also, the antenna must be consistent with the size and weight restrictions imposed on all components on the vehicle.

Since the antenna, which is shown in figure 176, is an electrically small, flushmounted, cavity-backed, dual-channel radiator, it is a most suitable element. Its primary radiation pattern is similar to that which would be obtained from a conventional half-wavelength radiator. The antenna is circular in cross section with two orthogonal slots used as the radiating element. Without tuning, the slot impedance is reactive and inductive in nature. The value of this reactance can be obtained by relating the impedance of the slot to the impedance of its complementary dipole,

$$Z_s = Z_o^2/Z_d^2$$

from which the following relations can be obtained:

$$R_s = 35{,}476/X_d^2$$

$$X_s = 35{,}476/X_d \quad .$$

From these equations, it can be shown that the reactance of the cruciform is inductive in nature. From this, it was deduced that a variable lumped capacitor was a feasible matching element. This, as well as distributed parameters, are used for impedance matching. At the center operating frequency of each operating band, a VSWR of less than 1.20:1 can be obtained with less than 2.0:1.00 at the edges of the operating bands. Physically, the cruciform is a small, rugged component constructed to survive in the severe environments of space flights. Its radome will be made of a lightweight ablative dielectric which will not impair the operation of the antenna in its descent toward the Martian surface.

Four cruciforms, spaced equally about the circumference of the vehicle and fed through a four-way power divider, will produce an omnidirectional array pattern for this size vehicle. Each point on the array pattern can be considered the vectorial sum of contributions from each element in the array. Because the phase front of each element will alternately add and cancel with that of the other

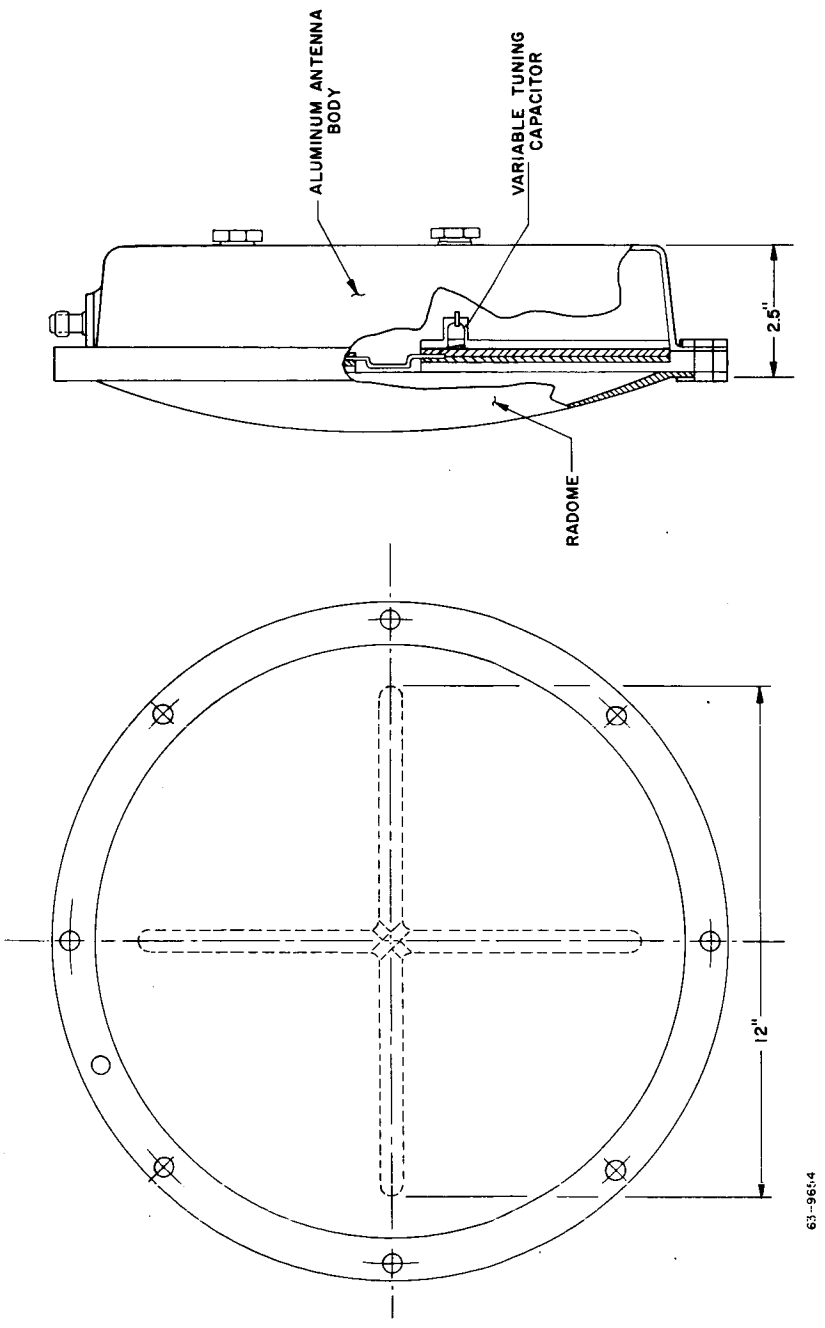

Figure 176 VHF RELAY ANTENNA

elements, the sphere surrounding the vehicle will contain a series of peaks and nulls of RF energy. With four elements mounted on a five-wavelength circumference, these variations will be gradual and of relatively shallow depths. They will not be abrupt and deep. A mean gain is computed for the sectors of interest and referenced to an isotropic radiator whose efficiency is, by definition, 100 percent. The calculation of mean gain is a statistical procedure. In the upper hemisphere, θ = 0 degrees to θ = 90 degrees, a mean gain of approximately -3db is anticipated from this array. The E-plane of opposing elements will be oriented 180 degrees out of phase with each other in order to ensure a continuous current flow around the surface of the vehicle. Figure 177 is a pattern of a two-element array whose elements are equally spaced on the circumference and fed 180 degrees out of phase. These patterns were measured on a vehicle approximately one-half the size of the lander. The nose coverage is relatively smooth at about the isotropic level. The relative smoothness of the pattern in this θ = 0 degree sector is indicative of a continuous current distribution around the nose of the vehicle. This has resulted from feeding the opposed elements in antiphase. These same results can reasonably be anticipated from a four-element array when the E fields of opposite pairs are 180 degrees out of phase.

A power divider which will split the input power equally four ways will have an insertion loss of less than 0.3 db and an input VSWR of less than 1.20 at the operating frequencies. It will consist of a folded quarterwave transformer whose impedance will be the geometric mean of the characteristic impedance of the line, 50 ohms, and the impedance as seen at the four-way junction, 16.6 ohms. Its physical configuration, both size and weight, will be consistent with the compactness of the other components on the vehicle. High power coaxial cable will be used to connect the transmitter with the power divider and antennas. These antennas will be evacuated and sealed with an ablative material which will serve both as a radome and heat shield. The power divider which will be the unit most susceptible to power breakdown in this system, will also be evacuated. The essential characteristics of the antenna system are given in table 31.

b. Lander relay/command antenna. The prime mission of the lander relay link antenna is the efficient generation of a nearly hemispherical radiation pattern to ensure long "playout" times for the transmission of telemetry data to the orbiter as it passes through the beam. The operation of this antenna is paramount should failures occur in the direct link to Earth via the 5-foot parabola.

The results of a study led to the selection of an antenna structure mounted in a 14-inch diameter glass "bubble". The bubble is mounted on a two-axis gimballed platform to ensure vertical orientation of the beam after deployment on the planet surface. This structure will house both VHF and S-band radiators. The size and weight restrictions imposed on the relay/command antenna configuration by the gimballed platform design require a loaded slot antenna design

TABLE 31

VHF ANTENNA ARRAY ON MARS LANDER VEHICLE

Antenna Type	12-inch cruciform with two orthogonal slots as radiating elements
Antenna Gain	3.0 db above an isotropic radiator
Antenna VSWR	Less than 1.20:1.00 at the center operating frequency and less than 2.0:1.0 at $f_o \pm 2$ mc.
Antenna - Radiation Pattern	Cardioid shaped pattern.
Array Pattern	Omnidirectional radiation coverage in the hemisphere above the vehicle.
Array Efficiency	Approximately 50 percent
Array VSWR	Less than 1.50:1.00 at the center operating frequency
Power Divider	VSWR will be less than 1.20:1.00 at the center operating frequency. Power shall be split equally into four antenna elements.
Power Input	50 watts
Bandwidth	4 mc
	Antenna shall have a transfer phase function which is linear with frequency.
Polarization	Linear

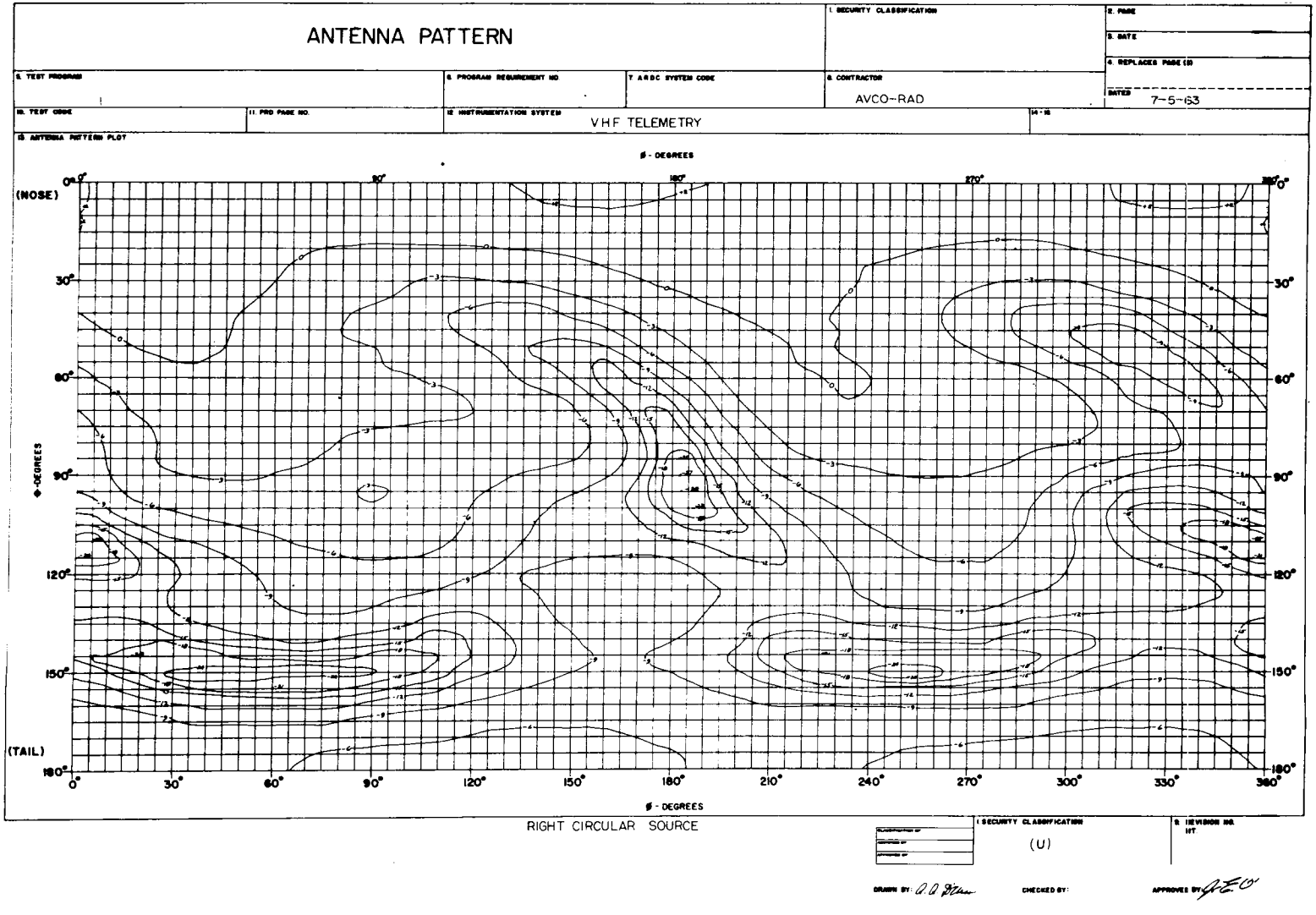

Figure 177 VHF ANTENNA PATTERN

for the VHF antenna. A conventional cavity-backed slot antenna at VHF frequencies will satisfy the pattern shape, gain, efficiency, and bandwidth requirements, but the physical size of such a unit operating at 300 mc is approximately 19.5 inches long by 10 inches deep, too large for use in this application. The possibility of dual channel operation was also considered. If a conventional slot configuration were used, diplexing components would be required and a high weight penalty would be incurred.

The bubble shape and size of the gimballed platform suggested the use of Avco RAD's cruciform antenna. The cruciform antenna is basically a crossed slot aperture, backed with a shorted cavity. Avco RAD has used antennas of this basic configuration on the early Titan reentry vehicle programs, the Mark 4 and the Mark 5 and Mark 11 reentry vehicle development programs. Because of the thermal and aerodynamic environments on the missile development programs and the severe limitations of conventional short slots at VHF frequencies, Avco developed the cruciform antenna. Figure 178 shows a typical VHF cruciform telemetry antenna.

One advantage of the cruciform slot over the conventional slot of equal physical length, is that diagonal excitation accomplishes an effective lengthening of the slot by a factor of $\sqrt{2}$. The bandwidth, for VSWR's of less than 2.00:1, of conventional loaded slots is severely limited for slot lengths of less than 0.3 wavelengths. Figure 179 shows the theoretical bandwidths for both the conventional and cruciform slots versus slot length. It should be noted also that dual channel operation can also be obtained by exciting the slots with orthogonal feeds.

Because of the size restriction, it was also decided to incorporate a dual-channel S-band cruciform into the same package with the VHF telemetry antenna. The prime mission of the S-band antenna is to supply a link to transmit data to the DSIF if the VHF telemetry relay antenna and S-band dish fail to function. In addition, the S-band antenna will provide the link to receive command signals from the DSIF.

The operating bandwidth requirement and the power handling capacity required indicate that an equivalent half wavelength cruciform is required. The slot length will be 14 inches and 1.82 inches for VHF and S-band antennas, respectively. To package this unit into the 14 inch diameter of the gimballed platform, the slots will be cut in a curved surface having a radius of curvature of 22 inches. The radiating elements will be energized by stripline feed across the slots. To match the impedances of the slots, series and shunt reactances are used. A unique tuning element which is relatively insensitive to temperature changes and has high constancy will be used to ensure stability of match during the sterilization cycle and also to prevent serious detuning during the landing process. Figures 180 and 181 show the external configuration of the antenna.

The pattern coverage provided by an antenna of this type is sufficient to meet the 140-degree beamwidth requirement. Figures 182, 183, and 184 are

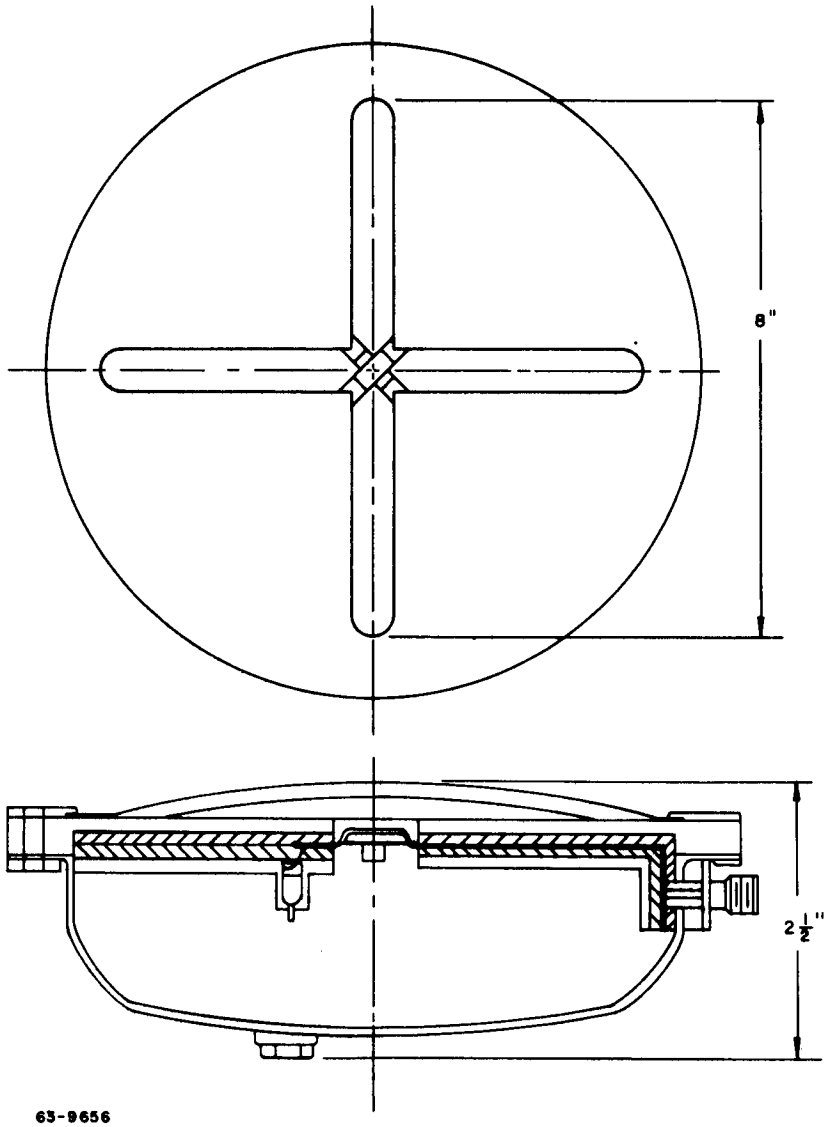

Figure 178 TYPICAL VHF ANTENNA

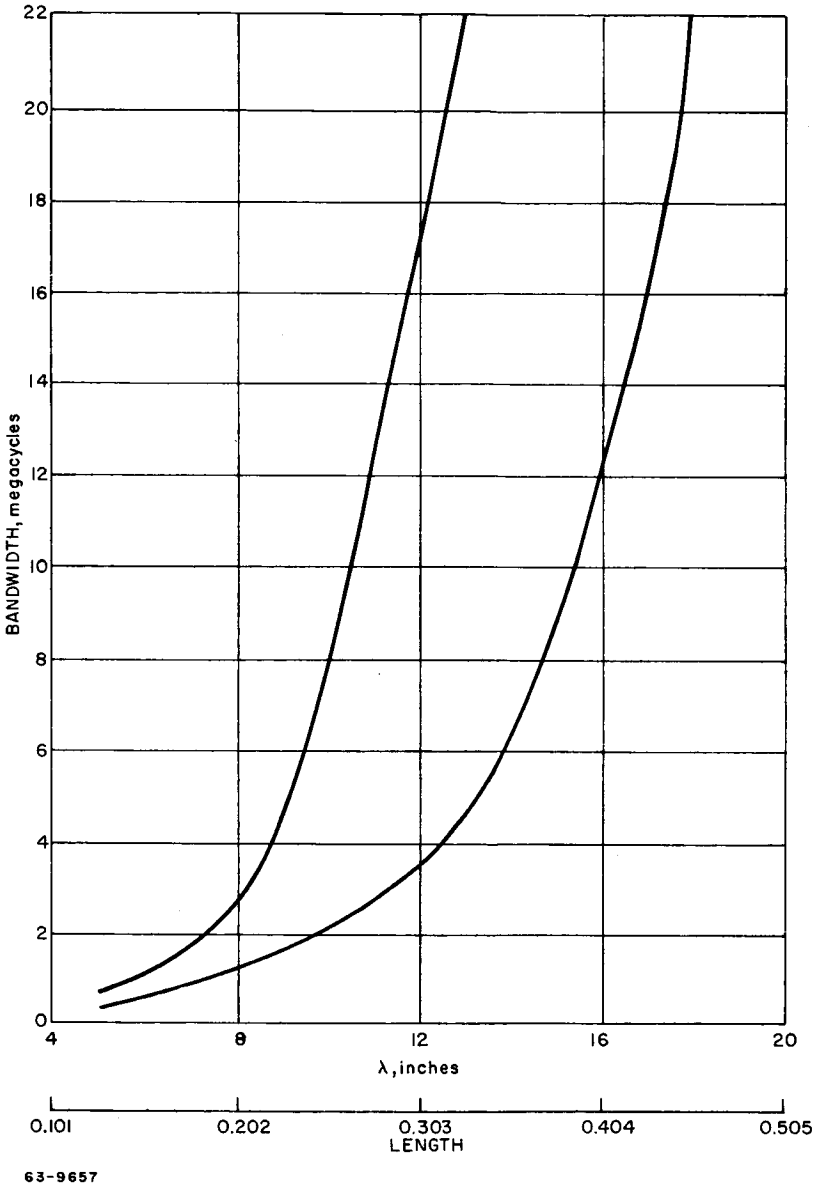

Figure 179 BANDWIDTH VERSUS SLOT LENGTH

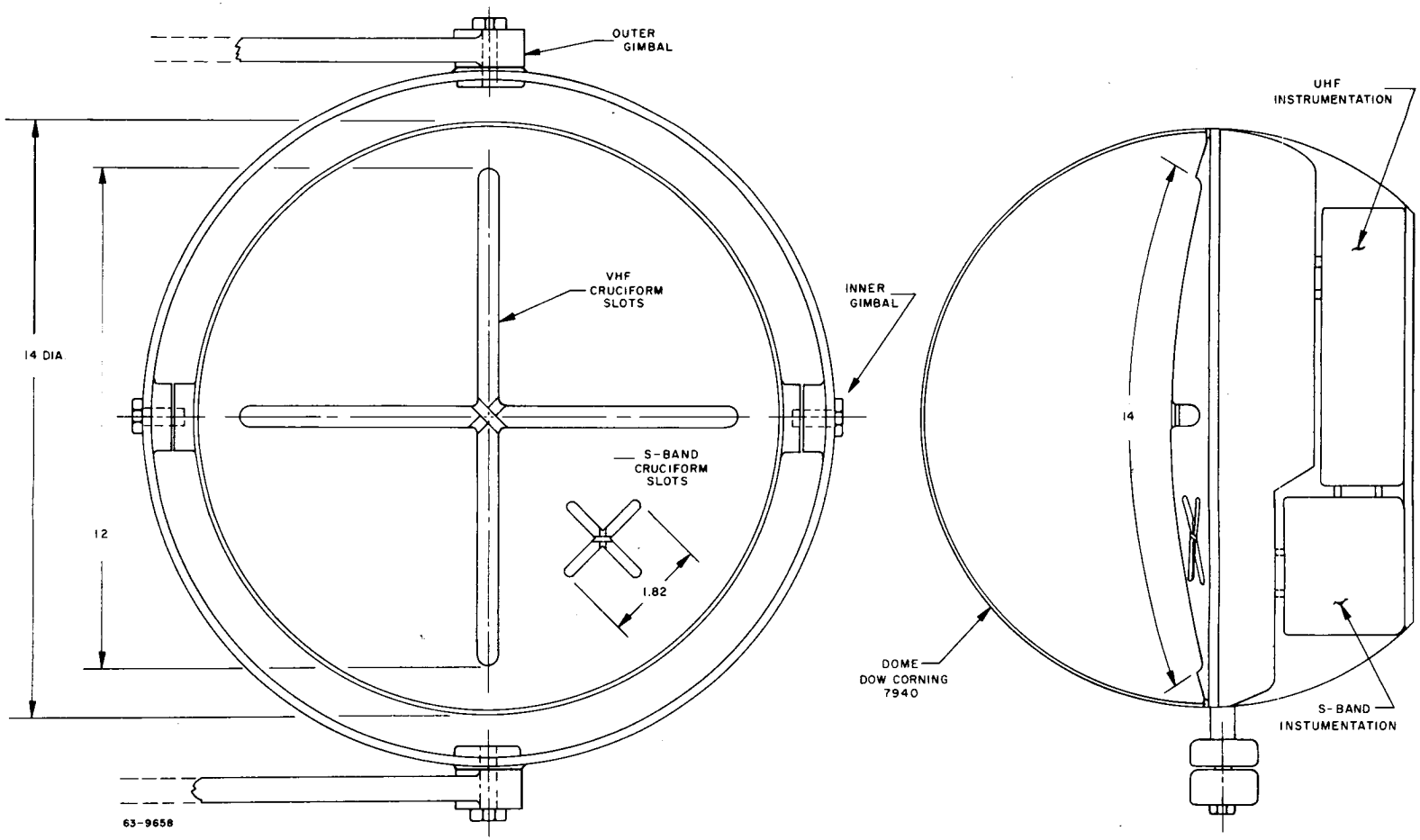

Figure 180 LANDER RELAY/COMMAND ANTENNA

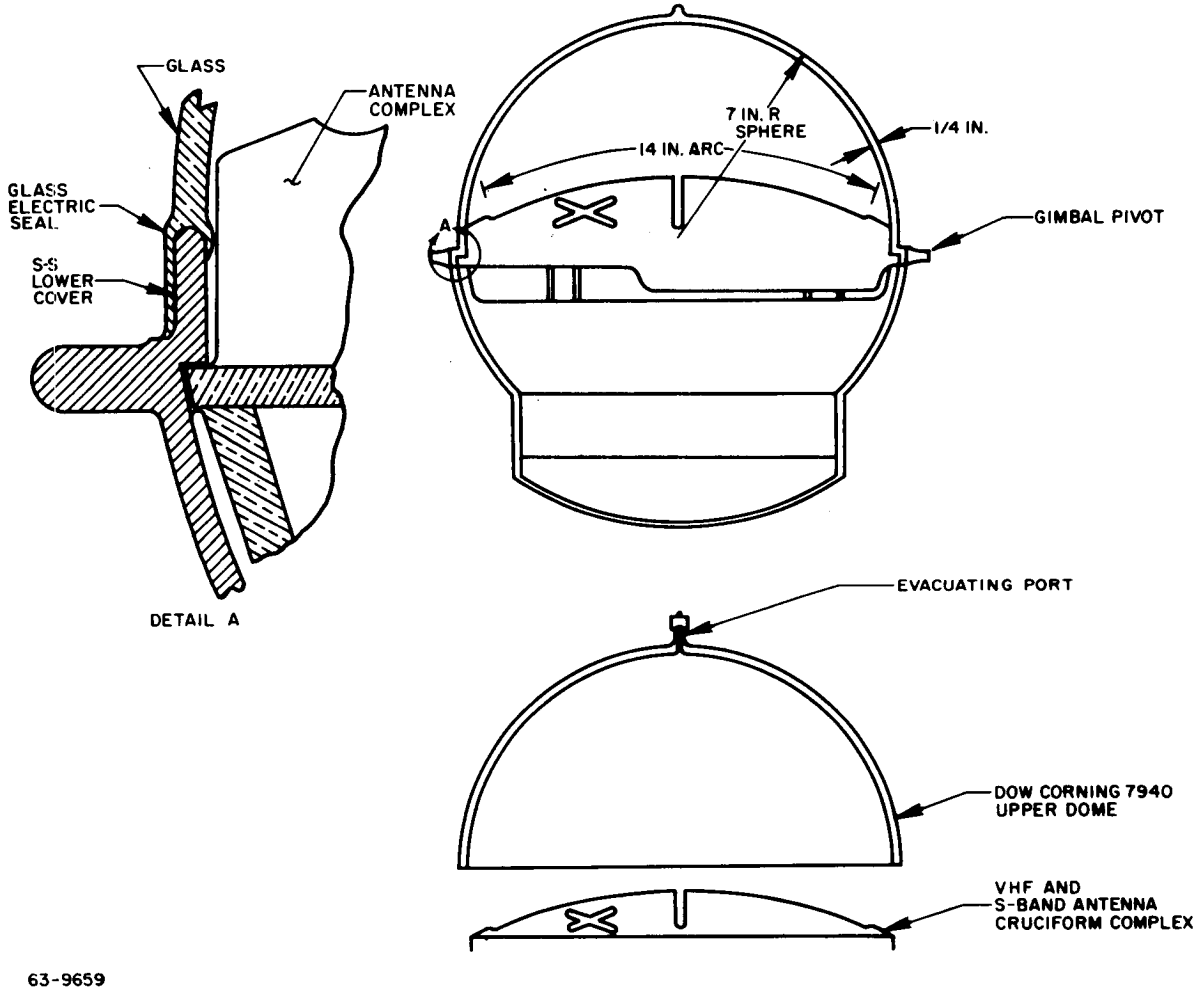

Figure 181 PICTORIAL ASSEMBLY RELAY/COMMAND ANTENNA

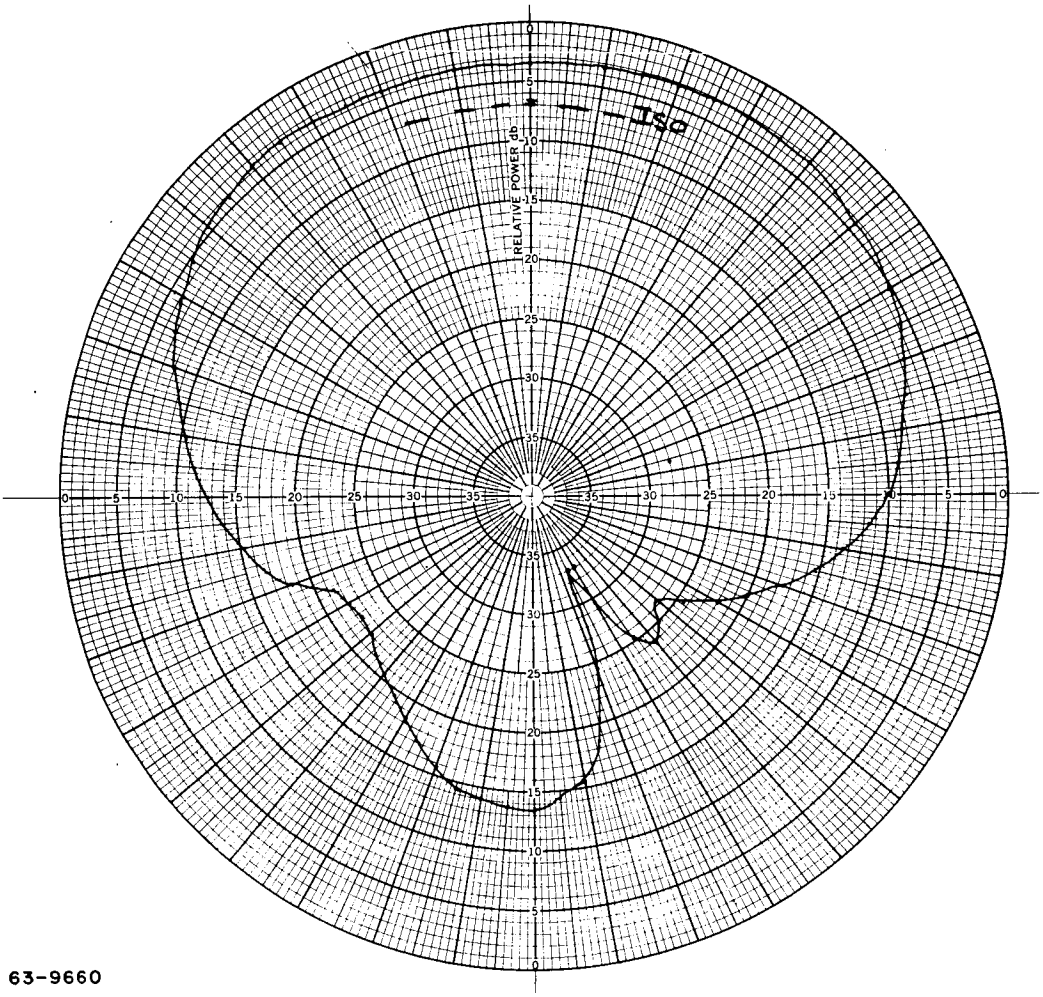

Figure 182 E PLANE PATTERN, VHF ANTENNA

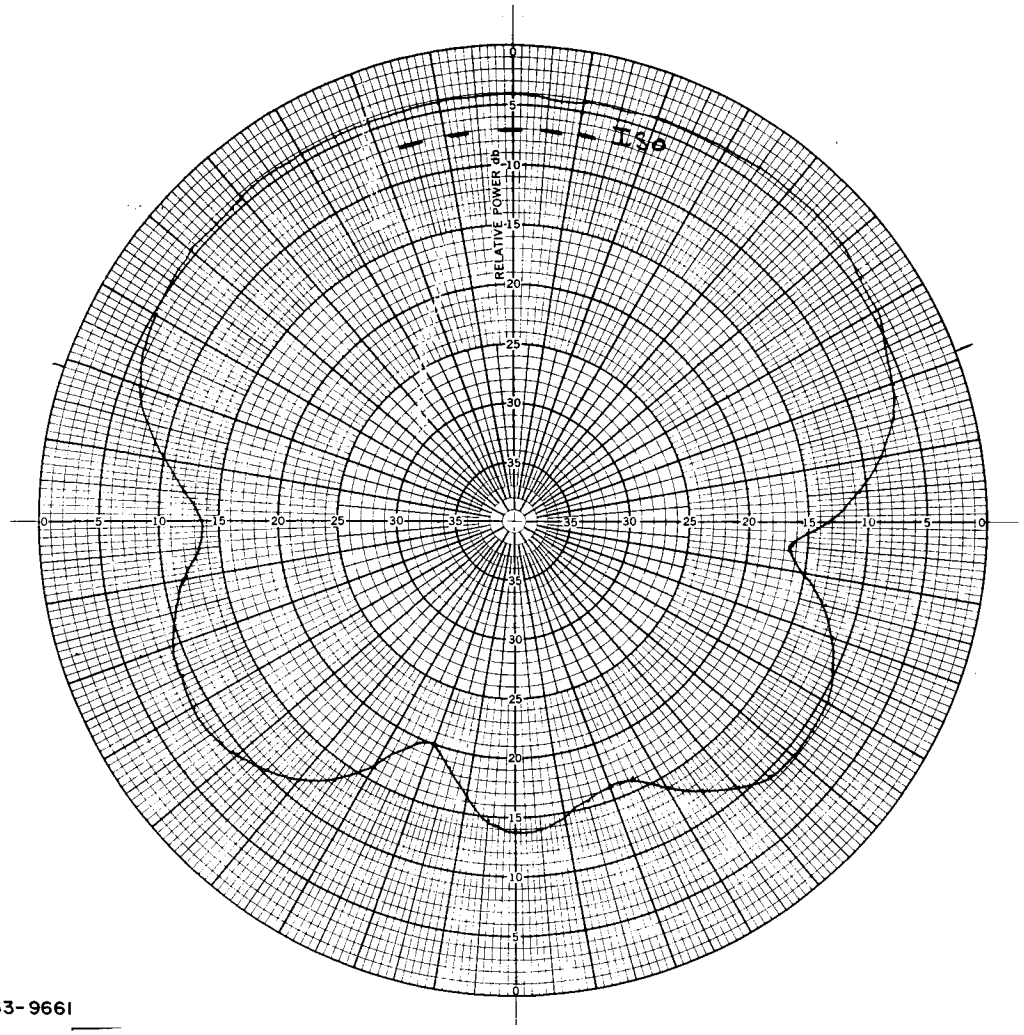

63-9661

Figure 183 H PLANE PATTERN, VHF ANTENNA

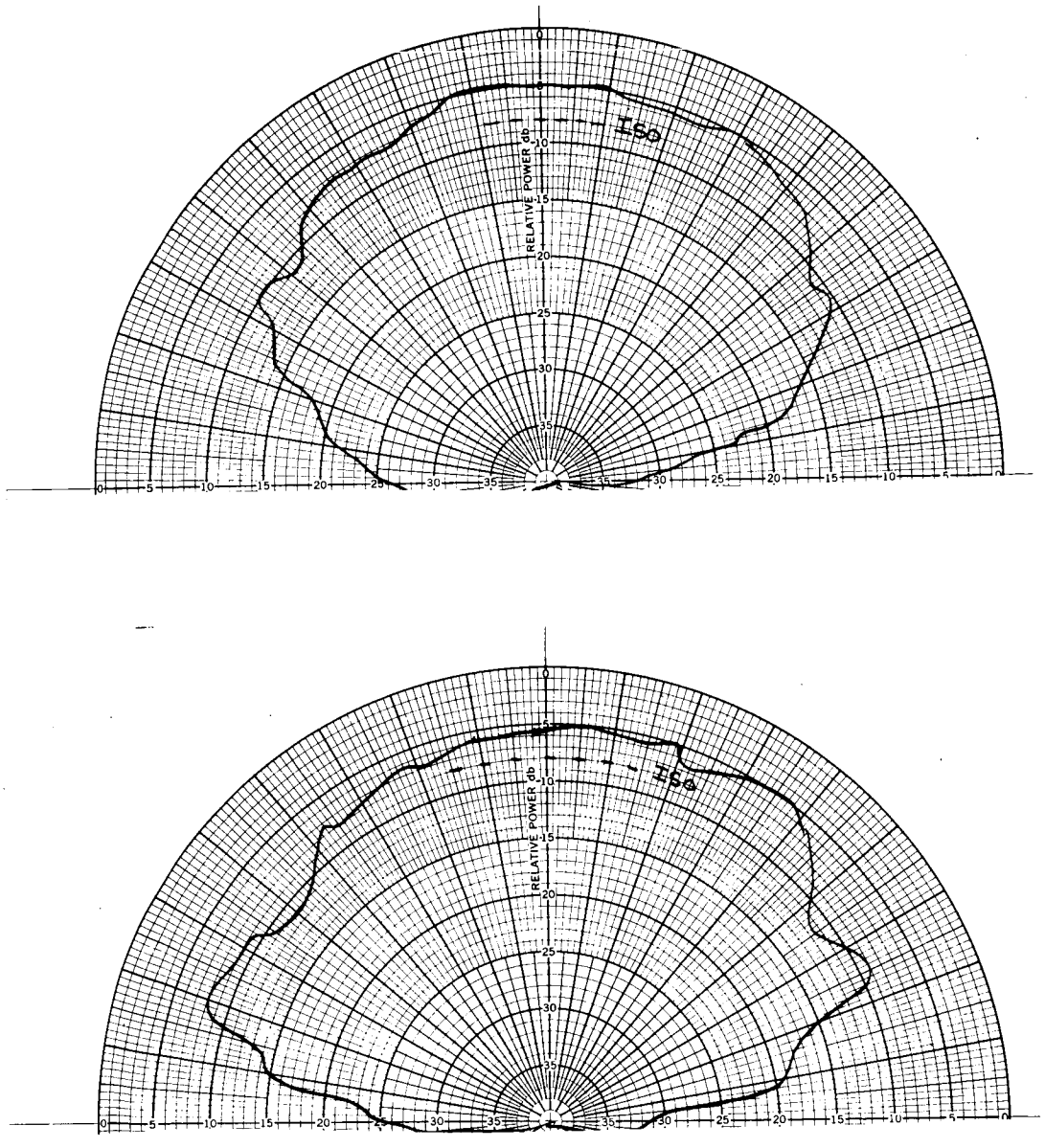

63-9662

Figure 184 E AND H PLANE PATTERNS, S-BAND ANTENNA

typical measured principle plane patterns. The pattern measurements were taken on an 18-inch ground plane for both frequencies. The position of the S-band aperture on the curved ground plane causes a slight tilting of the S-band pattern but this is not enough to compromise its mission.

Power breakdown is a problem which is enhanced by the predicted Martian atmosphere, i.e., density equivalent to a 90,000-foot altitude on Earth and a large content of argon gas. The proposed 50 watts cw, and 70 watts cw for VHF and S-band, respectively, also add to the breakdown problem. To overcome this problem, the antenna will be evacuated and sealed.

Antenna power breakdown measurements have been performed in Avco's high altitude space chamber, and the results of these tests indicate that a pressure of less than 1.747×10^{-2} mm H_g is required to ensure against breakdown. The choice of antenna materials now becomes important because of sublimation and outgassing when considering the use of a high vacuum system over a long duration.

Very little reliable information is available on the characteristics of materials under prolonged space flights and much of the choice is left to empirical design studies. Laboratory tests under simulated space environments indicate that the behavior of pure metals in space can be accurately predicted from the application of Langmuir equations for vapor pressures of materials in closed vacuum. On the basis of these equations, tin, aluminum, and stainless steel are considered stable enough for use in space structures. Outgassing and sublimation become extremely important in the choice of dielectric materials. Fluorocarbons have been flight tested and seem desirable. Both Teflon and Kel-F have been used extensively in satellites. This is an important area that must be investigated further, when considering the solution to the power breakdown problem. A more complete breakdown study may be found in appendix E.

To summarize, the relay/command link antenna will be mounted on a two-axis, gimballed platform. The antenna will be housed in a spherical glass bubble approximately 14 inches in diameter. The bubble will be constructed of Dow Corning 7940, fused silica. Dow Corning 7940 is a new material processed from noncrystalline materials of controlled purity. The material has excellent thermal, chemical, electrical, optical, and acoustical qualities.

Applicable properties: Dow Corning 7940, fused silica.

1) Thermal. Fused silica may be used at temperatures of 900 °C for long time service and 1100 °C for a short time. The average expansion coefficient per °C is 5.6×10^{-7} (from 0 to 300 °C) while the thermal conductivity at 25 °C ... 0.0032 cal/sec cm^2 °C/cm

2) Electrical. Dielectric constant: 1 kmc at 25 - 500 °C ... 3.85, Loss tangent: 1 mc at 385 °C ... 0.0001, 1 kmc at 490 °C ... 0.001

3) Mechanical. Modules of rupture: 7160 psi density, 2.202 gm/cc

4) Chemical. Excellent resistance to ordinary weathering. It also has typically high resistance to attack by nearly all chemical reagents.

5) Nuclear. Remains clear after 10^9 roentgens of gamma radiation from cobalt 60.

This material was chosen because it is a good microwave window; it does not discolor, nor do the dielectric properties change when subjected to heat and the predicted radiation environments. The fused silica also adapts quite readily to the glass-seal technique that will be used to seal the unit under vacuum. The glass dome assembly will be sealed using an electric sealing technique, i.e., the dome and seal ring will be heated in a gas flame, to near the softening point of the glass. An electric arc is struck into the glass and the current produced at the metal-glass interface raises the temperature of the glass to the fusion point. This accomplishes a smooth uniform seal. Figure 185 is a typical stress versus time characteristic curve for the fused silica.

The S-band and VHF telemetry antennas shall be incorporated in the same 14 inch diameter aperture. The weight of the total assembly will be less than 25 pounds. Both antennas are capable of dual-channel operation. The self-diplexing characteristics of the cruciform antenna reduces the need for bulky diplexing hardware since the cruciform design is capable of providing 30 db of isolation between channels. Table 32 lists some of the important electrical characteristics of this antenna design.

TABLE 32

ELECTRICAL CHARACTERISTICS
RELAY/COMMAND LINK ANTENNAS

Characteristic	VHF Telemetry	S-Band Telemetry/Command
Input Impedance	50 ohms nominal	50 ohms nominal
VSWR	Less than 2.0:1 over required operating band	Less than 1.5:1 over required operating band
Pattern Shape	$E_t = F\ (1 + \cos\theta)$	$E_t = F\ (1 + \cos\theta)$
Gain	+ 3 db	+ 3 db
Input Power	50 watts cw	70 watts cw
Channel Isolation	30 db	30 db

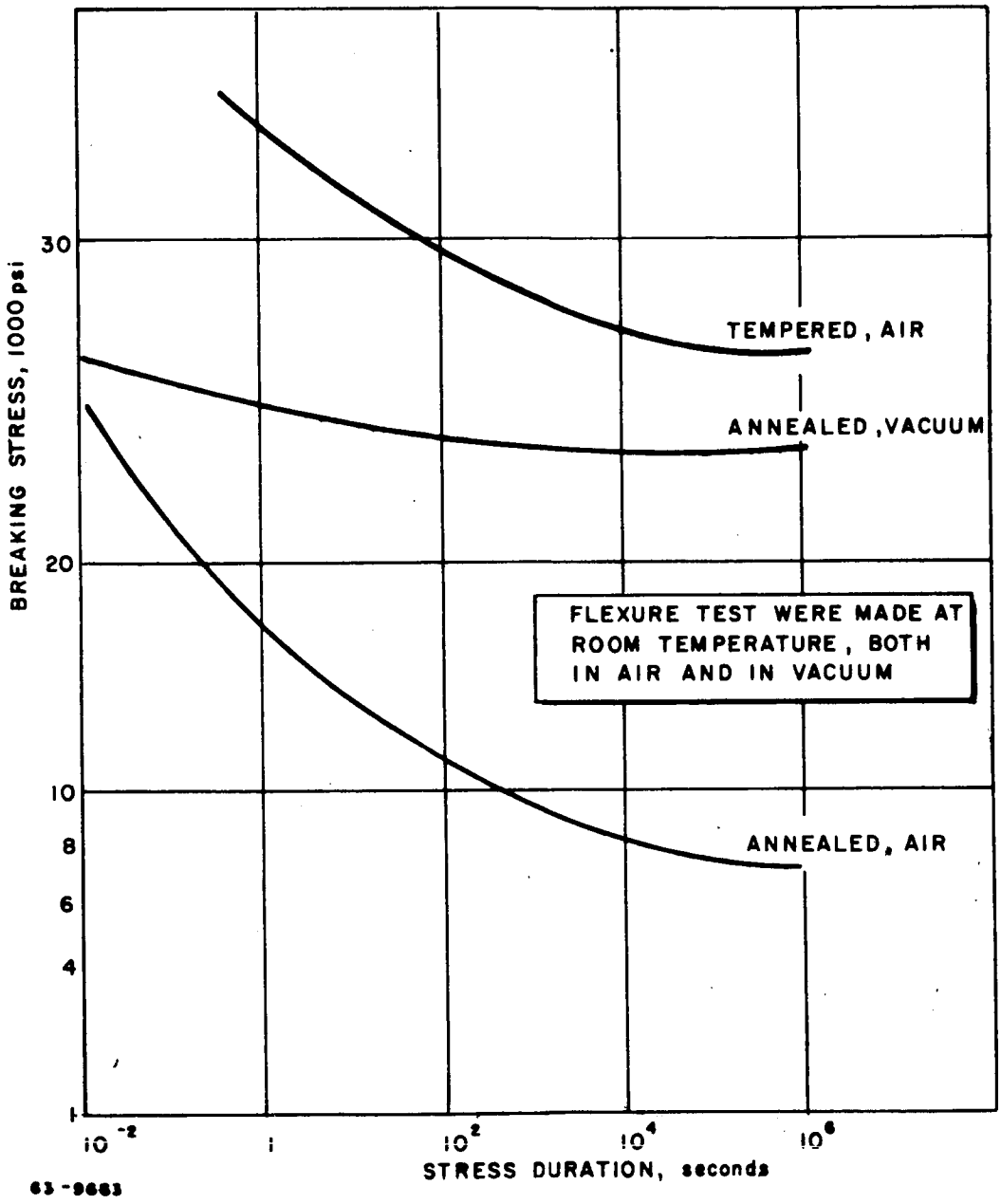

Figure 185 STRESS TIME CHARACTERISTICS OF GLASS

c. Altimeter antenna. An altimeter antenna is required on the lander vehicle which will remain operable from the beginning of entry to the actual landing of the vehicle on the surface of the planet. The antenna must be rugged enough to withstand severe entry environments and be fragile enough to crushup on landing in order not to push through the instrumentation canister on the lander. A study program has indicated that a glass antenna and glass transmission line with the inner surfaces coated with an 0.002-inch layer of silver is a feasible approach. The transition from metal to glass would be made forward of the crushup material. The transmission line will be run through the crushup material in such a manner that the impact of landing will tend to shatter the glass and not force the line and antenna up through the instrumentation canister. This crushup material through which this line is run will also afford sufficient vibration damping for the system.

The antenna and transmission line must be capable of carrying 1 kw peak power, and 10 watts average power. The 1.00 x 0.500 inch waveguide is adequate for these power levels. The altimeter system will operate at 9300 mc. The antenna itself will be a linearly polarized, pyramidal horn whose beamwidth at the half-power points in both the E and H plane will be 30 degrees. Figure 186 shows these calculated E and H plane patterns. This antenna has been designed to maintain phasing errors at the aperture below one-eighth of a wavelength since the main lobe of the radiation pattern becomes distorted when phasing errors at the aperture become excessive. The input VSWR will be under 1.25:1.00 at 9300 mc. Discontinuities will occur at the throat of the pyramidal horn, at the radiating aperture and at the surface of the heat shield. Small inductive or capacitive irises can be introduced in the flared portion of the horn to compensate for VSWR's caused by these discontinuities. The antenna will be evacuated and sealed with a glass cover fused over the aperture of the horn. The gain of this antenna will be approximately 15.5 db above an isotropic radiator.

Figure 187 is an assembly layout of the antenna system mounted in the lander vehicle, while table 33 presents the principle operating characteristics of the antenna system. The antenna design will be basically the same for either a Mars or a Venus mission.

TABLE 33

ALTIMETER ANTENNA OPERATING CHARACTERISTICS

Antenna Type	Pyramidal horn fabricated of glass with silver coating
Power Input	1 kw peak, 10 watts - average
Input VSWR	Less than 1.25:1.00 at the center operating frequency
Operating Frequency	9300 mc
Gain	15.5 db above an isotropic radiator
Beam Width	30 degree beamwidth in the E and H planes

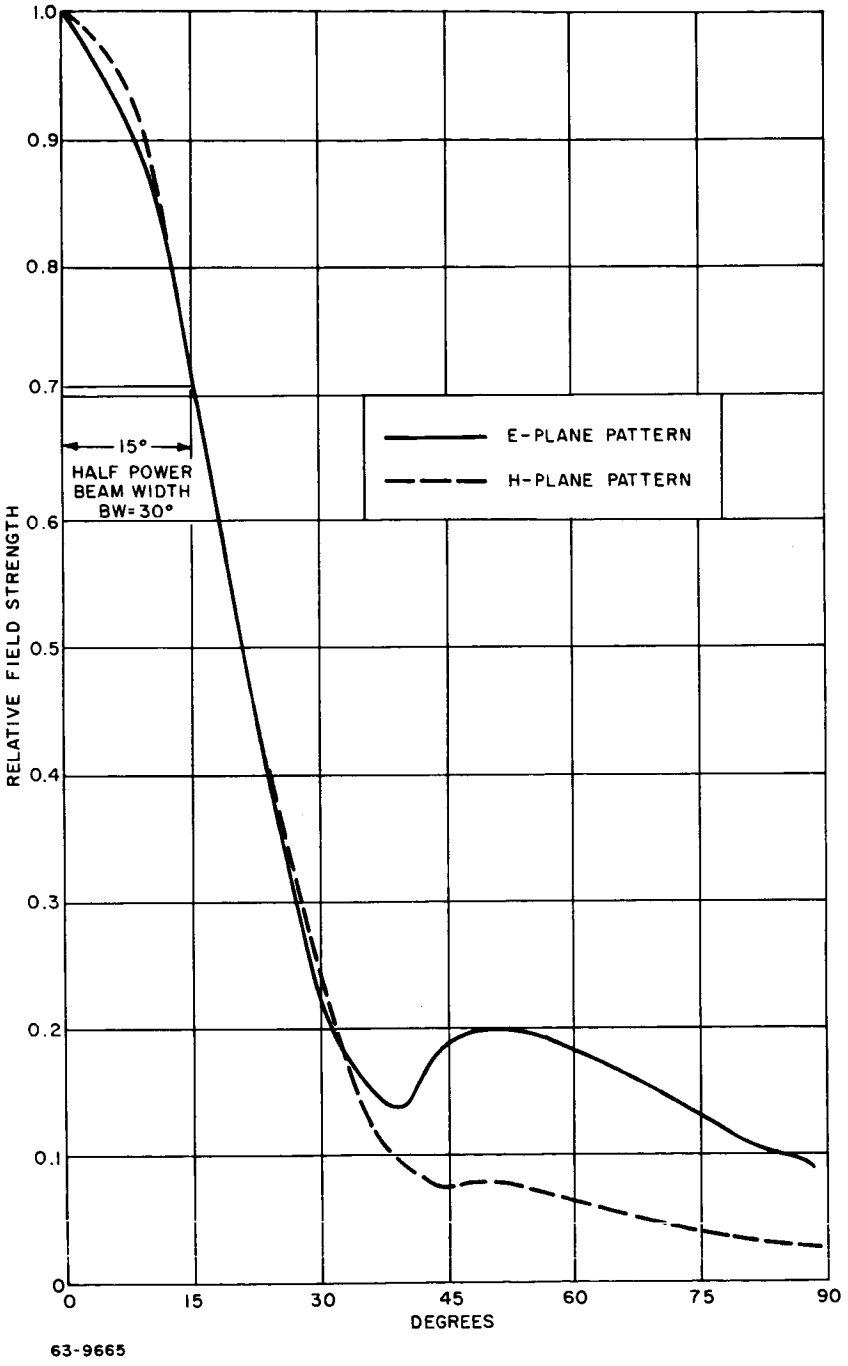

Figure 186 E AND H PATTERNS, ALTIMETER ANTENNA

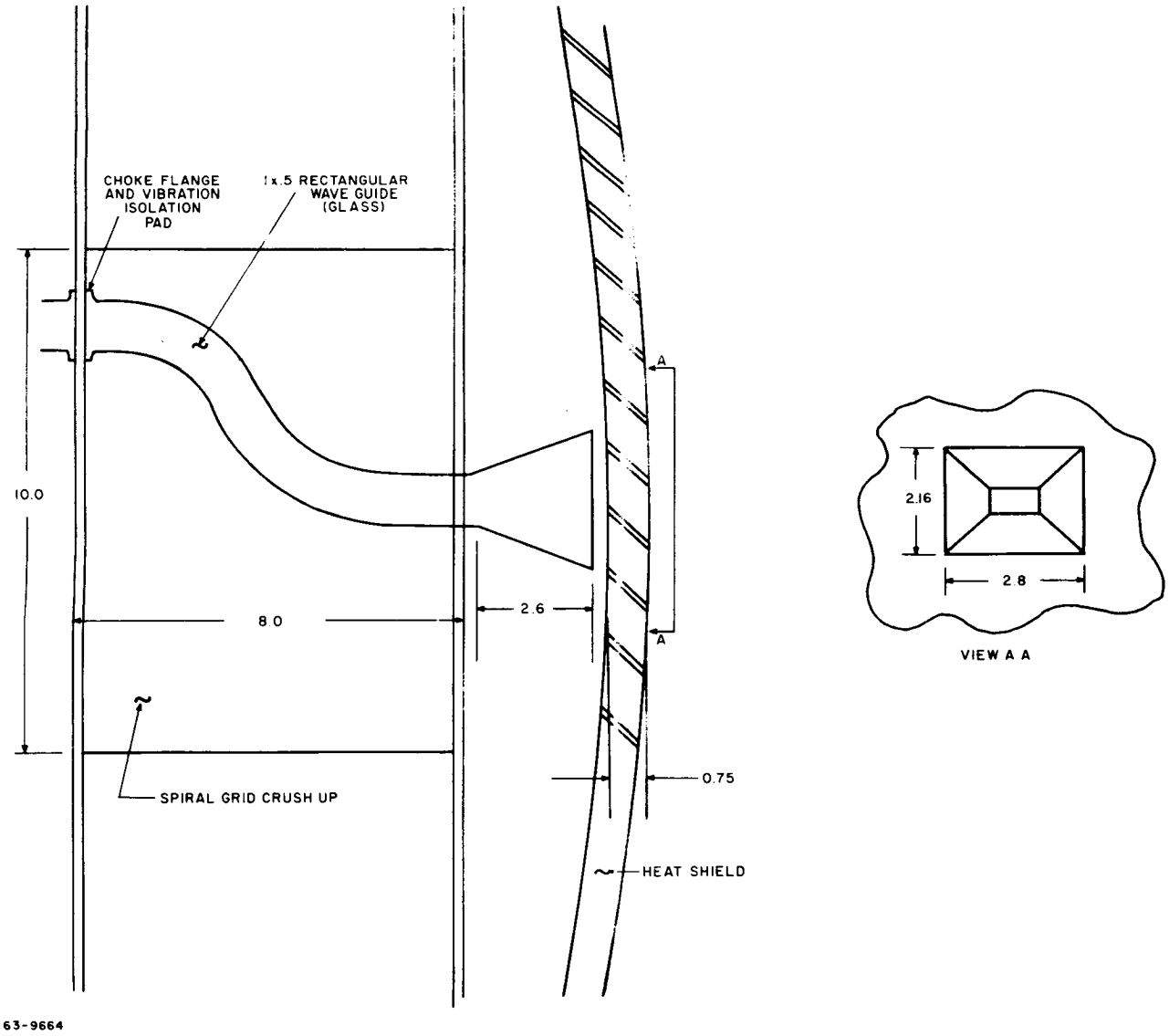

Figure 187 ALTIMETER ANTENNA ON LANDER VEHICLE

d. Direct link telemetry antenna. A cassegrain antenna system has been selected as most suitable for the direct telemetry link from the lander to Earth. This telemetry link is operative only after the landing on the surface of the planet has been successfully accomplished. The operating environments, therefore, are those of the surface of Mars.

Two factors in the proposed surface environments have the greatest impact on the antenna design; the low pressure and the low ionization potentials of the constituents of the Martian atmosphere result in a low power breakdown prediction at S-band transmission frequencies, and the high estimated wind velocities at the surface precludes the use of large solid, vertical reflector surfaces.

The power breakdown problem can best be solved by consolidating the final power amplifier, the feed line, and the feed horn into a single compact pressurized or evacuated assembly. The cassegrain system geometry is ideal for such an arrangement. The feed horn is mounted near the vertex of the main parabolic dish as shown in figure 188. The transmitter and receiver are mounted on the backside of the parabola adjacent to the feed horn. RF rotary joints are avoided as well as feedline losses by including all of the RF stages for transmission and reception in this package. Dc power and low frequency command and modulation frequencies are supplied through slip rings on the gimbal shafts.

The cassegrain system can be designed for a feedhorn with an E-plane aperture width in excess of three inches which is estimated to be necessary at 70 watts input to prevent corona discharge in the low pressure model of the Martian atmosphere. As the feed-horn aperture is made larger it must be placed closer to the vertex of the parabola to avoid excessive aperture blocking and consequent loss of efficiency.

The half power beamwidth of six degrees is determined by the 5-foot diameter paraboloid which fits into the cross sectional diameter of the lander. (Larger unfurlable antenna structures are not considered because of reliability factors.) A cassegrain system with a half-power beamwidth of more than a degree would normally be unattractive because of excessive aperture blocking resulting in gain loss and high sidelobes. Where operation can be restricted to a single linear polarization, a considerable reduction in the aperture blocking is possible (ref. 38). One method accomplishes this by a polarization twisting technique which renders a large feed invisible and permits the use of a small subdish (hyperboloid). The subdish incorporates a "twist reflector" which rotates the linear polarization 90 degrees on reflection. A vertically polarized feed is located behind the main dish and the central portion of the main dish includes a "transreflector" having a horizontal grating. The feed radiates through the transreflector toward the subdish; the subdish reflects this wave and twists its polarization to horizontal. The horizontally polarized wave is then completely reflected by the main dish. Since the feed is invisible, it can have a large aperture and a narrow beamwidth to reduce the size of the subdish and reduce the subdish blocking.

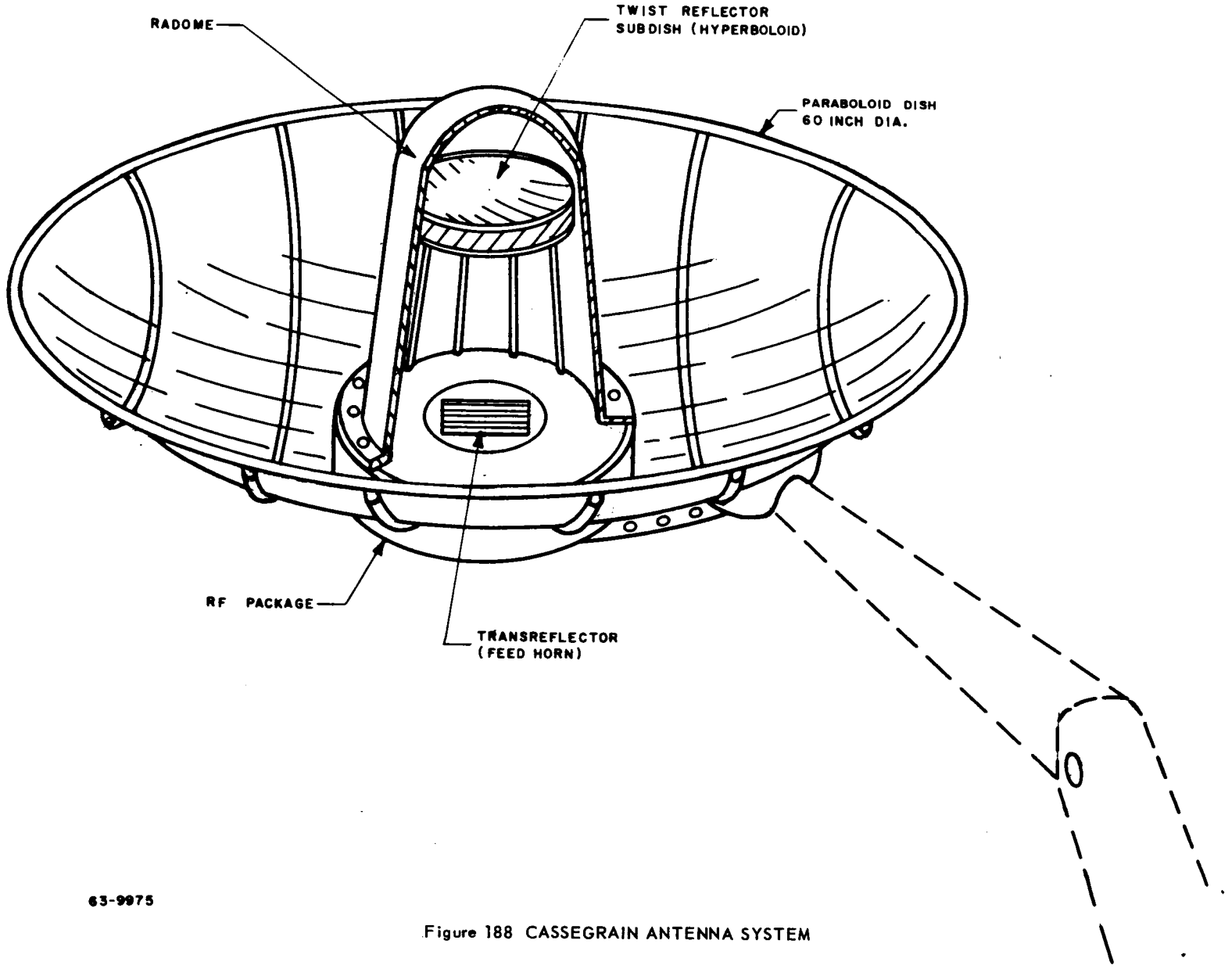

63-9975

Figure 188 CASSEGRAIN ANTENNA SYSTEM

Wind loading of the main dish can be kept low by maximizing the openness of the structure. Linear polarization requires a reflecting grid of wires parallel to the polarization only. The orthogonal wires can be omitted without degradation in the electrical performance. The parallel wires should be spaced less than 3/16 inch on centers for reflection efficiency. Stabilizing wires in the orthogonal direction can be spaced for mechanical considerations alone.

The twist reflector subdish is more complex in structure, but much smaller in diameter. For lightness, it is composed of two orthogonal gratings of wires which are separated by approximately 2 inches. The grating surface farthest from the feed requires approximately the same wire spacing as the main reflector (less than 3/16 inch). The orthogonal grid on the face of the subdish will have a wider spacing to permit one-half of the incident power to be transmitted through to the close spaced grid where it will be completely reflected. The twist reflection is obtained by orienting the grids at 45 degrees to the incident polarization.

The cassegrain system has another feature which makes it attractive for use in the lander. The double reflector system makes it possible to obtain a configuration which is very short in physical focal length while the performance is that of the much longer equivalent focal length.

TABLE 34

MARS LANDER DIRECT-LINK TELEMETRY ANTENNA

Antenna Type:	Cassegrain Reflector
Frequency:	2300 mc
Polarization:	Linear
Beamwidth (3 db):	6 degrees
Gain Above Isotropic:	28 db
Bandwidth:	40 mc
VSWR:	1.25
Power Handling Capability:	70 watts cw
Sidelobe Level:	-19 db
Weight:	18.5 pounds

8. MECHANICAL DESIGN -- VENUS

8.1 Capsule Entry From Orbit

1. System requirements. The large decrement in vehicle velocity requires sufficient propellant tankage, making it necessary to jettison the drained tankage (hence the external propulsion system location as shown in figure 189.) If the tankage had been packaged internally and retained, a larger entry vehicle and descent system would have been needed. Since a minimum size has been arrived at for the entry vehicle system, more than one system can be carried by the orbiter, giving added scientific interest to the mission. The detailed weight breakdown is show in table 35.

For minimum entry vehicle weight, an M/C_DA of 0.5 and the Apollo shape as shown in figure 190 were chosen. The scientific instrument payload for this mission was designed to provide data on atmospheric composition, temperature, and pressure. The vehicle must descend slowly enough through the atmosphere to allow sampling at approximately 5000-foot altitude increments but does not have to survive ground impact. Data are relayed back to the orbiter and thence sent to Earth.

The selection of the descent system for the Venus vehicle is quite different from the case of the Mars lander-vehicle descent system. The high atmospheric density of Venus permits the use of considerably smaller size deceleration devices. However, the high ambient temperature (between 800°F and 1050°F) at or near the surface of the planet makes the selection of the descent system dependent on the availability of materials to withstand these temperatures.

The mission requirements for the Venus vehicle dictate a decelerator capable of providing reasonably low vertical descent velocities at or above 300,000 feet altitude to permit atmospheric data collection from that altitude to ground impact. Since the vehicle is not designed to collect data after impact with the surface of the planet, the selection of a descent system is not primarily governed by the impact velocity, as in the case of the Mars lander vehicle.

In considering possible deceleration devices for the Venus lander, three approaches were considered: (1) use of a nylon or HT-1 parachute with acceptance of parachute destruction below a given altitude due to the increasing ambient temperature; (2) use of a metallic fabric parachute; and (3) use of a high-temperature ballute (ram "air" inflated conical balloon).

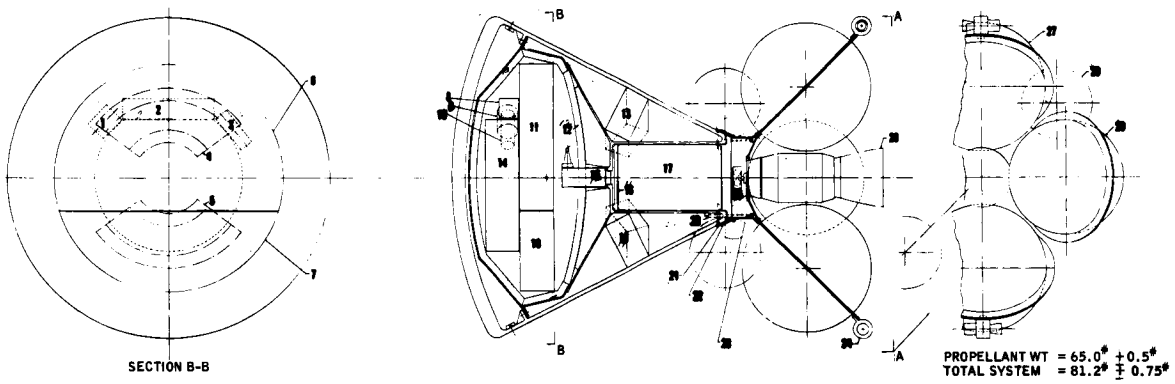

PROPELLANT WT = 65.0# ±0.5#
TOTAL SYSTEM = 81.2# ∓ 0.75#

1. ATMOS. PRESSURE 16" DIA. 2" LG. .31#
2. ATMOSPHERE DENSITY 15 IN^3 1.5#
3. ATMOS. TEMP. 1" DIA. 3" LONG .31#
4. OMNI ANTENNA
5. OMNI ANTENNA
6. ATMOSPHERIC COMPOSITION
7. COMMUNICATIONS PACKAGE
8. ATMOSPHERIC DENSITY
9. ATMOSPHERIC PRESSURE
10. ATMOSPHERIC TEMP.
11. ATMOSPHERE COMPOSITION
12. 384 IN^3 10# INSULATION
13. OMNI ANTENNA
14. COMMUNICATIONS AND BATTERY 5.6# 230 IN^3
15. GAS GEN.
16. SABOT
17. DROGUE BALLUTE 52# (IN CLOTH BAG)
18. COMMUNICATIONS 176 IN^3 TOTAL WEIGHT 31.4#
19. OMNI ANTENNA
20. CABLE CUTTER
21. CABLE
22. HINGED CLAMP
23. PROPELLANT SYSTEM SEPARATION SPRING
24. SPIN MOTOR (SOLID FUEL)
25. VALVES
26. 60# THRUST NOZZLE
27. OXIDIZER TANK (2 REQ'D) 9.53 IN. O.D.
28. PRESSURANT TANK (2 REQ'D) 5.55 IN. O.D.
29. FUEL TANK (2 REQ"D) 8.55 IN. O.D.

63-9762

Figure 189 ORBITAL INJECTION VENUS LANDER CROSS SECTION SHOWING INTERNAL DETAILS (W ENTRY = 85 POUNDS)

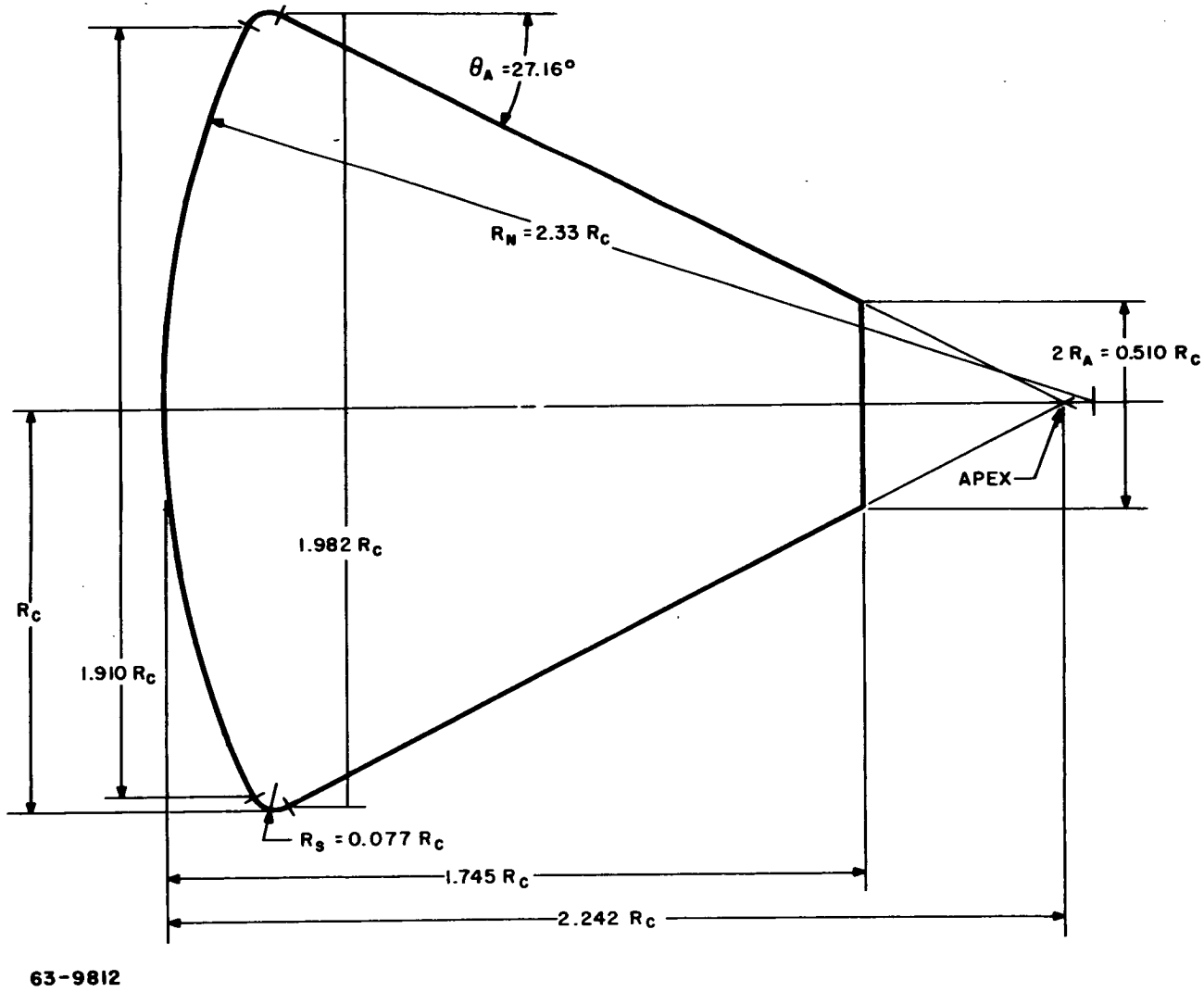

Figure 190 VOYAGER "APOLLO TYPE" ENTRY VEHICLE (VENUS ENTRY FROM ORBIT CONFIGURATION

TABLE 35

WEIGHT SUMMARY

VENUS ATMOSPHERIC PROBE REFERENCE DESIGN

$C_DA = 0.5$ $V_E = 28,000$ ft/sec			Weight (pounds)
Total lander weight (on orbiter)			174.7
Sterilization can and micrometeorite shield			
Aluminum cover sheets and foam metal core		8.0	
Spin rocket system			
4 solid rockets at 90°; Δ rpm = 40		0.5	
Main propulsion system			
Bipropellant liquid system			
Is_p = 315 seconds, λ_p = 0.795, ΔV = 5000 ft/sec			
Propellant weight (including residuals)		65.0	
Dry weight		16.0	
Pressurant (helium)		0.2	
Entry weight (2.12 feet diameter)			85.0
Heat shield, material 5026 (0.52-inch t on nosecap) γ_e = -5 degrees		10.6	
Substructure - aluminum honeycomb γ_e = -20 degrees		6.3	
Parachute, 2-foot unloaded diameter		5.2	
Heat shield bond - HT - 424 bonding compound		3.4	
Internal structure		8.0	
Miscellaneous		2.5	
Instrumentation		12.0	
Communications and battery		37.0	
Multiplex encoder	2		
VHF transmitter	12		
VHF antenna system (parachute phase)	3		
Central programmer and sequencer	3		
Power conditioning	6.4		
X-band altimeter	5		
Battery	5.6		

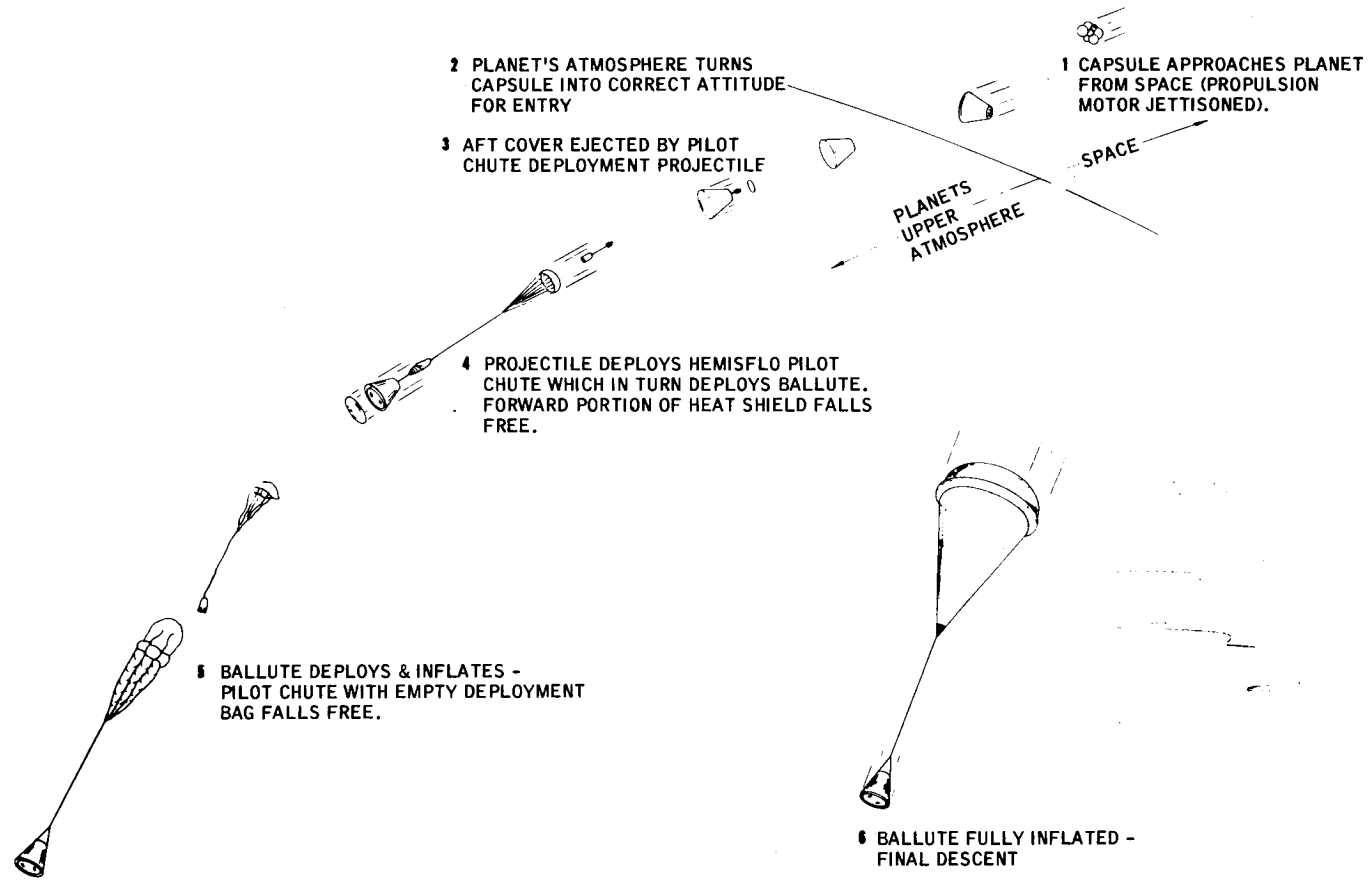

63-9764

Figure 191 DESCENT OPERATIONAL SEQUENCE

Approach number (1) was not given extensive consideration. Even with a parachute fabricated from HT-1 destruction of the chute could be expected to occur at an altitude from 180,000 feet (Kaplan "maximum temperature" atmosphere) to 75,000 feet (Kaplan "standard temperature" atmosphere). While the descent velocity established by the vehicle alone might be acceptable (assuming the parachute is disconnected when it is destroyed), the loss of the parachute could result in vehicle instability. With a tumbling vehicle, the atmospheric data collected would be of doubtful value.

Approaches (2) and (3) are both felt to be feasible within the mission requirements and the current knowledge of the Venusian atmosphere. Of the two, the high-temperature ballute appears to be far ahead of the metallic fabric parachute, in terms of state of development. The high-temperature ballute has been fabricated in sizes up to 9 feet in diameter, and has undergone wind tunnel testing at speeds varying from low subsonic to Mach 10. In these wind tunnel tests the ballute has demonstrated its ability to inflate and remain inflated and to possess the required aerodynamic stability throughout the Mach number range tested.

Metallic parachutes are, on the other hand, in the embryonic state of development. Several different types of metallic cloth have been produced in small quantities. However, there seems to be no evidence that parachutes have been fabricated from any of these metal cloths.

The use of metal cloth in a parachute for space missions appears, at least superficially, to pose some inherent problems. The metal cloths fabricated to date possess very low flexure strength. Therefore, packing of metal parachutes may required special techniques differing from those currently used in packing cloth parachutes.

2. Descent system. The proposed descent system for the Venus vehicle consists of a high-temperature ballute. The selection of the Venus descent system is based on a series of parameteric studies conducted by Northrop Ventura.

The proposed ballute in an isotensoid shape, fabricated of a skin woven of seven strand cables of 0.5-mil Rene 41, coated with high-temperature silicone-ceramic elastomer. To minimize the ballute system weight, deployment of the relatively heavy ballute will be accomplished by use of an 18-inch diameter HT-1 Hyperflo pilot parachute. The pilot chute is deployed by a pilot-chute deployment gun. Once inflated, the pilot chute exerts sufficient force to extract the ballute from its container.

The ballute size (about the same as the entry vehicle diameter) is selected to provide the minimum descent velocity from 300,000 feet altitude, consistent with a reasonable size and weight for the descent system.

The use of omnidirectional data-transmitting antenna, located on the entry package (which is suspended several vehicle diameters below the ballute), allows communications to be maintained with the orbiter throughout the atmospheric descent phase.

3. Descent operational sequence (figure 191)

a. Upon proper orientation of the orbiter bus, which has achieved orbit, the lander is separated at an optimum point on the orbit, and spun up to about 40 rpm and A velocity increment of about 5000 ft/sec is applied, slowing the vehicle. When the propellant has been expended, tankage and thrust chamber assembly are jettisoned prior to planetary atmospheric entry.

b. Planet's atmosphere turns capsule into correct attitude for entry. Location of vehicle c.g. is such that it is aerodynamically stable with the blunt face of the heat shield forward into the flow.

c. Aft cover is ejected by pilot chute deployment projectile. A g-sensing switch within the lander, and armed by rising entry g's, is closed at preselected descending g level while the vehicle is being aerodynamically decelerated. A deployment gun is explosively actuated and its projectile pushes off the rear thermal protection cover.

d. Projectile deploys hemisflo pilot chute, which in turn deploys ballute. Forward portion of heat shield falls free. A linear-shaped explosive charge also is actuated, which severs the heat shield front cap, allowing it to fall away and lowering the weight suspended from the ballute. Ballute deploys and inflates. Pilot chute with empty deployment bag falls free.

f. Ballute fully inflated --final descent. Atmospheric sampling experiments begin. Composition, temperature, and pressure measurements are made. Altimeter readings are made. Data are then transmitted to orbiter in real time on a time shared basis. The entry vehicle external aerodynamic shape is shown in figure 190.

4. Propulsion system. The Voyager Venus orbital-entry capsule propulsion system (figure 192) is a pressure-fed, storable, hypergolic bipropellant propulsion system with a total delivered impulse of 20,500 lb/sec. The system propellants are mixed oxides of nitrogen (MON composed of 85 percent nitrogen tetroxide and 15 percent nitric oxide) and an eutectic blended fuel (EMHF) compound of 87.6 percent monomethylhydrazine and 12.4 percent hydrazine. An all-welded configuration will be used to prevent leakage. The system is prepackaged with propellants and the fill and vent connections will be welded after filling.

The main thrust chamber is rigidly mounted, ablatively cooled, and is controlled for the one period of operation by normally closed squib valves, thrust terminating on propellant depletion. A radiation-cooled skirt is used on the expansion nozzle from an area ratio of 20 to the exit area ratio of 60 to satisfy minimum weight requirements. The chamber is designed to produce 60 pounds of thrust at a chamber pressure of 125 psia. Propellant tank pressure will be regulated to 175 psia. Thrust vector alignment tolerances are 0.01 inch for lateral displacement and 0.26 degree angular misalignment. The effect of these

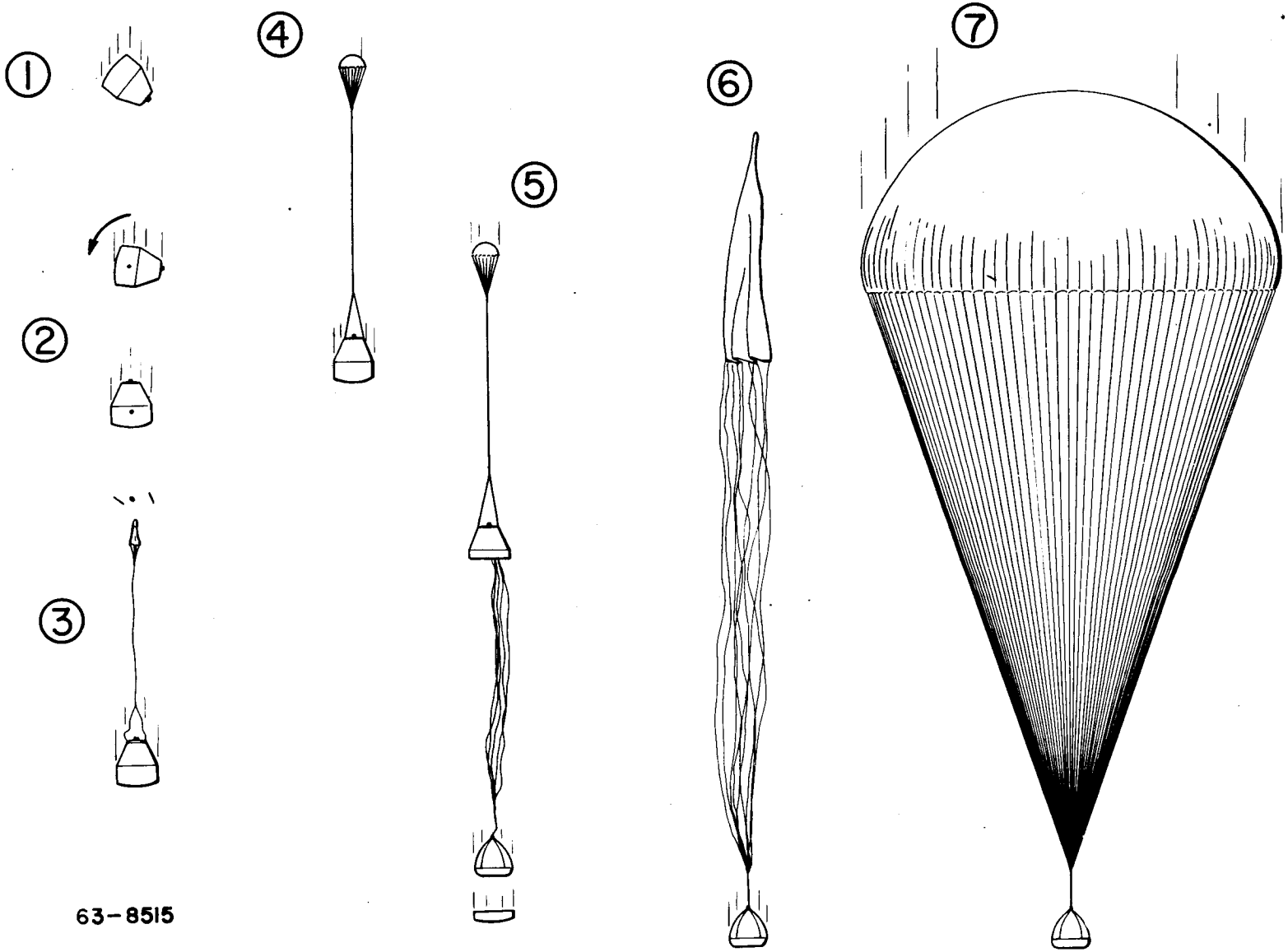

Figure 191a MARS DESCENT SEQUENCE

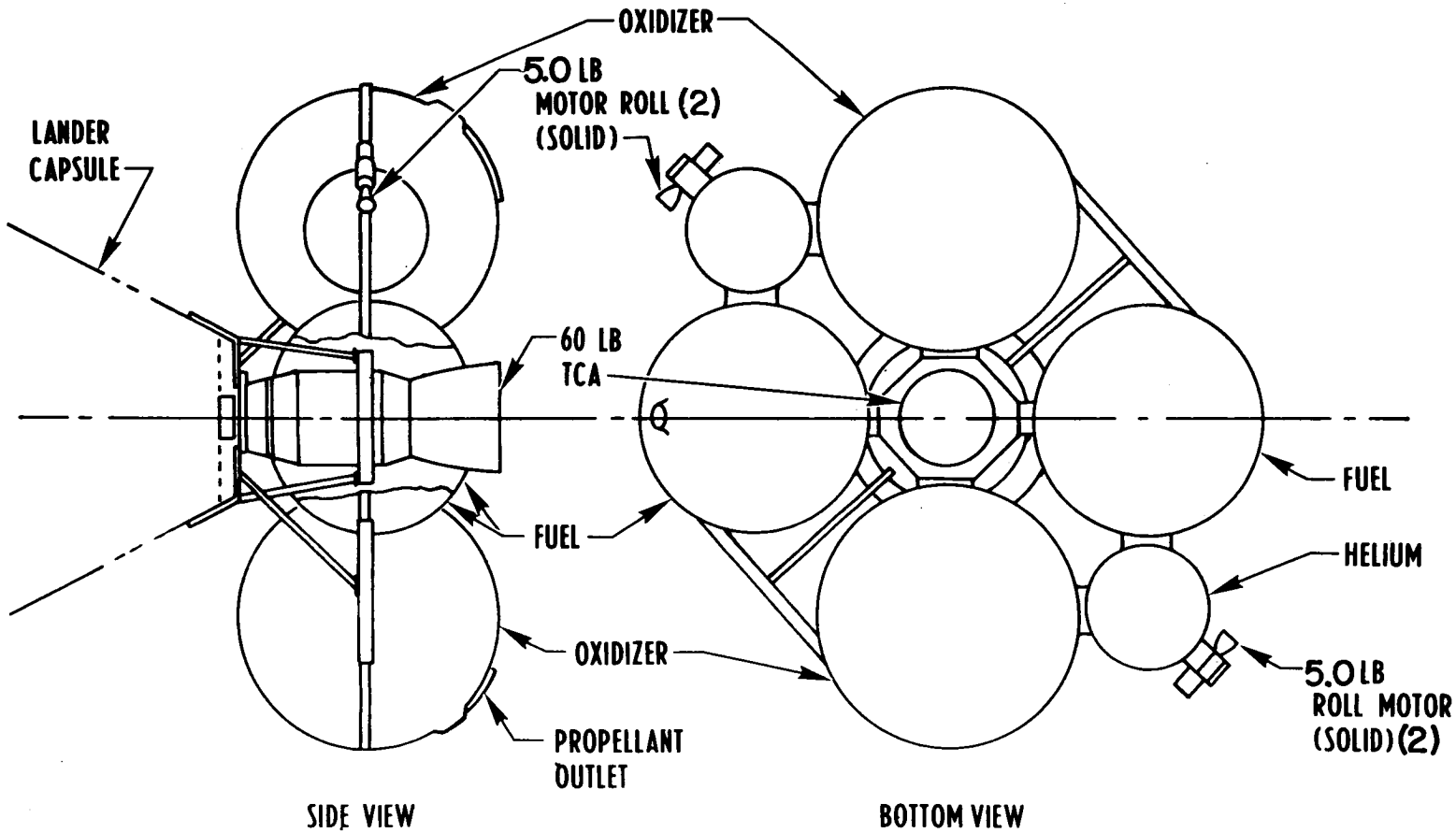

Figure 192 DESIGN LAYOUT OF VOYAGER VENUS LANDER PACKAGED PROPULSION SYSTEM

inaccuracies upon the velocity vector is reduced to an acceptable value by spinning the capsule at 40 rpm. Spinup and despin are accomplished by two pairs of solid-propellant rockets.

The propellant is contained in two equal-volume oxidizer tanks and two equal-volume fuel tanks balanced in oppostion about the system longitudinal axis. The capsule spin rate is utilized as a means of propellant orientation to give a dependable means of propellant expulsion. Tank outlets are positioned to allow maximum propellant utilization. A schematic is shown in figure 193

The two oxidizer tanks, as well as the two fuel tanks, are individually isolated by squib valves. The tanks are individually filled and sealed, resulting in a statically and dynamically balanced system. The normally closed squib valves prevent propellant migration from one tank to another, thus assuring a balanced system until actuation. The system is not actuated until capsule spinup has been accomplished by the solid-propellant spin rockets. Normally closed squib valves are used above the tanks rather than check valves because of the absence of diaphragms or bladder in the propellant tanks. The valves ensure isolating the propellants from one another.

Pressurization is provided by stored helium contained in two equal-volume spheres manifolded together. The two-tank configuration was chosen from dynamic balance considerations. Pressurant is isolated from the pressure regulator by a normally closed squib valve until the system is activated. Table 36 is a summary of the system performance parameters.

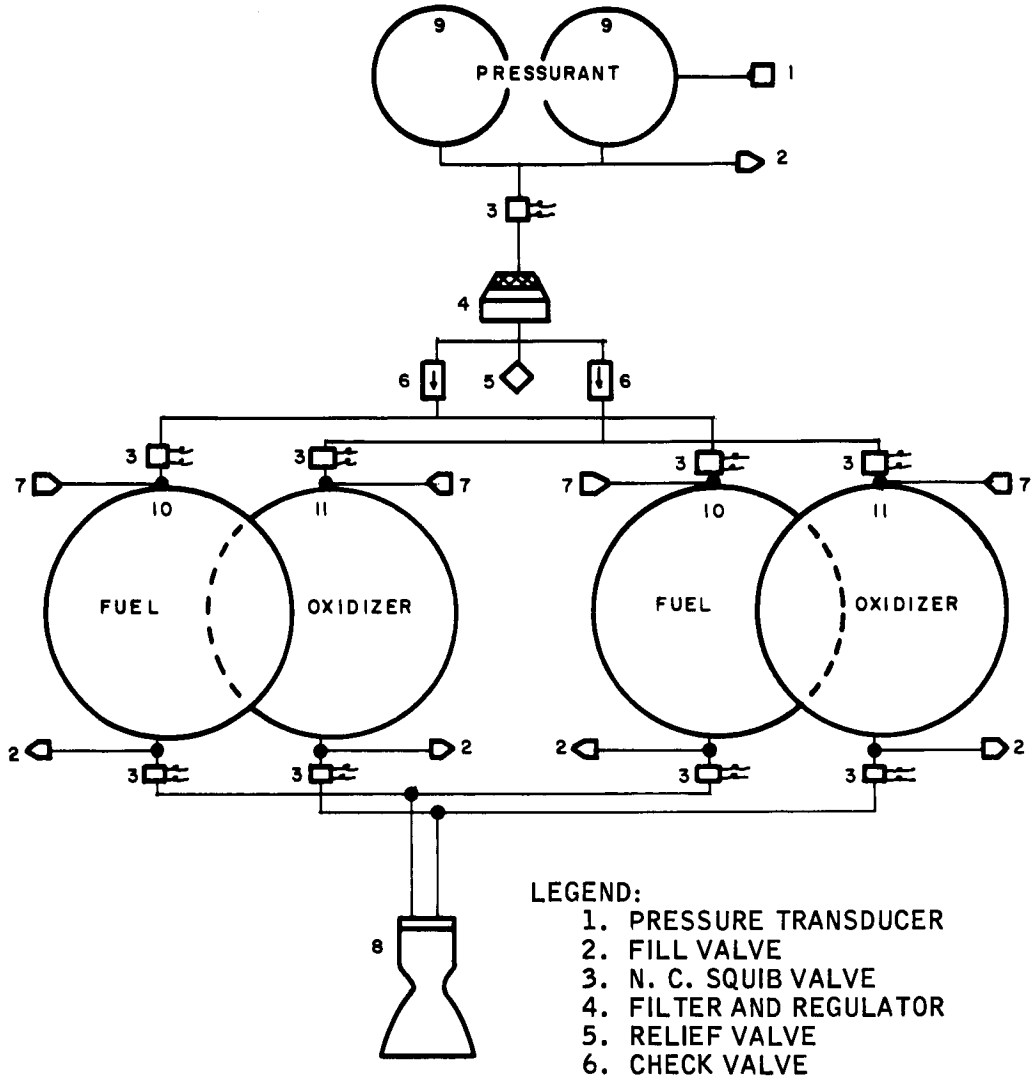

63-8446

Figure 193 VOYAGER VENUS LANDER PROPULSION SCHEMATIC

TABLE 36

SUMMARY OF PROPULSION SYSTEM PERFORMANCE PARAMETERS, VENUS ORBITAL ENTRY CAPSULE

Thrust, pounds	60
Chamber pressure, psia	125
Mixture ratio	2.15
Characteristics velocity (C*), ft/sec	5295
Thrust coefficient Cf	1.936
Specific impulse, seconds	318.5
C* efficiency	0.94
Cf efficiency	0.98
Throat area, $in.^2$	0.248
Expansion area ratio	60
Fuel flow rate, lb/sec	0.0598
Oxidizer flow rate, lb/sec	0.1286

8.2 Direct Entry Lander

As an alternate method for securing scientific data during a Venus mission, a direct entry lander design was investigated. A large decrease in propulsion weight was realized both on the orbiter and on the lander, as compared to the previously mentioned case where the entry vehicle was carried into orbit and then retropropelled to suborbital velocity. The direct entry lander was assumed to require a velocity increment of about 100 ft/sec when separated from the orbiter. A compromise between aerodynamic performance and data-securing capability was made with the selection of a modified V-2 shape. Figure 194 shows a cross section of the entry vehicle and table 37 shows the weight breakdown. Sufficient aerodynamic deceleration was obtained at an M/C_DA of 0.6 slugs/ft^2 to allow scientific data acquisition at altitudes in the neighborhood of 250,000 feet. The dense Venusian atmosphere also allows vehicle drag to play an important part in the deceleration time history. The entire entry vehicle is discarded at the time of parachute deployment, thus lowering the parachute size and weight required. The parachute itself must be resistant to the atmospheric heating effects, allowing the vehicle to impact prior to parachute failure. The use of a ballute was considered; however, it is felt that by the time of the Voyager mission, temperature-resistant textiles will be available for fabrication of a parachute lighter in weight than the ballute.

Atmospheric data sampled during the parachute phase is identical to that considered in the Venus orbital injection capsule in the previous section, namely, composition, temperature, pressure, and altitude at approximately 5000-foot altitude increments from about 260,000 feet to just above ground level. All data are recorded for playback to the orbiter vehicle at an opportune time. If the orbiter-lander relative positions are favorable during descent, some atmospheric data also may be relayed at that time.

During descent, an active thermal-control system is utilized to protect the internal instrument package. Minimizing the surface area of the instrument package and using a double-wall construction with an insulated and evacuated interspace, the thermal protection system's efficiency is kept at a maximum. Ten hours is predicated as the thermally controlled life of the instrument package. Atmospheric temperatures near the surface have been estimated to be up to 800° F, necessitating the choice of structural materials for the landed system which have sufficient strength at elevated temperature. Titanium sheet construction was chosen for the outer shell of the instrument box. Stainless-steel honeycomb protects the entire external surface of the instrument box at impact.

A toppling, nonerecting landed configuration using relay communication to the orbiting vehicle is detached from the parachute at ground impact. In its final attitude, one of the two large area sides of the instrument box will be up

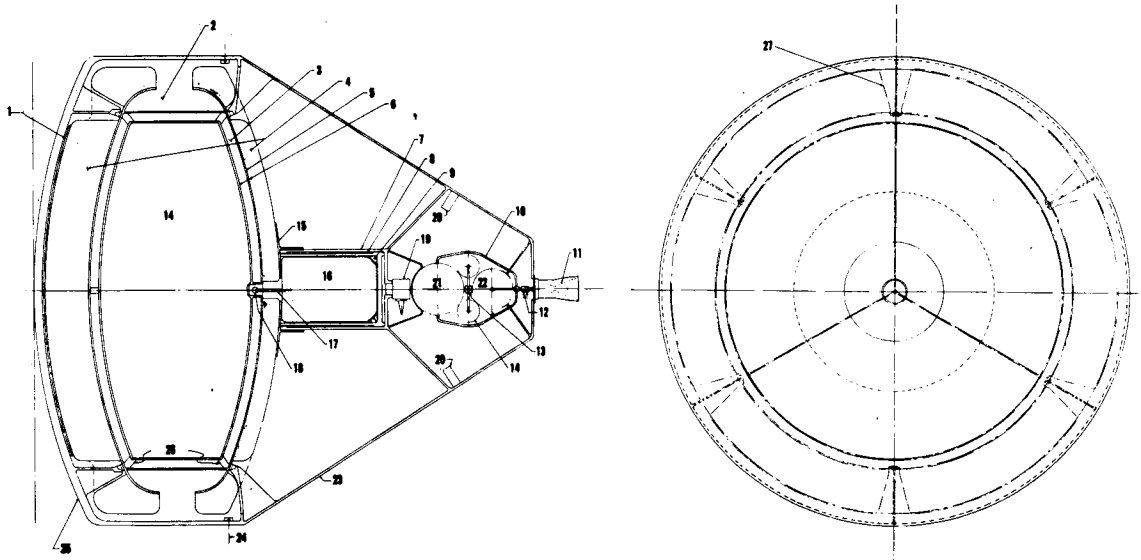

1. BASE PLT. FOR LOAD DISTRIBUTION
2. STOWAGE CAVITY FOR DEPLOYABLE INSTRUMENTATION
3. VACUUM & SUPER INSULATION
4. CRUSH-UP
5. VACUUM CASE (STRUCTURAL)
6. STRUCTURAL BOX
7. CANISTER
8. CAPTIVE SABOT
9. CLOTH BAG TIE-DOWN TO SABOT
10. LIQUID PROPELLANT MOTOR
11. THRUST CHAMBER
12. VALVES
13. PRESSURE REGULATOR
14. PRESSURANT (2)
15. LOAD DISTRIBUTION PLATE FOR CHUTE
16. PARACHUTE IN CLOTH BAG
17. PARACHUTE ATTACHMENT LINE
18. LANDER ATTACHMENT EYE
19. GAS GENERATOR
20. OMNI ANTENNA
21. OXIDIZER
22. FUEL
23. UPPER PORTION OF HEAT SHIELD
24. HEAT SHIELD SEPARATION PLANE
25. LOWER PORTION OF HEAT SHIELD
26. SPACERS
27. AXIAL AND LATERAL SUPPORT BRACKETS (6 ABOVE & 6 BELOW ENCLOSED INST. BOX)

63-9764

Figure 194 DIRECT - ENTRY VENUS LANDER CROSS SECTION SHOWING INTERNAL PACKAGING (W ENTRY = 1100 POUNDS)

with respect to the terrain. Several omnidirectional antennas are placed around the landed vehicle periphery, allowing communication with the orbiter regardless of final lander attitude.

Analysis of soil samples is accomplished through the use of an extendable sample acquisition device. A thermal lock is used to allow samples to be carried into the temperature-controlled interior of the instrument box for spectroscopic analysis.

TABLE 37

WEIGHT SUMMARY

VENUS LANDER, REFERENCE DESIGN

$M/C_DA = 0.6$ $V_E = 38,000$ ft/sec			Weight (pounds)
Total lander weight (on orbiter)			1219.4
Sterilization can and micrometeorite shield aluminum cover sheets and foam metal core		105	
Spin rocket system 4 solid rockets at 90 degrees, Δrpm = 10		2	
Main propulsion system Bipropellant liquid system I_{sp} = 315 seconds, λ_p = 0.7, ΔV = 100 ft/sec Propellant weight (including residuals)		12.4	
Entry weight (7.0-foot diameter)			1100
Heat shield material 5026 (1.8-inch t on nose cap) γ_e = -10 degrees worst condition		303	
Heat shield bond - HT-424 bonding compound		58.5	
Substructure - aluminum honeycomb (γ_e = -90 degrees, 340 g's)		264	
Parachute suspended weight			474.5
Parachute (50 ft/sec impact velocity, 12.9-foot diameter)		61.5	
Impact attenuation - stainless steel honeycomb, crushup pads		15.0	
Payload capsule structure-titanium sheet, stiffened		75.0	
Internal capsule structure (Dewar flask) aluminum sheet		35.0	
Thermal control system (internal)		35.0	
Residual weight (power supply, communications scientific experiments)			253.0
Power supply and communications		177.0	
Multiplex encoder	7.0		
Low-speed recorder	7.0		
VHF transmitter	12.0		
VHF transmitter	12.0		
S-band command receiver	4.0		
VHF omnidirectional antenna (heat shield)	3.0		
VHF loaded slot antenna (landed)	3.0		
S-band slot antenna	3.0		
Central programer and sequencer	3.0		
Power conditioning	6.5		
Battery	111.5		
X-band altimeter	5.0		
Science Payload		76.0	
Advanced mass spectrometer	20		
Emission spectrometer	12.0		
Temperature sensor	0.5		
Pressure sensor	0.5		
Atmospheric density sensor	1.5		
Television camera (descent and surface pictures)	17.0		
Surface sample acquisition subsystem	12.0		
Light scattering experiment (local source)	5.0		

9. DESCENT SYSTEM DESIGN

9.1 System Requirements

1. Orbital entry. The orbital entry case must allow the vehicle to descend slowly in such a way transmission of data to the orbital vehicle can be accomplished. Material selection of the drag device must be compatible with the transmitting antenna. Since deployment occurs at very high altitudes, the use of a parachute of HT-1 material may be acceptable. This parachute would very likely be destroyed at lower altitudes where the ambient temperature is high.

Deployment as early as possible is desirable to sample the cloud layer. Hence, supersonic deployment is desirable.

2. Direct entry((Figure 195). In the case of direct entry, where landing is desirable, the use of a ballute system appears attractive. This follows as a result of the higher temperature capabilities of a ballute system. However, a weight penalty is associated with the use of these high-temperature devices.

9.2 Reference

As a result of joint studies by Avco RAD and Northrop Ventura Division, a ballute was selected for the descent system due to the high ambient temperature (between 700°K and 840°K) at or near the surface of the planet. The high atmospheric density of Venus at lower altitudes permits the use of a relatively small device (ballute) to provide an acceptable descent velocity. A discussion of other system possibilities considered and a detailed description of the selected system are presented in themechanical design section and in appendix A.

Sensing for the ballute deployment could be accomplished with a single setting accelerometer. The setting would be determined by a minimum Mach number requirement due to vehicle dynamic characteristics for the normal entry trajectory. For shallow entries, the setting would cause deployment at higher Mach numbers. At this time, the deployment Mach number range being considered (M = 2.0 to 6.0) seems to be well within the capabilities of the ballute system.

9.3 Materials Reference

1. Introduction. A parachute descent through the Venusian atmosphere requires a fabric possessing extremely high-temperature resistance, since temperatures of roughly 800°F may be encountered. Nylon, with its low-melting

2. PLANET'S ATMOSPHERE TURNS CAPSULE INTO CORRECT ATTITUDE FOR ENTRY.

3. AFT COVER EJECTED BY PILOT CHUTE DEPLOYMENT PROJECTILE

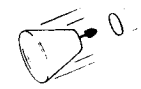

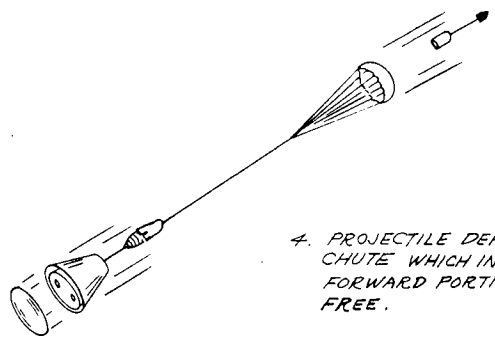

4. PROJECTILE DEPLOYS HEMISFLO PILOT CHUTE WHICH IN TURN DEPLOYS BALLUTE. FORWARD PORTION OF HEAT SHIELD FALLS FREE.

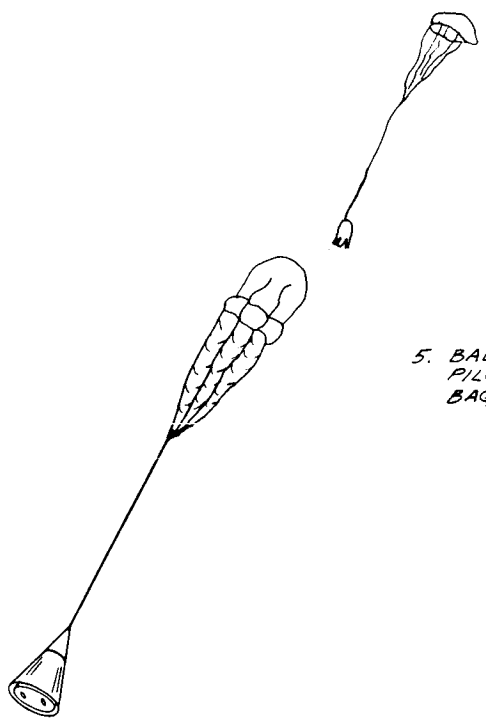

5. BALLUTE DEPLOYS & INFLATES - PILOT CHUTE WITH EMPTY DEPLOYMENT BAG FALLS FREE.

Figure 195 DIRECT ENTRY BALLUTE SYSTEM

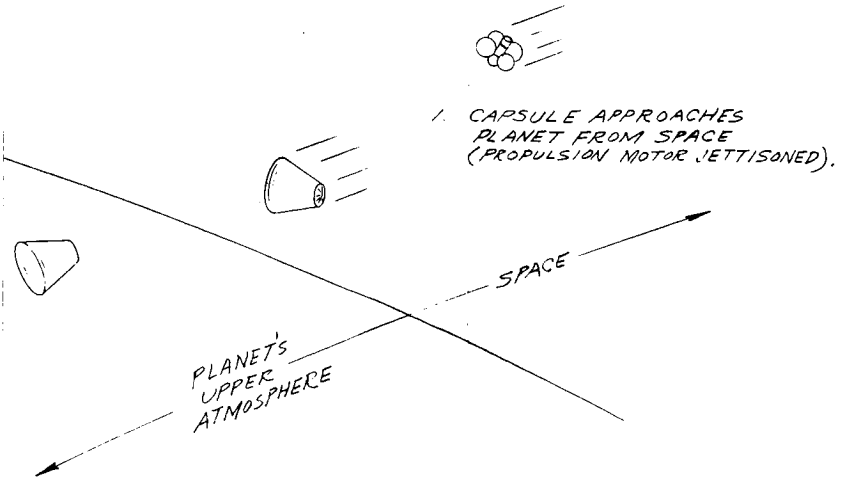

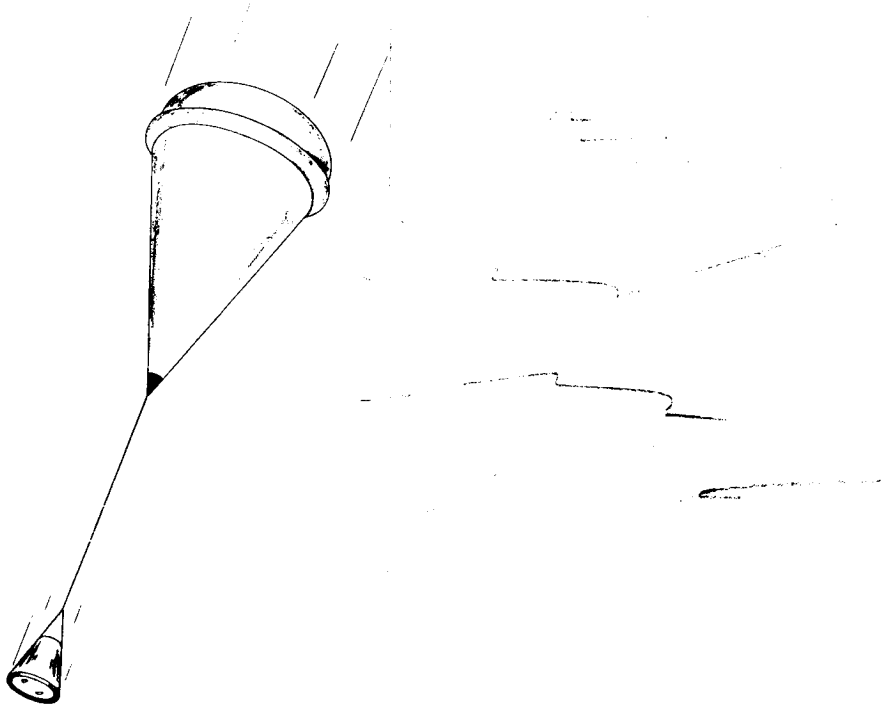

6. BA'LUTE FULLY INFLATED-
FINAL DESCENT

point near 400°F is obviously unsatisfactory. HT-1 fabric would be at best marginal. A new family of polymeric materials has recently been developed that may possess sufficient high-temperature stability. If additional information indicates that these fibers are still unsatisfactory, fabrics made from metal filaments may be used.

2. Organic fibers. Polybenzimidazole fibers have been produced with good strength retention at temperatures up to over 650°F in air. Some strength is retained after 1 to 2 hours aging at 750°F. More thermally stable fibers can be made from the polyoxadizoles (ref. 39). Figure 196 illustrates the thermal stability of a polyoxadizole fiber in air and nitrogen at 750°F. The higher strength retention in air is probably due to an oxygen induced crosslinking mechanism, resulting in a stronger but more brittle fiber. At 840°F, the samples degraded and partially carbonized under both atmospheres. It is concluded, therefore, that temperatures near 800°F may be the maximum use temperature for these fibers.

3. Metal filaments. Fabrics made from filaments of many high temperature metals have been woven. These metals include the super-alloys, such as Rene 41, Udimet 500 and 700, M-252, Waspalloy, Hastelloy, Inconel, Karma, Chromel R, and others. Strength versus temperature studies (ref. 40 and 41) indicate that these metals are relatively similar in high-temperature tensile behavior. Hot strengths of approximately 20,000 psi at 2200 °F were obtained for several fibers. Strengths of at least 120,000 psi were obtained at 800°F, which were nearly equal in most cases to room-temperature strengths. Therefore, the strength of the metal filament fabrics at 800°F should be adequate for parachute material. The ductility of these fibers varies considerably between materials, ranging from 1 to 30 percent at room temperature. Rene 41 (1-mil diameter) has a ductility of 26 percent at room temperature, 36 percent at 1500°F, and 8 percent 2000°F. Hastelloy X retained 17.6-percent ductility at 2200°F (but possessed only 13,000-psi tensile strength). The ductility and modulus of the fibers will govern the ability of the fabrics to be conveniently packaged in the lander without damage. Avco RAD has conducted studies on the use of metallic fabrics for decelerator purposes (ref. 42). Rene 41 wire (1.6-mil diameter) was woven into a plain weave 200 by 200-mesh cloth, demonstrating the practicability of super-alloy filament cloth. Methods for welding the wire cloth to itself and other structural members were developed.

The cloth was coated with a flexible, thermally stable, filled silicone to reduce the porosity of the cloth.

For environmental temperatures in excess of 800°F, it is probable that the coated wire-cloth materials will be sufficiently developed in the near future to serve as the parachute for the Venus lander.

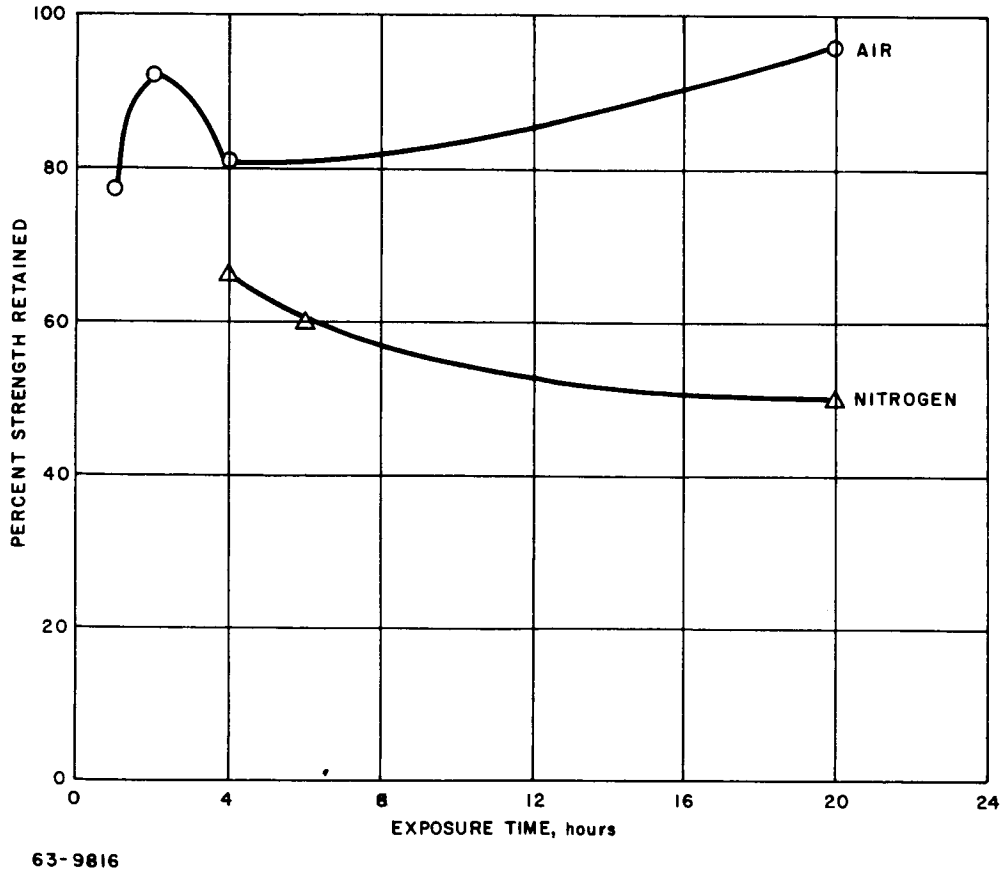

Figure 196 PERCENT STRENGTH RETAINED VERSUS TIME OF POLYOXADIAZOLE FIBERS IN AIR AND NITROGEN AT 750°F

10. AERODYNAMIC DESIGN -- VENUS

10.1 Entry Concepts

1. Atmospheric models. The limiting atmospheres which were used for the Venus entry study are those specified Kaplan (ref. 43) as the "maximum temperature" atmosphere ("K max T") and the "standard temperature" atmosphere ("K std T"). The atmospheric parameters utilized for input into trajectory and heating programs are presented in table 38. Two other atmospheres which were examined are similar to Kaplan's except for the assumed gas composition. These also are noted in the table and were used to determine entry radiative heating as a function of gas composition.

2. Trajectories. There are several lander-system requirements which are directly influenced by the atmospheric models. One of these requirements is the scientific goal of adequate measurement of the atmosphere and cloud layer. Thus, it is desired to deploy a deceleration device of some type as near the top of the cloud layer as possible in order that the vehicle will rapidly reach the low-velocity, stable descent necessary for atmospheric sampling. If the top of the cloud layer is assumed to lie at the tropopause of Kaplan's models, it is found that the relatively low-density stratosphere makes it very difficult for a vehicle to decelerate sufficiently for a drag device deployment before entry into the cloud layer. When the vehicle M/C_DA is lowered in an effort to achieve the necessary deceleration, the vehicle dimensions approach limits set by interface requirements.

The system requirement of high reliability also would be affected by any major portion of the high-velocity portion of flight occurring in the cloud layer. Little is known of heat shield performance of a vehicle traveling at high velocities through a cloud layer where turbulence and particles could damage the heat shield.

The cloud-layer top is assumed to lie at the tropopause which, for the atmospheric models utilized, is at an altitude of approximately from 320,000 to 420,000 feet. The altitude at which an aerodynamic decelerator can be deployed is a function of vehicle ballistic coefficient, entry angle, and atmospheric model and is relatively insensitive to entry velocity. Figure 197 indicates a drag device deployment altitude (assuming deployment at Mach = 2.5) for a γ = -90-degree entry as a function of M/C_DA. It is noted that the atmospheric model which provides the greatest deceleration at altitude also has the highest tropopause altitudes. The deployment altitude only begins to approach the tropopause at very low values of M/C_DA for each of the limiting atmospheres. The problem can be relieved somewhat by restriction of the entry angle (figures 198 and 199), although very low angles are required to produce a significant variation in deployment altitude.

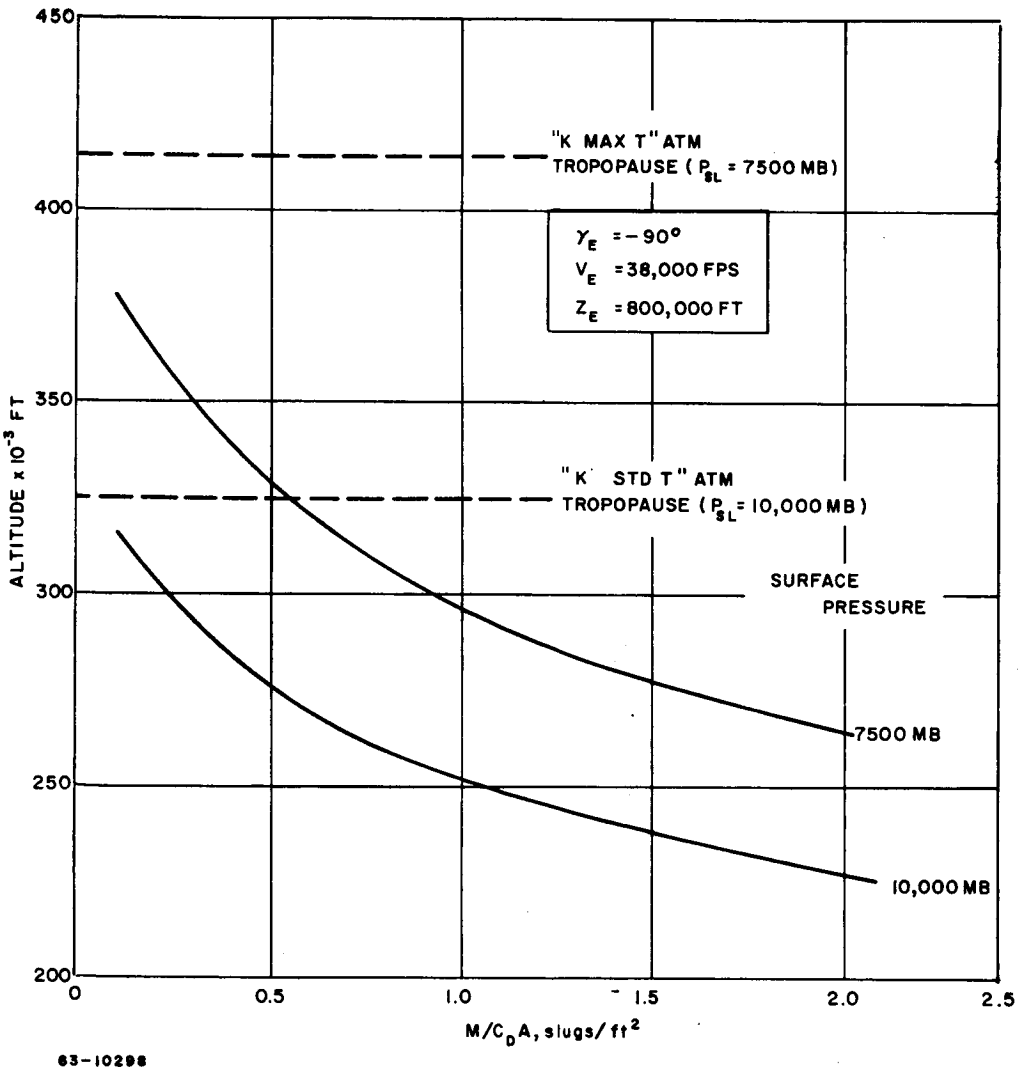

Figure 197 VENUS ATMOSPHERIC ENTRY: ALTITUDE AT M = 2.5 VERSUS VEHICLE M/C_DA

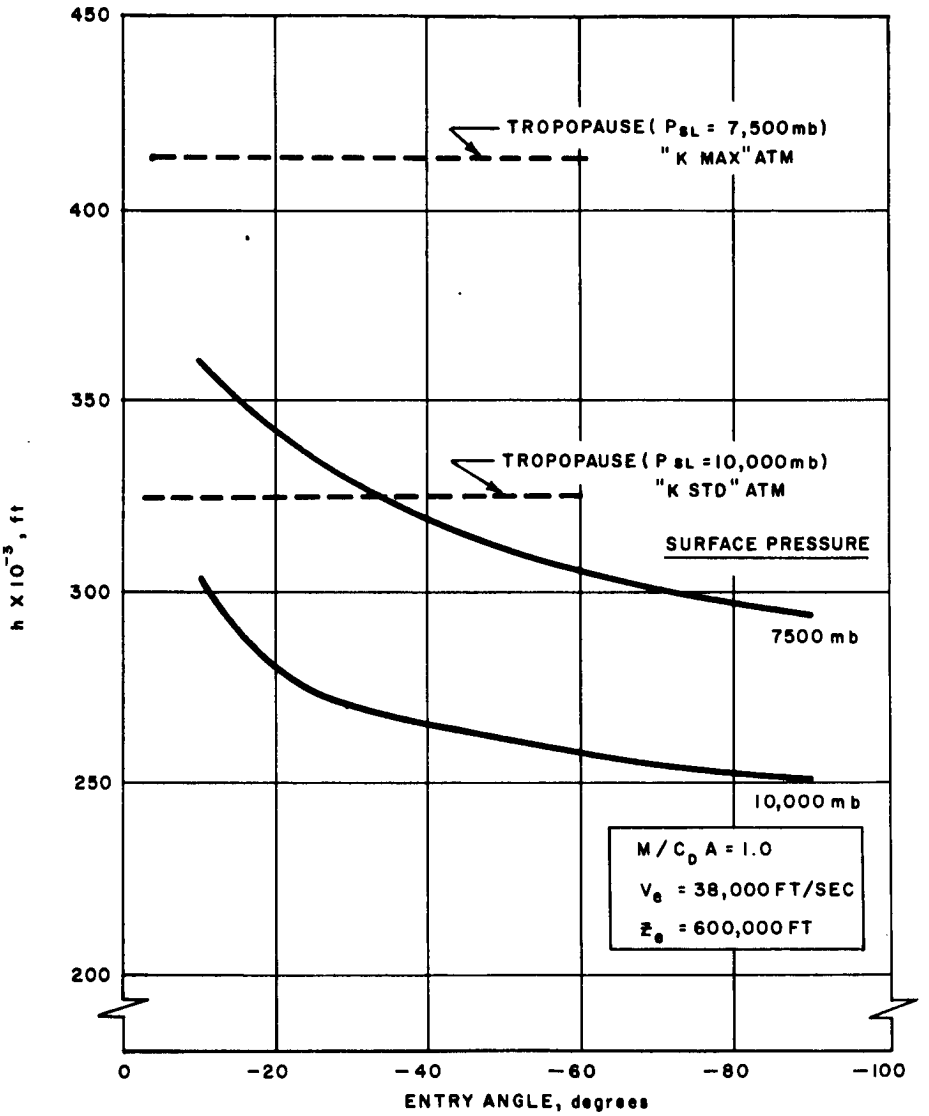

Figure 198 VENUS ENTRY: ALTITUDE AT M=2.5 VERSUS VEHICLE M/C_DA

63-9815

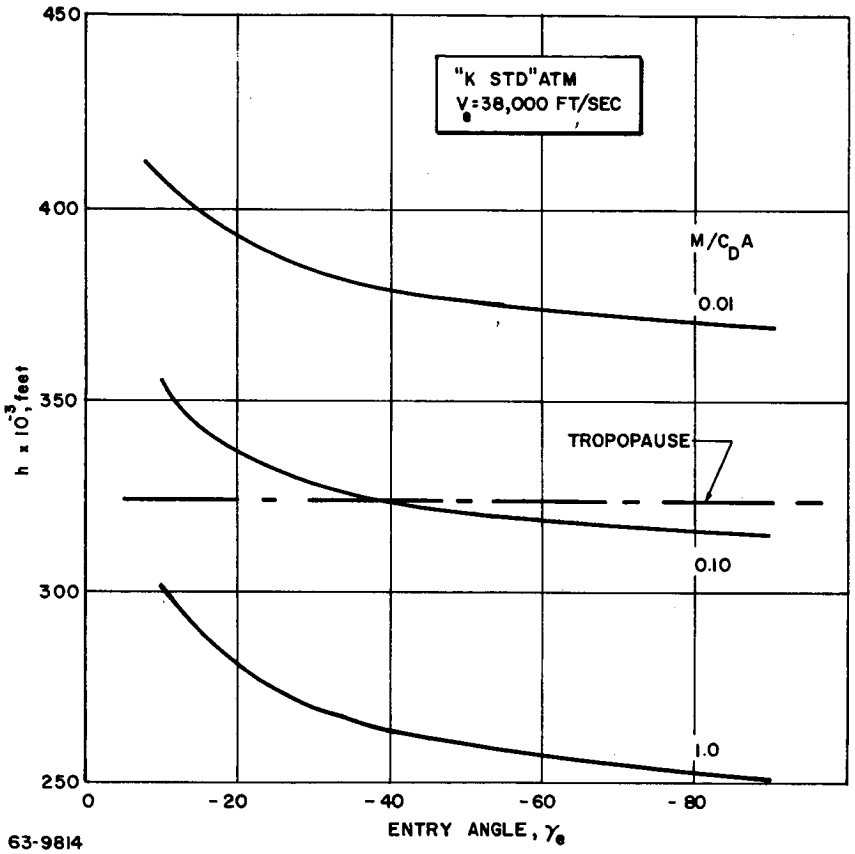

Figure 199 VENUS LANDER ALTITUDE AT M = 2.5 VERSUS ENTRY ANGLE

For a vehicle entering from orbit, the required deceleration is attained near the tropopause, as shown in figure 200, primarily because of the shallow entry angles.

3. Reference concepts. As a result of the scientific goals and due to the severity of the entry problem, two entry concepts were investigated: (1) a relatively low M/C_DA vehicle entering directly, and (2) a small vehicle entering from orbit.

10.2 Reference Designs

Two reference design were selected for the Venus study: (1) a small orbital entry vehicle, and (2) a larger direct entry vehicle.

1. Orbital entry vehicle. The Apollo shape (see figure 201) waschosen for this concept primarily for the blunt, low M/C_DA shape and the weight-saving conical afterbody. The required weight of 85 pounds and volume of the necessary instrumentation and communication package were the prime factors in the selection of the ballistic coefficient of 0.5 slugs/ft^2.

As shown previously (figure 200), the orbital entry concept allows deployment of an aerodynamic decelerator at or near the tropopause permitting measurement of the entire cloud layer. Also, the problem of significant heating rates while passing through clouds is avoided.

2. Direct entry vehicle. A modified V-2 vehicle (see figure 202)was selected to investigate the possibilities of using the same basic lander vehicle for both Mars and Venus entries. Heat shield and structure weights increase due to the more severe entry environment, but the required payload weight is decreased because of required lower scientific mission weights compared to the Mars mission. The net result is a total entry weight of 1100 pounds and a M/C_DA of 0.6 slugs/ft^2. The ballistic coefficient is a compromise between the very low M/C_DA required for parachute deployment at the cloud-layer top and the more efficient payload capabilities of higher M/C_DA vehicles.

Assuming a deployment of an aerodynamic decelerator at Mach numbers of 2.5 and above, the minimum deployment altitude for this concept is about 280,000 feet which is approximately 40,000 feet into the cloud layer (Kaplan's "standard temperature" atmosphere). The major portion of the heating pulse occurs above the clouds.

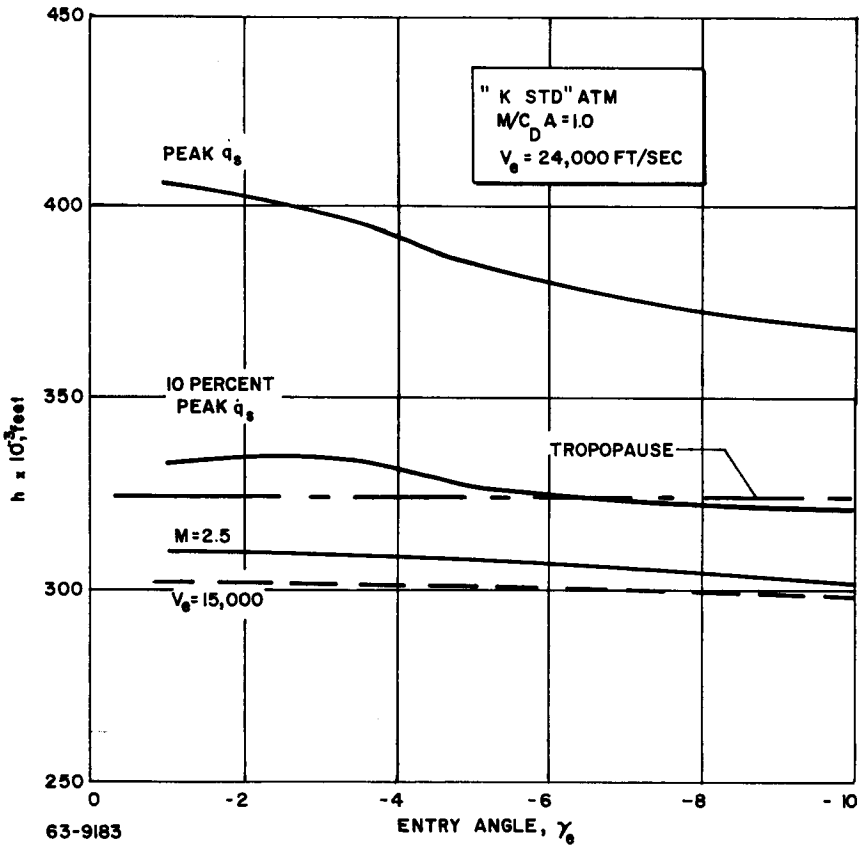

Figure 200 VENUS ORBITAL ENTRY: ALTITUDES AT PEAK HEATING, END OF HEATING PULSE, AND TYPICAL PARACHUTE DEPLOYMENT

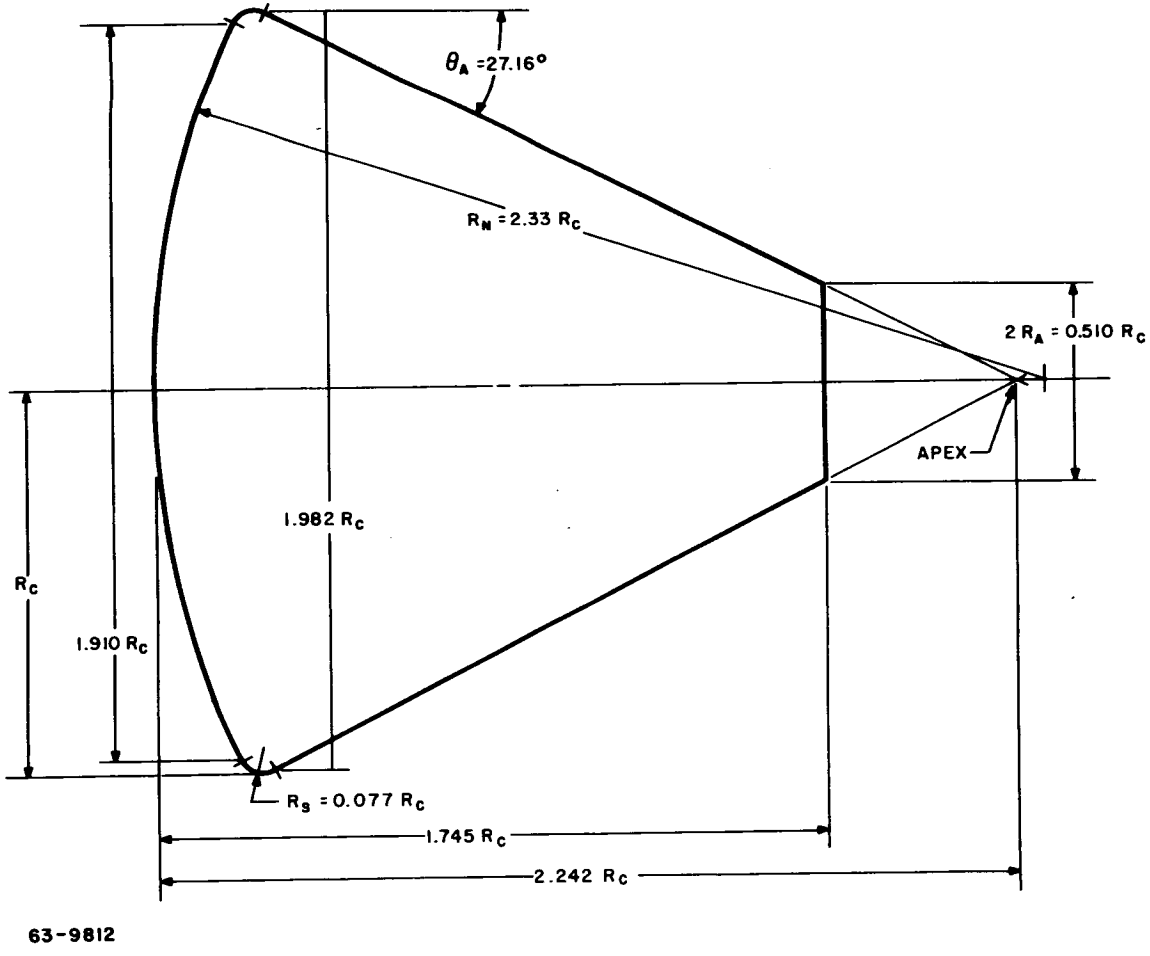

Figure 201 VOYAGER APOLLO-TYPE ENTRY VEHICLE (VENUS ENTRY FROM ORBIT) CONFIGURATION

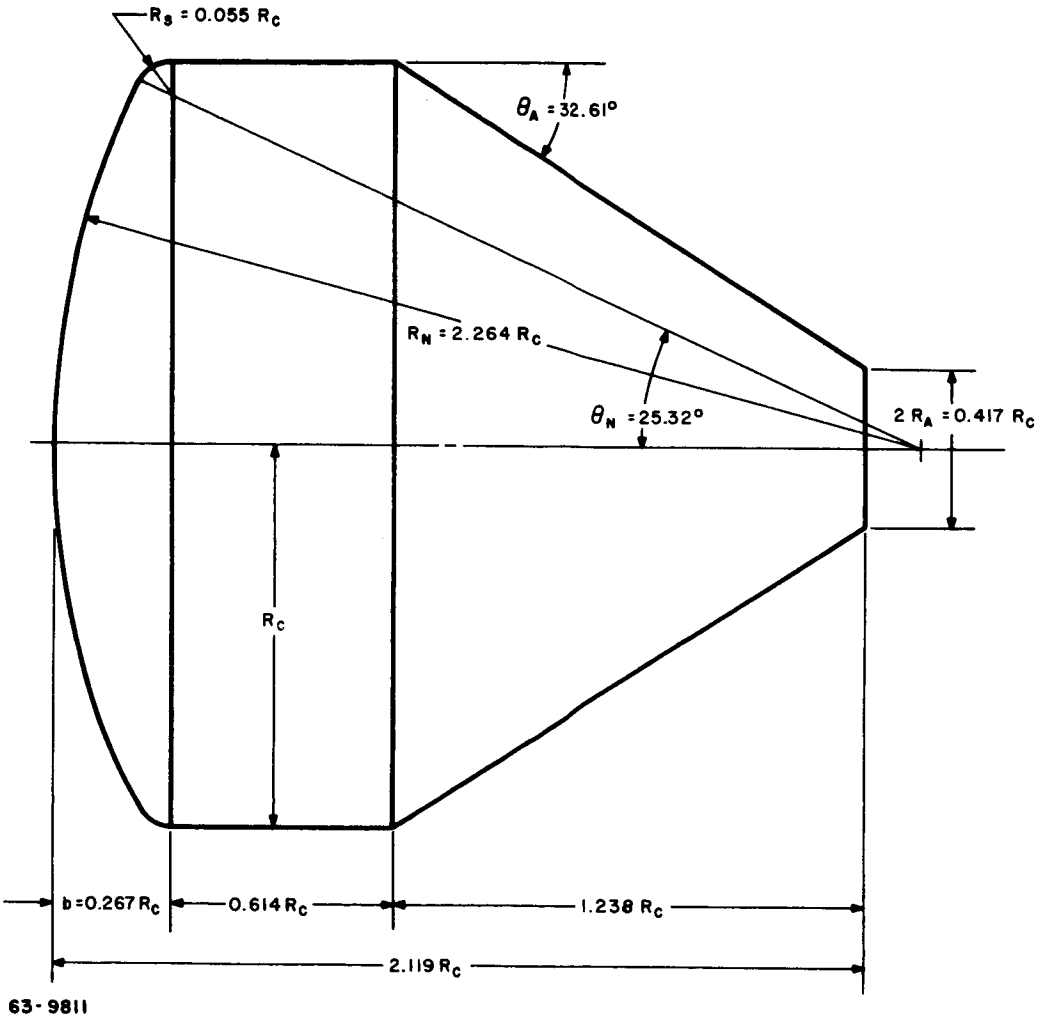

Figure 202 VENUS DIRECT ENTRY VEHICLE CONFIGURATION

TABLE 38

VENUS ATMOSPHERES

Models	M	T_{sl}	ρ_{sl}	P_{sl}	G_{sl}	L_1	L_2	X_n	X_o	X_c	T_{st}	P_{th}	ΔZ_{st}
Minimum Temperature (ref. 1)	29.62	560	15.43x10-3	26450	29.53	0.708	5.32×10^{-4}	0.90	0.0	0.10	160	6.35×10^{-3}	210,000
Standard Temperature (ref. 1)	29.62	700	9.876x10-3	21170	29.53	0.544	5.32×10^{-4}	0.90	0.0	0.10	215	6.35×10^{-3}	210,000
Maximum Temperature (ref. 1)	29.62	840	6.173x10-3	15880	29.53	0.523	5.32×10^{-4}	0.90	0.0	0.10	245	6.35×10^{-3}	210,000
Standard Temperature (ref. 2)	42.40	700	1.43x10-2	21170	29.53	0.416	5.32×10^{-4}	0.10	0.0	0.90	215	6.35×10^{-3}	210,000
Maximum Temperature (ref. 2)	28.64	840	6.036x10-3	15880	29.53	0.526	5.32×10^{-4}	0.96	0.0	0.04	245	6.35×10^{-3}	210,000

REFERENCES:

1. L. D. Kaplan, A Preliminary Model of the Venus Atmosphere. JPL Report No. 32-379, December 12, 1962.

2. NASA Presentation at RAD, April 24, 1963.

NOTE: $R_{sl} = 1.99 \times 10^7$

11. HEAT SHIELD DESIGN -- VENUS

11.1 Thermal Analysis

1. Entry heating

a. General results for direct entry. The radiative and convective heating calculations were performed in the same manner as for the Mars entry. A parametric heating study for a one-foot radius sphere was conducted with variables of entry conditions, atmospheric model, and vehicle ballistic coefficient. The results of stagnation convective and radiative heating (maximum rates and total integrated) and the ratio of integrated radiative heating to integrated convective heating are presented in figures 203 to 217. As expected, maximum heating rates increase with increasing M/C_DA, velocity, and entry angle with the high integrated heating occurring at shallow entry angles. As figures 215 to 217 indicate, the radiative contribution can be the major portion of the heating input for the higher velocity steep entries. It is noted that the ratio of radiative-to-convective heating will increase as larger blunt vehicles are considered.

Figures 218 and 219 present altitudes at peak heating and 10 percent of peak heating as a function of M/C_DA and entry angle to indicate where heat shield performance would be uncertain. For a vehicle of $M/C_DA = 1.0$ slug/ft^2 for example, it is seen that about half of the heating pulse occurs within the cloud layer for $\gamma_e = -90$-degree entry.

b. Orbital entry--reference design. The shallow entry angles and lower entry velocities for this concept result in low aerodynamic loads and heating. Figure 220 indicates a typical heating pulse, while maximum rates and integrated heating are shown in figures 221 and 222. The ratio of radiative-to-convective heating is shown in figure 223 to be relatively small for the lower entry angles.

c. Direct entry -- reference design. A typical heat pulse for the direct entry is presented in figure 224. The peak rates and integrated heating are summarized in figures 225 and 226 as a function of entry angle. Figure 227 illustrates the large radiative contribution as compared to the convective for the direct Venus entry.

2. Heat shield analysis

a. Method of calculation. The heat shield weights for the Venus lander were determined by the same methods employed for the Mars lander. The heat shield weights for the Venus lander were determined for a 600° F heat shield structure bondline temperature. The heat shield weight study for Venus was also limited to a zero angle of attack.

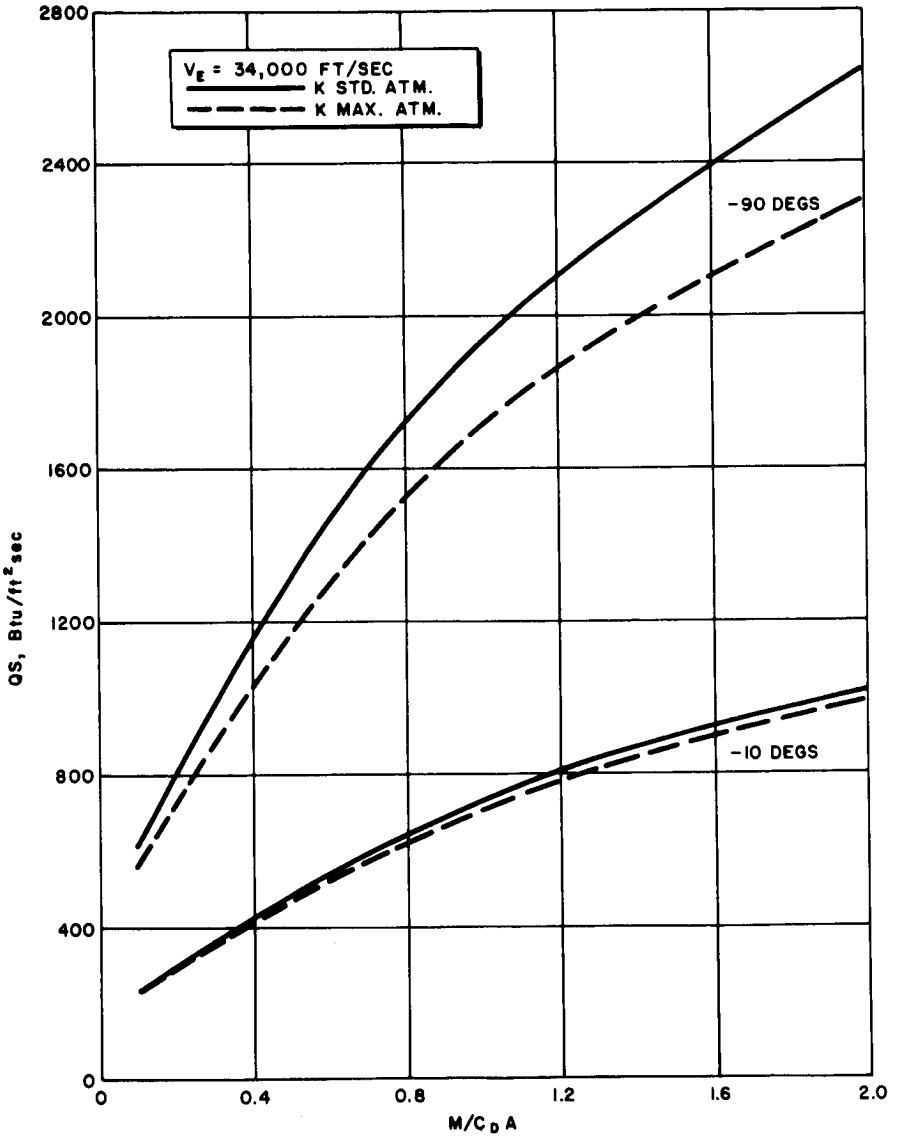

63-9810

Figure 203 VENUS ENTRY: MAXIMUM STAGNATION CONVECTIVE HEATING

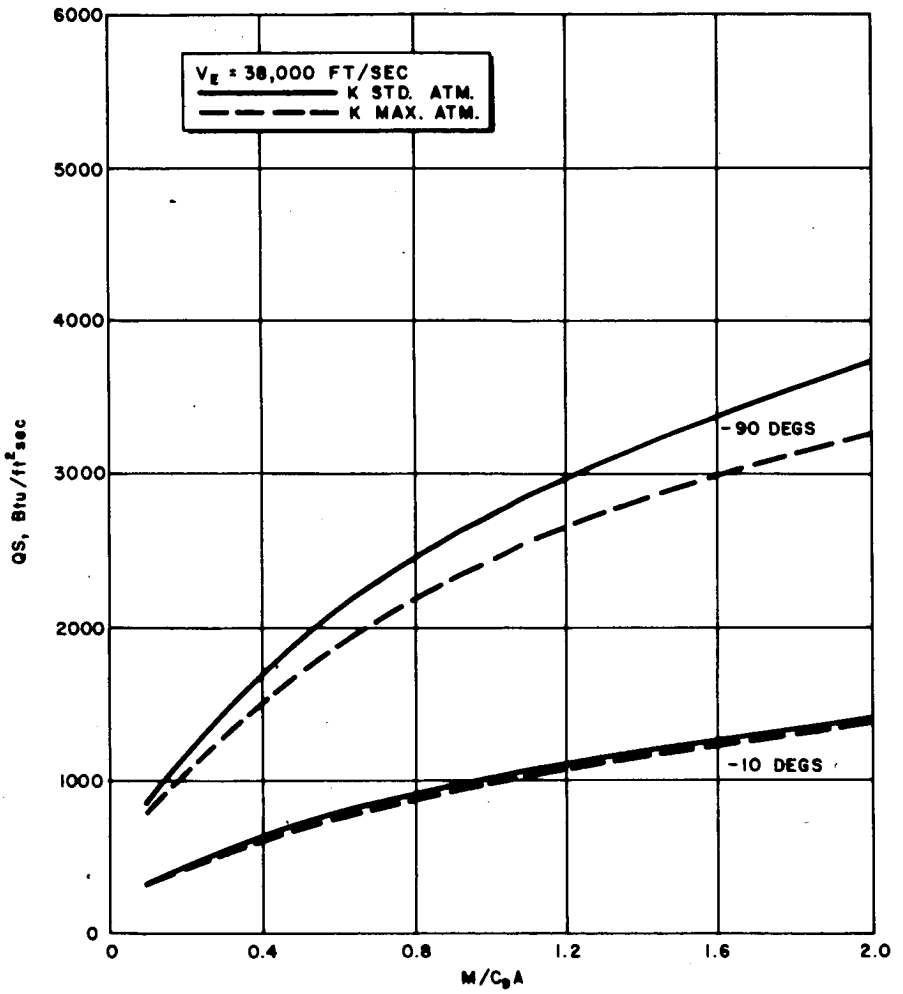

63-9809

Figure 204 VENUS ENTRY: MAXIMUM STAGNATION CONVECTIVE HEATING

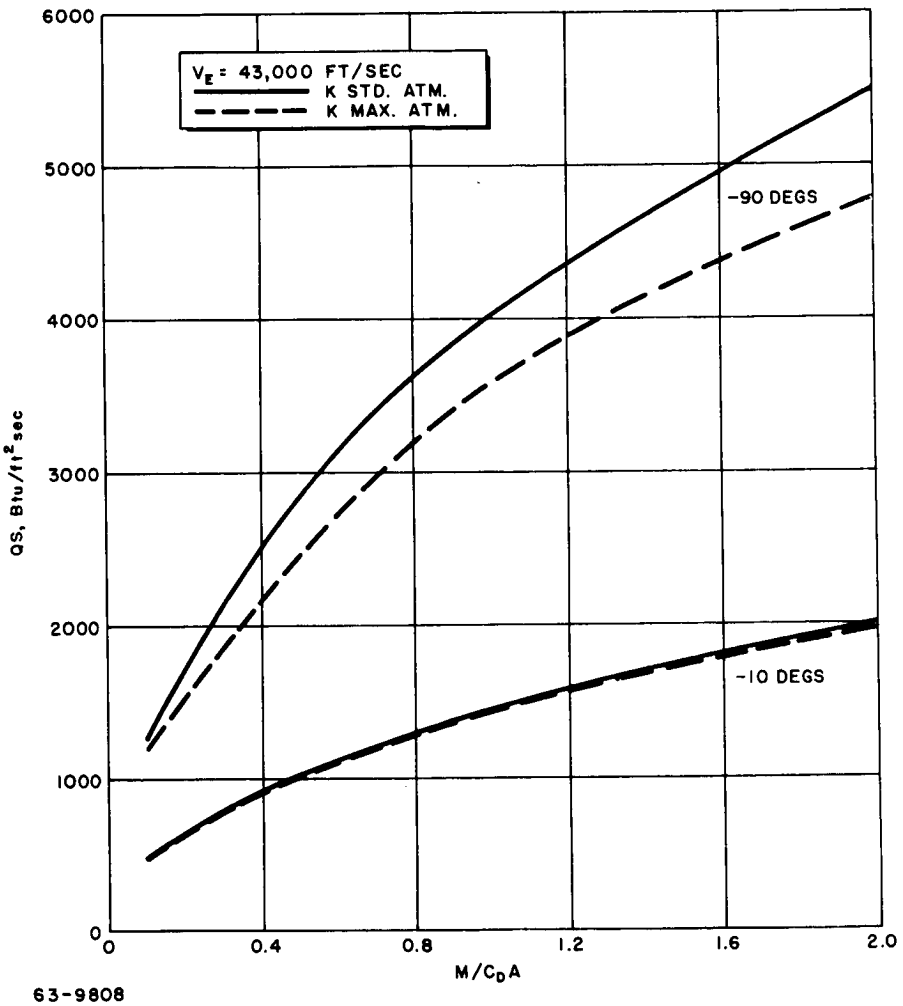

Figure 205 VENUS ENTRY: MAXIMUM STAGNATION CONVECTIVE HEATING

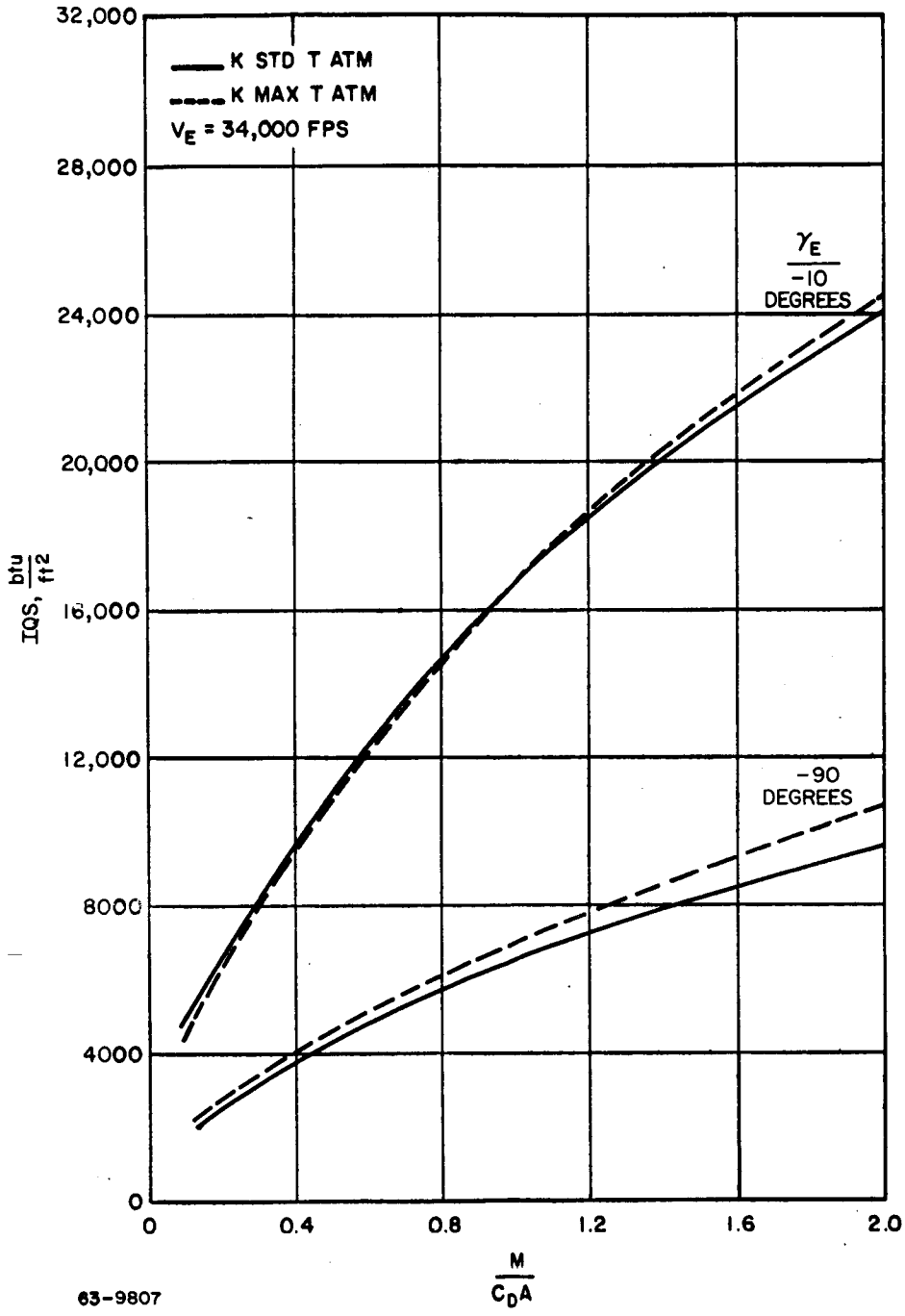

Figure 206 VENUS ENTRY: INTEGRATED STAGNATION CONVECTIVE HEATING

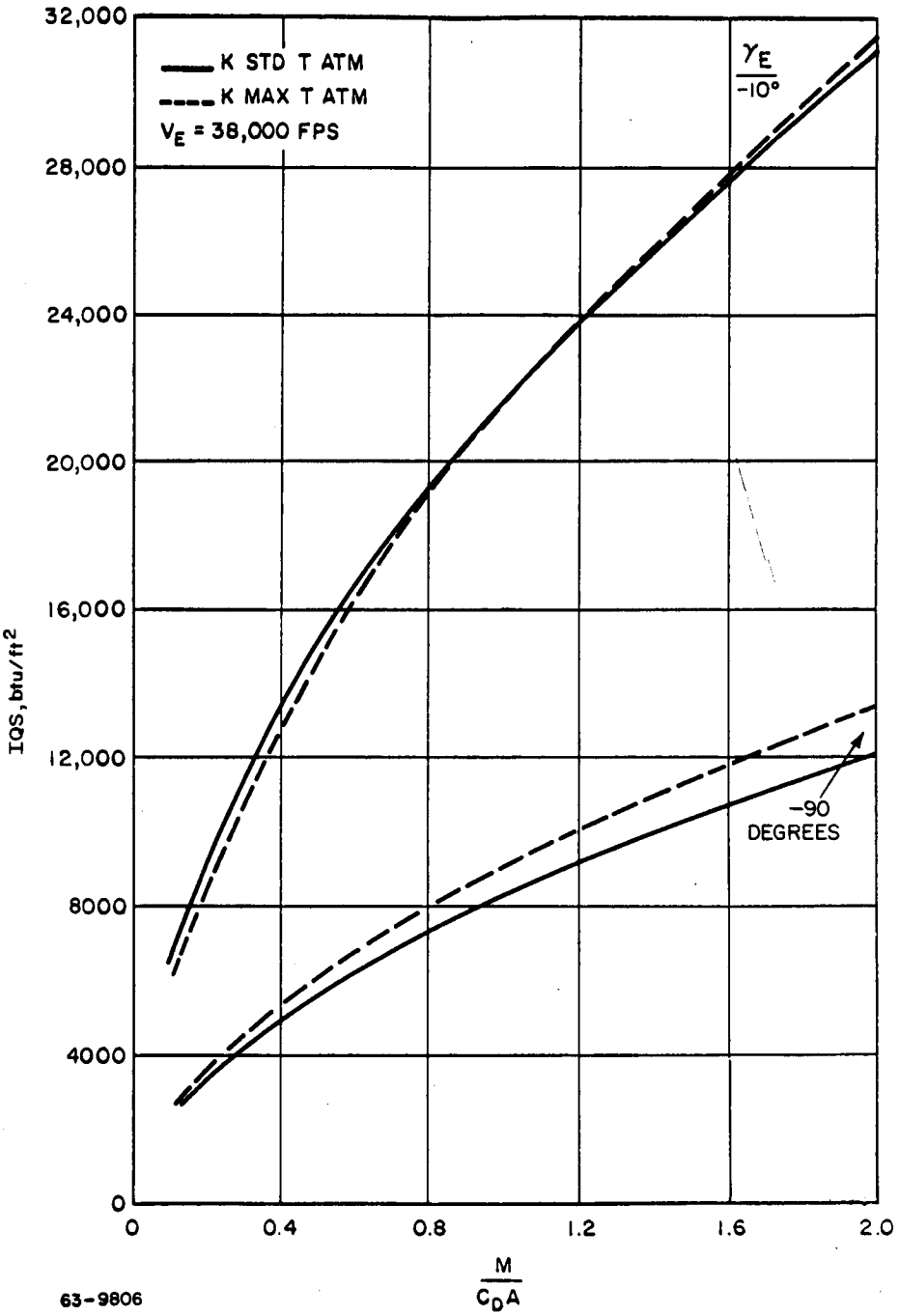

Figure 207 VENUS ENTRY: INTEGRATED STAGNATION CONVECTIVE HEATING

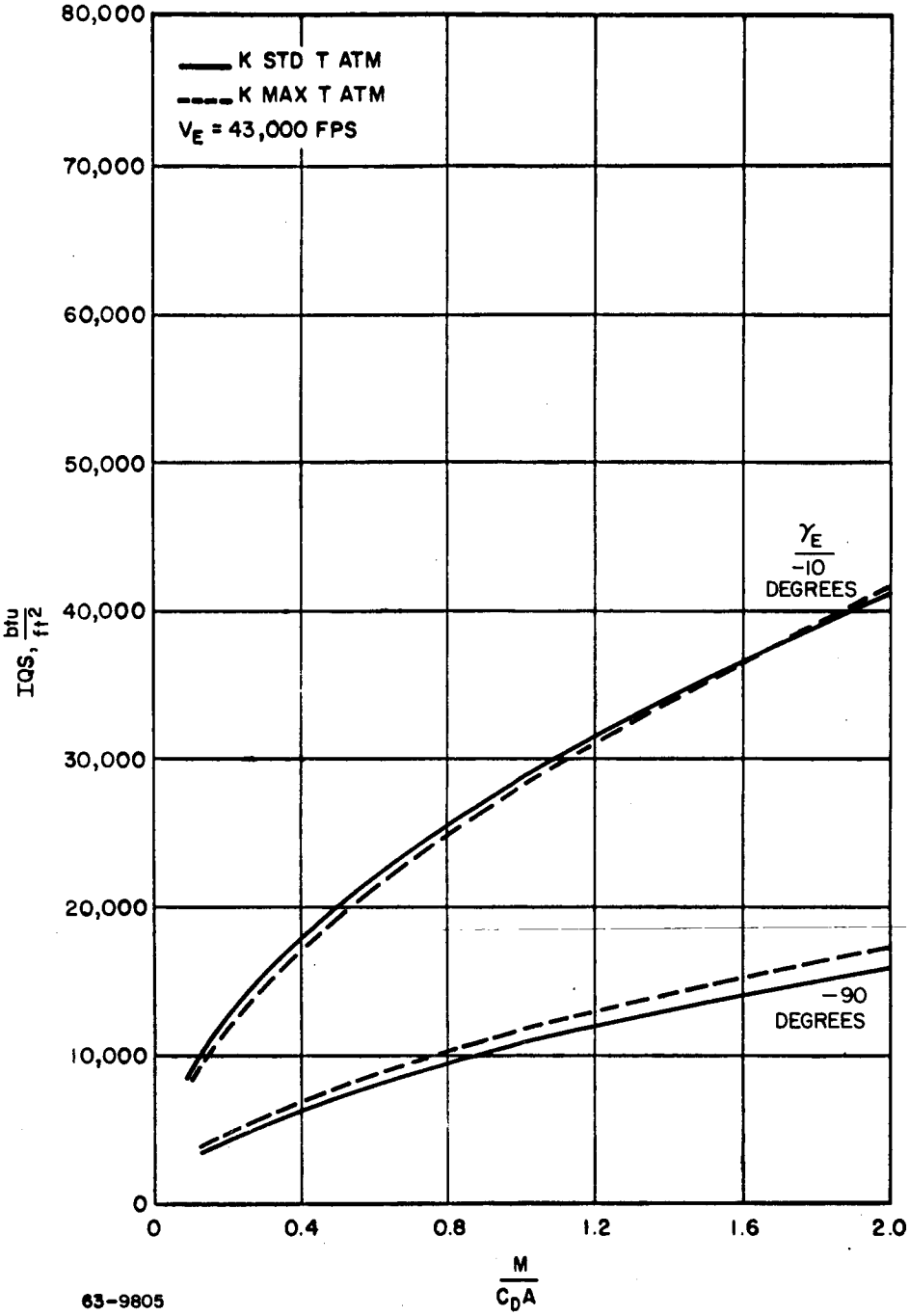

Figure 208 VENUS ENTRY:INTEGRATED STAGNATION CONVECTIVE HEATING

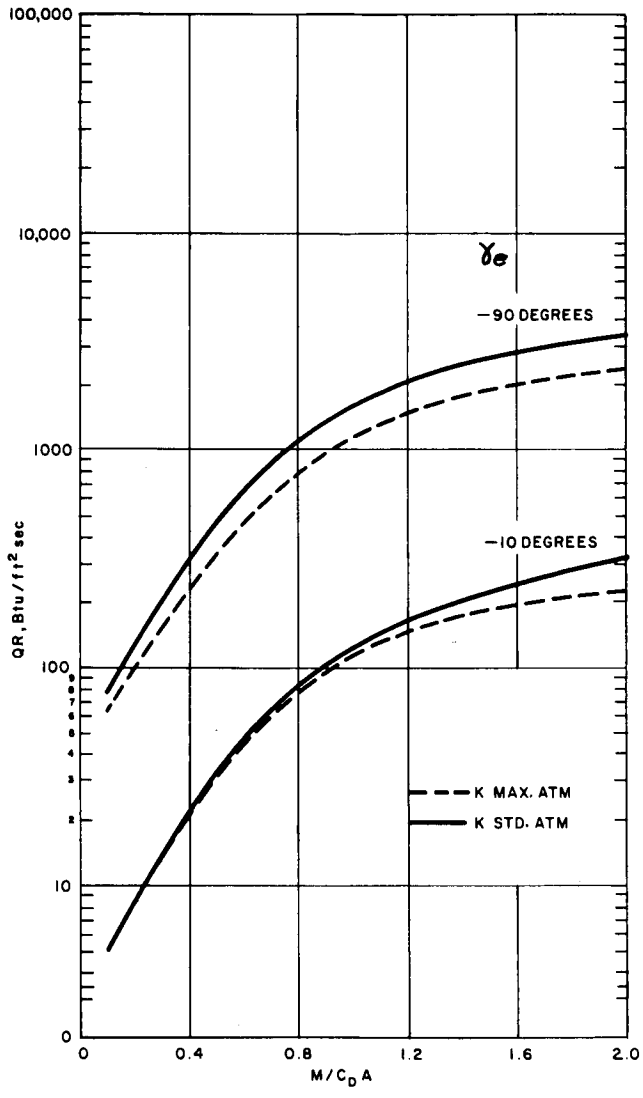

63-9804

Figure 209 VENUS ENTRY: MAXIMUM STAGNATION RADIATIVE HEATING

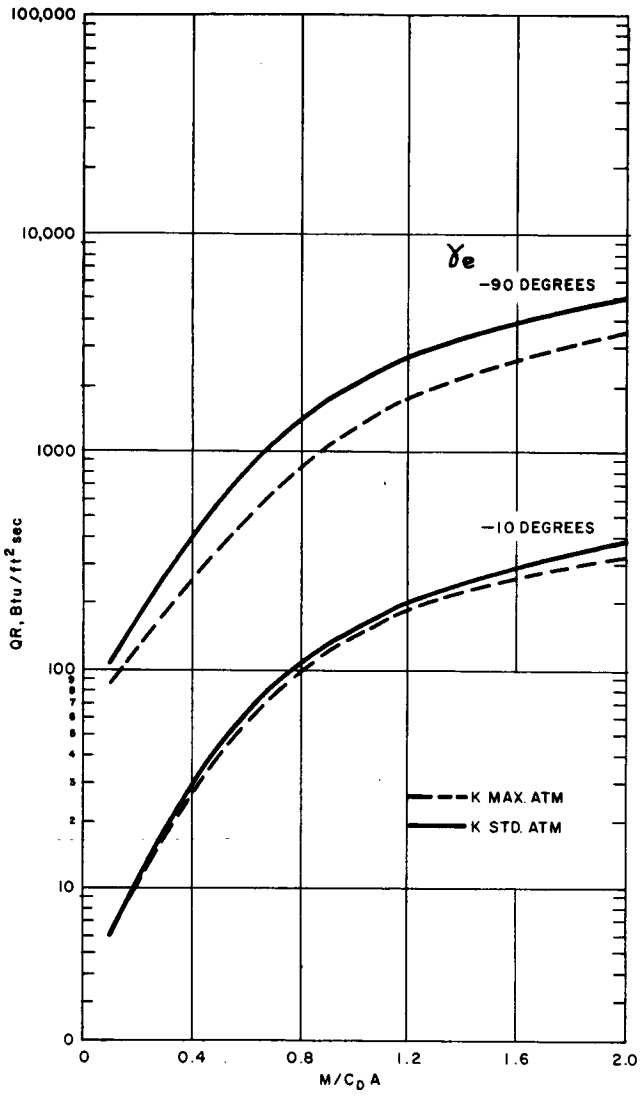

63-9803

Figure 210 VENUS ENTRY: MAXIMUM STAGNATION RADIATIVE HEATING

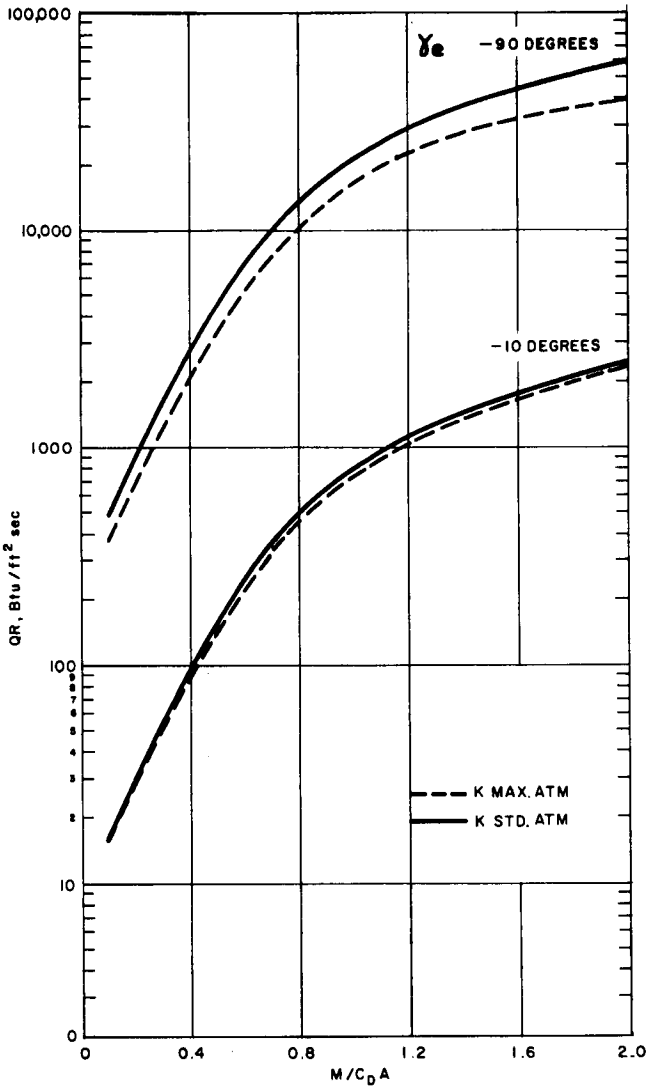

63-9802

Figure 211 VENUS ENTRY: MAXIMUM STAGNATION RADIATIVE HEATING

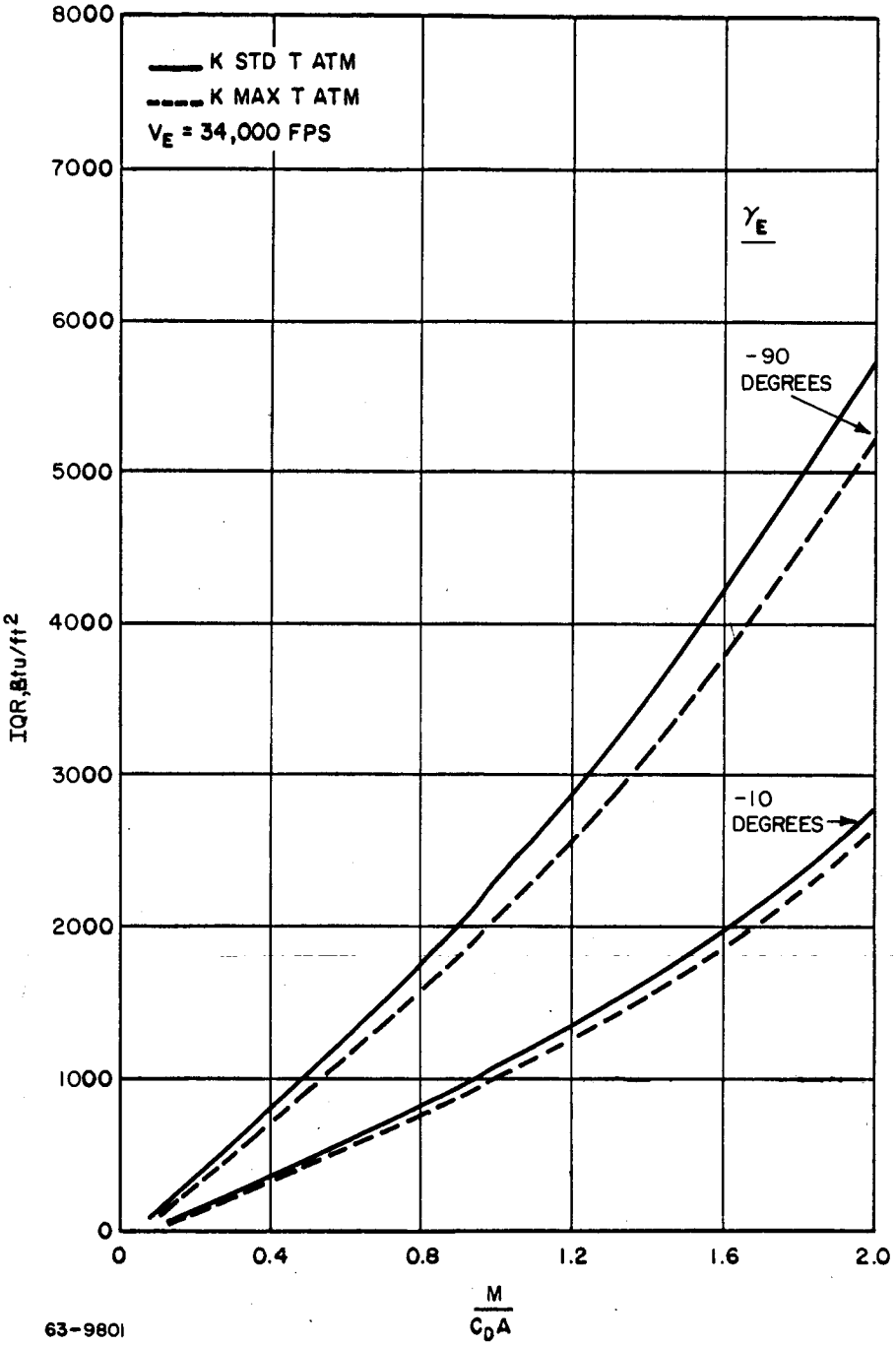

Figure 212 VENUS ENTRY: INTEGRATED STAGNATION RADIATIVE HEATING

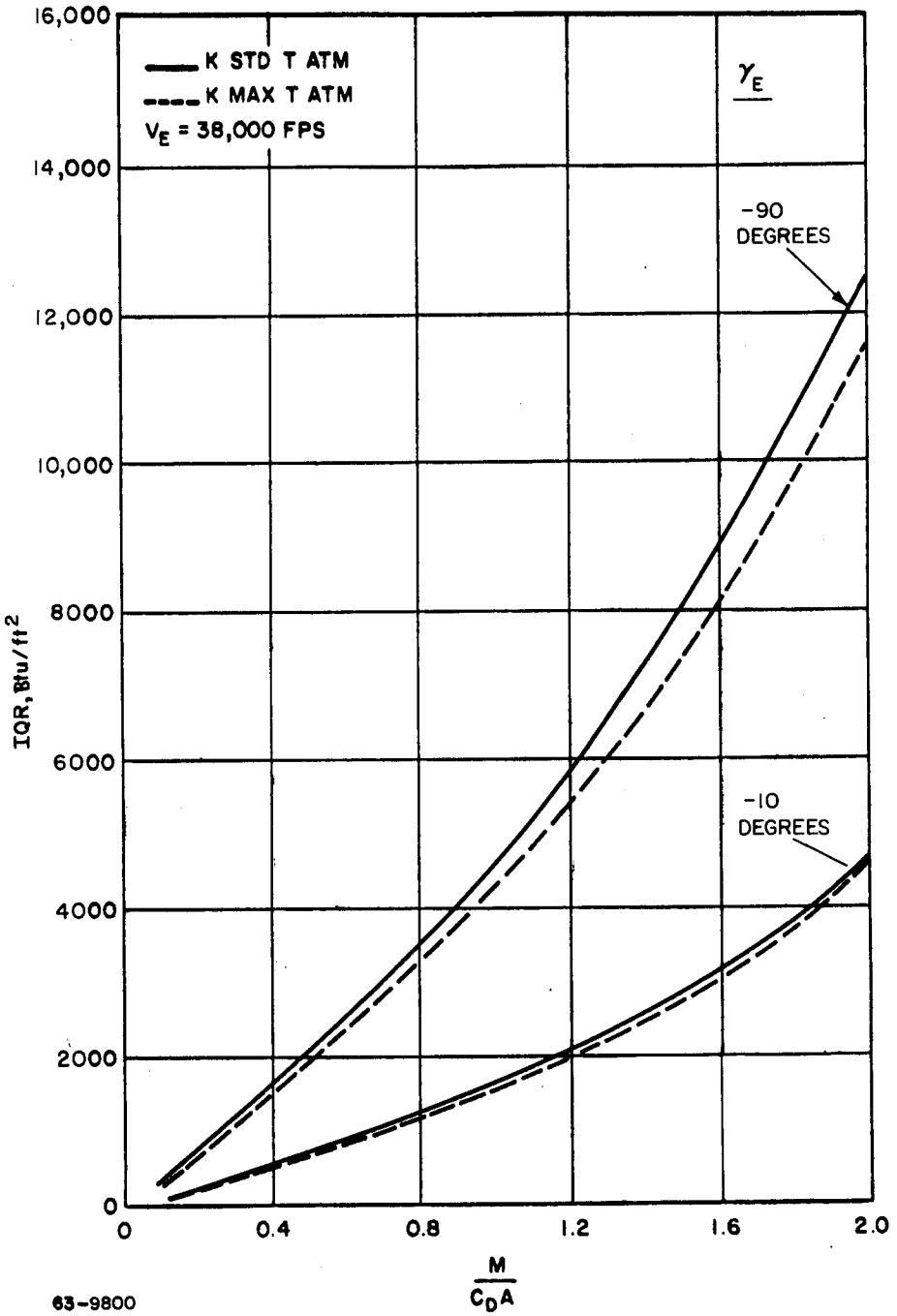

Figure 213 VENUS ENTRY: INTEGRATED STAGNATION RADIATIVE HEATING

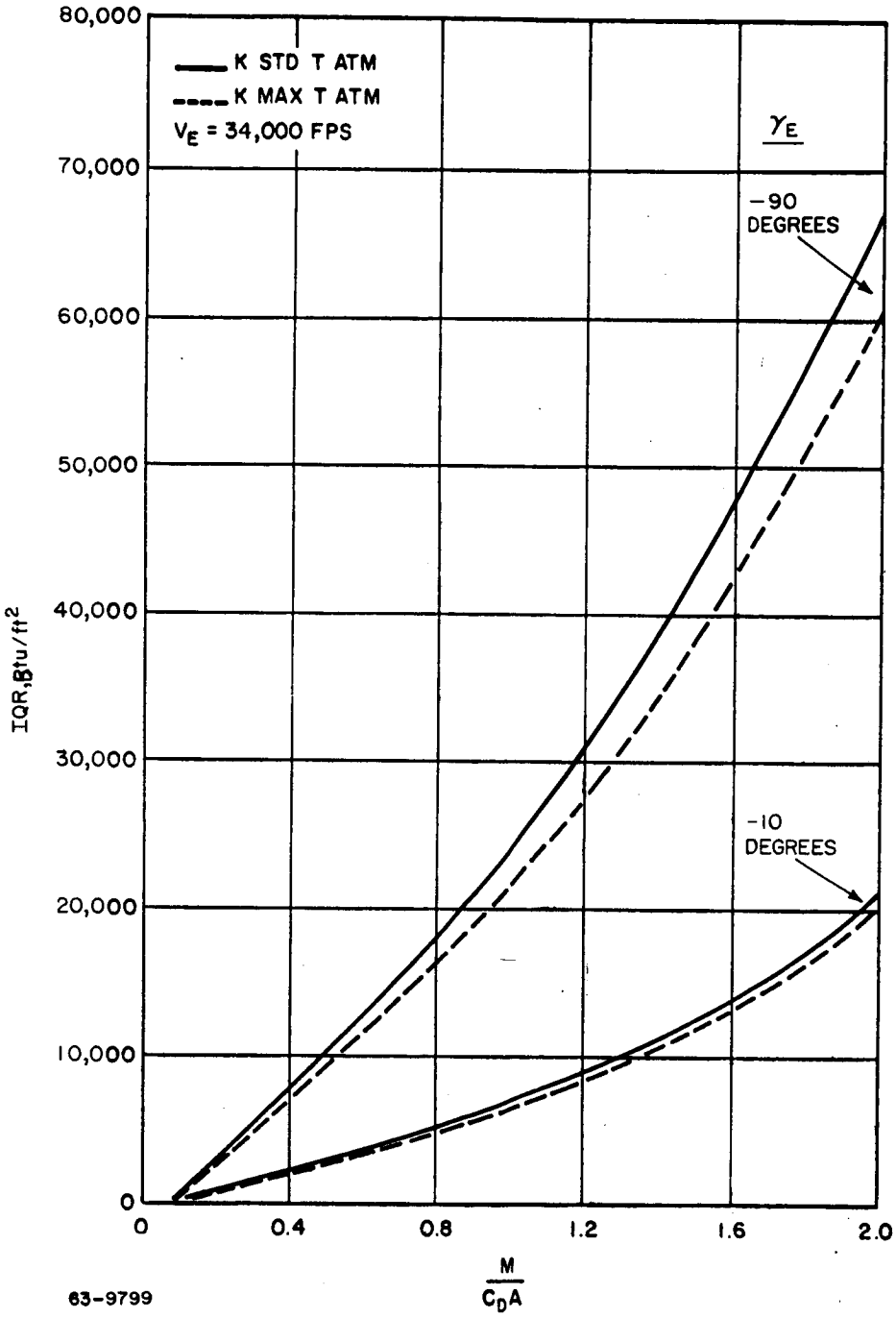

Figure 214 VENUS ENTRY: INTEGRATED STAGNATION RADIATIVE HEATING

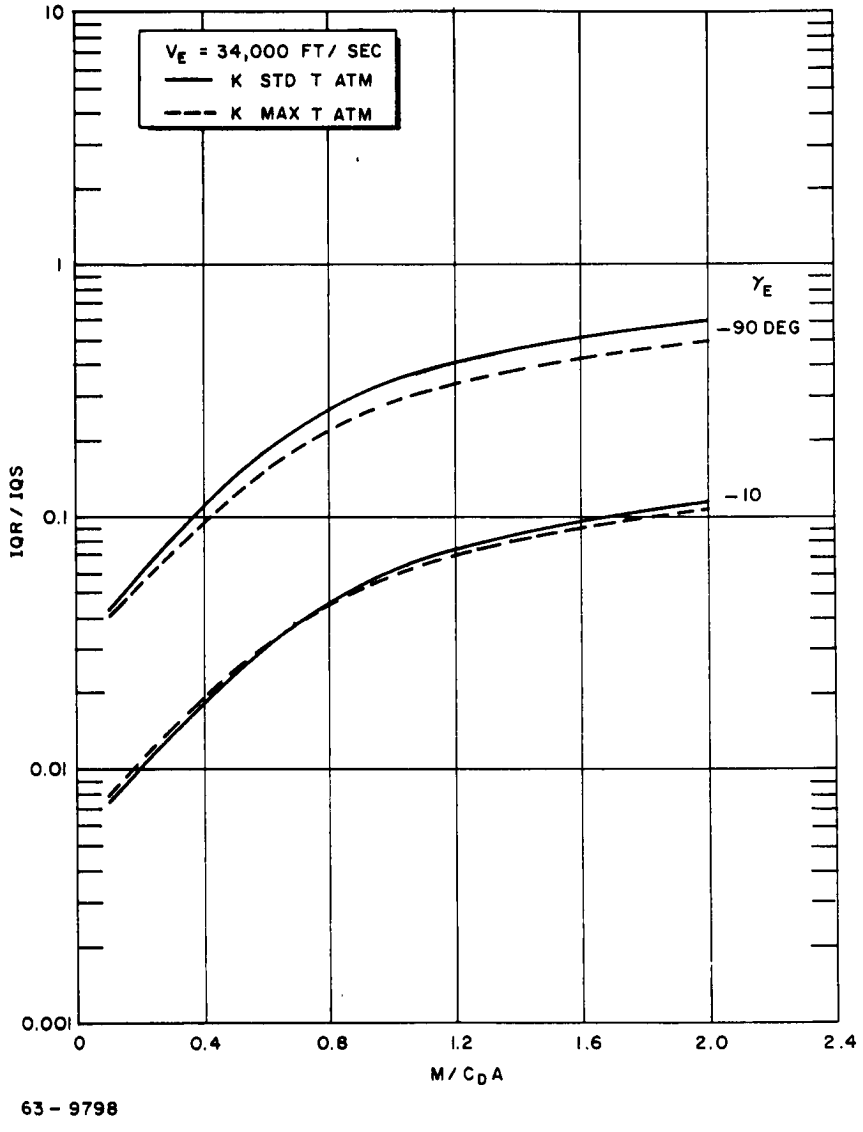

Figure 215 VENUS ENTRY: RATIO OF INTEGRATED STAGNATION RADIATIVE HEATING TO INTEGRATED STAGNATION CONVECTIVE HEATING

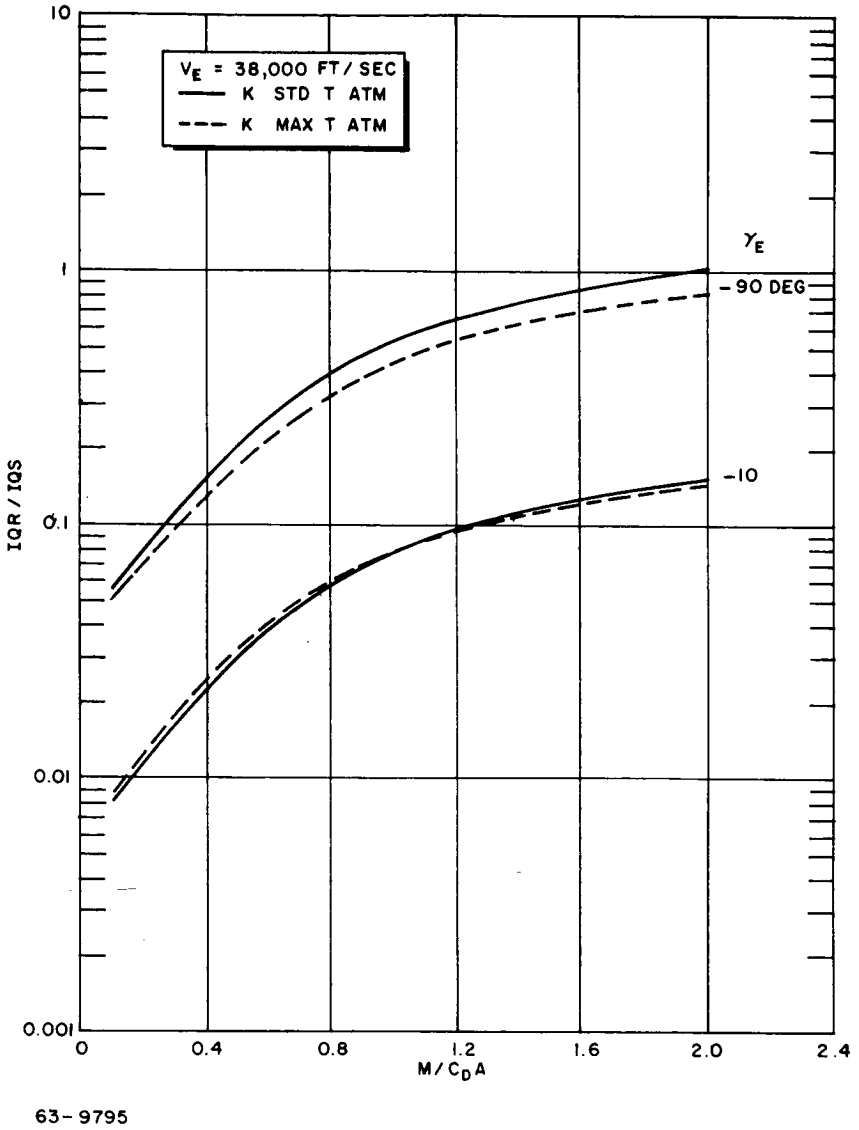

Figure 216 VENUS ENTRY: RATIO OF INTEGRATED STAGNATION RADIATIVE HEATING TO INTEGRATED STAGNATION CONVECTIVE HEATING

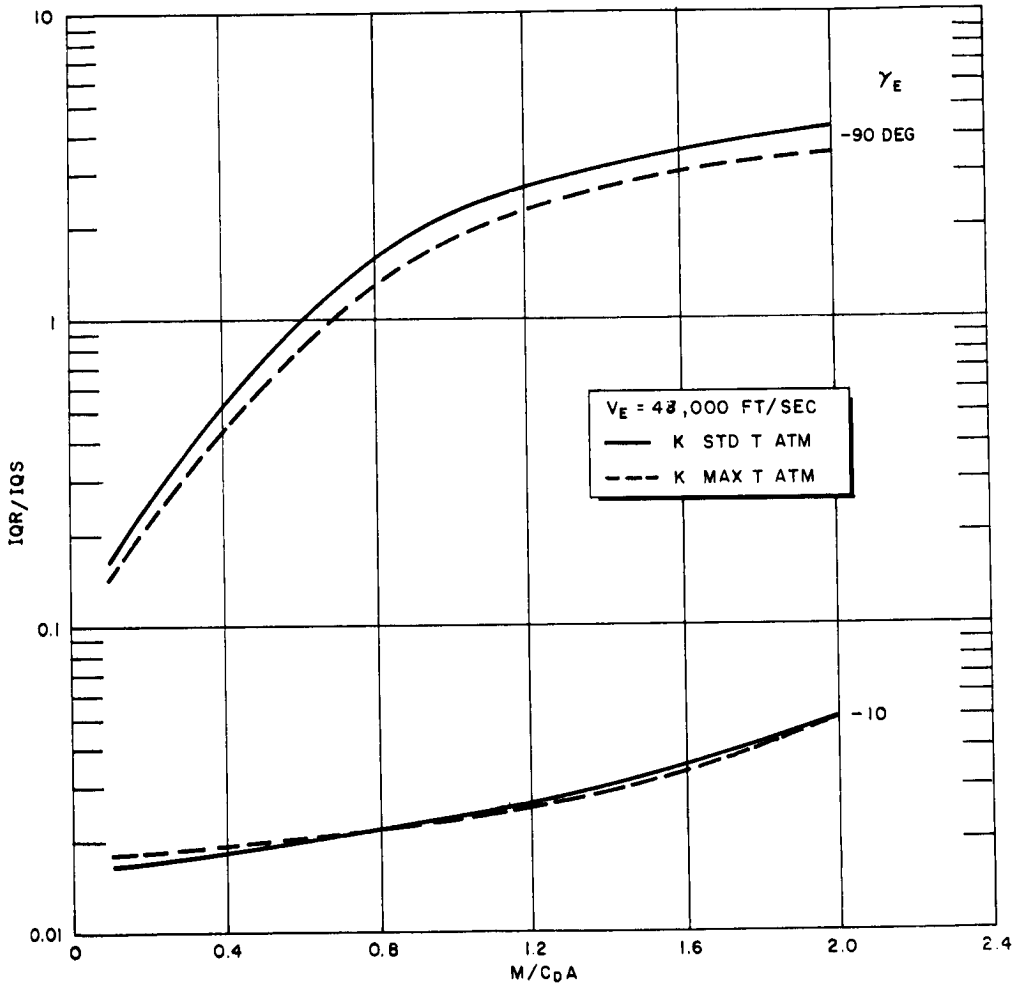

Figure 217 VENUS ENTRY: RATIO OF INTEGRATED STAGNATION RADIATIVE HEATING TO INTEGRATED STAGNATION CONVECTIVE HEATING

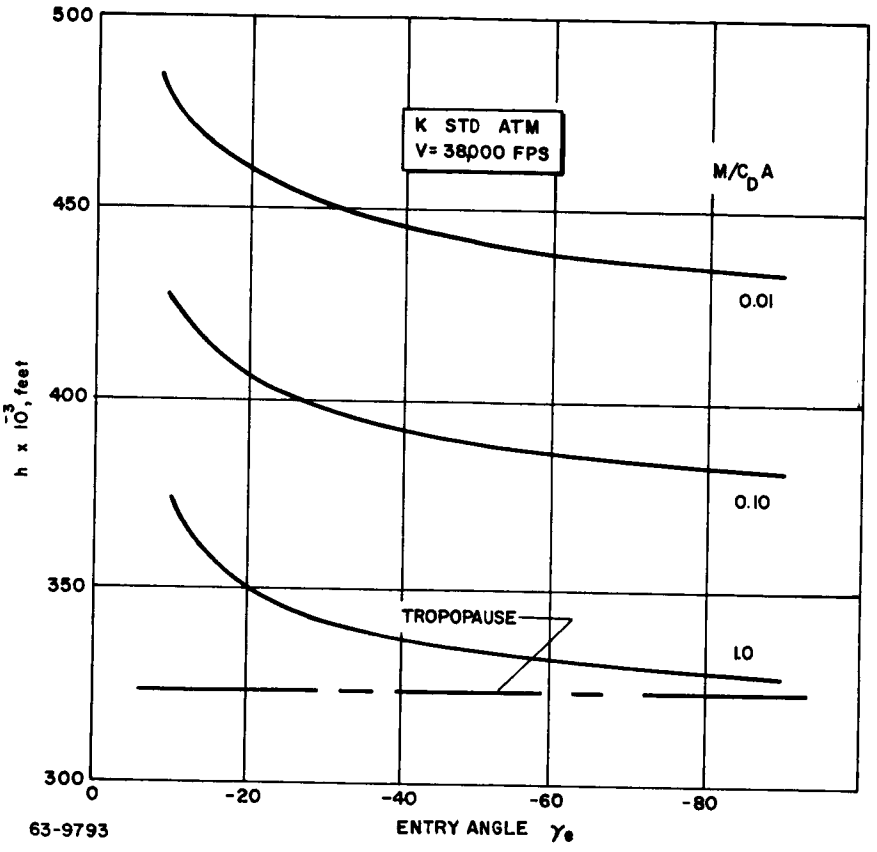

Figure 218 VENUS LANDER ALTITUDE AT MAXIMUM STAGNATION HEATING VERSUS ENTRY ANGLE

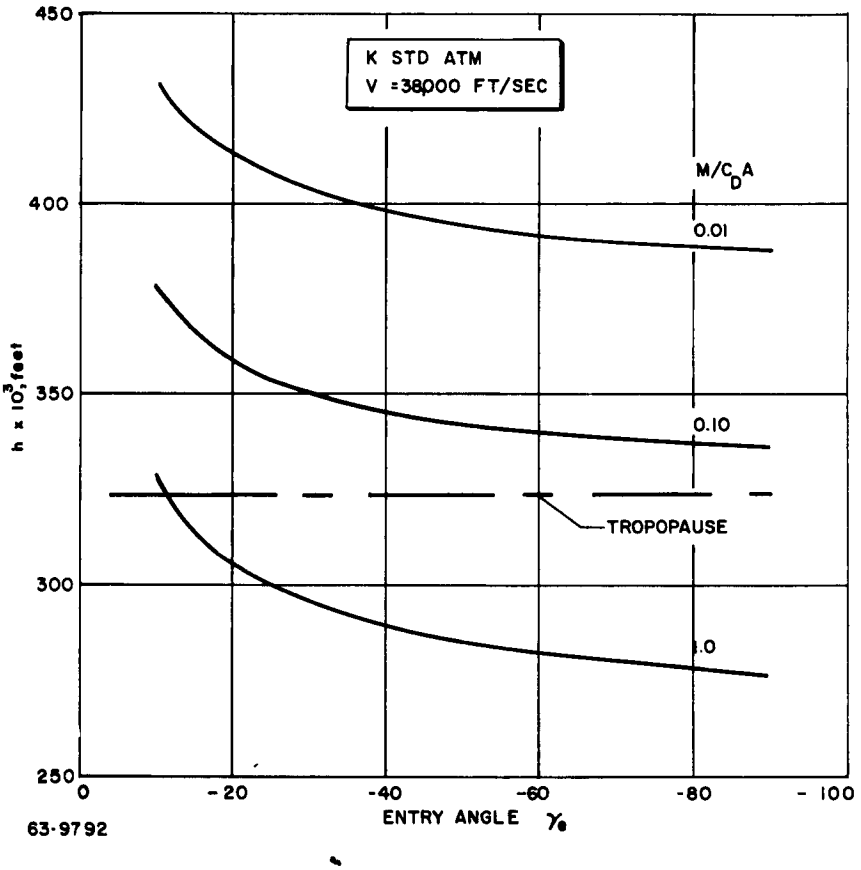

Figure 219 VENUS LANDER ALTITUDE AT 10 PERCENT MAXIMUM STAGNATION HEATING

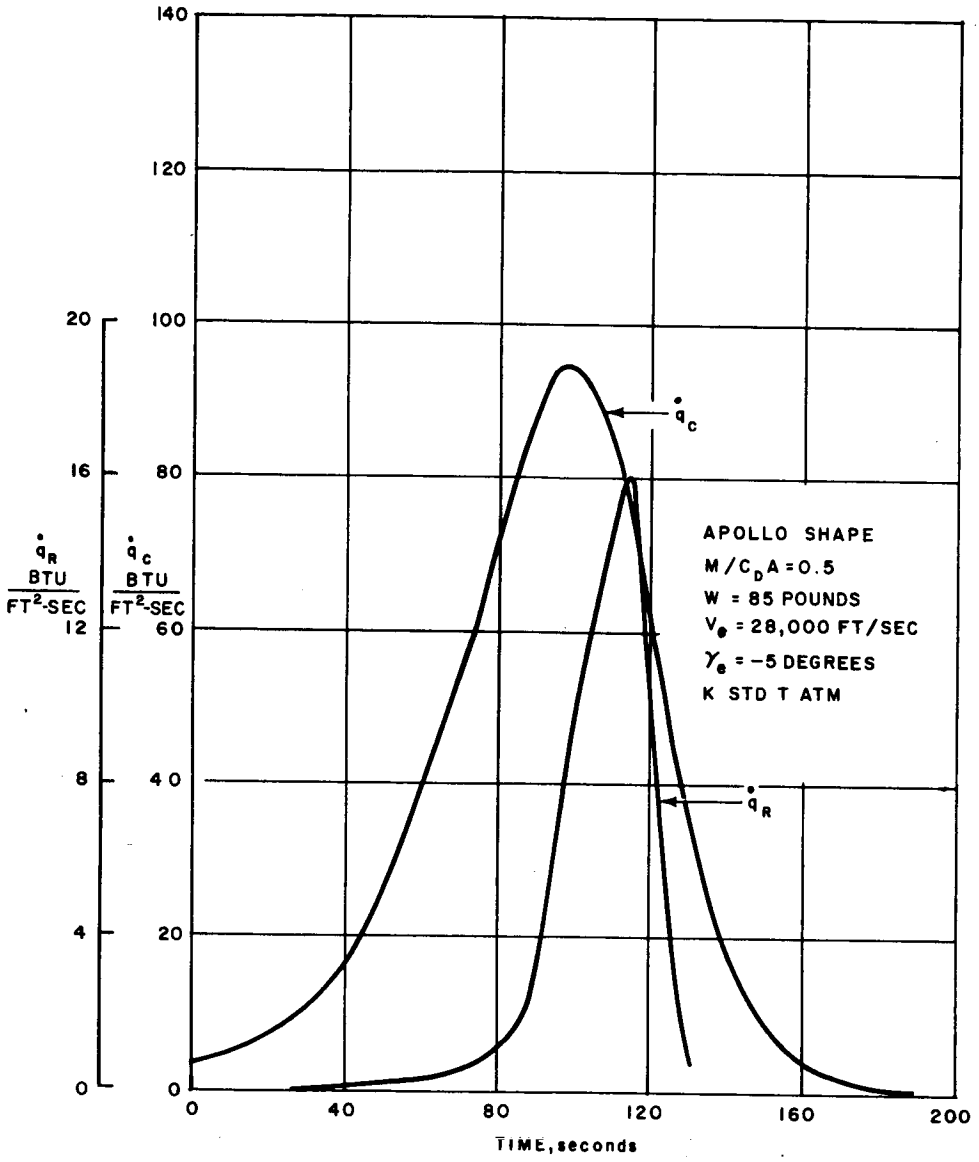

63-9791-652

Figure 220 VENUS ORBITAL ENTRY: RADIATIVE AND CONVECTIVE HEATING PULSES

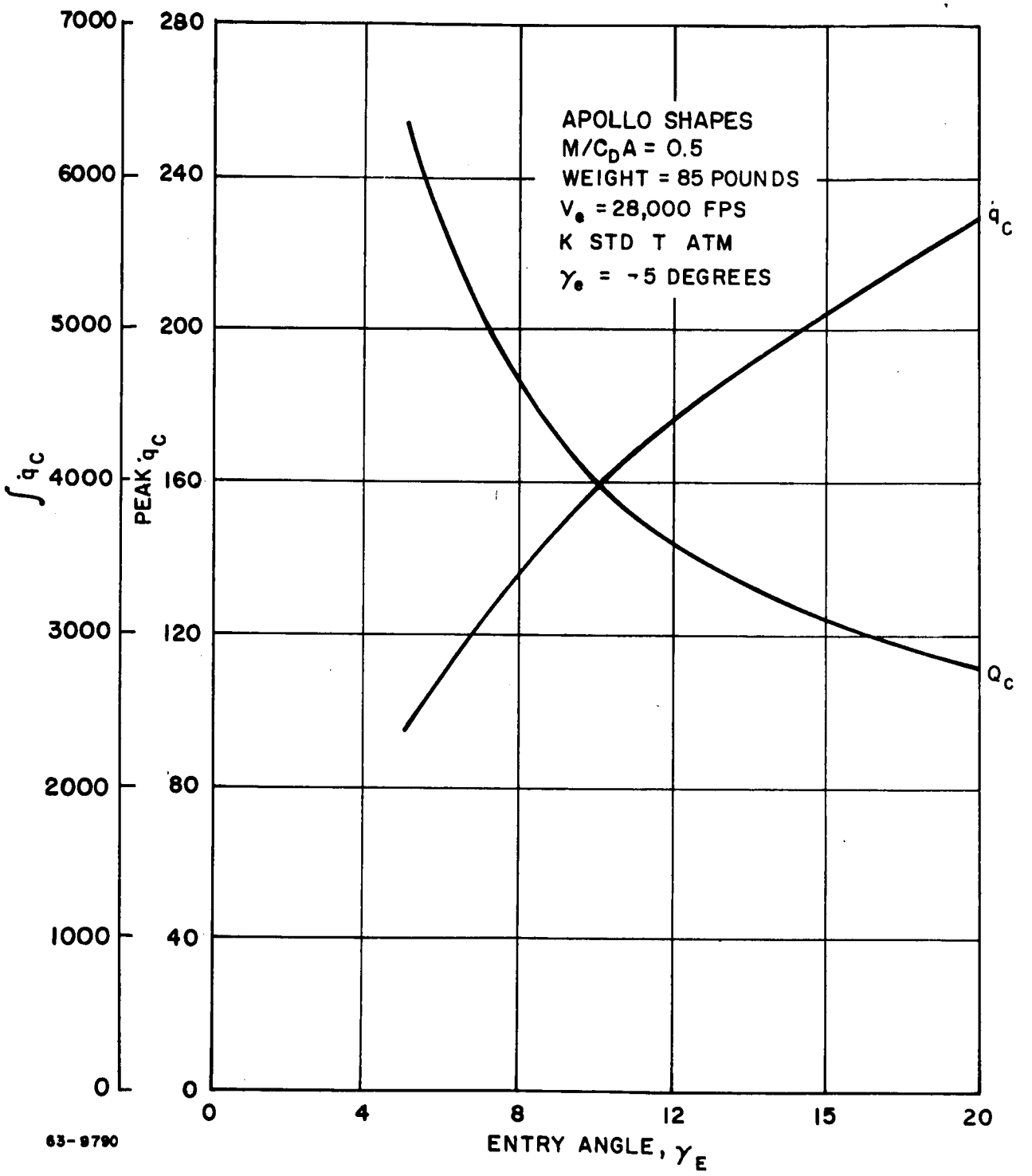

Figure 221 VENUS ORBITAL ENTRY: STAGNATION CONVECTIVE PEAK RATE AND TOTAL INTEGRATED INPUT

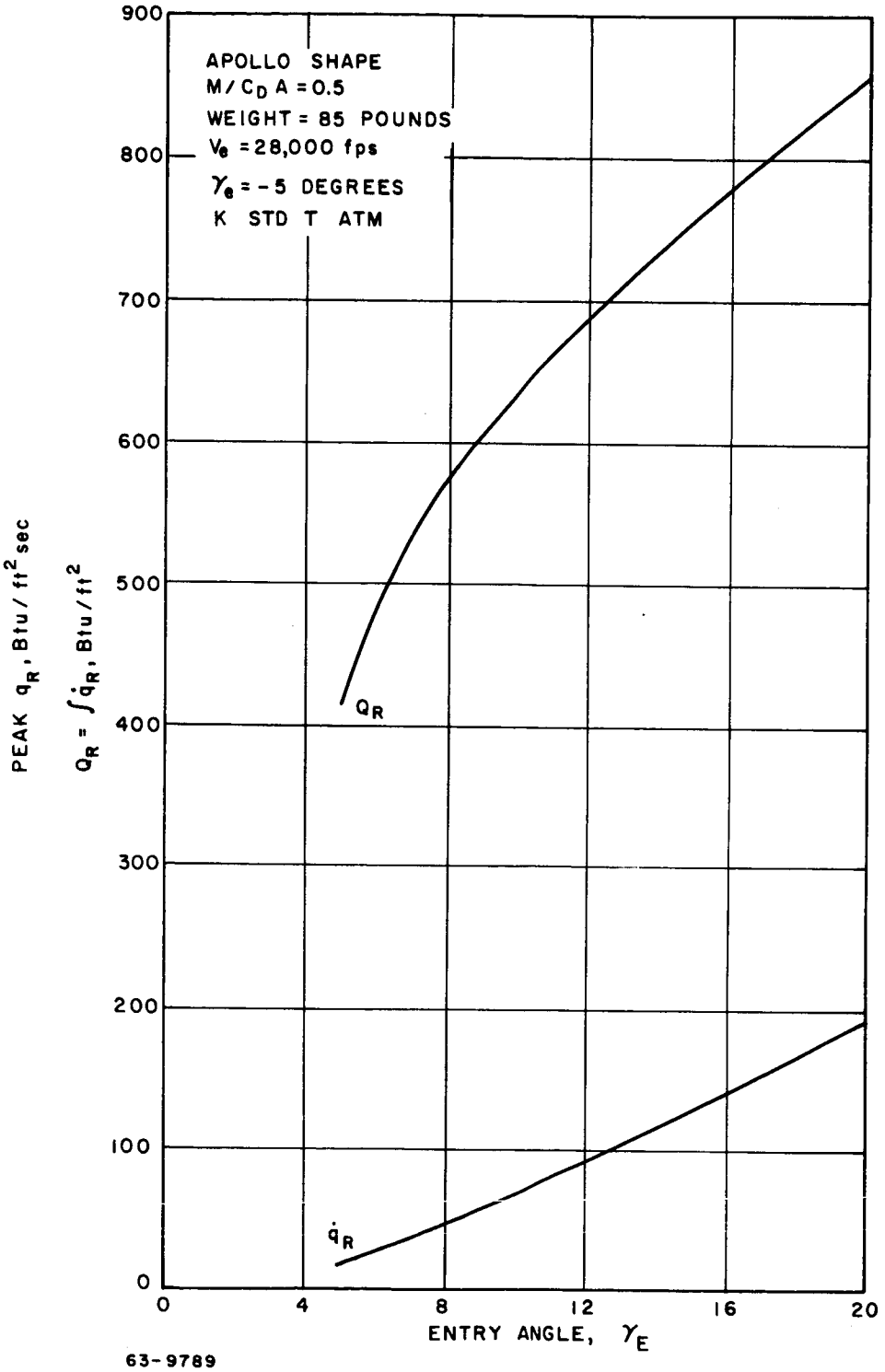

Figure 222 VENUS ORBITAL ENTRY: STAGNATION RADIATIVE PEAK RATE AND TOTAL INTEGRATED INPUT

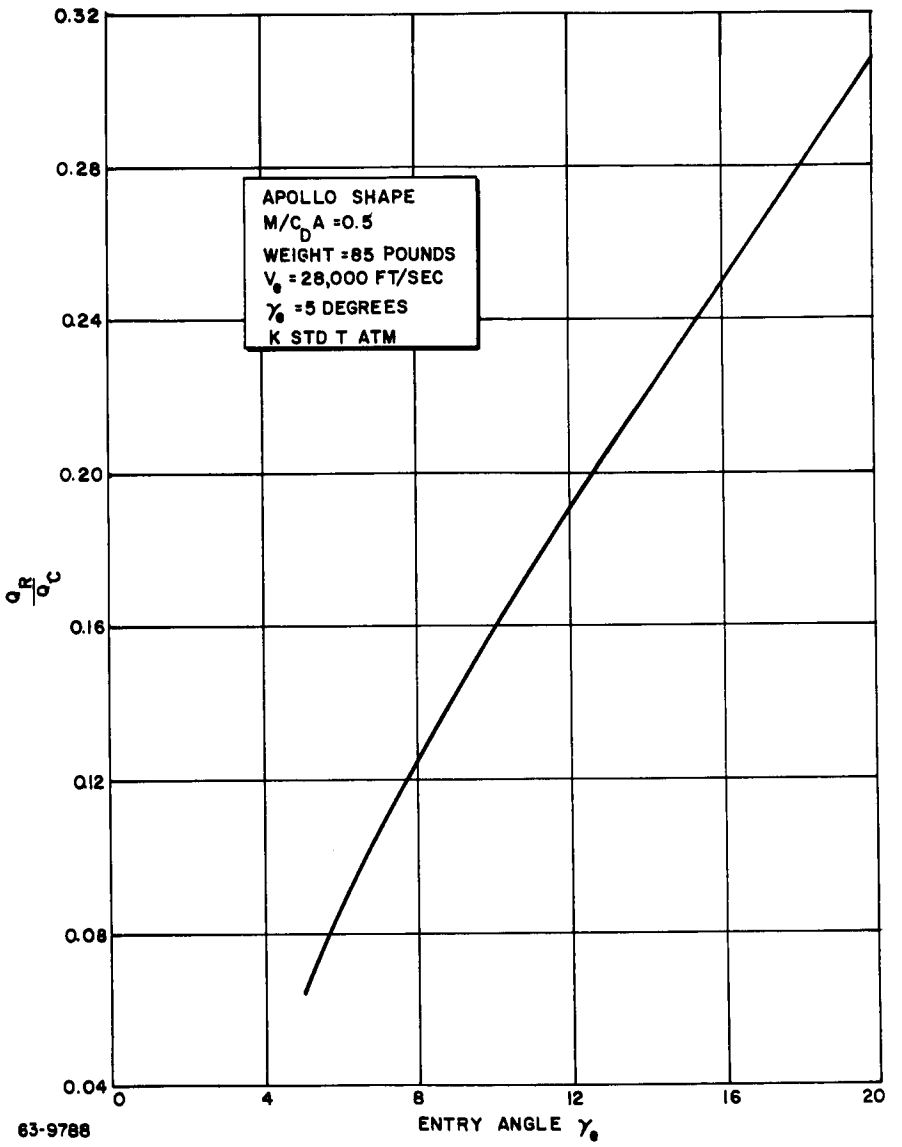

Figure 223 VENUS ORBITAL ENTRY RATIO OF INTEGRATED RADIATIVE HEATING TO INTEGRATED CONVECTIVE HEATING

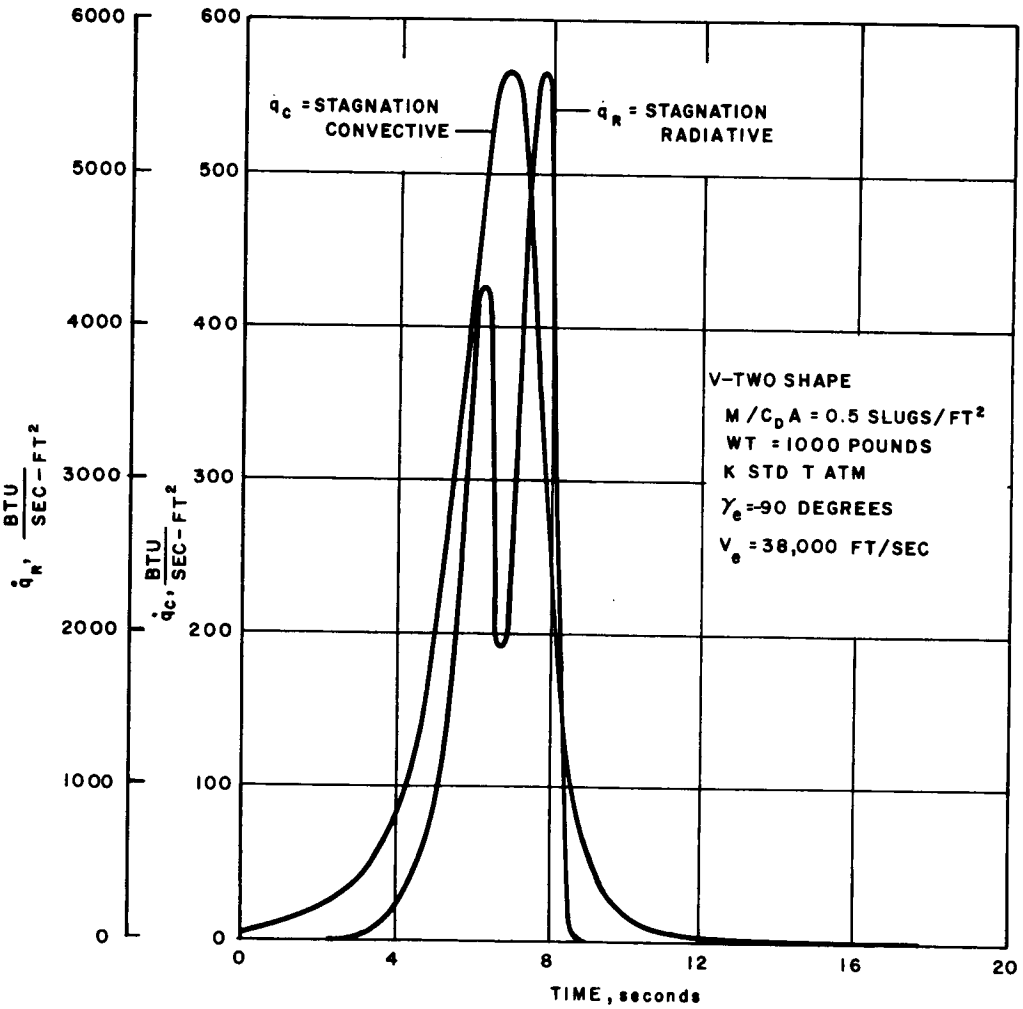

63-9787

Figure 224 VENUS ENTRY: RADIATIVE AND CONVECTIVE HEATING PULSES

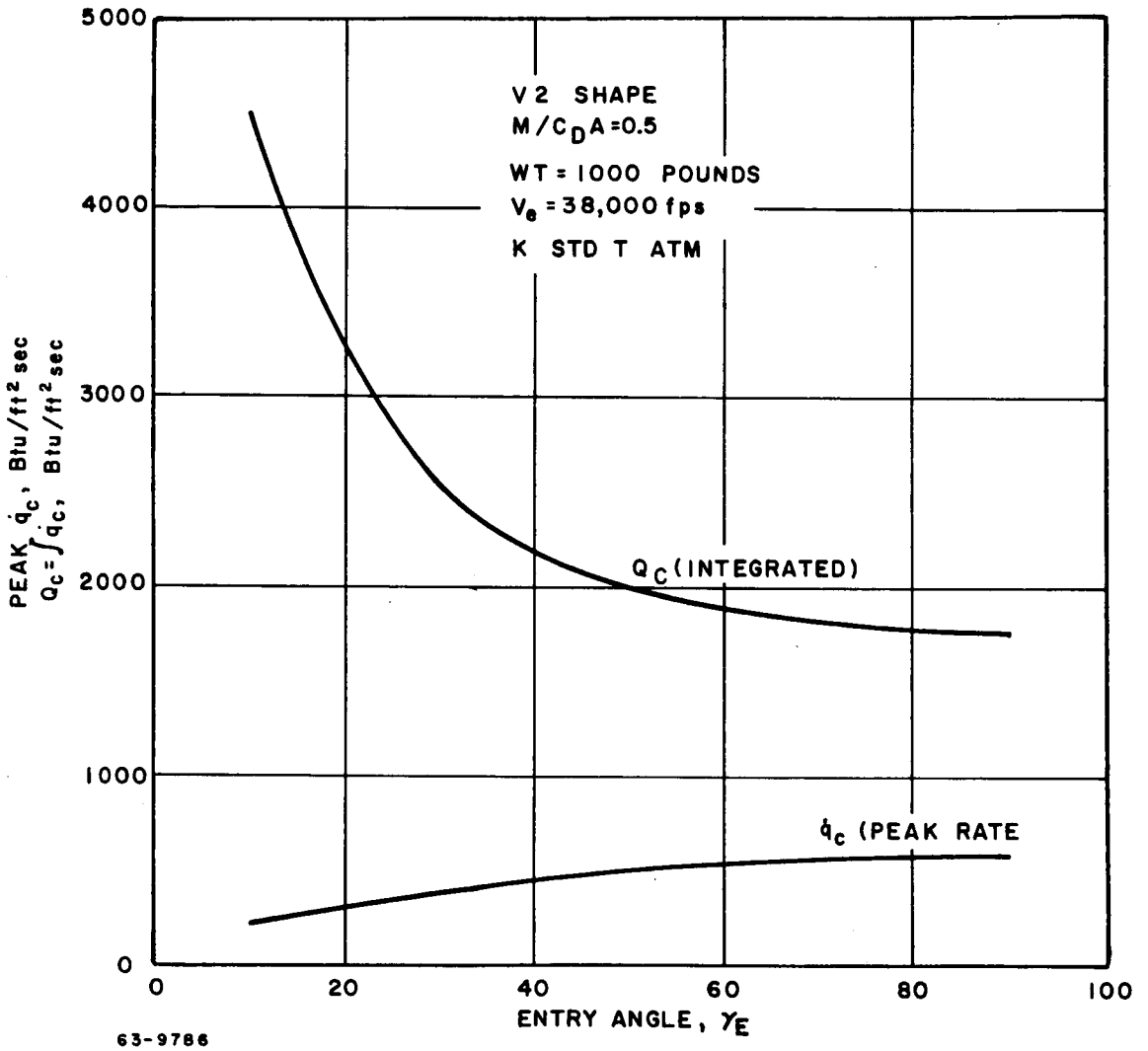

Figure 225 VENUS ENTRY: STAGNATION CONVECTIVE PEAK RATE AND TOTAL INTEGRATED INPUT

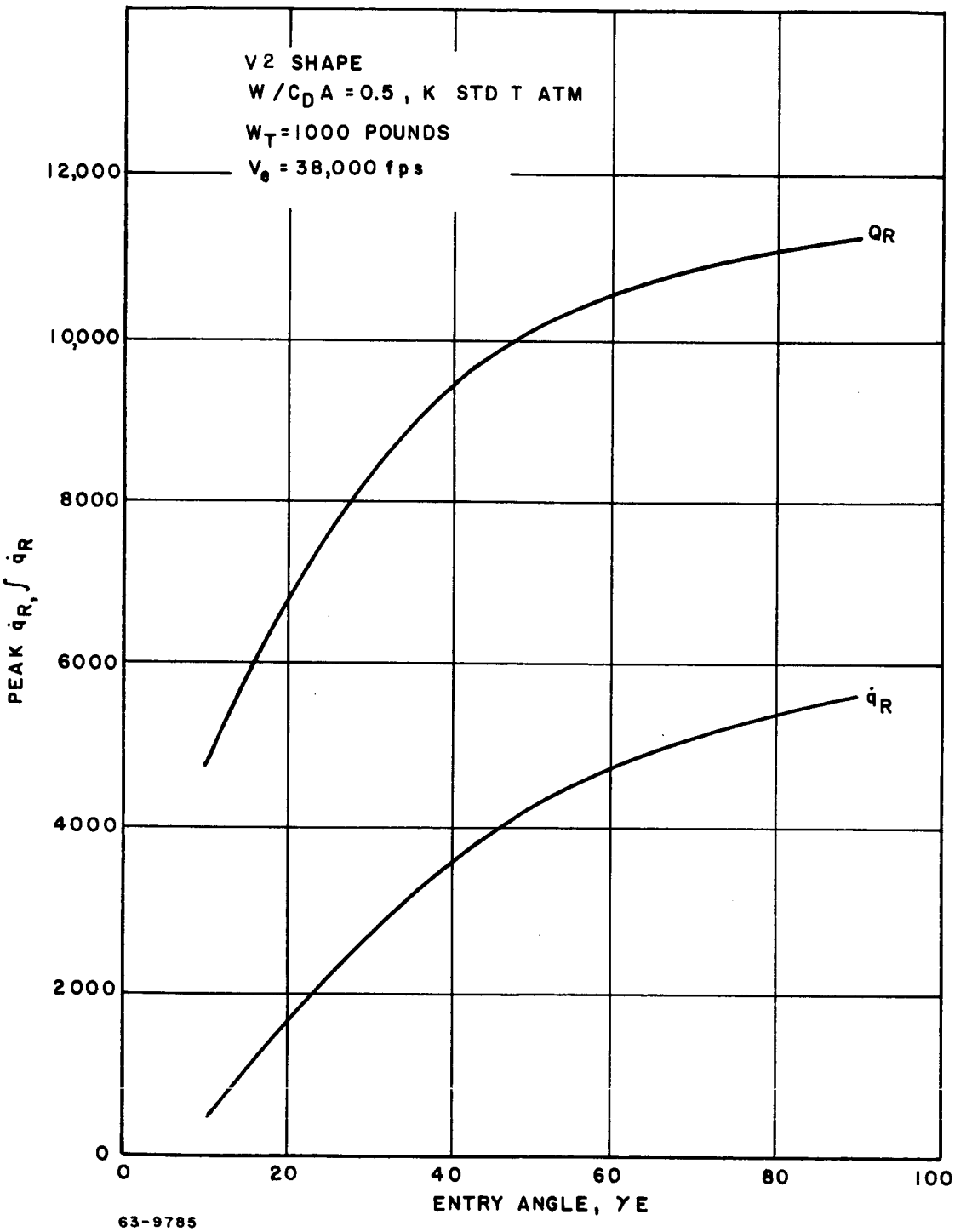

Figure 226 VENUS ENTRY STAGNATIVE RADIATIVE PEAK RATE AND TOTAL INTEGRATED INPUT

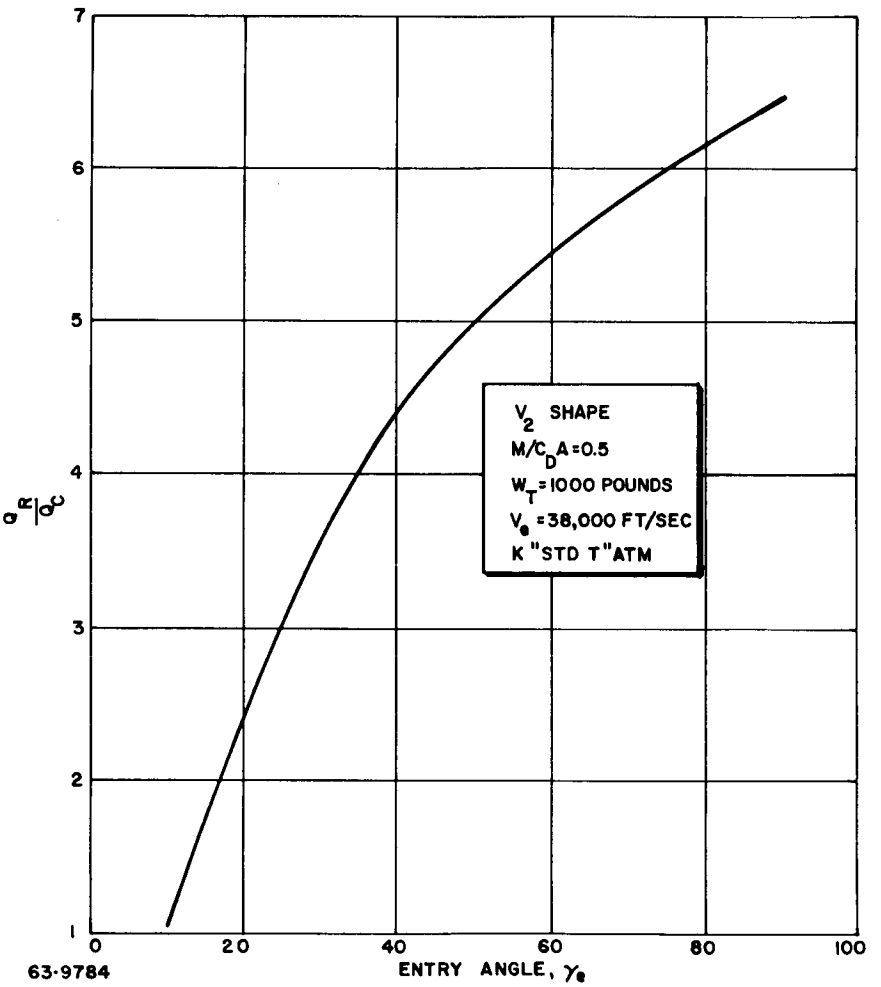

Figure 227 VENUS ENTRY RATIO OF INTEGRATED RADIATIVE HEATING TO INTEGRATE CONVECTIVE HEATING

b. Scope of study. The following configurations were considered in the analysis:

1) The V-2 Avco shape was analyzed for an M/C_DA range of 0.1 to 2.0 slugs/ft^2 with a lander weight variation of 500 to 2000 pounds for a 38,000-ft/sec entry condition. From this range of parameters, the reference direct-entry design lander was selected (M/C_DA = 0.6, lander weight = 1100 pounds). Also investigated was the heat shield variation with entry velocity (V_E = 34,000, 38,000, and 43,000 ft/sec) for an M/C_DA of 0.3 and a lander weight of 1000 pounds.

2) The V-1 shape for an M/C_DA range of 1.0 to 2.0 slugs/ft^2 and lander weights from 500 to 2000 pounds also were analyzed. The heating environment was taken for the 38,000 ft/sec entry condition.

3) The Apollo shape (orbital entry concept) was analyzed for M/C_DA of 0.5, a vehicle weight of 85 pounds and entry velocities of 24,000 and 28,000 ft/sec. This shape constitutes the second Venus lander reference design.

For the Venus heat shield analysis, two classes of materials were considered. One was a high-temperature ablator with very low conductivity and high thermochemical heat of absorption, the other was a very high temperature ablator with a low conductivity and a very high thermochemical heat of absorption. The two materials possessing these characteristics were an inorganic fibrous resin material 5026-39 and a reinforced carbonaceous material X-6008.

3. Heat shield material selection. The large amounts of convective and radiative heatings associated with an entry into the Venus atmosphere play an important role in the selection of the heat shield material. Thermal calculations have indicated that under severe radiative heating the blowing rates become very high, completely masking out the convective heating. Therefore, the mass-loss rates for a Venus entry environment can be very high.

From a thermal standpoint, it is desirable to have a material with the following characteristics:

a. High ablation temperature and heat of ablation.

b. High emissivity. (In areas of high radiative heating, good reflectivity could be significant, depending on capacity of the boundary layer.)

c. Low density and conductivity.

d. Good shear resistance in areas of high convective heating.

Also, the heat shield must be able to withstand the effects of sterilization and vacuum-flight deterioration.

The reference material for the high-heat input areas is a reinforced graphitic material X-6008. For low-heat input areas, the reference Mars material 5026 appears attractive.

4. Parametric study

a. V-2 design

1) Stagnation point. Figures 228 through 230 show the heat shield weight variation with M/C_DA at the stagnation point for the 5026 and X-6008 materials for entry angles of -10, -45, and -90 degrees, and vehicle weights of 500, 1000, and 2000 pounds. As is seen, the behavior of each material follows a certain pattern. For the shallow entry angle (-10 degrees) the heat shield weights of the 5026 are less than the X-6008, the degree of weight difference being significant for the 500 and 1000-pound vehicles and at the lower M/C_DA range. For the 2000-pound vehicle, the X-6008 material offers a greater weight savings at M/C_DA values larger than 1.6.

At the -45-degree entry angle condition, the 5026 material is better than X-6008 over a narrow band of small M/C_DA. This trend holds for all three vehicle weights. Beyond the M/C_DA value where both materials provide the same heat shield weight, the 5026 material becomes less desirable with increasing M/C_DA. The same trend can be seen for the -90-degree entry angle where once again the heat shield weight of the 5026 increases very rapidly compared to the X-6008. The large heat shield weights of 5026 are caused by the high radiation heating associated with increasing M/C_DA. For these cases, ablation makes up the bulk of the heat shield requirements with insulation being relatively unimportant.

It is worth noting that the value of M/C_DA for which both materials give the same weight varies with vehicle weight. For all three angles, as the vehicle weight increases the crossover point shifts to smaller values of M/C_DA. Therefore, one can conclude that for the Venus V-2 lander at the stagnation point, the 5026 is the better heat shield material for small landers with low M/C_DA and the X-6008 is better for large vehicles and high M/C_DA.

At this point, it is also of interest to observe the variation of the heat shield weight with velocity for the two materials. Figure 231 shows the trend between velocities of 34,000 and 43,000 ft/sec for a vehicle weight of 1000 pounds and an M/C_DA of 0.3. As is seen the 5026 material is better than the X-6008 where the radiative heating is low. This is true for small entry angles over the entire velocity range. As the entry angle increases and the radiative heating becomes larger with increasing velocity the 5026 material becomes progressively poorer. It must be mentioned here that figure 231 is representative of one M/C_DA (which is small) and that if the M/C_DA were to increase the radiative heating would increase rapidly. Therefore, at higher M/C_DA values the 5026 material will look less desirable over the entire velocity range than is shown in figure 231.

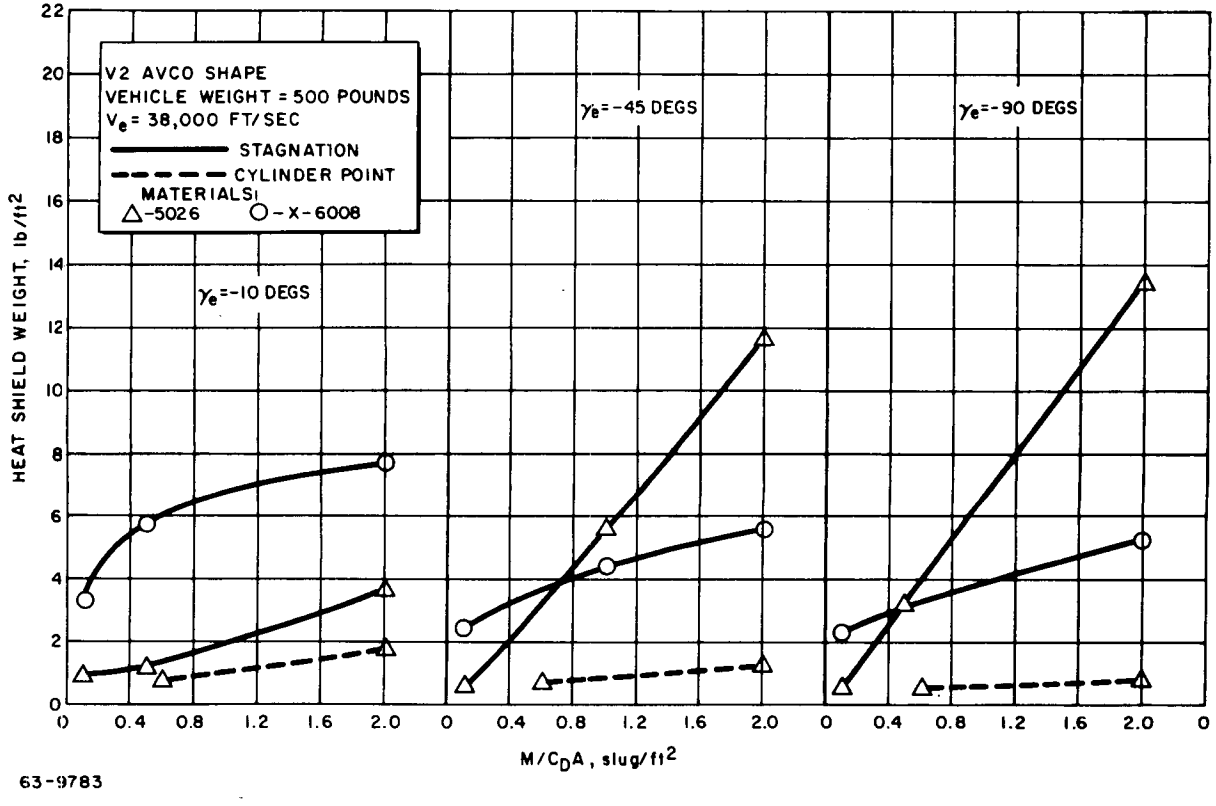

Figure 228 VENUS LANDER HEAT SHIELD WEIGHTS, KAPLAN STANDARD-TEMPERATURE ATMOSPHERE

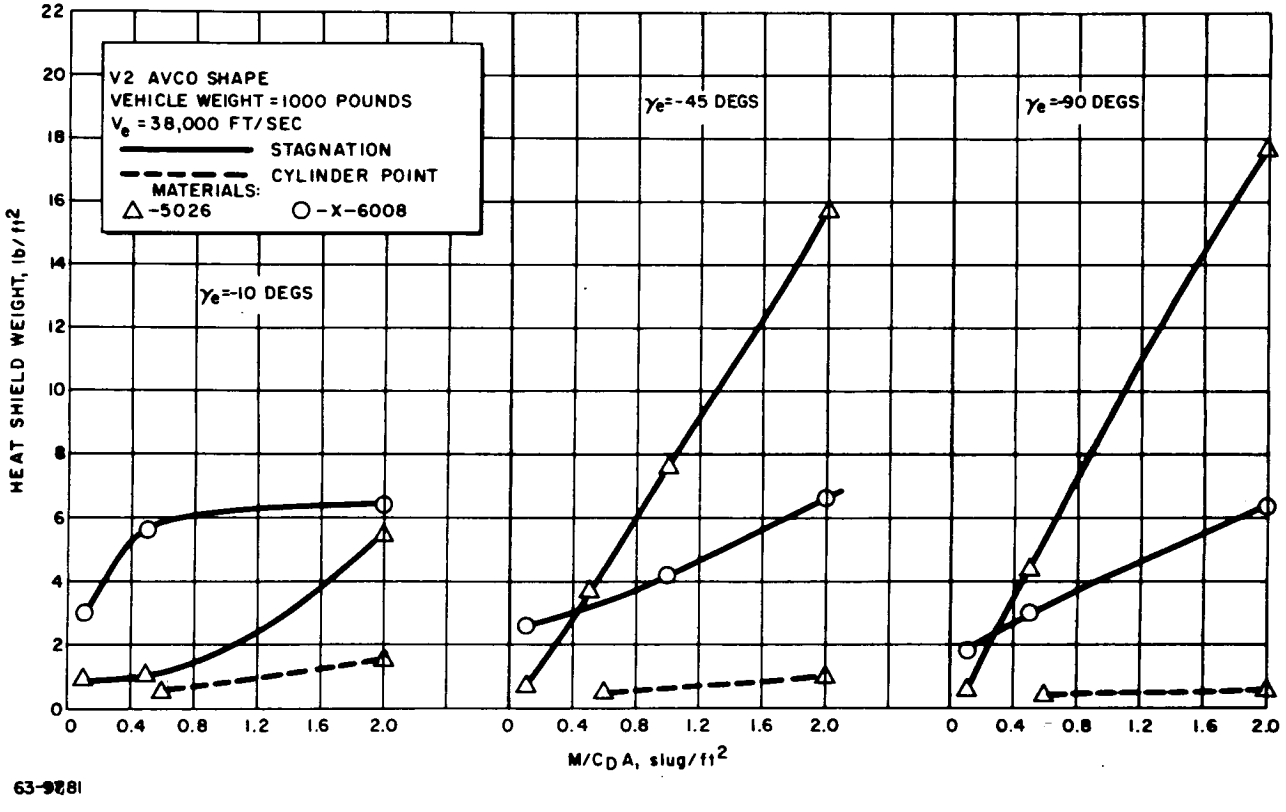

Figure 229 VENUS LANDER HEAT SHIELD WEIGHTS, KAPLAN STANDARD-TEMPERATURE ATMOSPHERE

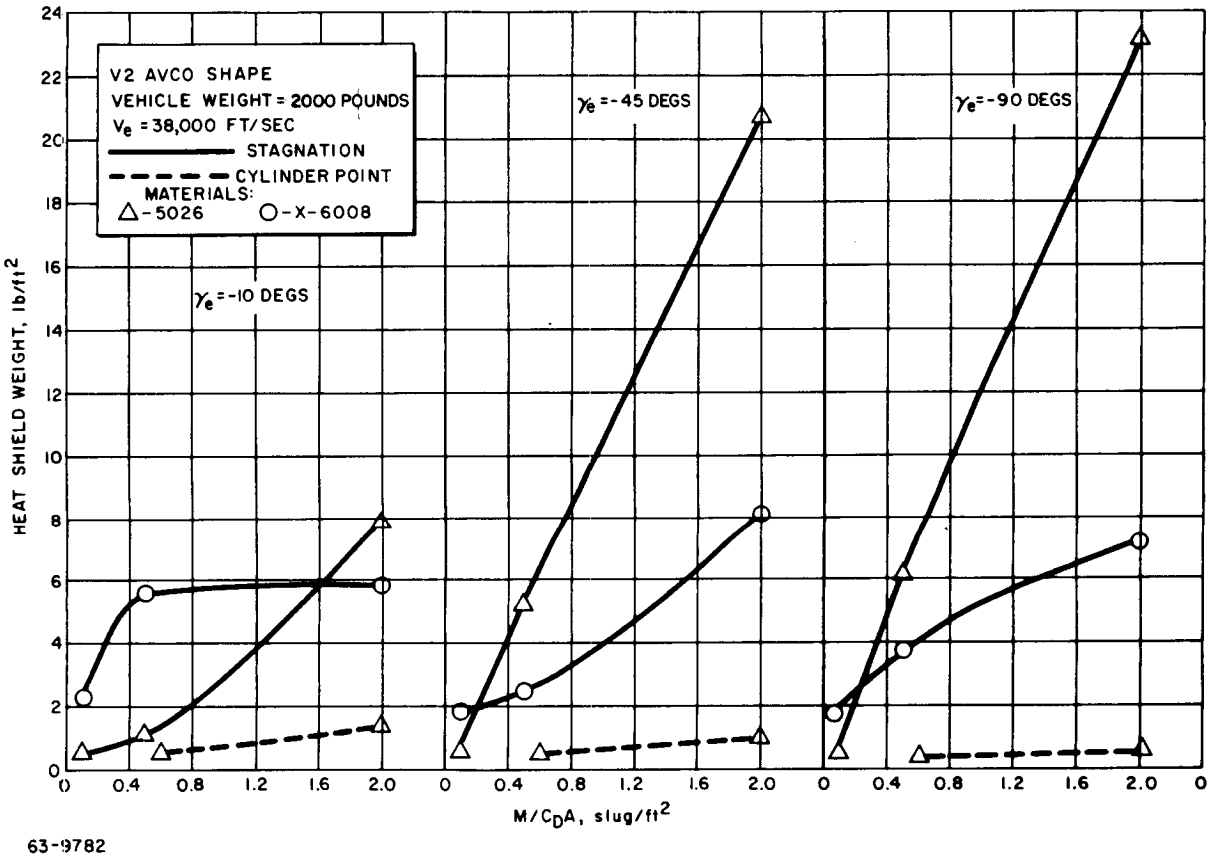

Figure 230 VENUS LANDER HEAT SHIELD WEIGHTS, KAPLAN STANDARD-TEMPERATURE ATMOSPHERE

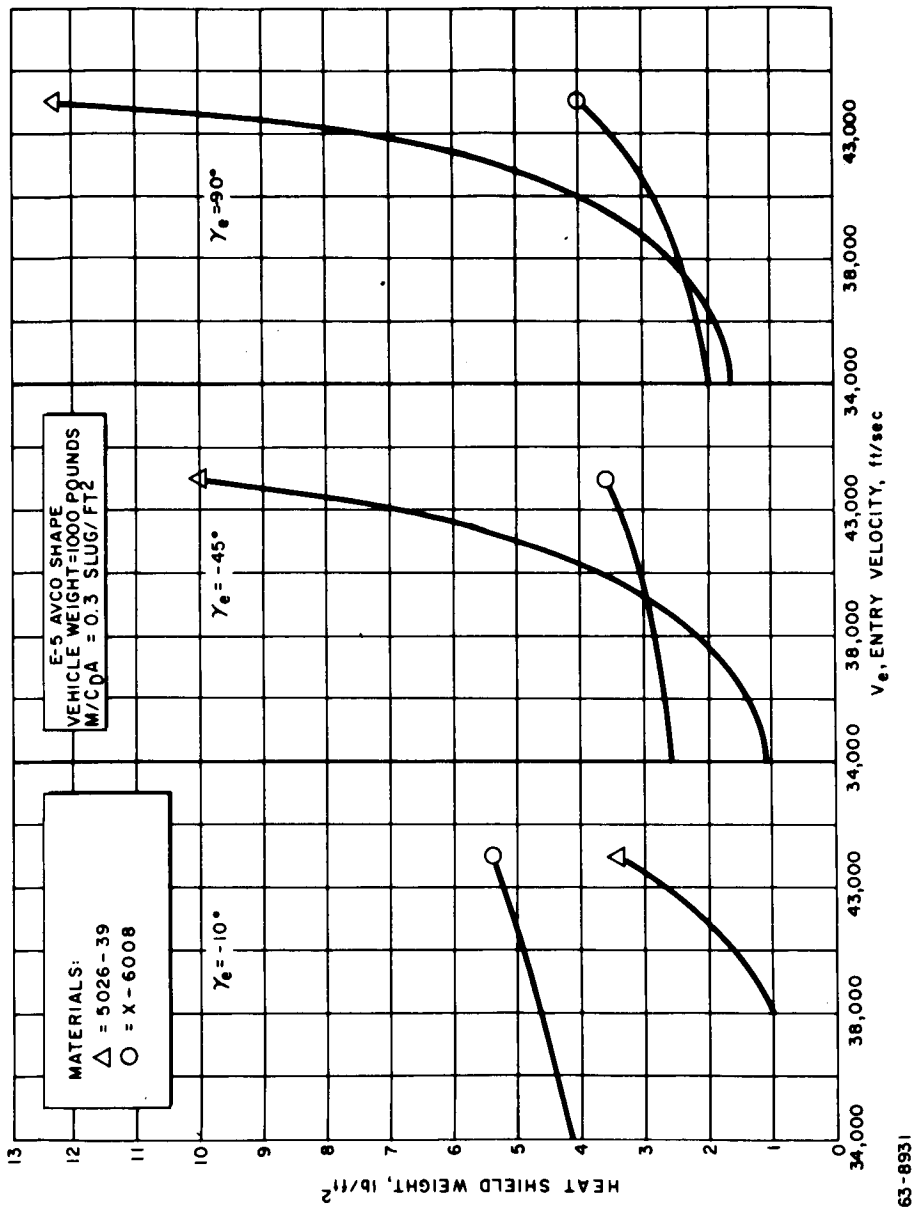

Figure 231 VENUS LANDER HEAT SHIELD WEIGHTS, STAGNATION POINT

2) Side points. At the side points of the V-2 shape for zero angle of attack, the heating is convective and an order of magnitude less than the convective heating at the stagnation point. In this region it is desirable to have for a heat shield material a good insulator since, in general, the magnitudes of the heating pulses will not produce ablation. Comparing the two materials we find that the 5026 material with its lower conductivity is best for the side points. Figures 228 through 230 show typical side point heat shield weights. The heat shield weights increase with increasing $M/C_D A$, decreasing vehicle weight and decreasing entry angle.

b. V-1 shape

1) Stagnation point. Figures 232 through 234 show the heat shield weight variation for a limited range of $M/C_D A$ at the stagnation point for both materials. If the curves are extended, the heat shield weight trend will be similar to the V-2 shape. That is, a crossover point exists where one material will be better than the other. The variation of heat shield weight with velocity is also similar to that shown for the V-2 shape.

2) Side points. At the side points of the V-1 shape the heating is convective and an order of magnitude greater than the heating on the side points of the V-2 shape.

Here in general the heat pulses are large enough to produce ablation in the 5026 material but not in the X-6008. For the cases where the heat pulses are low and no ablation occurs, the 5026 material is again a better heat shield material than X-6008. Figures 232 through 234 show the variation of side point heat shield weight with $M/C_D A$.

c. Apollo shape (85 pounds). One of the reasons for the selection of this shape concept was to take advantage of the reduction in radiation heating as $M/C_D A$ and vehicle weight are decreased. The vehicle will enter the Venus atmosphere with a velocity from 24,000 to 28,000 ft/sec. At these velocities, the relative length of the convective heat pulse will increase compared to the velocities discussed for the V-1 and V-2 shapes. Peak heating rates also will be comparably lower. Therefore, ablation does not occur. Figure 235 shows the variation of 5026 heat shield weight with entry angles from -5 to -20 degrees for entry velocities of 24,000 and 28,000 ft/sec.

d. Conclusions. Various ranges of entry conditions were analyzed with both materials considering the present shape concepts. For entry conditions where the total heating was high (high convective and radiative heating rates) and ablation was the prominent factor, the X-6008 material with its high heat of ablation appeared to be the better material. Under these high heating rates, the 5026 material produced very large ablation losses compared to the X-6008. When entry heating was moderately low, it was desirable to ablate rather than suffer the penalty of a large insulation weight; in this case, the 5026 material

with its lower conductivity and ablation temperature proved superior. In the case of the low side point heating, there was no ablation, the 5026 material again proved to be the better insulator.

The results presented here indicate that lander designs for a Venus entry can incorporate one heat shield material like 5026 for the entire surface of the lander when radiative heating is moderately low. Heating will be low for entry velocities of 34,000 and 38,000 ft/sec over certain ranges of $M/C_D A$ and lander weights. For a vehicle entering at a velocity of 43,000 ft/sec (radiation heating rates extremely high), an alternate heat shield material with high energy absorption characteristics must be selected for the stagnation region. This fact is clearly brought out by comparing the performance of the 5026 heat shield of the V-2 reference design for the three entry velocities. At 34,000 and 38,000 ft/sec the stagnation heat shield will survive all entry angles while for 43,000 ft/sec the heat shield will fail for entry angles above-12 degrees. Therefore, to cover the entire angle range of the 43,000-ft/sec launch window, X-6008 must be the heat shield material at the stagnation region.

11.2 Heat Shield Materials for Venus

1. Venus reference materials. Parametric studies of Venus entry thermodynamics indicate that very high heat fluxes may be encountered under the worst conditions. However, it is probable that the radiant flux will be less than 10,000 Btu/ft^2-sec, and the convective flux less than 3000 Btu/ft^2-sec. The higher heat fluxes require a high-performance heat shield material, such as a graphite cloth or fiber-filled epoxy or phenolic. The proposed Mars heat shield material appears to be the optimum material at the lower heat fluxes, and has been discussed elsewhere. For Venus, there appears to be a need for high-performance materials and, specifically, graphite reinforced heat shield materials, especially near the nose of the vehicle where the heating is high. In areas of low heating, the reference Mars material 5026 is attractive.

A graphitic surface is desirable for several reasons:

a. Carbon has a high heat of vaporization.

b. Carbon's high vaporization temperature results in high sensible heat, and high reradiation properties.

c. Pyrolytic graphite does not melt or flow like silica, and apparently is more stable to erosion than carbon.

2. Ablative properties of graphite materials. A series of high-performance heat shield materials has been developed that are based on carbon and graphite fibers combined with high-temperature epoxy and phenolic resins.

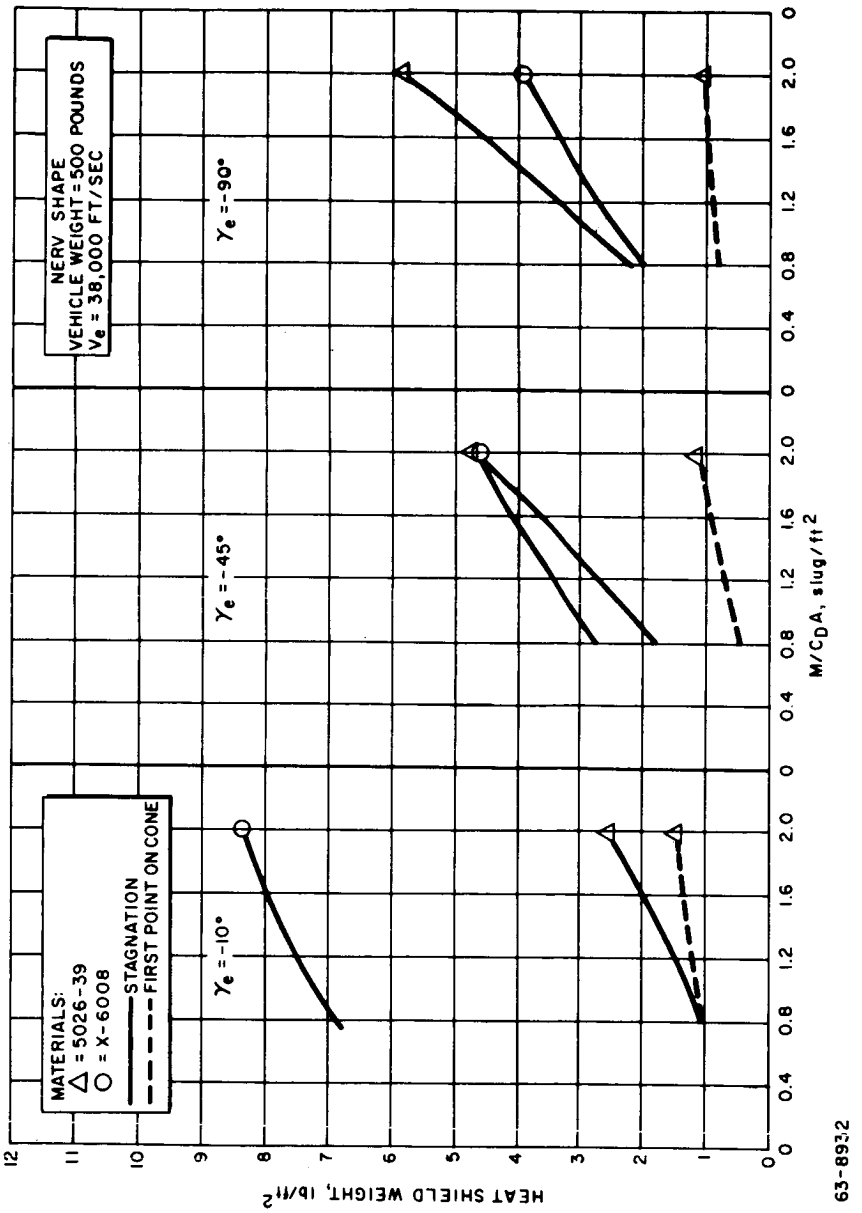

Figure 232 VENUS LANDER HEAT SHIELD WEIGHTS, KAPLAN
STANDARD-TEMPERATURE ATMOSPHERE

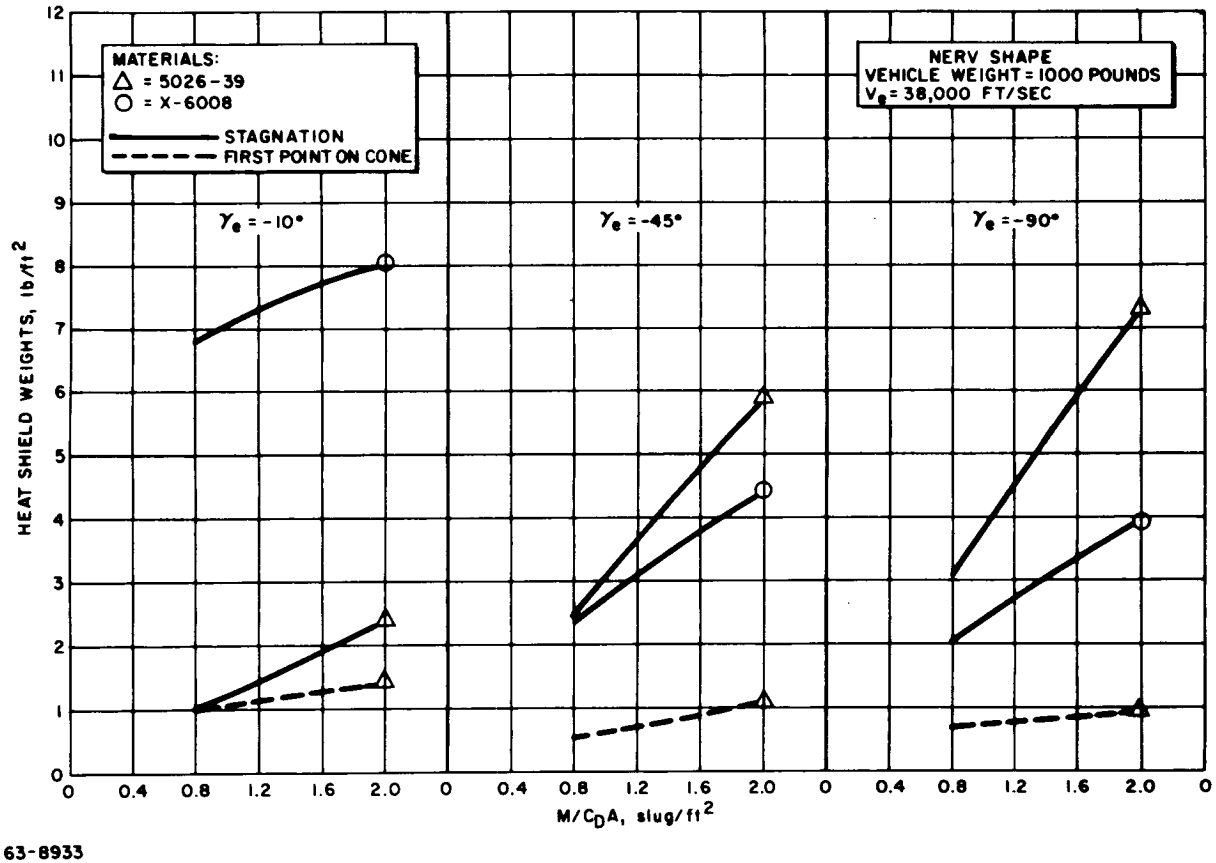

63-8933

Figure 233 VENUS LANDER HEAT SHIELD WEIGHTS, KAPLAN STANDARD-TEMPERATURE ATMOSPHERE

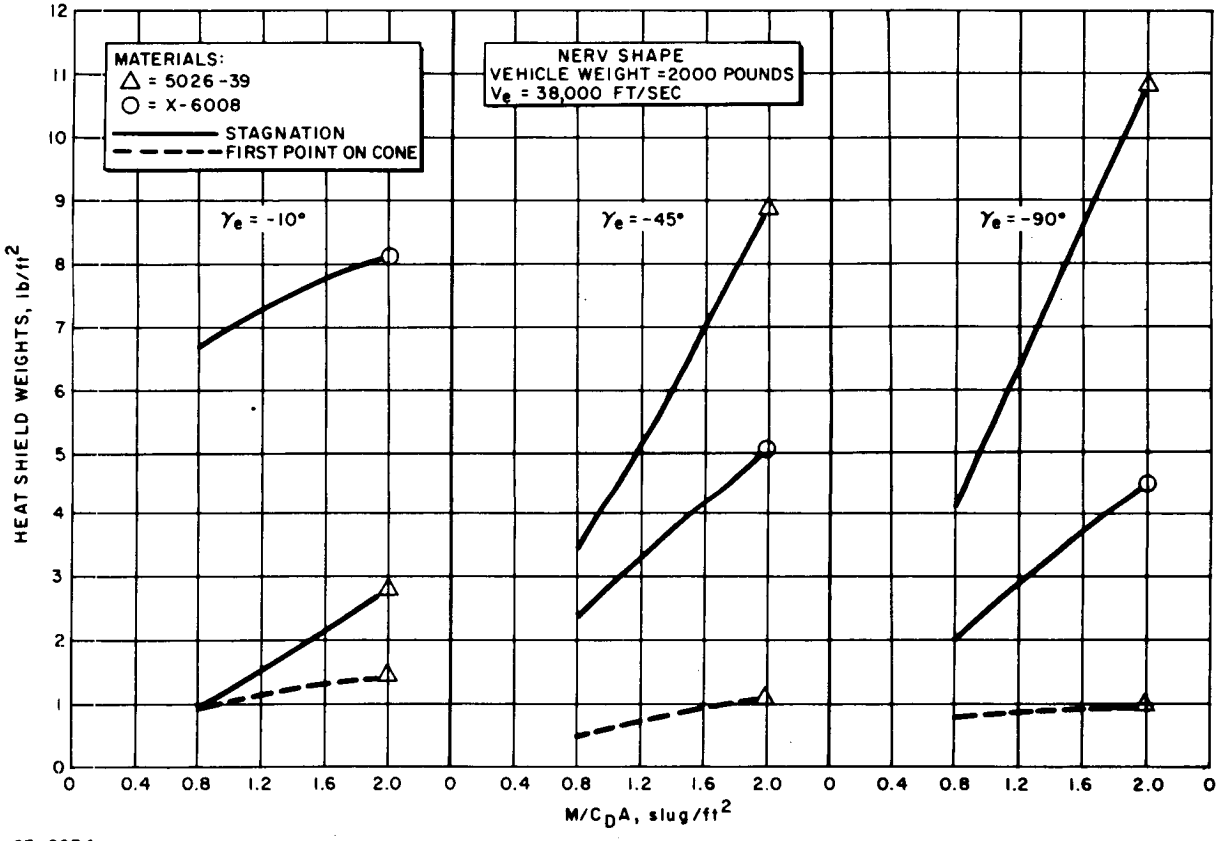

Figure 234 VENUS LANDER HEAT SHIELD WEIGHTS, KAPLAN STANDARD-TEMPERATURE ATMOSPHERE

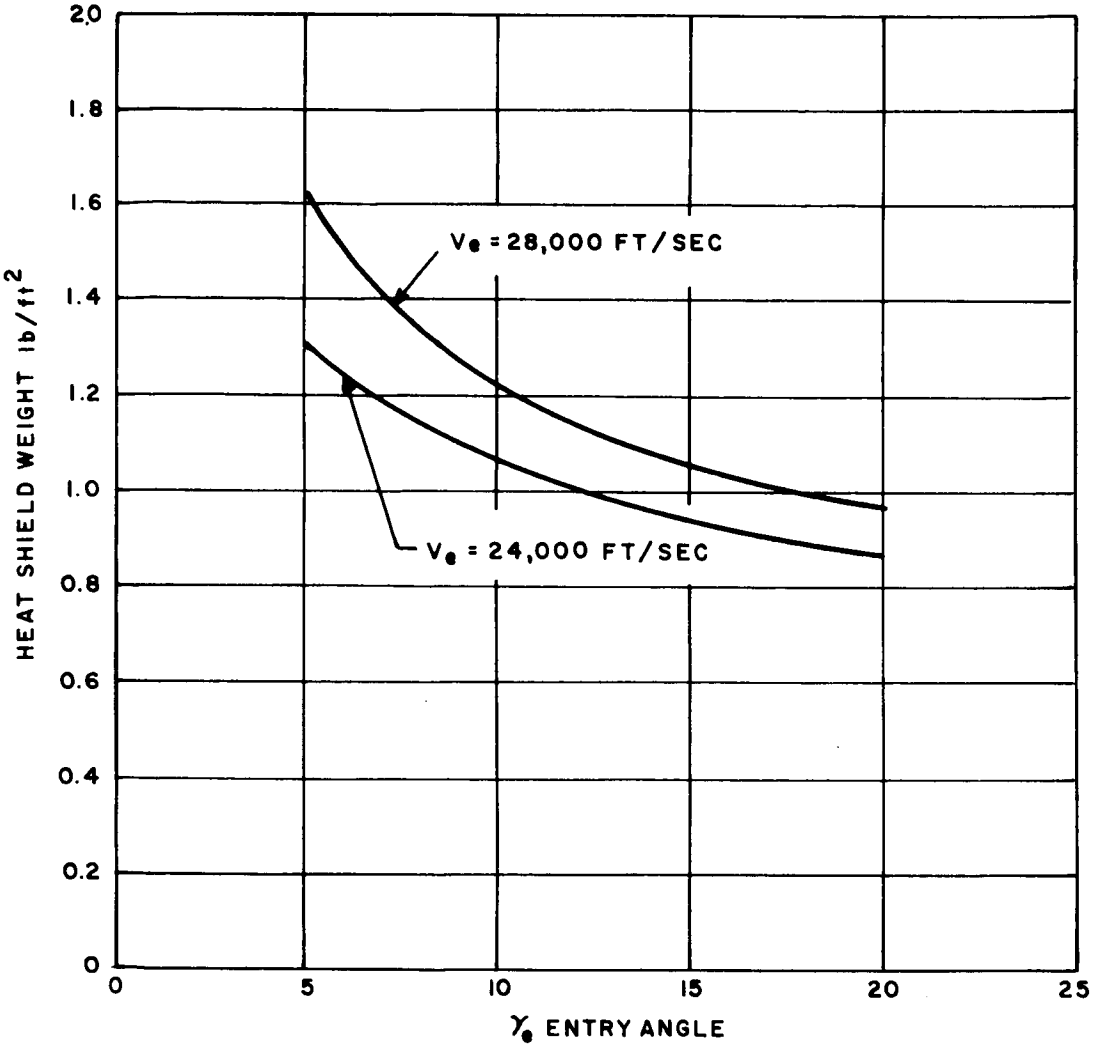

Figure 235 VENUS LANDER HEAT SHIELD WEIGHT, APOLLO SHAPE STAGNATION REGION

Ablative tests have been conducted under both convective and radiant-heat fluxes; however, a majority of the tests have been performed under convective heating (refs. 44 and 45). Carbon-based materials possess higher heats of ablation than silica-based materials, especially at the higher convective heat fluxes. The reasons for this behavior are well known and are based on the very high-vaporization temperature of carbon (7000°F) and its high heat of vaporization, resulting in low-erosion rates. Pure graphite has been used extensively in the linings of rocket nozzles because of its high-erosion resistance. At the lower heat fluxes, graphite-based composites do not erode; thus, that energy is not dissipated by the vaporization of carbon, and mass injection into the boundary is eliminated. The material then acts like a heat sink, which is a relatively inefficient thermal insulator. Therefore, graphite-based systems are useful only when the enthalpy is sufficient to produce ablation, which may be several thousands Btu/lb.

a. Convective heating. Two arc facilities have been extensively used at Avco RAD to evaluate these high-performance materials: the high enthalpy model-500 arc, and the 10-Mw arc.

1) High-enthalpy model-500 arc. The high-enthalpy model-500 arc has been briefly described in the Mars lander materials section. Heat fluxes up to 1500 Btu/ft^2-sec are generated in this arc. Generally, the graphite-based materials possess considerably higher heats of ablation (Q*) than the silica-based materials. Tests indicate that the phenolic-resin systems may be more thermally stable than epoxy resins. Phenolic-graphite specimens tend to reach steady-state ablation faster than epoxy-graphite specimens. In fact, epoxy-graphite specimens often do not reach a true steady-state ablation condition, as seen by increasing char depth with test time. The relatively high thermal conductivity of graphite-based materials tends to increase the heat-sink effect, thereby making the calculated Q* too high. Moreover, high-thermal conductivity tends to introduce errors in ablation temperature and reradiation measurements. Another difficulty with graphite-cloth-based systems is that swelling may occur anisotropically during the initial stages of ablation. Since the ablation velocities are generally quite low, small errors in length loss may result in fairly large Q* variations. Finally, at very low enthalpies combustion may occur, as has been discussed above.

In spite of these considerations, the large amount of data collected indicates that graphite-based composites are clearly superior in Q* and erosion resistance at medium- and high-heat fluxes over all other ablation materials. It is apparent that this results from the high heat of vaporization and high-vaporization temperature of carbon, resulting in high values of $[H_v + C_p\Delta T]$ and reradiation. Moreover, the mass injection into the boundary layer is quite high, with η usually greater than 2 (η = slope of Q* versus enthalpy curve). The use of phenolic and epoxy resins gives similar Q* values. Although phenolics may be slightly more thermally stable, epoxies are desirable because of ease of fabrication. Epoxies produce no products of condensation

as do phenolics, and these condensates must be removed by careful cure conditions. For the same reason, large shapes are more easily fabricated from epoxy-based composites.

It must be pointed out that increasing the amount of free oxygen in the boundary layer tends to decrease the heat of ablation of the graphite-charring materials. However, this also is true for other ablators, such as OTWR (oblique tape-wound refrasil), astrolite, and nylon-phenolic (ref. 46). For OTWR and astrolite, the slope of the Q* versus enthalpy curve (η) was relatively constant in nitrogen, nitrogen plus carbon dioxide (up to 10 percent), and air. However, η for nylon-phenolic was considerably lower in air than in nitrogen and combined nitrogen and carbon dioxide. It is apparent, therefore, that the atmospheric composition plays a significant role in the degradation of many, if not all, ablative materials.

Fiber orientation also has a significant effect on ablative properties. Generally, fiber orientation parallel to the gas flow results in a higher Q*. However, parallel fiber orientation also produces higher thermal conductivity in the direction of heat flow, which is disadvantageous for thermal insulation. Recent tests (on the 10-Mw arc) have shown that an oblique-angle fiber orientation (similar to OTWR) may give the best insulation efficiency.

2) 10-Mw arc. The 10-Mw arc produces turbulent gas flow in a pipe specimen with heat fluxes up to 1500 Btu/ft^2-sec. Tested samples of OTWR (a silica-phenolic tape-wound ablator) and two graphite-epoxy materials are shown in figures 236 and 237, respectively. Test conditions were approximately the same, except that the shear forces on the OTWR were slightly higher than those on the graphite materials. The delaminations noticed in the X-6023 material in figure 237 are caused by bondline delaminations. It is seen that the OTWR, while possessing good char stability, eroded considerably more than the graphite-based materials. The calculated heats of ablation were higher for the graphite-based materials.

b. Radiant heating. Radiant heating tests were carried out on various graphite-based materials on three different facilities: a low intensity arc, a high intensity arc, and the solar furnace.

1) The low-intensity arc. This radiant-arc facility and test results have been discussed in the Mars lander, materials section, of this report. The graphite-based materials did not erode significantly under a radiant flux of 450 Btu/ft^2-sec, although resin degradation occurred as shown by weight-loss measurements.

2) High-intensity arc. A high-intensity radiation, heat-transfer facility has been built and used at Avco-Everett Research Laboratory for a preliminary evaluation of materials at apparent radiant heat fluxes up to 50 kw/cm^2. This facility and the tests conducted are described by Louis, et al, in appendix C

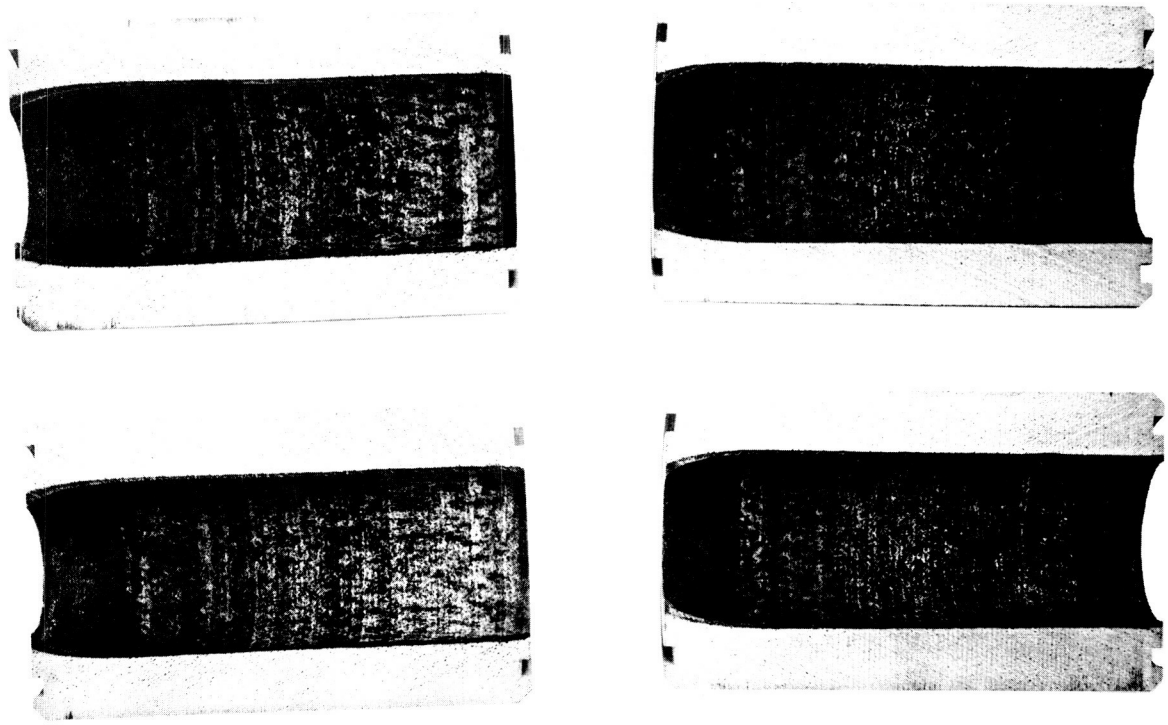

Figure 236 OBLIQUE TAPE-WOUND REFRASIL (OTWR) AFTER TESTING IN 10-MEGAWATT ARC
P-8925

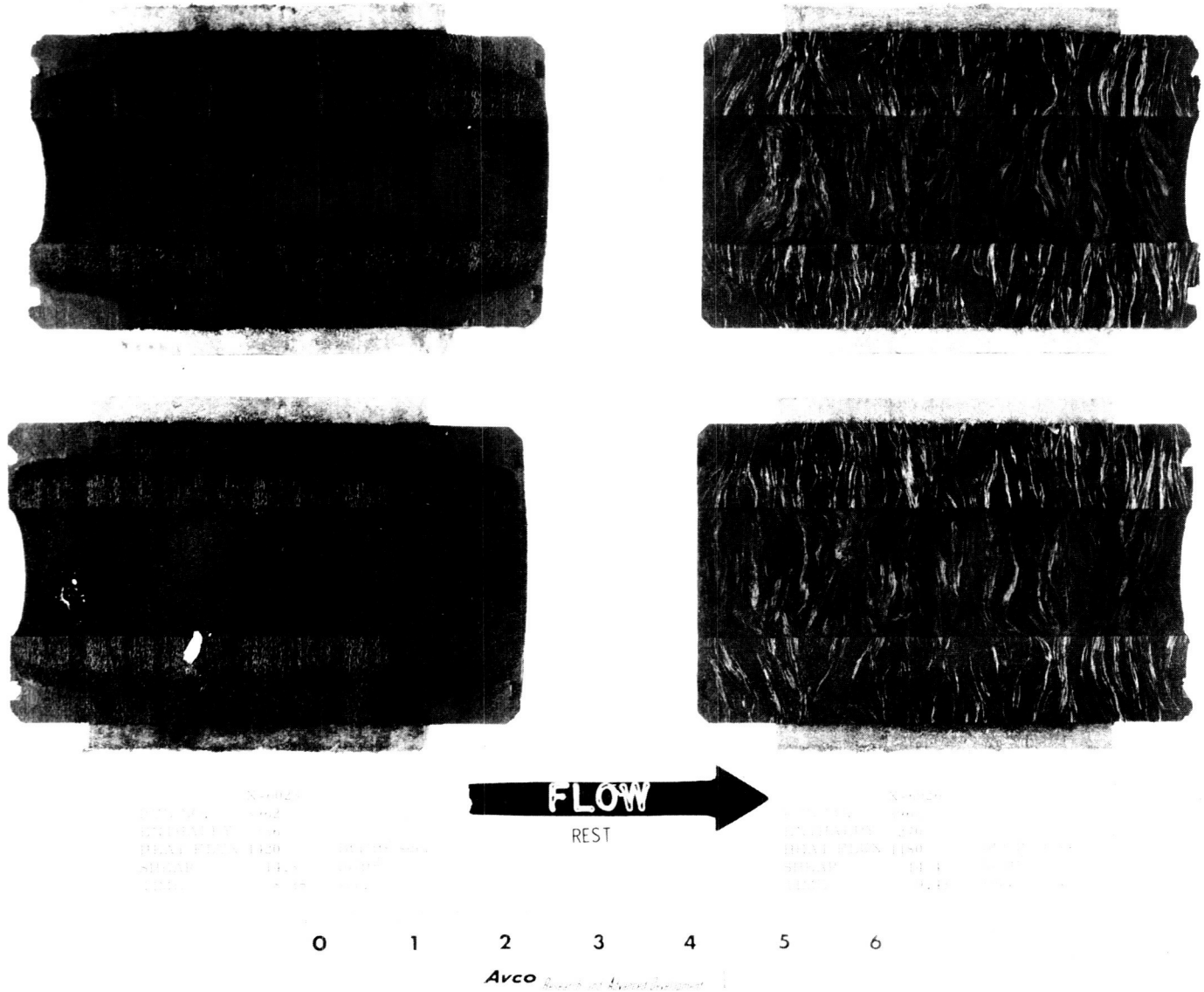

Figure 237 GRAPHITE-BASED MATERIALS AFTER TESTING IN
10-MEGAWATT ARC
P-9699A

and ref. 47. The arc is basically two carbon electrodes inserted into the ends of a pipe specimen. The power source is a battery bank capable of 3 Mw at a current up to 22,000 amperes for times up to 3 seconds. The facility has been operated for one minute at 500-kw input. There are three ways the power can be dissipated: electrode losses, absorption by the test material (heating, melting, vaporization), and superheating of the material vaporized from the test specimen (and electrodes).

As the pressure in the arc column rises above ambient pressure, the superheated ablated material is discharged through the passage between the electrodes and the test material. During a test, the total current is measured, as well as the voltage distribution along the wall using probes. Therefore, the average heat-transfer rate falling onto the test specimen can be determined for the center of the test section where stagnation conditions prevail. Preliminary heats of ablation can be calculated by dividing the apparent heat-transfer rate by the mass rate of ablation per unit area. However, these values should be treated with caution because of uncertainties in the data obtained. The establishment of steady state is not known, energy losses are not clearly defined, and the vaporized material may act as a shield to radiant energy into the test specimen. Spectroscopic studies indicated a column temperature in the vicinity of 14,000°K. Calculations (ref. 48) have indicated that significant radiant energy absorption by molecular species may occur at 10,000°K and above. This consideration would tend to make the calculated Q*'s high. However, this shielding effect may more closely simulate actual entry conditions than if it were eliminated.

The materials tested were graphite, Teflon, astrolite (silica-phenolic laminate), linen-phenolic, and a graphite-epoxy laminate. As expected, the graphite possessed the highest heat of ablation. The next best material appeared to be the graphite-epoxy laminate.

3) The solar furnace. The Avco RAD solar furnace is shown in figure 238. A 60-inch diameter paraboloidal reflector can generate heat fluxes up to 3000 Btu/ft^2-sec. under favorable weather conditions. It has an automatic guidance system to precisely follow the apparent motion of the sun.

Preliminary, uninstrumented tests were conducted to compare silica- and graphite-cloth-based phenolic and epoxy heat shield materials. The heat fluxes were approximately 2300 to 2900 Btu/ft^2-sec, and exposure times 3 to 10 minutes. In general, all the graphite-based materials possessed excellent resistance to the radiant heating, showing very little erosion, with no swelling or cracking, even after exposures of 7 to 10 minutes. The silica-based materials (OTWR and RAD 60) eroded significantly at lower test times of 2 to 4 minutes, with violent bubbling noticed. All tests were conducted under one atmosphere of nitrogen.

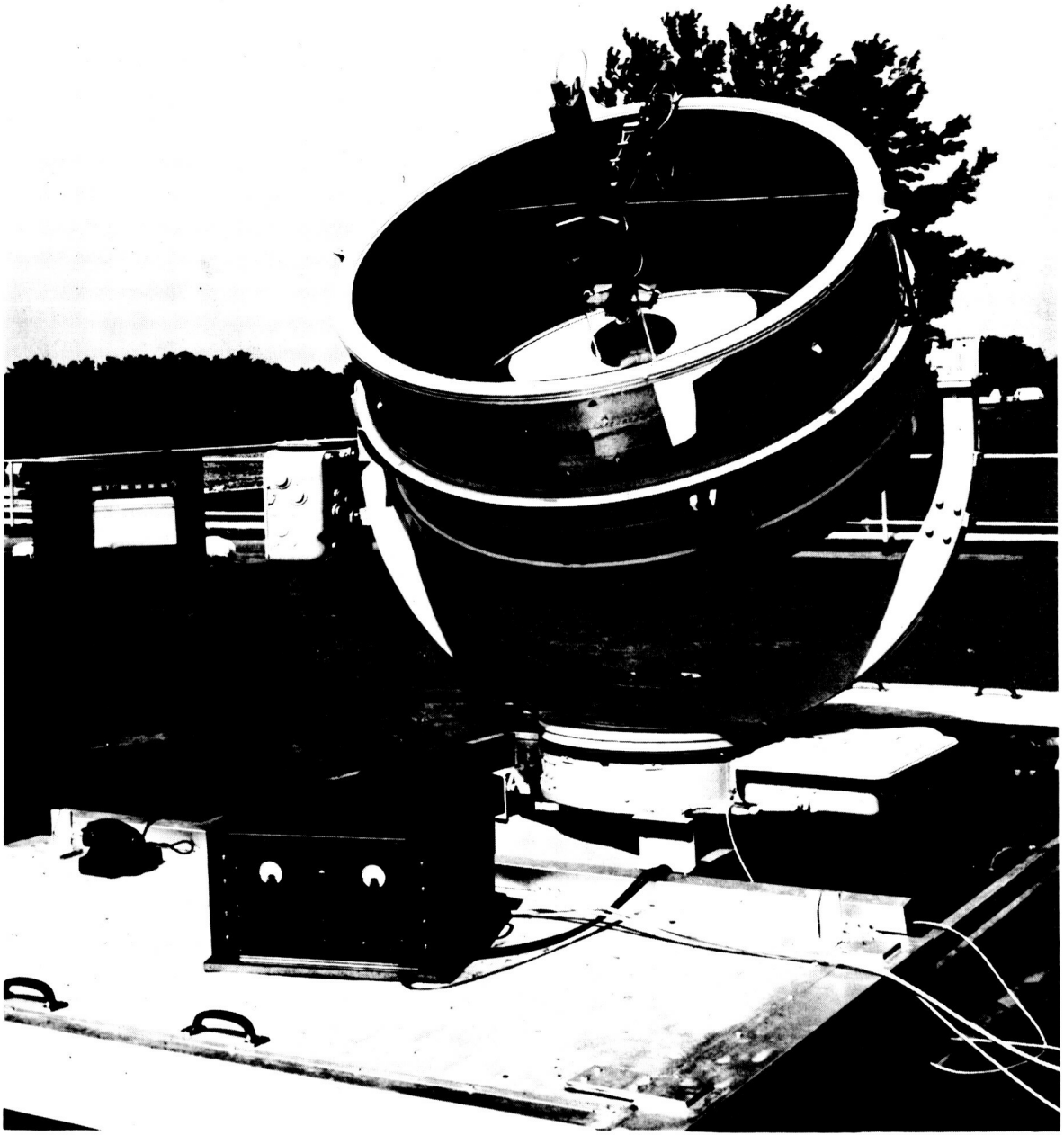

Figure 238 AVCO RAD SOLAR FURNACE
59-1192

Tests currently are underway with instrumented samples in an effort to obtain quantitative evaluation of material performance under a range of heat fluxes and atmospheres.

c. Combined radiant and convective heating. Test specimens of a typical graphite-cloth-epoxy laminate were sent to the Ames Research Center, NASA, Moffett Field, California, for testing on the high-intensity arc. This arc is reportedly capable of total radiant and convective heat fluxes up to 25,000/ft^2-sec. A few preliminary tests were conducted at combined heat fluxes up to 15,000 to 20,000 Btu/ft^2-sec (ref. 49). Lack of instrumentation and insufficient testing prohibit any conclusions on material performance at this time.

3. Physical properties. The physical properties of the graphite- and carbon-based materials vary considerably because of the large number of material variations. Table 39 lists some typical properties of one variation composed of graphite cloth and epoxy resin.

TABLE 39

TYPICAL PROPERTIES OF GRAPHITE- AND CARBON-BASED MATERIALS

	11		1
Density (gr/cc)		1.4	
Thermal conductivity at 250°F $\frac{\text{Btu}}{(\text{hr-ft-°F})}$	1.79		0.66
Specific heat $\frac{\text{Btu}}{\text{lb-°F}}$	0.29 to		--
Coefficient of thermal expansion (°F^{-1})	6 to 10		--
Ultimate tensile strength (psi) versus temperature			
-100°F	11,500		1200
78°F	10,000		1000
350°F	3,800		90
Tensile percent total strain versus temperature			
-100°F	0.89		0.10
78°F	0.77		0.10
360°F	2.47		0.10
Tensile modulus - Ex 10^{-6} (psi) versus temperature			
-100°F	2.07		1.34
78°F	2.16		1.13
350°F	0.58		0.14

11 - Test direction parallel to fiber orientation

1 - Test direction perpendicular to fiber orientation

These data are illustrative only and cannot be used for any design purposes.

As expected, the thermal conductivity and tensile properties are considerably less when measured perpendicular to the cloth orientation than when measured in the parallel direction. Composites made of essentially random orientated fibers possess more isotropic properties which are intermediate between parallel and perpendicular fiber orientation. An interesting composite is composed of HT-1 and carbon fibers in a semirigid epoxy binder. The mechanical properties of this material are far superior over a wide temperature range (-100°F to 350°F) than all other high-performance ablators. For example, at room temperature, tensile strengths of 17,000 psi and total strains of 13 percent are obtained, while at 350°F the strength has dropped to only 5000 psi and the total strain to near 9 percent. The char stability of this material is inferior to other systems and must be improved.

12. STRUCTURE DESIGN--VENUS

12.1 General Approach

1. External structure. The structure of the Venus direct-entry lander can be categorized into the same structural configuration as the Mars lander with the exception that there is no provision for reerection. The design considerations used in the evaluation of the structural integrity of the lander were the modes of failure experienced under planetary entry aerodynamic and inertia loads.

For direct entry into the Venus atmosphere two external configurations (V-1 and V-2) were examined. The entry vehicle external structure was of sandwich construction and two materials, aluminum and stainless steel, were evaluated. The study was directed at evolving an entry vehicle for Venus which would be essentially the same as the vehicle designed for Mars. It was determined that the V-2 shape was suitable for the external configuration of the Venus direct-entry vehicle. In order to minimize the structural design and development problems for a Venus lander, the aerodynamic load-bearing structure also was chosen to be an aluminum-sandwich construction. Although the sandwich construction of the Mars and Venus direct-entry vehicles differs in details (such as face sheet sizes, core thicknesses, and core densities), the vehicles are similar in that they have the same shape and basic diameter.

Due to the uncertainty of surviving direct entry into Venus, an alternate design was evaluated for a lander which enters from orbit. This configuration is a much smaller entry vehicle than the direct-entry lander and also is modified in that it does not survive impact. In order to save heat shield and structural weight, and since such constraints as packaging the payload and stroke for the impact attenuation system were relaxed, the afterbody of the V-2 shape was modified to an Apollo shape for the small Venus lander. The construction of the substructure of this lander is the same type as the other reference vehicles except for this modification.

2. Internal structure. The internal structure for the Venus direct-entry vehicle must have the ability to withstand the high surface temperatures proposed for Venus so it becomes necessary to use a titanium structure. In the design of the internal structure for Venus, it was attempted to provide the same load paths for the entry inertia loads of the payload as the Mars lander so that the effect of these loads on the external structure would be similar. The internal structure is complicated by the fact that a thermal control system must be provided for the payload of a survivable Venus lander. The high inertia loads imposed on the payload during entry must be transmitted through a thermal control system that requires that there be very little heat transmission along the load path. This requires a detailed analysis of the manner of support of

the payload and the thermal-protection system effectiveness which was not feasible at this stage of the study.

The impact attenuation system conceived for the direct-entry Venus capsule maintains the basic principle of a passive system using crushable material for energy absorption. The design mainly was influenced by two overriding considerations: the overall protection required for the much less sophisticated capsule compared to the Mars package, and the extremely high-surface temperature of Venus, presently believed to be in the neighborhood of 800°F.

The concept chosen for the reference design consists of a steel honeycomb expanded over top and bottom of the instrument package. The attempt to provide overall protection conflicts somewhat with the attempt to direct and impact loads into the same internal structural load paths as are used for atmospheric entry loads. The weight penalty incurred by necessitating additional structural members in the internal package is minor and could be eliminated by relieving the honeycomb in the vicinity of weak structural areas.

Steel was chosen as the reference material because of the high-temperature condition. Since the property which was the main influence on the crushing stress of the honeycomb is the yield stress of the steel, the particular steel used would be one which maintains a fairly constant yield stress up to 1000°F, such as Rene 41. Such a steel must be used; otherwise, should the surface temperature be lower or higher than the design value at 800°F, the system could fail. Thus, if a material whose crushing stress was strongly dependent on temperature were used, a surface temperature much less than 800°F could cause the material to be much stronger than anticipated, resulting in excessive decelerations. Conversely, a higher temperature could weaken the material to the extent that the impact energy could not be completely absorbed.

The weight of this system will be in the range of 4 or 5 percent of the total landed-package weight. This is fairly close to the weight ratio obtained for the Mars capsule.

3. Environmental criteria - Venus. The variation of the maximum dynamic pressure (γ_e = -90 degrees) is shown in figure 239 as a function of M/C_DA, atmospheric model, and entry velocity. Figure 240 indicates the maximum axial-deceleration variation for a constant velocity. The reduction in dynamic pressure when an orbital entry vehicle is considered is shown in figure 241. The peak entry loading conditions for the reference designs are:

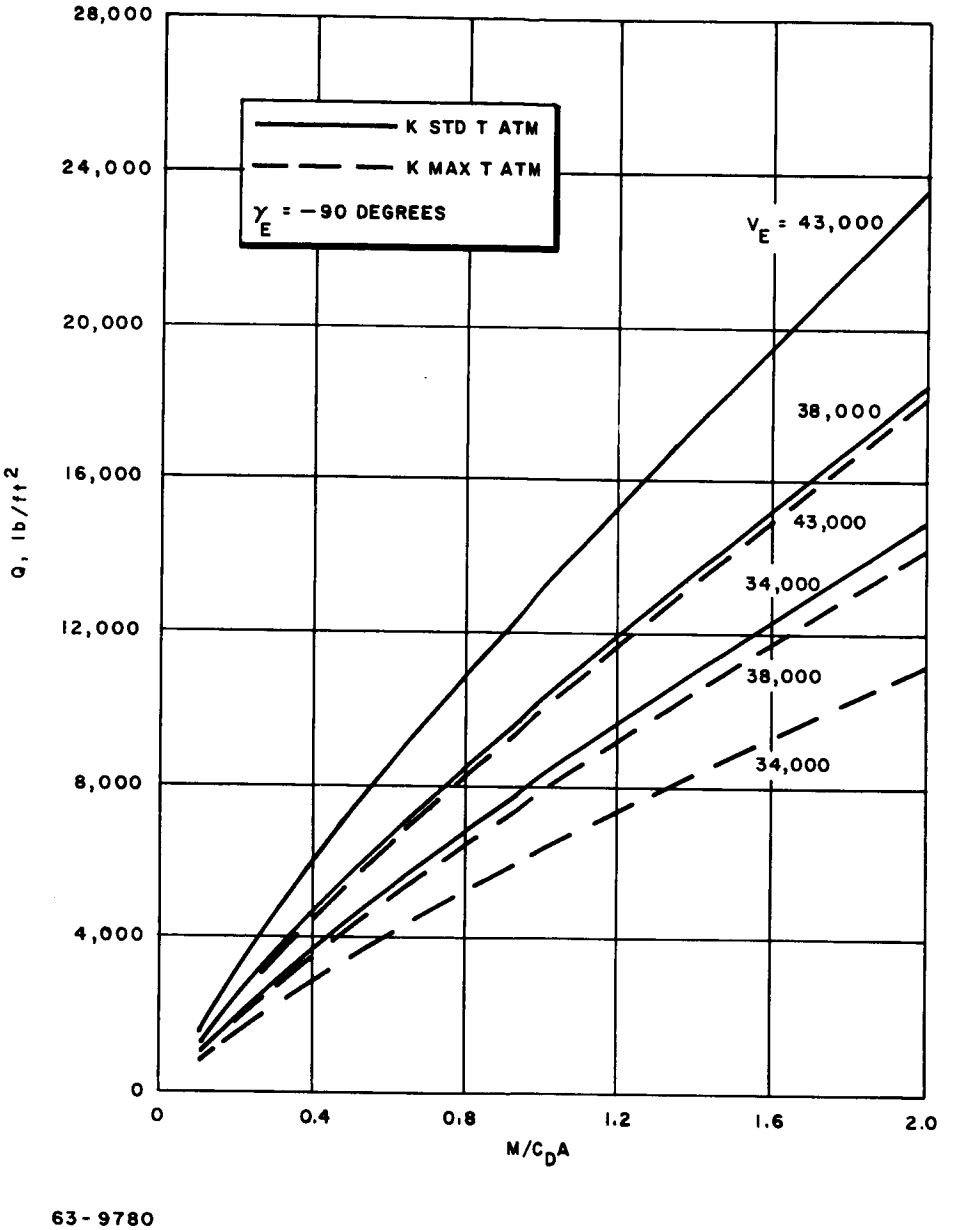

Figure 239 VENUS ENTRY: MAXIMUM DYNAMIC PRESSURE

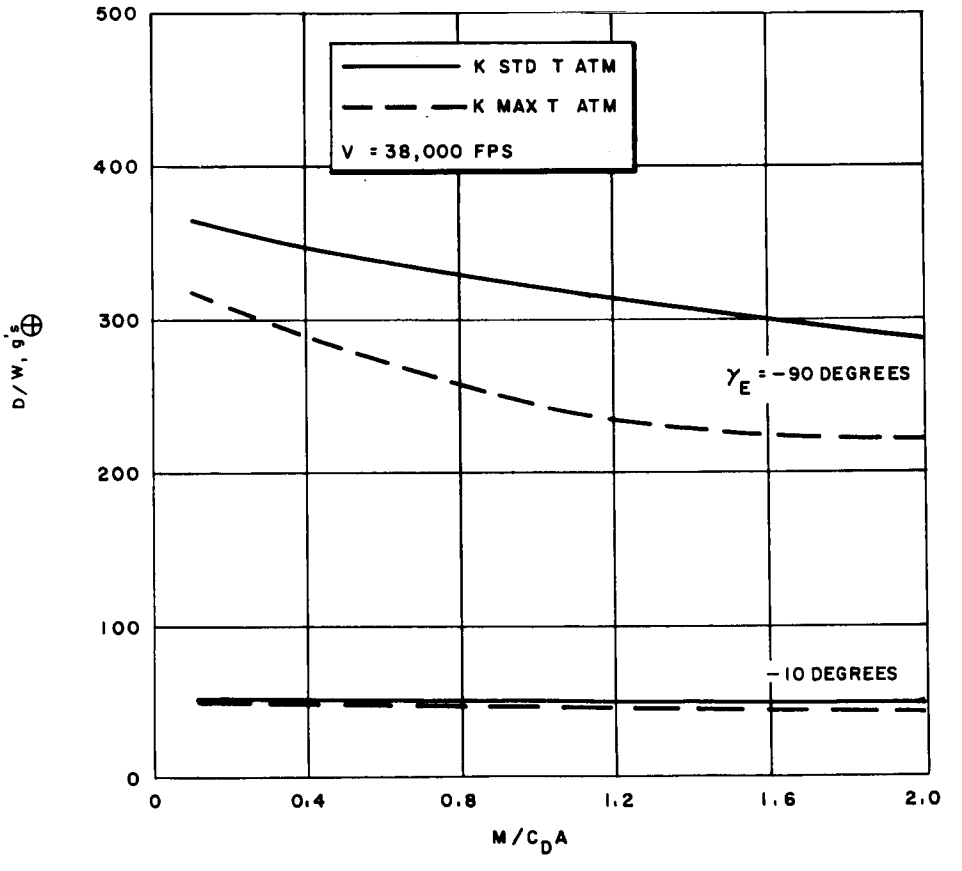

Figure 240 VENUS ENTRY MAXIMUM AXIAN LOAD FACTOR

Venus reference design--direct entry

V_e = 38,000 ft/sec	340 g (Earth) axial
γ_e = -10 to -90 degrees	55 g (Earth) lateral
M/C_DA = 0.6	q = 6,600 lb/ft^2

Venus reference design--orbital entry

V_e = 28,000 ft/sec	50 g (Earth) axial
γ_e = -5degrees -20 degrees	
M/C_DA = 0.5	q = 800 lb/ft^2

12.2 Analysis

1. External structure. The analysis performed on the entry vehicle accounted for two primary modes of failure, general instability and yielding caused by entry aerodynamic loading. The structures of the reference designs were evolved from these considerations.

Figures 242 and 243 depict the variation of the structural weight of the entry vehicle for the V-1 and V-2 shapes for aluminum sandwich construction. These figures demonstrate the significance of the increase in the weight of the structure for a decrease in M/C_DA. For a given M/C_DA, it can be seen that the V-2 vehicle has a weight advantage over the V-1 vehicle.

The use of stainless steel as the material for the known sandwich construction was evaluated and the results are shown in figure 242. It is apparent from the comparison of figures 243 and 244 that there is no significant difference in the weight of the structure for the entry vehicle if either stainless steel or aluminum are used as the structural material.

The use of aluminum-sandwich structure for the reference design of the direct-entry lander was determined by consideration of having structures for the Mars and Venus entry vehicles which were essentially the same. This conclusion resulted from the study of the entry vehicle and was further strengthened by the conclusion that the heat shield material (5026) used for entry into either planet could be similar over portions of the vehicle. The use of the same entry vehicle configuration facilitates the requirements for a detailed design analysis and also the requirements for structural testing of a final design. The modes of failure of the entry vehicles would be the same; therefore, the methods of analysis performed on one could be applied directly to the other.

2. Internal structure. A very preliminary analysis was performed on the internal structure. The structure was designed to introduce the inertia loads into the external structure in the same manner as the Mars lander so that the effect of these loads would have the same consequences on the design of both external structures.

It is necessary to perform a much more detailed analysis on the interaction of the thermal-control system and the method of structural support for the payload components.

The analyses performed thus far on the impact attenuation system for the Venus direct-entry capsule have been of necessity, of a very preliminary nature. They have consisted of, first, assuring that the volume of material crushed during the initial impact is sufficient to dissipate the kinetic energy (and the relatively minute potential energy) of the payload completely, and, secondly, of assuring that there exists no combination of load paths between the outer boundary of the impact attenuation system and the internal package which can impose excessive decelerations on the payload.

Systems satisfying these criteria have been found to fit satisfactorily in the volume available in the entry vehicle. In conclusion, since materials are known which can withstand the temperature environment, the feasibility of a simple, passive, crushable-material impact attenuation system has been established.

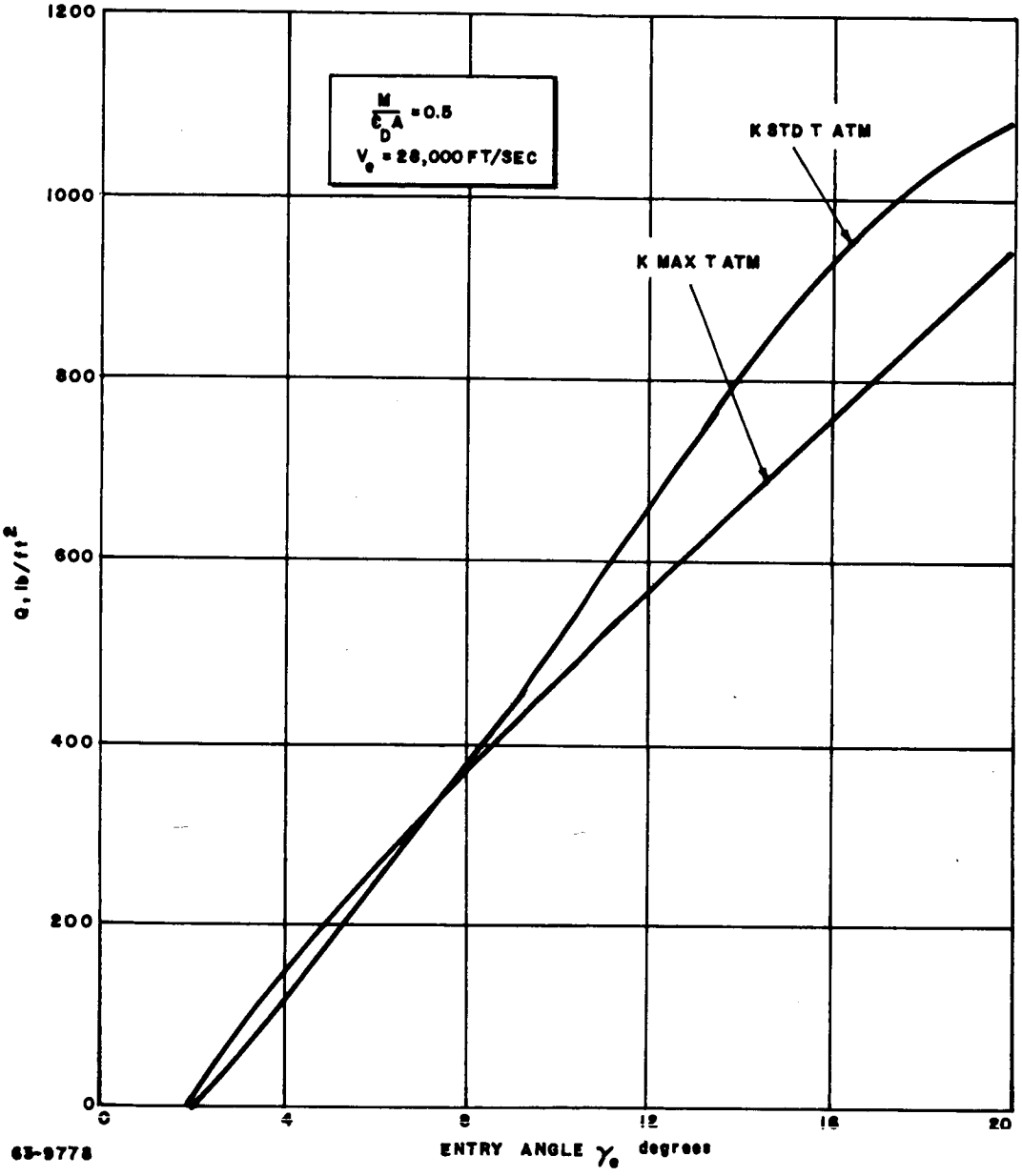

Figure 241 VENUS ORBITAL ENTRY MAXIMUM DYNAMIC PRESSURE

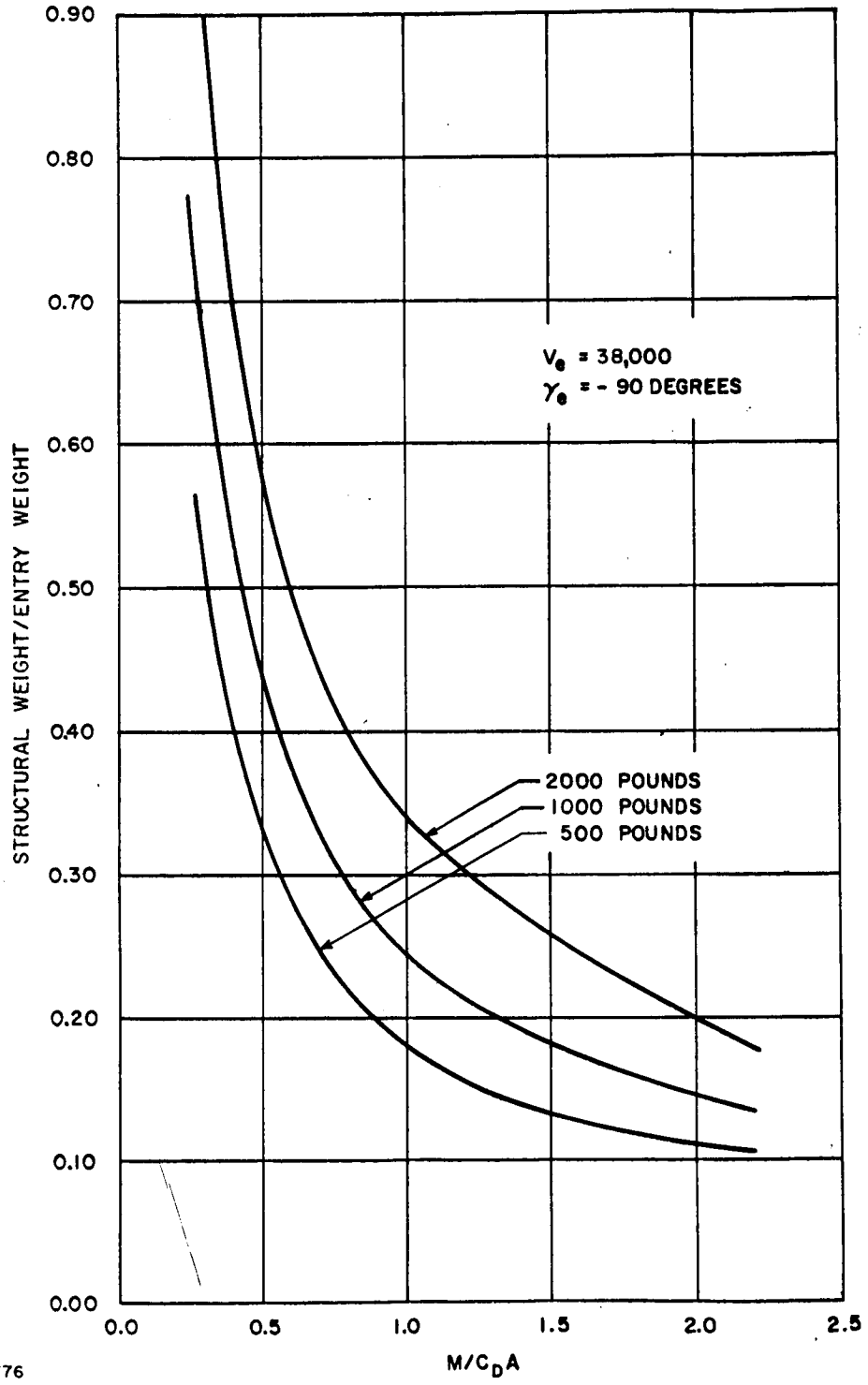

63-9776

Figure 242 VARIATION OF V-1 SHAPE ENTRY VEHICLE STRUCTURAL WEIGHT, FOR ALUMINUM SANDWICH CONSTRUCTION

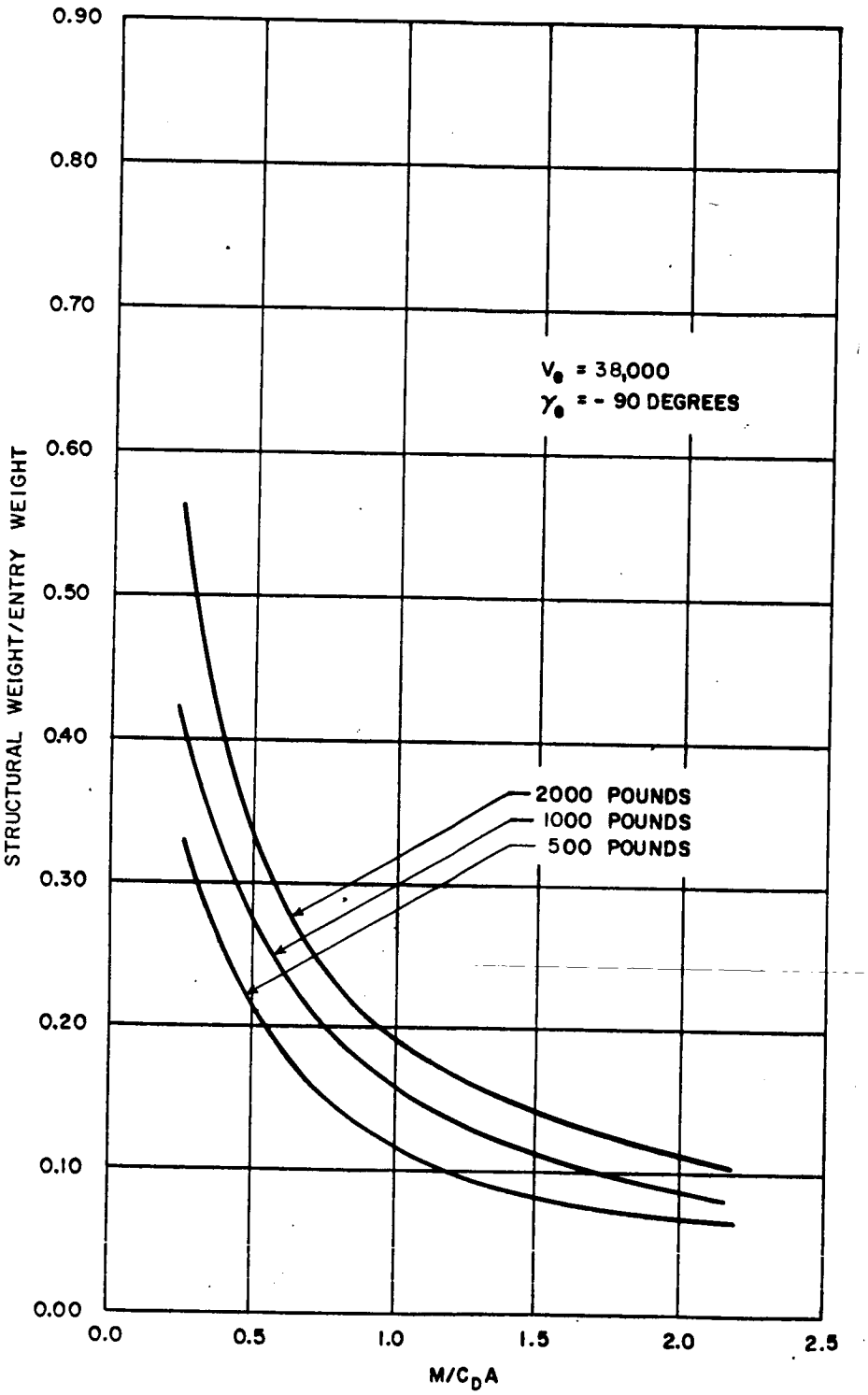

63-9877

Figure 243 VARIATION OF V-2 SHAPE ENTRY VEHICLE STRUCTURAL WEIGHT, FOR ALUMINUM SANDWICH CONSTRUCTION

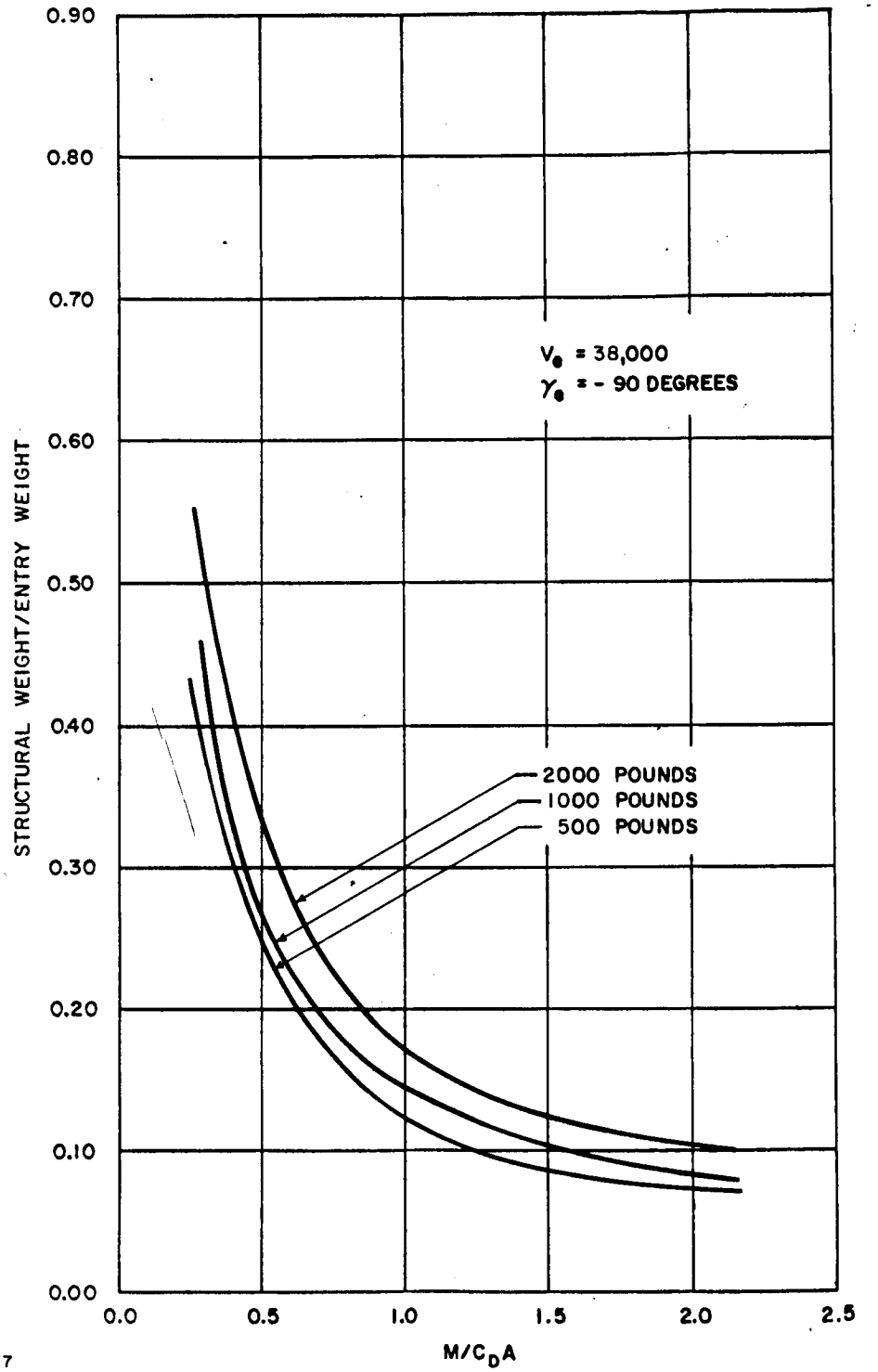

Figure 244 VARIATION OF V-2 SHAPE ENTRY VEHICLE STRUCTURAL WEIGHT, FOR ALUMINUM SANDWICH CONSTRUCTION

13. POWER SUPPLY--VENUS

13.1 Capsule

1. Constraints. The effective life of the Venus capsule from the point of view of power consumption is approximately one hour which begins at separation and ends at impact. As in the case of all Voyager landers, the power source must be heat sterilizable. Furthermore, the entire capsule weighs only 85 pounds.

2. Power source selection. Because the load requirement is small, a nickel-cadmium battery can be accommodated. There are two other power sources which might be suggested, the H_2-O_2 fuel cell and the berylium-thermionic heat engine, but neither is sufficiently developed and the thermionic engine has an inherent startup problem. Thermal batteries are limited to minutes of operating time and provide less watt hours per pound than do nickel cadmium.

3. Power system description. As provided by table 40, the power requirements for the capsule consist simply of an average 31-watt load for a duration of one hour.

TABLE 40

VENUS CAPSULE POWER-CONSUMPTION LIST

Major Subsystem	Power Consumed (watts)
Multiplex/Encoder	3
*VHF transmitter (B)	120
Central programer and sequencer	3
Science	5
*X-band altimeter (intermittent)	35
*Duty cycle of 20 percent	
This involves a battery weight of about $\frac{31 \text{ watt-hour}}{(14\text{wh/lb})\,(0.5)\,(0.9)\,(0.638)} = \frac{31 \text{ watt-hour}}{4.02 \text{ watt-hour/lb}} = 7.9$ pounds	

Where 0.5 is the discharge depth, 0.9 is the sterilization factor, and 0.635 is the discharge factor.

Much of the power shall be consumed at 600 volts for the VHF transmitter. The power-conditioning equipment weight needed for this dc-to-dc conversion and to provide other system voltages shall be about 3 pounds.

4. System weight. Total power-system weight:

Power Conditioning	3.0 pounds
Batteries	7.9 pounds
	10.9 pounds

13.2 Lander

1. Power source selection. The Venus surface temperature of approximately 800 of indicate a short mission powered by a system which is not Carnot cycle limited, as rejection of waste heat will be impossible with reasonably sized radiators. There are two currently available systems which appear to fall into this catagory: a windmill and storage devices.

a. Windmill. It is reasonable to consider a wind-powered device to supply power in a windy environment. A windmill, or wind turbine, is the only power device which is fundamentally insensitive to the extremely high-ambient temperatures. It would take particular advantage of the atmospheric density variously estimated to be between four and 100 times that of Earth and the wind velocity estimated to be greater than 20 mph and possibly much greater. This force represents a considerable driving potential and is shown quantitatively in figure 245. Note that the abscissa is in units of kilowatts. The data in the figure were prepared on the basis of an efficiency of conversion from kinetic energy to useful electrical energy of 40 percent. Theoretical maximum is 60 percent and 35 percent is achieved by Dutch windmills.

Load regulation could be accomplished by using governors and/or variable pitch blades along with electronic-voltage regulators. There is no orientation problem and very little development is necessary, since the existing technology certainly is adequate.

The great question, of course, is: How reliable are the estimates of surface conditions? After atmospheric density and wind velocity have been established, the anemometer is a clear prospect for a power source.

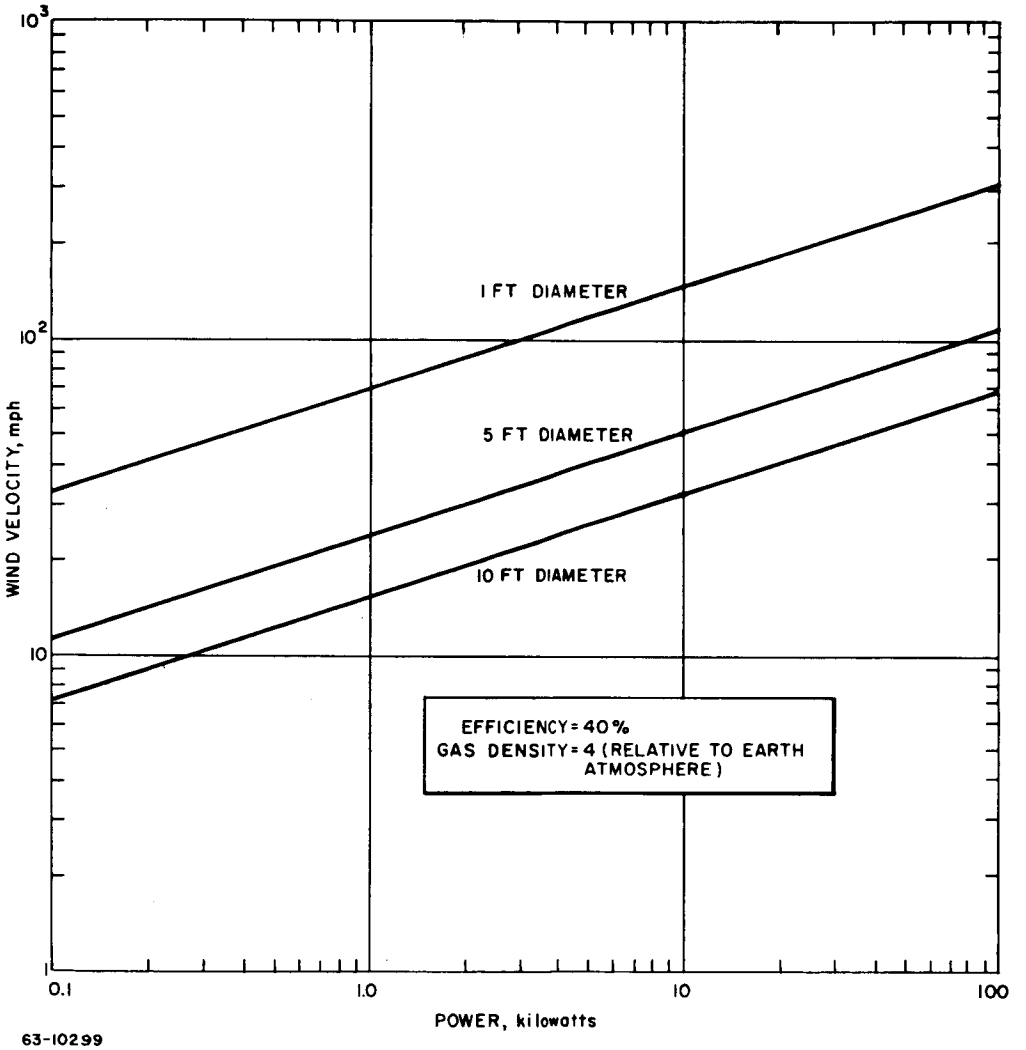

Figure 245 POWER AVAILABLE FROM A WINDMILL

b. Storage devices. The fact that the mission is restricted both by time and energy limitations, the possibility is admitted of using primary or secondary batteries (used as primary batteries) as a power source.

The hydrogen-oxygen fuel cell is similarly a candidate but, by the reasoning expressed earlier in this report, it cannot be considered at this time. Among the batteries, nickel-cadmium is the only type presently sterilizable. Silver zinc, when and if it becomes tolerant to this treatment, or if the requirement is removed for the Venus lander, would be a much more acceptable selection. Nickel-cadmium once again is the only present acceptable battery.

2. System description. The load profile is shown in figure 246, and the list of power users is provided in table 41. The nickel-cadmium battery weight necessary to accommodate the energy requirement is:

TABLE 41

POWER CONSUMPTION LIST

Major Subsystem	Power Consumed (watts)
Multiplex/Encoder	3
Lo Speed Recorder 5×10^5 bits	4
VHF Transmitter (a) (End of Transit)	120
VHF Transmitter (b)	120
S-Band Command Receiver	3
Cont. Prog. & Seq.	3
X-Band Altimeter	35

$$\text{Battery weight} = \frac{504 \text{ watt-hour}}{(14 \text{ watt-hour/lb})\ (0.4)\ (0.9)\ (0.85)} = 94 \text{ pounds}$$

Where 0.5 is the discharge depth, 0.9 is the sterilization factor, and 0.85 is the converter regulator efficiency

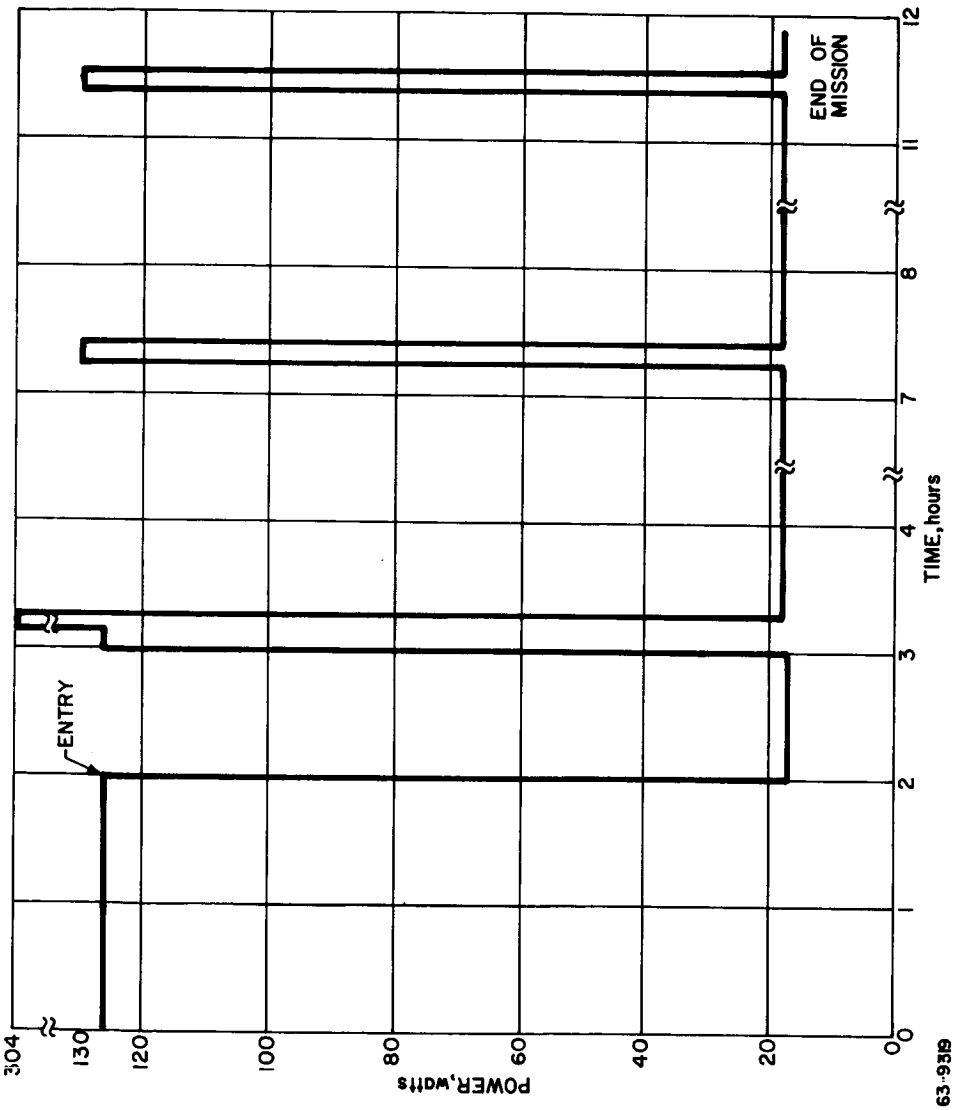

Figure 246 VENUS LANDER LOAD PROFILE

3. Power system weight. Assuming 40 percent redundancy in batteries the resultant system weight is:

Battery weight	131 pounds
Power conditioning	4 pounds
	135 pounds

14. COMMUNICATION SYSTEM--VENUS

14.1 Communication System Requirements

Two types of Venus atmospheric and surface probes are being considered: a capsule to acquire atmospheric data only, and a lander to acquire both atmospheric and surface data. The communication-system requirements for each type of probe are similar to the requirements of the Mars lander system; however, the data-handling requirements are reduced.

1. Lander. The communication-system requirements for the Venus lander are almost identical to those required of the Mars-lander system, with the major exception that the landed mission will last only 10 hours and the total data acquired will be approximately two orders of magnitude less.

2. Capsule. The capsule will be designed to enter the planetary atmosphere from orbiting spacecraft. The trajectories will be planned so that line-of-sight communications between the capsule and the orbiter is maintained throughout descent. The capsule will be required to acquire and transmit to the orbiter scientific data pertaining to the atmosphere only. The data will be played out as they are acquired. Data will be acquired only after parachute deployment, which will occur at about 300,000 feet. This will allow about one hour of descent time.

14.2 General System Description

1. Lander. The Venus-lander communications system will transmit all data acquired during the life of the lander by means of a VHF relay link through the orbiter. The system consists of loaded-slot VHF antennas located at the upward side of the disc-shaped instrumentation package. Antennas will be provided on both sides of the disc to allow for landed orientation contingencies; however, only those on the upward side will be used. The modulation scheme used in this link will be pulsed linear chirp. This modulation scheme is used to minimize the effects of multipath interference as discussed for the Mars lander. The system utilizes a 50-watt transmitter. Before impact, the system provides a bit rate of approximately 300 bits/sec at which a worst case performance margin of -0.8 db can be expected at the worst case range of 9,000 km. After impact the system provides a bit rate of approximately 10^4 bits/sec at which a worst case performance margin of +8.34 db can be expected at the worst case range of 2500 km. A separate-pulsed, linear-chirp system will be used to relay information to the orbiter prior to parachute deployment. This system also utilizes a 50-watt transmitter; however, it plays out through an omnidirectional antenna system located in the heat shield. For a bit rate of 20 bits/sec a

worst case performance margin of +1.2 db can be expected for a worst case range of 18,000 km.

A radar altimeter will be used by the lander to obtain altitude correlation of the atmospheric data and to provide signals for deployment of the parachutes and jettisoning the heat shield. The details of all subsystems are discussed in the section on the Mars lander.

A command receiver is required to ascertain the appropriate time for playout of surface data. This receiver will be a threshold detecting device designed to receive a VHF tone transmitted from the orbiter.

The data handling equipment on board the lander will be capable of operating in any one of three modes. Data requiring storage will be stored on an endless loop low speed tape recorder.

The source of power for the lander will be a 500-watt-hour nickle cadmium battery.

The total weights, volumes, and power consumptions of the lander communications system equipments are listed in table 42.

2. Capsule. The capsule communications system will transmit all data acquired during descent in real time to the orbiter by means of the pulsed linear-chirp system. The system consists of VHF omni-antennas located in the heat shield, and a 50-watt transmitter. This system provides a bit rate of 300 bits/sec at which a worst case performance margin of -0.8 db can be expected at the worst case range of 9000 km.

A radar altimeter will be used on the capsule for the same purpose it was used on the Venus lander. The power source will again be a battery.

The total weights, volumes and power consumptions of the capsule communications system equipments are shown in table 43.

14.3 Detailed System Description

1. Lander. A simplified block diagram of the lander communications system which will meet all of the requirements stated in section 1 is shown in figure 247. The system is capable of operating at any of three transmission rates with three corresponding data acquisition modes. These mode pairs are acquisition and playout of engineering data prior to parachute deployment, acquisition and playout of atmospheric data including TV pictures and acquisition and playout of surface data.

TABLE 42

VENUS LANDER
Subsystem Weights, Volumes, and Power Consumptions

Major Subsystem	Weight (pounds)	Volume (in.^{3})	Power Consumption (watts)
Multiplexer/Encoder	7	100	3
Tape Recorder 5 x 10^6 Bits Capacity	7	800	4
VHF Transmitter (A)	12	220	120
VHF Transmitter (B)	12	220	120
VHF Command Receiver	4	60	3
VHF Omni Antenna (in Heat Shield)	3	-	-
VHF Loaded Slot Antennas (Telemetry)	3	-	-
VHF Loaded Slot Antennas (Command)	3	-	-
Central Programmer and Sequencer	3	200	3
Power Conditioning	6.5	260	Dissipation figured in as battery capacity factor
X-Band Altimeter	5	30	35 (2-watt Average)
Battery	108	-	-
Totals	173.5	1890	Phase A - 126 watts* Phase C - 304 watts* Phase F - 130 watts*

*Includes Scientific Instruments Power Consumption

TABLE 43

VENUS CAPSULE
Subsystem Weights, Volumes, and Power Consumptions

Major Subsystem	Weight (pounds)	Volume ($in.^3$)	Power Consumption (watts)
Multiplexer/Encoder	2	100	3
VHF Transmitter (60W)	12	220	120
VHF Antenna System	3	-	-
Central Program and Sequencer	3	200	3
Power Conditioner	6.5	260	Efficiency of 0.85 used to calculate battery capacity required
X-Band Altimeter	5	30	35 (intermittant) (2-watt average)
Battery	6	-	-
Scientific Instruments	N/A	N/A	5 (Average)
Totals	37.5	810	123 for communications + 7 Average for instruments + 3 Continuous for central Prog. & Sequenc.

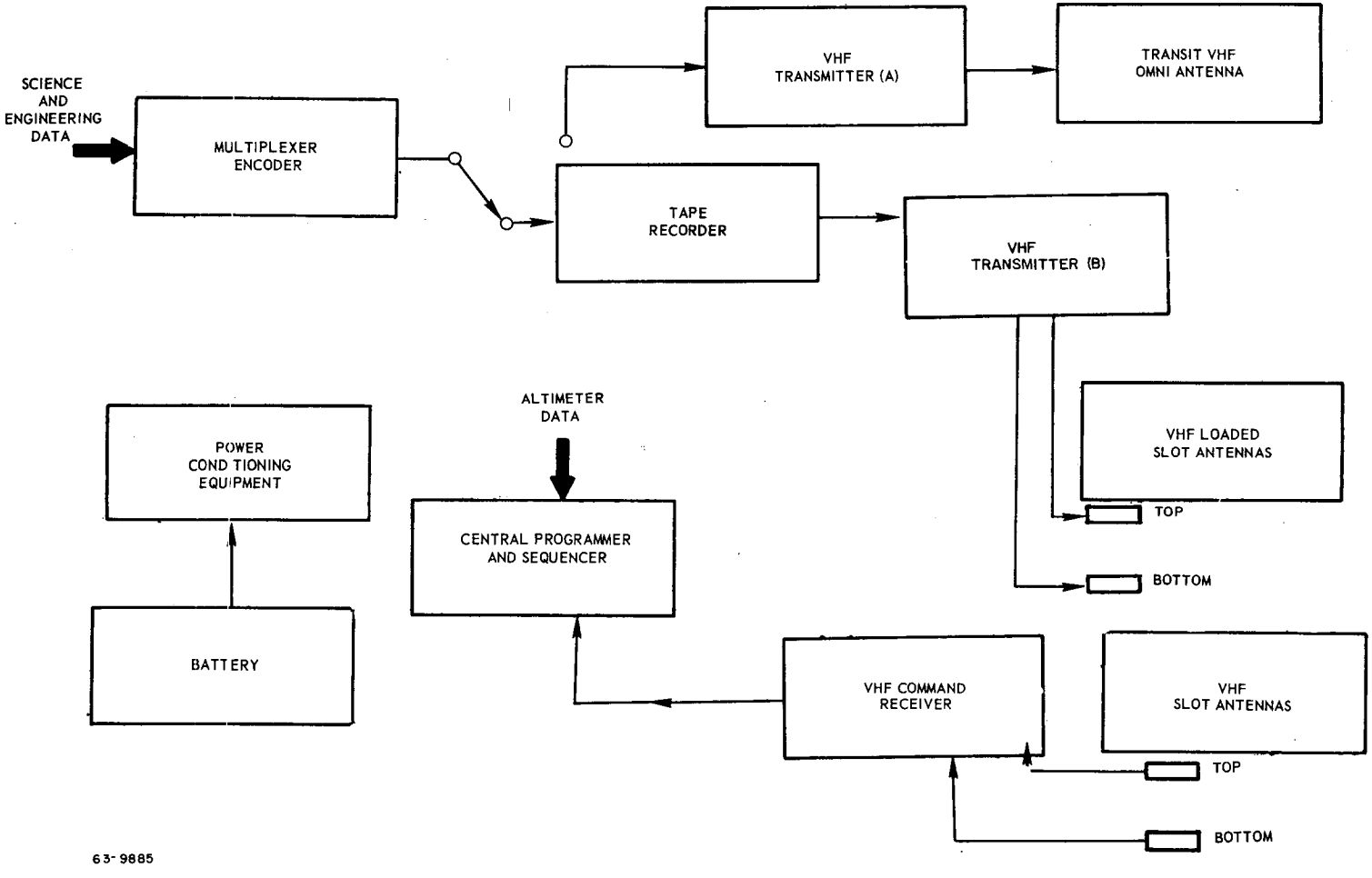

Figure 247 VENUS LANDER COMMUNICATION SYSTEM BLOCK DIAGRAM

a. VHF engineering data mode. The Venus lander engineering and status data will be transferred to the spacecraft during the two hours prior to atmospheric entry. Since the lander will not be attitude stabilized, transmission will be through omnidirectional antennas. The transmission range will be maximum at the time of transmission; however, the total quantity of data involved is small enough so that the bit rate can be kept quite low. Table 44 shows the design parameters for this link.

b. Atmospheric data mode. The atmospheric data acquired by the lander during its parachute descent will be stored on magnetic tape for transmission just before impact. Since the transmission range will be decreasing during the parachute descent the optimum time for transmission will be as close to impact as possible. Table 45 shows the design parameters for this link using a playout time of 10 minutes which is the minimum for transmitting all of the atmospheric data with the transmitter chosen.

c. Surface data mode. The surface data and the TV pictures, both of which are stored on magnetic tape, will be transmitted to the orbiting spacecraft when it passes over the lander. The trajectories of the lander and orbiter will be such that when the orbiter does pass over the lander it will be at periapsis. The transmission range will then be about 2500 km maximum. The design chart for this link (table 46) shows that a bit rate of 10^4 bits per second is possible. This value will allow playout of all the required data in 10 minutes.

2. Capsule. The atmospheric sampling capsule communications system is shown in block diagram form in figure 248. This system is designed to perform the single task of transmitting the atmospheric data, as it is acquired, to the orbiting Voyager spacecraft. The equipment used will be much the same in design and construction as that proposed for the lander.

The rate of data acquisition is uncertain so that the choice of transmitted bit rate was made on the basis of equipment size and weight and the required transmission range.

Although the orbit geometry is not absolutely predictable in advance, a maximum slant range of 9000 km has been chosen as a conservative value.

Table 47 shows the design parameters for this link. At a bit rate of 300 bits/sec, the worst case performance margin will be -0.8 db.

3. Hardware considerations. All of the electronic subsystems discussed for the Venus lander and atmospheric capsules will be adaptations of the systems described for the Mars lander. Most of these systems will be exactly as described there. The notable exceptions will be the multiplexer/encoders which will be very much simplified, and the tape recorder.

TABLE 44

SEPARATION TO ENTRY TELECOMMUNICATIONS DESIGN CONTROL CHART
(Lander To Orbiter, Separation To Entry (2 hour playout at end))

No.	Parameter		Nominal Value	Tolerance (decibels)	Source	Worst Value
1	Total transmitter power	50 watts	+47.0 dbm	+0.0 -0.5		+46.5 dbm
2	Transmitting circuit loss		-0.25 db	+0.0 -0.05		-0.3 db
3	Transmitting antenna gain	140-degree loaded slots	+4.5 db	+0.0 -0.5		+4.0 db
4	Transmitting antenna pointing loss		-1.5 db	±1.5		-3.0 db
5	Space loss = 32.46+20 log F+20 log R F 300 mc, R 18,000 km		-167.1 db	-		-167.1 db
6	Polarization loss		-0.0 db	±1.5		-1.5 db
7	Receiving antenna gain	Helix	+5.0 db	±0.5		+4.5 db
8	Receiving antenna pointing loss	84 degrees	-3.0 db	+0.0 -1.0		-4.0 db
9	Receiving circuit loss		-0.1 db	maximum		-0.1 db
10	Net circuit loss		-162.45 db	+3.5 -5.05		-167.5 db

TABLE 44 (Concl'd)

No.	Parameter	Nominal Value	Tolerance (decibels)	Source	Worst Value
11	Total received power	-115.45 dbm	+3.5 -5.5		-121.0 dbm
12	Receiver noise spectral density (N/B) T system_____NF 4 db	-169.8 dbm	+1.0 -0.0		-168.8 dbm
13	Predetection bandwidth (10^6 cps)	+60 db	-		+60 db
14	Required ST/N/E ($p_e = 5 \times 10^{-4}$)	+14.6 db	+1.0 -0.0		+15.6 db
15	Detector threshold power	-95.2 dbm	+2.0 -0.0		-93.2 dbm
16	Pulse compression gain	+20.0 db	+0.0 -1.0		+19 db
17	Integration improvement (500 bts/data bit)	+10.0 db	±1.0		+9.0 db
18	Required received power	-125.2 dbm	+3.0 -2.0		-122.2 dbm
19	Performance margin	+9.75 db	+5.5 -8.55		+1.2 db

TABLE 45

ATMOSPHERIC DATA MODE TELECOMMUNICATIONS DESIGN CONTROL CHART
(Lander to Orbiter, Transfer of Atmospheric Data (2×10^6 Bits in 10 Min.)

No.	Parameter	Nominal Value	Tolerance (decibels)	Source	Worst Value
1	Total transmitter power 50 watts	+47 dbm	+0.0 -0.5		+46.5 dbm
2	Transmitting circuit loss	-0.25 db	+0.0 -0.05		-0.3 db
3	Transmitting antenna gain 140-degree loaded slots	-4.5 db	+0.0 -0.5		-4.0 db
4	Transmitting antenna pointing loss	-1.5 db	±1.5		-3.0 db
5	Space loss = 32.46+20 log F+20 log R +2 db (Atmos) F 300 mc, R 9,000 km	-163.1 db	-		-163.1 db
6	Polarization loss	-0.0 db	±1.5		-1.5 db
7	Receiving antenna gain Helix	+5.0 db	±0.5		+4.5 db
8	Receiving antenna pointing loss 84 degrees	-3.0 db	+0.0 -1.0		-4.0 db
9	Receiving circuit loss	-0.1 db	maximum		-0.4 db
10	Net circuit loss	-158.45 db	+3.5 -5.05		-163.5 db

TABLE 45 (Concl'd)

No.	Parameter	Nominal Value	Tolerance (decibels)	Source	Worst Value
11	Total received power	-111.45 db	+3.5 -5.55		-117.0 dbm
12	Receiver noise spectral density (N/B) T system_____NF 4 db	-169.8 dbm	+1.0 -0.0		-168.8 dbm
13	Predetection bandwidth (10^6 cps)	+60 db	---		+60 db
14	Required ST/N/B ($P_e = 5 \times 10^{-4}$)	+14.6 db	+1.0 -0.0		+15.6 db
15	Detector threshold power	-95.2 dbm	+2.0 -0.0		-93.2 db
16	Pulse compression gain	+20.0 db	+0.0 -1.0		+19.0 db
17	Integration improvement	+3.0 db	---		+3.0 db
18	Required received power	-118.2 dbm	+2.0 -1.0		-116.2 dbm
19	Performance margin	+6.75 db	+4.5 -7.55		-0.8 db

TABLE 46

TRANSFER OF SURFACE DATA, TELECOMMUNICATIONS DESIGN CONTROL CHART
(Lander to Orbiter, Transfer of Surface Data, VHF Slot Antennas)

No.	Parameter		Nominal Value	Tolerance (decibels)	Source	Worst Value
1	Total transmitter power	50 watts	+47 dbm	+0.0 -0.5		+46.5 dbm
2	Transmitting circuit loss		-0.25 db	+0.0 -0.05		-0.3 db
3	Transmitting antenna gain	140-degree loaded slots	+3.5 db	+0.0 -0.5		+3.0 db
4	Transmitting antenna pointing loss		-1.5 db	±1.5		-3.0 db
5	Space loss = 32.46+20 log F+20 log R F 300 mc, R 2500 km		-149.96 db	---		-149.96 db
6	Polarization loss		0.0 db	±1.5		-1.5 db
7	Receiving antenna gain	65° Helix	+5.0 db	±0.5		+4.5 db
8	Receiving antenna pointing loss	84 degrees	-3.0 db	+0.0 -1.0		-4.0 db
9	Receiving circuit loss		-0.1 db	maximum		-0.1 db
10	Net circuit loss		-146.31 db	+3.50 -5.05		-151.36 db

TABLE 46 (Concl'd)

No.	Parameter	Nominal Value	Tolerance (decibels)	Source	Worst Value
11	Total received power	-99.31 dbm	+3.50 -5.55		-104.86 dbm
12	Receiver noise spectral density (N/B) T system_____ NF 4 db	-169.8 dbm	+0.0 -0.0		-168.8 dbm
13	Predetection Bandwidth (10^6 cps)	+60 db	---		+60 db
14	Required ST/N/B ($P_e = 5 \times 10^{-4}$)	+14.6 db	+1.0 -0.0		+15.6 db
15	Detector threshold power	-95.2 dbm	+2.0 -0.0		-93.2 dbm
16	Pulse compression gain	+20 db	+0.0 -1.0		+19.0 db
17	Integration improvement	+0.0 db	---		+0.0 db
18	Required received power	-115.2 dbm	+2.0 -1.0		-113.2
19	Performance margin	+15.89 db	+4.5 -7.55		+8.34 db*

*This becomes +6.34 db allowing 2 db for atmospheric absorption loss.

TABLE 47

CAPSULE TELECOMMUNICATIONS DESIGN CONTROL CHART
(Capsule to Orbiter, Transfer of Atmospheric Data (continuous playout, 1 hour, 2×10^5 bits)

No.	Parameter	Nominal Value	Tolerance (decibels)	Source	Worst Value
1	Total transmitter power 50 watts	+47.0 dbm	+0.0 -0.5		+46.5 dbm
2	Transmitting circuit loss	-0.25 db	+0.0 -0.05		-0 3 db
3	Transmitting antenna gain	+4.5 db	+0.0 -0.5		+4.0 db
4	Transmitting antenna pointing loss	-1.5 db	±1.5		-3.0 db
5	Space loss = 32.46+20 log F+20 log R +2 db (Atmos) F 300 MC, R 9,000 KM	-163.1 db	---		-163.1 db
6	Polarization loss	-0.0 db	±1.5		-1.5 db
7	Receiving Antenna gain HELIX	+5.0 db	±0.5		+4.5 db
8	Receiving Antenna pointing loss 84 degrees	-3.0 db	+0.0 -1.0		-4.0 db
9	Receiving circuit loss	-0.1 db	maximum		-0.1 db
10	Net circuit loss	-158.45 db	+3.5 -5.05		-163.5 db

TABLE 47 (Cont'd)

No.	Parameter	Nominal Value	Tolerance (degrees)	Source	Worst Value
11	Total received power	-111.45 dbm	+3.5 -5.55		-117.0 dbm
12	Receiver noise spectral density (N/B) T system _____ NF 4 db	-169.8 dbm	+1.0 -0.0		-168.8 dbm
13	Predetection Bandwidth (10^6 cps)	+60.db	---		+60.0 db
14	Required ST/N/B ($P_e = 5 \times 10^{-4}$)	+14.6 db	+1.0 -0.0		+15.6 db
15	Detector threshold power	-95.2 dbm	+2.0 -0.0		-93.2 dbm
16	Pulse compression gain	+20.0 db	+0.0 -1.0		+19.0 db
17	Integration improvement	+3.0 db	---		+3.0 db
18	Required received power	-118.2 dbm	+2.0 -1.0		-116.2 dbm
19	Performance margin	+6.75 db	+4.5 -7.55		-0.8 db

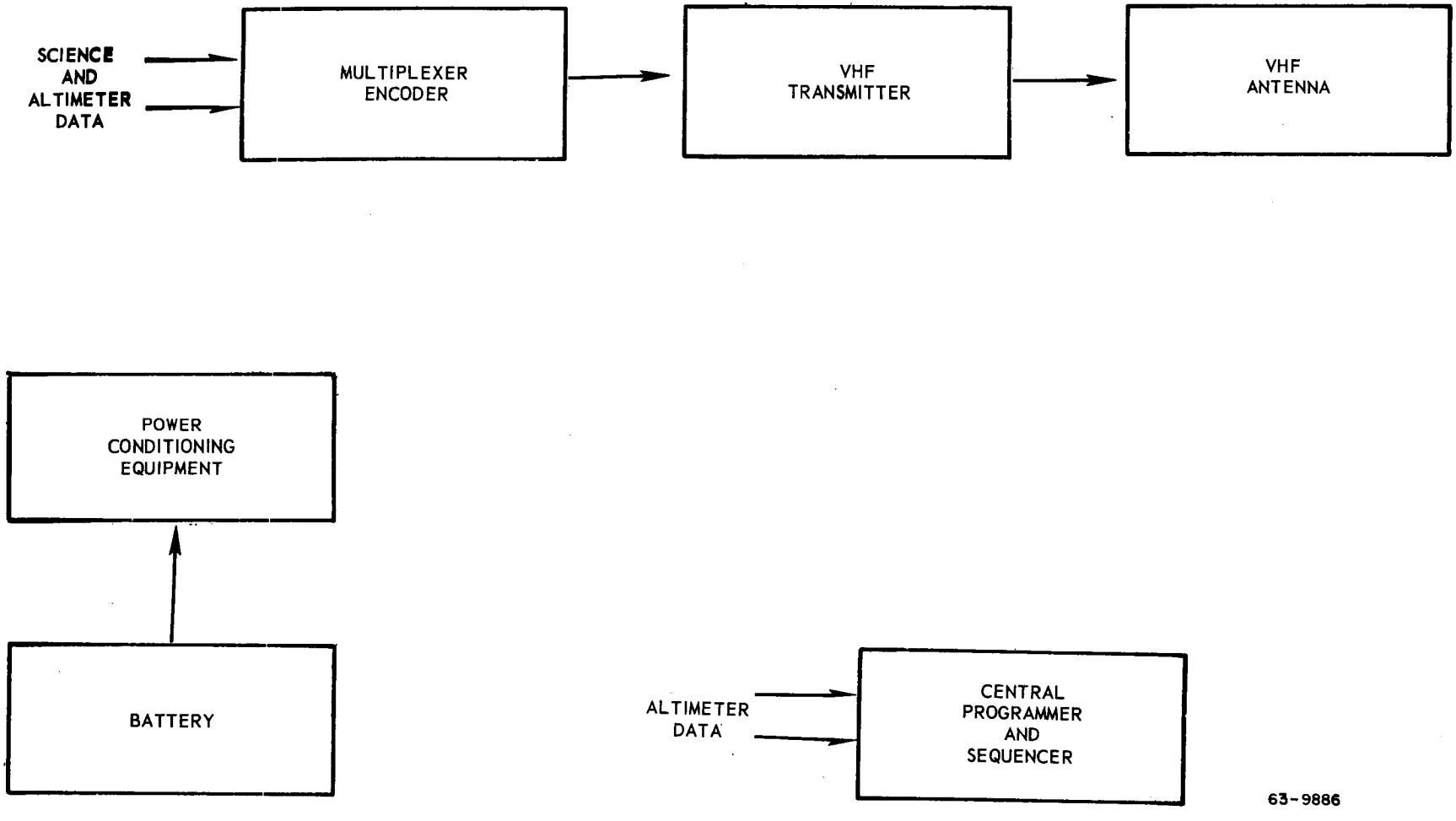

Figure 248 VENUS ATMOSPHERIC CAPSULE COMMUNICATION SYSTEM BLOCK DIAGRAM

The tape recorder used in the Venus lander will be an endless loop design of the type developed for the Mariner C program. This type of recorder will be significantly smaller and lighter than those required for the Mars lander but will be able to provide adequate capacity.

14.4 Antenna Designs

1. Lander antennas. A study was conducted to determine the most feasible antenna types for use on the Venus lander. The telmetry antenna required on the vehicle is to operate at 300 mc and will telemeter data back to the orbiter-bus.

The size and weight restrictions of the lander package led to the choice of the crossed-slot technique as the most feasible antenna design for use in the Venus lander. Some of the advantages of this type of antenna are:

a. The antenna is more compact than a conventional slot radiator.

b. Diagonal feeding results in an electrical length equivalent to 1.414 times the physical aperture.

c. This unit is 75 to 85 percent efficient.

d. It is flush mounted and rugged.

The basic principles involved in the theory of operation were presented in the Mars relay/command link section of the study report.

When considering a design for use in space systems, many factors must be investigated. Some of the more important factors are size and type of space structure, input power requirements, beamwidth, and the environments in which the antenna must operate. To date there is very little verified data on the atmospheric conditions on Venus; therefore, some basic assumptions must be made. An atmosphere consisting of 90 percent CO_2, 8 percent N_2, and 2 percent argon and a temperature ranging from 600 to 800° K at sea level was assumed.

The lander will be equipped with two antennas mounted on opposite sides of the vehicle. The system shall be designed such that each antenna will operate independently. The specific shape of the vehicle requires the use of a gravity switch network which ensures switching from one antenna to the other, depending upon which side of the lander is facing upward. A typical antenna installation is shown in figure 249.

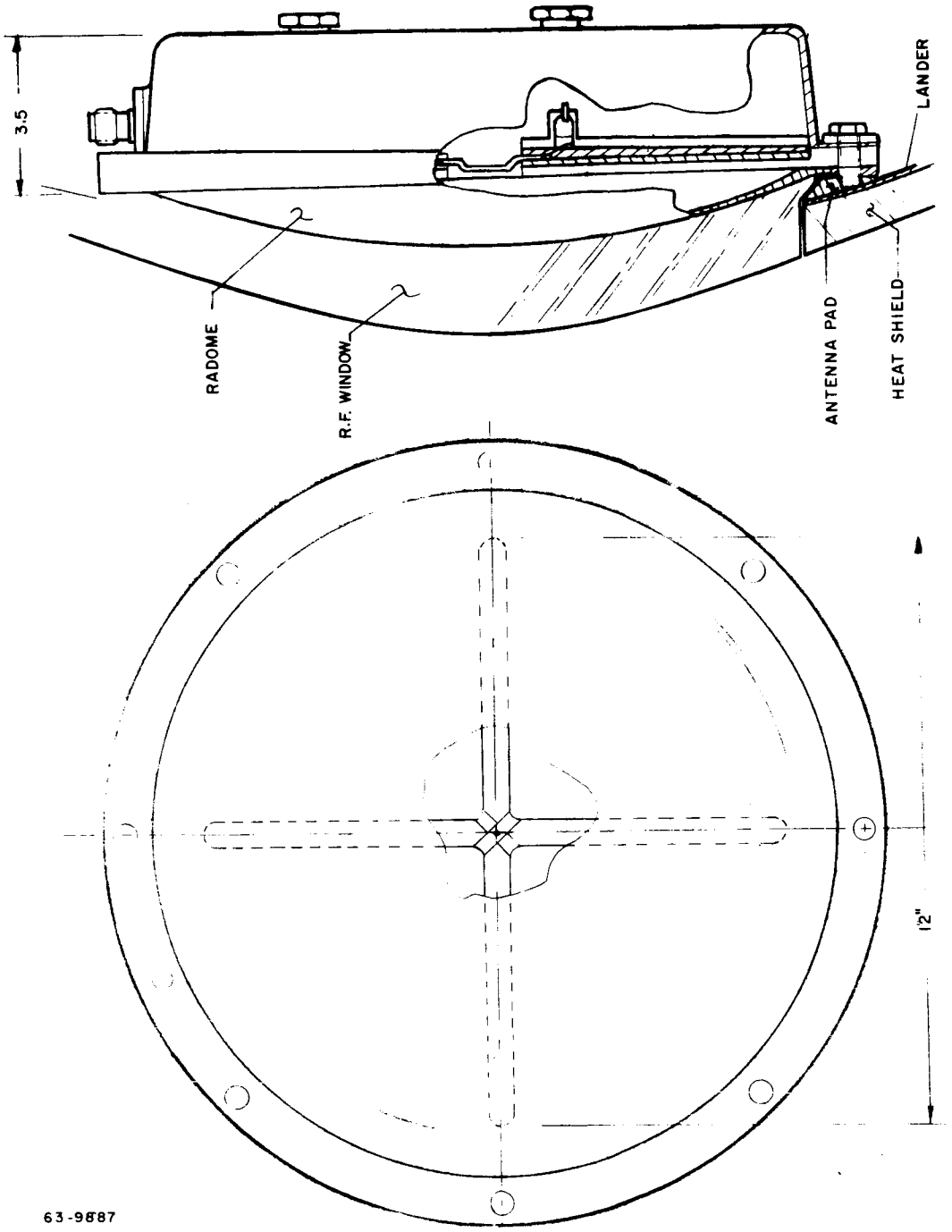

Figure 249 VHF ANTENNA INSTALLATION

The basic radiator to be used will be similar to the antenna used in the Mars lander array. This unit is a cruciform antenna with 12-inch crossed slots. A slight modification must be made to the mounting area and window aperture to adapt this design for use on the Venus heavy lander. This unit is also designed to take the shocks associated with the impact and reentry into the planet's atmosphere.

There is no appreciable power breakdown problem with the Venus lander because of the predicted high density to the Venus atmosphere. The unit will be sealed however, to insure against contaminants entering the antenna structure.

The pattern shape of this antenna is similar to that of a half wave dipole. Figures 250 and 251 are typical major plane patterns for a cruciform antenna mounted in a ground plane 48 inches in diameter.

Some of the basic characteristics of a design which is most desirable are listed in table 48.

TABLE 48

LANDER ANTENNA CHARACTERISTICS

Basic Type	Crossed-slots, cavity backed
Method of Feed	Stripline
Impedance	50 ohms nominal
VSWR	Equal to or less than 2.0:1 over the required operating band
Pattern Shape	Cardioid, $E_T = F(1 + \cos\theta)$, which provides essentially hemispherical coverage
Gain	+3 db above an isotropic source
Input Power	50 watts cw
Channel Isolation	30 db
Weight	4 pounds
Dimensions	14 inches in diameter - 3 inches deep

2. Heat Shield Antennas. The same requirements which applied to the Martian lander apply also to the Venus lander vehicle: (1) radiation coverage omnidirectional in the hemisphere above the lander, (2) an operating bandwidth of 4 mc. In the study of the omnidirectional array on the Mars lander vehicle, it was determined that a four element array fed through a fourway power divider would provide adequate radiation coverage. Any number less than a four element array, it was pointed out, would not be sufficient.

Since the circumference of the cylinder on which the array for the Venus lander is mounted is considerably smaller, (C = approximately 2.8 wavelengths), a 2-element array will provide adequate coverage. A contour plot of the radiation pattern of a 2-element array mounted on a cylinder approximately the same size as the Venus lander was presented with the discussion of the Mars lander. The units, consisting of a pair of 12-inch orthogonal slots, are small, rugged, dual channel radiators, especially suitable for this application.

The 2-way power divider will split the power equally into both antenna elements by means of a folded quarter-wave transformer whose impedance will be approximately 34 ohms. The power divider and antennas will be fed by a high power, high temperature, coaxial cable.

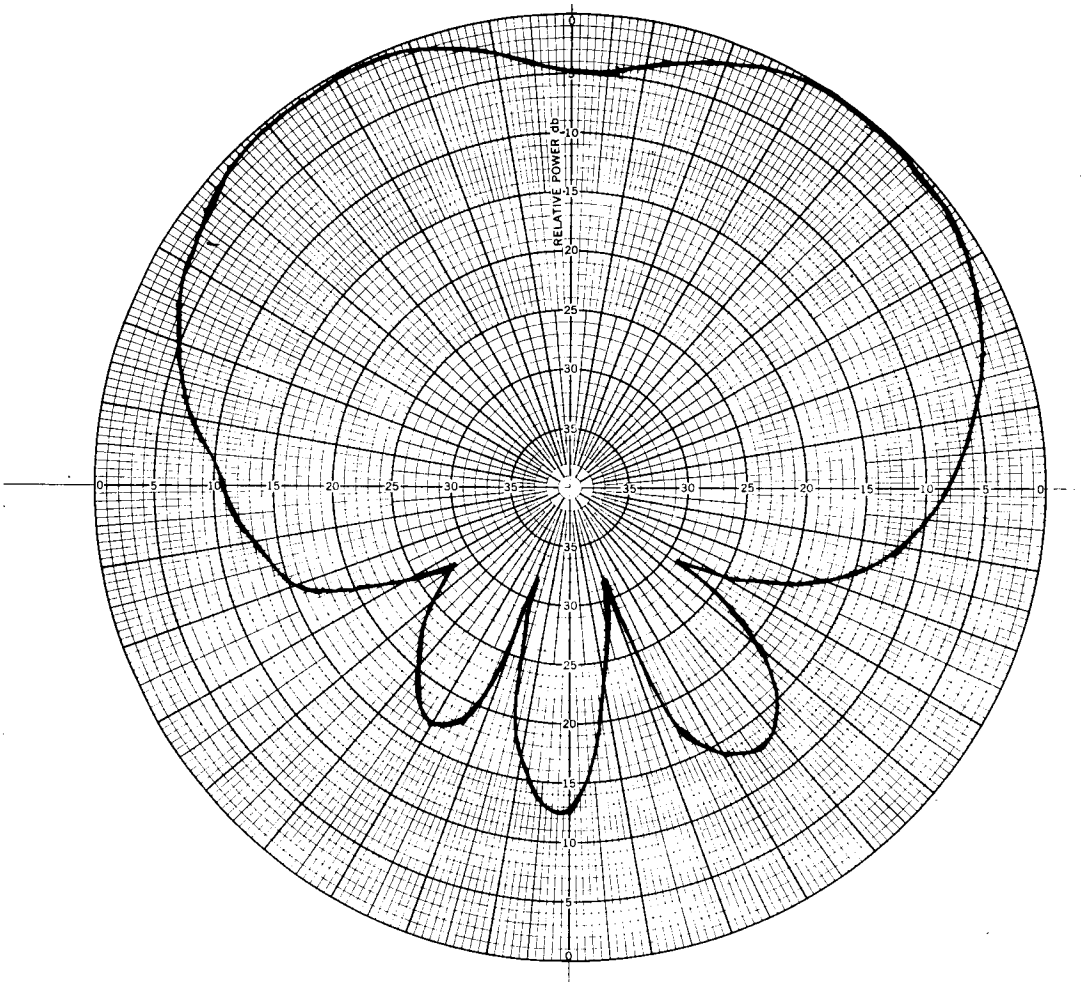

ANTENNA TYPE	LOCATION	USE	
TEST MODEL:		FREQUENCY: MCS	
MODEL SCALE:		SCALE FREQUENCY: MCS	
CONDITIONS: E-PLANE		POLARIZATION:	
CURVES PLOTTED IN:		Eθ:	°
VOLTAGE:		Eø:	
POWER:		PATTERN AREA:	
ENGINEER	OPERATOR	FILE NO.	DATE
			IC.3-PJB-2

ANTLAB #42410

63-9889

Figure 250 E PLANE PATTERN

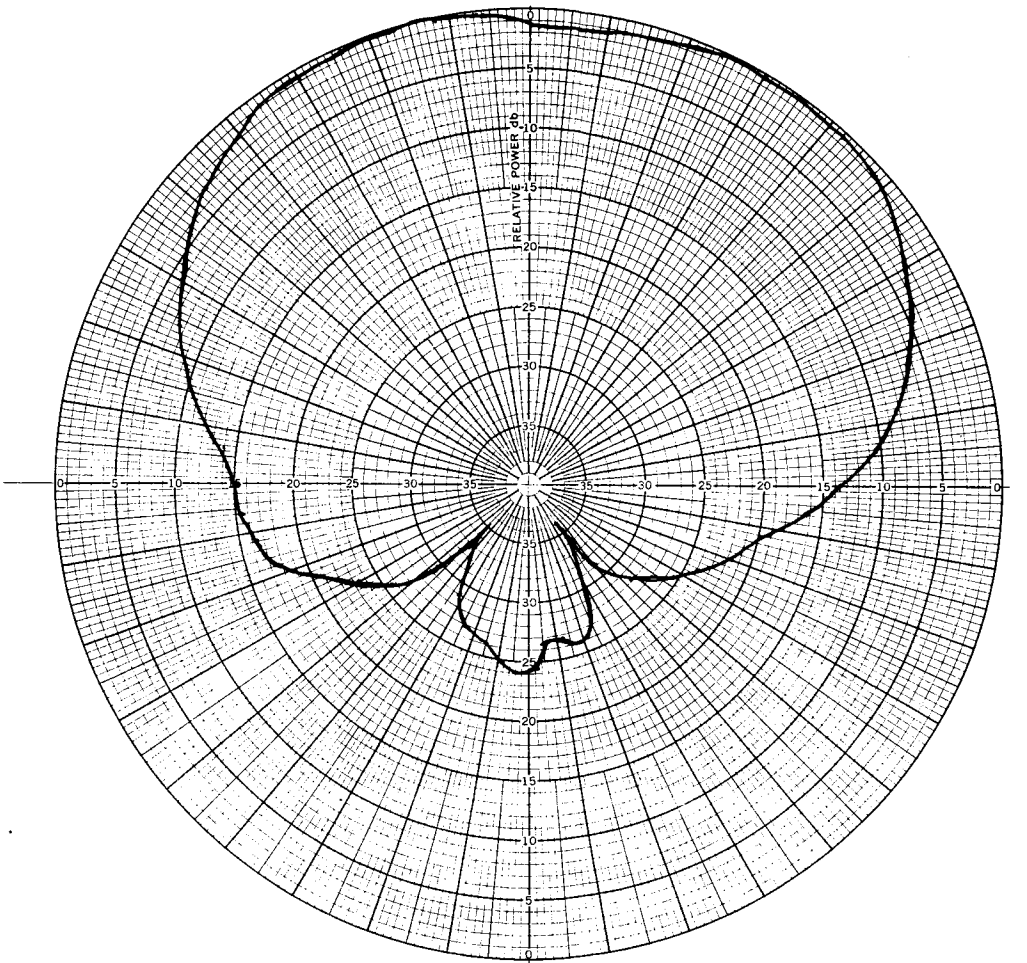

ANTENNA TYPE	LOCATION	USE	
TEST MODEL:		FREQUENCY: MCS	
MODEL SCALE:		SCALE FREQUENCY: MCS	
CONDITIONS: L. H. Plane		POLARIZATION:	
CURVES PLOTTED IN:		Eθ:	°
VOLTAGE:		Eφ:	
POWER:		PATTERN AREA:	
ENGINEER	OPERATOR	FILE NO.	DATE
		IC.3-PTB-3	

ANTLAB #42410

63-9889

Figure 251 H PLANE PATTERN

REFERENCES

1. Project Voyager Status Report, RAD TM-62-80, June-August 1962.

2. Stephenson, C. V., W. S. Wilcox, H. T. Crenshaw, H. L. Hancock, and E. B. Dismukes, Stanford Research Institute, ASD-TDR-63-57, February 1963.

3. McGrath, J. C., Aeronautical Systems Division, ASD-TDR-63-61, April 1963.

4. Neff, R. J., Phoenix Trimming Co., ASD-TDR-63-248, March 1963.

5. Schilling, G. F., Limiting Model Atmospheres of Mars, The Rand Corporation, R-402-JPL, August 1962.

6. Hill, F. J., Jr., and L. N. Morrissette, A Six-Degree-of Freedom Reentry Trajectory Program for Ballistic and Lifting Vehicles, Avco RAD-TM-62-70, September 1962.

7. McKinzie, D. J., Jr., Experimental Results of the LMSD E-5 Cornell 24-Inch Shock-Tunnel Tests, Avco RAD-TM-61-8, May 1961. Confidential

8. Schilling, G. F., Limiting Model Atmospheres of Mars, The Rand Corporation, R-402-JPL, August 1962.

9. Kaplan, L. D., A Preliminary Model of the Venus Atmosphere, JPL Technical Report 32-379, December 1962.

10. Detra, R. W., and H. Hidalgo, Generalized Heat Transfer Formulae and Graphs, AERL Research Report 72, March 1960.

11. Fay, J. A., and F. R. Riddell, Theory of Stagnation Point Heat Transfer in Dissociated Air, AERL Research Report 1, April 1957.

12. Rutowski, R. W., and K. K. Chan, Shock Tube Experiments Simulating Entry Into Planetary Atmospheres. Adv. in the Astronaut Sci. 5, Proceedings of the Second Western National Meeting, 1960.

13. Gilmore, F. R., Equilbirum Composition and Thermodynamic Properties of Air to 24,000°K, Rand Report RM-1543, 1955.

14. Hansen, F. C., Approximations for the Thermodynamic and Transport Properties of High Temperature Air, NASA TR R-50, 1959.

15. Raymond, J. L., Thermodynamic Properties of Carbon Dioxide to 24,000°K With Possible Application to the Atmosphere of Venus, Rand RM-2292, November 1958.

16. Treanor, C. E., and J. G. Logan, Jr., Thermodynamic Properties of Nitrogen from 2000°K to 8000°K, Cornell Aero Lab. Inc., Report BE-1008-A-5, January 1957.

17. Waldman, G., Blunt Body Velocity Gradients and Shock Detachment Distance, Avco RAD Memorandum, February 1961.

18. Chandrasekhar, S., Radiative Transfer, Dover Pub. Inc., New York, New York, 1960.

19. Flinn, D. J., A Solution of the Radiative Transfer Equation, Avco RAD TR-S230-DJF-209.

20. Patch, R. W., W. L. Shockleford, and S. S. Penner, Approximate Spectral Abosrption Coefficient Calculations for Electronic Band Systems Belonging to Diatomic Molecules, J. Quant. Spectrosc, Radiant Transfer, vol. 2, 1962, pp. 263-271.

21. Unsold, A., Continuous Spectrum of High-Pressure Hg. Lamp and Similar Gas Discharges. Ann. der. Physic, vol. 33, 1938, pp. 607-616.

22. Biberman, L. M., and G. E. Norman, Calculation of Photo-Ionization Absorption. Opt. i. Specktr. vol. 8, 1960, pp. 433-438.

23. Biberman, L. M., G. E. Norman, and K. N. Ulyanoo, On the Calculation of Photoionization Absorption in Atomic Gases. Opt. i. Spektr. vol. 10, pp. 565-569.

24. Bergess, A., and M. J. Seaton, A General Formula for the Calculations of Atomic Photoionization Cross-Sections. Monthly Notices of the Roy. Astron. Soc., vol. 120, 1960, pp. 121-151.

25. Kivel, B., and K. Bailey, Tables of Radiation from High Temperature Air. Avco Research Laboratory, RR 21.

26. Morris, J. C., Research On Radiation from Arc Heated Plasmas, Avco RAD, Quart. Progress Report 7, Contract AF 33 (616)-8390, 6 September 1963.

27. McAllister, L. E., J. C., Bolger, E. L. McCaffery, P. J. Roy, F. W. Ward, and A. C. Walker, Jr., Behavior of Pure and Reinforced Charring Polymer During Ablation Under Hypervelocity Reentry Conditions. From Applications of Plastic Materials in Aerospace, Chemical Engineering Progress, Symposium Series 40, vol. 59, 1963.

28. Apollo Heat Shield Monthly Progress Reports. Avco RAD, Avco Report Series 201. Confidential

29. Avco RAD Doc. 63-799. Internal Confidential

30. John, R. R., Internal Technical Release, Avco RAD, October 1959.

31. Avco RAD Doc. RAD-SR-63-136. Confidential

32. Ceccon, H., to R. Schlier, Avco RAD Internal Memo, Experimental and Theoretical Physics Section -62, 20 May 1963.

33. Rice, S. O., Selected Papers on Noise and Stochastic Processess, Edited by Wax, Nelson, p. 239.

34. Theory and Design of Chirp Radars. See B.S.T.J. July 1960, p. 745.

35. Springett, J. C., Command Techniques for the Remote Control of Interplanetary Spacecraft. National Telemetry Conference, vol. 2 proc. 1962.

36. Viterbi, On Coded Phase - Coherent Communications. IRE Trans. figure 8, for word error probability 5×10^{-3}, March 1961, p. 9.

37. Jaffee, Digilock Telemetry System, IRE Trans. Set, figure 6, March 1962, p. 48.

38. Hannan, P. W., Microwave Antennas Derived from Cassegrain Telescope, IRE Transactions on Antennas and Propagation, vol. AP-9, no. 2, March 1961, p. 147.

39. Frazer, A. H., J. J. Kane, and F. T. Wallenberger, E. I. duPont deNemours & Co., from Symposium on Fibrous Materials, Sponsored by Nonmetallic Materials Laboratory, ASD, October 1962.

40. Johnson, D. E., E. H. Newton, E. R. Benton, L. E. Ashman, and D. H. Knapton, Metal Filaments for High-Temperature Fabrics. Arthur D. Little, Inc., ASD-TR-62-180, February 1962.

41. Johnson, D. E., and E. H. Newton, Metal Filaments for High-Temperature Fabrics. Arthur D. Little, Inc., ASD-TR-62-180, Part II, February 1963.

42. Hritzay, D., and R. Wiant, Wire Cloth Structure for a Radiating Reentry Vehicle. Avco-Everett Research Laboratory, Research Report 123, March 1962.

43. Kaplan, L. D., A Preliminary Model of the Venus Atmosphere, JPL Technical Report 32-379, December 1962.

44. Avco RAD Doc. 63-288. Confidential

45. Avco RAD Doc. 63-1521. Confidential

46. Avco RAD Doc. 63-799. Confidential

47. Louis, J. F., R. Decker, R. A. Allen, and T. R. Brogan, Simulation of Reentry Radiation Heat Transfer. Avco-Everett Research Laboratory, August 1963.

48. Timmins, R. S., Private Communication, Avco RAD.

49. Carlson, W., Private Communication, Ames Research Center, NASA, 10 September 1963.

APPENDIX A

RECOMMENDED LANDING SYSTEMS FOR VOYAGER

1. Introduction. In support of a NASA-sponsored Voyager Study Program being conducted at Avco RAD, Wilmington, Massachusetts, Northrop Ventura has conducted an independent study project on the Voyager Landing System. The results of this independent study are reported in reference (1); based on reference (1), this report presents a proposed landing system for a specific Mars lander vehicle and a specific Venus lander vehicle, as defined by Avco RAD. The landing system for each vehicle is described, its sequence of operations outlined, and a weight and volume breakdown by system components presented. A program plan for the development, design, testing and fabrication of the landing system for each vehicle is also outlined, together with a program schedule for the accomplishment of the program plan.

For the case of the Mars vehicle landing system, the Schilling Model II Mars atmosphere has been used to define the system requirements. A brief discussion of the effect of the recently defined JPL "Minimum Density" Mars atmosphere on the proposed Mars vehicle landing system is presented in section 2 e of this appendix.

2. Mars lander vehicle landing system.

a. General discussion. In the selection of the proposed Mars vehicle landing system, certain basic assumptions have been made. These assumptions pertain to the vehicle itself, the anticipated range of vehicle entry trajectories, the range of atmospheric conditions surrounding Mars, the operational requirements of the vehicle during descent and touchdown, and the anticipated terrain and surface wind conditions on the surface of Mars. Briefly stated, these assumptions are as follows:

1) Gross vehicle Earth weight (W) is 1635 pounds*.

2) Vehicle ballistic coefficient (M/C_DA) is 0.9 slugs per square foot, based on a vehicle coefficient of drag (supersonic) of 1.5.

3) Vehicle weight at main parachute deployment is 1019 pounds, based on jettisoning of the fore and aft heat shields (575 lbs) and drogue parachute system (41 lbs) prior to main chute deployment.

4) Vehicle to enter the Mars atmosphere at a velocity between 20,000 to 29,000 feet per second and an angle between -20 to -90 degrees.

5) Vehicle to be provided with a 5-minute descent time for all conditions of entry and for the range of uncertainty of the Martian atmosphere considered.

*Preliminary Design Estimate.

6) The atmosphere of Mars to be in accordance with Schilling's Model II Atmosphere (ref. (2)).

7) Vehicle to impact on the surface of Mars with a deceleration not to exceed 100 Earth g's.

8) Vehicle to land upright or be capable of self-righting after impact, on terrain whose slope can vary from zero to 30 degrees, with surface winds from zero to 100 fps.

The proposed landing system is designed within the framework of the above listed assumptions, with the aim of providing a minimum weight system. To this end assumption (5) has been altered slightly to avoid a significant weight penalty on the main parachute subsystem.

The alteration to (5) above is as follows:

Vehicle to be provided with a 5-minute descent time for all conditions of entry in the Schilling atmosphere, except for the case of the vehicle entering the Schilling "Lower Limit" atmosphere at entry angles between -60 and -90 degrees. For this case the parachute descent time will decrease to a minimum value of 2.5 minutes for the vehicle entering the "Lower Limit" Mars atmosphere at an entry angle of -90 degrees.

The reason for the above alteration is as follows: the selection of a vehicle with a 0.9 ballistic coefficient in the Schilling "Lower Limit" Mars atmosphere seriously depresses the altitude at which an aerodynamic decelerator may be deployed. For vehicle trajectories with entry angles between -60 and -90 degrees, the altitude depression is sufficient to require a main parachute designed to provide a terminal velocity of about 30 fps in order to achieve a 5-minute descent time. On the other hand, parametric weight studies indicate that a significant landing system weight reduction can be achieved by designing the Mars vehicle landing system for a high impact velocity. For example, the landing system weight can be reduced 40 to 60 percent (depending on the descent/touchdown system combination employed), by increasing the impact velocity from 30 fps to 60 fps.

To minimize the landing system weight, the proposed landing system is based on an impact velocity of 60 fps. If further analysis indicates that the possible reduction in descent time is unacceptable, consideration should be given to the reduction of the vehicle ballistic coefficient to the range of 0.75 to 0.80. This reduction will permit a minimum 5-minute descent time for all entry conditions and atmospheres considered. However, an additional heat shield and structural weight is incurred.

b. Description of Mars vehicle landing system. The proposed landing system for the Mars vehicle consists of two basic subsystems; a parachute type

descent subsystem and a crushable material impact absorption-type touchdown subsystem. The selection of the individual subsystems, subsystem components, materials, and the mode of operation of each subsystem is based on a series of parametric studies conducted by Northrop Ventura and reported in reference (1). Each of the two subsystems is discussed in the following paragraphs.

1) Parachute descent subsystem. The parachute descent subsystem has two major assemblies - a drogue parachute assembly and a main parachute assembly - together with a sequence controller for proper control of initiation of deployment of each parachute.

The drogue parachute is sized to provide adequate vehicle deceleration and stabilization in the most unfavorable conditions of vehicle entry and atmosphere. To this end a 13-foot design diameter, "Hyperflo" parachute constructed of HT-1 material is proposed. The anticipated Mach number range at drogue chute deployment with the concomitant aerodynamic heating, plus the requirement of prelaunch heat sterilization make HT-1 a logical material choice for the drogue parachute.

The main parachute consists of a single, 50-foot nominal diameter, ringsail parachute, constructed of nylon and designed to provide a terminal velocity of 60 fps at impact with the Martian surface.

In the selection of the descent subsystem components for the Mars vehicle, one of the most difficult problems at this time is selection of the parachute materials. In terms of the anticipated Voyager program schedule, the number of candidate parachute materials can probably be narrowed to two - nylon and HT-1. The advantage of HT-1 over nylon, insofar as strength retention after exposure to heat (sterilization heating and, in the case of the drogue parachute, aerodynamic heating), must be balanced with the advanced state of manufacturing technology for nylon compared to HT-1. Nylon is currently available in a wide range of fabric weights and porosities which, in the case of the Mars lander vehicle, permits the design of lightweight parachutes to meet the operational requirements. HT-1 is not nearly so advanced insofar as availability of various fabric weights and porosities. Thus, the design of a parachute using HT-1 would tend to be considerably heavier than one fabricated from nylon.

In addition to the consideration of the effect of heat on parachute materials, the possible effects of long term high vacuum exposure on parachute materials are currently not well defined. It is felt that the forthcoming JPL program for the investigation of the effects of sterilization and long term space environment exposure on parachute materials will answer many of the questions which currently plague the designers of recovery systems for space applications.

Based on currently available data, the proposed parachute system uses HT-1 material for the drogue parachute and nylon for the main parachute. A somewhat

more detailed discussion of the current state-of-the-art of parachute materials for application to the Mars vehicle landing system is contained in reference (1).

2) Touchdown subsystem. The touchdown subsystem consists of an array of impact absorption material pads, suitably equipped with mounting fixtures and designed to accommodate both a vertical load and possible side loads due to surface winds and variations of the Martin terrain. In the case of the Mars vehicle the impact material selected is stainless steel honeycomb. By virtue of its high crushing stress, the use of stainless steel honeycomb offers the lowest weight decelerator system in comparison to other honeycomb materials, such as aluminum and paper.

c. Sequence of operations. The descent and landing sequence is shown functionally in figure A1 and pictorially in figure A2. Following the peak heating and deceleration period of entry, the drogue chute cover and cable covers are jettisoned at a signal from the G-switch assembly. After a two-second delay the drogue chute mortar is fired deploying the drogue chute in the wake of the vehicle at a maximum dynamic pressure of 160 psf. An 8-second timer is started at this time to prevent premature main chute deployment. The lander vehicle is decelerated by the drogue chute to a Mach number between 0.5 and 0.6. At a signal from the absolute altimeter (or the descent system baroswitches, if the absolute altimeter is not functioning) the shaped charges are fired to separate the fore and aft heat shields from the lander vehicle. The aft heat shield is pulled off the lander by the drogue chute, causing deployment of the main parachute. The main parachute deployment bag, attached by a bridle to the aft heat shield, is stripped off, and the main parachute opens fully. (Reefing of the main parachute is not required, due to the low dynamic pressure existing in a main chute deployment.) Deployment of the main parachute and subsequent deceleration of the lander vehicle causes separation of the forward heat shield from the lander vehicle, exposing the touchdown subsystem.

The lander vehicle, less heat shields, descends on the main parachute for a period of approximately five minutes. At ground impact the vehicle is decelerated by the crushing action of the honeycomb material in the touchdown subsystem.

d. Detailed weight and volume breakdown - Mars vehicle landing system.

	Weight-Lb	Volume-Cu In.
1) Descent subsystem.		
Main Parachute Assembly		
Canopy and Lines	39	
Riser Assembly	1	3050
Deployment Bag and Bridle	5	
Disconnect Fitting	2	10
Total	47.0	3060

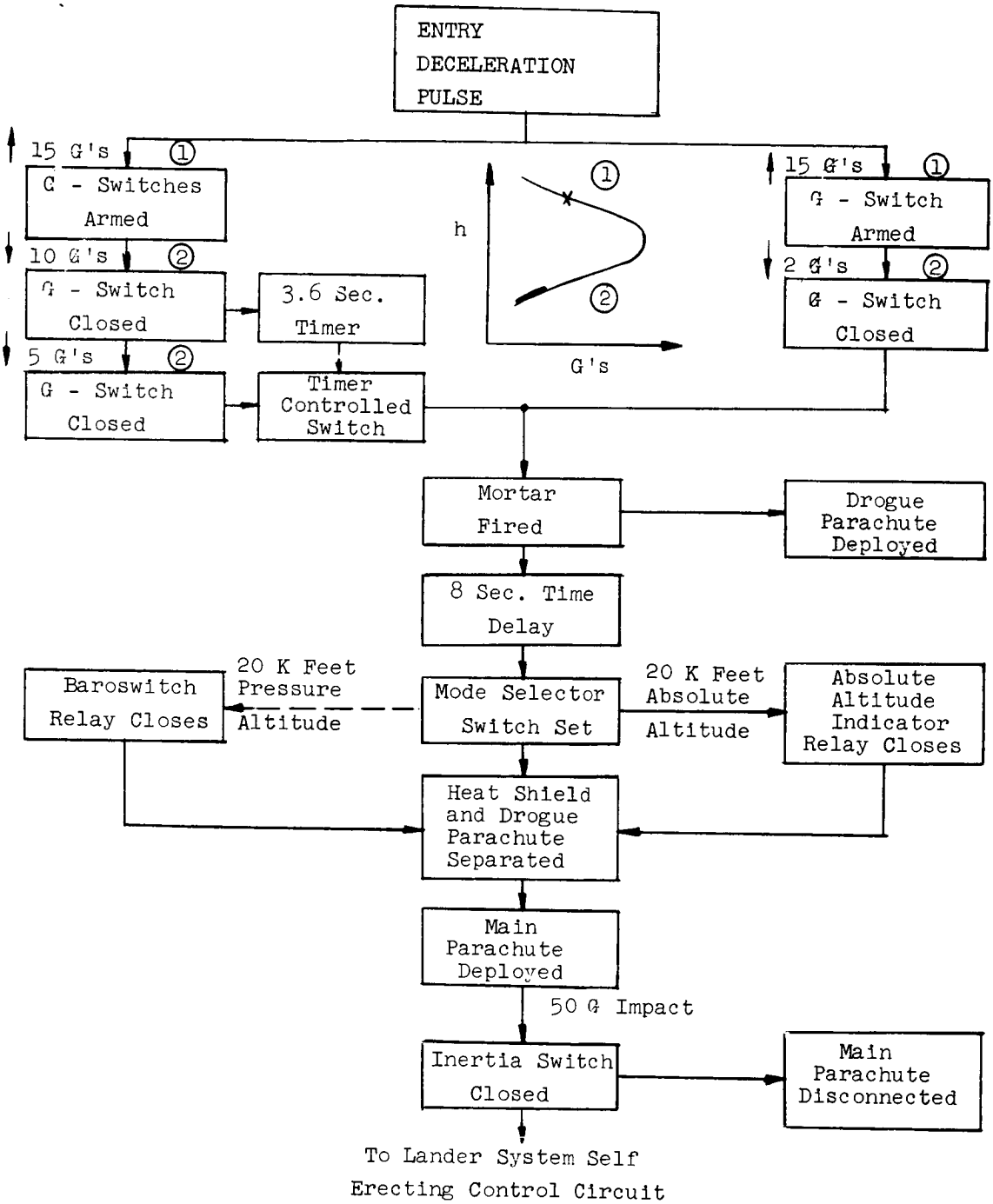

Figure A1 BLOCK DIAGRAM OF MARS VEHICLE DESCENT SYSTEM SEQUENCE CONTROLLER

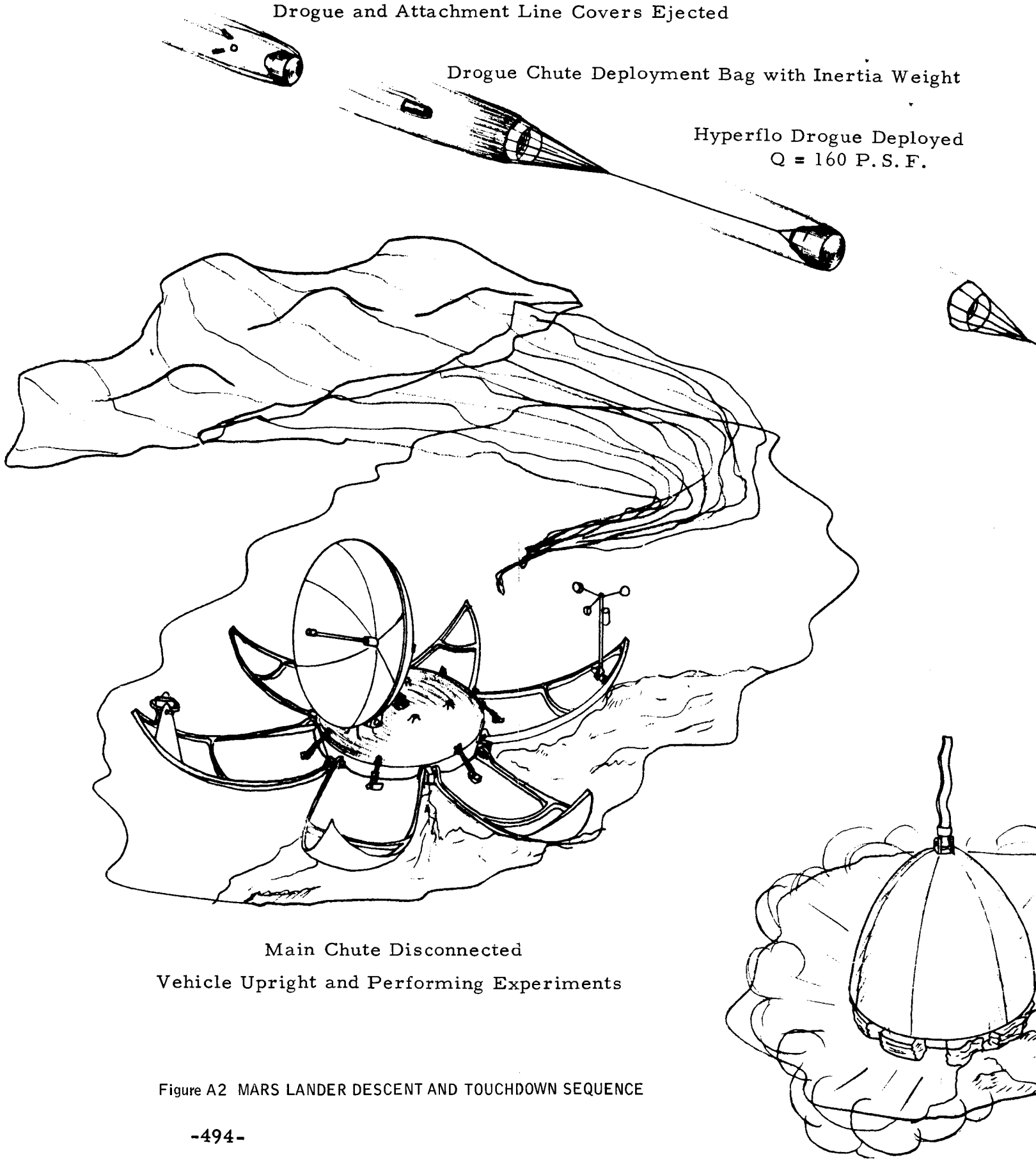

Figure A2 MARS LANDER DESCENT AND TOUCHDOWN SEQUENCE

Drogue Removes Aft Portion of Heat Shield
at Altitude Above 20, 000 Ft.

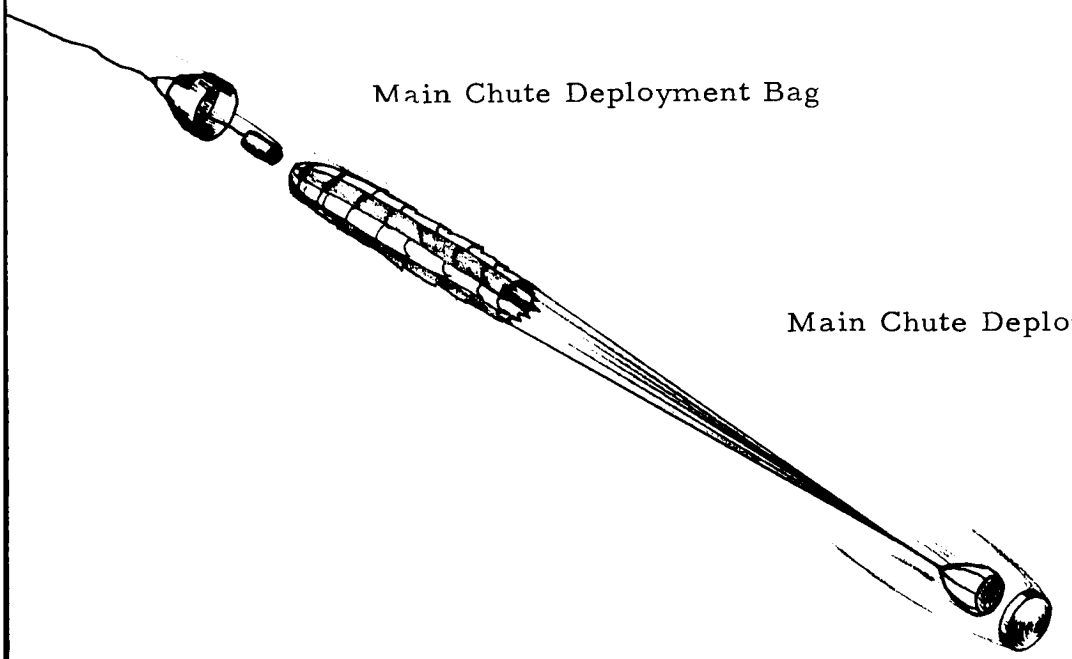

Main Chute Deployment Bag

Main Chute Deployed

Forward Portion of
Heat Shield
Falls Free

Main Chute (50' Ring Sail)

Fully Inflated

Final Descent:

60 Ft/Sec

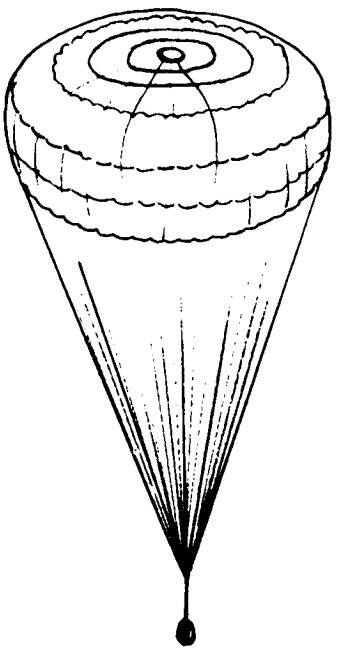

mpact

	Weight-Lb	Volume-Cu In.
Drogue Parachute Assembly		
Canopy and Lines	12.5	
Riser Assembly	9.5	1400
Deployment Bag and Bridle	2.5	
Harness Assembly	4.5	25
Mortar Assembly	12.0	
Total	41.0	1425
Sequence Controller		
G-Switch Assembly (2)	1.00	
Baroswitch (2)	.25	
Time Delay Relay (2)	.50	
Relays, Resistors, Connectors	.35	
Inertia Switch (2)	.50	
Container Assembly	3.20	
Wiring (Total System)	.30	
Total	6.1	
2) Touchdown subsystem.		
Impact Absorption Material	20.0	7000
Attachments and Redundant Material	8.0	2000
Total	28.0	9000
Landing System Total	122.1 Lbs	13,585 Cu In.

e. Effect of JPL's "Minimum Density" Mars atmosphere on the proposed Mars vehicle landing system. The recent redefinition of the Martian atmosphere by JPL has a profound effect on the design of both the lander vehicle itself and the vehicle landing system. While it is not possible in the current time schedule to completely reevaluate the landing system requirements for the newly defined atmosphere, certain factors are immediately apparent. The ballistic coefficient of 0.9 slugs per square foot selected for the vehicle in the Schilling atmosphere must be reduced to approximately 0.3 in the JPL "Minimum Density" atmosphere, in order to provide entry trajectories where the use of aerodynamic decelerators is feasible. Based on a ballistic coefficient of 0.3, a preliminary estimate of the size and weight of the landing system for a 1635-pound Mars lander vehicle in the JPL "Minimum Density" atmosphere has been made. Table A1 presents a comparison of this landing system with the currently proposed landing system, based on the Schilling Model II Mars atmosphere.

It will be noted in table A1 that the landing system weight increases by a factor of almost 2.5 in going from the Schilling to the JPL Mars atmosphere. The weight increase is due solely to the increased drogue and main parachute sizes required for the lower density atmosphere. The lower touchdown subsystem weight for the vehicle in the JPL atmosphere is due to lower vehicle weight at impact of that vehicle compared to the vehicle in the Schilling atmosphere.

3. Venus lander vehicle landing system.

a. General discussion. In the selection of the proposed Venus vehicle landing system, certain basic assumptions have been made. These assumptions pertain to the vehicle itself, the anticipated range of vehicle entry trajectories, the range of atmospheric conditions surrounding Venus and the operational requirements of the vehicle during descent. Briefly stated, these assumptions are as follows:

1) Gross vehicle Earth weight (W) is 85 pounds.

2) Vehicle ballistic coefficient (M/C_DA) is 0.5 slugs per square foot, based on a vehicle coefficient of drag (supersonic) of 1.5.

3) Vehicle to enter the Venus atmosphere from orbit.

4) Vehicle to be decelerated to a descent velocity suitable for atmospheric sampling and data transmission at or above the Venusian cloud layer (currently estimated at approximately 60 miles altitude).

5) The atmosphere of Venus to be in accordance with Kaplan's "Standard" and "Maximum Temperature" Model Atmospheres (ref. 3).

TABLE A1

COMPARISION OF THE LANDING SYSTEMS FOR A 1635 POUNDS MARS LANDER VEHICLE IN THE SCHILLING "LOWER LIMIT" ATMOSPHERE AND THE JPL "MINIMUM DENSITY" ATMOSPHERE

Parameter	Schilling Model II "Lower Limit" Atmosphere	JPL "Minimum Density" Atmosphere
Surface level density	1.44×10^{-4} slug /ft^3	0.42×10^{-4} slug/ft^3
Vehicle ballistic coefficient	0.9 slug/ft^2	0.3 slug/ft^2
Vehicle reference diameter	6.9 ft	12.0 ft
Drogue parachute diameter (D_p)	13 ft	24.1 ft
Drogue parachute assembly weight	41 lb	116 lb
Main parachute nominal diam (D_o) based on a terminal velocity of 60 fps	50.4 ft	93.1 ft
Main parachute assembly weight	47 lb	146 lb
Sequence controller weight	6 lb	6 lb
Touchdown subsystem weight	28 lb	23 lb
Total Landing System Weight	122 lb	291 lb
Landing System Weight Percentage	7.5%	17.8%

The selection of the descent system for the Venus vehicle is quite different from the case of the Mars lander vehicle descent system. The high atmospheric density of Venus permits the use of considerably smaller size deceleration devices. However, the high ambient temperature (between 800 °F and 1050 °F) at or near the surface of the planet makes the selection of the descent system heavily dependent on the availability of materials to withstand these temperatures.

The mission requirements for the Venus vehicle dictate a decelerator capable of providing reasonably low vertical descent velocities at or above 300,000 feet altitude to permit atmospheric data collection from that altitude to ground impact. Since the vehicle is not designed to collect data after impact with the surface of the planet, the selection of a descent system is not primarily governed by the impact velocity, as in the case of the Mars lander vehicle.

In considering possible deceleration devices for the Venus lander, three approaches were considered; (1) use of a nylon or HT-1 parachute with acceptance of parachute destruction below a given altitude due to the increasing ambient temperature; (2) use of a metallic fabric parachute; and (3) use of a high temperature Ballute.

Approach number (1) was not given extensive consideration. Even with a parachute fabricated from HT-1, destruction of the chute could be expected to occur at an altitude from 180,000 feet (Kaplan "Maximum Temperature" atmosphere) to 75,000 feet (Kaplan "Standard Temperature" atmosphere). While the descent velocity established by the vehicle alone might be acceptable (assuming the parachute is disconnected when it is destroyed), the loss of the parachute would result in vehicle instability. With a tumbling vehicle the atmospheric data collected would be of little value, and the mission would for all practical purposes be terminated at the point of parachute failure.

Approaches (2) and (3) are both felt to be feasible within the mission requirements and the current knowledge of the Venusian atmosphere. Of the two, the high temperature Ballute appears to be far ahead of the metallic fabric parachute, in terms of state of development. References (4) and (5) present a detailed description of the current efforts in the development of the high temperature Ballute. In brief, the high temperature Ballute has been fabricated in sizes up to 9 feet in diameter, and has undergone wind tunnel testing at speeds varying from low subsonic to Mach 10. In these wind tunnel tests, the Ballute has demonstrated its ability to inflate and remain inflated and to possess the required aerodynamic stability throughout the Mach number range tested.

Metallic parachutes are, on the other hand, in the embryonic state of development. Several different types of metallic cloth have been produced in small quantities. However, there seems to be no evidence that parachutes have been fabricated from any of these. The use of metal cloth in a parachute for space missions appears, at least superficially, to pose some inherent problems. The

metal cloths fabricated to date posess very low flexure strength. Therefore, packing of metal parachutes may require special techniques differing from those currently used in packing cloth parachutes. Also, the problem of metal seizure (cold welding) under prolonged exposure to high vacuum appears to be a very real consideration in the case of metallic cloth parachutes.

b. Description of Venus vehicle descent system. The proposed descent system for the Venus vehicle consists of a high temperature Ballute (ram-"air" inflated conical balloon). The selection of the Venus descent system is based on a series of parametric studies conducted by Northrop Ventura and reported in reference (1).

The proposed Ballute is a 4.5-foot diameter isotensoid shape, fabricated of a skin woven of seven-strand cables of 0.5-mil Rene 41, coated with high temperature silicone ceramic elastomer. To minimize the Ballute system weight, deployment of the relatively heavy Ballute will be accomplished by use of an 18-inch diameter HT-1 "Hyperflo" pilot parachute. The pilot chute is deployed by a pilot chute deployment gun. Once inflated, the pilot chute exerts sufficient force to extract the Ballute from its container.

The Ballute size is selected to provide the minimum descent velocity from 300,000 feet altitude, consistent with a reasonable size and weight for the descent system. The 4.5-foot-diameter Ballute system proposed will weigh an estimated 19 pounds, representing 22 percent of the gross vehicle weight. While this percentage appears high in comparison with descent systems provided on current Earth reentry vehicles, the small vehicle size, plus the requirement for materials capable of withstanding the high Venusian temperatures, results in this considerable weight percentage. A weight and volume breakdown for the proposed Ballute descent system is presented in section 3d of this report.

c. Sequence of operations. The descent system sequence of operations is shown functionally in figure A3 and pictorially in figure A4. The control circuit is armed by means of a latching relay which is closed by a signal from the g-switch during the rise portion of the vehicle deceleration curve. Following peak g, the g-switch closes another set of contacts when the g level decays to the preset level of 3 g's. Closure of these contacts initiates the pilot chute deployment gun 2-second delay cartridge and simultaneously fires the cover release cartridges. After 2 seconds the deployment gun fires, causing extraction of the pilot chute by the 1/2-pound slug. The pilot chute opens immediately and creates sufficient drag to extract the Ballute. During extraction, the 1/8-inch stainless steel Ballute riser cable is deployed from the bag in orderly fashion. At the fully extended position the bag is stripped off the Ballute by the pilot chute. The Ballute fills by means of ram pressure and decelerates the vehicle.

Figures 5 and 6 show the vertical descent velocity versus altitude for the vehicle-Ballute combination in the Kaplan "Maximum Temperature" and "Standard" atmospheres, respectively. Both of the plots are based on the vehicle

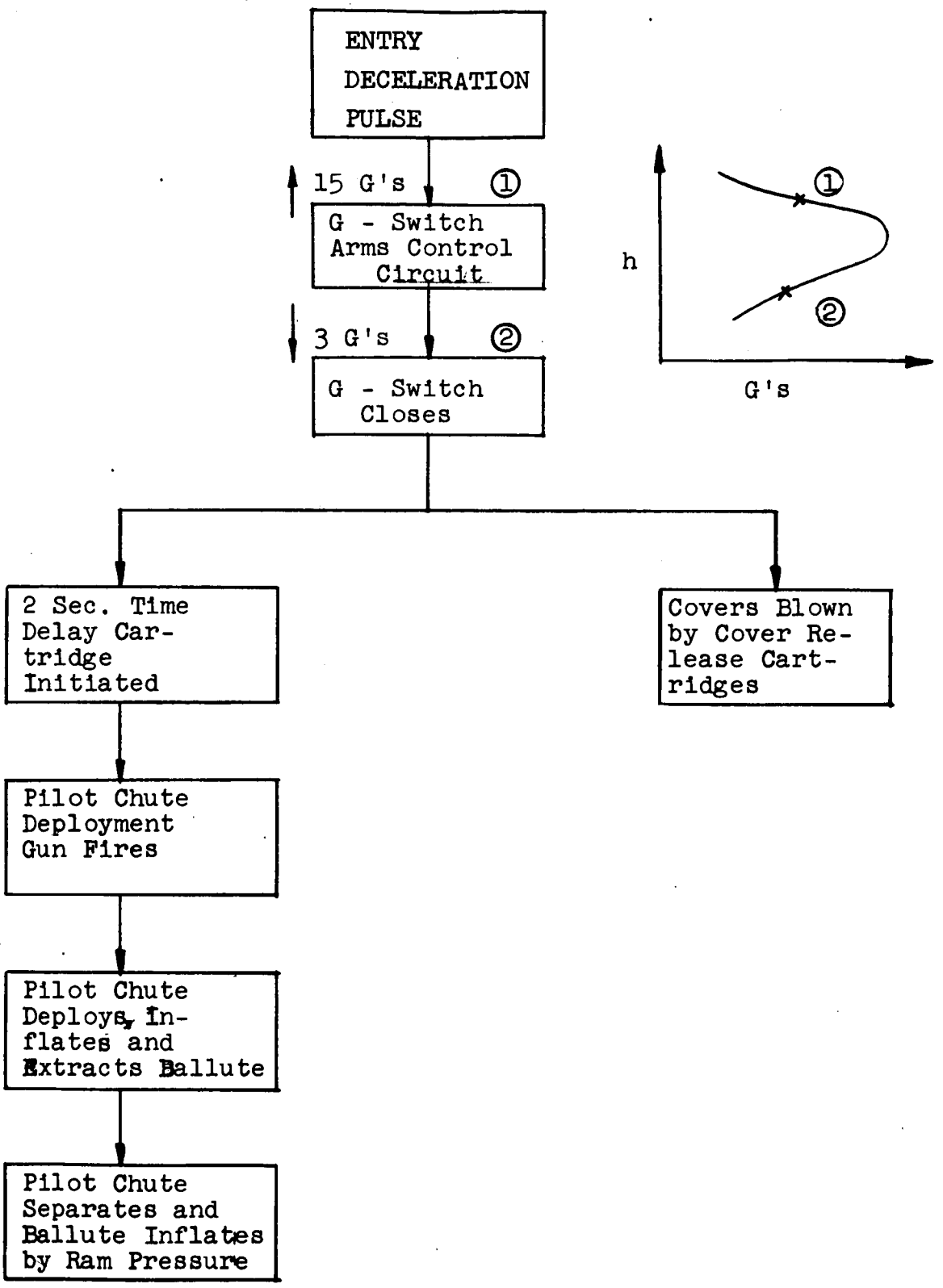

Figure A3 BLOCK DIAGRAM OF VENUS VEHICLE DESCENT SYSTEM SEQUENCE CONTROLLER

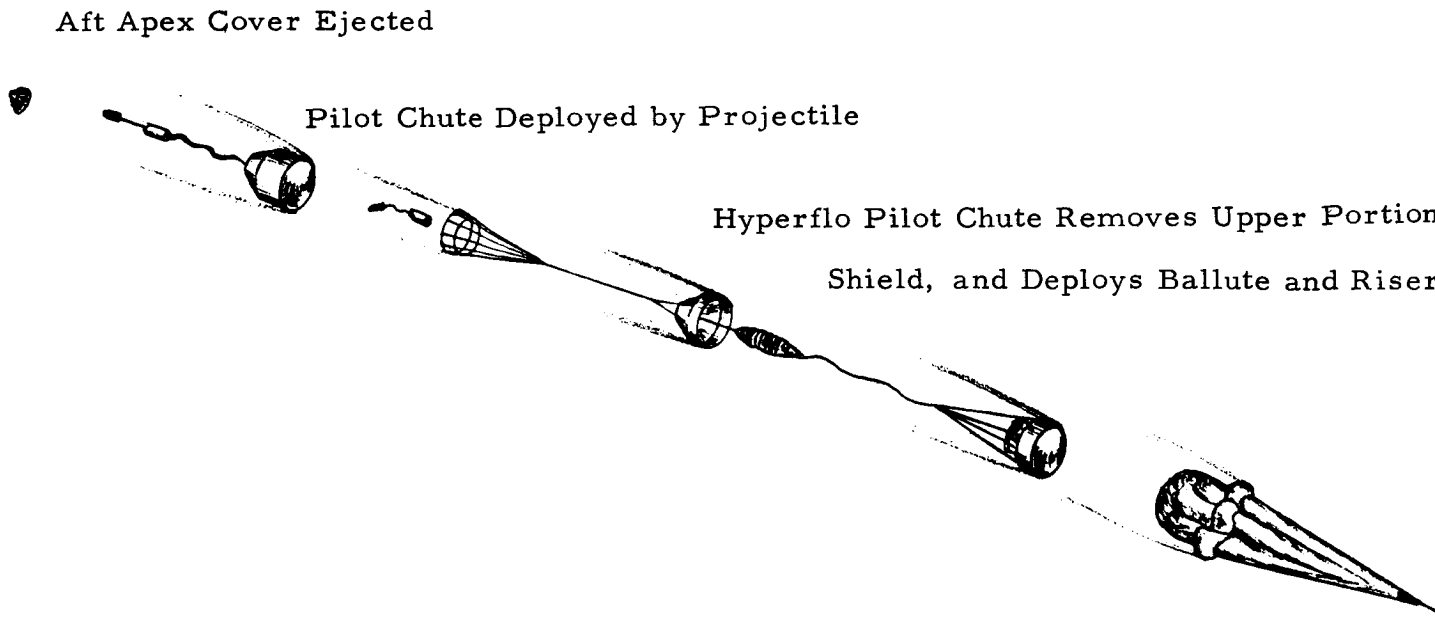

Figure A4 VENUS LANDER DESCENT SYSTEM

of Heat

Ballute Deployed and Inflating

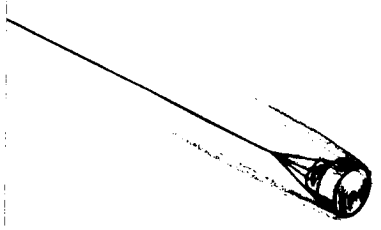

Ballute

Fully Inflated

Final Descent

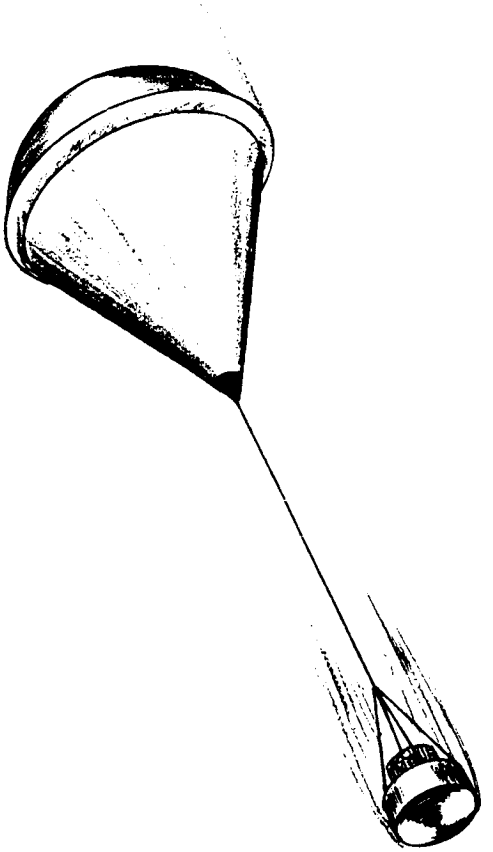

SEQUENCE

entering the Venusian atmosphere at -10 degrees and 38,000 feet per second. The solid line in figures A5 and A6 represents the proposed 4.5-foot diameter Ballute ($D_B/D_V = 3$). The dashed line represents a 9.0-foot diameter Ballute ($D_B/D_V = 6$), while the broken line shows the vertical descent velocity for the vehicle only.

d. Detailed weight and volume breakdown - Venus vehicle descent system.

	Weight-Lb	Volume-Cu In.
1) Ballute Assembly		
4.5-ft Ballute	12.0	720
Riser	.35	10
Deployment Bag	1.5	20
Riser Fittings	0.4	6
	14.25	756
2) Pilot Chute Assembly		
18-inch diam. HT-1 Pilot Chute	1.25	
Riser Bag and Bridle	1.0	
	2.25	50
3) Deployment Gun		
Gun and Cartridge Assembly	1.0	10
4) Sequence Controller	1.5	20
Descent System Total	19.0 Lb	836 Cu In.

4. Program plan for Mars lander vehicle landing system. The following pages present a program plan for the landing system for the Mars lander vehicle. The plan is divided into the following categories of effort:

1.0 Engineering analysis

2.0 Systems design

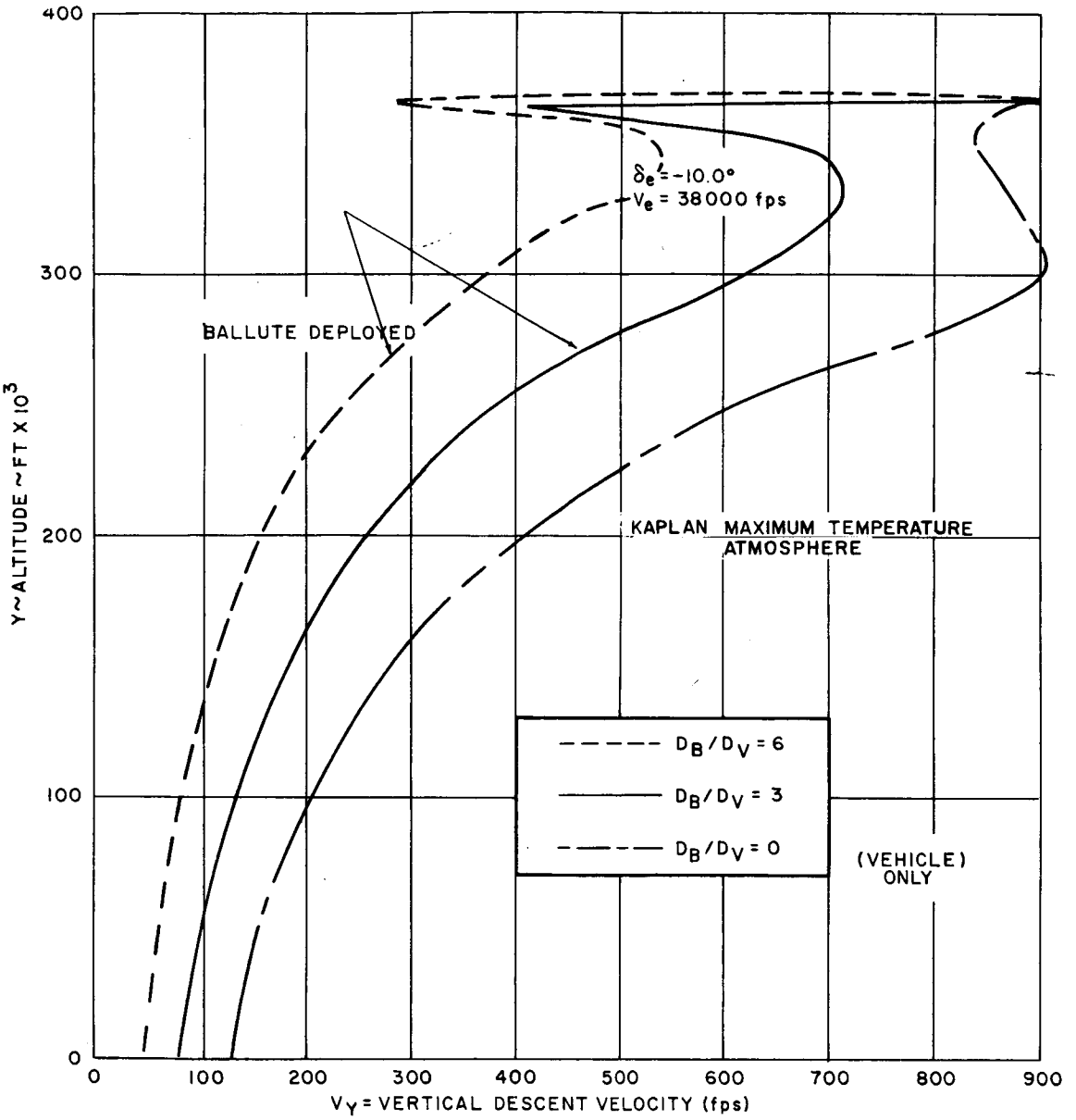

Figure A5 VERTICAL DESCENT RATE VERSUS ALTITUDE FOR THE VENUS VEHICLE WITH BALLUTE DECELERATOR

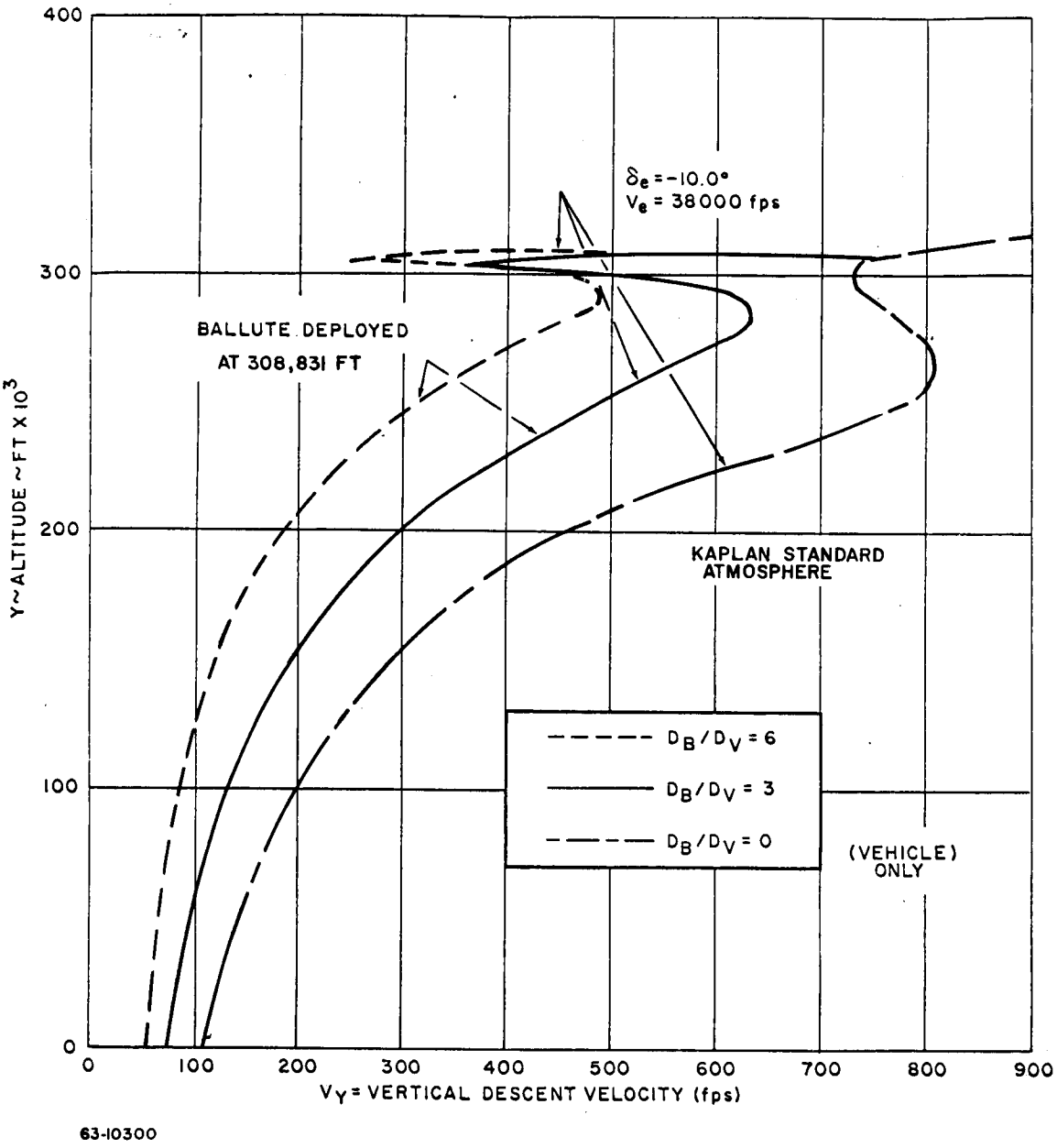

Figure A6 VERTICAL DESCENT RATE VERSUS ALTITUDE FOR THE VENUS VEHICLE WITH BALLUTE DECELERATOR

3.0 Test components and test vehicles design

4.0 Development tests - materials and components

5.0 Development tests - subsystems and systems

6.0 Qualification tests - components and subsystems

7.0 Reliability

8.0 Fabrication

9.0 Documentation.

1.0 Engineering analysis.

1.1 Descent systems. Aerodynamic, stability, aerothermodynamic and dynamic loading analyses of the drogue and the main parachute assemblies; sequence controller requirements analysis.

1.2 Touchdown system. Stability and dynamics analyses to determine the optimum materials, materials arrangement and mechanical design mounting details for variations of vehicle orientation at impact and conditions of Martian terrain in the impact area. (Northrop Ventura analysis will not include post impact orientation and self-righting vehicle design and operation.)

2.0 Systems design.

2.1 Descent system design.

2.1.1 HT-1 drogue parachute system.

2.1.1.1 Drogue parachute, riser.

2.1.1.2 Drogue mortar assembly.

2.1.1.3 Multiple g switch-timer control unit for drogue parachute deployment initiation control.

2.1.1.4 Integration of drogue parachute system into vehicle design. Solution of the interface problems.

2.1.2 Nylon main parachute system.

2.1.2.1 Main parachute, deployment bag, riser, and disconnect system.

2.1.2.2 True altitude sensing system's electrical coupling with main parachute deployment initiator. Also, backup aneroid deployment initiation controller. (Avco to supply true altitude sensing system as a part of vehicle instrument package.)

2.1.2.3 Integration of main parachute subsystem into vehicle design. Solution of interface problems.

2.2 Touchdown system design.

2.2.1 Size, placement and distribution of impact absorption material. Mechanical design of system to accommodate side loads and provide uniform distribution of the load to the impact absorption material array.

2.2.2 Integration of the touchdown system into the vehicle design. Solution of interface problems.

3.0 Test components and test vehicles design.

3.1 Descent system.

3.1.1 Design of windtunnel models of vehicle-drogue parachute combination for drag, stability and optimum riser length determination.

3.1.2 Design of multiple g-switch/timer switch drogue parachute deployment initiation controller unit.

3.1.3 Design of rocket boost vehicle for high Mach number drogue parachute testing.

3.1.3.1 Determination of required test program for best Mars entry simulation.

3.1.3.2 Selection of booster configuration to achieve test points.

3.1.3.3 Design of scaled test vehicle to carry experimental drogue chute system, including separate recovery system.

3.1.4 Design of aerial drop test vehicle. Vehicle to include prototype drogue and main parachute systems with modified deployment initiation controller. Vehicle to be dynamically scaled to Mars environment.

3.2 Touchdown system.

3.2.1 Design honeycomb impact pads for basic tests of various types of honeycomb impact absorption material.

3.2.2 Design boilerplate vehicle with means for replacement of impact attenuation units. (To be used for tower drop tests of touchdown system.)

4.0 Development tests - materials and components.

4.1 Descent system development tests.

4.1.1[1] Sterilization heat cycling tests on nylon, proposed pyrotechnic devices and deployment initiation controllers. For nylon, the effect of the required sterilization heat will be tested with an inert atmosphere on both material samples and full-or scale-model chute packs. Equipment required: minimum 4 x 4 x 4 ft test space temperature-altitude chamber (350° F range) with facility to evacuate chamber and purge with inert gas.

4.1.2[1] Long-term vacuum testing of nylon and HT-1. Complete packed chute testing desired, but may be difficult, due to large outgassing load of parachute. Possible scale-model parachute pack testing. Minimum test time - 30 days. Equipment required: 4 x 4 x 4 ft test space, high vacuum chamber with large ($Sp \geq 10^5$ liter/sec) pumping capacity at 10^{-6} Torr. Ultimate vacuum of chamber to be in the range of 10^{-8} Torr. Also, facility for solar heating of the test specimen during vacuum test is desirable. Capability for removal of test chute from pack after vacuum testing and physical testing of fabric in a Mars simulated environment (without exposure to air) appears mandatory for meaningful test results.

4.1.3 Acceleration testing of multiple g switch-timer drogue chute deployment initiation controller. Equipment required: centrifuge capable of 0 to 10 g's for a 1 to 2-lb test unit.

4.2 Touchdown system development tests.

4.2.1 Basic test program on various honeycomb materials (steel, aluminum, paper) to determine the applicability and optimum materials for application to the given system. Equipment required: impact machine, accelerometers, test samples of various impact absorption materials.

4.2.2 Materials investigation of possible degradation in a space environment and a sterilization environment of promising honeycomb materials, if these materials are organic in nature or use organic materials as a bonding agent. If brazed or welded honeycomb materials are used, this testing will not be required. Equipment required: (1) an 18-inch bell jar type high vacuum chamber, 10^{-7} to 10^{-8} Torr ultimate (2) a small oven (350°F range).

5.0 Development tests - subsystems and systems.

5.1 Descent system.

5.1.1 Windtunnel testing of vehicle - drogue parachute configuration per 3.1.1. Location: ARO or NASA Langley Unitary Plan wind tunnel.

[1] It is anticipated that some of these development tests will be made unnecessary in view of JPL's proposed program for sterilization and space environment testing of parachute materials.

Number of tests: 12 to 15 tests in the Mach number range from 0.5 to 4.5.

5.1.2 Aerial drop tests of prototype descent system with boilerplate vehicle and incorporated touchdown system. Drops will test drogue chute deployment including mortar operation, drogue-vehicle stability, drogue chute drag, main chute deployment, opening and final disconnect after impact.

No. of vehicles	2
No. of drops	12
No. of descent systems	8
No. of sequence control systems	4
No. of touchdown systems	12

Test location: El Centro, California

Test altitude: 50,000 feet or higher.

5.1.3 Rocket booster vehicle tests of drogue deployment and deceleration at high Mach numbers; will determine drogue deployment operations, drogue-vehicle stability.

No. of tests	6
No. of vehicles	6
No. of drogue sub-systems	6

Test location: Eglin AFB or WSMR

Test point range: 75,000 feet altitude and Mach 1.8 to 125,000 feet altitude and Mach 4.0.

5.2 Touchdown system.

5.2.1 Tower drop tests - to subject touchdown system to all anticipated horizontal-vertical velocity combinations and simulated Mars terrain conditions.

Location: Northrop Ventura, Newbury Park

No. of tests Minimum of 25

No. of vehicles 2

No. of impact systems 25 .

5.2.2 Aerial drop tests - can be accomplished in conjunction with 5.1.2. Boilerplate vehicle will have touchdown system incorporated. Will provide additional impact data including the effect of possible main chute oscillation at impact on the touchdown system operation.

6.0 Qualification tests - components and subsystems.

6.1 Purpose of the tests. To ensure operability of hardware after its being subjected to the anticipated environments.

6.2 Type of test.

Sterilization

High vacuum - Solar heating

Shock

Salt spray

Sand and dust

Vibration

Humidity

Fungus .

6.3 Items to be tested.

Pyrotechnic devices

Sequence controller

Drogue mortar assembly

Drogue parachute pack

Main parachute pack.

(Touchdown system will probably undergo qualification tests by Avco as part of vehicle qualification tests.)

7.0 Reliability.

7.1 Reliability analysis. Based on the reliability of the system components and the uncertainties of the entry trajectory, Martian atmosphere, and Martian terrain.

7.2 Reliability test program.

7.2.1 Environmental testing of components of the descent systems, particularly pyrotechnic and electromechanical devices, followed by operational tests as applicable. Type of testing as listed in 6.2.

7.2.2 Aerial drop tests to determine reliability of landing system:

No. of vehicles	2 (Avco to supply)
No. of drops	12
No. of landing systems	12
Test location:	El Centro, California
Test altitude:	50,000 feet or higher .

8.0 Fabrication.

8.1 Test components and test vehicles fabrication.

8.1.1 Fabrication of windtunnel models of vehicle-drogue parachute configurations per 5.1.1; quantity - 3.

8.1.2 Breadboarding and prototype fabrication of sequence controller; quantity - 1 breadboard, 3 prototype for testing per 4.1.3.

8.1.3 Fabrication of rocket-boosted drogue chute system test vehicle with drogue subsystem, plus booster vehicle interface per 5.1.3.

8.1.4 Fabrication of tower drop test vehicle and touchdown systems, per 5.2.1; quantity - 2 boilerplate vehicles, 25 touchdown systems. Additional equipment required: accelerometers, recorders, strain gauges, motion picture cameras.

8.1.5 Fabrication of aerial drop test vehicles and landing systems, including prototype drogue parachute subsystem with modified deployment initiation control, main parachute subsystem and dynamically scaled boilerplate vehicle with prototype impact system, per 5.1.2.

8.1.6 Fabrication of prototype descent systems for reliability aerial drop tests, per 7.2.2.

8.2 Production fabrication

Fabrication of twelve production landing systems for the Mars vehicle.

9.0 Documentation

9.1 Reports

9.1.1 Monthly Progress Reports

9.1.2 Quarterly Technical Progress Reports

9.1.3 Engineering Reports at Significant Milestones

9.1.4 Development Test Reports

9.1.4.1 Sterilization Study Report

9.1.4.2 Vacuum Testing Report

9.1.4.3 Tower Drop Test Report and Film

9.1.4.4 Aerial Drop Test Report and Film

9.1.4.5 Rocket Boost Test Report and Film

9.1.5 Qualification Test Report

9.1.6 Reliability Analysis and Test Report

9.1.7 Final Program Report.

9.2 Specifications

9.2.1 Qualification Test Specification

9.2.2 Reliability Test Specification.

9.3 Drawings

9.3.1 Test Vehicle Drawings

9.3.2 Prototype System Drawings

9.3.3 Production System Drawings.

2. Program plan for Venus lander vehicle descent system

The following pages present a program plan for the descent system for the Venus lander vehicle. The plan is divided into the following categories of effort:

1.0 Engineering Analysis

2.0 Systems Design

3.0 Test Components and Test Vehicles Design

4.0 Development Tests - Materials and Components

5.0 Development Tests - Subsystems and Systems

6.0 Qualification Tests - Components and Subsystems

7.0 Reliability

8.0 Fabrication

9.0 Documentation.

1.0 Engineering analysis

Aerodynamic, stability, aerothermodynamic and dynamic loading analyses of the ballute assembly and the pilot chute assembly; sequence controller requirements analysis.

2.0 Systems design

2.1 Pilot chute system design

2.1.1 Pilot chute (HT-1)

2.1.2 Pilot chute riser

2.1.3 Pilot chute deployment gun.

2.2 Ballute system design

2.2.1 Ballute (to be furnished by Goodyear Aircraft Corporation)

2.2.2 Ballute riser

2.2.3 Ballute bag

2.2.4 Integration of the ballute system into the vehicle design. Solution of the interface problems.

2.3 Sequence controller design

3.0 Test components and test vehicles design

3.1 Design of windtunnel models of vehicle-Ballute combination for drag, stability and optimum riser length determination.

3.2 Design of aerial drop test vehicle. Vehicle to include prototype Ballute system with modified deployment initiation controller. Vehicle to be dynamically scaled to Venus environment. Supplementary recovery system to be furnished.

3.3 Design of rocket boost vehicle for high Mach number ballute system testing.

3.3.1 Determination of required test program for best Venus entry simulation.

3.3.2 Selection of booster configurations to achieve test points.

3.3.3 Design of test vehicle to carry experimental Ballute system, including separate recovery system.

4.0 Development tests - materials and components

4.1[1] Sterilization heat cycling tests on Ballute material, pilot chute (HT-1) material, proposed pyrotechnic and deployment initiation controllers. Equipment Required: See Paragraph 4.1.1 of Mars Vehicle Landing System Work Statement.

4.2[1] Long term vacuum testing of Ballute material and pilot chute material. Equipment Required: See Paragraph 4.1.2 of Mars Vehicle Landing System Work Statement.

5.0 Development tests - subsystems and systems

5.1 Windtunnel testing of vehicle - Ballute configuration per 3.1

Location: ARO or NASA, Langley Unitary Plan wind tunnel.

No. of Tests: 12 to 15 at Mach nos. between 0.1 and 5.0.

5.2 Aerial drop tests of prototype descent system with boilerplate vehicle. Drops will test pilot chute deployment, Ballute deployment, and inflation characteristics, Ballute-vehicle stability and Ballute drag measurement.

No. of Vehicles 2

No. of Drops 8

No. of Descent Systems 5

No. of Sequence Control Systems 3

Test Location El Centro, California.

Test Altitude 50,000 feet or higher (supplementary recovery system required.)

5.3 Rocket boosted vehicle tests of Ballute deployment and deceleration at high Mach numbers. Tests will determine pilot chute deployment, Ballute deployment, and inflation characteristics, Ballute-vehicle stability and Ballute drag measurement.

No. of Vehicles 6

No. of Descent Systems 6

Test Locations Eglin AFB or WSMR

Test Point Range 75,000 feet to 125,000 feet altitude in the Mach number range of 3 to 4.

6.0 Qualification tests - components and subsystems

6.1 Purpose of the qualifications tests: To ensure operability of the hardware after being subjected to the anticipated environments.

6.2 Type of test:

Sterilization

High Vacuum - Solar Heating

Shock

Salt Spray

Sand and Dust

Vibration

Humidity

Fungus .

6.3 Items to be tested:

Pilot chute assembly

Electromechanical deployment initiation controls Ballute assembly

Pyrotechnic devices.

7.0 Reliability

7.1 Reliability analysis, Based on the reliability of the system components and the uncertainties of the entry trajectory and the Venusian atmosphere, as these uncertainties affect the landing system operational reliability.

7.2 Reliability test program

7.2.1 Environmental testing of components of the landing system, particularly pyrotechnic and electromechanical devices, followed by operational tests as applicable. Types of tests are as listed in 6.2.

7.2.2 Aerial drop tests to determine reliability of descent system.

No. of Vehicles 2

No. of Drops 12

No. of Descent Systems 12

Test Location El Centro, California

Test Altitude 50,000 feet or higher (supplementary recovery system required).

8.0 Fabrication

8.1 Test components and test vehicles fabrication

8.1.1 Windtunnel models of vehicle - Ballute configuration per 3.1: Quantity -3.

8.1.2 Fabrication of aerial drop test vehicles, including pilot and Ballute system with modified deployment initiation control and supplementary recovery system to be applied per 5.2.

8.1.3 Fabrication of 6 rocket-boosted Ballute system test vehicles with recovery system plus booster vehicle interface, per 5.3.

8.1.4 Fabrication of 12 prototype landing systems for reliability aerial drop tests per 7.2.2.

8.2 Production fabrication

Fabrication of 9 production landing systems for the Venus vehicle.

9.0 Documentation

9.1 Reports

9.1.1 Monthly Progress Reports

9.1.2 Quarterly Technical Progress Reports

9.1.3 Engineering Reports at Significant Milestones

9.1.4 Development Test Reports

9.1.4.1 Sterilization Study Report

9.1.4.2 Vacuum Test Report

9.1.4.3 Windtunnel Test Report

9.1.4.4 Aerial Drop Test Report and Film

9.1.4.5 Rocket Boost Test Reports and Film

9.1.5 Qualification Test Report

9.1.6 Reliability Analysis and Test Report

9.1.7 Final Program Report.

9.2 Specifications

9.2.1 Qualification Test Specification

9.2.2 Reliability Test Specification.

9.3 Drawings

9.3.1 Test Vehicle Drawings

9.3.2 Prototype System Drawings

9.3.3 Production System Drawings.

6. Program schedule

The program schedule for the accomplishment of the Program Plans outlined in Sections 4 and 5 of this report is shown in figure A7. The schedule is based on a "go-ahead" for the programs in January 1965, with delivery of the first three Mars vehicle production landing systems to Avco in June 1968, and delivery of the first three Venus vehicle production landing systems to Avco in June 1969.

As shown on the program schedule the program tasks for the Mars and Venus systems are integrated and carried out coincidentally. This arrangement will provide major economies in eliminating duplication of effort. This will be particularly true in the case of development tests, qualification tests and reliability tests. In the development tests, single test crews can be utilized, together with concurrent testing where applicable, of materials and components to reduce test engineering and test equipment time. For the qualification and reliability tests, a single field crew can be utilized to carry out the test programs for both systems. It is currently felt that a single rocket -boosted test vehicle can be designed to flight test both the Mars lander drogue parachute subsystem and the Venus lander Ballute system.

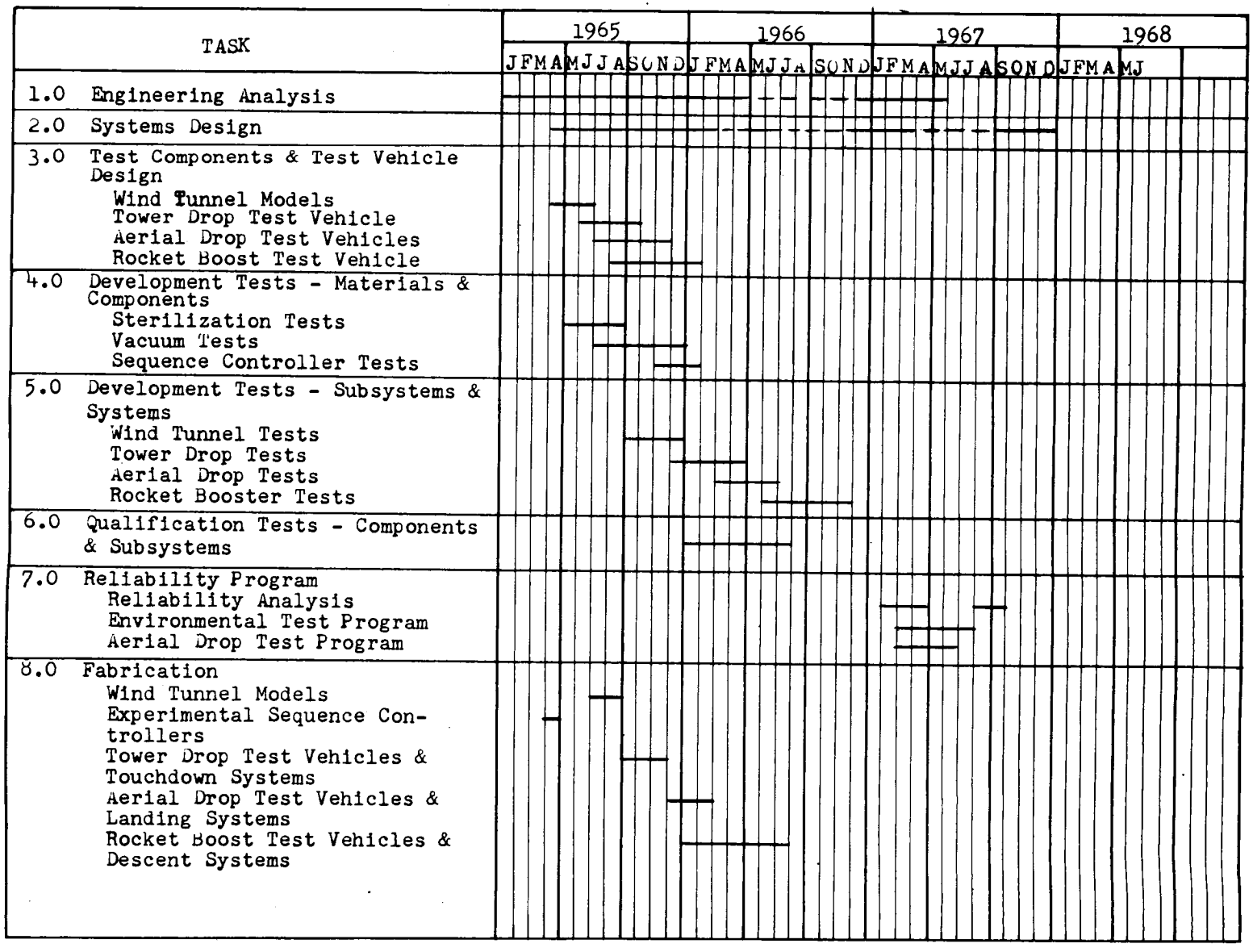

Figure A7 PROGRAM SCHEDULE

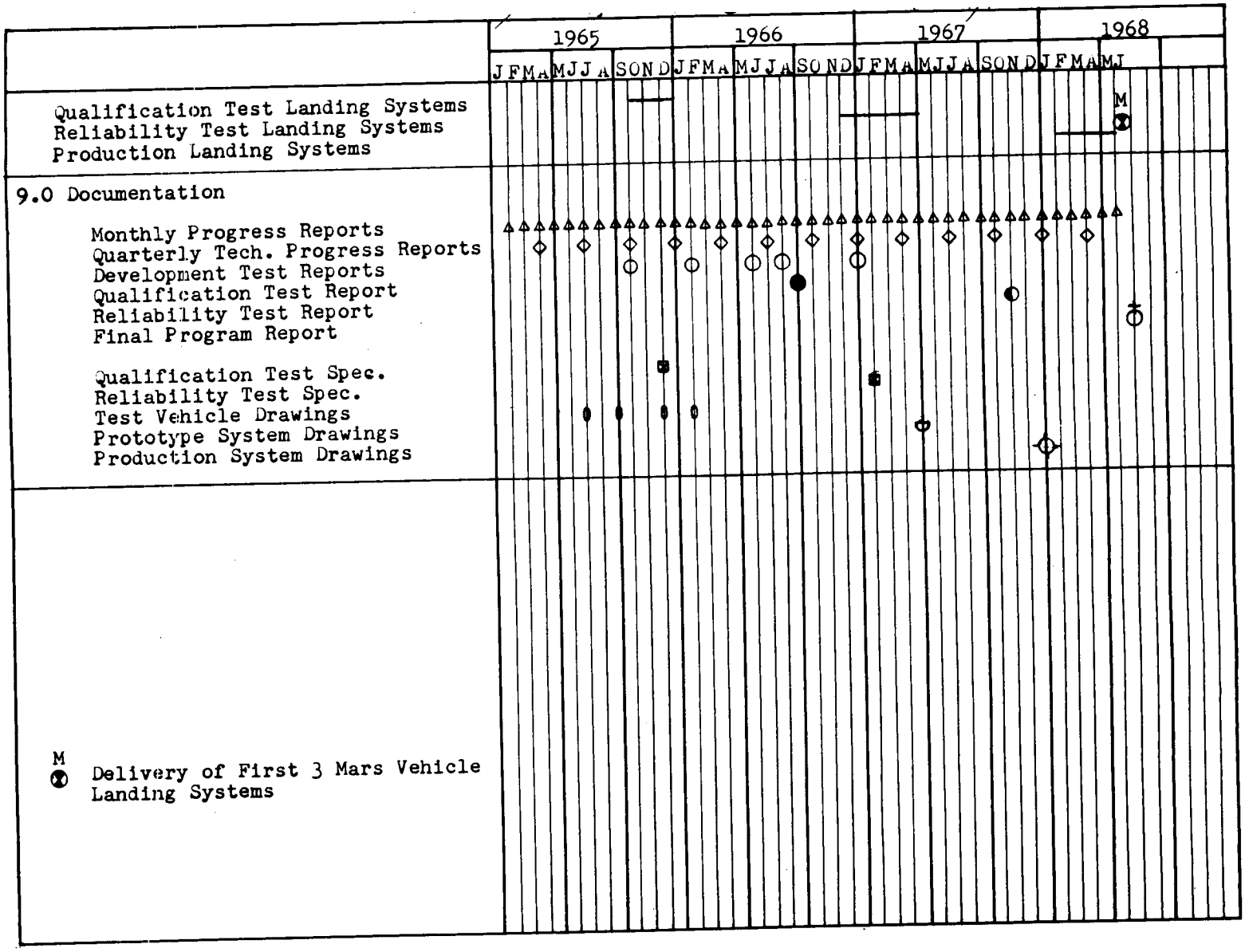

Figure A7 PROGRAM SCHEDULE (CONCL'D)

7. References

1. Moeller, J., M. Neustadt, and H. Bixby, Parametric Study for the Optimization of Voyager Landing Systems; Northrop-Ventura Report No. 2807 (20 September 1963).

2. Schilling, F. G., Limiting Model Atmospheres of Mars; JPL Report No. R-402-JPL (August 1962)

3. Kaplan, L. D., A Preliminary Model of the Venus Atmosphere; JPL Tech. Report No. 32-379 (December 1962).

4. Nebiker, F. R., Feasibility Study of an Inflatable Type Stabilization and Deceleration System for High-Altitude and High-Speed Recovery; WADD Technical Report 60-182 (December 1961).

5. Aebischer, A. C., Investigation to Determine the Feasibility of Using Inflatable Balloon Type Drag Devices for Recovery Applications in the Transonic Supersonic, and Hypersonic Flight Regime, Parts I and II, ASD-TDR-62-702 (October 1962, December 1962).

APPENDIX B

SUMMARY OF ROCKETDYNE STUDIES ON LANDER PROPULSION SYSTEMS

PART I -- MARS LANDER PROPULSION SYSTEM DESIGN REQUIREMENTS

The design requirements for the Mars lander propulsion system were defined by Avco as follows:

1. System design duration of 1 year with capability of extending the duration to 18 months without significant modifications

2. Environmental temperature range of 0 to 100° F for pressurant and propellant tanks

3. System adequacy for vacuum environment and space-radiation conditions

4. Meteoroid protection for tanks to be provided by the system structure

5. Vibration and g-loading as shown in the orbiter propulsion system design section

6. The system must provide a velocity increment of 100 fps when integrated into a vehicle weighing 1670 pounds at entry

7. The system period of operation may be varied by a command signal but will consist of a single thrusting period

8. The propulsion system operation will occur while the vehicle is rotating at 10 rpm. Precession angles during rotation may be as large as 15 degrees

9. Special sterilization requirements for the structurally integrated propulsion unit will require heating the structure and propulsion unit to 295° F for 24 hours. Propellants and pressurants are to be loaded in the system prior to heating.

1. Propulsion system description. The Mars lander propulsion system is a pressure-fed, storable, hypergolic, bipropellant system with a total delivered impulse of 5150 lb-sec. The system propellants are mixed oxides of nitrogen (MON) composed of 85 percent nitrogen tetroxide and 15 percent nitric oxide and a eutectic fuel (EMHF) consisting of 87.6 percent monomethylhydrazine and 12.4 percent hydrazine by weight. An all-welded configuration will be used to prevent leakage. The system is prepackaged with propellants, and the fill and vent connections will be welded after filling. This system is capable of

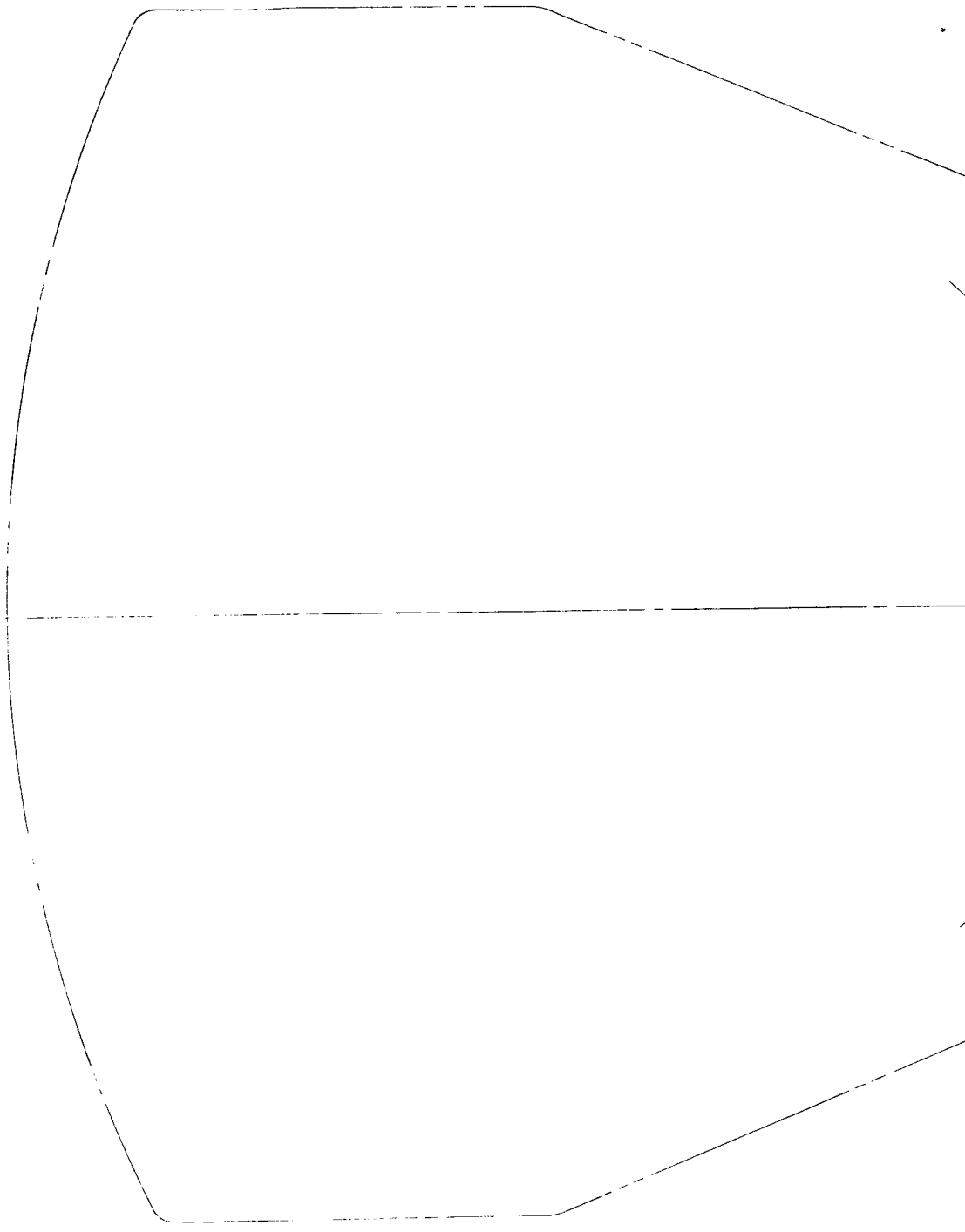

Figu

63-9428

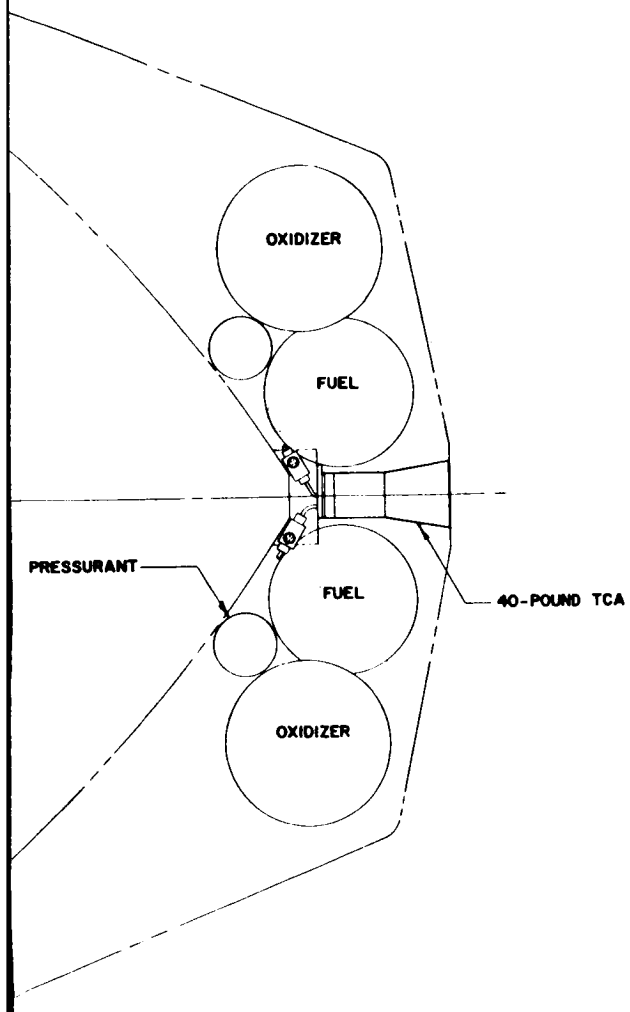

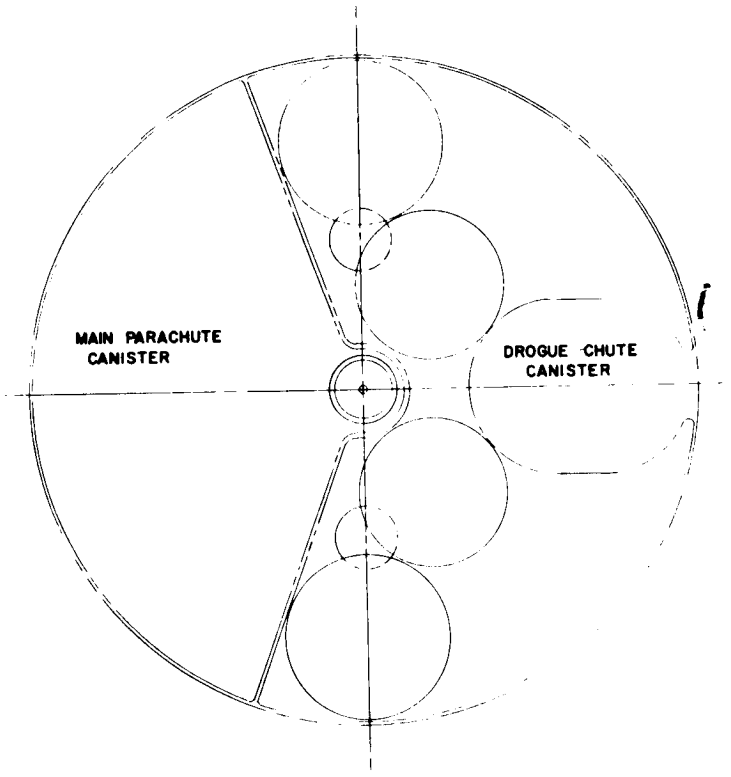

re B1 PROPULSION SYSTEM LAYOUT

being sterilized with loaded propellants at a temperature of 295° F for a period of 24 hours. An installation drawing of the system is shown in figure B1. The system weight and power requirements are shown in Tables B1 and B2.

TABLE B1

WEIGHT SUMMARY

Pressurant System		
Pressurant Tank (2)	0.8	
Pressure Transducer	0.3	
Fill Connection	0.2	
Normally Closed Squib Valve (3)	0.8	
Filter and Regulator	1.0	
Relief Valve	0.8	
Check Valve (2)	0.4	
Vent Valve	0.4	
Plumbing and Miscellaneous Fittings	0.5	
		5.2
Propellant System		
Fuel Tank (2)	0.6	
Oxidizer Tank (2)	2.5	
Fill Connection (2)	0.4	
Normally Closed Squib Valve (2)	0.6	
Normally Open Squib Valve (2)	0.6	
Filter (2)	0.4	
Plumbing and Miscellaneous Fittings	0.5	
		5.6
Thrust Chamber Assembly		2.1
Fluids		
Pressurant, Helium	0.05	
Oxidizer, MON	12.1	
Fuel, EMHF	5.6	
Total Dry Weight, pounds		12.9
Total Wet Weight, pounds		30.6
Usable Propellant-to-System Weight Ratio (λ_p)		0.55

TABLE B2

POWER REQUIREMENTS

Unit	Number and Component	
	5 Normally Closed Squib Valves (4, 8, 13)*	2 Normally Open Squib Valves (14)
Voltage, volts	1.8	1.8
Operating Current, amperes	2	2
Maximum No-Fire Current, amperes	0.15	0.15
Response, milliseconds	2	2
Maximum Power, watts (0 to 100°F)	3.6 each	3.6 each

*Numbers in parentheses indicate location on schematic

The main thrust chamber is rigidly mounted, ablatively cooled, and is controlled for the single period of operation by normally closed and normally open squib valves in series. The chamber is designed to produce 40 pounds of thrust at a chamber pressure of 100 psia. Propellant tank pressure will be regulated at 140 psia. Thrust vector alignment tolerances are 0.01 inch for lateral displacement and 0.26 degree angular misalignment, as shown in the orbiter thrust vector analysis section. The effect of these inaccuracies upon the velocity vector is reduced to an acceptable value by spinning the lander at 10 rpm. Spin-up is accomplished by a pair of solid-propellant rockets attached to the lander sterile container. The solid rockets are not provided with the propulsion system. The propellant is contained in two equal-volume oxidizer tanks and two equal-volume fuel tanks. The tanks are packaged in a nearly dynamically balanced arrangement within the space allowed. The lander spin rate is utilized as a means of propellant orientation to give a dependable means of propellant expulsion. Tank outlets are positioned to allow maximum propellant utilization.

The propellant tanks are filled with the required amount of propellant before sterilization. During sterilization at 295°F, the oxidizer will generate a high vapor pressure. The generated pressure is a function of ullage volume; in this case, the design was based on a pressure of 1300 psia with a 10 percent ullage volume. A stainless steel, which is compatible with the oxidizer at the sterilization temperature, was chosen for the tank material. At 295°F, the steel has

such high strength that manufacturing minimum thickness is the governing factor in determining wall thickness. The vapor pressure of the fuel is 75 psia at 295° F, which is well below tank design pressure of 140 psia. Aluminum was chosen for the fuel tank material with wall thickness governed again by manufacturing capability rather than stress requirements. Normally closed squib valves are used above the tanks for propellant isolation because of the absence of diaphragms or bladders in the propellant tanks. The valves ensure propellant isolation until system activation. Check valves will then provide assurance of isolating the propellant from one another during system operation.

Pressurization is provided by stored helium contained in two equal-volume spheres manifolded together. The two-tank configuration was chosen from packaging and dynamic balance considerations. The pressurant is sealed by a normally closed squib valve until the system is activated.

2. System operation. The propulsion system is operated as described below. The numbers in parentheses refer to the system schematic diagram (figure B2). The system is activated and fired by signals to the control components in the following sequence:

1. The normally closed squib valves (4), (8), and (13), are fired simultaneously. This permits pressurant to flow through the regulator (5), check valves (7), valves (8), and into propellant tanks (10) and (11). The propellants flow through valves (13) and (14) and hypergolically ignite in the chamber (15), providing rated thrust.

2. Thrust is terminated by a signal, firing valves (14) to stop propellant flow. The pressurant, at this time, will be exhausted externally through the relief valve (6).

3. Less than full total impulse may be achieved by timing the signal to valves (14) for thrust termination.

3. Analysis. Analysis of the lander propulsion system was conducted to permit optimization of system design parameters. It was determined that requirements for sterilization present no unusual problems. Vehicle spin stabilization was used as a method of propellant orientation for expulsion, and propellant diaphragms were not required.

3.1 Optimization of Design Parameters

Engine mixture ratio, chamber pressure, and expansion area ratio were examined to determine optimum values for these parameters for minimum propulsion system weight. For the analysis, items considered to be of variable weight were thrust chamber, propellants (due to specific impulse variations),

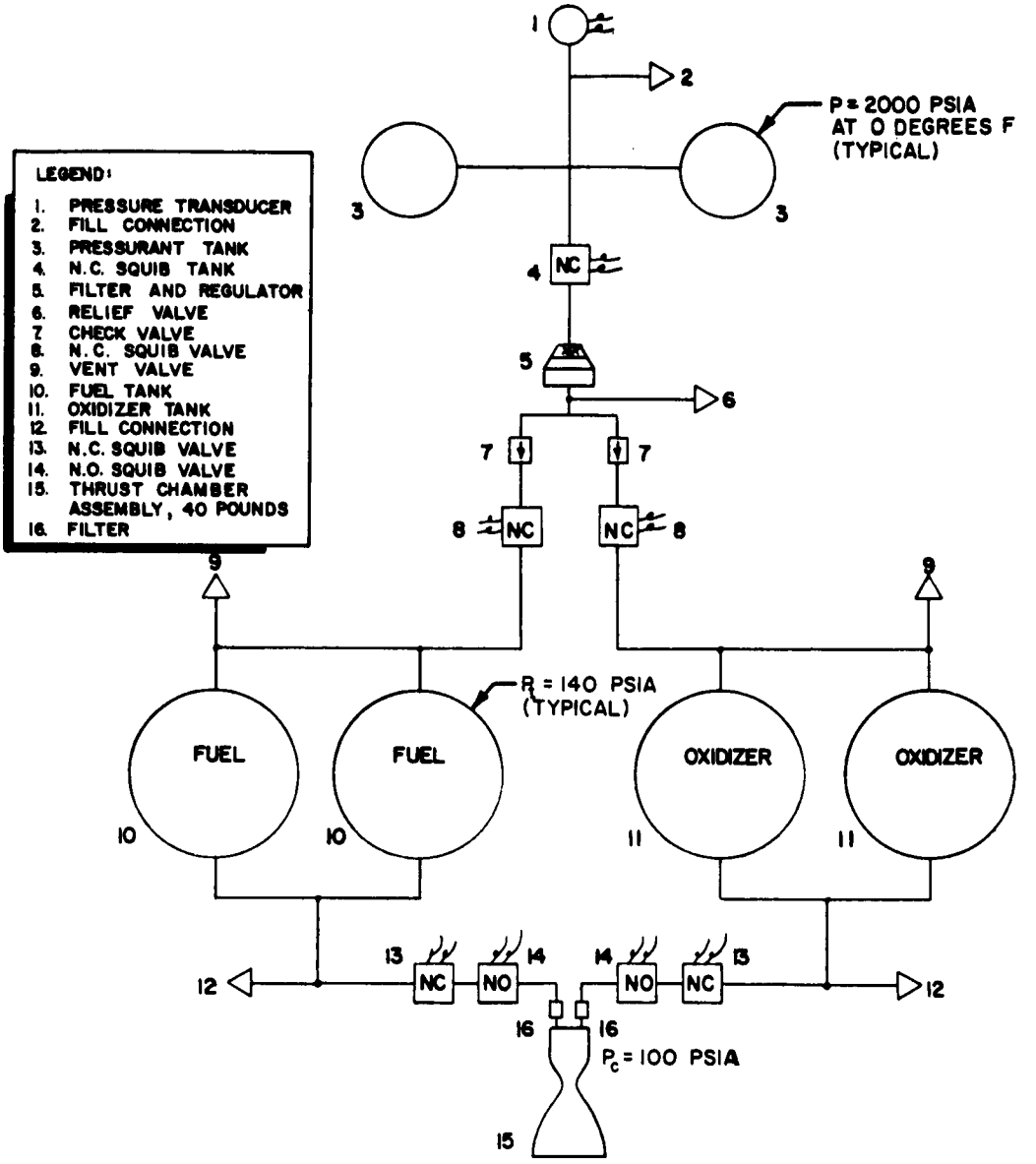

Figure B2 PROPULSION SYSTEM SCHEMATIC

63-9429

propellant tanks, pressurant, and pressurant tanks. Mixture ratio optimization was necessary because of the significant weight of the high-pressure oxidizer tanks. The results of the analysis are presented in figures B3 through B5. Examination of the figures indicates a rather wide range over which each of the parameters may be varied without deviating significantly from the point of minimum weight.

The performance parameters resulting from the optimization of design parameters are shown in table B3. These were used for the system preliminary design.

3.2 Reliability Analysis

The results of a preliminary reliability analysis of the proposed lander propulsion system are presented in table B4. The estimated system reliability represents a potential level which the propulsion system can expect to achieve at the conclusion of the qualification test phase. This reliability is the probability that the propulsion system will successfully perform start, operation, shutdown as required in the mission.

The propulsion system is designed for maximum reliability; it incorporates redundant components in the pressurization system and propellant feed system to guard against internal leakage during an extended mission. An all-welded configuration will be used to prevent external leakage. Fill and vent connections will be positively sealed after servicing.

The failure rates in this analysis are derived from Rocketdyne experience with components of similar design and/or performing similar functions. Consideration is given to the mission and environmental requirements of the component, criticality of component operation, and the projected state of the art. A few basic assumptions necessary in estimating component failure rates and system reliability are:

1. The reliability of a component is inherent in the function it performs and will therefore be similar to components with similar functions and proved reliabilities.

2. No insurmountable problems will be encountered in the development of the new system; therefore, the inherent functional reliability will be achieved in a normal development program.

3. The wearout life of the components will be sufficiently longer than the operational life of the system so that wearout failure will not be encountered and only chance failure will occur.

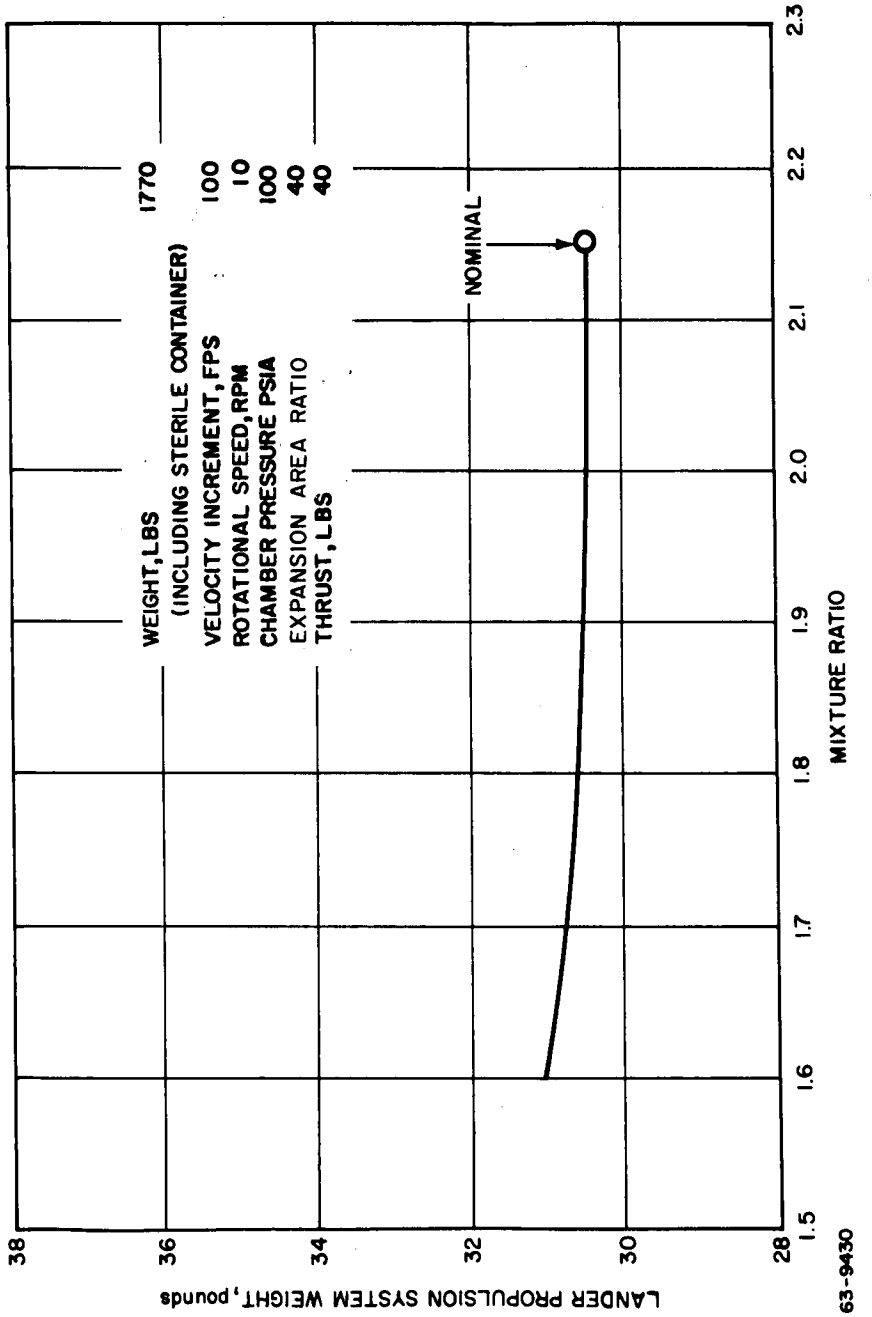

Figure B3 MARS LANDER PROPULSION SYSTEM WEIGHT VERSUS MIXTURE RATIO

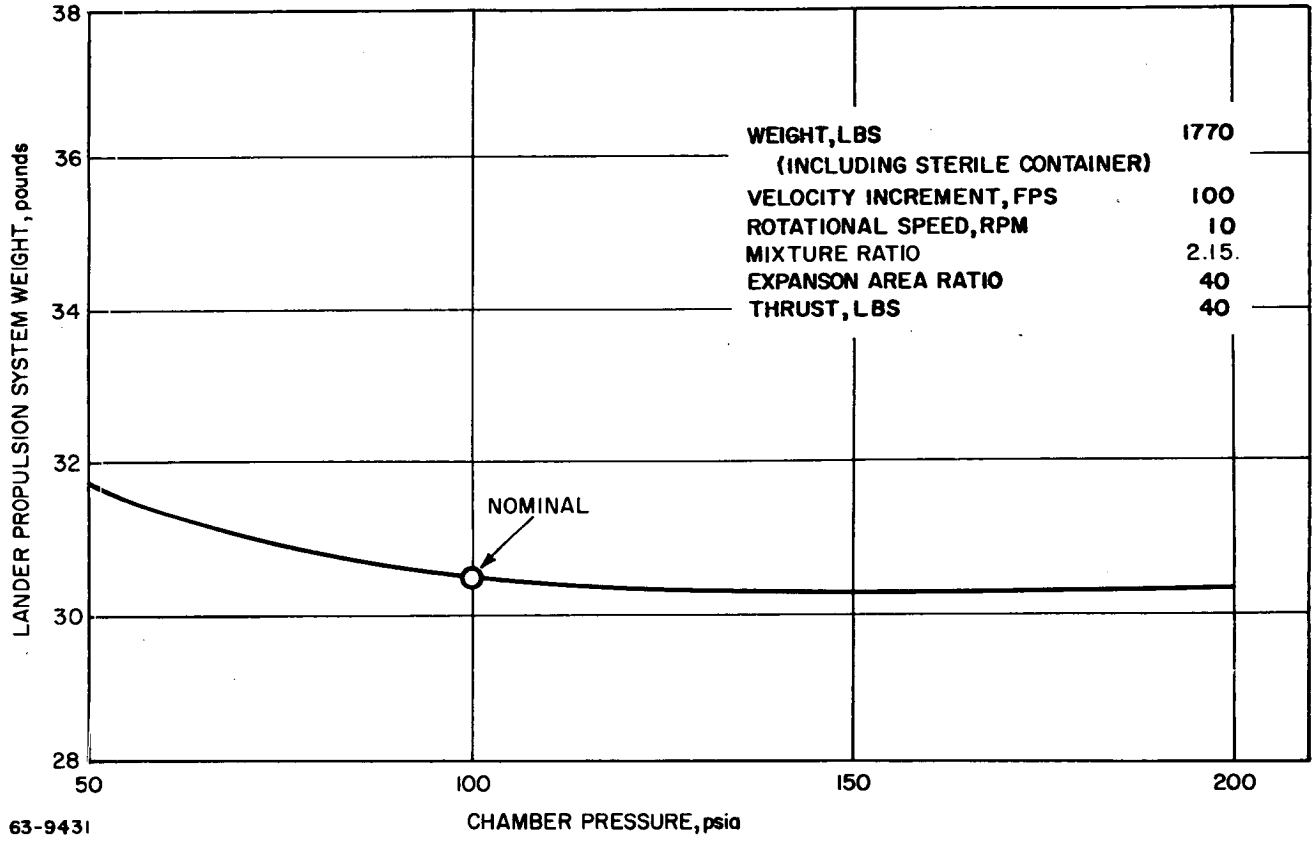

Figure B4 MARS LANDER PROPULSION SYSTEM WEIGHT VERSUS CHAMBER PRESSURE

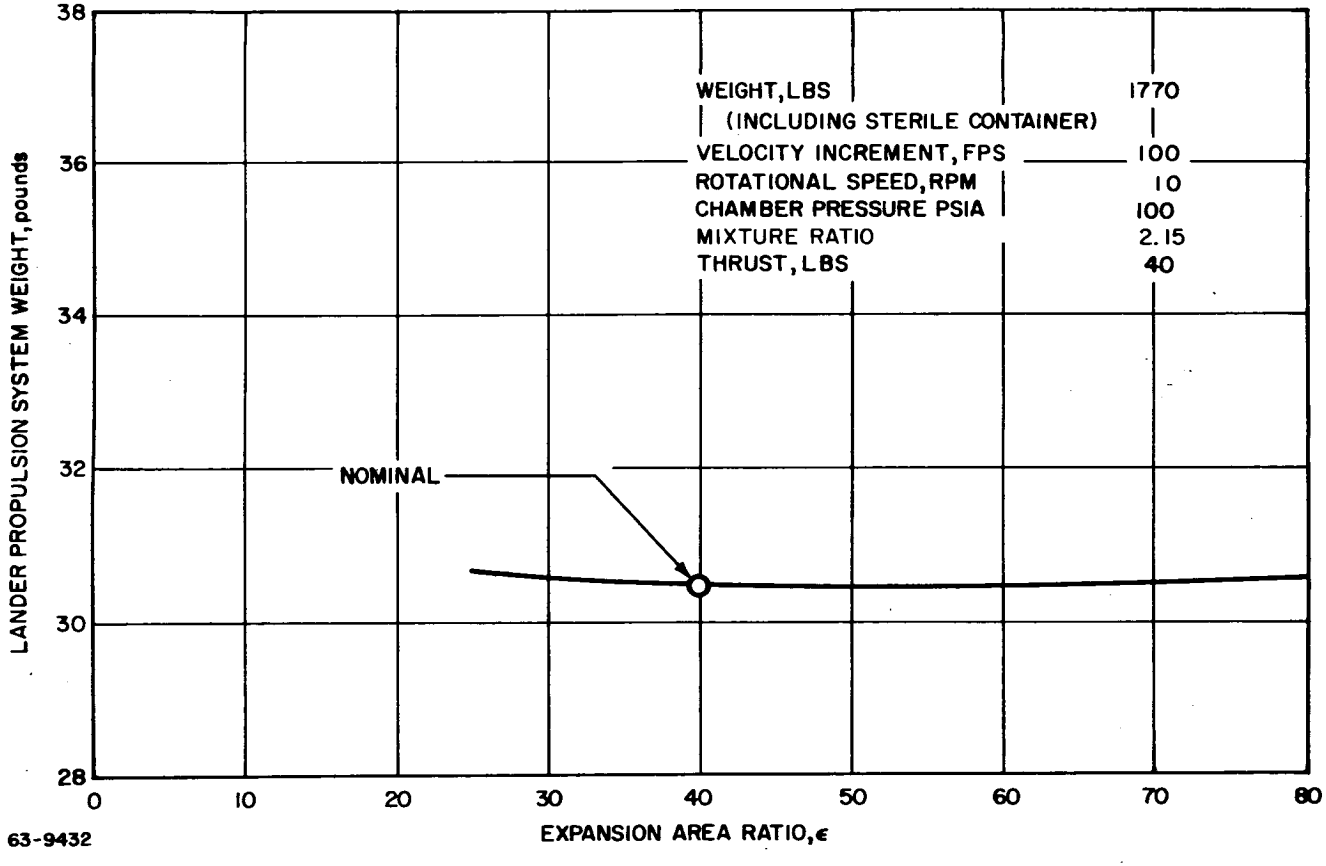

Figure B5 MARS LANDER PROPULSION SYSTEM WEIGHT VERSUS EXPANSION AREA RATIO

TABLE B3

SUMMARY SYSTEM PERFORMANCE PARAMETERS

Thrust, pounds	40
Chamber Pressure, psia	100
Mixture Ratio	2.15
Characteristic Velocity (c*), fps	5313
Thrust Coefficient (C_F actual)	1.850
Specific Impulse (I_{sp}), seconds	305.5
I_s Efficiency	0.900
c* Efficiency	0.945
C_F Efficiency	0.952
Throat Area, sq in.	0.216
Expansion Area Ratio	40:1
Oxidizer Flowrate, lb/sec	0.088
Fuel Flowrate, lb/sec	0.042

TABLE B4

PREDICTED COMPONENT FAILURE RATES AND SYSTEM RELIABILITY

Subsystem Unit	Number Required	P_c, x 10^{-5}	P_s, x 10^{-5}	Total
Subsystem I--Pressurization				
Pressure Transducer	1	15	15	
Fill Connection	1	5	5	
Pressurant Tank	2	8	16	
Isolation Valve, Normally Closed Squib	1	5	5	
Filter and Regulator Assembly	1	32	32	
Relief Valve	1	12	12	
Check Valve	2	10	20	
Isolation Valve, Normally Closed Squib	2	5	10	
Vent Valve	2	5	10	
Subtotal				125
Subsystem II--Propellant Feed System				
Propellant Tank Assembly	4	35	140	
Fill Connection	2	5	10	
Isolation Valve, Normally Closed Squib	2	5	10	
Isolation Valve, Normally Open Squib	2	5	10	
Subtotal				170
Subsystem III-Thrust Chamber Assembly				
Thrust Chamber Assembly	1	60	60	60
Total			355	355

Reliability Estimate

$$R = \exp - [\Sigma P_s] = \exp - [355 \times 10^{-5}] = e^{-0.00355} = 0.99645$$

P_c = estimated probability of failure for one component

P_s = estimated probability of failure for the components in the system based on the number of components required, $P_s = n \times P_c$

4. SYSTEM DESIGN

This section presents a detailed description of the components in the repropulsion system. The following paragraphs include a comprehensive description of their function, materials, and construction. All components are designed to withstand the sterilization requirements of 295°F for 24 hours as well as the rotational effects of the 10-rpm vehicle spin.

4.1 Thrust Chamber Assembly

The Mars lander engine (figure B6) is a 40 pound, 140-second-duration, 40:1 epsilon thruster consisting of a fiberglass-wrapped, lined, ablative combustion chamber, with a refractory silicon carbide throat. The basic design parameters may be found in table B5.

The optimum configuration for the lander mission was determined after a detailed examination was made to select the recommended thrust chamber.

The thrust chamber is designed so that, with 140 seconds duration, insulative material remains between the char and fiberglass to give a maximum outer wall temperature of 500°F. Once the char depth is determined, asbestos-phenolic insulator is wrapped and cured over the ablative material. The insulator reduces the rate of heat flux to the structural fiberglass shell.

Tests run on the Gemini program indicate that the effects of the 295°F temperature for 24 hours will have a negligible effect on the thrust chamber ablative material.

1. Throat. Silicon carbide is the throat-insert material proposed for Voyager and is presently being used at Rocketdyne. However, other materials under consideration and investigation are silicon carbide backed by a molybdenum sleeve, and silicon diffused into graphite.

Silicon carbide has a high melting point (4400°F), excellent thermal shock characteristics, relatively high thermal conductivity (115 Btu/hr/ft^2/in.), low coefficient of thermal expansion (2.4 x 10^{-6} in./in.-°F), excellent oxidation resistance, and high abrasion resistance. A molybdenum backup and sleeve are used only in those cases where the silicon carbide insert cannot conduct the heat sufficiently.

2. Combustion chamber. After the optimum chamber pressure was determined, the combustion chamber geometry was established. The dimensions of the combustion zone are such that the gases mix thoroughly upstream of the throat. In many cases, however, the high-silica glass in the ablative material becomes fluid enough to be swept downstream and deposited in the throat section. This causes thrust variances and the possibility of an unsymmetrical velocity

profile in the deposition area. Prevention of this phenomenon is accomplished by inserting a liner of JTA (45 percent graphite, 45 percent zirconium diboride, and 10 percent silicon) in the combustion zone. The liner, which proved highly successful on the Gemini program, is segmented to provide a path for the pyrolyzed ablative gases which reduces the ΔP across the liner and prevents cracks which might otherwise occur in an expanding unsegmented liner.

TABLE B5

THRUST CHAMBER DESIGN PARAMETERS

Thrust, pounds	40
Chamber Pressure (P_c), psia	100
Throat Area, sq in.	0.216
Throat Diameter, inches	0.525
Contraction Area Ratio (ϵ_c)	4.0:1
Combustion Chamber Area, sq in.	0.86
Combustion Chamber Diameter, inches	1.050
Characteristic Length (L^*), inches	14
Expansion Area Ratio (ϵ)	40:1
Exit Diameter, inches	3.32
Thrust Coefficient (C_F, actual)	1.850
Exit Cone Contour	80 percent Bell
Duration, seconds	140
Mixture Ratio ($\dot{w}_o / \dot{w}_f$)	2.15
Oxidizer Flowrate ($\dot{w}_o$), lb/sec	0.088
Fuel Flowrate ($\dot{w}_f$), lb/sec	0.042

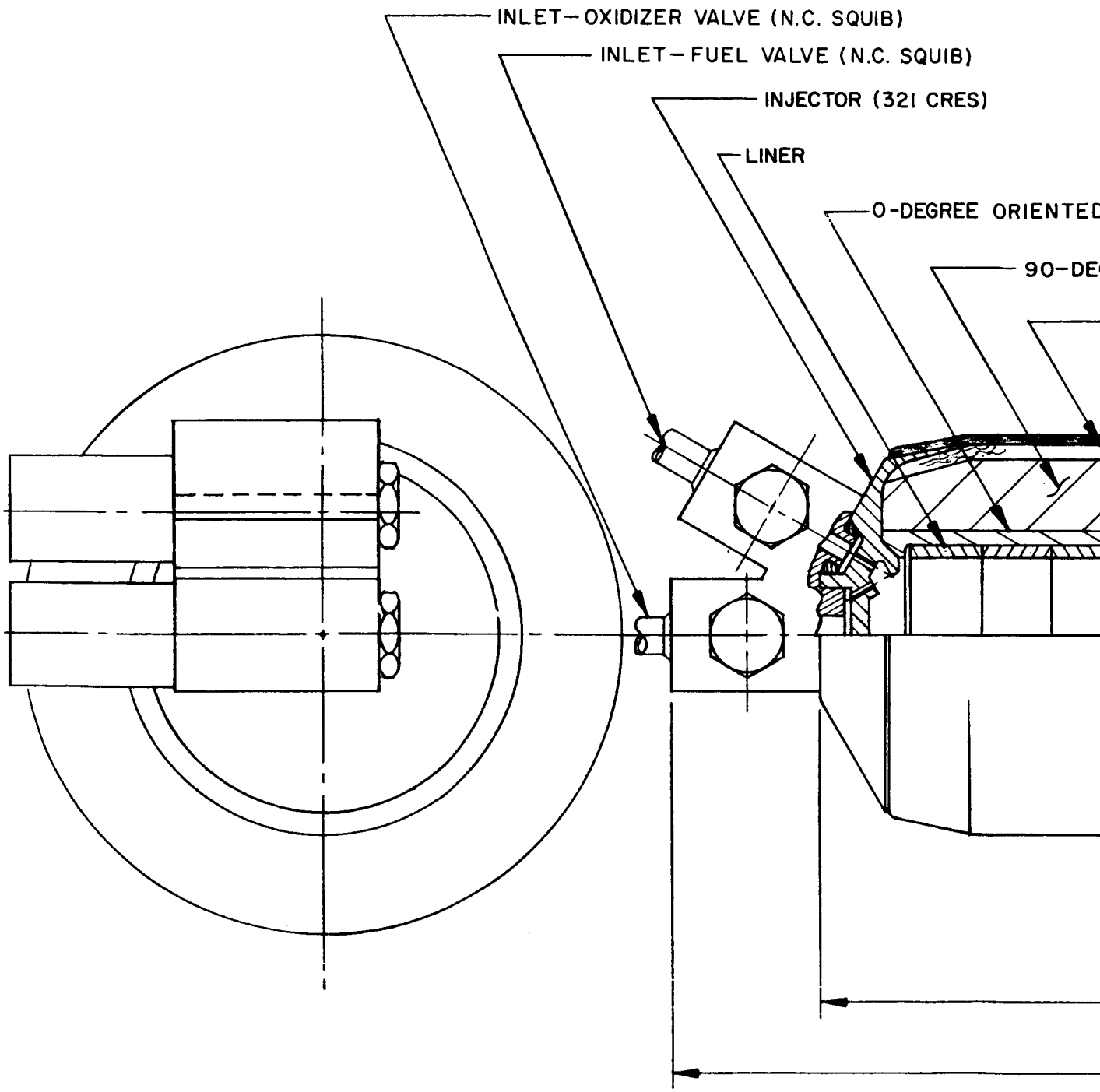

Figure B6 THRUST CHAM

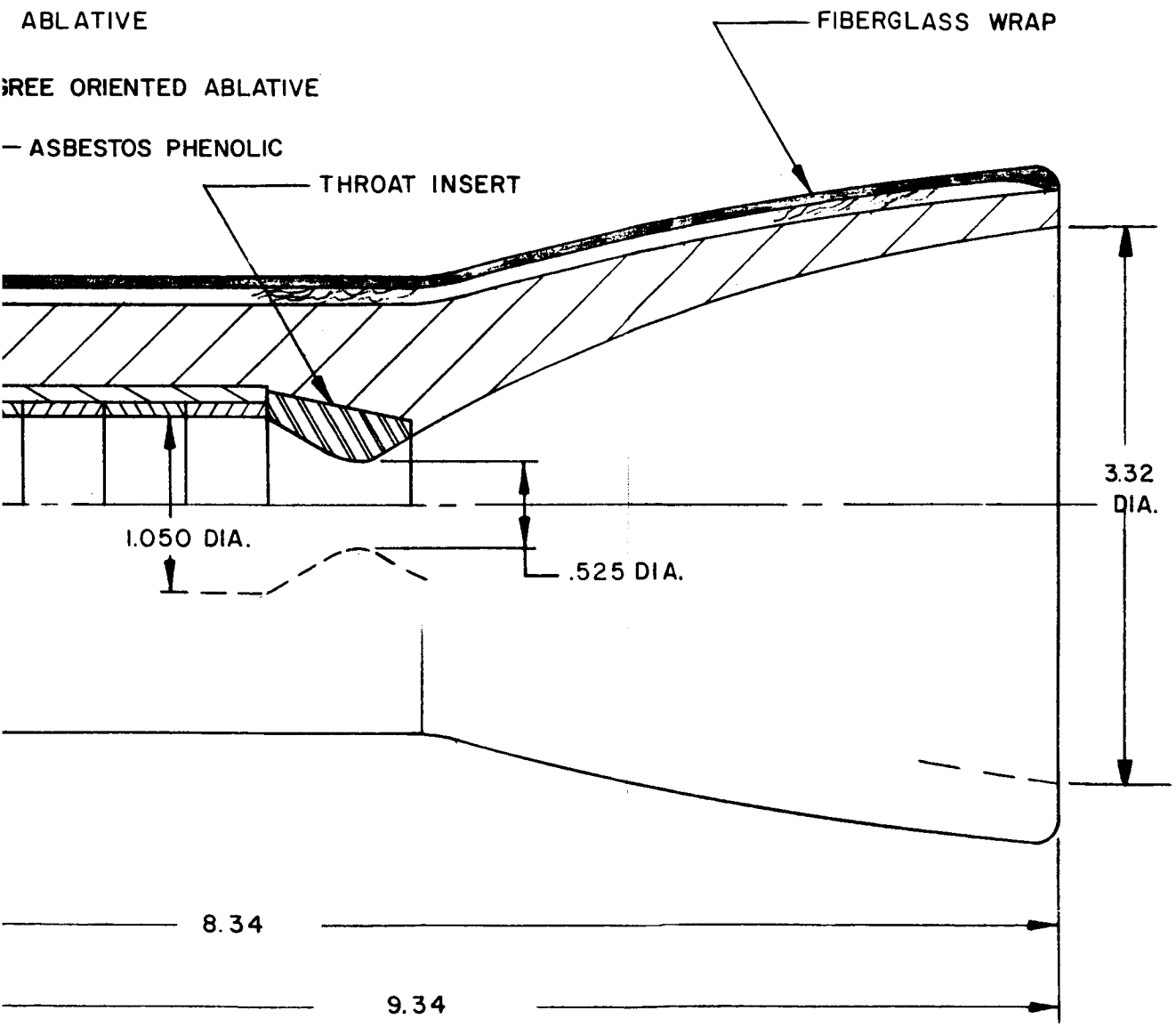

BER ASSEMBLY

3. Fiberglass. As the ablative chamber and nozzle sections char, the radius at which the operating pressure acts will increase. The minimum insulation provided thereafter will carry little load; hence, the fiberglass, which is filament-wound to accept hoop stresses and longitudinally wrapped to contend with meridional stresses, is designed to carry all the resultant chamber forces.

4. Injector. The injector selected for the lander thrust chamber is machined from 321 corrosion-resistant stainless steel. It conforms to a conventional, fixed-orifice, single-ring, impinging unlike doublet, splash-plate type. The splash plate is utilized because of improved performance obtained at this thrust level. The injector is designed to inject propellant into the combustion zone so that the resultant momentum vector is parallel to the centerline of thrust. The propellant manifolding provides minimum downstream volume and, therefore, maximum response. External considerations of the injector design are thrust chamber attachment and mounting provisions for the explosively actuated propellant valves.

Several types of injectors (single ring) were investigated for this application: impinging unlike doublets, like-on-like and fuel-on oxidizer; and impinging triplets (with and without the splash plate). However, the combustion chamber is of such a size as to enable the use of a simple, efficient, and proved unlike doublet configuration to ensure initial and complete liquid-phase mixing of the propellant. Because of the simple configuration (single fuel and oxidizer manifolds), convenient lathe-turned fabrication and injector inspection is permitted. Quality of the injector is controlled by inspection methods which include radiography, water-flow calibration of ΔP, and hot-fire calibration of mixture ratio.

4.2 Pressurant Tank

The two pressurant tanks (figure B7) are designed to store helium at a pressure of 2000 psia at 100°F. However, the sterilization requirements of the lander consist of elevating the system to a temperature of 295°F and maintaining this temperature for 24 hours. The tanks therefore were designed to a maximum pressure of 3200 psia and a temperature of 295°F.

The two pressurant tanks are machined from hemispherical, solution heat-treated, 6Al-4V titanium forgings. The two hemispherical halves are joined at the equator by tungsten electrode arc welding within an inert-gas-filled chamber. They are designed with an ultimate stress of 130,000 psi at 295°F and a safety factor of 1.8. Wall thickness at the weld joint is increased to compensate for loss of structural strength resulting from a weld efficiency of 83 percent.

Titanium was chosen as the tank material because of its high strength-to-weight ratio (970,000 inches). Several tanks of this type have been successfully

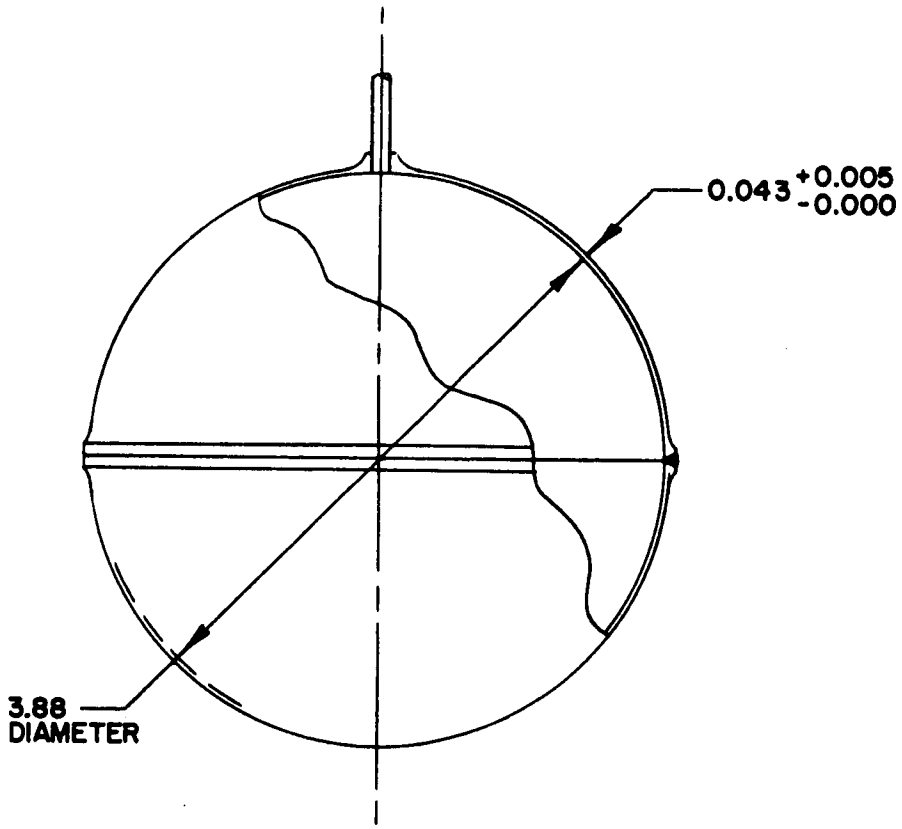

Figure B7 PRESSURANT TANK

63-9434

incorporated in each Atlas missile without a single failure. This design is also being used on the currently contracted SE-6 and SE-7 man-rated Gemini program.

4.3 Oxidizer Tank

The oxidizer used in the lander propulsion system is mixed oxides of nitrogen (MON). Sterilization requirements for the lander consist of elevating the system to a temperature of 295°F and maintaining this temperature for 24 hours. At this temperature, the vapor pressure of MON is 1300 psia. Therefore, the tanks (figure B8) are designed to withstand this pressure, thereby permitting the propulsion system to be sterilized as a self-contained unit with no subsequent addition of sterilized propellants. The material selected for this application was PH 15-7 Mo CRES because of its high strength at 295°F, its compatibility with MON, and its good weldability and machinability.

The two oxidizer tanks are machined from two hemispherical, heat-treated, PH 15-7 Mo CRES forgings and are welded at the equator. They are designed with an ultimate tensile stress of 196,000 psi at 295°F with a safety factor of 1.8. Wall thickness at the weld joint is increased to compensate for loss of structural strength resulting from the weld efficiency.

The outlet and inlet port bosses are integral parts of the forged hemispheres. The outlet port is located at an appropriate angle in order to provide maximum utilization of the oxidizer, considering the effects of rotational and axial acceleration loadings.

Table B6 gives comparative data on the tank materials considered for this application.

4.4 Fuel Tank

The fuel used in the lander propulsion system is a eutectic mixture of hydrazine fuels (EMHF). Although sterilization is required on the lander propulsion system, elevating the temperature of the system to 295°F for 24 hours only causes the vapor pressure of the fuel to increase to 75 psia. Because the ultimate tensile strength of 6061-T6 aluminum drops to 84 percent of its room temperature value at 295°F, it is seen that the maximum stress conditions occur at the operating conditions of 100°F maximum and a tank pressure of 140 psia. The tanks (figure B8) therefore are designed with 42,000 psi ultimate tensile stress at 100°F with a safety factor of 1.8. However, these calculations indicate that the tank wall would be prohibitively thin from a manufacturing standpoint. Consequently, materials of a higher strength-to-weight ratio were not required and the tank was designed with 0.020-inch-thick walls of 6061-T6 aluminum.

TABLE B6

COMPARISON OF CANDIDATE PROPELLANT TANK MATERIALS

Material	Ultimate Strength-to-Weight Ratio at 295 F ($\times 10^{-5}$)	Compatibility With Propellants	Ease of Manufacturing	Development Risk	Comments
6AL-4V Titanium	8.1	Compatible with fuel but not with oxidizer at 275 F	Reasonable for forgings	Extensive experience on cylindrical (SE-6) and spherical (SE-7) propellant tanks	High strength-to-weight ratio. However it is not compatible with MON at 275 F.
AM 350 Stainless Steel	6.2	Compatible with both propellants	Reasonable	Low risk; experience on similar tankage	Lower strength-to-weight ratio makes this material second choice; however offers good backup.
PH 15-7 Mo Stainless Steel	7.1	Compatible with MON; however long term storage with EMIF produces etching	Reasonable	Moderate experience on tankage	Poor compatibility with fuel makes this material poor choice for fuel tanks but optimum choice for oxidizer tanks
2014-T6 Aluminum	5.2	Compatible with both propellants	Low cost	Extensive production experience; also presently utilized on Rocketdyne's Lance program	Low strength-to-weight ratio offsets favorable cost
Inconel - X	4.8	Compatible with both propellants	Unfavorable cost factor	High cost per tank assembly produces poor development and delivery schedules	Low strength-to-weight ratio and high cost eliminates this material
6066-T6 Aluminum	4.2	Compatible with both propellants	Low cost	Experience on SE-9 transtage program	Low strength-to-weight ratio offsets favorable cost
6061-T6 Aluminum	3.5	Compatible with both propellants	Minimum cost	Experience on Atlas start system, SE-1-1, SE-5-1, SE-5-2, study for transtage, and in-house study 6011-0005	Minimum cost, maximum experience, and ease of manufacturing makes this optimum choice for fuel tanks because thin walls preclude use of higher strength materials.

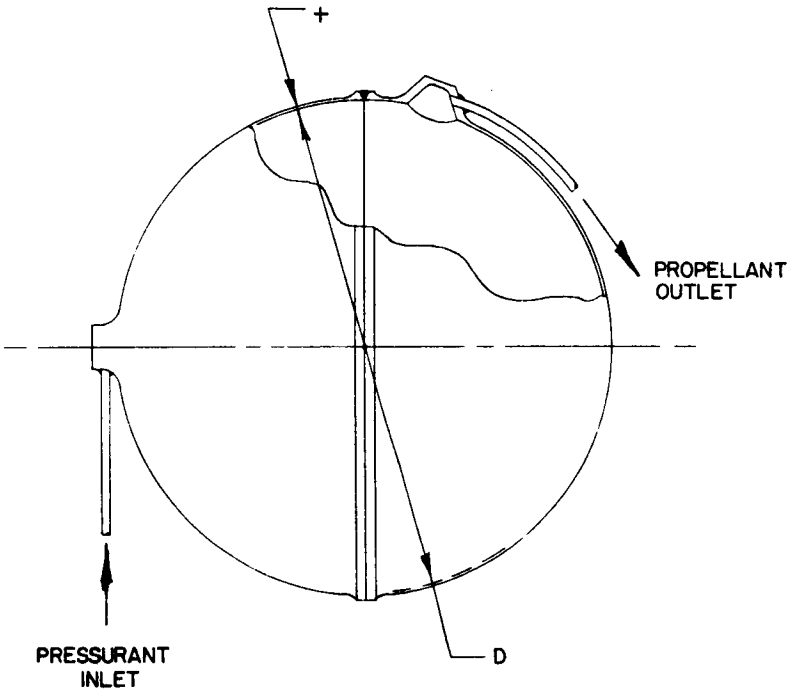

	D	+	MATERIAL
FUEL	5 68	0.020 $^{+\ 0.005}_{-\ 0.000}$	6061-T6 AL
OXIDIZER	7.06	0.020 $^{+\ 0.005}_{-\ 0.000}$	PH15-7MO CRES

Figure B8 PROPELLANT TANKS

63-9435

The two fuel tanks are machined from hemispherical halves and welded at the equator. The outlet and inlet bosses are integral parts of the forged hemispheres. The outlet port is located at the appropriate angle in order to provide maximum utilization of the fuel, considering the effects of rotational and axial acceleration loadings.

4.5 Pressure Tranducer

A pressure transducer, rated at 0 to 5000 psia, is located in the pressurization system. The proposed unit is presently being used on the SE-5 engine system and conforms to Rocketdyne specification NA5-27283.

4.6 Pressure Regulator

The pressure-reducing component proposed for this system (figure B9) is a single-stage, dome-loaded, spring reference regulator similar to, but smaller than, that used on the SE-5 engine system. The dome-loading feature is incorporated for higher accuracy and improved response characteristics. The housing will be made of 6061-T6 aluminum and will incorporate an integrated filter element.

4.7 Fill and Vent Connections

After the pressurant and propellant tanks have been loaded, the fill and vent lines are crimped and welded closed, providing a hermetically sealed system. This technique for closing the fill and vent lines has been used on the SE-1-1 engine system and is currently being used on the Lance program.

4.8 Pressure Relief Valve

A pressure relief valve is incorporated in the event overpressurization occurs. The valve is a pilot-operated, spring-loaded, poppet type and is made of 6061-T6 aluminum, with an incorporated hard-soft seat combination. The cracking pressure is adjustable over a 60-psi range, with the reseat pressure designed for 6 to 10 psi below cracking pressure. A similar valve, conforming to Rocketdyne specification NA5-26842, is being used on the SE-5 engine system.

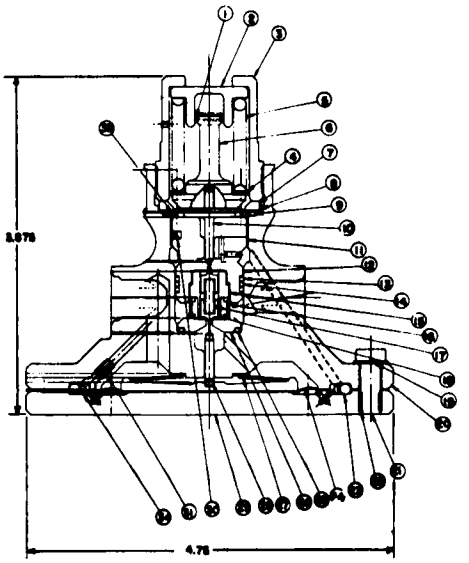

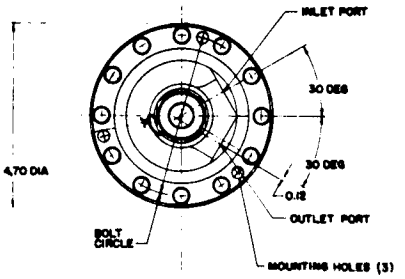

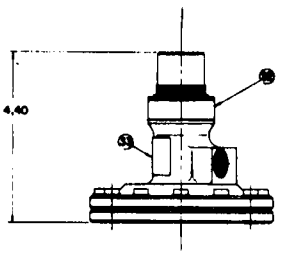

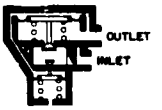

REGULATOR SCHEMATIC

1	Ring, Damper
2	Retainer
3	Housing
4	Shim (2 Places)
5	Spring
6	Retainer
7	Collar
8	Diaphragm Assembly
9	Packing
10	Push Rod
11	Retainer
12	Seat Assembly
13	Retainer
14	Packing
15	Guide
16	Filter Assembly
17	Spring
18	Poppet
19	Washer
20	Body
21	Screw

22	Heli-Coil Insert	29	Cover
23	Packing	30	Fellet
24	Diaphragm	31	Restrictor
25	Packing	32	Nameplate
26	Seat Assembly	33	Caution-Spring Loaded
27	Spring Disk	34	Retainer
28	Push Pin	35	Retainer

Figure B9 PRESSURE REGULATOR

63-9436

4.9 Explosively Actuated Valves

Both normally open and normally closed, explosively actuated valves are incorporated throughout the system to initiate and terminate flow. These valves, complying with North American Aviation, Inc., specification, will be procured from commercial sources. Similar components (NA5-28084 normally open and NA5-28069 normally closed) are presently being used on the SE-5, SE-6, SE-7, and SE-9 systems.

The proposed valves are rated for 4500 psig, with a proof pressure of 7800 psig and a burst pressure of 10,400 psig. Each valve will be actuated by a pyrotechnic charge which will ignite at a current of 4 amperes, providing complete operation in 2 milliseconds. The charge will contain two independent initiating squibs for high reliability; either of the squibs is capable of actuating the charge. The squibs will not fire when 1 ampere is passed through both squibs for 5 minutes. The squibs contain a specially prepared charge which will withstand the sterilization requirement of 295° F for 24 hours. These squibs are commercially available. The valve body is of 300 series CRES, with the pyrotechnic charge housed in an aluminun alloy casting. The cutting ram is heat-treated 17-7PH steel.

4.10 Propellant Filters

The propellant filters, located upstream of the thrust chamber, will be made of woven, stainless-steel wire mesh of nominal 10-micron size. The wire mesh is formed in a wave shape to increase rigidity and the exposed surface area. The filter element will be encased in a stainless-steel ring which acts as a structural support and also protects the element during handling.

The filter housing is desinged so as to guide all the flow from the outside to the inside of the filter, thus, preventing entrapment of contaminants. The housing material is 300 series CRES for environmental and structural compatibility. The inlet and outlet ports will be suitable for welded connections, and the pressure drop across the filter element will be less than 2 psi. This type of filter is currently being used on the SE-5 and Gemini engine systems.

4.11 Check Valves

Two pneumatic check valves (figure B10) will be required to prevent reverse flow of pressurant gas and the possible mixing of propellant vapors. The proposed valves are a spring-loaded, Telfon poppet type similar to those which have passed qualification for the SE-5 engine system according to North American Avaition, Inc., specification NA5-26842.

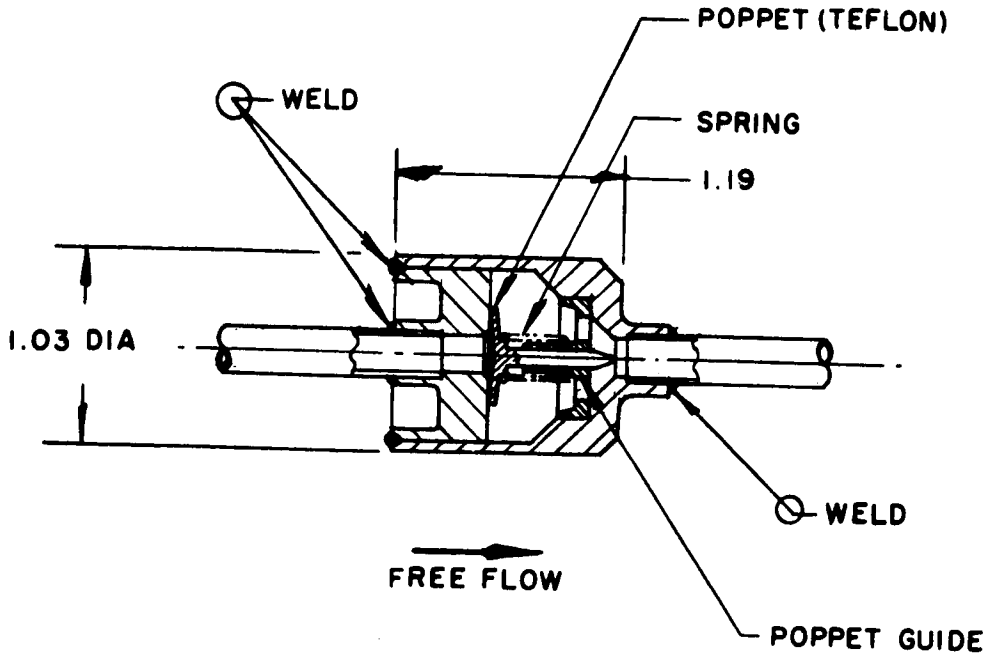

Figure B10 CHECK VALVE

63-9437

The valve body is made of a 300 series CRES to withstand the effects of corrosive propellants. Cracking pressure of the valve will be less than 2 psi and the pressure drop across the valve will be less than 5 psi.

PART II -- VENUS CAPSULE PROPULSION SYSTEM, DESIGN REQUIREMENTS

The design requirements for the Venus capsule propulsion system were defined by Avco as follows:

1. System design duration of 1 year with capability of extending the duration to 18 months without significant modifications.

2. Environmental temperature range of 0 to 100°F for pressurant and propellant tanks.

3. System adequacy for vacuum environment and space-radiation conditions.

4. Meteoroid protection for tanks to be provided by the system structure.

5. Vibration and g-loading as shown in the orbiter propulsion system design section.

6. The system must provide a velocity increment of 5000 fps when attached to a capsule weighing 85 pounds.

7. The system will operate for a single period to propellant depletion.

8. The propulsion system operation will occur while the combined capsule and propulsion module are rotating at 40 rpm. Precession angles should be limited to 4 degrees.

9. Sterilization requirements were not included in the design. Sterilization requirements similar to those for the Mars lander propulsion system can be incorporated in the design.

1. Propulsion system description. The Avco Voyager Venus capsule propulsion system is a pressure-fed, storable, hypergolic, bipropellant propulsion system with a total delivered impulse of 21,000 lb-sec. The system propellants are mixed oxides of nitrogen (MON) composed of 85 percent nitrogen tetroxide and 15 percent nitric oxide and a eutectic fuel (EMHF) consisting of 87.6 percent monomethylhydrazine and 12.4 percent hydrazine by weight. A system layout drawing is presented in figure B11. An all-welded configuration is used to prevent leakage. The system is prepackaged with propellants and the fill-and-vent connections are welded after filling. This system is not sterilized. A system weight summary is shown in table B7. Power requirements are listed in table B8.

The main thrust chamber is rigidly mounted, ablatively cooled, and is controlled for the single period of operation by normally closed squib valves, with

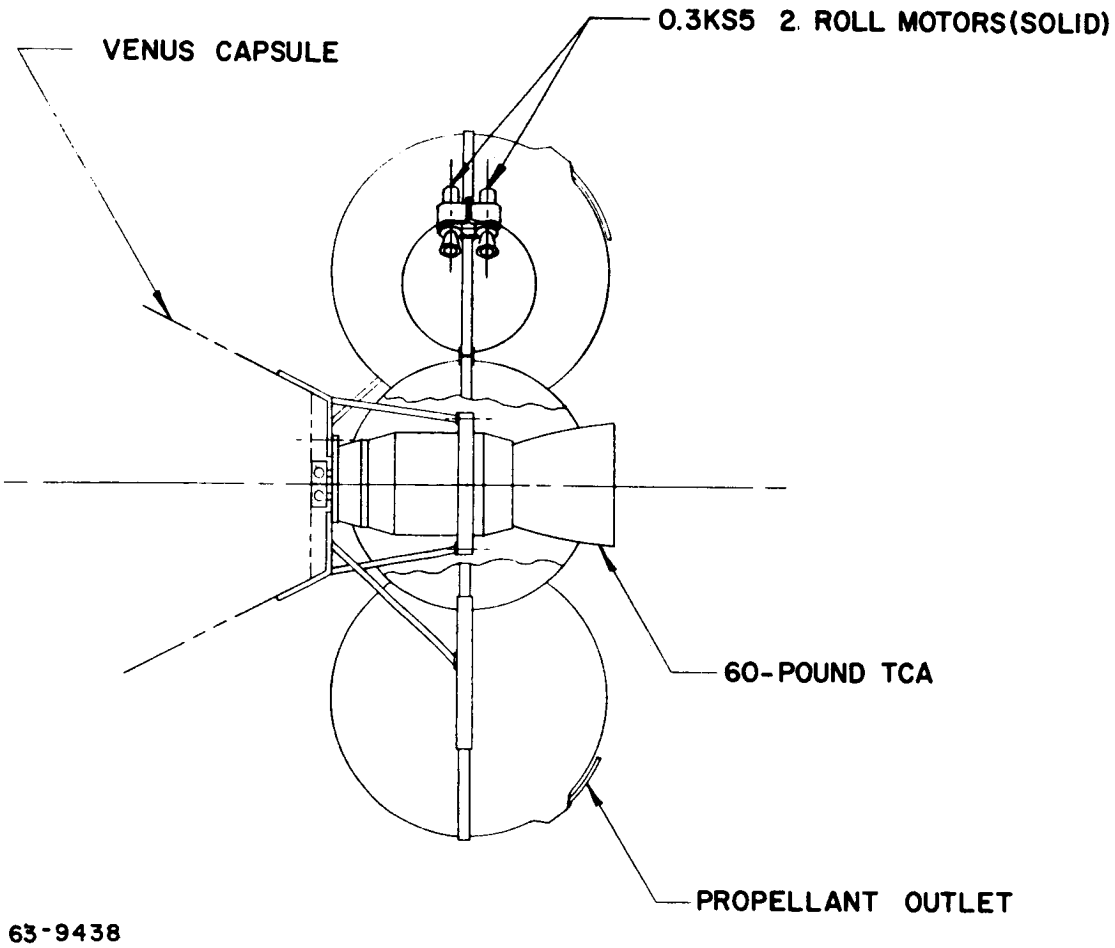

Figure B11 PROPULSION SYSTE

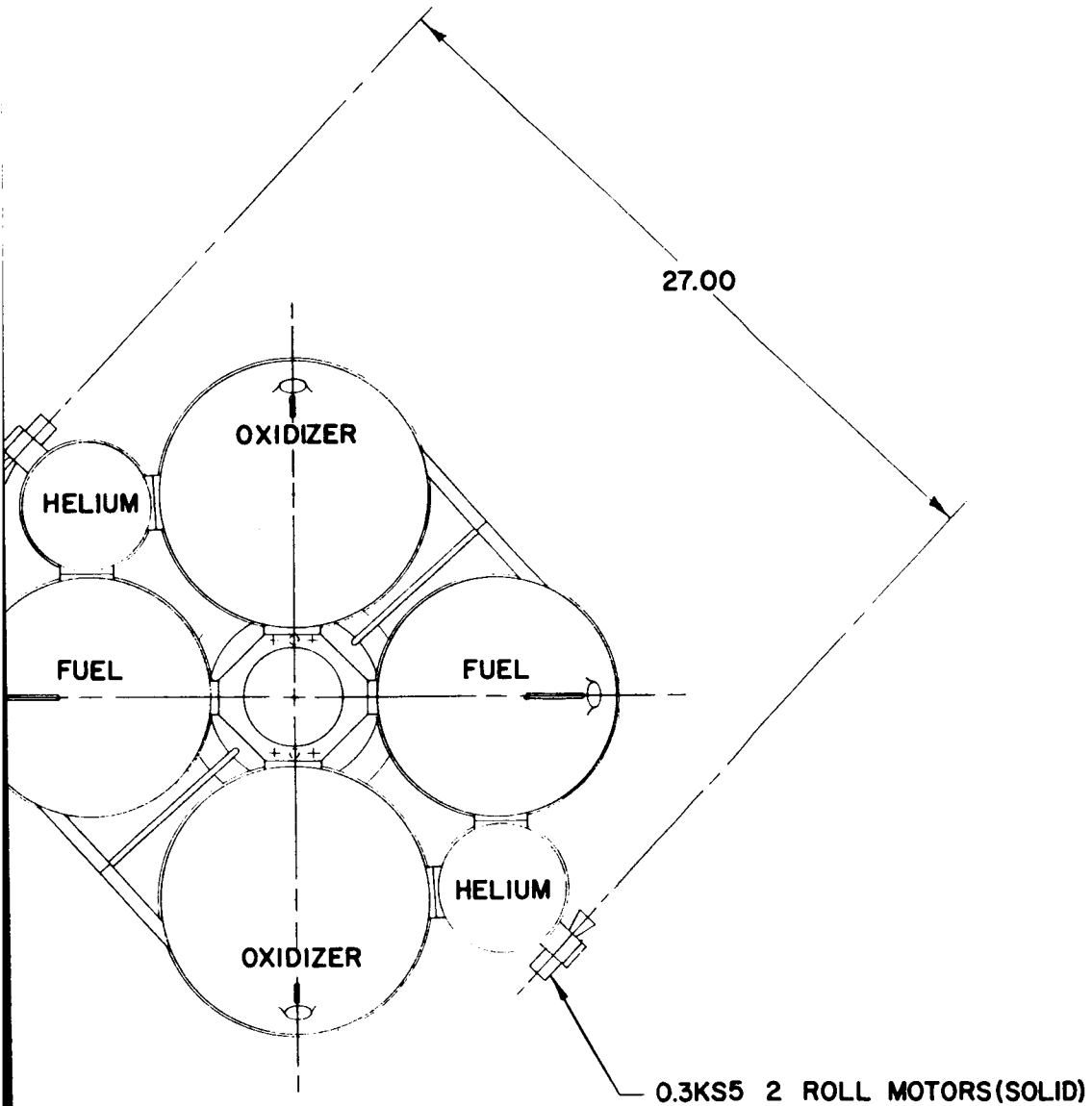
27.00
OXIDIZER
HELIUM
FUEL
FUEL
HELIUM
OXIDIZER
0.3KS5 2 ROLL MOTORS(SOLID)

ΣM LAYOUT

TABLE B7

WEIGHT SUMMARY

Pressurant System		
Pressurant Tank (2)	1.7	
Pressure Transducer	0.3	
Fill Connection	0.2	
Normally Closed Squib Valve	0.3	
Filter and Regulator	1.0	
Relief Valve	0.8	
Check Valve (2)	0.4	
Normally Closed Squib Valve (4)	1.0	
Vent Valve (4)	0.8	
Plumbing and Miscellaneous Fittings	0.5	
		7.0
Propellant System		
Fuel Tank (2)	1.3	
Oxidizer Tank (2)	1.6	
Fill Connection (4)	0.8	
Normally Closed Squib Valve (4)	1.2	
Filter (2)	0.4	
Plumbing and Miscellaneous Fittings	0.5	
		5.8
Thrust Chamber Assembly		4.3
Support Structure and Solid Motors		2.0
Fluids		
Pressurant, Helium	0.23	
Oxidizer, MON	46.4	
Fuel, EMHF	21.6	
Total Dry Weight, pounds		19.1
Total Wet Weight, pounds		87.3
Usable Propellant to System Weight Ratio (λ_p)		0.77

thrust terminated by propellant depletion. A radiation-cooled skirt is used on the expansion nozzle from an area ratio of 20 to the exit area ratio of 60 to satisfy minimum weight requirements. The chamber is designed to produce 60-pounds of thrust at a chamber pressure of 125 psia. Propellant tank pressure will be regulated to 175 psia. Thrust vector alignment tolerances are 0.01 inch for lateral displacement and 0.26-degree angular misalignment. The effect of these inaccuracies upon the velocity vector is reduced to an acceptable value by spinning the lander of 40 rpm. Spin-up is accomplished by two pairs of solid propellant rockets.

The propellant is contained in two equal-volume oxidizer tanks and two equal-volume fuel tanks balanced in opposition about the system longitudinal axis. Centrifugal force due to the lander spin rate is utilized as a means of propellant orientation to give dependable propellant expulsion. Tank outlets are positioned to allow maximum propellant utilization.

TABLE B8

POWER REQUIREMENTS

Unit	Number and Component Nine Normally Closed Squib Valves (4, 8, 13)*
Voltage, volts	1.8
Operating Current, amperes	2
Maximum No-Fire Current, amperes	0.15
Response, milliseconds	2
Maximum Power, at 0°F, watts	3.6 each

*Numbers in parentheses indicate location on schematic

The two oxidizer tanks, as well as the two fuel tanks, are individually isolated by squib valves. The tanks are individually filled and sealed, resulting in a statically and dynamically balanced system. The normally closed squib valves prevent propellant migration from one tank to another, thus ensuring a balanced system until actuation. The system is not actuated until lander spinup has been accomplished by the solid propellant spin rockets. Normally

closed squib valves are used above the tanks rather than check valves because of the absence of diaphragms or bladders in the propellant tanks. The valves ensure propellant isolation until system activation. Check valves will then provide assurance of isolating the propellants from one another.

2. System Operation.

The propulsion system is operated as described below, with the numbers in parenthesis referred to the system schematic diagram (figure B12).

The system is activated and fired by a signal firing all valves (4), (8), and (13). This permits pressurant to flow through the regulator (5), check valves (7), and pressurizes the propellant tanks (10) and (11). Propellants flow through the opened valves (13), and hypergolically ignite in the thrust chamber (14), providing rated thrust. Thrust continues to propellant depletion.

3. Analysis.

Analysis of the Venus capsule propulsion system was performed to determine an optimum system size to perform the specified mission. The mission specifications require imparting a 5000-fps velocity increment to the vehicle. It was further specified that the engine could run to propellant depletion as a means of thrust termination. The capsule weight exclusive of propulsion is 85 pounds. The propulsion system will not be subjected to heat sterilization. The quantity of propellant loaded provides for 1/2 percent above the amount required to balance the tolerance on mixture ratio variations. There will be no significant impulse generated by the pressurant as it escapes after propellant depletion. Vehicle spin will be provided by two pairs of 0.3-KS5 solid propellant rocket motors (not furnished by Rocketdyne).

The performance parameters resulting from the parametric analyses of the system are shown in table B9. These were used for the system preliminary design.

3.1 Reliability Analyses

The results of a preliminary reliability analysis of the proposed Avco Voyager Venus capsule propulsion system are presented in table B10. The estimated system reliability represents a potential level, which the propulsion system can expect to achieve at the conclusion of the qualification test phase. This reliability is the probability of the propulsion system successfully performing start, operation, and shutdown as required in the mission.

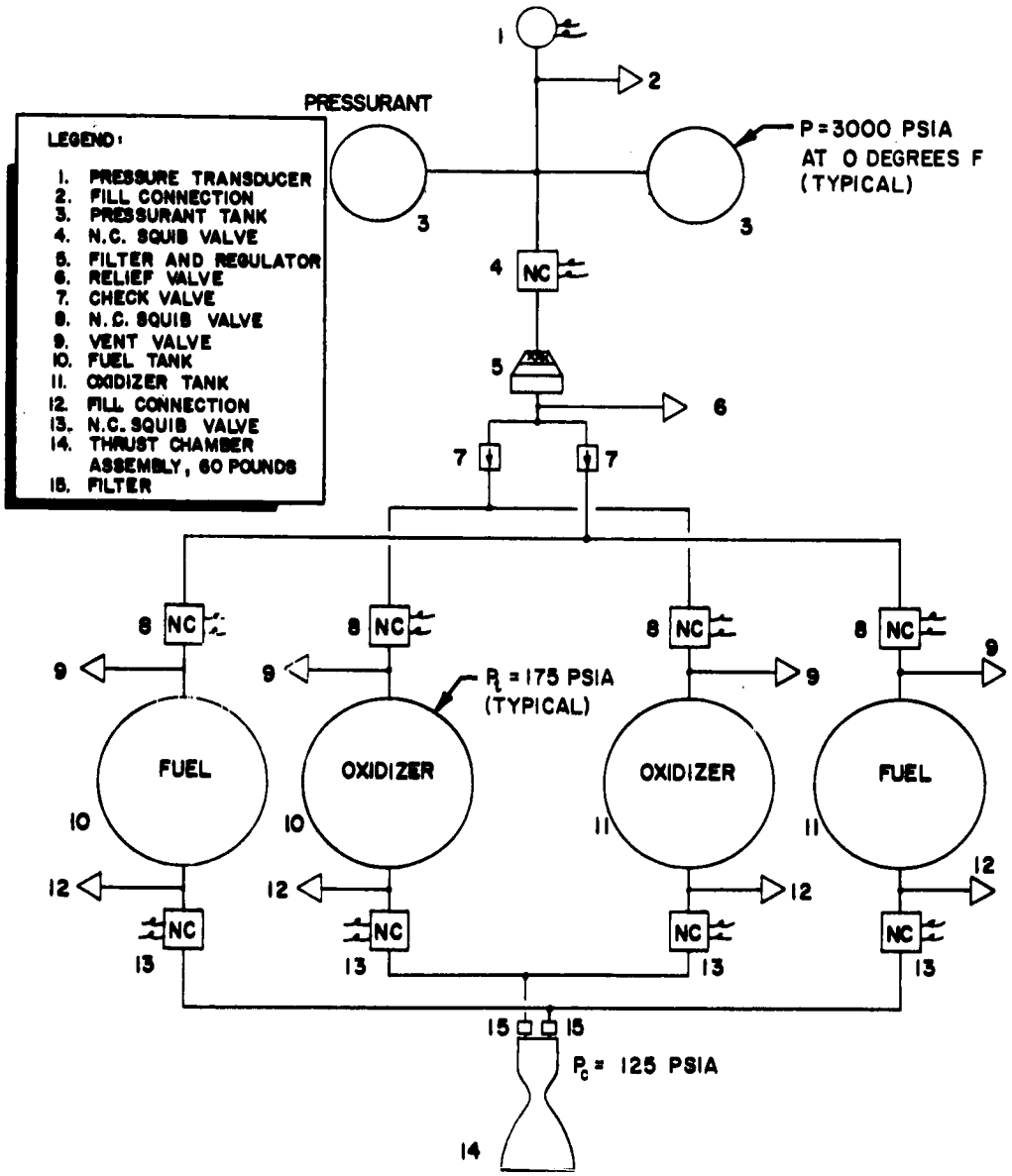

Figure B12 PROPULSION SYSTEM SCHEMATIC

63-9438

TABLE B9

SUMMARY OF SYSTEM PERFORMANCE PARAMETERS

Thrust, pounds	60
Chamber Pressure, psia	125
Mixture Ratio	2.15
Characteristic Velocity (c*), fps	5323
Thrust Coefficient (C_F, actual)	1.880
Specific Impulse (I_{sp}), seconds	311.3
Specific Impulse Efficiency	0.900
c* Efficiency	0.945
C_F Efficiency	0.952
Throat Area, sq in.	0.256
Expansion Area Ratio	60:1
Oxidizer Flowrate, lb/sec	0.132
Fuel Flowrate, lb/sec	0.061

TABLE B10

PREDICTED COMPONENT FAILURE RATES AND SYSTEM RELIABILITY

	No. Required	P_c, × 10^{-5}	P_s, × 10^{-5}	Totals
Subsystem I--Pressurization				
Pressure Transducer	1	15	15	
Fill Connection	1	5	5	
Pressurant Tank	2	8	16	
Tank Isolation Valve, Normally Closed Squib	1	5	5	
Filter and Regulator Assembly	1	32	32	
Relief Valve	1	12	12	
Check Valve	2	10	20	
Tank Isolation Valve, Normally Closed Squib	4	5	20	
Vent Valve	4	5	20	
Subtotal				145
Subsystem II--Propellant Feed System				
Propellant Tank Assembly	4	35	140	
Fill Connection	4	5	20	
Tank Isolation Valve, Normally Closed Squib	4	5	20	
Subtotal				180
Subsystem III--Thrust Chamber Assembly				
Thrust Chamber Assembly	1	60	60	60
Total			385	385

Reliability Estimate

$$R = \exp - [\Sigma P_s] = \exp - [385 \times 10^{-5}] = e^{-0.00385} = 0.99614$$

P_c = estimated probability of failure for one component

P_s = estimated probability of failure for the components in the system based on the number of components required, $P_s = n \times P_e$

The propulsion system is designed for maximum reliability incorporating redundant components in the pressurization system and propellant feed system to guard against internal leakage during an extended mission. An all-welded configuration will be used to prevent external leakage. Fill-and-vent connections will be positively sealed after servicing.

The failure rates in this analysis are derived from Rocketdyne experience with components of similar design and/or performing similar functions. Consideration is given to the mission and environmental requirements of the component, criticality of component operation, and the projected state of the art. A few basic assumptions that are necessary in estimating component failure rates and system reliability are as follows:

1. The reliability of a component is inherent in the function it performs and will, therefore, be similar to components with similar functions and proved reliabilities.

2. No insurmountable problems will be encountered in the development of the new system; therefore, the inherent functional reliability will be achieved in a normal development program.

3. The wearout life of the components will be sufficiently longer than the operational life of the system such that wearout failures will not be encountered and only chance failures will occur.

An extensive discussion regarding the method of predicting engine system reliability based on Rocketdyne space engines experience, component redundancy, failure mode data, and failure data is given in Appendix A.

4. SYSTEM DESIGN

A propulsion module (figure B7) consisting of a thrust chamber, propellant and pressurant tanks, value components, associated plumbing, and structure, is proposed for the Boyager Venus capsule. The module will be externally attached to the Venus capsule. Provision is made for attaching solid-propellant motors to the module to provide a vehicle spin of 40 rpm.

The following paragraphs present a comprehensive description of each of the component functions, materials and construction.

4.1 Thrust Chamber Assembly

The Venus capsule thrust chamber (figure B-13) is a 60-pound-thrust, 350-second-duration, fiberglass-wrapped, lined, ablative thrust chamber with a refractory, silicon-carbide throat insert, and a Hastelloy-X radiation skirt. Table B11 lists the basic design parameters. After a detailed appraisal was made to determine the optimum configuration for the capsule mission, the thrust chamber was selected.

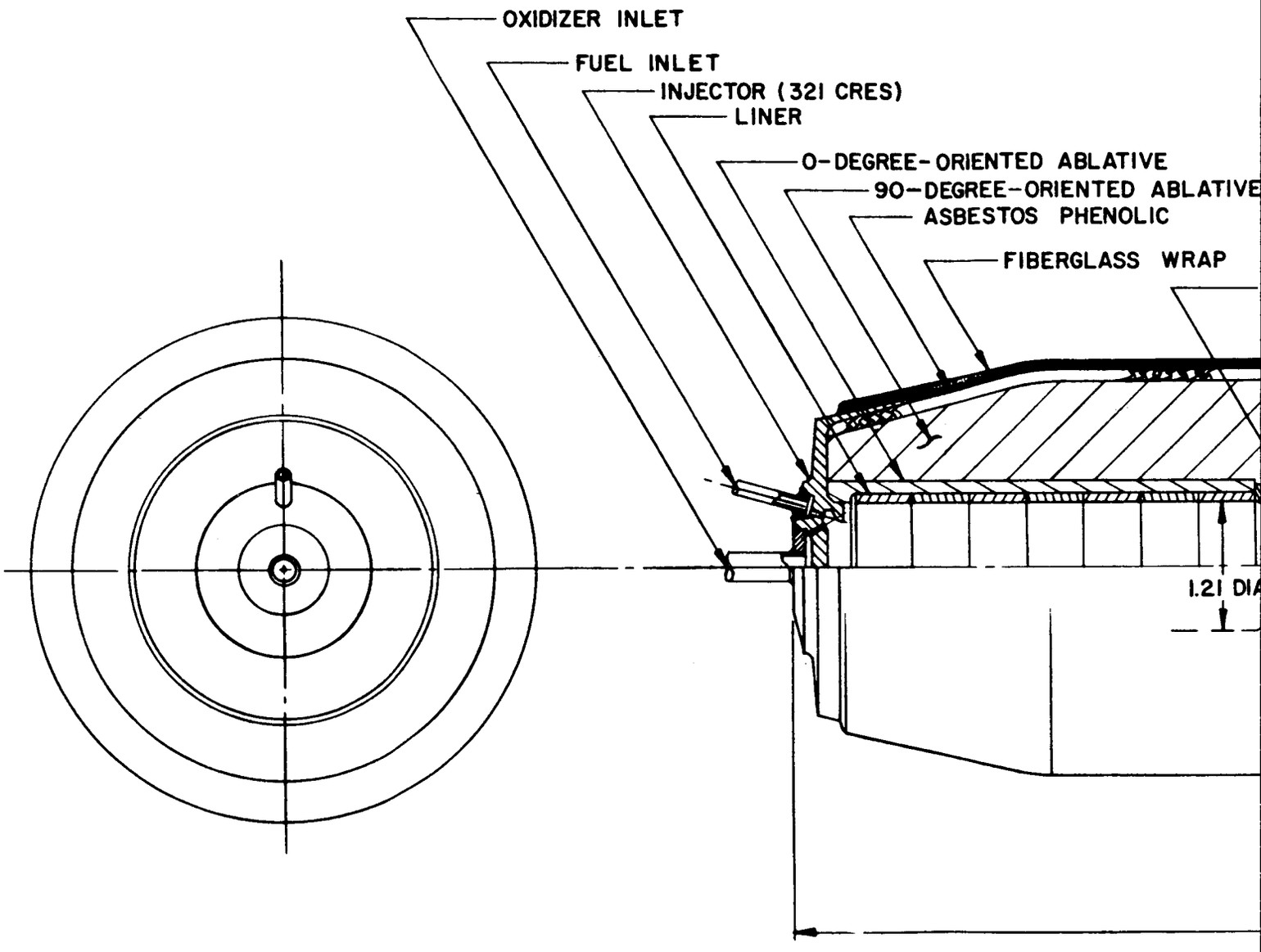

Figure B13 THRUST CHAMBER ASSEMB

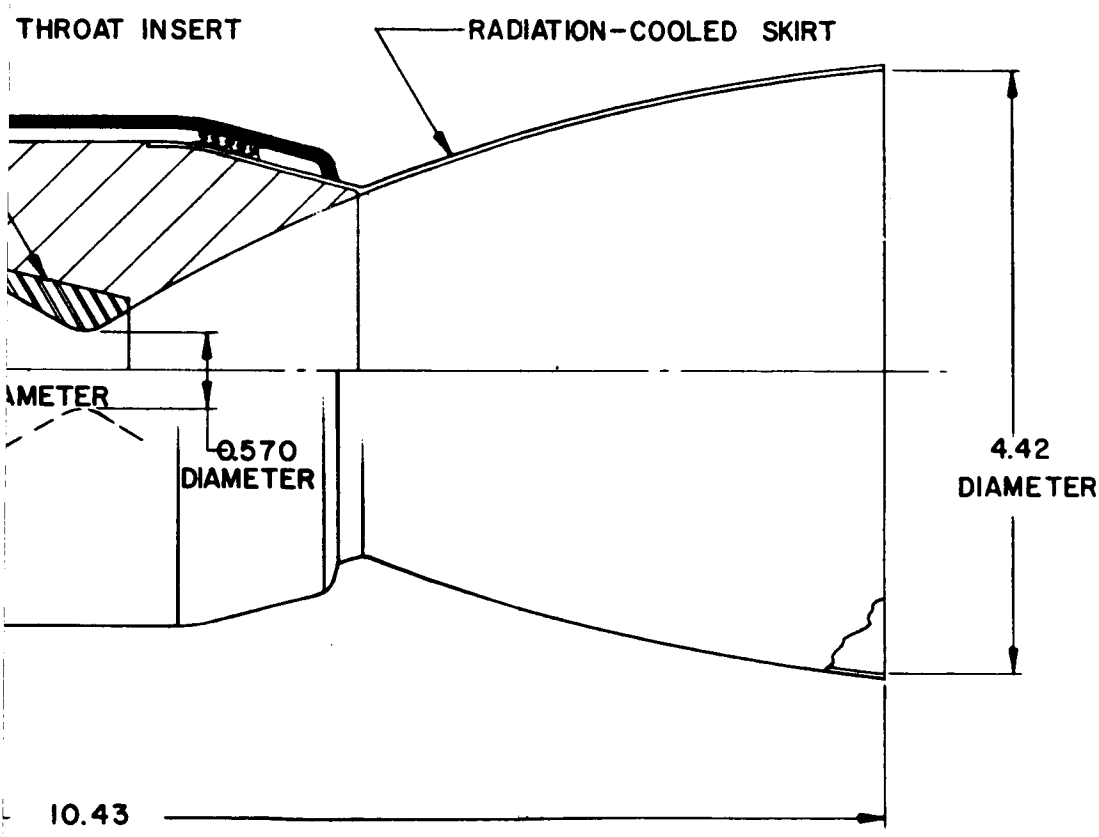
THROAT INSERT
RADIATION-COOLED SKIRT
AMETER
0.570
DIAMETER
4.42
DIAMETER
10.43

LY

TABLE B11

THRUST CHAMBER DESIGN PARAMETERS

Thrust, pounds	60
Chamber Pressure, psia	125
Throat Area, sq in.	0.255
Throat Diameter, inch	0.570
Contraction Area Ratio (ϵ_c)	4.5:1
Combustion Chamber area, sq in.	1.15
Combustion Chamber Diameter, inches	1.21
Characteristic Length (L*), inches	18
Expansion Area Ratio (ϵ)	60:1
Exit Diameter, inches	4.42
Thrust Coefficient (C_F, actual)	1.880
Exit Cone Contour	80 percent Bell
Skirt Attachment (ϵ_r)	20:1
Duration, seconds	360
Mixture Ratio ($\dot{w}_o / \dot{w}_f$)	2.15
Oxidizer Flowrate ($\dot{w}_o$), lb/sec	0.132
Fuel Flowrate ($\dot{w}_f$), lb/sec	0.061

The thrust chamber is designed so that with 360 seconds duration, insulation material remains between the char and fiberglass to give a maximum outer-wall temperature of 500°F. Once the char depth is determined, an asbestos-phenolic ablative insulator may be used to keep the outer wall at the required temperature. The asbestos insulator is wrapped and cured over the ablative material and reduces the rate of heat flux to the structural fiberglass shell.

4.2 Throat

Silicon carbide is the throat-insert material proposed, and is presently being used at Rocketdyne. However, other materials under consideration and investigation are silicon carbide backed by a molybdenum sleeve, and silicon diffused into graphite.

Silicon carbide has a high melting point (4400°F), excellent thermal shock characteristics, relatively high thermal conductivity (115 Btu/hr-ft^2-°F/in.), low coefficient of thermal expansion (2.4 x 10^{-6} in./in.-°F), excellant oxidation resistance, and high abrasion resistance.

A molybdenum backup and sleeve are used only in those cases where the silicon carbide insert cannot conduct the heat sufficiently.

4.3 Combustion Chamber

After the optimum chamber pressure was determined, the combustion chamber geometry was established. The dimensions of the combustion zone are such that the gases mix thoroughly upstream of the throat. In many cases, however, the high-silica glass in the ablative material becomes fluid enough to be swept downstream and deposited in the throat section. This causes thrust variances and the possibility of an unsymmetrical velocity profile in the deposition area. Prevention of this phenomenon is accomplished by inserting a liner of JTA (45 percent graphite 45 percent zirconium diboride, and 10 percent silicon) in the combustion zone. The line (proved highly successful on the Gemini program) is segmented to provide a path for the pyrolyzed ablative gases which reduces the ΔP across the liner and prevents cracks that might otherwise occur in an expanding unsegmented liner.

1. Fiberglass. As the ablative chamber and nozzle sections char, the radius at which the operating pressure acts will increase. The minimum insulation remaining will carry little load; thus, the fiberglass, which is filament-wound to accept hoop stresses and longitudinally wrapped to contend with meridional stresses, is designed to carry all the resultant chamber forces.

2. Radiation Skirt. The nozzle skirt section, as opposed to a full-radiation engine, is not confronted with the large stresses caused by high temperatures in the combustion zone and throat, thrust transmission, and injector attachment. The skirt is designed to accept and emit the heat flux transmitted by the expanding gases, in addition to withstanding loads imposed by thrust transmission. It is made of a 0.030-inch Hastelloy-X sheet, and is tape-wrapped to the thrust chamber at an expansion area ratio of 20:1. The nozzle exit contour is an 80 percent bell extending to a 60:1 expansion area ratio.

3. Injector. The injector selected for the thrust chamber is machined from 321 corrosion-resistant stainless steel. It conforms to a conventional fixed-orifice, single-ring, impinging-unlike-doublet, splash-plate type.

The splash plate is utilized because of improved performance obtained at this thrust level. The injector is designed to inject propellants into the combustion zone so that the resultant momentum vector is parallel to the centerline of thrust. The propellant manifolding provides minimum downstream volume and, therefore, maximum response. External considerations of the injector design are thrust chamber attachment and mounting provisions for the explosively actuated propellant valves.

Several types of injectors (single ring, impinging unlike doublets, like-on-like, and fuel-on-oxidizer; impinging triplets with and without the splash plate) were investigated for this application. However, the combustion chamber is of such size to enable the use of a simple, efficient, and proved unlike doublet configuration to ensure initial and complete liquid phase mixing of the propellant.

Because of the simple configuration (single fuel and oxidizer manifolds), convenient lathe-turned fabrication and injector inspection is permitted. Quality of the injector is controlled by inspection methods that include radiography, water-flow calibration of ΔP, and hot-fire calibration of mixture ratio.

4. Pressurant tanks. The two pressurant tanks (figure B14) are designed to store helium at a maximum pressure of 3650 psia. Each is machined from two hemispherical, solution heat-treated, 6Al-4V titanium forgings. The two hemispherical halves are joined at the equator by tungsten electrode arc welding within an inert-gas-filled chamber. They are designed with an ultimate tensile stress of 155,000 psi and a safety factor of 1.8. Wall thickness at the weld joint is increased to compensate for loss of structural strength resulting from a weld efficiency of 83 percent.

Titanium was chosen as the tank material because of its high strength-to-weight ratio (970,000 inches). Several tanks of this type have been successfully incorporated in each Atlas missile without a single failure. This design is also being used on the currently contracted SE-6 and SE-7 man-rated Gemini program.

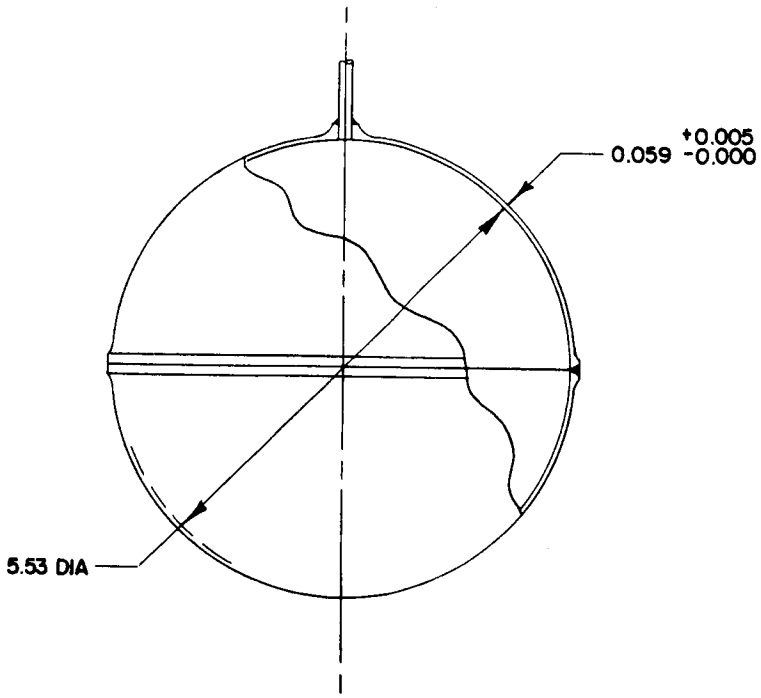

Figure B14 PRESSURANT TANK

63-9441

5. Propellant tanks. The propellants used in the Venus propulsion system are a eutectic mixture of hydrazine fuels (EMHF) for the fuel and mixed oxides of nitrogen (MON) for the oxidizer. The tanks (figure B15) are designed for the temperature range of 0 to 100°F and a maximum pressure of 175 psia.

Because the propulsion system for the Venus capsule is extremely weight critical, 6Al-4V titanium was selected for both propellant tanks.

The tanks are machined from hemispherical, solution heat-treated forgings. The two hemispherical halves are joined at the equator by tungsten electrode arc welding with an inert-gas-filled-chamber.

6. Pressure transducer. A pressure transducer, rated at 0 to 5000 psia, is located in the pressurization system. The proposed unit is presently being used on the SE-5 engine system and conforms to Rocketdyne specification NA5-27283.

7. Pressurant regulator. The pressure-reducing component proposed for this system (figure B16) is a single-stage, dome-loaded, spring-reference regulator, similar to, but smaller than, that used on the SE-5 engine system. The dome-loading feature is incorporated for higher accuracy and improved response characteristics. The housing is made of 6061-T6 aluminum, and incorporates an integrated filter element.

8. Fill-and-vent connection. After the pressurant and propellant tanks have been loaded, the fill-and-vent lines are crimped and welded closed providing a hermetically sealed system. This technique for closing the fill-and-vent lines has been used on the SE1-1 engine system and is currently being used on the Lance program.

9. Pressure relief valve. A pressure relief valve is incorporated in the event that overpressurization should occur. The valve is a pilot-operated, spring-loaded, poppet type, and is made of 6061-T6 aluminum, with an incorporated hard-soft seat combination. The cracking pressure is adjustable over a 60-psi range, with the reseat pressure designed for 6 to 10 psi below cracking pressure. A similar valve, conforming to Rocketdyne specification NA5-26842, is presently being used on the SE-5 engine system.

10. Explosively actuated valves. Both normally open and normally closed explosively actuated valves are incorporated throughout the system to initiate and terminate flow. These valves complying with a North American Aviation, Inc. specification, will be procured from commercial sources. Similar components (NA5-28084, normally open and NA5-28069, normally closed) are presently being used on the SE-5, SE-6, SE-7, and SE-9 systems.

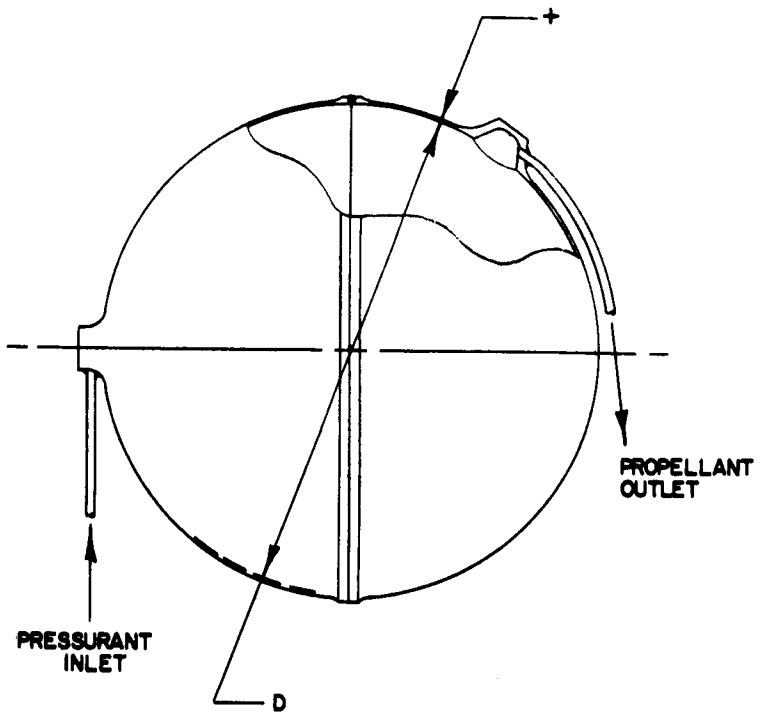

6AL-4V TITANIUM

	FUEL	OXIDIZER
D	8.69	9.69
+	0.015 $^{+.0005}_{-.0000}$	0.015 $^{+0.005}_{-0.000}$

Figure B15 PROPELLANT TANKS

63-9442

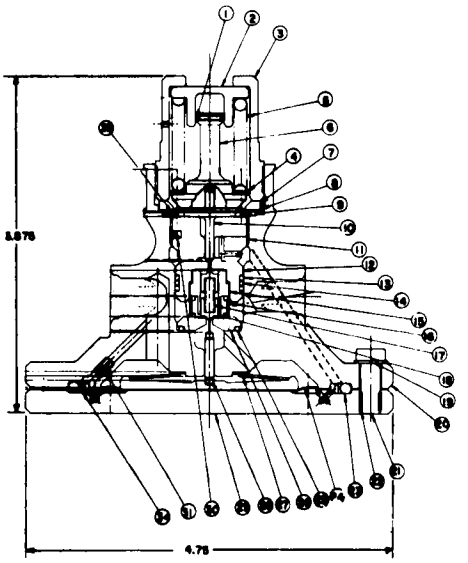

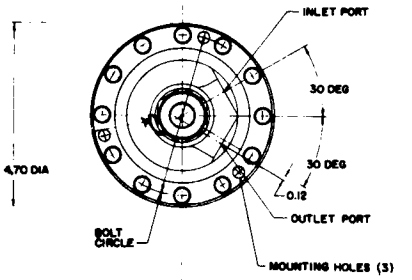

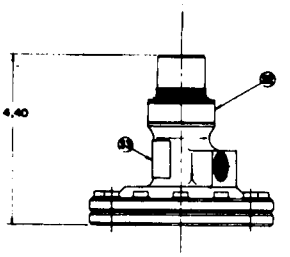

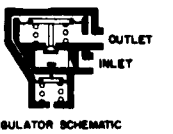

REGULATOR SCHEMATIC

1	Ring, Damper
2	Retainer
3	Housing
4	Shim (2 Places)
5	Spring
6	Retainer
7	Collar
8	Diaphragm Assembly
9	Packing
10	Push Rod
11	Retainer
12	Seat Assembly
13	Retainer
14	Packing
15	Guide
16	Filter Assembly
17	Spring
18	Poppet
19	Washer
20	Body
21	Screw

22	Heli-Coil Insert	29	Cover
23	Packing	30	Pellet
24	Diaphragm	31	Restrictor
25	Packing	32	Nameplate
26	Seat Assembly	33	Caution-Spring Loaded
27	Spring Disk	34	Retainer
28	Push Pin	35	Retainer

Figure B16 PRESSURE REGULATOR

63-9443

The proposed valves are rated for 4500 psig, with a proof pressure of 7800 psig, and a burst pressure of 10,400 psig. Each valve will be actuated by a pyrotechnic charge (NA5-26875) that will ignite at a current of 4 amperes providing complete operation in 2 milliseconds. The charge will contain two independent initiating squibs for high reliability; either of the squibs is capable of actuating the charge. The squibs will not fire when 1 ampere is passed through both squibs for 5 minutes.

The valve body is of 300-series CRES, with the pyrotechnic charge housed in an aluminum alloy casting. The cutting ram is heat-treated 17-7PH steel.

11. Propellant filters. The propellant filters, located upstream of the thrust chamber, will be made of woven, stainless-steel wire mesh of nominal 10-micron size. The wire mesh is formed in a wave shape to increase both rigidity and the exposed surface area. The filter element will be encased in a stainless-steel ring, which acts as a structural support and also protects the element during handling.

The filter housing is designed so as to guide all the flow from the outside to the inside of the filter, thus preventing entrapment of contaminants. The housing material is 300-series CRES for environmental and structural compatibility. The inlet and outlet prototypes will be suitable for welded connections, and the pressure drop across the filter element will be less than 2 psi. This type filter is currently being used on the SE-5 and Gemini engine systems.

12. Check valves. Two pneumatic check valves (figure B17) are required to prevent reverse flow of pressurant gas and the possible mixing of propellant vapors. The proposed valves are a spring-loaded, Teflon-poppet-type similar to those that have passed qualification for the SE-5 engine system per North American Aviation, Inc., specification NA5-26842.

The valve body is made of a 300-series CRES to withstand the effects of corrosive propellants. Cracking pressure of the valve will be less than 2 psi and the pressure drop across the valve will be less than 5 psi.

13. Structure. A strong, lightweight structure of 6Al-4V titanium is proposed for the Venus capsule propulsion module. The propulsion system is completely self-contained and is attached externally to the capsule. The structure supports the tanks, valving, thrust chamber, and solid propellant roll motors as well as providing a mount to the capsule.

The structural loads imposed are quite small. Neither the axial nor the centrifugally induced loadings exceed 1 g.

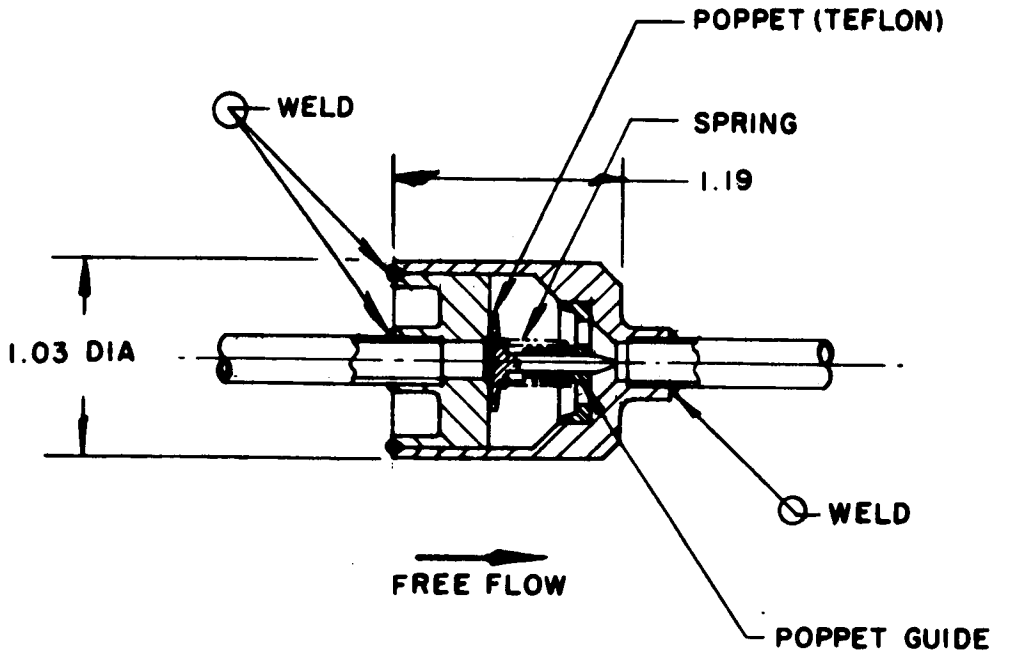

Figure B17 CHECK VALVE

63-9444

APPENDIX C

SIMULATION OF REENTRY RADIATION HEAT TRANSFER

1. INTRODUCTION

At the entry velocities typical of interplanetary flights, it is likely that very high heat-transfer rates to the entering vehicle will be encountered due to radiation from the hot gases surrounding the body (refs. 1, 2). These rates can approach 50 kw/cm^2 in some cases. In order to study the behavior of protective materials for this environment, it is desirable that steady-state simulation of the conditions be provided in the laboratory. This work has been directed to this simulation. Under the program, a method of simulation has been developed, and materials have been subjected to radiative heat pulses at varying levels up to 51 kw/cm^2 (44, 500 Btu/ft^2-sec) and at ambient pressures up to 4 atmospheres absolute. Values for heats of ablation (Q*) have been obtained. More work is required to understand the results and, in particular, to relate them directly to the flight situation.

2. PRINCIPLE OF THE SIMULATOR

Figure C1 is a schematic diagram of the simulator which has been developed in the present program. It consists of a high-powered arc surrounded by the material to be tested. A cylindrical hole is bored through the test sample and the electrodes are located at its ends. When the arc is struck, the discharge column fills most of the volume of the hole. The total power into the arc is equal to the product of the current I by the arc voltage V. With the enclosed arc configuration, there are three ways the power can be dissipated:

a. Electrode losses

b. Absorption by the test material (heating, melting, vaporization)

c. Superheating of material vaporized from the test specimen (and electrodes).

In actual operation, the arc burns in the vaporized material ablated from the test specimen and the electrodes. The pressure in the arc column rises above the ambient pressure, and the superheated ablated material is discharged through the passage between the electrode and the test material.

The pressure is determined by the rate of material vaporization, the temperature of the arc, and the size of the clearance between the electrodes and the test sample. In the center of the test section, stagnation conditions prevail and the joule heat dissipated in the center of the arc column falls onto the boundary, i.e., low-temperature vaporized material and the wall. The streamlines shown in figure C1 indicate that convection of ablated material plays an important

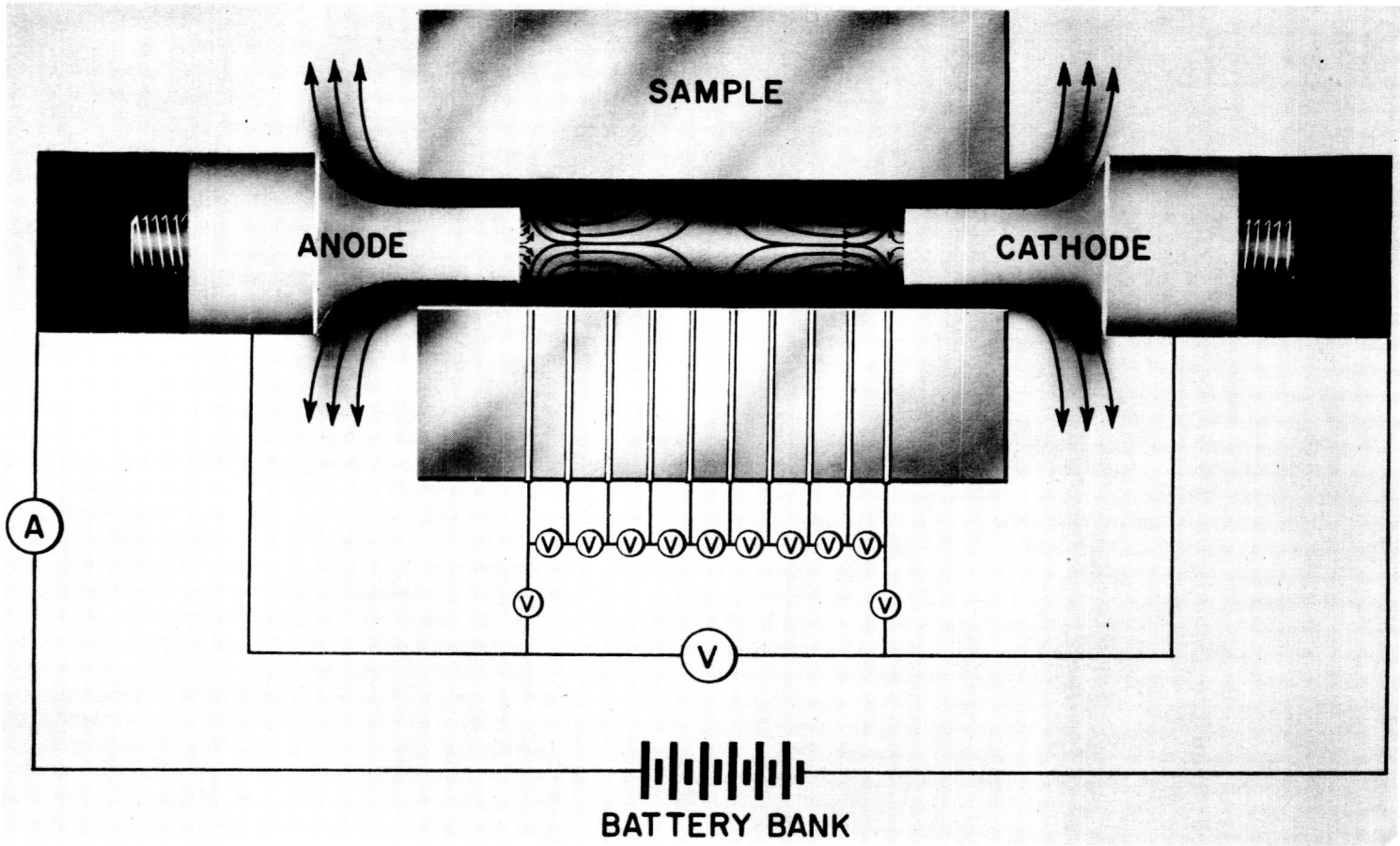

Figure C1 SCHEMATIC VIEW OF THE REENTRY RADIATION HEAT-TRANSFER SIMULATOR

role on the heat actually transferred to the test specimen. In this respect, the simulation strongly resembles the flight situation where the combination of radiation from the hot gas through the ablated material to the body, absorption of this radiation in the cooler gas near the body, and aerodynamic convection will determine the performance of the material.

During a test, the total current is measured as well as the voltage distribution along the wall using the probes shown in figure C1. Thus, the local power dissipated in the arc column is determined by the product of the current density by the local electric field found from the probe voltages. Therefore the average heat-transfer rate $\dot{q}$, falling onto the test specimen can be determined for the center of the test section where stagnation conditions prevail. In the usual manner, the effective heat of ablation Q^* is then equal to the ratio of the apparent heat-transfer rate to the mass rate of ablation per unit area.

3. TEST FACILITIES

Two versions of the arc-powered simulation apparatus have been built to date at AERL where power from a 3.3-Mw battery bank was conveniently available.

Figure C2 shows a view of the first facility. The facility handles a total power of up to 3 Mw at a current up to 22,000 amperes for 3 seconds and has been operated for 1 minute at 500 kw input. The time limitation is due to lack of cooling and electrode feed as well as to gross change in test specimen dimension. It was found that at high current density (2500 amp/cm^2), only the anode would need to be fed as the cathode is cooled by electron vaporization. A transit pipe with a viewing window surrounds the arc. At the end of the run, nitrogen is introduced to quench any spontaneous combustion of the graphite electrodes and test material. However, this has not been completely effective, as the nitrogen entrains some air. Therefore, it was decided to build a second version with an enclosed test section where the material would remain in a nitrogen atmosphere after shutdown. Figure C-3 is a diagram of the second facility, and figure C-4 is a photo of it. This second facility has basically the same configuration as the previous except for its size and internal atmosphere control.

4. EXPERIMENTAL DATA

As mentioned above and shown in figure C1, the voltage distribution throughout the sample and the current are measured to determine the power density. For electrically insulating test materials, voltage probes are introduced in the sample (figure C1). For electrically conducting materials such as graphite, the test section is made of thin washers coated with a thin layer of arc-sprayed alumina to provide the insulation. A voltage tap can be made

Figure C2 VIEW OF THE FIRST ARC FACILITY

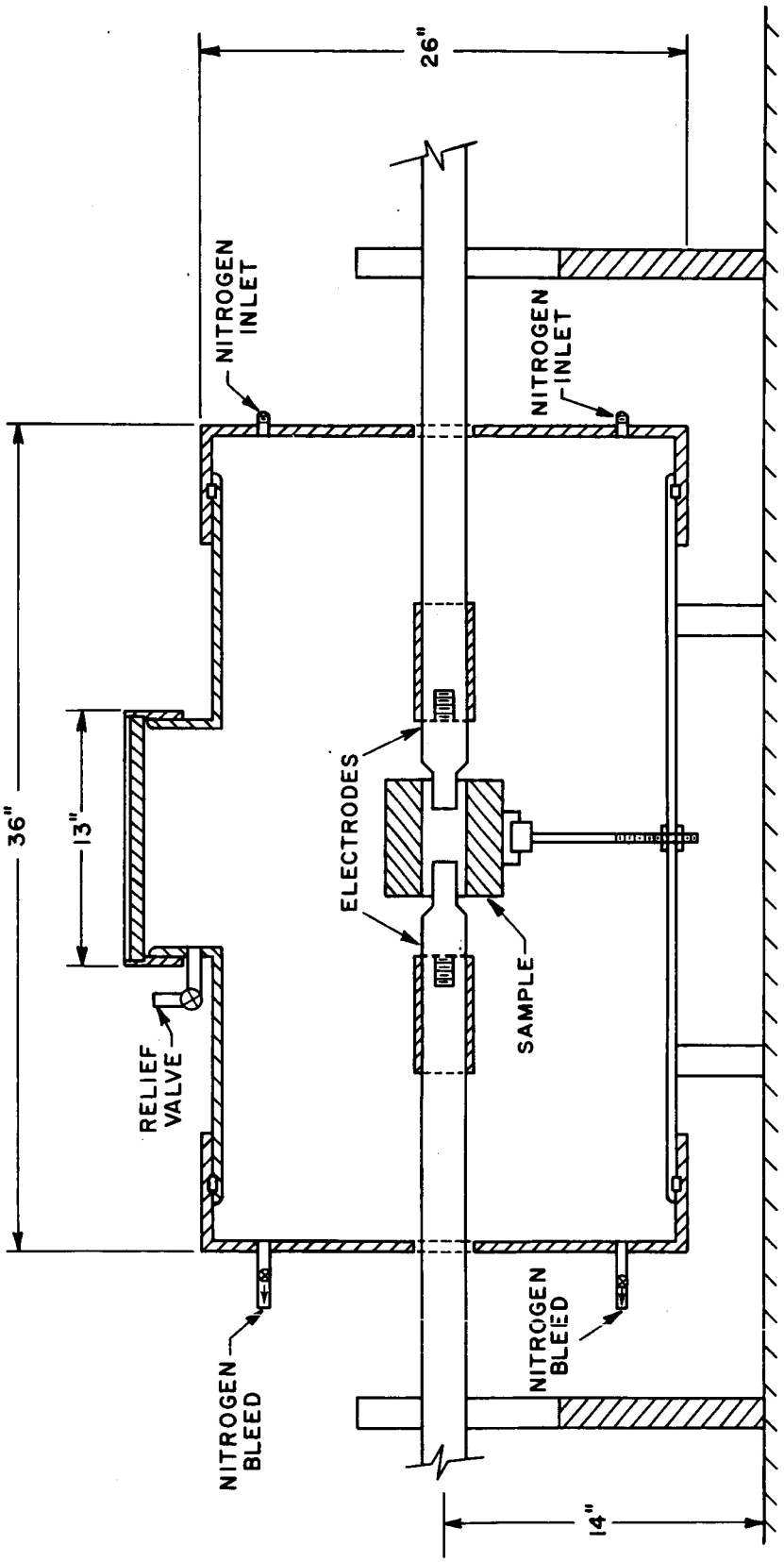

Figure C3 SCHEMATIC DIAGRAM OF THE SECOND ARC FACILITY

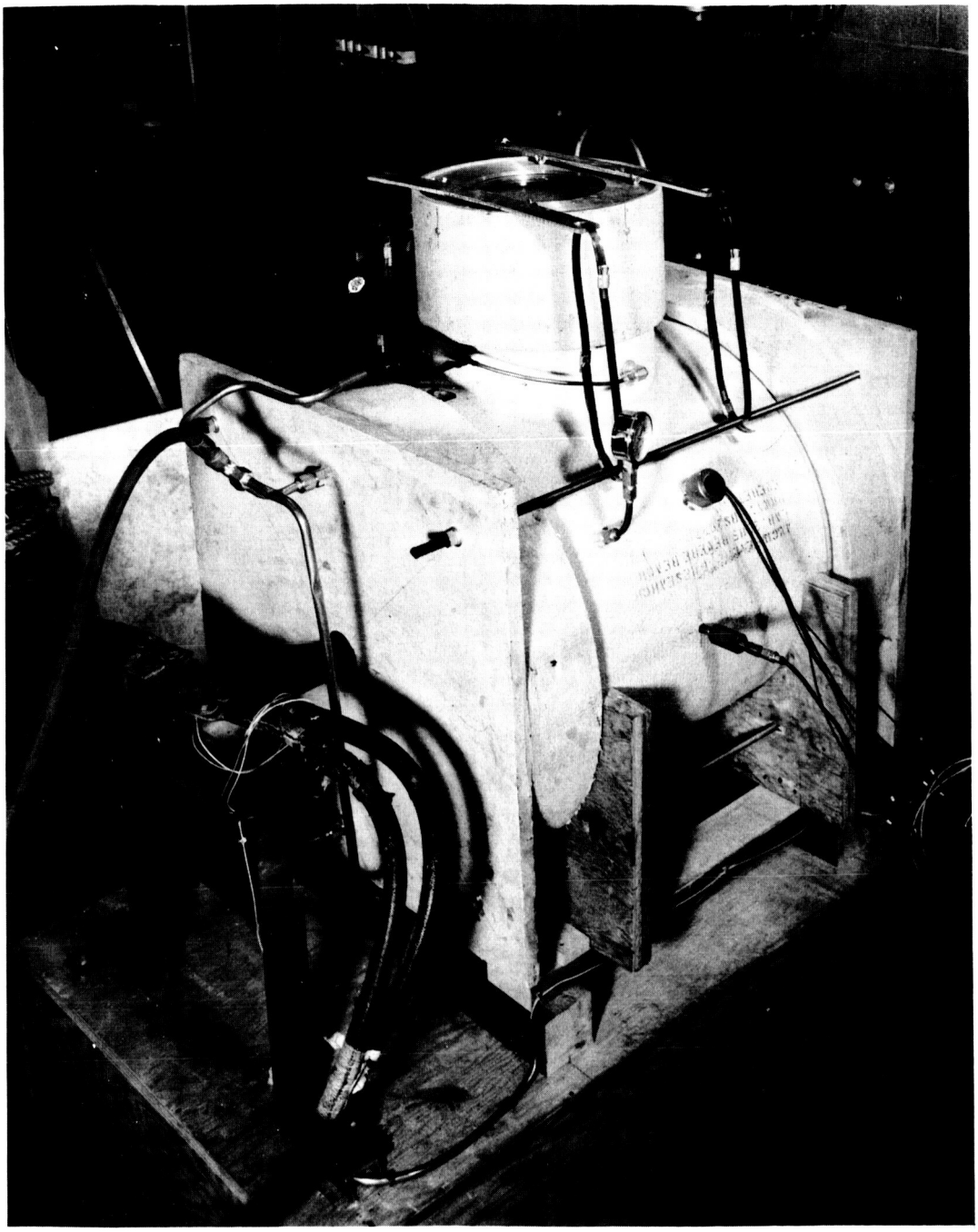

Figure C4 VIEW OF THE SECOND ARC FACILITY

on the washer and power density determined. Pressure measurements have been carried out using a Kistler gauge.

The effective conductivity of the gas can be calculated from the ratio of the current density of the electric field and an effective temperature deduced from this measurement using the Saha equation. An approximate temperature can also be deduced from the arc pressure and ablating mass flow through the throat of known area. Figure C5 shows the arc in operation with the flow of high temperature gas streaming through the end clearance over the electrodes.

Spectra of the arc were taken of the arc column for linen phenolic test samples. The spectrum (figure C6) indicated Stark broadening of the H_β line which has been studied theoretically by Griem, Kolb, and Shen (ref. 3). From the comparison of experimental measurement of the H_β line (figure C7) and its theoretical broadening, an electron concentration of $1.8 \times 10^{17}/cm^{-3}$ was determined at a total pressure of 1.54 atm. By assuming that the linen phenolic was 40 percent carbon of much lower energy of ionization than the other constituents, one can deduce a column temperature of 14,000°K. Again, this temperature has to be considered as an effective temperature as the spectograph was focused on the center line of the test section by looking through the thickness of the gas slab. This measurement agrees (within 7 percent) with the values calculated from the gas conductivity and pressure and ablating flow as described above.

A spectrum (figure C6) of a higher pressure arc at 3.6 atm shows a Stark broadening of the H_β line (figure C7) which indicates an electronic concentration of 8.5×10^{17} cm^{-3}. In the spectrum, several absorption bands of CN and C_2 and the rate of decrease of intensity from the band's head can be determined. This measurement allows a determination of the vibrational temperature (in equilibrium with the translational) of the gas close to the wall. This determination indicates a variation of vibrational temperature between 4000° and 6500°K.

The measurement of the arc temperature was also accomplished by comparison of the H_a and H_β lines and corroborated the previous data.

Preliminary tests have been carried out on maple wood, astrolite, Avco X6023, carbon, and white teflon. Table C1 summarizes these results, giving the total power, the heat transfer rate, and the heat of ablation. Heat transfer rates up to 51 kw/cm^2 and heats of ablation up to 40,000 cal/g were recorded. After the test, the samples were cut and examined for change in dimensions. Figure C-8 shows such samples cut after test and the ablation patterns are apparent.

Testing was carried out on linen phenolic at different pressures by changing the power density and the size of the throat area. Table C2 recaptiluates these results. These results are plotted on figure C9 and show that the heat of ablation increases with the pressure roughly up to 1.45 atm. At pressures higher than 1.45 atm, the heat of ablation Q^* is essentially constant within the scatter of the data.

TABLE C-1

PRELIMINARY RESULTS

Materials	Arc Power Input (kw)	σ (mho/cm)	$\dot{q}$ (kw/cm^2)	Q*	
				cal/g	Btu/lb
Astrolite	2860	3600	51	17300	31400
Astrolite	324	3600	2.88	4400	8000
Astrolite	965	7160	8.3	6400	11620
Astrolite	2250	6480	18	7680	13900
Astrolite	3110	6800	22.6	6180	11250
Avco X6023	2860	3600	51	30000	54500
Maple Wood	2320	5100	33	7200	13100
Graphite	2225	3200	20.5	42400	77000
Teflon	2225	3200	20.5	8600	15650

TABLE C-2

LINEN PHENOLIC

Arc Pressure (atm abs)	Arc Power Input (kw)	$\dot{q}$ (w/cm^2)	Q^*	
			Cal/g	Btu/lb
3.85	2620	31500	20000	38100
2.225	1125	14350	10800	20600
1.58	2620	27700	24300	46400
1.53	2200	23300	23900	45500
1.41	892	11000	23500	44800
1.35	1.990	19200	19250	36700
1.28	1.625	16000	17450	33200
1.25	953	9680	16850	32150
1.02	420	5500	13800	26500
1.78	1000	12800	20200	38800
3.31	1790	34600	23300	44700
1.75	2180	30050	23700	45500
1.070	463	8650	14700	28200
3.78	2240	43500	23300	44700
1.103	790	12300	14700	28200

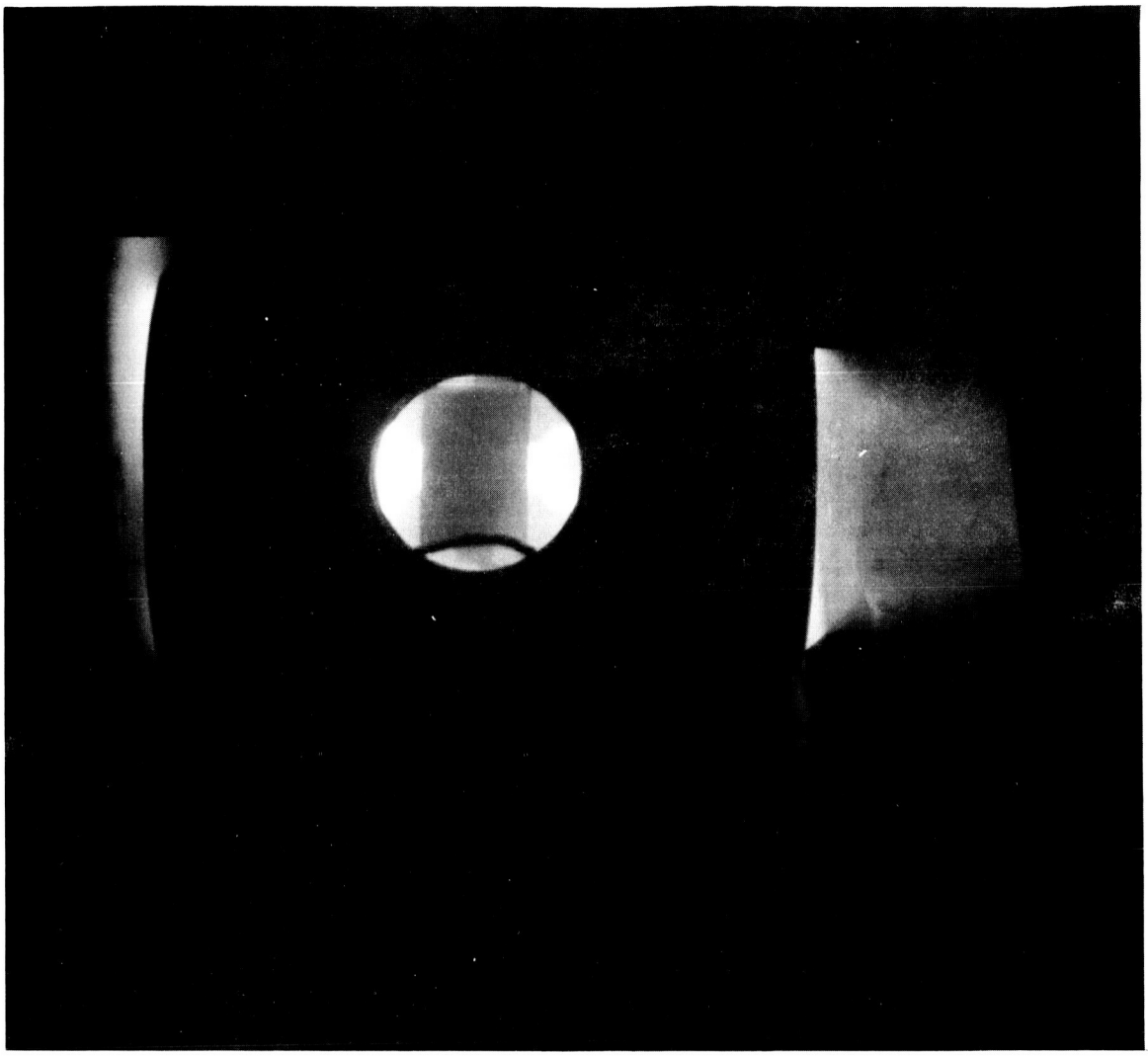

Figure C5 ARC IN OPERATION

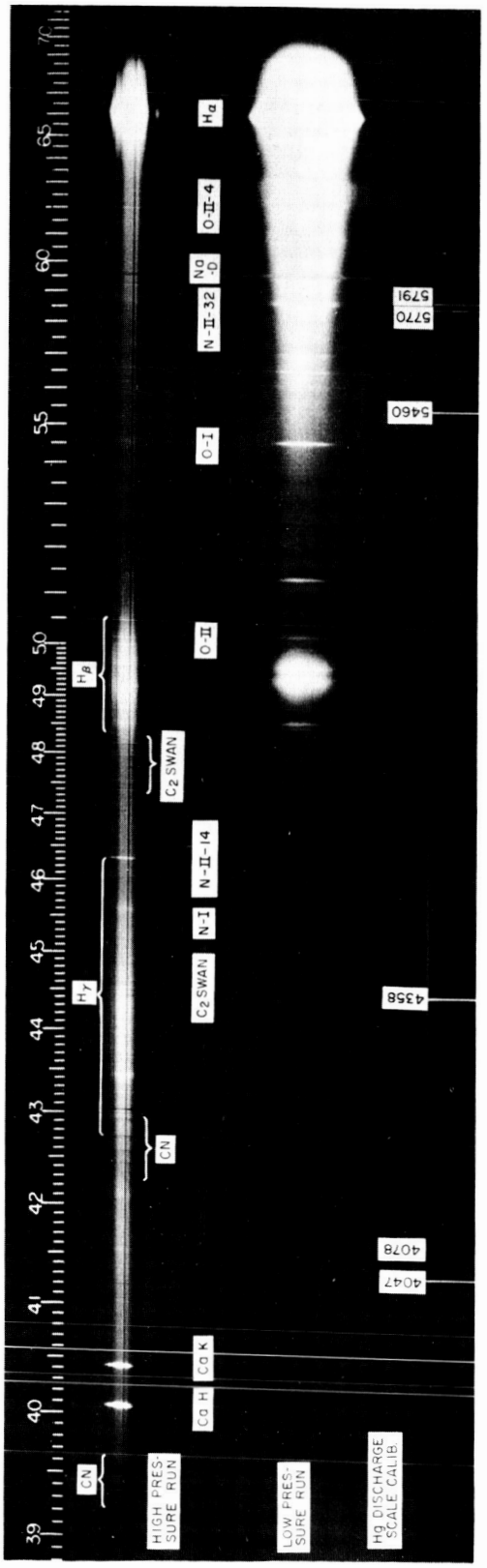

Figure C6 RADIATION SPECTRA OF HIGH-POWERED ARC AT 1.5 ATM AND 3.78 ATM

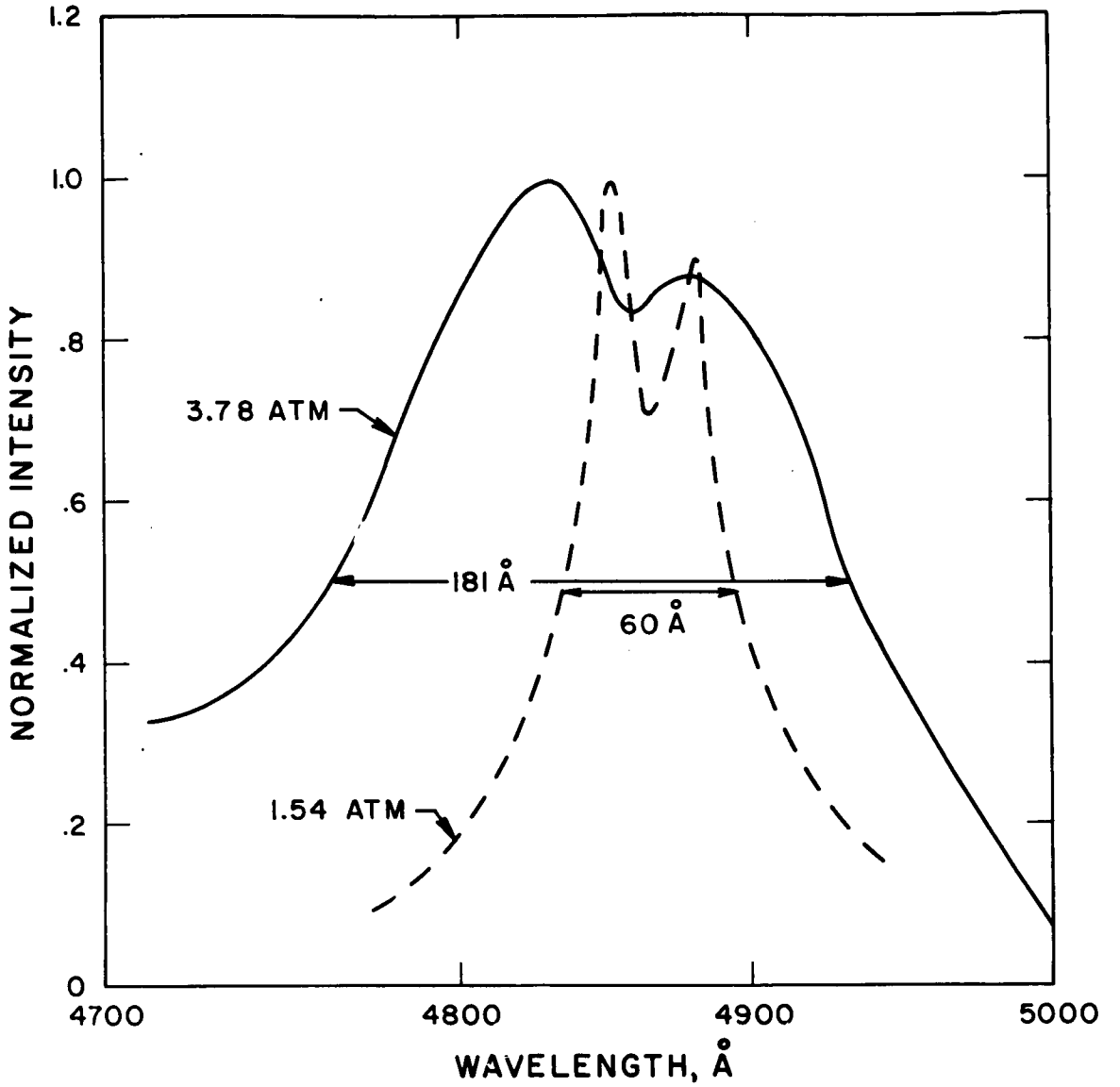

Figure C7 BROADENING OF THE H_β LINE

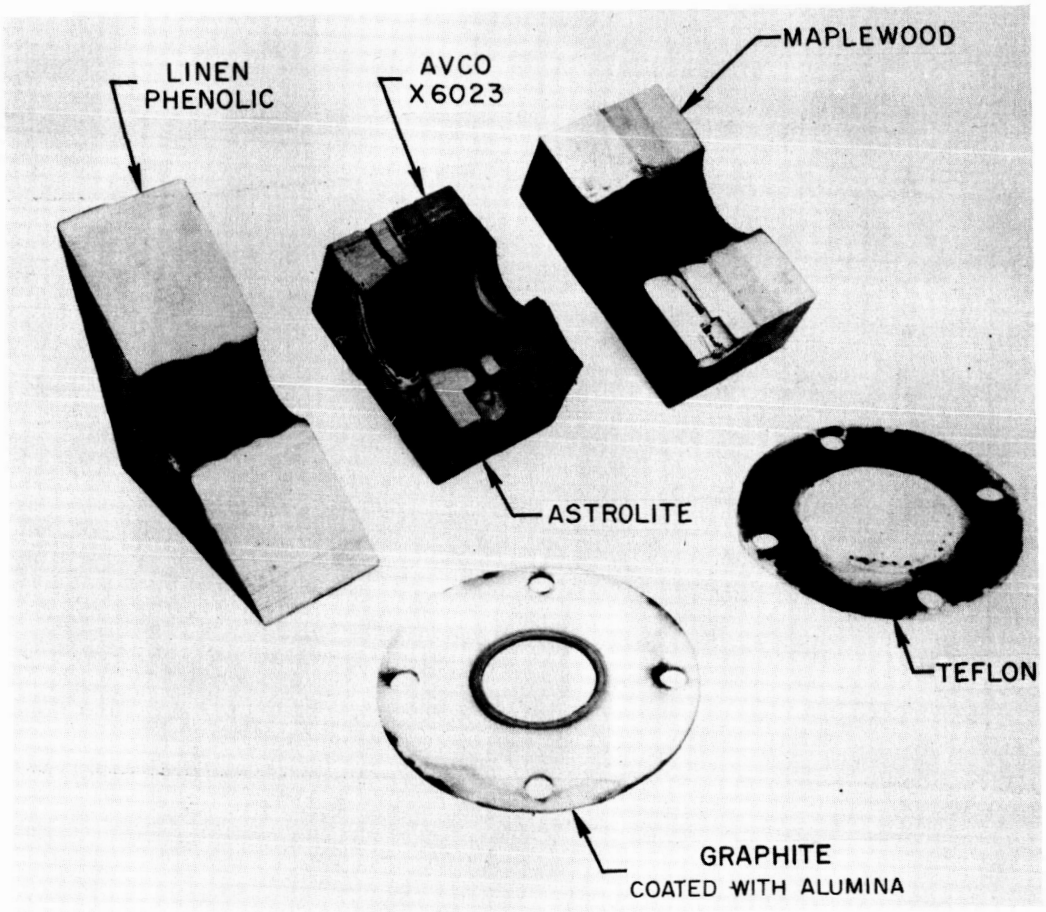

Figure C8 VIEW OF SAMPLES AFTER TEST

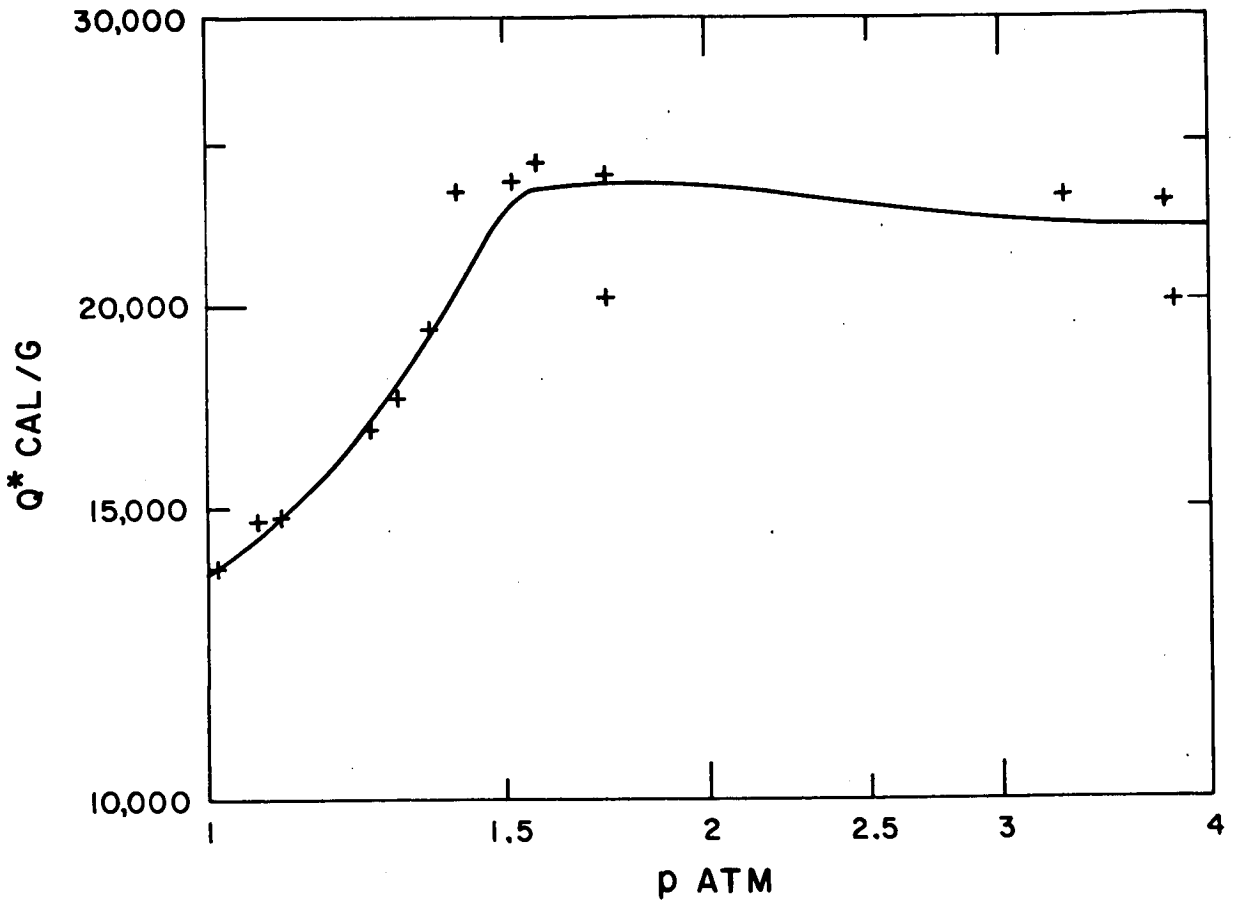

Figure C9 HEAT ABLATION OF LINEN PHENOLIC AS A FUNCTION OF PRESSURE

Generally speaking, the effective heats of ablation are quite high indicating an important shielding of the body due to the presence of vaporized material between the body and the hot gas, and/or to blowing.

5. GAS RADIATION CALCULATION

Figure C10 compares the blackbody and the carbon gas continuum radiation densities as a function of the wave number for operating conditions at 16,000°K and 3 atm (as determined from apparent gas conductivity and measured pressure), the optical depth was taken to be 3 cm. The continuum radiation density for the carbon gas was determined using Ünsold's theory (ref. 4) as modified by Biberman and Norman (ref. 5) for the free-free and free-bound radiation. The carbon gas behaves as a blackbody for wavelengths larger than 1 micron and the emissivity is high over most of the visible. It appears that blackbody radiation would have been achieved at a pressure of about 6 atm.

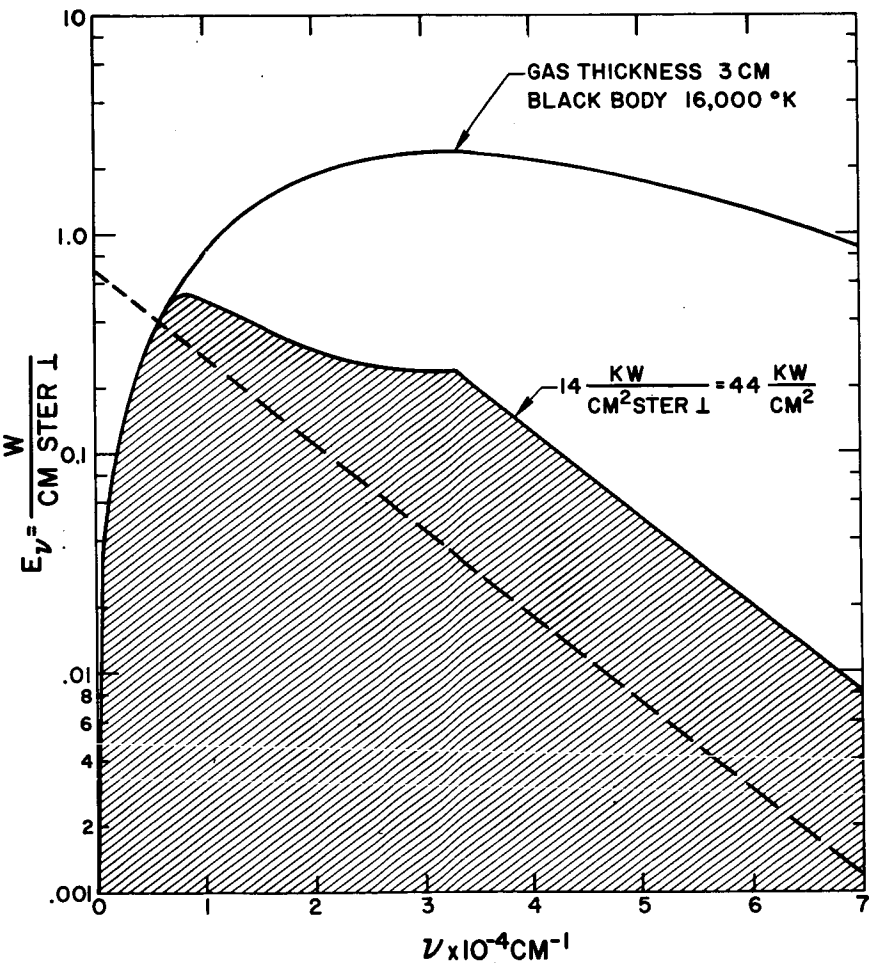

Figure C10 COMPARISON BETWEEN BLACKBODY AND HIGH-TEMPERATURE GAS-RADIATION DENSITIES AT OPERATING CONDITIONS

By integrating the spectral curve for the carbon gas, a power density of 44 kw/cm^2 is found to be falling on the boundary compared to 51 kw/cm^2.

6. AERODYNAMIC HEAT TRANSFER

The high area ratio between test cross section and the throat is such that the maximum Mach number is equal to 0.1 when the flow is choked. The pressurization of the test cell can be used to control the velocity within the test section. The aerodynamic heat transfer in the center section results from stagnation laminar convection. In this section, the high-temperature gas is ionized and the high-diffusivity electrons influence the diffusion of ion-electron pairs to the walls where recombination may occur with the release of the ionization energy. The influence of stagnation heat transfer rate due to ionization has been considered in ref. 6. The results of this investigation indicate, for the conditions of stagnation enthalpy existing in this experiment, the nondimensional heat-transfer parameter $Nu/\sqrt{Re}$ would be close to 0.3. The heat-transfer rate can be derived for conditions existing in test section with graphite walls at the sublimation temperature and for a carbon gas at 16,000°K. This yields a value of 2600 w/cm^2. This heat-transfer rate is much smaller than the radiative (44 kw/cm^2) and does not account for the blowing effect taking place in this experiment.

7. CONCLUSION

An experimental setup has been developed for the production of intense radiation heat pulses which can be used to simulate the very high heat transfer rates due to radiation from the hot gases surrounding bodies at reentry velocities typical of interplanetary flights. Radiation heat transfer up to 50 kw/cm^2 were determined. The effective temperature of the gas column was determined by several methods and the results concur. A theoretical calculation of the radiation heat transfer agrees roughly with experimental, and it is also found that the aerodynamic heat transfer is much smaller. Different materials were tested in this experimental setup and the high values obtained for the heat of ablation indicate an important shielding of the material by the vaporized matter between the wall and the arc column. More work remains to be done to understand the detailed mechanism of heat transfer and to relate the results to actual flight situations.

8. REFERENCES

1. Kivel, B. and K. Bailey: Tables of Radiation from High Temperature Air. Avco-Everett Research Laboratory, Research Report 21, December 1957.

2. Allen, R. A., P. H. Rose, and J. C. Camac: Non-equilibrium and Equilibrium Radiation at Super-Satellite Re-entry Velocities. Avco-Everett Research Laboratory, Research Report 165, September 1962.

3. Griem, H. R., A. C. Kolb, and K. Y. Shen: Stark Broadening of Hydrogen Lines in Plasma. NRL Report 5455, March 1962.

4. Ünsold, A.: Ann. Physik, Vol. 33, 607 (1938).

5. Biberman, L. M., and G. E. Norman: Opt. i Spektr. Vol. 8, 433 (1960); Optics and Spectroscopy, Vol. 8, 230 (1960).

6. Fay, J. A. and N. H. Kemp: Theory of Stagnation Point Heat Transfer in a Partially Ionized Diatomic Gas. Avco-Everett Research Laboratory, Research Report 144, April 1963.

APPENDIX D

HIGH ALTITUDE BREAKDOWN

The mechanics of high-altitude microwave breakdown have been thoroughly investigated in the past. In particular, a gread deal of effort has been expended on antenna breakdown, and the work by Morita, Schorfman, and Chown is well known.

It might be thought that with the present knowledge of low-pressure breakdown, the design and prediction of performance of aerospace antennas is a "cookbook" problem. This largely would be true if antennas with a known field configuration, such as the horn and dipole, were used in standard terrestrial atmospheres. However, the antenna commonly used on the aerospace vehicle is a highly sophisticated, high temperature, miniaturized, dielectric embedded radiator the near field of which is seldom, if ever, known. The proposed cruciform antennas for the lander-orbiter relay link are, in addition, self-diplexing, which is a further complication. The near field is incalculable; and thus, even in the known Earth atmosphere, knowledge of power-handling characteristics in empirical.

Breakdown, from the physicists standpoint, is a matter of solving:

$$\frac{\partial n}{\partial t} = (V_i - V_a)\, n + S + \nabla^2 (Dn) + \alpha n^2$$

where

n = electron density

V_i = ionization rate

V_a = attachment rate

S = ionization from external source

D electron diffusion coefficient

α recombination rate

The αn^2 is not generally considered at sea level, but becomes increasingly important at low pressures and in high electron densities (n^2).

Here, the constant parameters used are measured values of the Earth atmosphere and are not applicable to any other gaseous mixture.

To theoretically predict the power handling capability of an antenna, say, on the surface of Mars, accurate knowledge of the antenna's near field, and the physical constants for the above equation for the Martian atmosphere are required.

Recognizing the above problem, the Avco RAD Aerospace Antenna Section undertook a modest company-sponsored research program in 1962 to investigate high power breakdown in non-Earth atmospheres. It was belived that a simple relationship might exist between the major constituents of various atmospheres and antenna breakdown characteristics, e.g., between sparking potentials or ionization potentials. This, however, was not the case, as is shown in the following discussion.

1. Experimental procedure and results. As the successful operation of the Avco RAD cruciform antenna on numerous reentry flights has proven its applicability and versatility it was chosen as one type of antenna for utilization in the extraterrestrial antenna study. Its superior characteristics under extreme environments also had been proven, and the numerous test records are available for use.

The second type of antenna chosen for study was the horn, as the fields are known, and data may be used in determining the equation constants for various atmospheres.

The third study item was an investigation of cables and connectors which have been subjected to a prolonged high vacuum and then to high RF power at low pressures. This is to check out gassing effects and subsequent gas absorption and power-handling degradation.

The instrumentation and the simulation sphere used are shown in figure D1. The facility is capable of simulating atmospheric pressures from a few atmospheres to approximately 350,000 feet, and any desired gaseous constituent may be introduced into the system.

In figure D2, power breakdown versus altitude is shown for the cruciform antenna in atmospheres of air, N_2, and A. This is a direct inversion of the results obtained with dc or at very low-frequency, where argon, with its low ionization potential is the first to corona. The curves were taken using the high-frequency channel (900 mc) of a scaled antenna.

Figure D3 shows the results of three supposedly identical antennas in an a argon atmosphere. It is seen that one antenna closely approaches the expected curve of air, while the other three curves show phenomena not obtained in air. For instance, if the curve of the No. 1 antenna at 900 mc were typical of one taken in air, it would break down at about 1 or 2 watts in the 140-kilofoot region; however, a secondary ionization apparently occurs in and around the feed dielectric. An almost indiscernible ionization occurs here and keeps the field strength at

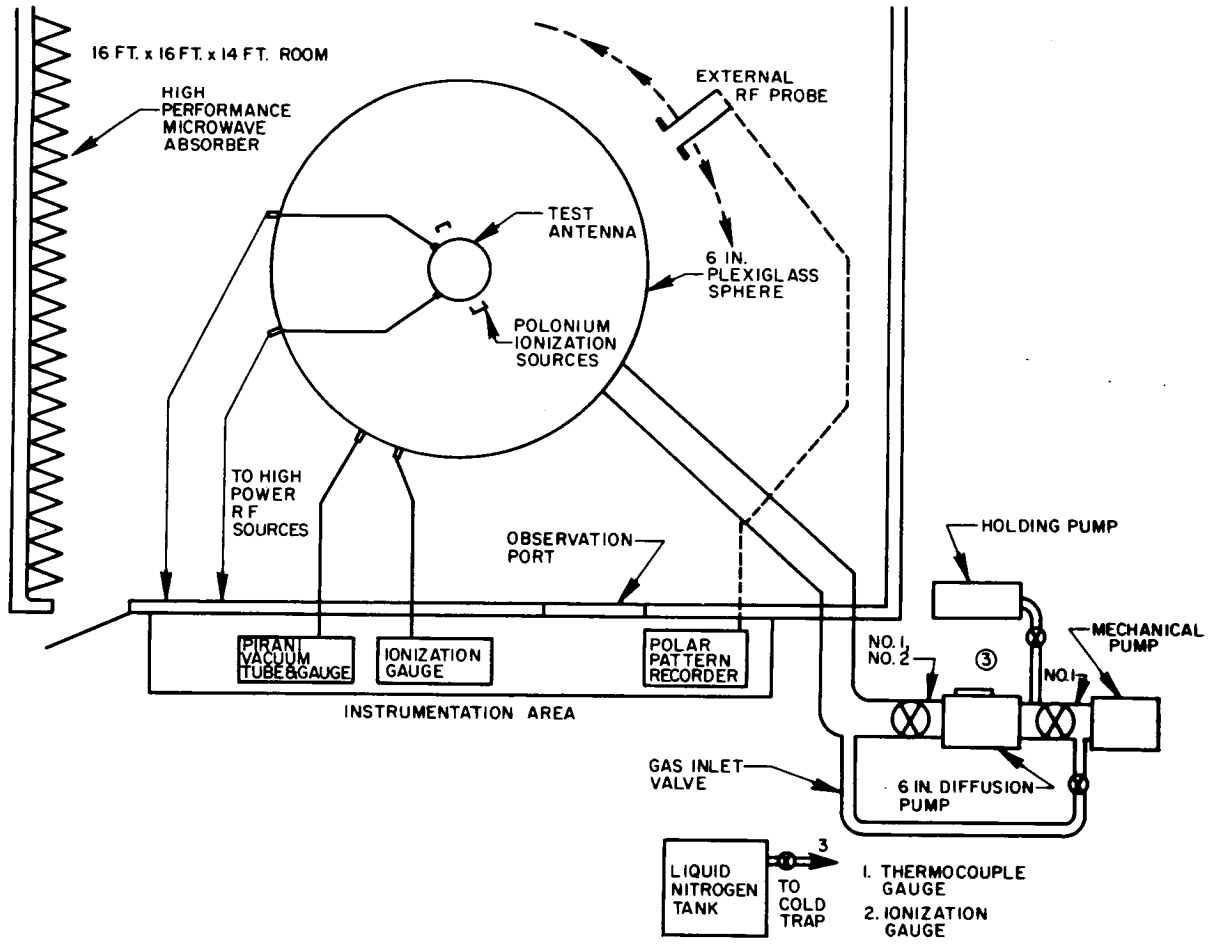

Figure D1 CRUCIFORM ANTENNA WITH LOW TEMPERATURE WINDOW

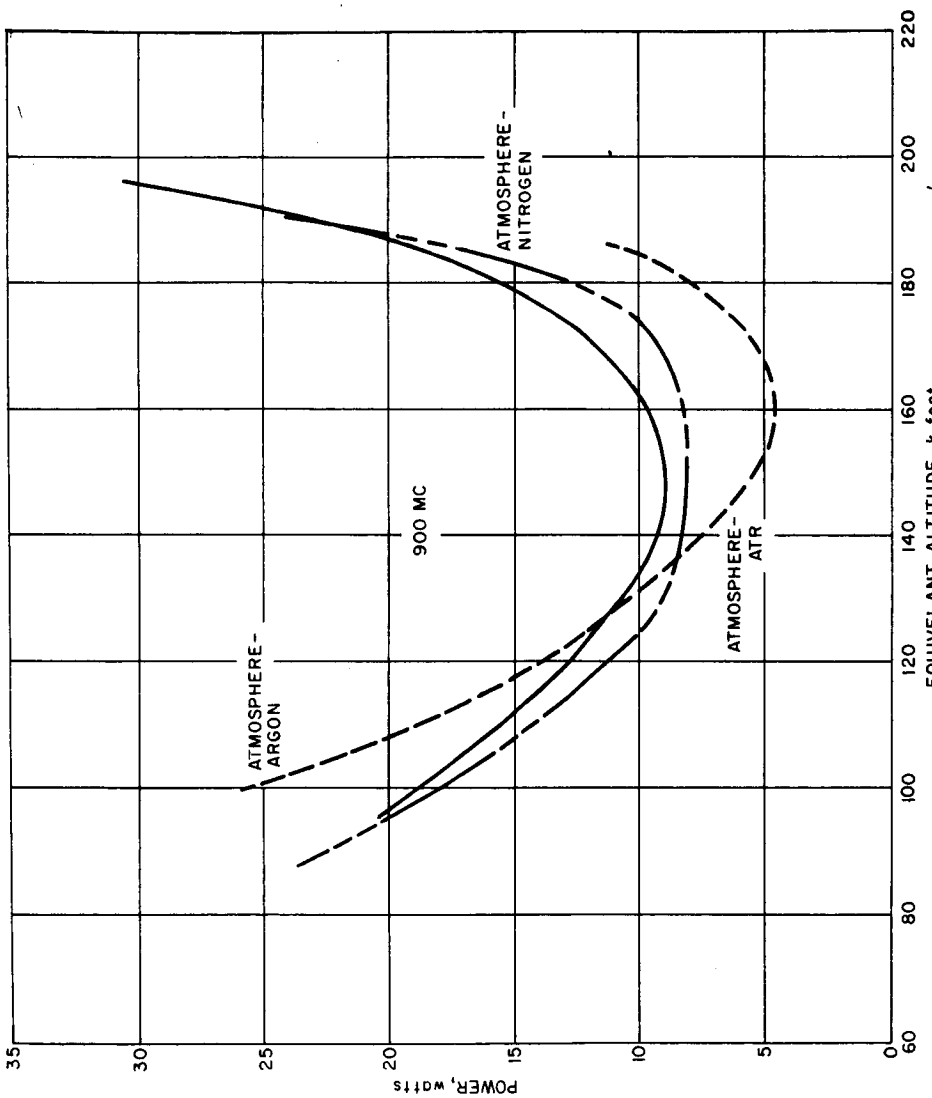

Figure D2 POWER/ALTITUDE BREAKDOWN CURVES, AIR, N_2, AND A, AT 900 MC

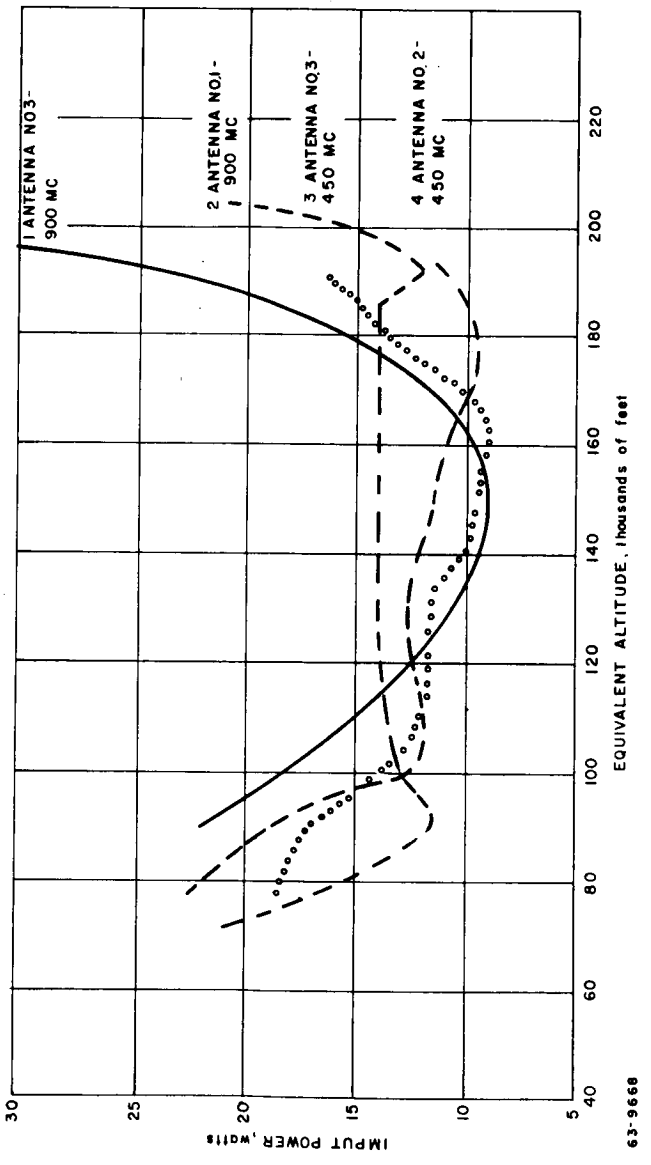

Figure D3 POWER/ALTITUDE BREAKDOWN CURVES, ARGON 450 AND 900 MC

the aperture low enough to avoid ionization there until several times the normal power is applied. Patterns, impedance measurements, and gain measurements will need to be made before this phenomenon can be fully evaluated. The phenomenon also is illustrated at 450 mc, again in an argon atmosphere, with two "identical" antennas in figure D 4.

The major constituent of the Martian surface is believed to be either felsitic rhyolite or limonite. It was not known whether a layer of sand of either material over the antenna window would enhance breakdown. A sample of each, therefore, was prepared and tested. A fine coating of the felsitic rhyolite produced no discernible change, and about an 1/8-inch cover of limonite produced the curve of figure D 5.

Tests on connectors have shown them to be unreliable and breakdown to be generally umpredictable. The long-term exposure of the cables to high-vacuum tests has not yet been done, but it is anticipated that a solid dielectric such as Teflon will be necessary. Trouble may be met if Teflon's susceptibility to inhomogeneities and subsequent pinhole arcing is experienced.

2. Summary of results. Traditional critical points of radiating systems, i.e., feeds and connectors, are the critical areas in low pressure, high power designs. In addition, it is suspected from dc tests in argon, that transmitters and power supplies will have to pressurized if over 50 volts dc is used.

A new breakdown phenomenon was observed when argon was used. The slope of the curve was reversed in the normally, most critical region. This has not yet been fully explained.

The normal power-breakdown-versus-altitude curves for various atmospheres may not mean as much in an atmosphere of high argon content because of the anomalous phenomenon experienced.

Tests of an antenna similar to the one proposed proved its ability to handle 50 watts without breakdown for all external pressures. A cover of sand (limonite) over the antenna surface did not lead to degradation of power-handling capability.

3. Conclusion. The Avco RAD VHF cruciform antenna will fulfill requirements at a 50-watt power level, which is the maximum that can be recommended with the given conditions.

The 70-watt, S-band, horn-feed antenna is practical with regards to power-handling capabilities, if the given configuration is kept or improved.

Connectorless coaxial lines should be considered for reliability.

A thorough study of coaxial cables subjected to a long period of high vacuum and then introduced to a very light atmosphere must be undertaken before reliability can be determined.

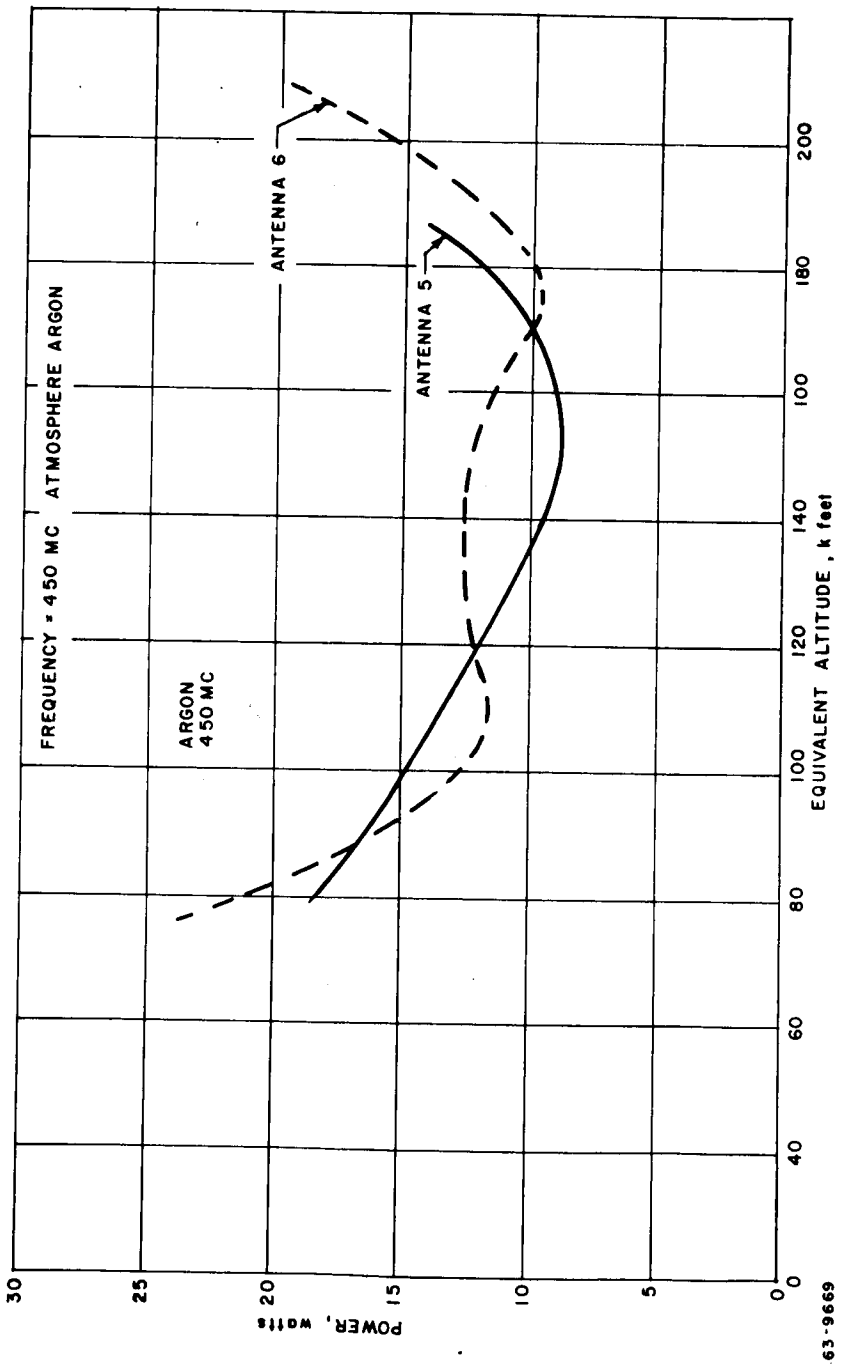

Figure D4 POWER/ALTITUDE BREAKDOWN CURVES, ARGON 450 MC

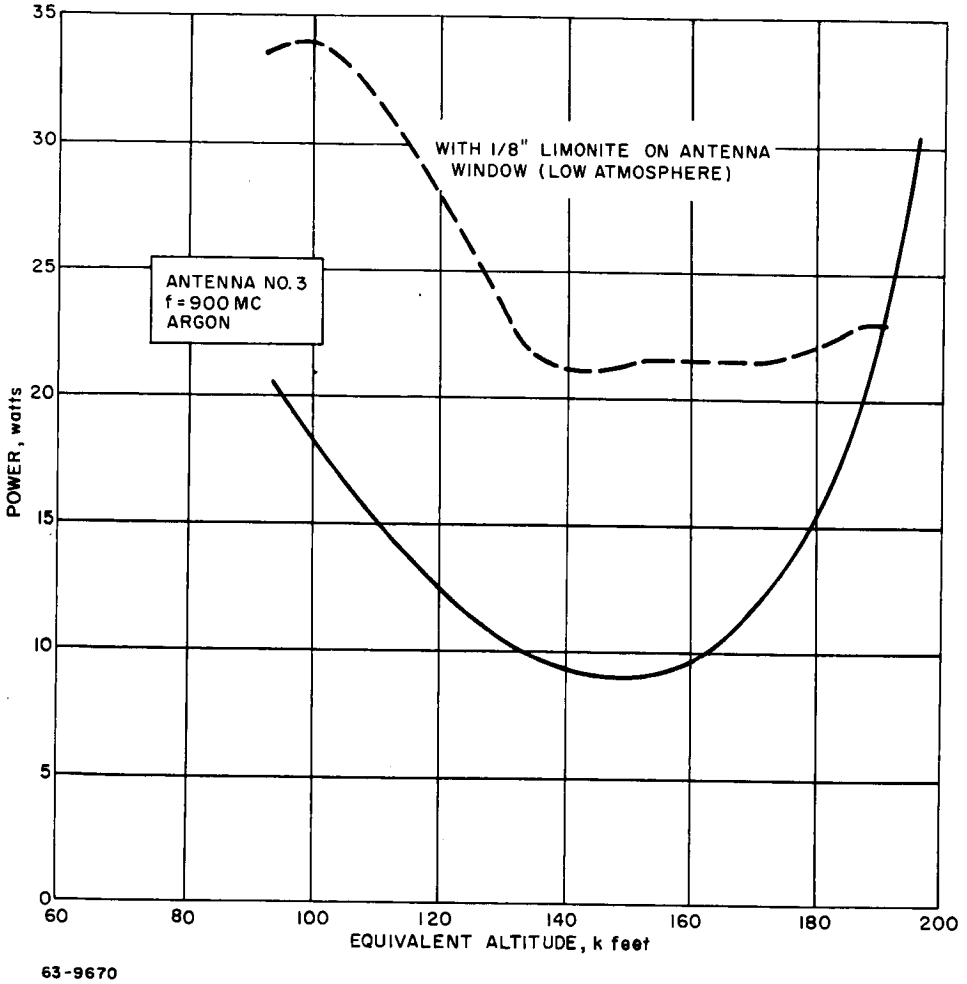

Figure D5 POWER/ALTITUDE BREAKDOWN CURVES, ARGON AT 900 MC WITH 1/8-INCH LIMONITE OVER ANTENNA WINDOWS

TABLE D1

	Frequency (mc)	Presterile VSWR	Poststerile VSWR		Equipment
Power divider C-band 306115	5400 5555 5900	1.30:1 1.30:1 1.23:1	1.30:1 1.30:1 1.21:1		H. P. Amp. 415B Tag 2499 H. P. Osc. S/N 02874 Narda D.S. Tuner 231 Narda Slotted Line Mod 231 Astrolab Load 8067F1
Cable 74	5400 5555 5900	1.05:1 1.21:1 1.14:1	1.10:1 1.21:1 1.15:1		
Antenna C-band 308201	5400 5555 5900	1.35:1 1.10:1 2.0:1	1.10:1 1.18:1 1.65:1		
Antenna C-band 335490	5400 5765 5900	1.75:1 1.26:1 1.45:1	1.75:1 1.28:1 1.50:1		
	High Frequency (mc)	Presterile VSWR	Poststerile VSWR	Poststerile No. 2	Equipment
Antenna UDOP 335109	901 900 899	1.22:1 1.17:1 1.18:1	1.45:1 1.33:1 1.24:1	1.21:1 1.18:1 1.26:1	H.P. Osc. 612A H.P, Amp. H.P. Slotted Line S/N 1658 Cable Ser A39819
	Low Frequency (mc)				
UHF Power Divider 305137	451 450 449 440 450 460	3.0:1 1.20:1 2.40:1 1.32:1 1.50:1 1.51:1	8.0:1 4.8:1 2.2:1 1.30:1 1.45:1 1.50:1	1.88:1 1.45:1 3.40:1	

TABLE D2

LIST OF AVCO COMPONENTS TESTED

Mark 5, Mod 5B CTLI C-band antenna	308201
Mark 11, Mod 4A C-band antenna	335490
Mark 11 UDOP	335109
Teflon cable assembly with connectors C-band	No. 74
C-band power divider	306115
UHF power divider	305137

The peculiarities of the low-pressure, argon-rich atmosphere should be considered perhaps even more than the normal altitude-versus-breakdown curves.

Transmitters and any component with 20 volts or more should be subjected to similar high-altitude simulation tests.

The above investigation represents only a start and the program must be expanded before much of the necessary data is acquired.

Table D1 gives pertinent antenna data, and table D2 lists Avco components tested.

REFERENCES

D1. Voyager Spacecraft LA 5553.

D2. Development of International Efforts to Avoid Contamination by Extra-terrestrial Exploration, Science, Vol. 128, No. 887.

D3. Jaffe, L. D., Sterilization of Unmanned Planetary and Lunar Space Vehicles An Engineering Examination, Jet Propulsion Laboratory, Technical Report No. 32-325 (Rev.)(25, March 1963).

D4. Davis, R. W., and Comuntzis, M. G., The Sterilization of Space Vehicles to Prevent Extraterrestrial Biological Contamination, Xth International Astronautical Congress, London (1959).

D5. Phillips, C. R., and Hoffman, R. K., Sterlization of Interplanetary Vehicles, Science, Vol.132 14, (October 1960).

D6. Jaffee, L. D., Sterilizing Unmanned Spacecraft, Jet Propulsion Laboratory, Astronautics and Aerospace Engineering (August 1963).

DISTRIBUTION

Addressee	No. of Copies
NASA Director, Lunar and Planetary Programs 400 Maryland Avenue SW Washington 25, D. C. Attn: D. P. Hearth, Code SL (+1 reproducible)	10
Central Files	1
Document Control	5
Research Library	134